Selectively fluorinated compounds as bioactives and biomolecular probes

Dominic Eamon Spurling

A thesis submitted for the degree of PhD
at the
University of St Andrews

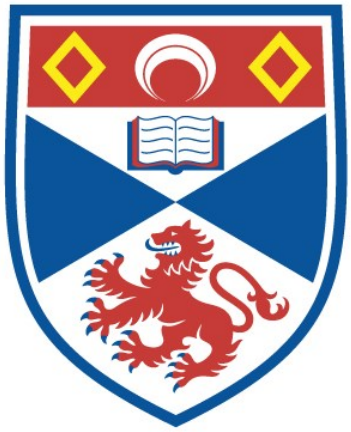

2024

Candidate's declaration

I, Dominic Eamon Spurling, do hereby certify that this thesis, submitted for the degree of PhD, which is approximately 66,000 words in length, has been written by me, and that it is the record of work carried out by me, or principally by myself in collaboration with others as acknowledged, and that it has not been submitted in any previous application for any degree. I confirm that any appendices included in my thesis contain only material permitted by the 'Assessment of Postgraduate Research Students' policy.

I was admitted as a research student at the University of St Andrews in September 2020.

I received funding from an organisation or institution and have acknowledged the funder(s) in the full text of my thesis.

12/06/24

Date Signature of candidate

Supervisor's declaration

I hereby certify that the candidate has fulfilled the conditions of the Resolution and Regulations appropriate for the degree of PhD in the University of St Andrews and that the candidate is qualified to submit this thesis in application for that degree. I confirm that any appendices included in the thesis contain only material permitted by the 'Assessment of Postgraduate Research Students' policy.

12/06/24

Date Signature of supervisor

Permission for publication

In submitting this thesis to the University of St Andrews we understand that we are giving permission for it to be made available for use in accordance with the regulations of the University Library for the time being in force, subject to any copyright vested in the work not being affected thereby. We also understand, unless exempt by an award of an embargo as requested below, that the title and the abstract will be published, and that a copy of the work may be made and supplied to any bona fide library or research worker, that this thesis will be electronically accessible for personal or research use and that the library has the right to migrate this thesis into new electronic forms as required to ensure continued access to the thesis.

I, Dominic Eamon Spurling, have obtained, or am in the process of obtaining, third-party copyright permissions that are required or have requested the appropriate embargo below.

The following is an agreed request by candidate and supervisor regarding the publication of this thesis:

Printed copy

No embargo on print copy.

Electronic copy

No embargo on electronic copy.

12/06/24
Date

Signature of candidate

12/06/24
Date

Signature ~~of~~ supervisor

Underpinning Research Data or Digital Outputs

Candidate's declaration

I, Dominic Eamon Spurling, understand that by declaring that I have original research data or digital outputs, I should make every effort in meeting the University's and research funders' requirements on the deposit and sharing of research data or research digital outputs.

12/06/24
Date Signature of candidate

Permission for publication of underpinning research data or digital outputs

We understand that for any original research data or digital outputs which are deposited, we are giving permission for them to be made available for use in accordance with the requirements of the University and research funders, for the time being in force.

We also understand that the title and the description will be published, and that the underpinning research data or digital outputs will be electronically accessible for use in accordance with the license specified at the point of deposit, unless exempt by award of an embargo as requested below.

The following is an agreed request by candidate and supervisor regarding the publication of underpinning research data or digital outputs:

No embargo on underpinning research data or digital outputs.

12/06/24
Date Signature of candidate

14/06/24
Date Signature of supervisor

Abstract

Fluorine's role in medicinal chemistry and biochemistry cannot be overstated. Its small atomic radius and high electronegativity make fluorine a versatile tool for the design of novel drugs and biomolecular probes.

In Chapter 1 a history of fluorine chemistry is presented, followed by a general discussion of the dominant interactions associated with organofluorine compounds. Fluorine's role in medicinal chemistry, specifically its use in antibiotics is explored, which is followed by a deeper look into the drug resistant bacterium *Mycobacterium abscessus*. Both the all *syn* pentafluoro cyclohexane and binding methods of molecules to DNA will also be examined, foreshadowing the work done in the following chapters.

Chapter 2 details the design, synthesis, and testing of a collection of novel fluorinated β-lactam lactamase inhibitors and antibiotics. Synthesised β-lactams are assayed against an array of drug resistant bacteria, predominantly *M. abscessus* strains. The mechanism of action is also investigated through chemical hydrolysis of the β-lactam ring, which is studied through multiple NMR time courses.

In Chapter 3 the interaction between an all *syn* pentafluoro cyclohexane "Janus face" molecule and both double strand and single strand DNA is investigated. Using biophysical methods centred around Förster resonance energy transfer (FRET), an interaction between DNA and the Janus face motif is described. Chapter 3 also details the synthesis of multiple pentafluoro cyclohexane "building blocks" and biological probes.

Chapter 4 reports the synthesis of a radiotracer which constitutes a pentafluoro cyclohexane motif. The enzymatic radiolabelling *via* the fluorinase enzyme is reported, and evidence of a radioactive pentafluoro cyclohexane probe is reported. Synthesis of additional biomolecular probes for use in a medicinal setting is also described.

Finally, Chapter 5 explores the synthesis of novel A_{2A} receptor agonists which posses a pentafluoro cyclohexane motif. The agonists are subsequently assayed in a radiotracer displacement experiment which showcases the relatively high affinity of the agonists for the human A_{2A} receptor.

Table of Contents

Abbreviations

[H]	Reduction
[O]	Oxidation
A	Alanine
Å	Angstrom
A.u.	Arbitrary Unit
Ac	Acetyl
ACS	American Chemical Society
ADA	Azodicarbonamide
AdoMe	S-Adenosyl-L-methionine
AdoSeMet	Adenosylselenomethionine
Ar	Aromatic
Arg	Arginine
Asp	Aspartic acid
AT	Adenine-thymine
ATCC	American Type Culture Collection
ATR	Attenuated total reflectance
BCG	Bacillus Calmette-Guérin
BDE	Bond Dissociation Energy
Bn	Benzyl
Boc	*tert*-Butyloxycarbonyl
bp	Boiling Point
br	Broad
Bu	Butyl
C	Cystine
c(RGDfK)	*cyclo*(-Arginine-Glycine-Aspartic acid-d-Phenylalanine-Lysine-)
CAAC	Cyclic (Alkyl)(Amino)Carbene
Cat.	Catalyst
CCD	Charge Coupled Device
CFC	Chlorofluorocarbons
ClDA	5'-chloro-5'-Deoxyadenosine
ClDEA	5’-chloro-‘5-deoxy-2-ethynyladenosine
CNS	Central Nervous System
COSY	Homonuclear correlation Spectroscopy
CuAAC	Copper(I)-catalysed azide–alkyne cycloaddition

Cy3	Cyanine 3
Cy5	Cyanine 5
d	Doublet
DAST	Diethylaminosulfur trifluoride
DBO	Diazabicyclooctane
DCM	Dichloromethane
dd	Doublet of doublets
ddd	Doublet of doublet of doublets
dec.	Decomposed
DFT	Density Functional Theory
DIBAL-H	Diisobutylaluminium hydride
DIPEA	N, N-Diisopropylethylamine, Hünig's base
DMAP	4-Dimethylaminopyridine
DMEM	Dulbecco's Modified Eagles Medium
DMF	Dimethylformamide
DMP	Dess–Martin periodinane
DMSO	Dimethylsulfoxide
DNA	Deoxyribonucleic acid
DOI	Digital Object Identifier
DOPr	Δ-opioid receptor
DOX	Doxorubicin
DP	Differential Power
dq	Doublet of quartets
dsDNA	Double stranded deoxyribonucleic acid
dt	Doublet of triplets
EDCI	1-Ethyl-3-(3-dimethylaminopropyl)carbodiimide
EDTA	Ethylenediaminetetraacetic acid
E_{FRET}	Förster Resonance Energy Transfer efficiency
EI	Electron impact
EMCCD	Electron-Multiplying Charge Coupled Device
equiv.	Equivalent
ES	Enzyme Substrate
ESBL	Extended Spectrum Beta-Lactamase
ESI	Electron Spray Ionisation
Et	Ethyl

FDA	5’fluoro-5’-deoxyadeonosine
FDEA	5’-Fluorodeoxy-2-ethynyladenosine
FDG	2-Fluoro-2-deoxyglucose
FDM	2-Fluoro-2-deoxy-D-mannose
FRET	Förster Resonance Energy Transfer
g	Gram/s
G	Guanine
Gly	Glycine
GPCR	G-Protein-coupled receptor
GSK	GlaxoSmithKline
h	Hour/s
HD	High Definition
HF.Pyr	Hydrogen Fluoride Pyridine
HFC	Hydrofluorocarbon
HOMO	Highest Occupied Molecular Orbital
HPLC	High Performance Liquid Chromatography
HRMS	High-Resolution Mass Spectroscopy
HSQC	Heteronuclear Single Quantum Coherence
HWE	Horner-Wadsworth-Emmons
Hz	Hertz
IC_{50}	Half maximum inhibitory concentration
IR	Infrared
ITC	Isothermal Titration Calorimetry
J	Coupling Constant
K	Capacity factor OR Equilibrium constant
Kcal	Kilocalories
L-Met	L-Methionine
L-SeMet	L-Selenomethionine
L	Litre/s
lit.	Literature
Log *P*	Partition coefficient (logarithmic)
LOR	Line of response
LUMO	Lowest Unoccupied Molecular Orbital
Lys	Lysine
m	Meter
m	*Meta*

M	Molarity
m/z	Mass/charge ratio
MBC	Minimum bactericidal concentration
MDPI	Multidisciplinary Digital Publishing Institute
Me	Methyl
mg	Milligram
MIC	Minimum Inhibitory Concentration
min	Minute
mL	Millilitre
mM	Millimolar
mm	Millimetre
mmol	Millimolar
mol	Mole
MP	Melting Point
Ms	Mesyl
ms	Millisecond
MS	Molecular Sieves
NBO	Natural Bond Orbital
NBS	N-Bromosuccinimide
NCTC	National Collection of Type Cultures
NDB	Nucleic Acids Database
NECA	5'-N-Ethylcarboxamidoadenosine
NHC	N-Heterocyclic carbene
nm	Nanometre
NMR	Nuclear magnetic resonance spectroscopy
NTM	Nontuberculous mycobacteria
o	*Ortha*
OD	Optical Density
p	*Para*
PBP	Penicillin Binding Proteins
PBS	Phosphate-Buffered Saline
PCA	Protocatechuic acid
PCD	Protocatechuate 3,4-dioxygenase
PEG	Polyethylene glycol
PET	Positron Emission Tomography
PFAS	Per- and polyfluoroalkyl substances

Ph	Phenyl
Phe	Phenylalanine
pH	Hydrogen dissociation potential
pKa	Acid dissociation constant
pK_i	Inverse log dissociation constant
ppm	Parts per millions
Pr	Propyl
PTFE	Polytetrafluoroethylene
pulv.	Pulverised
q	Quartet
RDS	Rate Determining Step
R_f	Retention Factor
RGD	Arginylglycylaspartic acid
RGM	Rapidly Growing Mycobacteria
RNA	Ribonucleic acid
RP	Reverse Phase
RT	Room Temperature
R_t	Retention time
S	Second/s
SAR	Structure-Activity Relationship
sat.	Saturated
SDS-PAGE	Dodium Dodecyl Sulfate–Polyacrylamide Gel Electrophoresis
SEM	Standard error of the mean
smFRET	Single molecule Förster Resonance Energy Transfer
S_N2	Bimolecular nucleophilic substitution
S_NAr	Nucleophilic aromatic substitution
solv.	Solvent
SPS	Solvent Purification System
ssDNA	Single stranded deoxyribonucleic acid
t	Triplet
T	Theanine
$t_{1/2}$	Half life
TBAB	Tetrabutylammonium bromide
TBAF	Tetrabutylammonium fluoride
TBAI	Tetrabutylammonium iodide

TCI	Tokyo Chemical Industry
TEA	Triethylamine
tert	Tertiary
TFA	Trifluoroacetic acid
THF	Tetrahydrofuran
TIR	Total Internal Reflection
TLC	Thin Layer Chromatography
TMS	Trimethylsilane
Tris	Tris(Hydroxymethyl)aminomethane
TROLOX	6-Hydroxy-2,5,7,8-tetramethylchroman-2-carboxylic acid
Ts	Tosyl
UTI	Urinary tract infection
UV-Vis	Ultraviolet Visible light
Vol.	Volume
w	Week
ΔH°	Standard enthalpy change
δ	Chemical shift
µg	microgram
µL	microlitre
µM	Micromolar
µm	Micrometre
µmol	Micromole

Acknowledgements

First and foremost, I would like to thank my supervisor Prof David O'Hagan for his support and guidance throughout my PhD. His dedication towards fluorine chemistry is unmatched, and his determination and perseverance towards my projects encouraged me to keep going when I would otherwise throw in the towel. I would also like to thank the O'Hagan group for their support and motivation. Although the group has seen many people come and go over the past four years, their memories will be memorialised in the group lore through bard songs and oral tradition. Specifically, I want to thank Dr Rifahath Mon for his mentorship during the early stages of my PhD, Dr Phillip Lowe for teaching me a large deal of biology and being a source of emotional support and guidance, Dr Joshua Clark for saving me from hypothermia, Tommy Poskin, Josephine Stewart, Pusk, Bun, and George Kingsley-Moore for their constant love, support, encouragement and brain rot which kept me going through some of the most stressful times of my PhD.

I also want to thank the many staff of the Chemistry department, specifically Dr Tomas Lebl for his assistance with NMR, Dr Kevin Jones for his aid with safety and patching me up after a few close calls, and Dominic Stewart, for his assistance and great company in the teaching labs while I was demonstrating. I would also like to thank the many collaborators I have worked with over the years, specifically Dr Johnathan Cox and Emily Baker from Aston University, Sergio Dall'angelo from the University of Aberdeen, Prof Carlos Penedo from the University of St Andrews, and Dr Rongfang Liu from Leiden University. Without their time and assistance none of the work in this thesis would be possible.

A massive thank you to the University of St Andrews Athletics and Cross-Country Club. I cannot overstate how much of an impact this club has had on me and my growth during my PhD, and how I will look back on the many memories made with this club with great fondness (especially Manchester 0161 manny on the map). This extended family not only made me a sub-par runner, but also introduced me to amazing people I will cherish forever, specifically; Shaun Allen, Daniel Boulton-Jones, Joshua Corcoran, Owen Crew, Seb Dickie, Armaan Gheewala, Sarah Knight, Ayman Qureshi, Alex Robinson, Samuel Thom, Jasmine Whittaker, Bartek Witkowski, Callum Young, and most importantly, Jessica MacLeod. Thank you also to the St Andrews Catholic Society and Fr Michael John Galbraith for helping me grow in my faith and welcoming me into a fantastic community. I will look back on the many CathSoc events fondly and I am eternally thankful for the constant work done by its selfless members.

I see this PhD thesis not only as the conclusion to the four years spent at St Andrews, but as a culmination of all the academic work which I have done throughout my decade of higher education. To this end, I thank the many mentors which have taught me so much about the world of chemistry and helped me grow academically, most notably Dr Will Unsworth and Dr Mike Edwards. I also thank Mr Ryan Bathew for his constant belief in my talents and encouragement to be the best version of myself.

I would also like to thank everyone who helped me achieve and persevere through my highest of highs and lowest of lows over this past decade, who helped me overcome mental illness, addiction, and grief. Specifically I would like to thank; Dan Aberg for his lukewarm music takes, Aaron Barrett for keeping my ego in check, Esme Callander for her great chat, Nischa Dosanjh for her support during my undergraduate years, Rachael Esh for her hospitality and kindness, James Juxon for showing me how not to approach a woman, Aidan Lynch for knocking my IQ down a few points, Becky Orr for driving me all the way to Dundee, Pryesh Patel for putting up with me for the longest time, Connor Spicer for dragging me in and out the SU, Elliott Stevens for shouting at me for putting my drinks on pool tables, Jed Williams for living in London, and Daisy Wright for believing in me when no one else did. Without these people my life would be a great deal worse, and for this I owe them everything.

Thank you to my extremely intelligent gf Tori *Shona* Fraser for her constant love, compassion, and kindness, and for also proof reading this. Thank you to my aunt Lynn Harmon for being like a second mother to me, showering me with love, support, and encouragement throughout my journey. Finally, thank you to my beautiful mother Marina, who, despite the circumstances we were in, gave me an amazing upbringing and continues to be the most kind hearted woman on this earth.

The research underpinning this thesis has received funding from The Wellcome Trust (Wellcome Trust Institutional Strategic Support Fund, Grant number 105621/Z/14/Z)

Soli Deo gloria

Dedicated to my secondary school chemistry
teacher, Dr. Holroyd, who said I would amount to nothing.

Chapter 1
Introduction

1.1 – Fluorine in organic chemistry

1.1.1 – A brief history of fluorine

The origin of fluorine chemistry can be traced back to the first synthesis of hydrofluoric acid (HF) by Carl Wilhelm Scheele in 1771.[1] Scheele treated the mineral fluorite (calcium fluoride) with sulfuric acid to generate HF gas, a compound which was to form the basis of all organic fluorine chemical production. Electrolysis of hydrogen fluoride also forms the only practical method for the generation of elemental fluorine (F_2 gas).[2] Elemental fluorine was isolated over 100 years later in 1886 by French chemist Henri Moissan, who electrolysed a solution of potassium hydrogen difluoride (KHF_2) in hydrofluoric acid at -23 °C, using platinum-iridium electrodes.[1] For the isolation of this highly reactive element, Moissan was awarded the Nobel Prize in chemistry in 1906.

The first organofluorine compound (and in turn the first carbon-fluorine bond) was synthesised in 1891 by Frederic Swarts,[3] who prepared trichlorofluoromethane using a mixture of antimony trifluoride (SbF_3) and HF to perform a halogen exchange with tetrachloromethane. Giving his name to the reaction,[3] Swarts went on to synthesise many other organofluorine compounds using this procedure, including; trifluoroacetic acid, phenylfluoroform, and monofluoro-ethanol.[3] Notably, many of the compounds synthesised by Swarts would be the first organofluorines to be commercialised, known as “Freons”, a class of compounds that were subsequently employed as refrigerants. Chlorofluorocarbons (CFC) would go on to dominate the refrigerant market, most notably dichlorodifluoromethane.[4] However, when it was established that the halogens in CFC’s was responsible for ozone depletion in the upper atmosphere, these compounds were banned for commercial use in 1987 under the Montreal Protocol and were replaced with hydrofluorocarbon (HFC) alternatives.[5]

Organofluorine compounds make up a large percentage of medicinal and agrochemical products on the market today.[6–10] Fluorinated molecules also appear prominently in materials chemistry, most notably in the form of fluoropolymers such as Teflon™, arguably the most widely used perfluorinated material.[11] However, the growing awareness of research into the persistence of per- and polyfluorinated alkyl substances (PFAS) has found that due to their resistance to degradation they persist in the environment indefinitely, and as such there is an emerging acknowledgement of their risk to biodiversity and human health.[12]

The widespread use of organofluorines can be attributed to the intrinsic properties of the fluorine atom itself, and how its unique place within the Periodic Table underpins the need for continued development of fluorine chemistry.

1.1.2 – Atomic fluorine

Fluorine is the most electronegative element, with the highest Pauling value of 4.0.[13] This high electronegativity originates from its high nuclear charge to atomic radius ratio, and hence high electron affinity, generating fluoride ions with a filled valence shell. The electronegativity of fluorine is compared to other elements in Figure 1.1.[14]

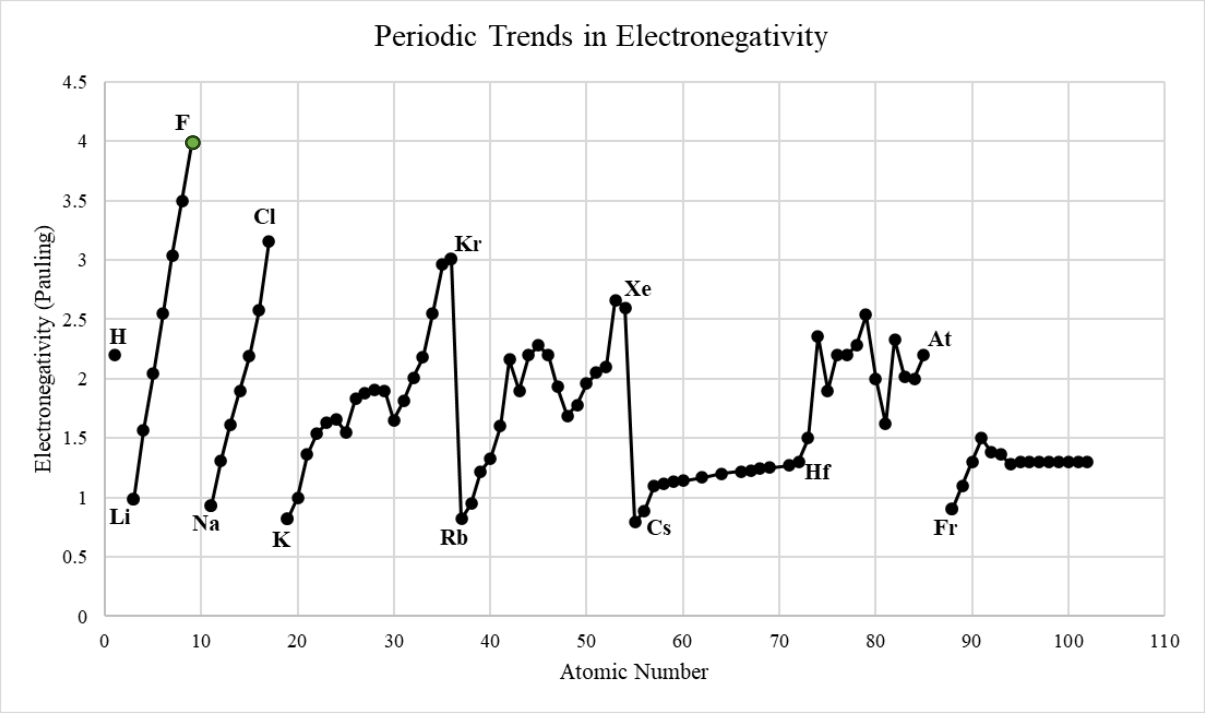

Figure 1.1: Periodic trends in electronegativity. Fluorine (green) is the most electronegative element.[14]

It follows that fluorine has one of the smallest Van der Waals radii (1.47 Å), second only to hydrogen (1.20 Å), and similar to that of oxygen (1.52 Å).[15] Fluorine's small atomic radius allows it to be utilised in place of hydrogen in pharmaceutical development without a significant change in steric impact (see Chapter 1.2.4), but with a significantly increased polarity.

1.1.3 – The carbon-fluorine bond

The carbon-fluorine bond has the highest bond-dissociation energy (BDE) of any element bonded to carbon. A comparison of BDEs for common elements to carbon is shown in Table 1.1.[16]

Table 1.1: Bond dissociation energies for common covalent carbon bonds.[16]

Bond	Bond Dissociation Energy (BDE)/kcal mol^{-1}
C-F	105.4
C-H	98.8
C-O	84.0
C-C	83.1
C-Cl	78.5
C-N	69.7

The electron density of the C-F bond is drawn towards fluorine, producing a highly polarised bond. This leads to significant $C^{\delta+}$–$F^{\delta-}$ electrostatic attraction which accounts for its strength and relatively short bond length (1.385 Å for H_3C-F).[17] The unique properties of the C-F bond lead to its high stability and often low reactivity, especially when compared to other halogens. This is most apparent in S_N2 reactions, where the high barrier to cleavage impacts the rate dramatically, leading to reaction rates which are orders of magnitude slower than the other halogens progressing from chlorine (Table 1.2).

Table 1.2: Relative reaction rate of S_N2 reactions with different halogen leaving groups.

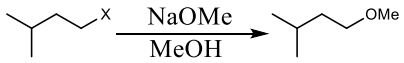

1a - 1d **2**

Halide Leaving Group (X)	Relative Reaction Rate
F (**1a**)	1
Cl (**1b**)	71
Br (**1c**)	3500
I (**1d**)	4500

Interestingly, the opposite is true in S_NAr reactions. When compared to other halogens, aryl fluorines promote faster rates of reaction, as nucleophilic addition is the rate determining step (RDS) of S_NAr. The polar nature of the C-F bond generates an electropositive carbon, and for 2,4-dinitrofluorobenzene **3a**, this leads to a 400-fold increase in relative rate when compared to the next halogen in the series, chlorine (**3b**), as illustrated in Table 1.3.[18]

Table 1.3: Relative S_NAr reaction rates with different halogen leaving groups.[18]

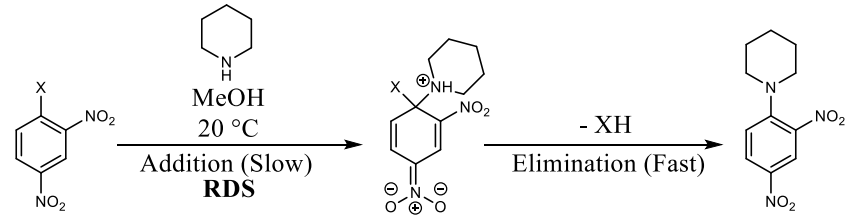

3a - 3d **4a - 4d** **5**

Halide Leaving Group (X)	Relative Reaction Rate
F (**3a**)	1613
Cl (**3b**)	4
Br (**3c**)	4
I (**3d**)	1

Fluorine forms thermodynamically favourable bonds with atoms that have a higher degree of polarizability. This is a consequence of its high electronegativity. The electrons in carbon are more polarisable in orbitals with greater p-character (sp^3 over sp^2) due to the distance of the p orbital and shielding from the nucleus. This in turn allows fluorine to preferentially form stronger bonds with sp^3 hybridised over sp^2 hybridised carbons. This characteristic was illustrated by Dolbier in the example shown in Scheme 1.1.[19] It was demonstrated that the equilibrium lay towards the sp^3 hybridised carbon bound fluorine (**7**) in a Cope rearrangement of **6** to **7**.

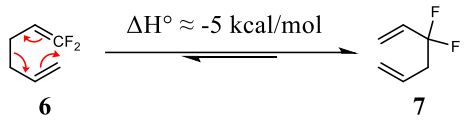

Scheme 1.1: Cope rearrangement of **6** demonstrating preferential formation of sp^3 hybridised C-F bonds.[19]

The efficiency of fluoride ion elimination under basic conditions creates a challenge for the synthesis of many organofluorine compounds. Deprotonation β to fluorine is promoted by the electron withdrawing nature of fluorine. The negative charge of the resultant carbanion is then transferred to fluoride through an $E1_{CB}$ elimination reaction, forming a π-bond (Scheme 1.2).[20] However, elimination is the rate determining step, as the propensity for fluoride to leave is relatively low when compared to the $E1_{CB}$ elimination of other halogens in the series.[20]

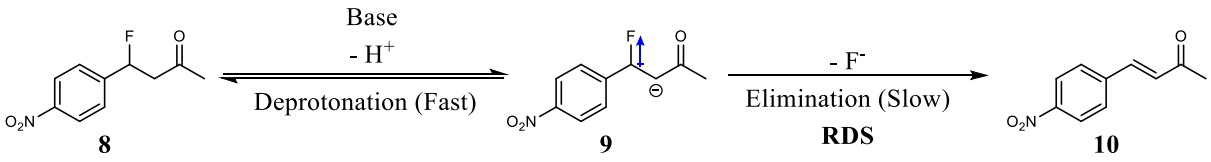

Scheme 1.2: $E1_{CB}$ elimination of fluoride under basic conditions.[20]

1.1.4 – Stereoelectronic effects of the carbon-fluorine bond

Hyperconjugation is a feature of aliphatic organofluorine compounds. The low energy σ* C-F antibonding LUMO can accept electron density from the adjacent higher energy σ C-H bond HOMO in a stabilising hyperconjugation interaction (Figure 1.2). This interaction often impacts favoured conformations and is the basis for widely discussed effects in organofluorine compounds, such as the "gauche effect" and fluorine anomeric effects.

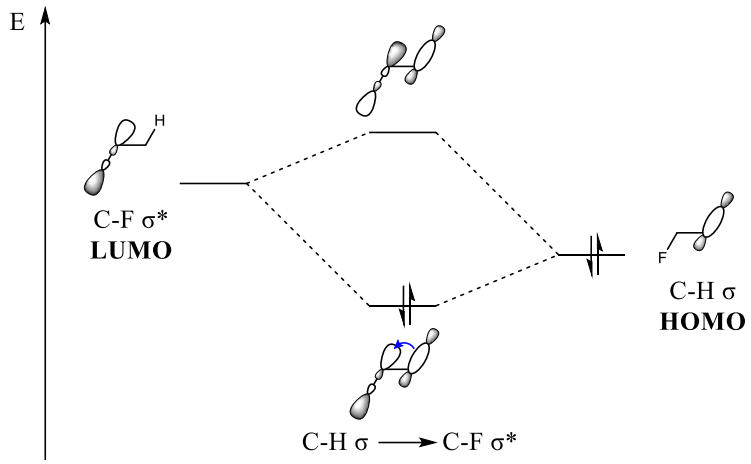

Figure 1.2: Molecular orbital diagram demonstrating energy change from hyperconjugation between C-H σ → C-F σ*.

The anomeric effect rationalises why heteroatom substituents in six membered rings such as dihydropyrans prefer an axial conformation in contrast to the sterically less demanding equatorial conformation. This effect can largely be explained by hyperconjugation; the non-bonding electron pair of the endo-cyclic heteroatom can donate electron density into the LUMO (σ*) of the geminal substituent. Figure 1.3 demonstrates this with a fluorine substituent α to the cyclic oxygen atom. An oxygen lone pair most readily donates electron density into the C-F σ* orbital when the fluorine is axial due to favourable orbital overlap. However, when the fluorine is equatorial, the overlap is significantly reduced, weakening the degree of hyperconjugation, and generating a less stable conformer. In one theory study density functional theory (DFT) predicted a stabilisation of the axial over the equatorial conformer for 2-fluorotetrahydropyran **11** by 2.89 kcal/mol^{-1}. [21]

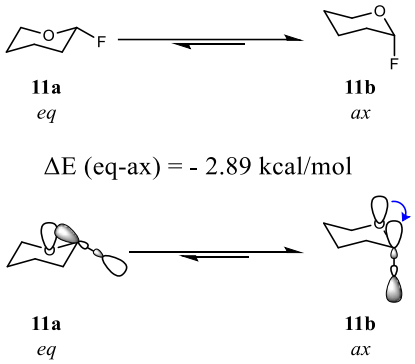

Figure 1.3: Fluorine anomeric effect: Energy difference (ΔE) between the axial and equatorial conformations of 2-fluorotetrahydropyran **11**.[21]

Hyperconjugation also contributes to the conformational preferences of linear fluorinated molecules, such as vicinal difluoroalkanes. The gauche effect recognises that 1,2-difluoroethane **12a** has a lower energy conformation rather than the perhaps expected *anti*

conformation (Figure 1.4).[16] This is in contrast to other 1,2-dihaloethanes which, due to their larger size and electrostatic repulsion, adopt the more obvious *anti*-conformation. For difluoroethane, stability is provided through C-H σ to C-F σ* hyperconjugative interactions which are maximised in the *gauche* conformation. The *anti*-conformer does not offer the required orbital proximity, thus these hyperconjugative interactions are not significant, leading to a less stable conformer.

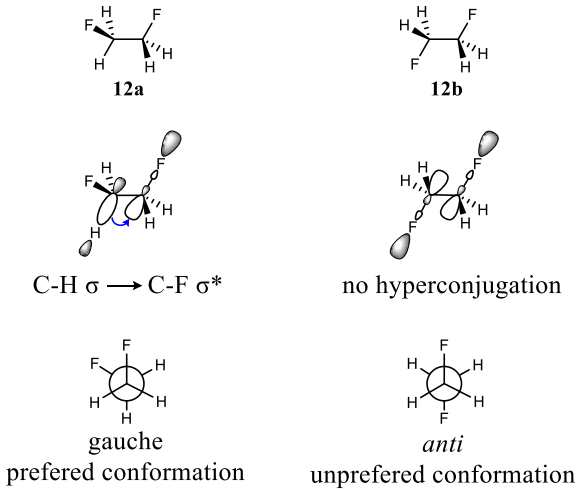

Figure 1.4: Hyperconjugation in the gauche conformation of 1,2-difluoroethane **12**.[16]

Although hyperconjugation is the most articulated explanation of this phenomenon, and natural bonding orbitals (NBO) indicate it is a significant contributor, the true nature of the gauche effect is still a topic of discussion. For example, electrostatic interactions between the fluorines and their electropositive β-carbons is also a stabilising factor. [22,23]

1.1.5 – Dipole-dipole and charge-dipole interactions

Although hyperconjugation may be used to rationalise certain phenomena, it is only one effect that can influence a favoured conformational preference in organofluorine compounds. For example, 1,3-difluoropropane **13** has four vicinally staggered conformers providing a range of relative energies, with the highest energy conformer accommodating electrostatic repulsion between two aligned C-F bonds. interactions (Figure 1.5).[24]

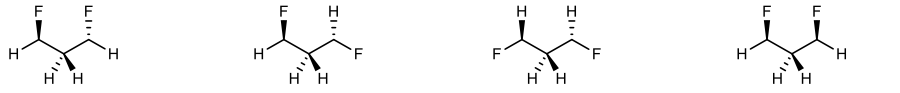

Figure 1.5: Relative energies of four vicinally staggered conformers of 1,3-difluoropropane.[24]

The lowest energy conformer **13a** has two hyperconjugative interactions with minimal dipolar repulsion between the two fluorines whereas the conformers of intermediate energy (**13b** and **13c**) again minimise dipolar repulsion, however, they have one (**13b**) and no (**13c**)

hyperconjugative (C-H σ to C-F σ*) interactions respectively. Thus, the relative energies arise as a consequence of both stereoelectronic and electrostatic effects.

α-Fluoro carbonyls have a clear conformational preference towards the *anti*-conformer due to relaxation between the C=O and C-F bond dipoles. For α-fluoro amides the energy difference between conformers is substantial (-7.5 kcal mol^{-1} from *syn* to *anti*), however this energy difference decreases progressing amide to ester (-4.5 kcal mol^{-1}), to ketone (-2.2 kcal mol^{-1}) and finally to an aldehyde (-1.7 kcal mol^{-1}) (Figure 1.6).[25–28] This trend can be rationalised by a progressive weakening of the dipole strength of the carbonyl which increases electrostatic repulsion between the carbonyl oxygen and the fluorine.

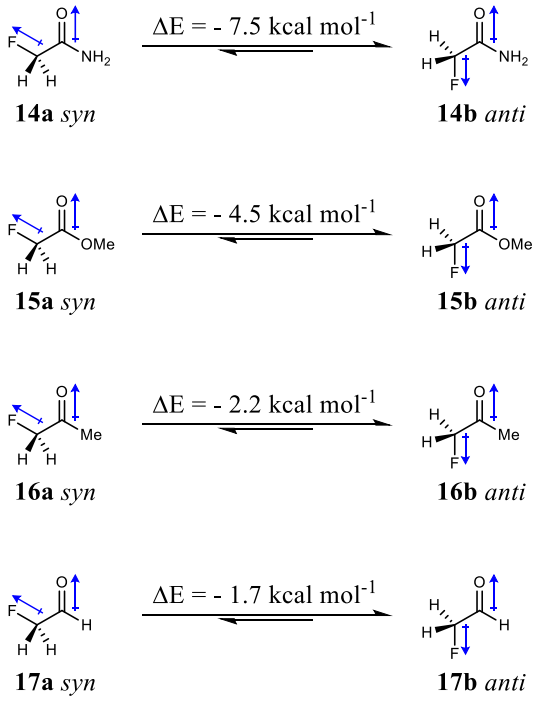

Figure 1.6: Energy differences between the *syn* and *anti*-conformers of given α-fluoro carbonyls.

Conformational preferences of the C-F bond may also arise in positively charged organofluorine compounds. A good illustration of this is the large axial preference for fluorine in 3-fluoropiperidinium ring systems (Figure 1.7).[29]

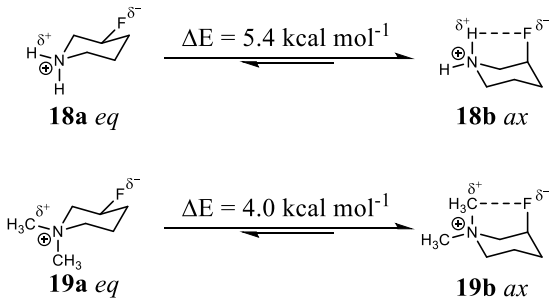

Figure 1.7: Axial preference of the C-F bond in 3-fluoropiperidines **18** and **19**.[29]

The axial conformation of the C-F bond allows for relatively strong electrostatic interactions between the fluorine and the protonated amine (**18**) or with one of the methyl groups of the quaternary amine (**19**). This electrostatic effect results in energy differences of 5.4 or 4.0 kcal mol^{-1} respectively, relative to the corresponding equatorial conformers.

Charge-dipole interactions of fluorine with positively charged species can also lead to changes in bond angles. The four-membered ring azetidinium cation **21** "puckers" if a β-fluorine replaces hydrogen. This can be accounted for by an electrostatic interaction between the electronegative fluorine and the charged (protonated) amine (Figure 1.8).[30]

20 **21**

Figure 1.8: Change in azetidinium ring pucker due to fluorine charge-dipole interaction.[30]

1.1.6 – Fluorine as a hydrogen bond acceptor

A hydrogen bond is defined as an electrostatic interaction between a hydrogen donor (-XH) and a hydrogen acceptor (-Y:) where there is evidence of an interaction between the hydrogen and the acceptor.[31] However, in the case of fluorine, hydrogen bonding is rare. C-F is generally a poor hydrogen bond acceptor, due to its low proton affinity (low-lying lone pair orbitals and electron shell tightness) and its inability to undergo intramolecular electron delocalisation.[32] There are, however, some rare examples of fluorine engaging in hydrogen bonding as evidenced by short F-H contacts from X-ray crystallography. One such example is shown in (Figure 1.9), which shows an intra-fluorine hydrogen bond with a distance of 1.86 Å (**22**).[33]

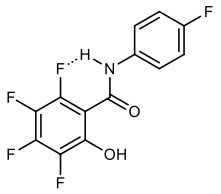

22

Figure 1.9: Example of a hydrogen bond to fluorine in **22**. [33]

An example of a good hydrogen bond to fluorine is found in a "proton sponge" as illustrated by Johnson *et. al* (Scheme 1.3).[34] The trend in basicity illustrated above can be explained by the fact that the conjugate acid of the most basic proton sponge (**25b**) is stabilised by a hydrogen bond with the fluorine. This fluorine-hydrogen bond was further verified by NMR spectroscopy ($^{1}H,^{19}F$-HSQC) which gave a coupling constant similar to predicted ($^{1}H_{(JF)}$ = 44.3 Hz to 43.7 Hz predicted). The conjugate acid was also characterised by X-ray crystallography which validated the presence of a hydrogen bond to fluorine (d_{HF} = 2.13 Å).

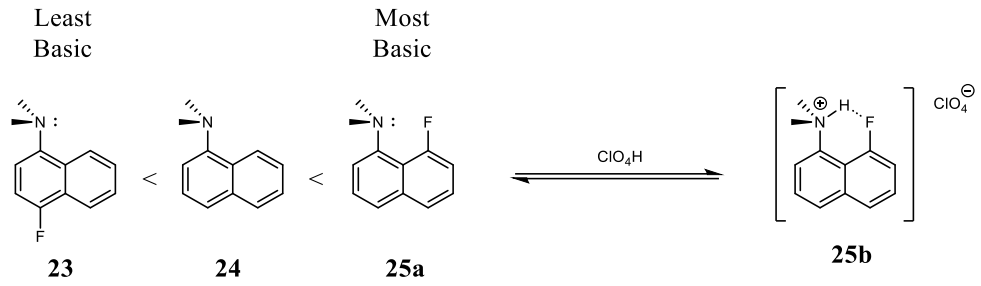

Scheme 1.3: Relative basicity of selected "proton sponges" and the fluorine-hydrogen bond of conjugate acid **25b**.[34]

1.2 – Fluorine in medicinal compounds

The role of fluorine in medicinal chemistry cannot be overstated. It is estimated that 20% of pharmaceutical drugs on the market contain at least one fluorine atom.[9] The first commercially available fluoro-pharmaceutical was Florinef acetate **26** (Figure 1.10),[35] a synthetic corticosteroid that exhibits potent mineralocorticoid properties and high glucocorticoid activity. It is used for the treatment of adrenogenital syndrome, adrenal insufficiency and postural hypotension.[36] Since then, there have been numerous examples of fluorine incorporation into pharmaceuticals, a significant class being the fluoroquinolone based antibiotics.

One such pharmaceutical is the fluoroquinolone antibiotic levofloxacin **27**, an important drug in the history of fluoro-pharmaceuticals. Introduced in the 1980's, fluoroquinolones act as antibacterial agents which inhibit the activity of DNA gyrase and topoisomerase, a mechanism of action entirely different to classical β-lactam antibiotics such as the penicillins, which operate by directly inhibiting bacterial cell wall biosynthesis.[9] Perhaps the biggest fluoropharmaceutical success is the blockbuster pharmaceutical Lipitor **28**. First sold in 1997, Lipitor is mostly prescribed as a statin for the prevention of cardiovascular disease. Lipitor is one of the most widely prescribed medications in the world, with 114 million prescriptions in 2020 alone.[7,37]

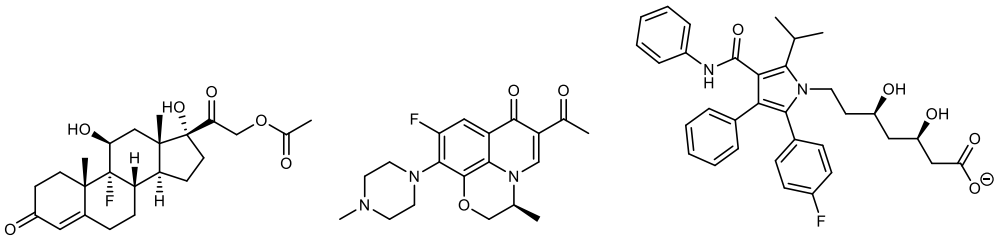

Figure 1.10: Landmark fluoro-pharmaceuticals; Florinef acetate **26**, Levofloxacin **27**, and Lipitor **28**.

It is no surprise that fluoro-pharmaceuticals continue to heavily influence the market, especially when fluorine can be used for the fine tuning of the pharmacokinetics of a drug candidate (eg. lipophilicity, pK_a, conformational bias, slowing metabolism, hydrogen bonding ability etc). Some of these characteristics are described below.

1.2.1 – Fluorine's effect on lipophilicity

Lipophilicity is defined as the ability of a molecule to dissolve in fats, oils or lipids, and is often expressed as the partition coefficient (Log *P*) of an n-octanol/water system. More lipophilic compounds are partitioned in the n-octanol layer and have a larger Log *P* value.[38] In a now legendary assessment of ideal drug candidates, Lipinski's "rule of five" states that the Log *P* of a drug candidate should not exceed 5.[39] This is a partition ratio or 1:100,000 between water and octanol. In order to assist membrane permeability, it may be necessary to increase or decrease a drug candidates lipophilicity, whilst maintaining the drugs bioactivity. As fluorine is similar in size to hydrogen, it can be discreetly introduced into drug candidates to increase or decrease the lipophilicity.

In general, a decrease in lipophilicity is most often seen after replacing sp^3 bound hydrogens with fluorine in saturated aliphatics.[40] On the other hand, selective fluorination and trifluoromethylation of aromatic hydrocarbons, such as benzene tends to increase lipophilicity (Figure 1.11).[41]

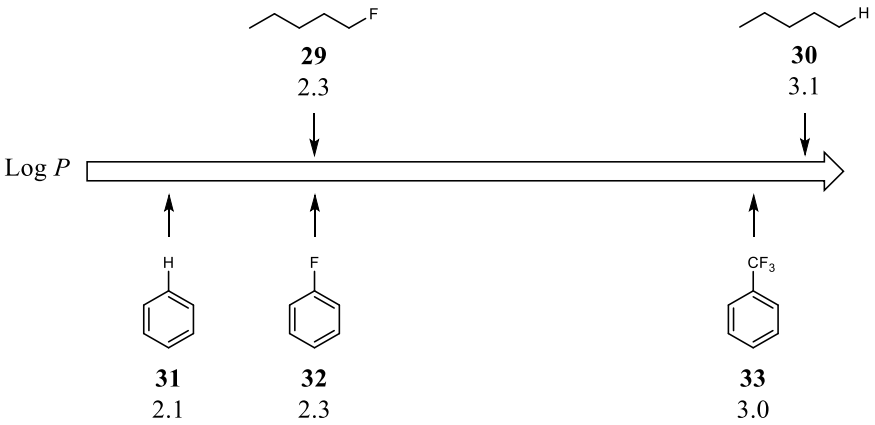

Figure 1.11: Log *P* of selected aliphatic and aromatic compounds.[41]

However, fluorines effect on lipophilicity becomes more complex when heteroatoms are introduced. Jeffries *et. al.* studied the change in lipophilicity of fluorinated alcohols when compared to their non-fluorinated analogues (Figure 1.12),[42] and found that in specific instances there was a decrease in measured Log *P* between the "parent" compound and the fluoro-analogue. Replacement of the terminal CH_2 group in butanol with a CF_2 group led to an increase in polarity of the alcohol **37** in Figure 1.12. This is caused by polarising the proximate OH group and in turn increasing its hydrogen bonding donor ability with water. This effect lessens the further the CF_2 group is from the alcohol, as the electron withdrawing impact the CF_2 group has on the OH weakens. However, the CF_2 polarises the adjacent hydrogens and this leads to a significant effect on increasing polarity, and thus decreasing lipophilicity.

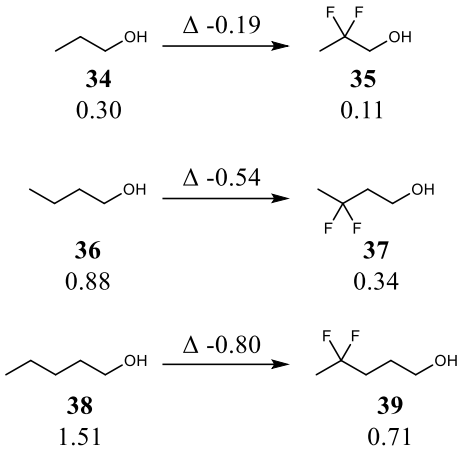

Figure 1.12: Log *P* change upon fluorination of alcohols.[42]

Jeffries *et. al.* also found that progressively replacing the terminal CH_3 with a CF_3 in a range of alcohol lengths resulted in a consistent increase in lipophilicity, as summarised in Figure 1.13.[42] This is caused by the CF_3 creating a hydrophobic surface on the molecule, due to a lack of hydrogen bonding potential, leading to an increase in lipophilicity.

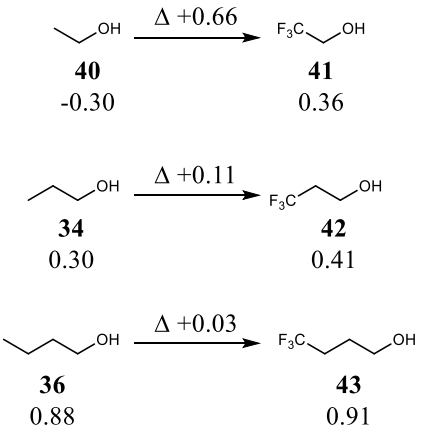

Figure 1.13: Log *P* change upon trifluorination of alcohols of different lengths.[42]

However, effects on lipophilicity can be somewhat difficult to predict for multi-substituent aromatic systems, such as those illustrated in Figure 1.14.[43] When a single fluoro-substituent is placed *ortho* to the hydroxyl group of paracetamol **44** the Log *P* increases, and as expected, difluoro-*ortho*-substitution (**46**) increases lipophilicity further. This is again caused by the withdrawal of electron density from the oxygen. However, when difluoro-substitution occurs *meta* to the hydroxyl (**47**), there is little change to lipophilicity, due to the inability of fluorine to effectively withdraw electron density from the oxygen.

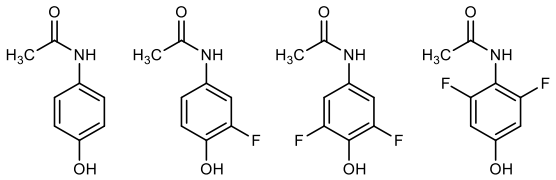

Figure 1.14: Log $D^{3.0}$ of Paracetamol **44** and it's fluorinated analogues.[43]

A broad scope study of 293 proprietary aromatic compounds taken from the Roche in-house collection found that, on average, the substitution of a single hydrogen atom for a fluorine increases lipophilicity by 0.25 Log *D* units.[44]

1.2.2 – Fluorine's effect on pK_a

pK_a is the standard method of measuring the ability of a proton to dissociate from a molecule in solution. It gives insight into the strength of acids and bases (by way of a bases conjugate acid), where a lower pK_a correlates to a stronger acid on a logarithmic scale.

The effect of fluorine on pK_a is dependent on its proximity to functional groups, and due to the electronegativity of the fluorine atom, it can influence the pK_a value through inductive effects. Thus, fluorine substitution can decrease the basicity of aliphatic or aromatic amines. For example Figure 1.15.i compares the relative basicities of ethylamine to its fluorinated analogues.[44] The pK_a of the protonated amine decreases in a linear fashion with progressive substitutions of hydrogens for fluorines (from 10.7 to 5.7).

A lower basicity is often required to improve a compound's ability to pass through a cell membrane and can also be utilised as a tool to solve a host of biochemical challenges. Van Niel *et al.*[45] demonstrated how the selective incorporation of fluorine was used to significantly lower the pK_a of $5Ht_{1D}$ receptor ligand **53**, modestly reducing the compounds binding affinity of **52** but dramatically increasing its bioavailability (Figure 1.15.ii).

i

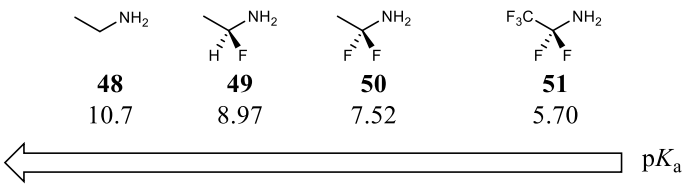

ii

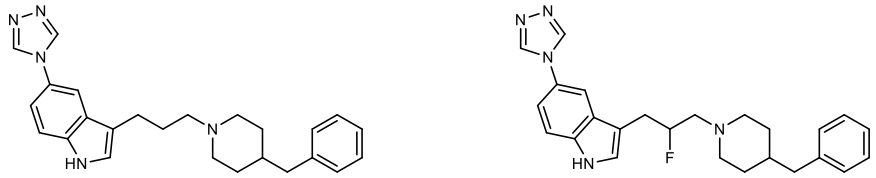

52
IC_{50} = 0.3 nm
pK_a = 9.7
low bioavailability

53
IC_{50} = 0.9 nm
pK_a = 8.7
high bioavailability

Figure 1.15: i) Progressive relationship between amine basicity and fluoro-substitution.[44] **ii)** utilization of fluoro-substitution for bioavailability optimisation of $5Ht_{1D}$ receptor ligand **53** *via* lowering of pK_a.[45]

Increased acidity of functional groups (such as carboxylic acids) may also be desirable in drug discovery. In a complementary manner to amines, fluorine substitution adjacent to an acidic group will decrease its pK_a due to electron withdrawal. This is most apparent when comparing the acetic acid (pK_a = 4.76) series through mono, di and trifluoracetic acid (TFA) (pK_a = -0.25) (Figure 1.16).

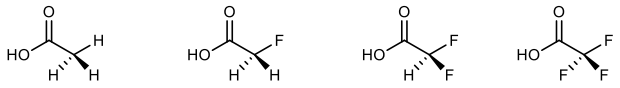

54 4.76 **55** 2.66 **56** 1.33 **57** -0.25

Figure 1.16: Progressive relationship between carboxylic acid acidity and fluoro-substitution.

This relationship was utilised by Kokuryo *et al.*[46] for the development of the rheumatoid arthritis drug **59** (Figure 1.17). The non-fluorinated analogue **58** shows high levels of toxicity due to poly-glutamylation (polymerisation with glutamic acid) at the terminal carboxylic acid, but after introduction of a fluorine atom α- to the carboxylic acid group the amount needed for a lethal dose was increased by a factor of 15. The increased acidity of the terminal carboxylic acid substantially reduced the compound's ability to undergo poly-glutamylation whilst maintaining good levels of T and B cell inhibition.

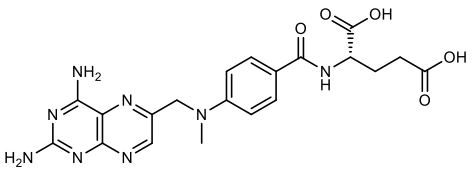

58

IC_{50} (T Cell) = 6.1 ng/mL
IC_{50} (B Cell) = 12.5 ng/mL
Lethal dose in mice = 40 mg/kg

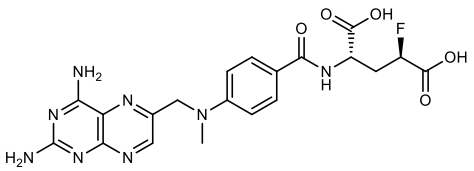

59

IC_{50} (T Cell) = 25.9 ng/mL
IC_{50} (B Cell) = 21.0 ng/mL
Lethal dose in mice = 600 mg/kg

Figure 1.17: IC_{50} and lethal dose values of methotrexate **58** and its fluorinated analogue **59**.[46]

1.2.3 – The effect of fluorine on metabolism

Before a drug candidate can be considered for human use its metabolism needs to be understood. Many fluorinated compounds can produce harmful metabolites when absorbed into the human body, and at high enough concentrations these metabolites can accumulate and become toxic. The simplest fluorine containing metabolite is fluoride, generated from C-F bond cleavage. While fluoride can be beneficial in small doses, amounts of over 10 mg/day can result in undesirable side effects, such as skeletal fluorosis.[47] A highly problematic fluoro-metabolite is fluoroacetic acid, produced primarily from the oxidation of fluoroamines and fluoroethers. Fluoroacetic acid is among the most toxic compounds known and has an LD_{50} = 10 mg/kg in humans. Fluoroacetic acid at this concentration disrupts the Krebs cycle, a central process in respiration, in turn leading to death.[47]

Despite the risk of generating harmful fluoro-metabolites, substitution of labile C-H bonds with more inert C-F bonds can be employed to inhibit metabolism. A good example is illustrated by the development of Ezetimibe **61** (Figure 1.18).[48] When interacting with cytochrome P450 monooxygenases, the first generation of Ezetimibe **60** was oxidised and produced a complex metabolic mixture which proved to be more toxic than the pre-metabolised drug itself. This "non-productive" metabolic pathway is blocked by the introduction of fluorine at the *para* positions of two aromatic rings, protecting the labile sites of the molecule from unwanted oxidation. In addition, the electron withdrawing capacity of fluorine also withdraws electron density from the aromatic ring, leading to a more electrophilic lactam carbonyl and an improved mechanism of action. These factors, as well as incorporation of other functionalisation to encourage active metabolism, increased the potency of Ezetimibe 400-fold.[8]

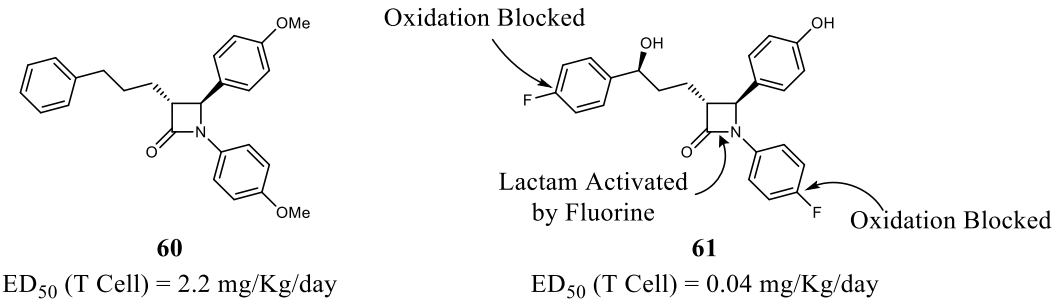

60
ED_{50} (T Cell) = 2.2 mg/Kg/day

61
ED_{50} (T Cell) = 0.04 mg/Kg/day

Figure 1.18: Optimisation of Ezetimibe **61**.[8]

Incorporation of fluorine into drugs can also substantially increase the half-life of a molecule under physiological conditions. This in turn leads to enhanced metabolic stability and thus extends the activity of the administrated drug. This is seen clearly in the case of the potent platelet aggregating agent Thromboxane A_2 **62** (Figure 1.19).[49] Incorporation of a CF_2 group into the oxetane ring reduces the rate of acid hydrolysis of the epoxy-acetal linker 10^8-fold. This is due to the CF_2 group destabilising any adjacent formed carbocation, in turn reducing the rate of hydrolysis.

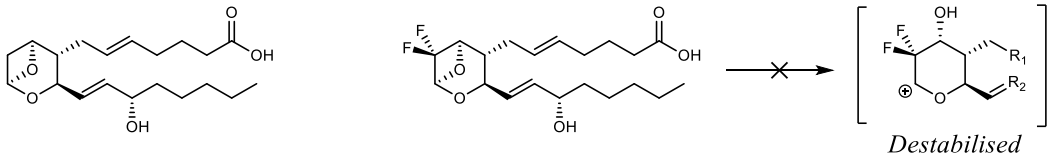

Thormboxane A_2 **62**
Ring hydrolysis half-life = 32 s

7,7-Difluoro Thormboxane A_2 **63**
Ring hydrolysis half-life = 101 yr

Figure 1.19: The CF_2 group stabilises Thromboxane A_2 **63** *in vivo*. [49]

1.2.4 – Fluorine as an isostere

The concept of isosteres was first conceived by Langmuir in 1919 and they are loosely defined as substituents with similar steric and electronic properties compared to the parent compound.[50] Isosterism is now mainly associated with medicinal chemistry and drug development. Bioisosteres are chemical substituents of similar size and electronics with broadly similar biological properties, and are employed in drug development to reduce toxicity, improve bioavailability, and alter metabolism. Fluorine is comparable in size to oxygen, allowing the opportunity to incorporate fluorine in place of oxygen within functional groups to generate bioisosteres.

The replacement of a carbonyl bond with fluorine is of particular interest to medicinal chemists, as the C-F bond preserves the dipole of the parent compound whilst preventing unwanted biochemical reactions such as hydrolysis or reduction. This is demonstrated with camptothecin **64** and its fluorinated analogues (Figure 1.20).[51] Camptothecin **64** acts as an inhibitor of topoisomerase I and shows substantial antitumour activity.[52] However, the hydrolytically

susceptible lactone ring generates a biologically inactivate carboxylate under physiological conditions. Replacement of the lactone with an α-fluoro ether led to a substantial increase of *in-vivo* half-life (**65**), removing the possibility of hydrolysis whilst maintaining a dipole moment similar to that of the lactone. However, fluorine substitution led to decreased inhibitory activity against the three cancer cell lines A459, MD-MB-435, and HCT-116. This was remedied by incorporating a cyclohexyl moiety on the quinoline ring (**66**), restoring similar levels of inhibitory activity (Figure 1.20).

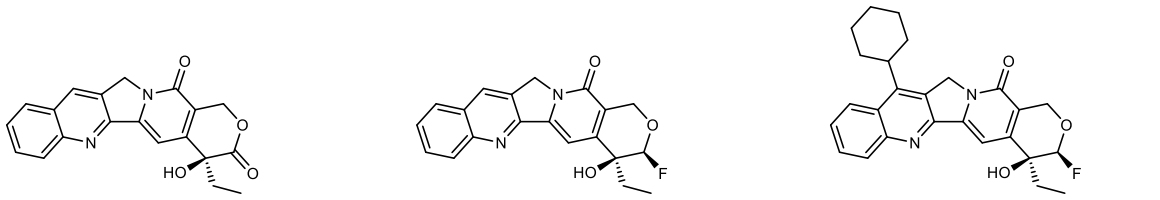

64	**65**	**66**
Lifetime (pH 7.4): 43.7% after 6 h	Lifetime (pH 7.4): 96.0% after 6 h	Lifetime (pH 7.4): > 99.0% after 6 h
A459 EC_{50} = 0.65 μM	A459 EC_{50} = 9.95 μM	A459 EC_{50} = 0.71 μM
MD-MB-435 EC_{50} = 0.45 μM	MD-MB-435 EC_{50} = 58.3 μM	MD-MB-435 EC_{50} = 0.41 μM
HCT-116 EC_{50} = 0.07 μM	HCT-116 EC_{50} = 6.35 μM	HCT-116 EC_{50} = 0.07 μM

Figure 1.20: Data associated with camptothecin **64** and fluorine analogues **65** and **66**.[51]

Another example is demonstrated with the optimisation of Leu-Enkephalin **67**, which activates the Δ-opiod receptor (DOPr) (Figure 1.21).[53] Although Leu-Enkephalin **67** has a good pharmacodynamic profile, the peptide does not produce analgesia when injected intravenously. This is due to the inability of the peptide to cross the blood-brain barrier and reach the opioid receptors in the central nervous system (CNS). This is in part due to the molecule's low lipophilicity (Log $D_{7.4}$ = -0.95). However, when the second amide bond is substituted with a *trans*-fluoroalkene isostere (**68**), the drugs lipophilicity was increased (Log D = -0.11) whilst maintaining similar H-bond acceptor ability and good bioactivity levels (K_i = 43 ± 14 nM).

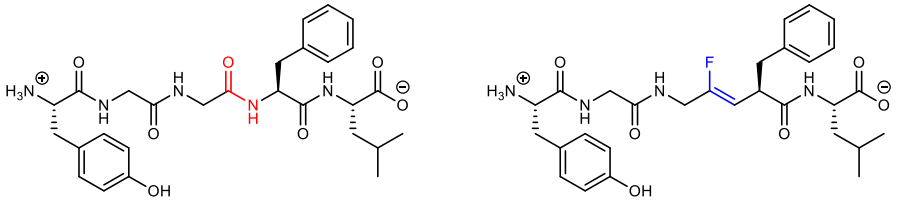

Leu-Enkephalin **67**	**68**
K_i = 6.9 ± 2.3 nM	K_i = 43 ± 14 nM
Log $D_{7.4}$ = -0.95	Log $D_{7.4}$ = -0.11

Figure 1.21: Lipophilicity and bioactivity relationship between Leu-Enkephalin **67** and fluoroalkene isostere **68**.[53]

1.3 – β-Lactam antibiotics and β-lactamase inhibitors

1.3.1 – β-Lactam antibiotics

Antibiotics are the most common and effective method of choice to combat bacterial infections. An important class of antibiotics are β-lactams, which include penicillins.[54] Pharmaceuticals containing a β-lactam core are some of the most common and accessible in the antibacterial market. β-Lactam antibiotics are distinguished by their structure; all molecules belonging to this family contain the 4-membered β-lactam ring (Figure 1.22, blue). In 2014 it was reported that drugs containing a β-lactam core constitute a large percentage of N-heterocyclic drugs approved by the FDA, with drugs containing cephem and penam moieties making up 10% of the 640 pharmaceuticals possessing an N-heterocycle.[55]

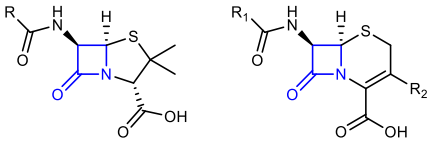

Penams **69** Cephems **70**

Figure 1.22: Core structures of penams **69** and cephems **70** with the β-lactam ring in blue.

β-Lactams operate by preventing the synthesis of bacterial cell walls *via* inhibition of *trans*-peptidases, cross linking enzymes, known as penicillin binding proteins (PBP).[56] Target bacteria are encased by a membrane comprised of layers of peptidoglycan, a covalently cross-linked polymer matrix which endows the bacteria with mechanical stability and dictates the cell shape.[57] It is the activity of *trans*-peptidases, and PBPs, that maintains the peptidoglycan layer *via* the addition of disaccharide pentapeptides which extend the peptidoglycan layer and cross-link adjacent peptide strands.[58] β-Lactams interfere with the homeostatic maintenance of the peptidoglycan layer by blocking the cross-linkage of peptidoglycan units by inhibiting peptide bond formation catalysed by PBPs.[59,60] Figure 1.23 summarises this process,[61–63] with penicillin **69** used as an example β-lactam drug.

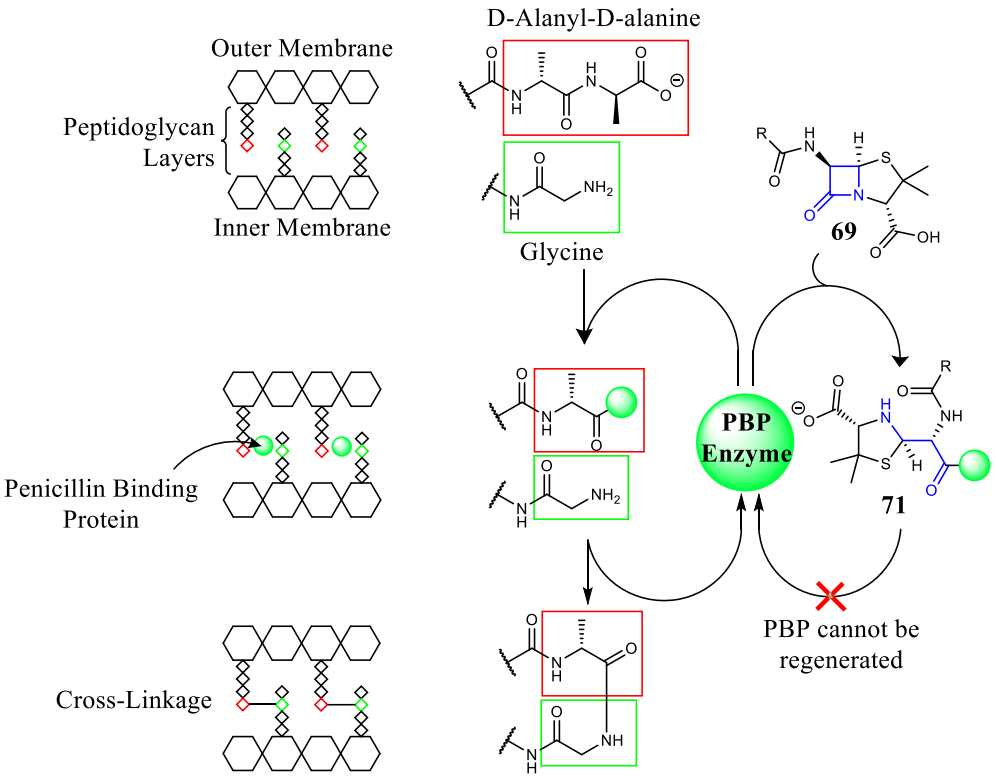

Figure 1.23: Schematic for peptidoglycan cross-linkage catalysed by a PBP enzyme. Left shows the intended cross link between D-alanyl-D-alanine and glycine. Right shows the inhibition of the PBP enzyme by a penicillin.[61–63]

Peptidoglycan cross-linking (Figure 1.23, left) is the standard homeostasis mechanism which takes place in the absence of a PBP inhibitor. D-Alanine is cleaved from the D-alanyl-D-alanine subunit of peptidoglycan *via* hydrolysis to give an enzyme complex which can then undergo cross-linking with an adjacent glycine unit to give a complete peptidoglycan linkage. However, when a PBP inhibitor is introduced, such as a β-lactam antibiotic, the PBP attacks the β-lactam ring masquerading as an analogue of the terminal D-alanyl-D-alanine dipeptide of the peptidoglycan, to give the covalently bound enzyme-substrate complex **71**. This process (termed penicilloylation[56]) inhibits further turnovers of the PBP enzyme and halts cell wall biosynthesis and results in lysis.[64,65] Lysis caused by PBP inhibition is a complex process and consists of two main phases. The first is inhibition of peptidoglycan synthesis by the β-lactam antibiotic which prevents production of the bacterial membrane, however, this alone does not result in lysis.[66] Autolysins, membrane associated enzymes found in bacteria, also play a role in bacterial cell lysis. Autolysins breaks down cross-linked peptide bonds between peptidoglycan strands, allowing for cell membrane turnover and maintenance of the cell shape.[57] However, when peptidoglycan production is halted by antibacterial β-lactams, autolysins will continue to hydrolyse cross-linked peptides, leading to lysis and cell death.

1.3.2 – β-Lactamases

Antibiotic resistance is an ever-growing problem in the healthcare sector. Constantly evolving bacteria possess several intricate mechanisms which increase their drug resistance, some of which are: lowering cell wall permeability,[67] upregulating drug efflux pumps,[68,69] and genetic polymorphism of drug targeted genes to circumvent drug specificity.[70] Another crucial mode of action involves the expression of enzymes such as β-lactamases, capable of modifying drugs or drug-targets, and the strategy has provided drug resistance, particularly toward β-lactam antibiotics.[71]

β-Lactamase enzymes operate by hydrolysing the β-lactam ring of antibiotics such as cephalosporins, carbapenems, and penams, rendering these antibiotics ineffective against the target bacteria.[72] The most common β-lactamases are categorised by the Ambler classification, based on amino acid sequence homologies.[73] Ambler class A β-lactamases are the most common group found in penicillin resistant bacteria and generally operate using a serine residue to hydrolyse the β-lactam ring. Scheme 1.4 shows a reaction scheme of *E. coli* TEM1 β-lactamase reacting with a β-lactam substrate.[74–76]

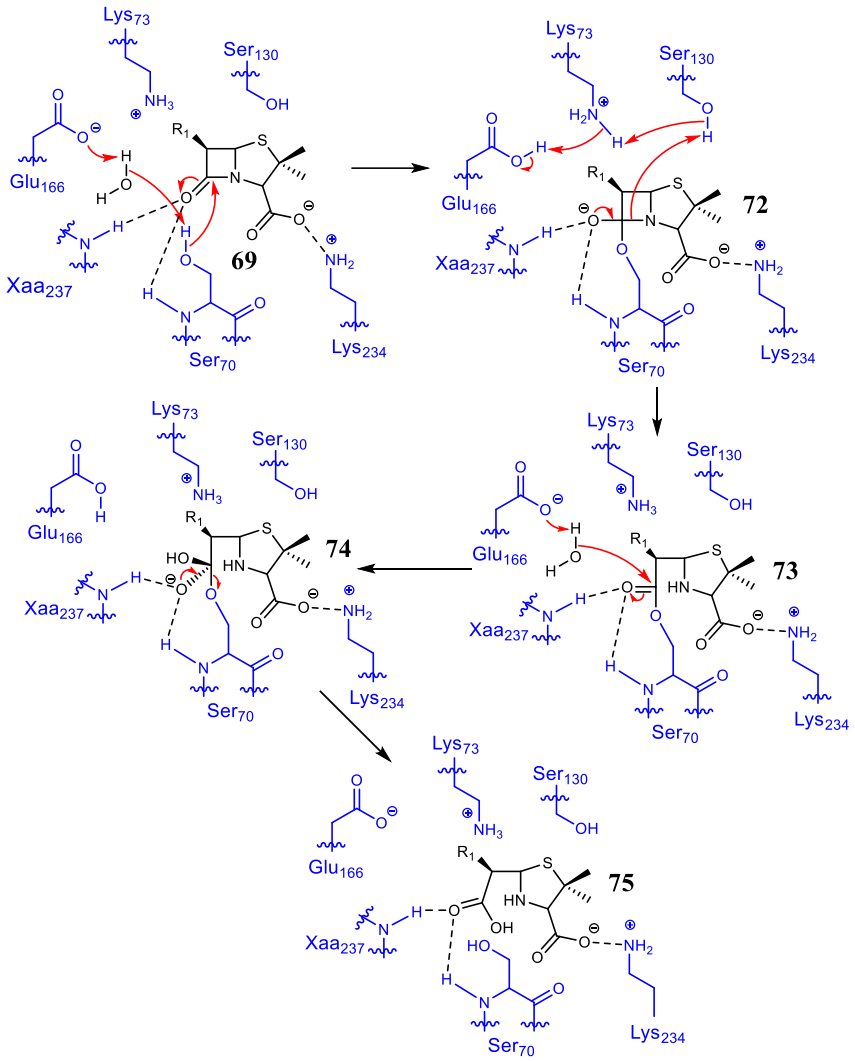

Scheme 1.4: Hydrolytic β-lactam ring opening and subsequent antibiotic deactivation by *E. coli* TEM1 serine protease, The penicillin core shown in black and the enzyme residues are shown in blue.[74–76]

The β-lactamases use a serine OH as the nucleophile and progress through a classical Td intermediate, stabilised by intimate hydrogen bonding in the active site. This intermediate collapses to an acyl-enzyme complex **73** and opening of the β-lactam ring. Glutamic acid then activates a nearby water molecule enabling hydrolysis to a ring opened carboxylic acid **75** and inactivation of the antibiotic.

The acylation and inactivation of a β-lactamase can be represented by Equation 1.1,[77] where; E represents the β-lactamase enzyme, S represents the substrate (in this case a β-lactam drug), E:S is the Michaelis complex, the association of the substrate with the enzyme, E – S is the covalently bonded acyl-enzyme complex, and P is the reaction product devoid of antibacterial capabilities. Rates k_1 and k_{-1} describe the association and dissociation rate constants respectively for the Michaelis complex; k_2 describes the acylation rate constant; and k_3 describes the deacylation rate constant.

$$\mathrm{E} + \mathrm{S} \underset{k_{-1}}{\overset{k_1}{\rightleftharpoons}} \mathrm{E{:}S} \overset{k_2}{\longrightarrow} \mathrm{E} - \mathrm{S} \xrightarrow{k_3, \mathrm{H_2O}} \mathrm{E} + \mathrm{P} \qquad 1.1$$

With Equation 1.1, the kinetic behaviour of β-lactamases can be better understood. The Michaelis constant, K_m, is used to represent the relative affinity of E and S to generate the ES complex and k_2, k_3 the rate at which ES is converted to P.[78] The Michaelis constant, K_m, is defined by

$$K_m = \frac{k_3 K_s}{(k_2 + k_3)} \qquad 1.2$$

Where the kinetic constant, K_s, is defined by;

$$K_s = \frac{(k_{-1} + k_2)}{k_1} \qquad 1.3$$

Using Equation 1.2, the Michaelis constant K_m can be calculated, enabling greater insight into the enzyme kinetics of β-lactamases.

1.3.3 – β-Lactamase inhibitors

One strategy commonly employed to combat the degradation of antibiotics by β-lactamase is to co-administrate β-lactamase inhibitors with the antibiotic. Alone, the β-lactamase inhibitor provides little or no antibacterial activity, however, when paired with the appropriate β-lactam drug the combination can be effective in killing drug resistant bacteria. β-Lactamase inhibitors bind to the active site of β-lactamases, disabling the enzyme, thus allowing the co-administered drug to inhibit PBP.[79,80] β-Lactamase inhibitors can display reversible or irreversible inhibition (the latter also known as "suicide" inhibition).[74,81] Reversible inhibitors are described as those which bind to an enzyme in such a manner that the enzyme activity is eventually restored. These inhibitors generally have a high enzyme-substrate affinity and form sterically bulky acyl-enzyme complexes that are hydrolysed at a slow rate. Examples of reversible inhibitors are monobactams and carbapenems (Figure 1.24). Equation 1.4 describes the relationship between a reversible inhibitor with an enzyme counterpart, where I_{rev} describes a reversable β-lactamase inhibitor and $E{:}I_{rev}$ describes the Michaelis complex. For reversible inhibitors, an equilibrium constant can be evaluated ($K \approx k_{-1}/k_1$) to estimate the affinity of the inhibitors.

$$\mathrm{E} + \mathrm{I}_{rev} \underset{k_{-1}}{\overset{k_1}{\rightleftharpoons}} \mathrm{E{:}I}_{rev} \qquad 1.4$$

Irreversible inhibitors (or suicide inhibitors) permanently inactivate β-lactamase enzymes through covalent modifications at the enzyme active site. Once these secondary reactions take place, neither the inhibitor nor the enzyme can be regenerated. Examples of irreversible inhibitors are clavulanic acid **76**, sulbactam **77**, and tazobactam **78** (Figure 1.24). The equation below describes the relationship between an irreversible inhibitor with an enzyme counterpart where; I_{irr} describes the irreversible inhibitor; $E{:}I_{irr}$ describes the Michaelis complex; $E–I_{irr}$ describes the acyl-enzyme complex, and $E–I_{irr}$* describes the inactive enzyme-substrate complex. The affinity of irreversible inhibitors is best described by its first order rate constant.[82]

$$E + I_{irr} \underset{k_{-1}}{\overset{k_1}{\rightleftharpoons}} E{:}I_{irr} \xrightarrow{k_2} E - I_{irr} \xrightarrow{k_3} E - I_{irr}{}^{*} \qquad 1.5$$

A common notation used when discussing the effectiveness of β-lactamase inhibitors is the half maximum inhibitory concentration (IC_{50}), which details how much of an inhibitor is needed to suppress a biological process by 50%. Although the IC_{50} is an indicator of performance, it does not fully reflect the effectiveness of any individual inhibitor and is often presented with other data such as first order rate constants and minimum inhibitory concentration (MIC), the lowest concentration of an antimicrobial that will inhibit the visible growth of a microorganism after overnight incubation.[83]

The increasing threat of bacterial resistance over the past four decades has driven the discovery of a diverse library of β-lactamase inhibitors, each designed to overcome a new obstacle presented by the rapid adaption of bacteria in modern clinical environments. Figure 1.24 shows a small selection of these β-lactamase inhibitors.

Clavam and Sulphone ß-Lactamase Inhibitors

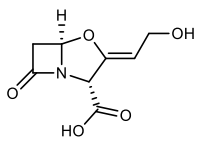

Clavulanic Acid **76**

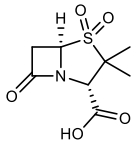

Sulbactam **77**

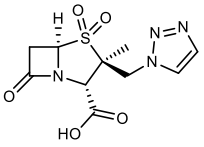

Tazobactam **78**

Diazabicyclooctane (DBO) ß-Lactamase Inhibitors

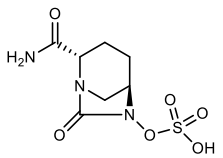

Avibactam **79**

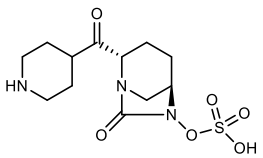

Relebactam **80**

Figure 1.24: Examples of commonly used Ambler class A β-lactamase inhibitors.

A key consideration in the design and administration of β-lactamase inhibitors is the choice of the accompanying β-lactam drug.[84] Both the β-lactamase inhibitor and β-lactam drug must possess similar pharmacokinetic properties in order to be administered together effectively. This presents a challenge in the design process as the target β-lactamase must have a greater affinity for the β-lactamase inhibitor when compared to the β-lactam drug.[80] Table 1.4 shows the established pairings of widely prescribed β-lactam drugs and β-lactamase inhibitors as well as the trade name that the drug combination is sold under.[79,84]

Table 1.4: Widely prescribed β-lactam drug and β-lactamase inhibitor combinations.[79,84]

Structural Group	β-Lactamase Inhibitor	Accompanying β-Lactam Drug	Trade Name (Manufacturer)
Clavam and Sulphone	Clavulanic Acid **76**	Amoxicillin	Augmentin (GlaxoSmithKline)
	Sulbactam **77**	Ampicillin	Unasyn (Pfizer)
	Tazobactam **78**	Piperacillin Ceftolozane	Zosyn (Pfizer) Zerbaxa (Merck)
DBO	Avibactam **79**	Ceftazidime	Avycaz/ Zavicefta (Pfizer)
	Relebactam **80**	Imipenem and Cilastatin	Recarbrio (Merck)

1.3.4 – First generation β-lactamase inhibitors

Clavulanic acid **76** was isolated from the bacteria *Streptomyces clavuligerus* in 1976.[85] It was the first β-lactamase inhibitor used in a clinical setting. The most common pairing for clavulanic acid **76** is amoxicillin **81** (Augmentin, GSK, Figure 1.25), and together they are the only lactam-lactamase drug combination still available for oral use. Augmentin is used to treat a wide spectrum of bacterial infections, such as those caused by *S. aureus, H. influenzae, M. catarrhalis, Bacteroides spp., N. gonorrhoeae, E. coli, Klebsiella spp.,* and *P. mirabilis*.[74,86]

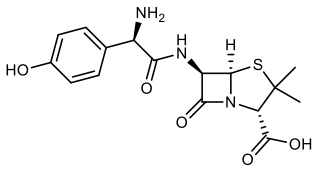

Amoxicillin **81**

Figure 1.25: Amoxicillin **81**.

After the initial success of clavulanic acid, structurally similar analogues were investigated, with sulbactam **77** emerging from this effort. First synthesised in 1978,[87] the sole administration of this inhibitor showed no antibacterial activity, with the exception of the drug having potent effects on resistant strains of *N. gonorrhoeae*. When compared to clavulanic acid **76** and tazobactam **78**, sulbactam **77** has the highest turnover number (the number of molecules

hydrolysed during each inactivation event) when tested against a wide spectrum of β-lactamases.[88] Ampicillin is the β-lactam drug most commonly coupled with sulbactam (Unasyn®), first marketed in 1987. This drug combination is administered parenterally and used to treat urinary tract infections (UTI) and intra-abdominal infections.[74] Unasyn® has proven effective against a variety of bacteria, including *S. aureus, H. influenzae, M. catarrhalis, E. coli, Proteus spp., Klebsiella spp*., and several anaerobes.[86,89,90] Unfortunately, due to the ever increasing resistance of bacteria, clinically isolated strains of *E. coli* have shown a particular resistance to Unasyn®,[91] further demonstrating the need for discovery of new antibacterial drug combinations.

In 1984 an analogue of sulbactam possessing a triazole moiety was found to show inhibitory activity against a wide spectrum of pathogens.[92] Later named Tazobactam **78**, it exhibits a comparable spectrum of activity as a β-lactamase inhibitor to both clavulanic acid **76** and sulbactam **77**. However, Tazobactam **78** has greater inhibitory activity than sulbactam **77**, although it possesses no notable antibacterial activity on its own.[93] Piperacillin is the antibacterial drug most commonly administered with Tazobactam **78**, sold under the trade name Zosyn®. This combination is predominantly used for the treatment of pelvic inflammatory disease.[94] Alone, piperacillin has demonstrated activity against *P. aeruginosa, pneumococci, streptococci, anaerobes,* and *Enterococcus faecalis*,[80] however when paired with Tazobactam **78** it exhibits activity against most strains of *Enterobacteriaceae*, *H. influenzae, N. gonorrhoeae*, and *M. catarrhalis*.[95]

Clavulanic acid **76**, sulbactam **77** and tazobactam **78** are all suicide inhibitors operating through a similar mode of inhibition and they are most efficacious against the ambler class A β-lactamases. Scheme 1.5 shows the mechanism by which clavulanic acid **76** inhibits an A class β-lactamase isolated from *S. aureus via* covalent modification of Ser_{70}.[96–99]

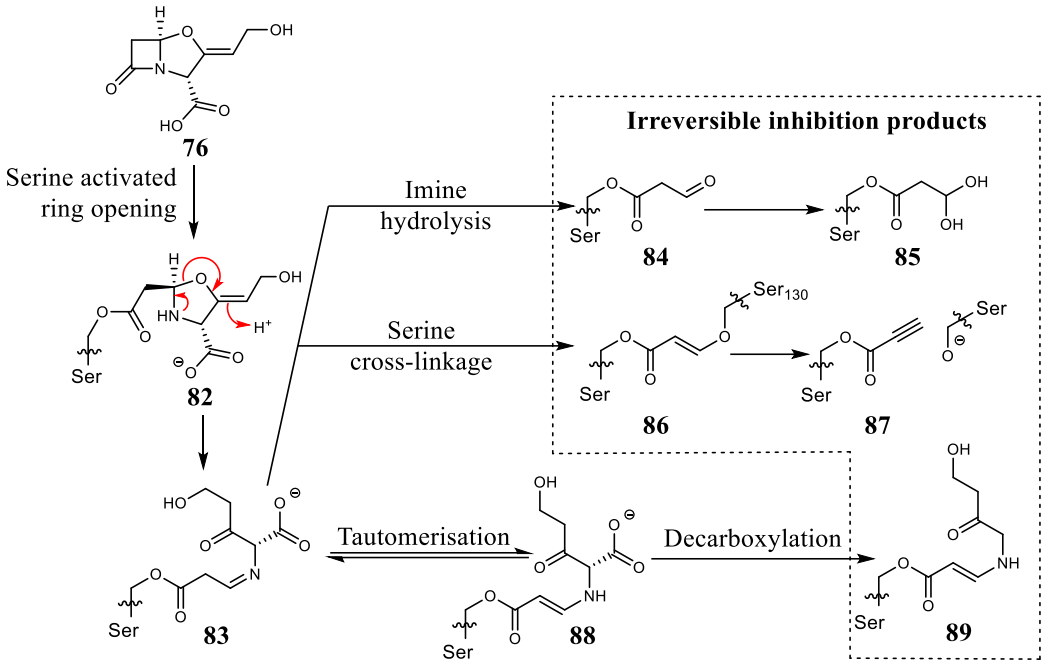

Scheme 1.5: Mechanism for inhibition of class A β-lactamase by clavulanic acid **76**.[96–99]

The β-lactam ring of clavulanic acid **76** is hydrolysed in the same way as a β-lactam antibiotic (Scheme 1.4). The acetyl-serine intermediate **83** can then take several different pathways to form reactive intermediates, which in turn leads to inhibition. One pathway involves imine hydrolysis to form aldehyde **84**, which becomes hydrate **85**. The imine intermediate **83** can also react with another serine in a cross-linking reaction to irreversibly form adduct **86**. The enol ether present in **86** is cleaved to give the propynyl-enzyme inhibition product **87**. Intermediate **83** is also prone to tautomerisation, yielding enamine **88**, which is then decarboxylated to form adduct **89**. With the formation of any of the listed irreversible inhibition products, the β-lactamase is no longer able to hydrolyse β-lactam antibiotics, allowing for effective treatment of pathogens.

Kinetic and mass spectrometry analysis of inactivation mechanisms, as well as several crystallographic studies, have shown that the β-lactamase inhibitors sulbactam **77** and tazobactam **78** follow similar mechanistic pathways to that shown in Scheme 1.5.[100] Clavulanic acid **76** is used for the treatment of Ambler class A β-lactamases PC1, TEM-1, and SHV-1, which found in several bacteria species.[99–101]

1.4 – All *syn* pentafluoro cyclohexane "Janus face"

1.4.1 – History and synthesis

All-*cis* 1,2,3,4,5,6-hexafluorocyclohexane ring **90** possesses a fluorine atom on each carbon with a configuration that orientates each fluorine towards one face of the ring (Figure 1.26). This stereochemistry and the chair conformation associated with cyclohexanes, affords **90** an

exceptionally large dipole moment (μ = 6.2 D),[102] due to the co-alignment of the three axial and highly polarised C-F bonds. This results in an electronegative fluorine face and an electropositive hydrogen face. Due to these two faces looking in different directions, the cyclohexane is referred to as a "Janus face" molecule,[103] named after the Roman mythos, Janus who had two faces.

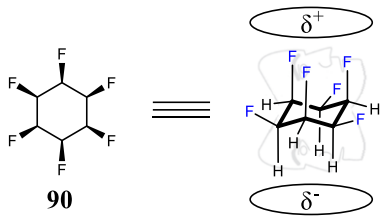

90

Figure 1.26: "Janus face" all-*cis* 1,2,3,4,5,6-hexafluorocyclohexane **90**.

First synthesised in 2015 by Dr Neil Keddie in St Andrews, the original route comprised a 12-step protocol starting from inositol **91** (Scheme 1.6).[102] The overall yield however was less than 1%.

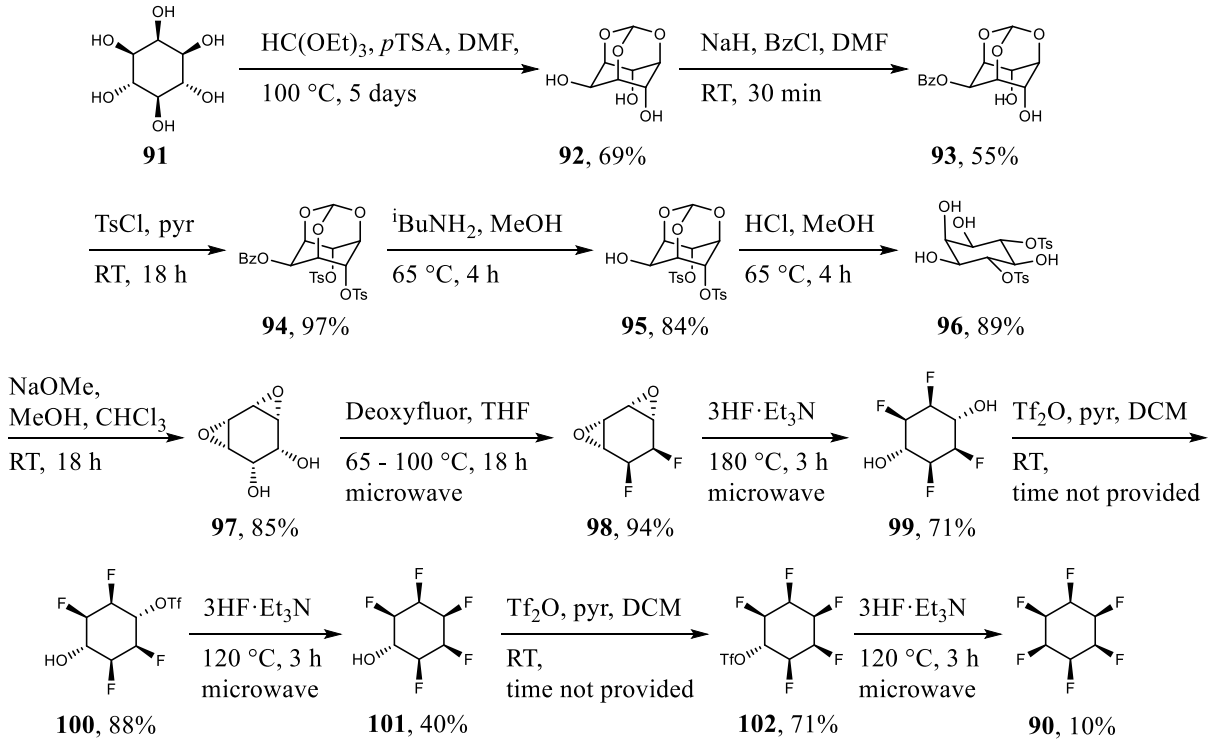

91, **92**, 69%, **93**, 55%, **94**, 97%, **95**, 84%, **96**, 89%, **97**, 85%, **98**, 94%, **99**, 71%, **100**, 88%, **101**, 40%, **102**, 71%, **90**, 10%

Scheme 1.6: The first synthesis of all-*cis* 1,2,3,4,5,6-hexafluorocyclohexane **90**.[102]

X-ray structure analysis revealed that **90** sits in a classic chair conformation with alternating axial and equatorial C-F bonds. Although the synthesis of the first Janus face cyclohexane **90** was something of a landmark, it is not practical for access to material for significant experimental work, or to make derivatives. Shortly after, the Glorius group in 2017 disclosed a much more practical approach towards the synthesis of this class of Janus face compounds (Scheme 1.7).[104]

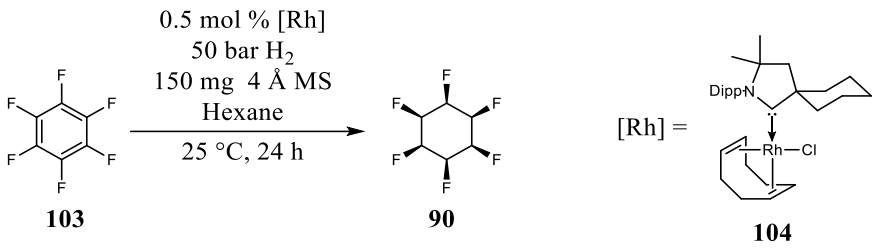

Scheme 1.7: Direct access to Janus face **90** *via* arene hydrogenation.[104]

The synthesis of **90** was achieved by a high pressure hydrogenation of readily available hexafluorobenzene **103**, catalysed by rhodium–cyclic (alkyl)(amino)carbene (CAAC) **104**. This *N*-heterocyclic carbene (NHC) catalyst was previously discovered by the Zeng group and was used for selective hydrogenation of functionalised aromatics.[105]

Direct access to **90** provided an opportunity for futher investigation into the properties of this cyclohexane. This work was built upon in St Andrews, with the synthesis of pentafluoro cyclohexane derivatives possessing functionalised substituents (Scheme 1.8).[106]

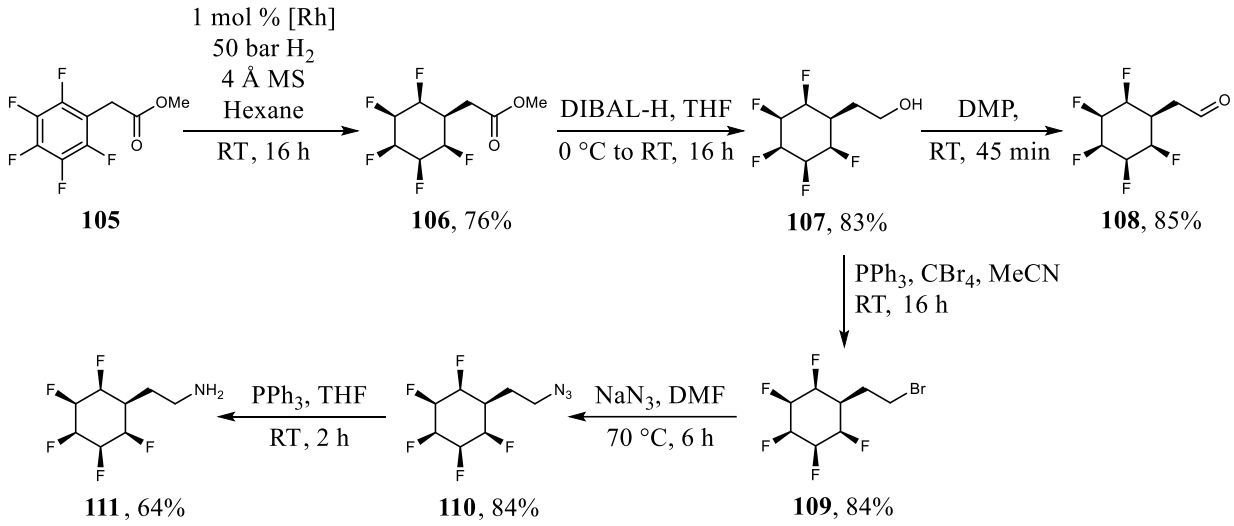

Scheme 1.8: Synthesis of all-*cis* pentafluorocyclohexane Janus face building blocks.[106]

Using conditions previously described by Glorius *et al.,* pentafluoroaryl methyl ester **105** was subjected to an all *syn* hydrogenation to afford methyl ester **106**. With access to this Janus face intermediate, a range of different functional group interconversions were explored, including conversions to alcohols (**107**), aldehydes (**108**), bromides (**109**), azides (**110**), and amines (**111**). These building blocks can in turn be used as reagents for a variety of reactions, such as substitutions, "click" [3+2] Copper(I) catalysed Azide-Alkyne cycloaddition (CuAAC) reactions to form triazoles, couplings to form amides, and inclusion in Ugi multicomponent reactions.[106] This catalogue of now accessible Janus face building blocks allows for their direct incorporation into larger, more complex molecular architectures.

1.4.2 – Intermolecular interactions of Janus face cyclohexanes

The recorded melting point of the original Janus face cyclohexane **90** is 206 °C (dec), which actually refers to the temperature at which the compound sublimes rather than melts. Such a high temperature is perhaps more indicative of an ionic zwitterion such as an amino acid, than an organic compound, and gives some indication of the unusual properties of **90**. There are clearly strong electrostatic interactions between the electropositive and electronegative faces in the solid state and this is reinforced in the crystal packing from the X-ray structure of **90** as shown in Figure 1.27.[102]

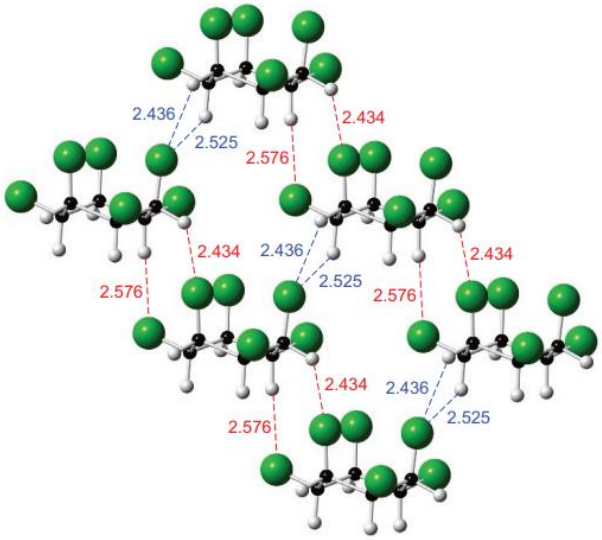

Figure 1.27: X-ray structure of **90**, Reprinted with permission from Springer Nature.[102] *Copyright © 2015, Springer Nature Limited.*

The crystal structure shown in Figure 1.27 reveals an "offset stacking" of individual molecules of **90**, with the fluorine faces contacting the hydrogen faces of adjacent molecules. The packing is clearly ordered electrostatically and notably there are no fluorine to fluorine or hydrogen to hydrogen interactions which would be expected in more hydrophobic compounds.

The interaction of isolated molecules of **90** with ions has been explored in the gas phase, which showcased the electrostatic nature of the ring. Negative mode mass spectroscopy revealed chloride ion complexes and positive ion mode revealed sodium ion complexes. Analysis of the isolated ions in an ion chamber with a free electron laser revealed that it is exclusively the electronegative fluorine face of **90** that complexes to the Na^+ cation, and the electropositive hydrogen face that complexes to Cl^- anion.[107] Theory supporting this experimental data allowed calculations of the complexation energies and a proposed structure of the ion complexes, as shown in Figure 1.28.[107]

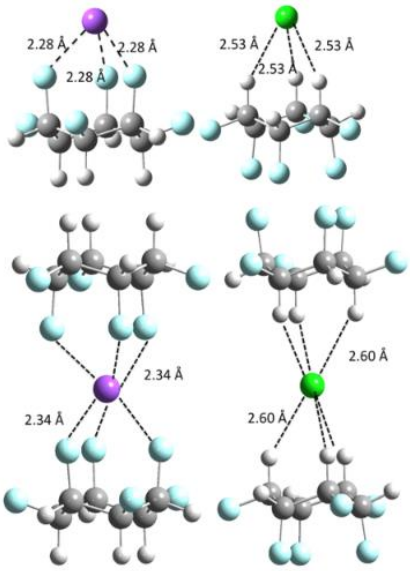

Figure 1.28: Structures of Na^+ (magenta) and Cl^- (green) ions coordinating to Janus cyclohexane **90**. Reprinted with permission from ACS Publications.[107] *Copyright © 2016, American Chemical Society.*

The complexation energies are remarkably large for the Na^+ (-41 kcal mol^{-1}) and Cl^- (-37 kcal mol^{-1}) complexes, although they are maximum values as they are in the gas phase. The sodium and chloride ion complexes form either as 1:1 or 1:2 adducts. Interestingly, chloride ion complexation resulted in a lengthening of both the axial and equatorial C-F bonds, due to the electron density being pushed into the ring from the halide ion. In the case of the Na^+ ion complex, the axial C-F bonds lengthened, but the equatorial C-F bond shortened. Table 1.5 shows the resulting bond length changes from complexation with ions.[107]

Table 1.5: Bond distances (Å) for Janus face **90** ion complexes.

	90	MNa^+	M_2Na^+	MCl^-	M_2Cl^-
C-C	1.532	1.530	1.530	1.526	1.527
$C\text{-}H_{ax}$	1.098	1.097	1.097	1.099	1.097
$C\text{-}H_{eq}$	1.094	1.090	1.091	1.093	1.093
$C\text{-}F_{ax}$	1.380	1.418	1.409	1.396	1.392
$C\text{-}F_{eq}$	1.384	1.377	1.378	1.400	1.397
X-H/F	-	2.282	2.341	2.532	2.604

1.4.3 – Aggregation of the Janus face

The packing and aggregation of the Janus cyclohexane fatty acid **117** and a saturated hydrocarbon counterpart **121** has been explored, as illustrated in Scheme 1.9.[108] Interestingly, the melting point of fatty acid **117** was 100 °C higher than that of the cyclohexyl hydrocarbon counterpart **121**, again indicative of strong electrostatic interactions between the Janus face cyclohexanes.

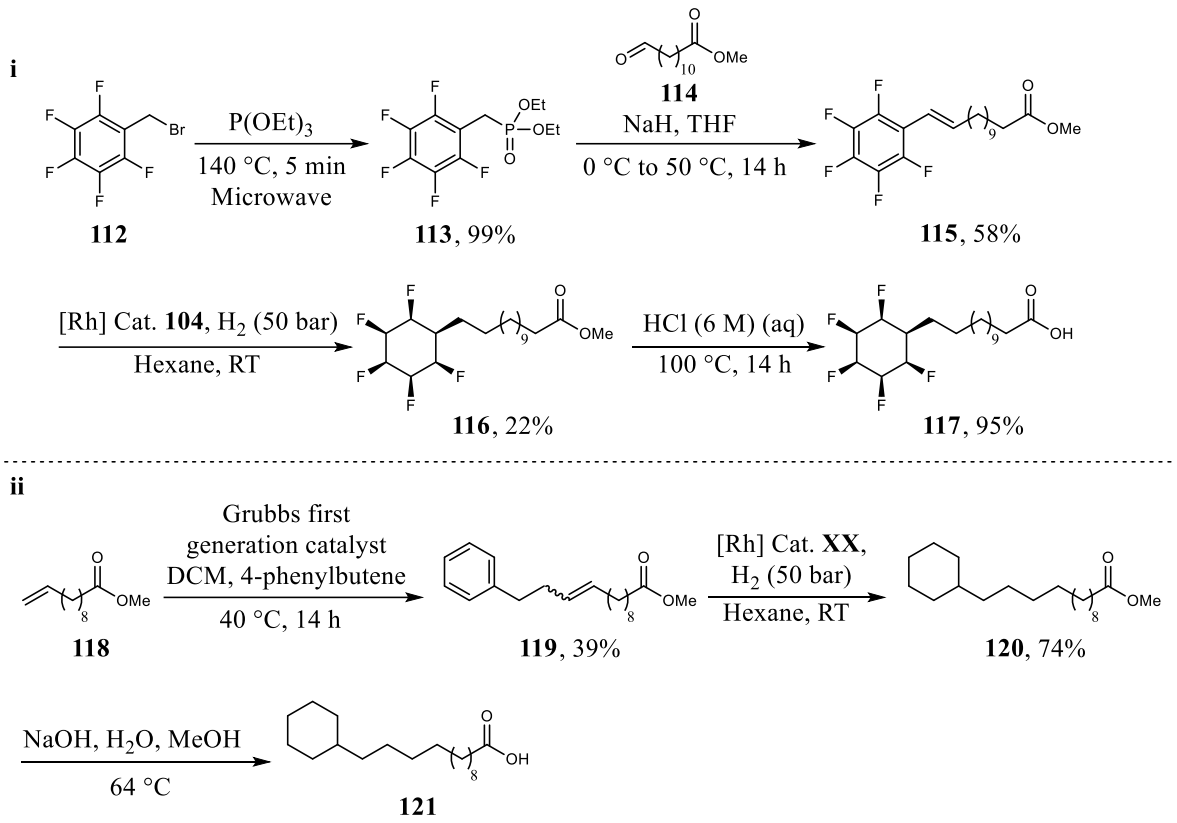

Scheme 1.9: i) Synthesis of fatty acid **117** and **ii)** of hydrocarbon counterpart **121**.[108]

Synthesis of fatty acid **117** was achieved through a Horner-Wadsworth-Emmons (HWE) olefination between pentafluoroaryl phosphonate **113** and long chain ester-aldehyde **114** to generate ester **115**. Direct hydrogenation at 50 bar H_2 yielded the saturated ester **116** which was then hydrolysed to form the target fatty acid **117**. Synthesis of the hydrocarbon fatty acid **121** was achieved through cross-metathesis between 10-undecenoate **118** and 4-phenylbuntene to yield ester **119**. Once again direct hydrogenation gave the saturated ester **120** which was then converted to fatty acid **121** after hydrolysis.

A Langmuir trough is used to measure surface pressures by compressing monolayers on a sub-surface (usually water), by reducing the surface area and measuring pressure-area isotherms. In this case it was used to investigate monolayer behaviour of Janus cyclohexane terminated fatty acid **117** relative to its hydrocarbon counterpart **121** (Figure 1.29).

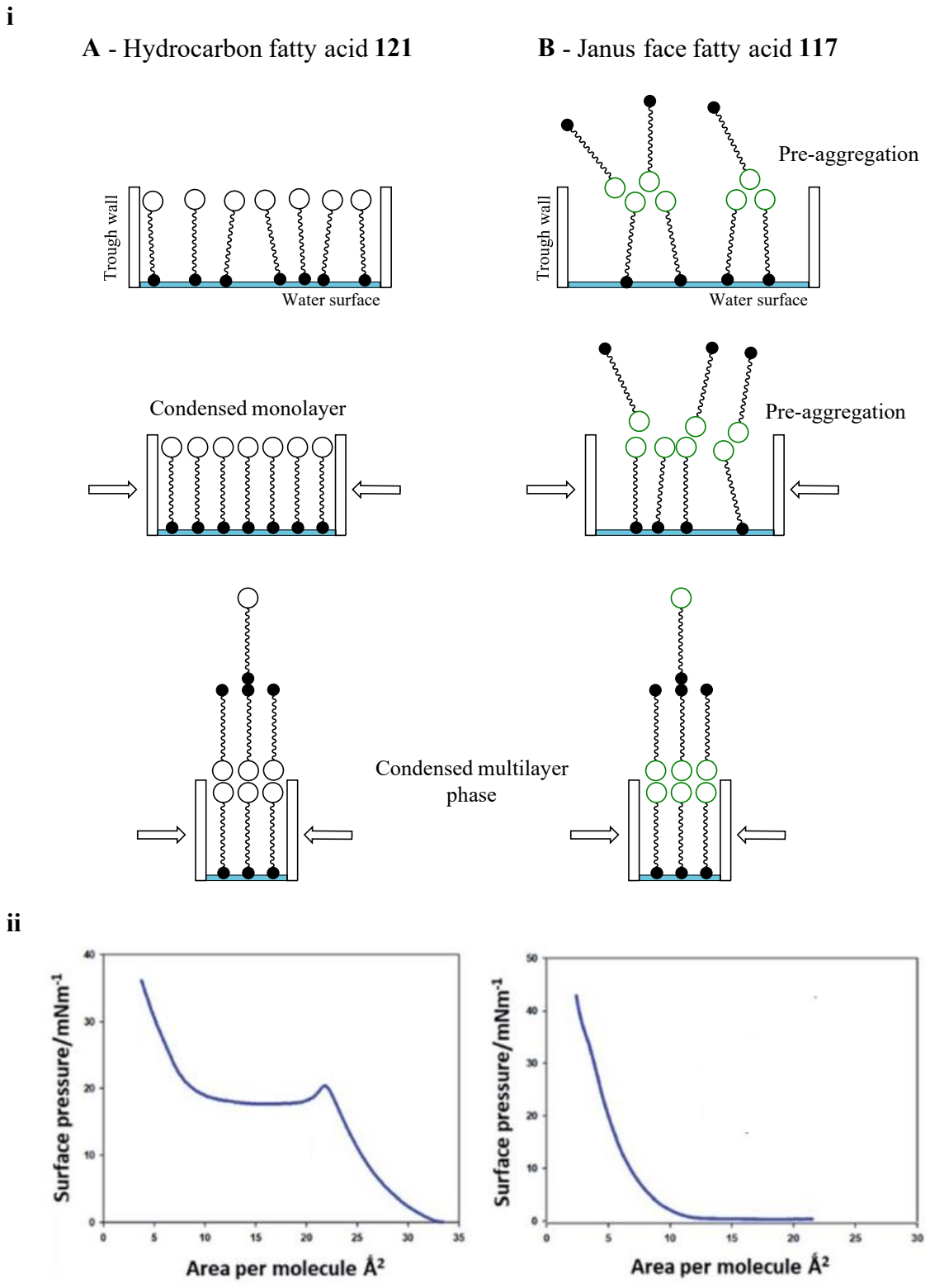

Figure 1.29: i) Illustration of the behaviour of hydrocarbon fatty acid **121** (column A) and Janus face fatty acid **117** (column B) during the Langmuir trough experiment on a water subphase. Arrows represent the movement of the trough walls to reduce surface area.[108] **ii)** Respective pressure-area isotherms with the hydrocarbon fatty acid **121** on the left and Janus face fatty acid **121** on the right. Reproduced with permission from the Royal Society of Chemistry.[108] *Copyright © The Royal Society of Chemistry 2021.*

Hydrocarbon **121** formed stable monolayers, whereas the fatty acid **117** formed multilayers with no evidence of a coherent monolayer. These findings suggest that the Janus fatty acid **117** pre-aggregates and forms bilayers directly, indicating that the Janus face ring systems are self-

associating, and these interactions are at least similar in magnitude if not greater than the interaction of the carboxylate with the water subphase. The interaction energy between Janus face cyclohexanes has been calculated to be between 6-8 kcal mol^{-1},[109] which is comparable to very healthy hydrogen bond interaction (~5.0 kcal mol^{-1}) between hydrophilic head groups and water.

1.5 – Overview of ligand–DNA binding

The ability of molecules in solution to bind to deoxyribonucleic acid (DNA) has been a topic of intense research over the past five decades. Ligand-DNA interactions have been shown to disrupt replication/transcription resulting in cell death. It follows that DNA binding ligands have potential to be used as anti-cancer or anti-viral agents.[110] For this reason, understanding DNA-ligand interactions is of great importance, and drives a constant effort from drug discovery teams to synthesis new DNA binding ligands.[111]

There are several categories for non-covalent reversibly binding ligands with dsDNA: (1) electrostatic interactions with the phosphate backbone, (2) DNA major groove binding, (3) DNA minor groove binding, (4) DNA minor groove intercalation, (5), DNA major groove intercalation and (6) DNA threading intercalation.[112] These interactions are illustrated in Figure 1.30.

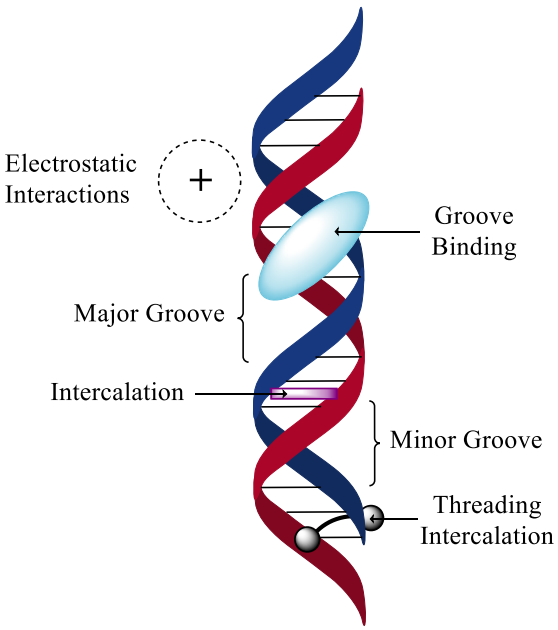

Figure 1.30: Schematic illustration of non-covalent binding modes to dsDNA.

1.5.1 – Electrostatic interactions to the phosphate backbone of dsDNA

The conformational stability of folded DNA depends on ionic interactions with cations (such as Na^+ or Mg^{2+}) through a process termed 'counterion condensation'. Binding of cationic ligands to DNA neutralizes the anionic phosphate charges and results in the release of these condensed counterions into the surrounding area. This release provides an entropic contribution to the binding energy between the ligand and DNA.[113]

This form of non-covalent binding is highly dependent on the salt concentration of the medium, and electrostatic DNA binding is generally weak under physiological conditions for mono-cationic ligands without other binding modes. However, for highly charged molecules, such as proteins or multi-cationic ligands, the number of counter-cations released is substantial, resulting in a significant entropic contribution to the binding energy and good affinity between the ligand and DNA.[112]

This form of DNA binding is often paired with other modes, as alone it does not yield strong interactions. Therefore, when designing small molecule DNA ligands an electrostatic element is usually incorporated into its structure, such as a carboxylate or an amine salt.[114] These ionic molecules in turn show greater binding with DNA at lower salt concentrations.

1.5.2 – Major and minor groove binding

Both minor and major groove DNA binding arises as a result of direct hydrogen bonding to base pair edges, van der Waals interactions with the groove walls, and generalized electrostatic interactions between the ligand and the groove.[115] Protonated polyamines meet this criteria and bind well with DNA *via* groove binding. An example of a good major groove binder is spermine **122** shown in Figure 1.31.

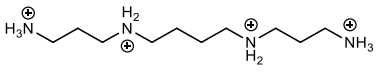

Spermine **122**

Figure 1.31: Spermine **122**.

The highest concentration of negative potentials in dsDNA is located in the grooves of DNA duplexes, rather than within the anionic phosphate backbone.[113] These negative potentials are most concentrated in the proximity of guanine-cytosine (GC) base pairs found in the major groove. A flexible cationic molecule such as spermine **122** can take advantage of these areas of high negative potential by complexing within these grooves. However, whilst spermine **122** is a major groove binder, derivatives of spermine with terminal thiols have shown a greater

tendency to bind to the minor groove, suggesting that polyamines may also act as minor groove binders.[116]

Minor groove binders often contain non-conjugated aromatic rings connected by bonds with torsional freedom. These characteristics can be seen in the selection of minor groove binders shown in Figure 1.32. The torsional freedom of these binders allows the ligand to adopt the appropriate conformation to fit the curved groove without compromising the DNA structure. Free rotation of the aromatic rings of these ligands also allows for van der Waals interactions between the ligand and the walls of the groove, as well as hydrogen bonding with adenine-thymine (AT) base pairs found in the minor groove.[112] Both the major and minor groove binders discussed here are also amine salts, which benefit from electrostatic interactions with the phosphate backbones, as previously discussed (Chapter 1.5.1).

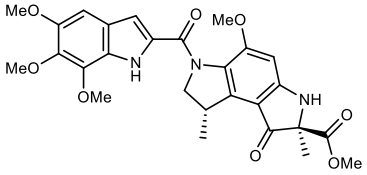

Duocarmycin A **123**

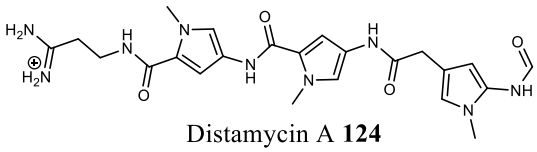

Distamycin A **124**

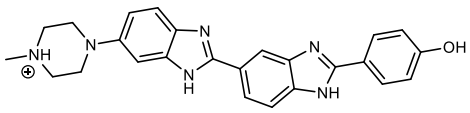

Hoechst 33258 **125**

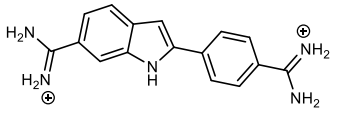

Hoechst 33258 **126**

Figure 1.32: DNA Minor groove binding ligands.

Groove binding ligands can change the conformation of the DNA double helix structure, however conformational change is not a requirement for this mode of binding. Minor groove binding ligands such as **123 – 126** cause negligible conformational change whilst the major groove binder spermine **122** may cause localised bending of the DNA helix to facilitate DNA counterion condensation and improved binding affinity.[117]

1.5.3 – Major, minor, and threading intercalation

Despite there being a wealth of structural data available for DNA-ligand intercalation complexes, the intermolecular forces responsible for intercalation are not fully understood. It has been proposed that hydrophobic aromatic ligands associate with the hydrophobic aromatic base pairs of DNA, in turn shielding the ligand from the aqueous environment surrounding the DNA.[118,119] However, electrostatic, allosteric, hydrogen bonding, HOMO-LUMO interactions, and/or van der Waals interactions can also play a role in binding interactions.[120]

Traditional intercalators all share a similar structure; a fused-ring aromatic core with cationic atoms attached *via* a side chain or incorporated into the aromatic core itself.[121] A selection of classical intercalator ligands is illustrated in Figure 1.33.

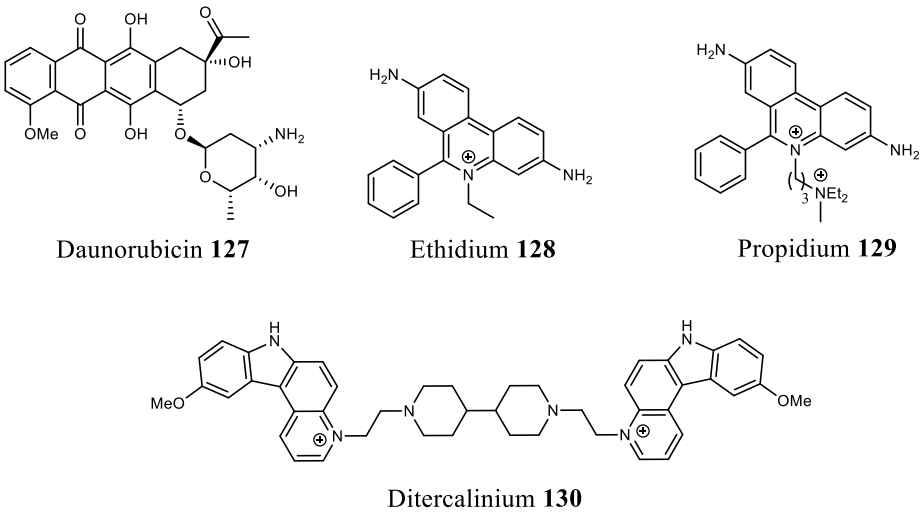

Figure 1.33: DNA Intercalator ligands.[112]

The planar aromatic cores of these intercalators **127** – **130** fit into the gap between base pairs, stacking through π-π interaction without disrupting Watson-Crick hydrogen bonding. Intercalating ligands obey the nearest neighbour exclusion principle,[122] which states that when dsDNA is fully saturated with intercalators, every second potential intercalation site is empty, despite an excess of intercalation ligands. Additionally, adjacent base pairs of duplex DNA increase their separation by 2.4 Å, forming a cavity which accommodates the intercalating ligand. To form this cavity, duplex DNA must reduce the degree to which it twists, causing it to unwind upon intercalation. This unwinding varies depending on the size and shape of intercalating ligands. Figure 1.34 shows a visualisation of ethidium **128** intercalating between two base pairs of dsDNA.[123]

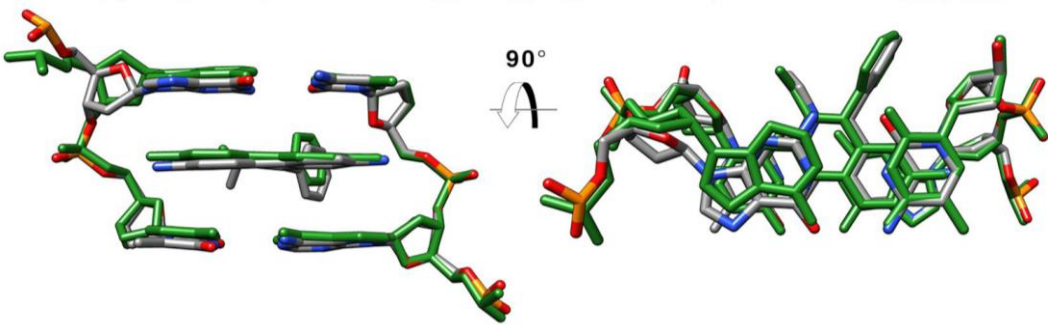

Figure 1.34: Overlay of the X-ray structure (NDB code drbb12) and a molecular dynamics simulation average structure (green) from the intercalation of ethidium **128** between two base pairs of dsDNA. Reprinted with permission from Oxford University Press.[123] *Copyright © 2021, Oxford University Press © The Author(s) 2021.*

Threading intercalators have some similarity to classical intercalators but differ with respect to the ligand's substituents. Naphthalene diimide **129** is a well-known threading intercalator as

shown in Figure 1.35. It possesses a fused aromatic core and two aliphatic side chains terminating in protonated (charged) tertiary amines.

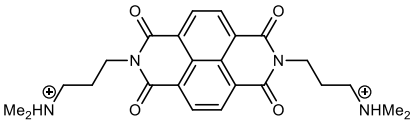

Naphthalene diimide **129**

Figure 1.35: Naphthalene diimide **129**.

Threading intercalators bind to dsDNA by insertion of the planar aromatic core between adjacent base pairs (similar to classical intercalators). One cationic substituent binds to the major groove and the other to the minor groove on the opposite face of the DNA duplex.[112] Threading intercalators both associate and dissociate from DNA slower than classical intercalators whilst maintaining similar equilibrium binding constants.[124]

1.6 – Summary

This thesis will explore a number of interrelated topics associated with organofluorines in biochemistry. The synthesis of a new class of β-lactam derivatives, designed as suicide inhibitors of β-lactamase enzymes or the transpeptidase enzyme responsible for bacterial cell wall biosynthesis. Another focus will explore interactions of the Janus face cyclohexane motif with DNA and also methods to prepare such probes that are radiolabelled with fluorine-18 as potential traceable ligands for biological imaging. More specifically Chapter 2 will describe the work on the novel β-lactam class. Chapter 3 will explore interactions between the Janus face motif and both single and double stranded DNAs using biophysical techniques, predominantly Förster resonance energy transfer (FRET). Chapter 4 will describe work on fluorine-18 labelling of Janus face containing ligands, and particularly using the fluorinase enzyme to introduce ^{18}F-fluoride. Finally, Chapter 5 will showcase the incorporation of the Janus face motif into adenosine core molecules for use as A_{2A} receptor agonists, as well as investigating their affinity for A_{2A} receptors *via* radioligand displacement assays.

1.7 – References

1 M. E. Weeks, *J. Chem. Educ.*, 1932, **9**, 1915.

2 G. Villalba, R. U. Ayres and H. Schroder, *J. Ind. Ecol.*, 2007, **11**, 85–101.

3 G. B. Kauffman, *J. Chem. Educ.*, 1955, **32**, 301.

4 J. M. Calm, *Int. J. Refrig.*, 2008, **31**, 1123–1133.

5 J. G. Anderson, D. W. Toohey and W. H. Brune, *Science*, 1991, **251**, 39–46.

6 T. Fujiwara and D. O'Hagan, *J. Fluor. Chem.*, 2014, **167**, 16–29.

7 J. Han, A. M. Remete, L. S. Dobson, L. Kiss, K. Izawa, H. Moriwaki, V. A. Soloshonok and D. O'Hagan, *J. Fluor. Chem.*, 2020, **239**, 109639.

8 S. Purser, P. R. Moore, S. Swallow and V. Gouverneur, *Chem. Soc. Rev.*, 2008, **37**, 320–330.

9 M. Inoue, Y. Sumii and N. Shibata, *ACS Omega*, 2020, **5**, 10633–10640.

10 J.-P. Bégué and D. Bonnet-Delpon, *Bioorganic and Medicinal Chemistry of Fluorine*, John Wiley & Sons, Hoboken, New Jersey, 2008.

11 J. Gardiner, *Aust. J. Chem.*, 2014, **68**, 13–22.

12 I. T. Cousins, J. C. DeWitt, J. Glüge, G. Goldenman, D. Herzke, R. Lohmann, C. A. Ng, M. Scheringer and Z. Wang, *Environ. Sci. Process Impacts*, 2020, **22**, 2307–2312.

13 L. Pauling, *J. Am. Chem. Soc.*, 1932, **54**, 3570–3582.

14 L. Pauling, *The Nature of the Chemical Bond and the Structure of Molecules and Crystals: An Introduction to Modern Structural Chemistry*, Cornell University Press, Itchaca, New York, 1960.

15 A. S. Batsanov, *Encyclopaedia of Spectroscopy and Spectrometry*, ed. J. C. Lindon, Academic Press, Oxford, 2nd edn, 2010, pp. 2550–2558.

16 D. O'Hagan, *Chem. Soc. Rev.*, 2008, **37**, 308–319.

17 F. H. Allen, O. Kennard, D. G. Watson, L. Brammer, A. G. Orpen and R. Taylor, *J. Chem. Soc., Perkin Trans. 2*, 1987, S1–S19.

18 N. A. Senger, B. Bo, Q. Cheng, J. R. Keeffe, S. Gronert and W. Wu, *J. Org. Chem.*, 2012, **77**, 9535–9540.

19 W. R. Dolbier, A. C. Alty and O. Phanstiel, *J. Am. Chem. Soc.*, 1987, **109**, 3046–3050.

20 P. Ryberg and O. Matsson, *J. Org. Chem.*, 2002, **67**, 811–814.

21 M. L. Trapp, J. K. Watts, N. Weinberg and B. M. Pinto, *Can. J. Chem.*, 2006, **84**, 692–701.

22 D. Rodrigues Silva, L. de Azevedo Santos, T. A. Hamlin, C. Fonseca Guerra, M. P. Freitas and F. M. Bickelhaupt, *ChemPhysChem*, 2021, **22**, 641–648.

23 C. Thiehoff, Y. P. Rey and R. Gilmour, *Isr. J. Chem.*, 2017, **57**, 92–100.

24 D. Wu, A. Tian and H. Sun, *J. Phys. Chem. A*, 1998, **102**, 9901–9905.

25 J. W. Banks, A. S. Batsanov, J. A. K. Howard, D. O'Hagan, H. S. Rzepa and S. Martin-Santamaria, *J. Chem. Soc., Perkin Trans. 2*, 1999, 2409–2411.

26 B. J. van der Veken, S. Truyen, W. A. Herrebout and G. Watkins, *J. Mol. Struct.*, 1993, **293**, 55–58.

27 R. J. Abraham, A. D. Jones, M. A. Warne, R. Rittner and C. F. Tormena, *J. Chem. Soc., Perkin Trans. 2*, 1996, **0**, 533–539.

28 H. V. Phan and J. R. Durig, *J. Mol. Struct. THEOCHEM*, 1990, **209**, 333–347.

29 L. Hunter, *Beilstein J. Org. Chem.*, 2010, **6**, DOI:10.3762/bjoc.6.38.

30 N. E. J. Gooseman, D. O'Hagan, M. J. G. Peach, A. M. Z. Slawin, D. J. Tozer and R. J. Young, *Angew. Chem.*, 2007, **119**, 6008–6012.

31 P. A. Champagne, J. Desroches and J.-F. Paquin, *Synthesis*, 2015, **47**, 306–322.

32 J. D. Dunitz and R. Taylor, *Chem. Eur. J.*, 1997, **3**, 89–98.

33 J. A. K. Howard, V. J. Hoy, D. O'Hagan and G. T. Smith, *Tetrahedron*, 1996, **52**, 12613–12622.

34 M. T. Scerba, C. M. Leavitt, M. E. Diener, A. F. DeBlase, T. L. Guasco, M. A. Siegler, N. Bair, M. A. Johnson and T. Lectka, *J. Org. Chem.*, 2011, **76**, 7975–7984.

35 J. Fried and E. F. Sabo, *J. Am. Chem. Soc.*, 1954, **76**, 1455–1456.

36 J. Elks, *The Dictionary of Drugs: Chemical Data: Chemical Data, Structures and Bibliographies*, Springer, New York, NY, 2014.

37 D. O'Hagan, *J. Fluor. Chem.*, 2010, **131**, 1071–1081.

38 M. Tredwell and V. Gouverneur, *Comprehensive Chirality*, eds. E. M. Carreira and H. Yamamoto, Elsevier, Amsterdam, 1st edn, 2012, vol. 1, ch. 5, pp. 70–85.

39 C. A. Lipinski, *Drug Discov. Today Technol.*, 2004, **1**, 337–341.

40 B. E. Smart, *J. Fluor. Chem.*, 2001, **109**, 3–11.

41 S. Swallow, *Progress in Medicinal Chemistry*, eds. G. Lawton and D. R. Witty, Elsevier, 1st edn, 2015, vol. 54, ch. 2, pp. 65–133.

42 B. Jeffries, Z. Wang, J. Graton, S. D. Holland, T. Brind, R. D. R. Greenwood, J.-Y. Le Questel, J. S. Scott, E. Chiarparin and B. Linclau, *J. Med. Chem.*, 2018, **61**, 10602–10618.

43 S. Barnard, R. C. Storr, P. M. O'Neill and B. K. Park, *J. Pharm. Pharmacol.*, 1993, **45**, 736–744.

44 H.-J. Böhm, D. Banner, S. Bendels, M. Kansy, B. Kuhn, K. Müller, U. Obst-Sander and M. Stahl, *ChemBioChem*, 2004, **5**, 637–643.

45 M. B. van Niel, I. Collins, M. S. Beer, H. B. Broughton, S. K. F. Cheng, S. C. Goodacre, A. Heald, K. L. Locker, A. M. MacLeod, D. Morrison, C. R. Moyes, D. O'Connor, A. Pike, M. Rowley, M. G. N. Russell, B. Sohal, J. A. Stanton, S. Thomas, H. Verrier, A. P. Watt and J. L. Castro, *J. Med. Chem.*, 1999, **42**, 2087–2104.

46 Y. Kokuryo, K. Kawata, T. Nakatani, A. Kugimiya, Y. Tamura, K. Kawada, M. Matsumoto, R. Suzuki, K. Kuwabara, Y. Hori and M. Ohtani, *J. Med. Chem.*, 1997, **40**, 3280–3291.

47 J. L. Kyzer and M. Martens, *Chem. Res. Toxicol.*, 2021, **34**, 678–680.

48 S. B. Rosenblum, T. Huynh, A. Afonso, H. R. Davis, N. Yumibe, J. W. Clader and D. A. Burnett, *J. Med. Chem.*, 1998, **41**, 973–980.

49 J. Fried, E. A. Hallinan and M. J. Szwedo, *J. Am. Chem. Soc.*, 1984, **106**, 3871–3872.

50 I. Langmuir, *J. Am. Chem. Soc.*, 1919, **41**, 1543–1559.

51 Z. Miao, L. Zhu, G. Dong, C. Zhuang, Y. Wu, S. Wang, Z. Guo, Y. Liu, S. Wu, S. Zhu, K. Fang, J. Yao, J. Li, C. Sheng and W. Zhang, *J. Med. Chem.*, 2013, **56**, 7902–7910.

52 M. E. Wall, M. C. Wani, C. E. Cook, K. H. Palmer, A. T. McPhail and G. A. Sim, *J. Am. Chem. Soc.*, 1966, **88**, 3888–3890.

53 J.-F. Nadon, K. Rochon, S. Grastilleur, G. Langlois, T. T. H. Dao, V. Blais, B. Guérin, L. Gendron and Y. L. Dory, *ACS Chem. Neurosci.*, 2017, **8**, 40–49.

54 N. Kardos and A. L. Demain, *Appl. Microbiol. Biotechnol.*, 2011, **92**, 677–687.

55 E. Vitaku, D. T. Smith and J. T. Njardarson, *J. Med. Chem.*, 2014, **57**, 10257–10274.

56 M. A. Kohanski, D. J. Dwyer and J. J. Collins, *Nat. Rev. Microbiol.*, 2010, **8**, 423–435.

57 J. V. Höltje, *Microbiol. Mol. Biol. Rev.*, 1998, **62**, 181–203.

58 J. T. Park and T. Uehara, *Microbiol. Mol. Biol. Rev.*, 2008, **72**, 211–227, table of contents.

59 D. J. Tipper and J. L. Strominger, *Proc. Natl. Acad. Sci. U.S.A.*, 1965, **54**, 1133–1141.

60 E. M. Wise and J. T. Park, *Proc. Natl. Acad. Sci. U.S.A.*, 1965, **54**, 75–81.

61 D. J. Waxman, R. R. Yocum, J. L. Strominger, J. Baddiley and E. P. Abraham, *Philos. Trans. R. Soc. Lond. B Biol. Sci.*, 1980, **289**, 257–271.

62 M. M. Miyachiro, C. Contreras-Martel and A. Dessen, *Macromolecular Protein Complexes II: Structure and Function*, ed. J. R. Harris and J. Marles-Wright, Springer International Publishing, Cham, 1st edn, 2019, vol. 93, ch. 8, pp. 273–289.

63 H. R. Josephine, I. Kumar and R. F. Pratt, *J. Am. Chem. Soc.*, 2004, **126**, 8122–8123.

64 A. Tomasz, *Annu. Rev. Microbiol.*, 1979, **33**, 113–137.

65 T. P. T. Cushnie, N. H. O'Driscoll and A. J. Lamb, *Cell. Mol. Life Sci.*, 2016, **73**, 4471–4492.

66 A. Tomasz, A. Albino and E. Zanati, *Nature*, 1970, **227**, 138–140.

67 J. Trias, V. Jarlier and R. Benz, *Science*, 1992, **258**, 1479–1481.

68 G. E. Louw, R. M. Warren, G. van Pittius, C. R. E. McEvoy, P. D. V. Helden and T. C. Victor, *Antimicrob. Agents. Chemother.*, 2009, **53**, 3181–3189.

69 E. D. Rossi, J. A. Aínsa and G. Riccardi, *FEMS Microbiol. Rev.*, 2006, **30**, 36–52.

70 I. Guillemin, V. Jarlier and E. Cambau, *Antimicrob. Agents. Chemother.*, 1998, **42**, 2084–2088.

71 R. Urban-Chmiel, A. Marek, D. Stępień-Pyśniak, K. Wieczorek, M. Dec, A. Nowaczek and J. Osek, *Antibiotics*, 2022, **11**, 1079.

72 R. Fernandes, P. Amador and C. Prudêncio, *Rev. Res. Med. Microbiol.*, 2013, **24**, 7.

73 R. P. Ambler, J. Baddiley and E. P. Abraham, *Philos. Trans. R. Soc. Lond. B Biol. Sci.*, 1980, **289**, 321–331.

74 S. M. Drawz and R. A. Bonomo, *Clin. Microbiol. Rev.*, 2010, **23**, 160–201.

75 S. O. Meroueh, J. F. Fisher, H. B. Schlegel and S. Mobashery, *J. Am. Chem. Soc.*, 2005, **127**, 15397–15407.

76 C. Jelsch, L. Mourey, J.-M. Masson and J.-P. Samama, *Proteins: Struct., Funct., Bioinf.*, 1993, **16**, 364–383.

77 K. A. Johnson and R. S. Goody, *Biochem.*, 2011, **50**, 8264–8269.

78 M. Galleni and J.-M. Frère, *Enzyme-Mediated Resistance to Antibiotics: Mechanisms, Dissemination, and Prospects for Inhibition*, ed. R. A. Bonomo and M. Tolmasky, ASM Press, Washington, D.C., 1st edn, 2007, ch. 12, pp. 195–213.

79 K. Bush and P. A. Bradford, *Cold Spring Harb. Perspect. Med.*, 2016, **6**, DOI:10.1101/cshperspect.a025247.

80 D. M. Livermore, *J. Antimicrob. Chemother.*, 1998, **41**, 25–41.

81 K. Bush, *Clin. Microbiol. Rev.*, 1988, **1**, 109–123.

82 K. Bush, *Drugs Exp. Clin. Res.*, 1986, **12**, 565—576.

83 J. M. Andrews, *J. Antimicrob. Chemother.*, 2001, **48**, 5–16.

84 K. Bush and P. A. Bradford, *Nat. Rev. Microbiol.*, 2019, **17**, 295–306.

85 C. Reading and M. Cole, *Antimicrob. Agents. Chemother.*, 1977, **11**, 852–857.

86 L. M. Bush and C. C. Johnson, *Infect. Dis. Clin. North Am.*, 2000, **14**, 409–433.

87 A. R. English, J. A. Retsema, A. E. Girard, J. E. Lynch and W. E. Barth, *Antimicrob. Agents. Chemother.*, 1978, **14**, 414–419.

88 A. B. Shapiro, *Antimicrob. Agents. Chemother.*, 2017, **61**, 1612–1617.

89 J. A. Retsema, A. R. English, A. Girard, J. E. Lynch, M. Anderson, L. Brennan, C. Cimochowski, J. Faiella, W. Norcia and P. Sawyer, *Rev. Infect. Dis.*, 1986, **8**, S528–S534.

90 H. M. Wexler, B. Harris, W. T. Carter and S. M. Finegold, *Antimicrob. Agents. Chemother.*, 1985, **27**, 876–878.

91 K. S. Kaye, A. D. Harris, H. Gold and Y. Carmeli, *Antimicrob. Agents. Chemother.*, 2000, **44**, 1004–1009.

92 S. C. Aronoff, M. R. Jacobs, S. Johenning and S. Yamabe, *Antimicrob. Agents. Chemother.*, 1984, **26**, 580–582.

93 K. Bush, C. Macalintal, B. A. Rasmussen, V. J. Lee and Y. Yang, *Antimicrob. Agents. Chemother.*, 1993, **37**, 851–858.

94 R. Sweet, S. Roy, S. Faro, W. O'Brien, J. Sanfilippo, and M. Seidlin, *Obstet Gynecol*, 1994, **83**, 280–286.

95 R. N. Jones, M. A. Pfaller, P. C. Fuchs, K. Aldridge, S. D. Allen and E. H. Gerlach, *Diagn. Microbiol. Infect. Dis.*, 1989, **12**, 489–494.

96 R. P. A. Brown, R. T. Aplin and C. J. Schofield, *Biochem.*, 1996, **35**, 12421–12432.

97 S. M. Drawz, C. R. Bethel, K. M. Hujer, K. N. Hurless, A. M. Distler, E. Caselli, F. Prati and R. A. Bonomo, *Biochem.*, 2009, **48**, 4557–4566.

98 M. Kalp, M. A. Totir, J. D. Buynak and P. R. Carey, *J. Am. Chem. Soc.*, 2009, **131**, 2338–2347.

99 U. Imtiaz, E. Billings, J. R. Knox, E. K. Manavathu, S. A. Lerner and S. Mobashery, *J. Am. Chem. Soc.*, 1993, **115**, 4435–4442.

100 J. Fisher, R. L. Charnas, S. M. Bradley and J. R. Knowles, *Biochem.*, 1981, **20**, 2726–2731.

101 R. L. Charnas, J. Fisher and J. R. Knowles, *Biochem.*, 1978, **17**, 2185–2189.

102 N. S. Keddie, A. M. Z. Slawin, T. Lebl, D. Philp and D. O'Hagan, *Nat. Chem.*, 2015, **7**, 483–488.

103 N. Santschi and R. Gilmour, *Nat. Chem.*, 2015, **7**, 467–468.

104 M. P. Wiesenfeldt, Z. Nairoukh, W. Li and F. Glorius, *Science*, 2017, **357**, 908–912.

105 Y. Wei, B. Rao, X. Cong and X. Zeng, *J. Am. Chem. Soc.*, 2015, **137**, 9250–9253.

106 J. L. Clark, R. M. Neyyappadath, C. Yu, A. M. Z. Slawin, D. B. Cordes and D. O'Hagan, *Chem. Eur. J.*, 2021, **27**, 16000–16005.

107 B. E. Ziegler, M. Lecours, R. A. Marta, J. Featherstone, E. Fillion, W. S. Hopkins, V. Steinmetz, N. S. Keddie, D. O'Hagan and T. B. McMahon, *J. Am. Chem. Soc.*, 2016, **138**, 7460–7463.

108 J. L. Clark, A. Taylor, A. Geddis, R. M. Neyyappadath, B. A. Piscelli, C. Yu, D. B. Cordes, A. M. Z. Slawin, R. A. Cormanich, S. Guldin and D. O'Hagan, *Chem. Sci.*, 2021, **12**, 9712–9719.

109 S. M. Pratik, A. Nijamudheen and A. Datta, *ChemPhysChem*, 2016, **17**, 2373–2381.

110 J. Portugal and F. Barceló, *Curr. Med. Chem.*, 2016, **23**, 4108–4134.

111 A. Rescifina, C. Zagni, M. G. Varrica, V. Pistarà and A. Corsaro, *Eur. J. Med. Chem.*, 2014, **74**, 95–115.

112 L. Strekowski and B. Wilson, *Mutat. Res. Fundamental Mol. Mech. Mutagenesis*, 2007, **623**, 3–13.

113 G. S. Manning, *Biophys. Chem.*, 2002, **101–102**, 461–473.

114 S. B. Howerton, A. Nagpal and L. Dean Williams, *Biopolymers*, 2003, **69**, 87–99.

115 A. Lauria, A. Montalbano, P. Barraja, G. Dattolo and A. M. Almerico, *Curr. Med. Chem.*, 2007, **14**, 2136–2160.

116 D. Sy, C. Durand, S. Hugot, C. Savoye, C. Swenberg, M. Charlier and M. Spotheim-Maurizot, *Theor. Chem. Acc.*, 1999, **101**, 114–120.

117 V. A. Bloomfield, *Biopolymers*, 1997, **44**, 269–282.

118 L. S. Lerman, *J. Mol. Biol.*, 1961, **3**, 18-IN14.

119 V. Luzzati, F. Masson and L. S. Lerman, *J. Mol. Biol.*, 1961, **3**, 634–639.

120 A. A. Almaqwashi, T. Paramanathan, I. Rouzina and M. C. Williams, *Nucleic Acids Res.*, 2016, **44**, 3971–3988.

121 A. Mukherjee and W. D. Sasikala, in *Advances in Protein Chemistry and Structural Biology*, ed. T. Karabencheva-Christova, Elsevier, Netherlands, 1st edn., 2013, vol. 92, pp. 1–62.

122 J. D. McGhee and P. H. von Hippel, *J. Mol. Biol.*, 1974, **86**, 469–489.

123 R. Galindo-Murillo and T. E. Cheatham III, *Nucleic Acids Res.*, 2021, **49**, 3735–3747.

124 F. A. Tanious, S. F. Yen and W. D. Wilson, *Biochem.*, 1991, **30**, 1813–1819.

Chapter 2
Novel β-lactams inhibitors and antibiotics against *M. abscessus* and other drug resistant bacteria

2.1 – Introduction

2.1.1 – *Mycobacterium abscessus*

Mycobacterium abscessus was first identified in 1953 by Frerichs and Moor,[1] and in 2009 its full genome was sequenced by Gaillard *et al*.[2] It is a rapidly growing mycobacterium (RGM) that has garnered significant interest over the past decade.[3–6] As a human pathogen, *M. abscessus* is one of the most common non-tuberculosis mycobacterium (NTM) species that is responsible for a wide spectrum of soft tissue infections,[7] with the most notable diseases being broncho-pulmonary infections found in patients with cystic fibrosis and bronchiectasis.[8–12] However, *M. abscessus* infections have also been found in patients without any detected underlying health conditions, and it has also been identified in lung transplant recipients.[13,14] Several cases of *M. abscessus* infection outbreaks in both medical and non-medical settings have also been reported,[15–18] all of which demonstrate the impact that *M. abscessus* has had in the healthcare environment. Disturbingly, the pathogen has become most prevalent over the past two decades, with the number of *M. abscessus* infections found in patients with cystic fibrosis escalating dramatically.[19]

Three subspecies constitute the *M. abscessus* group; *M. absessus*, *M. bolletii,* and *M. massiliense*.[20] The subspecies of the *M. abscessus* group have been differentiated using RNA polymerase beta-subunit encoding (rpoB) gene sequencing techniques,[21] revealing a heterogeneity of the *M. abscessus* group. However, assigning clinical strains from the *M. abscessus* group to their respective subspecies has proven difficult.[22] This issue has been of considerable concern, as the genotypic and phenotypic heterogeneity of the *M. abscessus* group has been shown to cause a variance in antibiotic resistance between subspecies. One example is *M. massiliense* which shows susceptibility to the antibiotic drug clarithromycin, whereas *M. abscessus* and *M. bolletii* both show clarithromycin resistance.[23] This in turn increases the complexity of treating patients with *M. abscessus*, in spite of treatment regimens for *M. abscessus* related diseases being already difficult, with one meta-analysis study showing the success rate of *M. abscessus* pulmonary disease treatment was as low as 45.6%.[24]

Antibiotic resistance is a major concern posed by pathogenic bacteria, and this includes the *M. abscessus* group.[3,25] This ever-growing problem in the healthcare sector has previously led to instances of *M. abscessus* infections causing fatality.[26] It is thought that the *M. abscessus* group possess several intricate mechanisms which allow for drug resistance, with the most noteworthy being low cell wall permeability,[27] drug efflux pumps,[28,29] and genetic polymorphism of drug targeted genes.[30] However, it is the expression of enzymes which are able to modify drugs or drug-targets that allows the *M. abscessus* group to possess an extraordinary resistance to most known classes of antibiotics used to fight disease.[31]

2.1.2 – β-Lactamase Bla_{Mab} enzyme

One notable drug modifying enzyme expressed by *M. abscessus* is β-lactamase Bla_{Mab}, encoded by the MAB_2875 gene.[32] The broad-spectrum activity of this enzyme allows effective hydrolysis of first- and second-generation β-lactam antibiotics such as cephalosporins, carbapenems, and penams,[31,32] in turn rendering these antibiotics ineffective against controlling *M. abscessus*.[33] Bla_{Mab} is class A on the Ambler scale,[32] a scale used to categorise the amino acid sequence homology of a given enzyme. A 3D model of the active site is shown in Figure 2.1, which highlights the key serine (Ser70) residue which acts as a nucleophile.[34] Although the mechanism of action of Bla_{Mab} is thought to be similar to other Ambler class A lactamase inhibitors, no specific mechanism studies have been carried out with Bla_{Mab}.

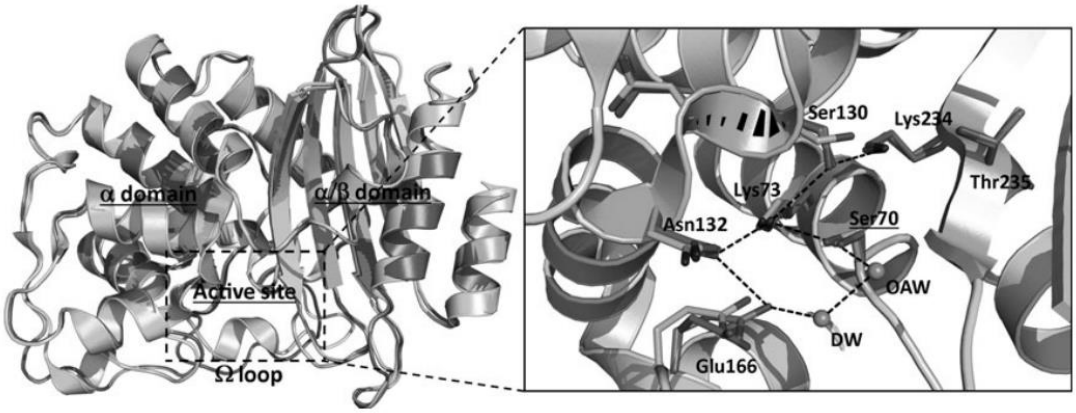

Figure 2.1: 3D model of β-lactamase Bla_{Mab} produced by *M. abscessus.* Left shows the overall structure of the protein whilst right details the active sight with hydrogen bonding between essential residues.[34] Reprinted with permission from Mary Ann Liebert, Inc.[34] *Copyright © 2017, Mary Ann Liebert, Inc.*

In an effort to negate the effect of Bla_{Mab}, β-lactam antibiotics which are hydrolysed at a much slower rate can be used, such as the dual administration of cefoxitin **130** and imipenem **131**, a combination which is currently used for treatment of *M. abscessus* infections (Figure 2.2).[35,36] However, cefoxitin **130** and imipenem **131** are still active substrates of Bla_{Mab}, and the clinical success of these antibiotics is still not ideal.[37]

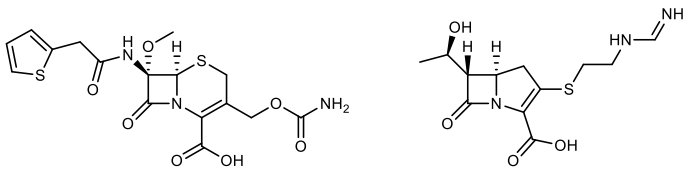

Cefoxitin **130** Imipenem **131**

Figure 2.2: Cefoxitin **130** and Imipenem **131**.

2.1.3 – Bla_{Mab} Enzyme inhibitor drugs in use

Clinical isolates of *M. abscessus* show strong resistance to almost all conventional antibiotics, and there is an emerging absence of drug treatments for the pathogen.[38] Despite this, recent studies have shown that avibactam **79**, a non β-lactam lactamase diazabicyclooctane (DBO) inhibitor, is effective against Bla_{Mab}.[36,39] Research by Dubée *et. al.*[39] indicates that avibactam **79** significantly lowers the minimum inhibitory concentration (MIC) of the accompanying β-lactam drug amoxicillin **81**. The combination of both avibactam **79** and amoxicillin **81** is also effective in treating macrophages and zebra-fish embryos infected with *M. abscessus*. It is thought that avibactam **79** possesses a better inhibition efficiency for class A serine β-lactamases, including the *M. abscessus* Bla_{Mab} enzyme. The general mechanism of action of avibactam **79** for the inhibition of KPC-2, a serine β-lactamase from *Klebsiella pneumoniae*, is shown in Scheme 2.1.[40–42]

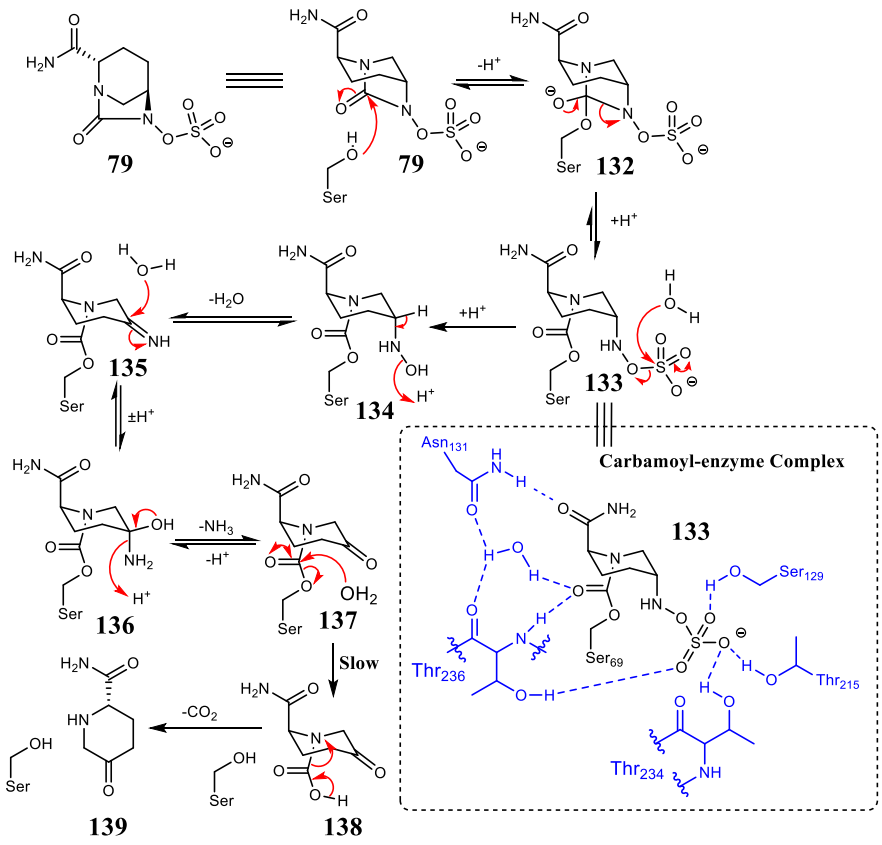

Scheme 2.1: Mechanism of action for avibactam **79**.[40–42]

Avibactam **79** is hydrolysed by a serine moiety to the urea carbonyl of avibactam, to form hemiketal **132**, which then collapses into acetyl-enzyme intermediate **133**. This carbamoyl-enzyme complex **133** is the key inhibitory complex formed during the β-lactamase and avibactam **79** interaction and is also the sole inhibitory complex. It is thought that carbamoyl-enzyme complex **133** is stable due to the polar interactions and hydrogen bonding between the complex and the surrounding residues in the active site.[43]

Similar to other β-lactamase inhibitors, the inhibition complex can be hydrolysed further,[44] allowing for release of the active β-lactamases. This is demonstrated in Scheme 2.1, with water attacking into the sulfonate of a carbamoyl-enzyme complex **133**, forming the hydrolysis product **134**. An E2 type elimination then occurs, with deprotonation α to the hydroxylamine, in turn causing elimination of the alcohol to form the cyclic imine **135**. Imine hydrolysis with water (**135** → **137**) gives ketone **137**, and then the carbamic is hydrolysed, to give carbamic acid **138**. This recovers the serine residue, which is then free to react with other antibiotics/inhibitors. Carbamic acid **138** can undergo decarboxylation to give the stable end metabolite **139**.

Relebactam **80**, first synthesised in 2014 under the name MK-7655,[45] is another non β-lactam DBO lactamase inhibitor, and is an analogue of avibactam. Like avibactam **79**, relebactam **80** contains a urea core which is hydrolysed during β-lactamase inhibition. It also has a sulfonate group allowing for covalent stability of the intermediate enzyme-complex during inhibition. However, relebactam **80** also possesses a piperidine moiety, which is hypothesised to reduce efflux from bacterial cells by sustaining a positive charge (Figure 2.3).[45]

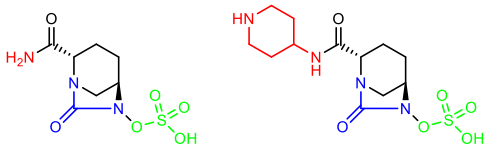

79 Avibactam **80** Relebactam

Figure 2.3: β-Lactamase inhibitors avibactam **79** and relebactam **80**. Blue indicates the urea core, green indicates the sulphonate group, and red indicates different moieties.

Relebactam **80** is also an inhibitor of the β-lactamase enzyme Bla_{Mab}, improving the efficiency of β-lactam drugs when co-administered, including several carbapenems and cephalosporins,[46,47] both of which are β-lactam core containing drug groups. Although relebactam **80** shows a notably lower inhibition efficacy of Bla_{Mab} when compared to avibactam **79**, relebactam **80** dramatically increases the efficiency of the β-lactam drug with imipenem showing the highest activity against *M. abscessus*,[48] in turn leading to a 88% microbial death rate of the bacterium.[46,47]

The mechanism of action for relebactam **80** is similar to that of avibactam **79** (Scheme 2.1), however, the specific protein interactions and active sight binding is subtly different when bound to Bla_{Mab}. Figure 2.4 displays the known protein-ligand interactions between relebactam **80** and the main active site residues of β-lactamase Bla_{Mab}.[49]

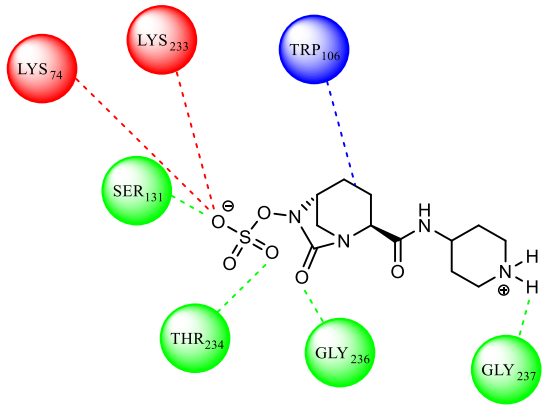

Figure 2.4: Representation of relebactam **80** protein-ligand interactions in the active site of Bla_{Mab}.[49] Green represents hydrogen bonding interactions, red represents charged ion interactions, blue represents π-alkyl interactions.

Although the dual administration of relebactam **80** with imipenem **131** (sold under the brand name Recarbrio®) has been approved by the FDA for urinary tract and intra-abdominal infections,[50] imipenem is associated with severe side effects and toxicity.[51,52] The drug is prescribed as a last-resort treatment in small dosages. However, recent studies have shown that administration of a second β-lactam drug, amoxicillin **81**, to a relebactam **80** and imipenem **131** cocktail can reduce the concentration of imipenem-relebactam needed in treatments four-fold, whilst still maximising the inhibitory effect of Bla_{Mab},[49] reducing the needed dose for the patient. The combination of these two β-lactam drugs with a β-lactamase inhibitor is improving outcomes in the fight against *M. abscessus*,[53] and is becoming an increasingly common treatment strategy.

2.1.4 – Aims and objectives

The O'Hagan group observed that the benzylic fluorine on the trifluoro-cyclopropane ring of anisole **140** was converted to phenol **141** after reaction work up, specifically when it was treated with boron tribromide. This was rationalised by an elimination-addition process, caused initially by boron trifluoride promoted methyl ether cleavage and then elimination of fluoride due to electron donation from the phenol, as illustrated in Scheme 2.2. Subsequent nucleophilic attack from water generated the tertiary alcohol **143**.[54]

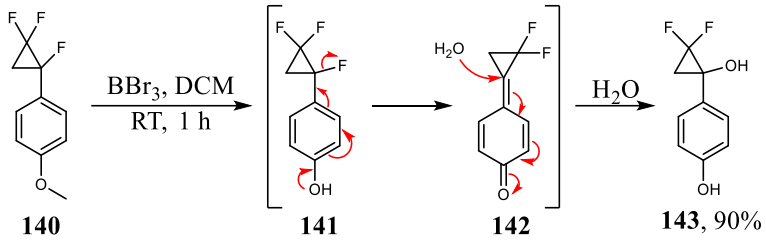

Scheme 2.2: Mechanistic rationale for the conversion of trifluoro-cyclopropyl **140** to alcohol **143**.[54]

This observation suggested a strategy for enzyme inhibition. If a β-lactam was installed at the *para* position to the cyclopropane ring, such as lactam **144**, then the β-lactamase induced ring opening of the β-lactam ring should trigger fluoride ejection through a similar mechanism. Such a process would constitute a novel "suicide" inhibitor strategy for β-lactamase enzymes. Scheme 2.3 illustrates this mechanistic hypothesis.

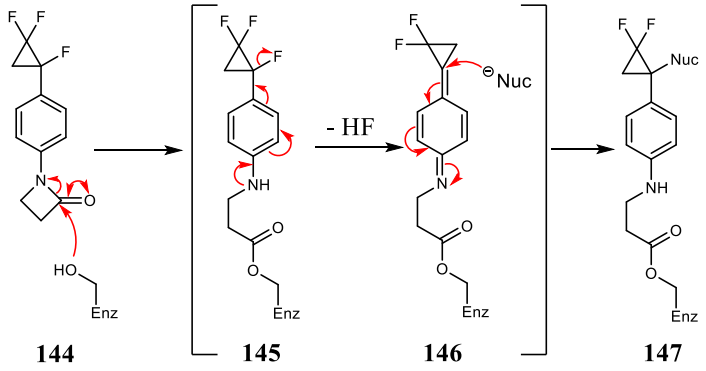

Scheme 2.3: Hypothesis for β-lactamase inhibition with β-lactam **144**.

This chapter describes the synthesis of a set of novel β-lactams of this class as candidate β-lactamase inhibitors. The lactams were screened against *M. abscessus* and other common drug resistant bacteria as novel β-lactamase inhibitors. The proposed chemical mechanism of action was also studied in model reactions by exploring the reactivity of the candidate β-lactams using a series of nucleophiles.

2.2 – Results and discussion

2.2.1 – Synthesis of novel trifluoro-cyclopropane lactams

The first β-lactam to be considered for synthesis was trifluoro-cyclopropane **144**. A proposed synthesis route towards this target is outlined in Scheme 2.4.

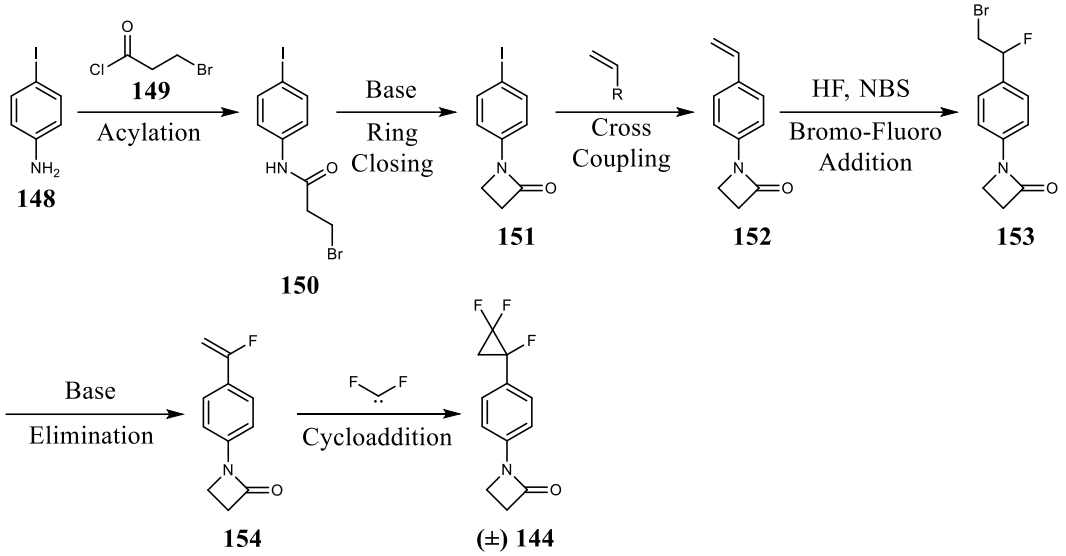

Scheme 2.4: Proposed route to tri-fluorocyclopropane **144**.

Acylation of iodoaniline **148** with 3-bromopropanoyl chloride **149** would give amide **150**. Lactam **151** would then be formed by ring closing substitution of the terminal alkyl bromine under basic conditions. This would be followed by vinyl cross-coupling with aryl iodide **151** to give styrene **152**. Bromo-fluoro addition across the styrene **152** would generate **153** which when exposed to base should result in fluoro-styrene **154** after hydrogen bromide elimination. Finally, a [2+1] cycloaddition with difluoro-carbene would generate cyclopropane **144**.

With this synthetic strategy outlined, work began on the acylation of aniline **150**. The first reaction is summarised in Scheme 2.5.

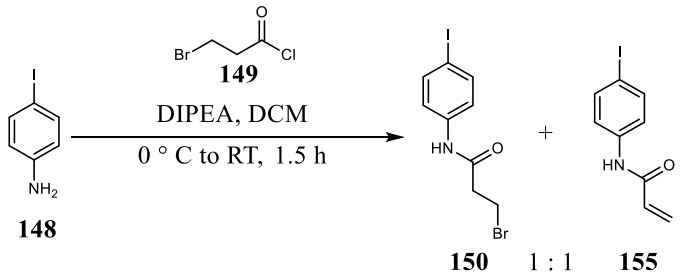

Scheme 2.5: Synthesis of amide **150** and acrylamide **155**.

With N,N-diisopropylethylamine (DIPEA) as a base, the reaction of 3-bromopropanoyl chloride **149** with aniline **148** resulted in a 1:1 mixture (calculated from ^{1}H NMR spectroscopy) of both the desired amide **150** and side product acrylamide **155**. The formation of acrylamide **155** can be rationalised after hydrogen bromide elimination as shown in Scheme 2.6.

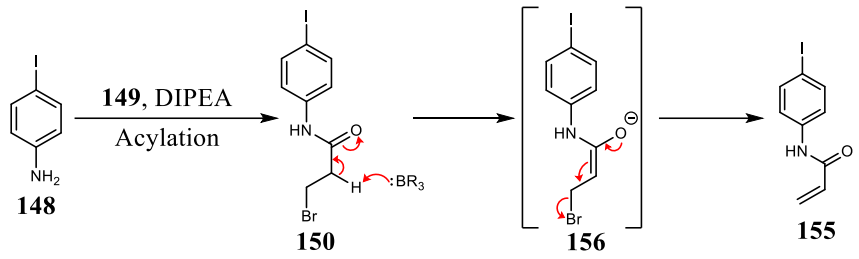

Scheme 2.6: α, β-Elimination of hydrogen bromide to generate acrylamide **155**.

Due to the high ratio of the undesired product, and difficulty in separating the products by chromatography, a weaker base was explored, as illustrated in Scheme 2.7.

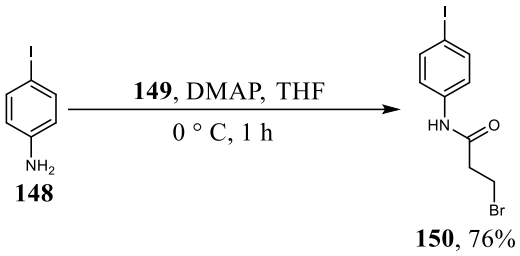

Scheme 2.7: Acylation of aniline **148**.

Accordingly, 4-dimethylaminopyridine (DMAP) was employed as both a nucleophilic catalyst and as a weaker base. This resulted in only the formation of amide **150** and none of the unwanted acrylamide **155**. With access to amide **150** established, attention was directed to ring closure to generate β-lactam **151** (Table 2.1).

Table 2.1: Reaction conditions explored for the cyclisation of amide **150**.[55]

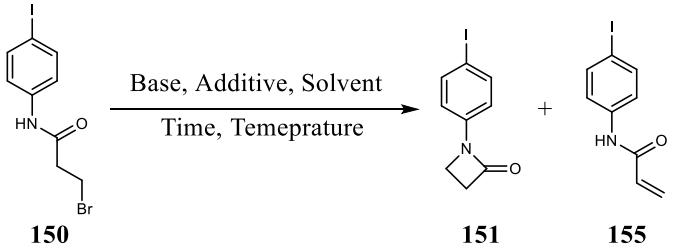

Entry	Base	Additive	Solvent	Time/h	Temperature	Ratio **151:155**	Isolated Yield
1	^{t}BuONa	-	DMF (1 M)	2	0 °C	79:21	34%
2	NaH	-	DMF (0.2 M)	3	0 °C	56:44	46%
3	KOH	TBAB	MeCN:DCM (0.001 M)	6	RT	100:0	92%

Initial conditions (entry 1) used sodium *tert*-butoxide as a relatively weak base. This resulted in a significant presence of the undesired acrylate by-product **155** as well as a poor yield (34%). Sodium hydride was trialled (entry 2) as an alternative base, however, this generated a much higher ratio of acrylamide **155** (56:44). Finally, potassium hydroxide was used in conjunction with tetrabutylammonium bromide (TBAB) as a phase transfer catalyst with high dilution

(entry 3).[55] This resulted in both an excellent yield (92%) and no formation of acrylamide **155** at all. The higher dilution appears to have led to the kinetically favoured β-lactam **151** whilst a more concentrated solution led to base promoted acrylamide **155** formation.[56]

The next step in the route involved formation of styrene **152** *via* a Stille cross coupling reaction (Scheme 2.8).

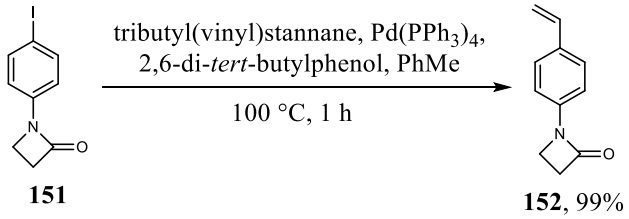

Scheme 2.8: Stille cross-coupling to form styrene **152**.

The synthesis of **152** was achieved in an excellent yield under classic Stille conditions, which used 2,6-di-*tert*-butylphenol as an antioxidant.[57] Moving forward, bromo-fluorination and then successive hydrogen bromide elimination was attempted (Scheme 2.9).

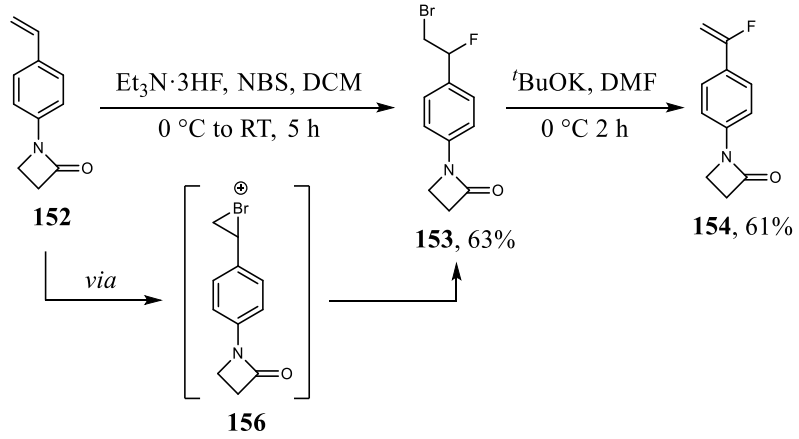

Scheme 2.9: Bromofluorination of styrene **152**.

Bromo-fluorination of styrene **152** was achieved in good yield using *N*-bromosuccinimide (NBS) and triethylamine trihydrofluoride as an electrophilic bromine source and a nucleophilic fluoride source respectively.[58] The regiochemistry favours fluorination at the α-carbon of intermediate **156** due to greater stabilisation of the pseudo cation by the adjacent phenyl ring. The bromofluorinated product **153** was isolated in good yield (63%). Finally, elimination of hydrogen bromide from **153** was achieved using potassium *tert*-butoxide as a sterically bulky base. This was designed to limit β-lactam ring opening and gave the required vinyl fluoride **154**, again in good yield.

Finally, the [2+1] carbene cycloaddition with difluorocarbene and vinyl fluoride **154** was explored (Scheme 2.10), using a protocol previously reported by the St Andrews group,[54] which

used the Ruppert-Prakash reagent (trifluoromethyltrimethylsilane) as a difluorocarbene source.[59]

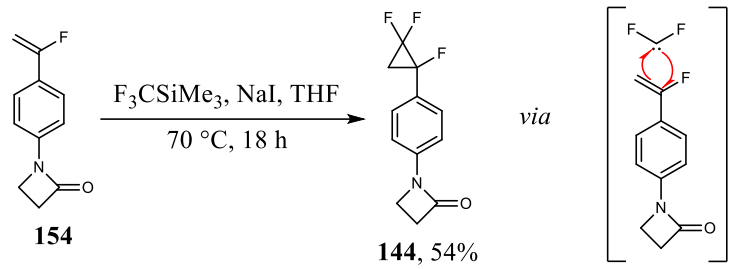

Scheme 2.10: [2+1] Cycloaddition of vinyl fluoride **154** with difluorocarbene.[54,59]

In situ generation of a difluoromethyl carbene *via* the treatment of trifluoromethyltrimethylsilane with sodium iodide resulted in a [2+1] cycloaddition with vinyl fluoride **154** to yield the trifluoro-cyclopropane **144** in modest yield (54%).[54,59] This was a final product, and cyclopropane **144** could be synthesised in six steps with an overall yield of 15%.

With this synthesis a general synthetic route towards β-lactam trifluoro-cyclopropane analogues was established, and four additional fluoro-aryl analogues **181** – **184** were then synthesised, as summarised in Scheme 2.11.

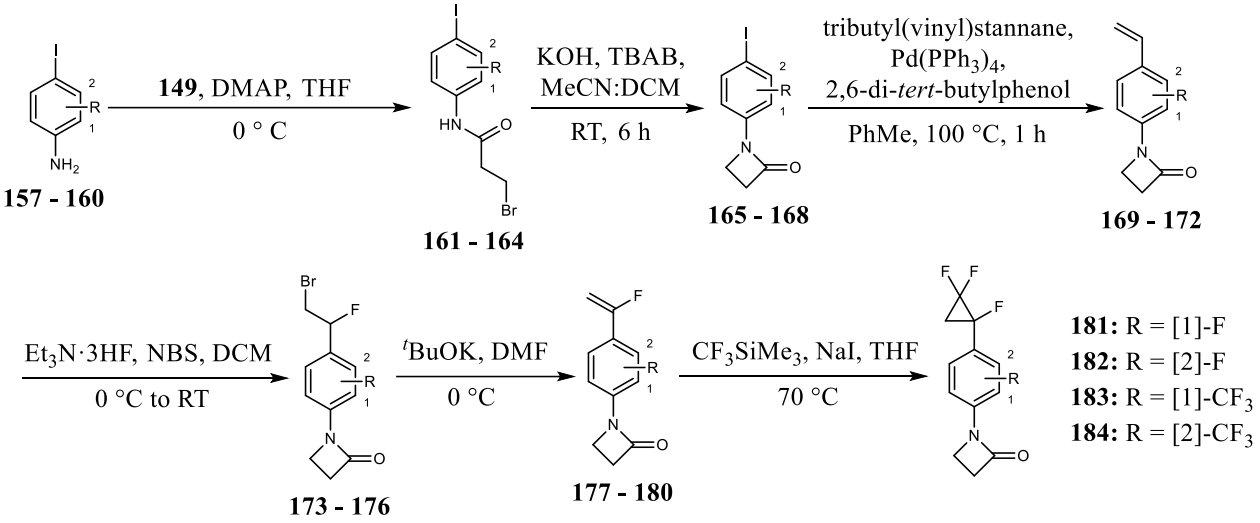

Scheme 2.11: Synthesis of fluoroaryl β-lactams **181 – 184**.

In each case the fluoroaryl β-lactams **181** – **184** were prepared using the six step protocol with overall yields comparable to the synthesis of β-lactam **144** (8%–13%).

The synthesis of an additional trifluoro-cyclopropane analogue was also explored (difluoroaryl **190**, Scheme 2.13), however, this used a slightly modified route. This new approach involved the direct introduction of a vinyl fluoride motif in the cross-coupling reaction as illustrated in Scheme 2.12. Success would shorten the route by two steps, but also depended on the commercial availability of (1-fluorovinyl)(methyl)diphenylsilane **185**.

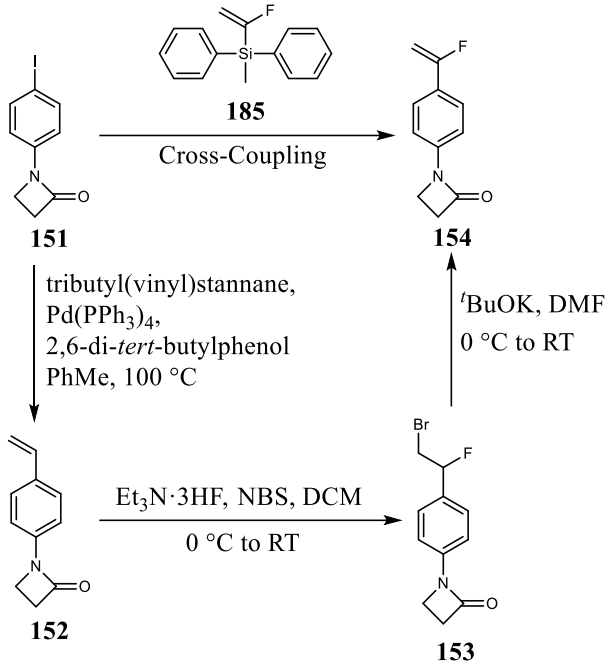

Scheme 2.12: One-step synthesis of vinyl fluoride **154** from iodoaryl **151**.

In order to explore this route a synthesis of difluoroaryl **188** was required (Scheme 2.13).

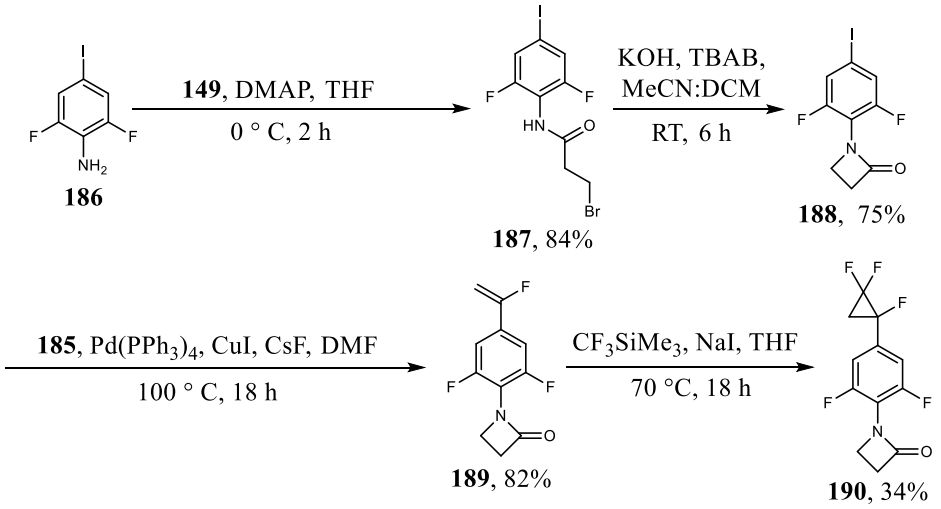

Scheme 2.13: Four-step synthesis of trifluoro-cyclopropane **190** from difluoroaryl aniline **186**.[60]

The synthesis of β-lactam **188** from aniline **186** was achieved over two steps using the previous β-lactam synthesis (see Scheme 2.11). Hiyama cross-coupling with iodoaryl **188** was attempted with (1-fluorovinyl)(methyl)diphenylsilane **185** as the vinyl fluoride coupling partner.[60] The reaction proceeded in high yield (82%), and with subsequent cyclisation, trifluoro-cyclopropane **190** was successfully prepared over four steps in an overall yield of 18%.

This completed the preparation of a family of six trifluoro-cyclopropane β-lactams to be explored for their bioactivity (Figure 2.5).

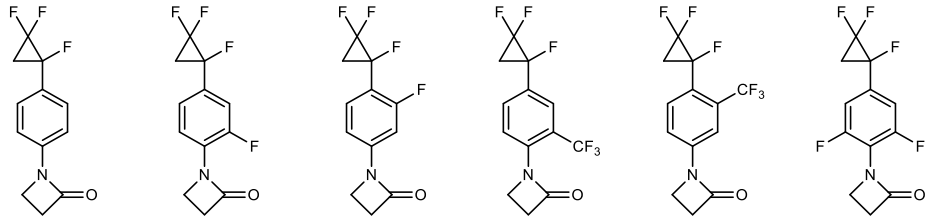

Figure 2.5: Prepared trifluoro-cyclopropane β-lactams.

Each candidate β-lactamase inhibitor differed in their aryl substituents. The differing electron withdrawing capacities (-CF_3 vs -F) and position of the substituents may result in a structure activity profile and also inform on the reactivity of the system in each case.

2.2.2 – β-Lactam assay against *M. abscessus* and other bacteria

In collaboration with the Dr Jonathan Cox group based at Aston University, our collection of β-lactamase inhibitor candidates were screened against several different antibiotic resistant bacteria; *Mycobacterium abscessus* NCTC 13031*, Escherichia coli* ATCC 25922, J53 2138E, J53 2140E, 1496 ESBL, *Pseudomonas aeruginosa* ATCC, and *Salmonella sp*. Each bacterium was individually incubated with a chosen β-lactamase candidate and with the β-lactam antibiotic, amoxicillin **81**. Assays were conducted in a 96-well plate format with varying concentrations of the inhibitor. The optical density of each culture was recorded at 16, 24, 72, or 96 hours as a measure of bacterial cell growth, and the absorbance values of these wells were plotted against time (for further detail see Chapter 7.3.3). Figure 2.6 details the results of these assays with *M. abscessus.*

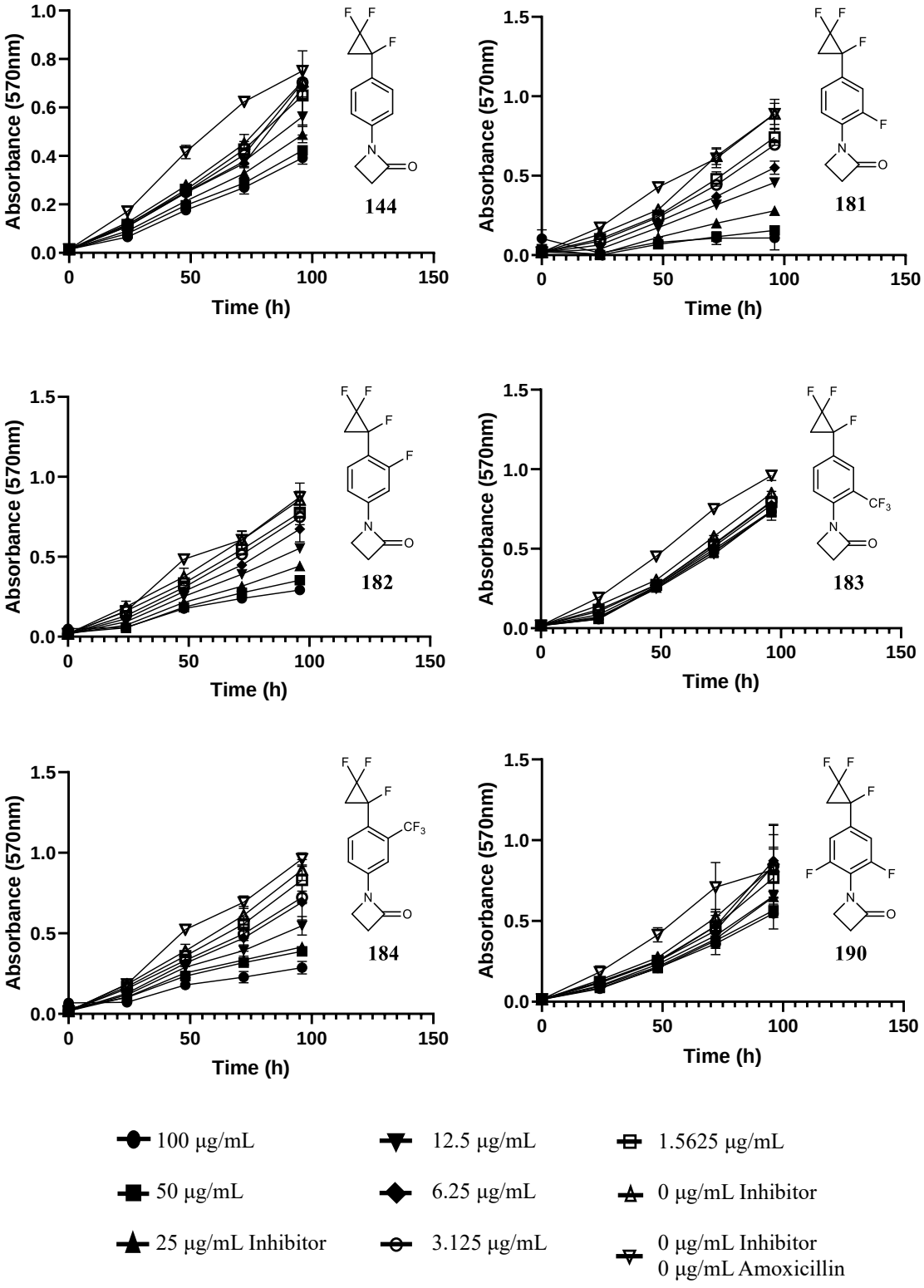

Figure 2.6: Optical density of *M. abscessus* cultures incubated with 100 µg/mL of amoxicillin at different concentrations of β-lactamase inhibitor.

The assays show that the β-lactamase inhibitors enhance amoxicillin efficacy, to varying degrees, against *M. abscessus* over a 96 h period. *O*-Fluoroaryl lactam **181** is the most successful inhibitor trialled, as culture growth is slowed significantly at increased lactam concentrations. Most notably, at 100 µg/mL the optical density of the *M. abscessus* culture

decreases from 72 h to 96 h, indicating that the inhibitor is enhancing the effect of amoxicillin **81** beyond restricting its growth. Importantly, there was no observed change in optical density when the *M. abscessus* was incubated with the β-lactams without the presence of amoxicillin **81**, and vice versa. This suggests that the new β-lactams may function as β-lactamase inhibitors, and not as antibiotics in their own right.

O-Fluoroaryl lactam **181** also showed the highest enhancement of amoxicillin **81** activity against all other tested bacteria compared to its analogues, with an MIC of 100 μg/mL. Figure 2.7 shows the outcomes of these assays over 24 hours with several antibiotic resistant bacteria.

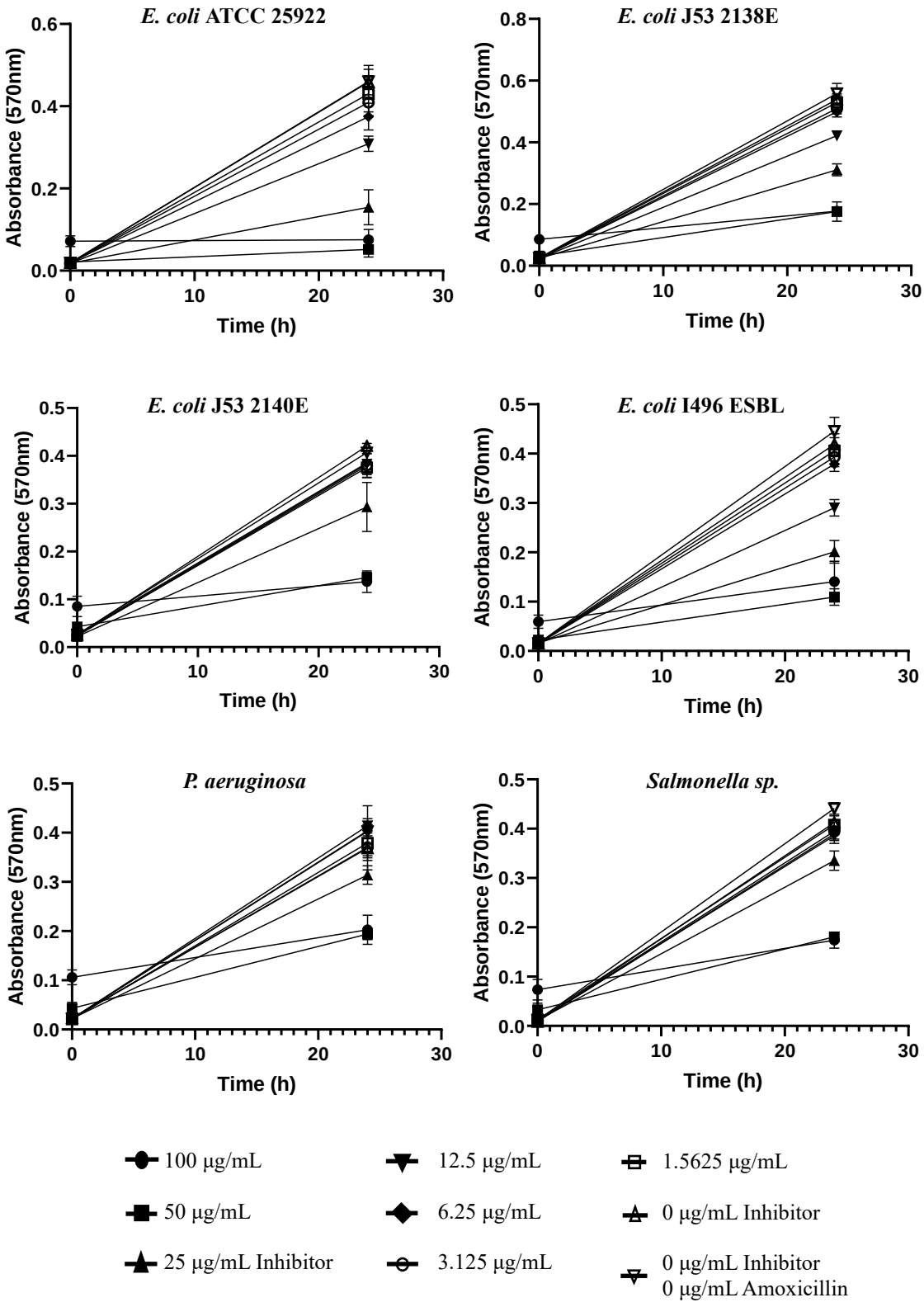

Figure 2.7: Optical density of various bacteria strains incubated with amoxicillin and β-lactamase inhibitor **181** over 24 h.

The above data shows that to varying degrees inhibitor **181** enhances the efficacy of amoxicillin **81** against a panel of bacteria. For almost all the bacteria screened, their rate of growth is slowed at relatively high concentrations (>50 µg/mL) of **181**. However, inhibitor **181** shows total

inhibition of *E. coli* ATCC 25922 (a common reference strain for antibiotic susceptibility) at concentrations of 50 μg/mL and higher.

This study confirmed that a selection of the synthesised β-lactams enhanced the efficacy of amoxicillin **81**, most notably with *M. abscessus*. It was of interest at this stage to evaluate if a possible mechanism of action may be related to fluoride ion elimination accompanied by β-lactam ring opening. This was explored in model chemical reactions.

2.2.3 – Trifluoro-cyclopropane ring opening experiments

In an attempt to observe if the fluoride ion was released in conjunction with β-lactam ring opening (see Scheme 2.3), the hydrolysis of selected inhibitors was explored. In an initial experiment, the appropriate β-lactam (1.0 equiv.) was dissolved in deuterated methanol (0.5 mL) and then sodium methoxide (1 M, 1.5 equiv.) was added. The reaction course was followed by NMR spectroscopy. The ^{1}H and $\{^{1}H\}^{19}F$ NMR experiments were run at multiple time intervals to monitor the reaction progression (for further detail, see Chapter 7.4). Figure 2.8 shows stacked $\{^{1}H\}^{19}F$ NMR spectra taken from a ring opening experiment using inhibitor **181** over 24 hours.

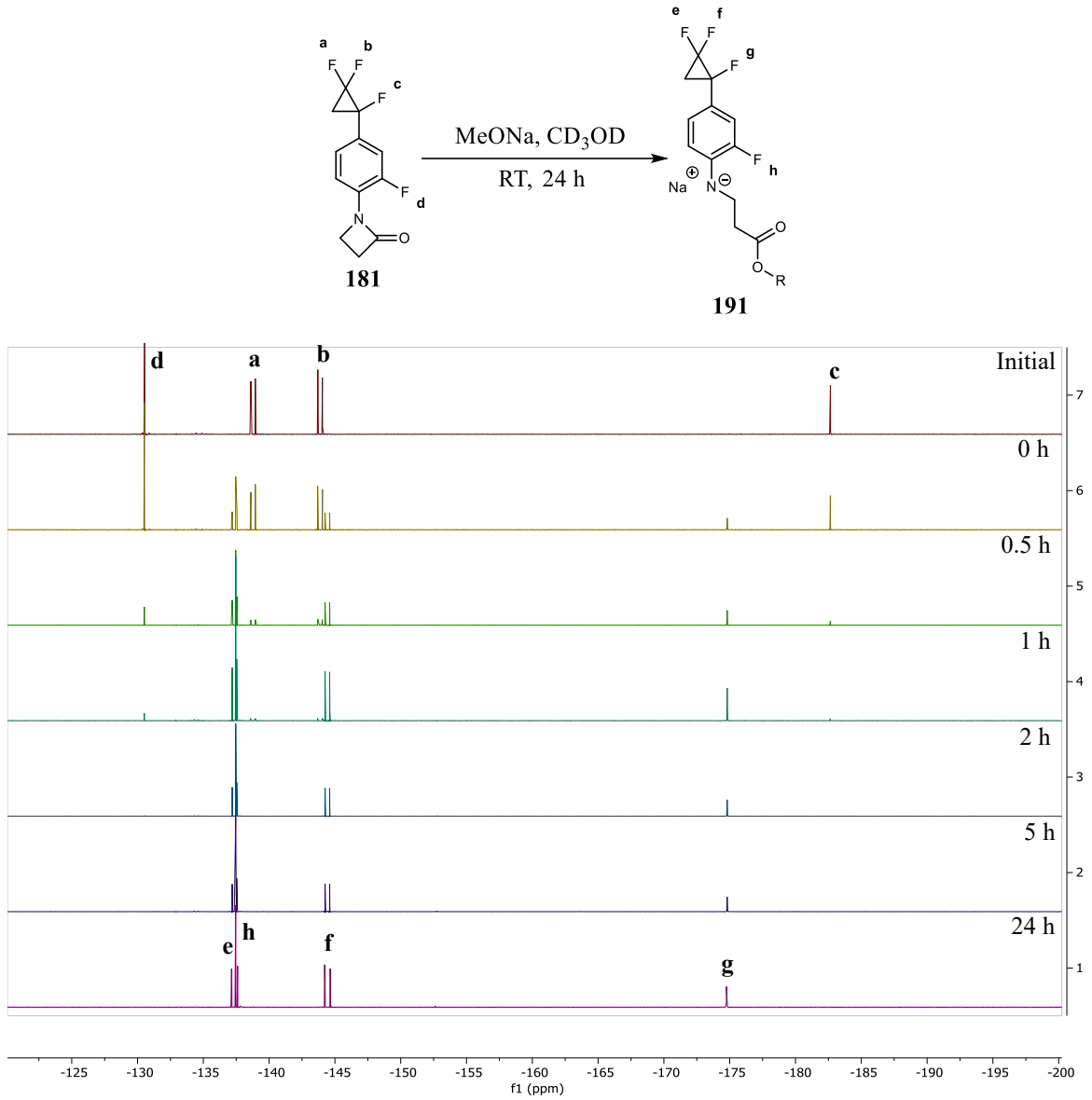

Figure 2.8: Stacked $\{^{1}H\}^{19}F$ NMR spectra taken at intervals up to 24 h after treatment of β-lactam **181** with sodium methoxide.

The time course from Figure 2.8 indicates that the ring of β-lactam **181** is opened by sodium methoxide. There is a clear chemical shift for all fluorine environments in the ^{19}F NMR spectra, with the most significant change in shift associated with the peak corresponding to the α-cyclopropane fluorine environment which moves from -183 ppm to -175 ppm (**c** → **g**). However, there was no observed change in couplings between the trifluoro-cyclopropane system (**a, b** and **c** → **e, f** and **g**), indicating that the cyclopropane ring remains intact and retains all three fluorines after β-lactam ring opening. The retention of all the cyclopropane fluorines is also indicated by the ^{1}H NMR spectrum (Figure 2.9).

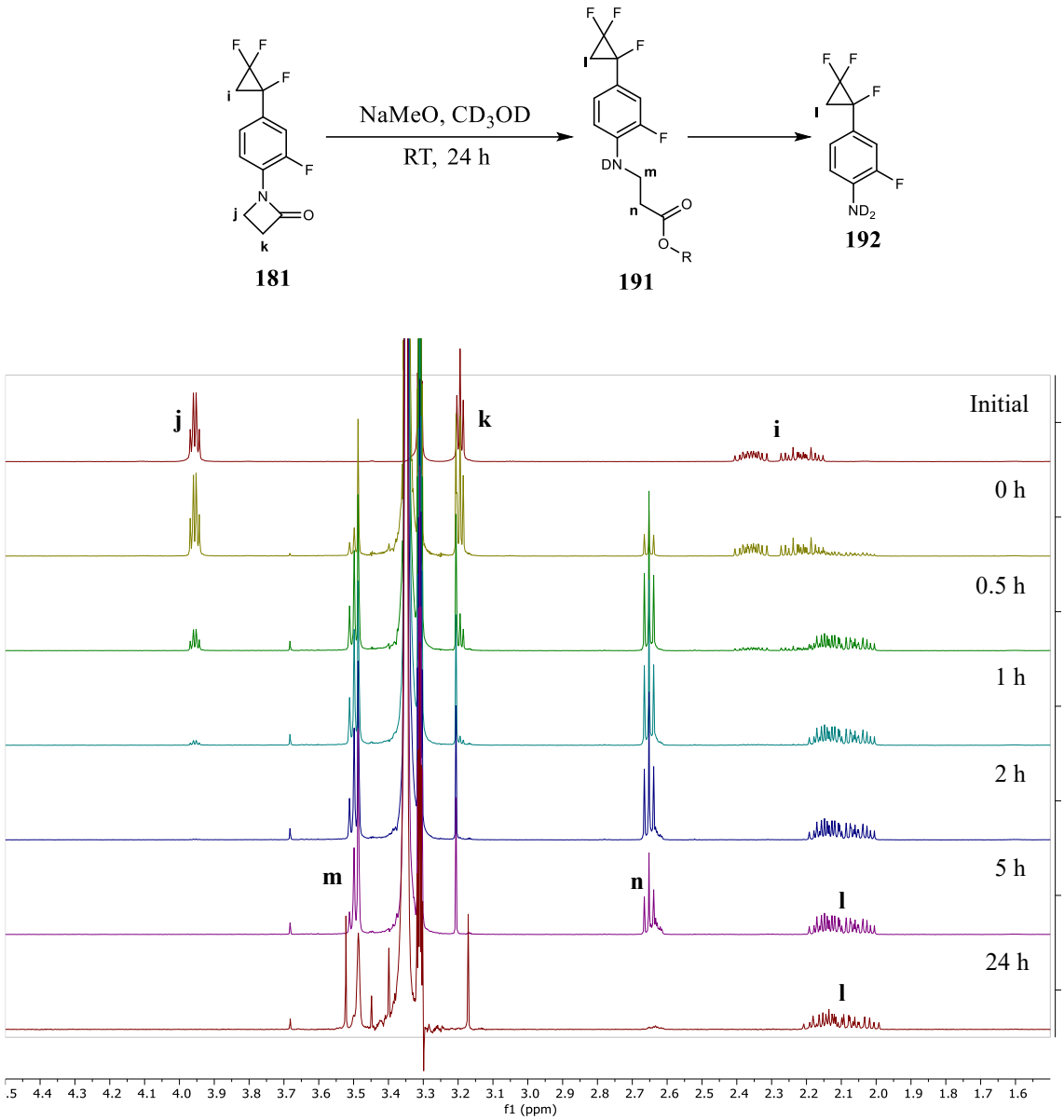

Figure 2.9: Stacked ^{1}H NMR spectra taken at intervals up to 24 h from the treatment of β-lactam **181** with sodium methoxide (1.5 equiv.).

The stacked ^{1}H NMR spectra show a shift in the ppm of several peaks. Peaks corresponding to the β-lactam ring shift upfield, 3.96 ppm (**j**) and 3.20 ppm (**k**) to 3.49 ppm (**m**) and 2.65 ppm (**n**) respectively, whilst maintaining the same coupling patterns, consistent with ring opening of the β-lactam. The same is true for the cyclopropane protons, which also shift upfield (2.41 – 2.15 (**i**) to 2.19 – 2.01 (**l**)) whilst maintaining an identical coupling pattern, again suggesting a significant electronic change but an intact cyclopropane with no loss of fluorine.

The ^{1}H NMR spectrum at the 24 h point does not show any evidence of the methylene group of the β-amino propionate residue (3.49 ppm (**m**) and 2.65 ppm (**n**)) (Figure 2.9), however, the cyclopropane (2.19 – 2.01 ppm (**l**)) remains intact, and the corresponding $\{^{1}H\}^{19}F$ NMR spectrum (Figure 2.8) shows the aryl fluorine (**h**) is also intact. This suggests that the alkyl unit has degraded under prolonged basic conditions, presumably by base induced elimination to

generate the free aniline **192** and also acrylate (not observed). As there was no evidence of fluorine ejection, the resulting product was not investigated further.

When similar ring opening experiments were performed under acidic conditions with hydrochloric acid (1M, 1.5 equiv.), no change was observed by either ^{1}H NMR or $\{^{1}H\}^{19}F$ NMR spectra after 24 hours.

In a similar manner, base and acid catalysed ring opening experiments were performed on all of the synthesised β-lactams (**144**, **181-184**, and **190**) (see Chapter 7.4.2 for ^{1}H NMR and $\{^{1}H\}^{19}F$ NMR time courses). All β-lactam rings were hydrolysed when treated with sodium methoxide after one hour, yet most proved stable under hydrochloric acid, with lactams **144** and **183** showing only minor conversions to the ring opened product in hydrochloric acid after 24 h. However, there was no evidence of fluoride ion elimination by ^{1}H NMR or $\{^{1}H\}^{19}F$ NMR spectra, even when treated with a ten-fold equivalent of sodium methoxide over the course of a week. This data suggests that the cyclopropane is stable to fluoride ion release after β-lactam hydrolysis. Fluorine ion release may be suppressed by the presence of the inductively withdrawing CF_2 group in the cyclopropane ring, which could be a significant stabilising factor. Therefore, it is concluded that the observed bioactivity is not a consequence of suicide inhibition through the anticipated mechanism.

2.2.4–Synthesis of a monofluoro-cyclopropane lactam

If the inductively withdrawing CF_2 group was replaced by a CH_2 group, a developing carbocation intermediate would be more stabilised, in turn promoting release of fluoride (Scheme 2.14).

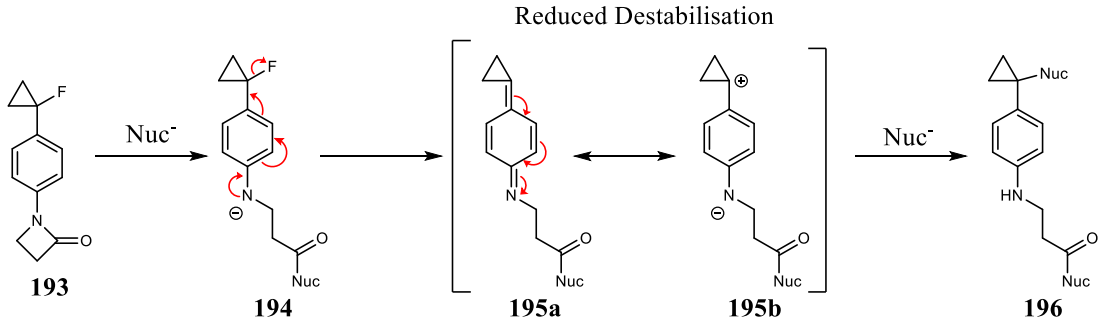

Scheme 2.14: Mechanistic reasoning for lack of fluoride ejection and proposed monofluoro-cyclopropane analogue **193** to circumvent destabilised intermediate.

In order to promote fluoride ion release, attention turned to the synthesis of monofluoro-cyclopropane analogue **193**, which only possessed a benzylic fluorine in the cyclopropane, without the CF_2 group. An initial synthesis envisioned vinyl fluoride **154** as a substrate to instal

a CH_2 group *via* carbene [2+1] cyclisation. Two sets of conditions were explored for carbene cycloaddition, as illustrated in Scheme 2.15.

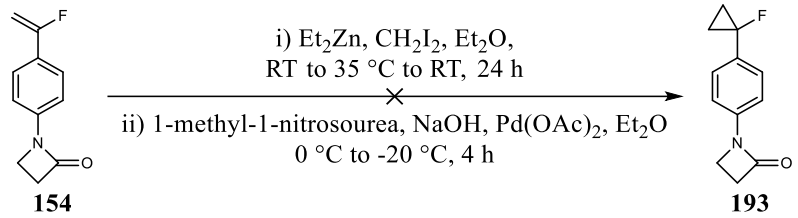

Scheme 2.15: Attempts at the synthesis of cyclopropane **193** from vinyl fluoride **154**.

The two approaches involved were: (i) a Simmons Smith reaction,[61] and (ii) a palladium catalysed carbene addition.[62] Both reactions failed to provide product, with no evidence of any conversion by ^{1}H or ^{19}F NMR spectra. It is hypothesised that the fluorine deactivates the alkene, rendering it unsuitable for cycloaddition. Notably, no literature could be found for the conversion of an aryl vinyl fluoride to a mono fluorinated cyclopropane.

The synthetic route towards monofluoro-cyclopropane **193** was therefore re-evaluated. In collaboration with a fellow group member George Kingsley-Moore (MChem student), the synthetic route was revised to the four-step process illustrated in Scheme 2.16.[63]

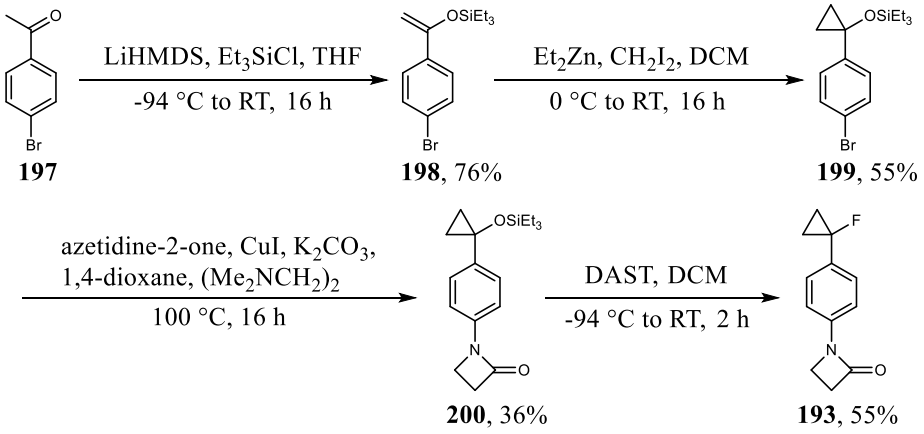

Scheme 2.16: Route towards the synthesis of monofluoro-cyclopropane **193** conducted by G. Kingsley-Moore.[63]

Acetophenone **197** was enolised and subsequently trapped with triethylsilyl chloride to give silyl enol ether **198**. This was then used as a substrate for a Simmons-Smith transformation to successfully install the CH_2 group, forming cyclopropane **199**. The lactam ring was generated using an Ullmann cross coupling reaction to give aryl lactam **200**. In a final step **200** was treated with diethylaminosulpher trifluoride (DAST), to give the target monofluoro-cyclopropane **193** in an overall yield of 8% over the four steps.

This initial synthesis established the viability of the route, however, it did not yield enough material for biological assays, therefore the synthesis was revised and scaled up. A more optimised route is illustrated in Scheme 2.17.

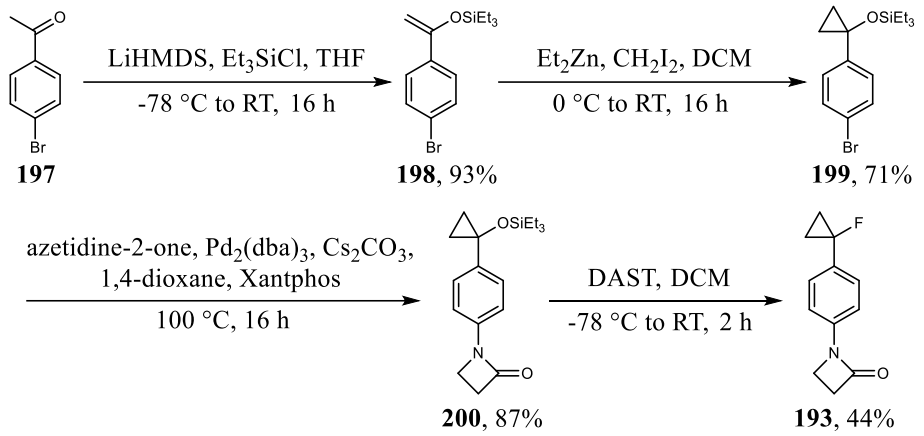

Scheme 2.17: Revised route towards monofluoro-cyclopropane **193**.

The most significant change in the synthesis addressed the cross-coupling reaction **199** → **200**. The Ullmann reaction with copper was changed to a higher yielding Buchwald-Hartwig cross-coupling with palladium. This proved to be highly efficient (87% yield) and more than doubled the overall yield to 25%, allowing for the synthesis of sufficient quantities of **193** for assays.

Monofluoro-cyclopropane **193** was assayed for inhibition activity against multiple antibiotic resistant bacteria, again in collaboration with the Cox group at Aston University. In an assay similar to that described in Chapter 2.2.2, monofluoro-cyclopropane **193** was incubated with a panel of subspecies of *M. abscessus*. Surprisingly, it was discovered that there was a lack of culture growth in wells without the accompanying antibiotic amoxicillin **81**. This indicates that lactam **193** possesses antibiotic properties in its own right and can be used without accompanying drugs to inhibit bacterial growth. Figure 2.10 summarises the results of the conducted assays.

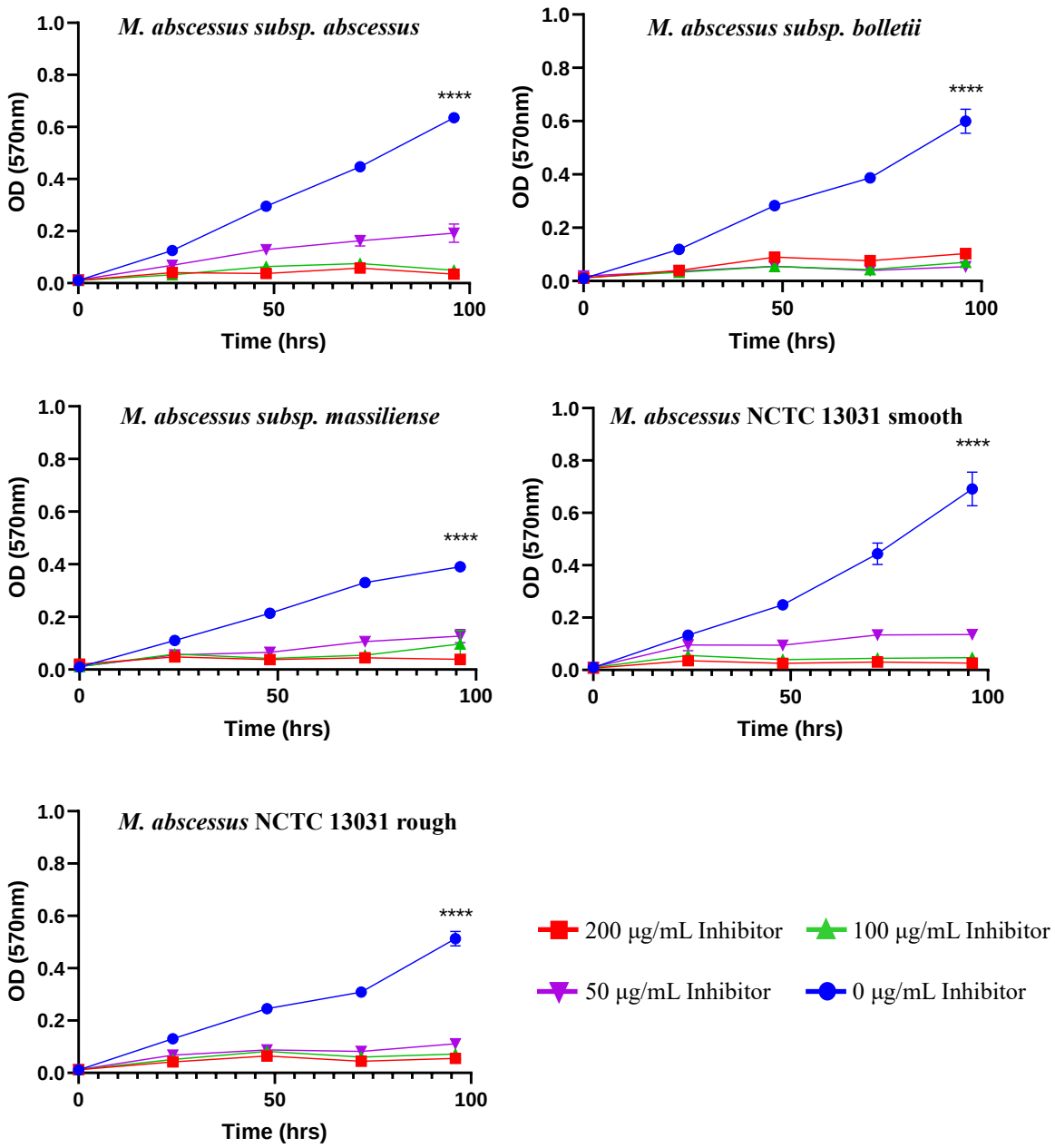

Figure 2.10: Optical density of several *M. abscessus* strains incubated with monofluoro-cyclopropane **193** over 96 h.

For all of the tested strains and subspecies of *M. abscessus* the MIC of antibiotic candidate **193** is less than 100 µg/mL, and the minimum bactericidal concentration (MBC), the lowest concentration at which bacterial cell death occurs, is lower than 100 µg/mL for selected strains. However, when antibiotic **193** was tested against *Mycobacterium bovis* bacillus Calmette-Guérin (BCG) (a strain used for tuberculosis immunisation) the MIC and MBC was 0.39 µg/mL, a lower dosage than for any *M. abscessus* strain. The results from this assay are illustrated in Figure 2.11**.**

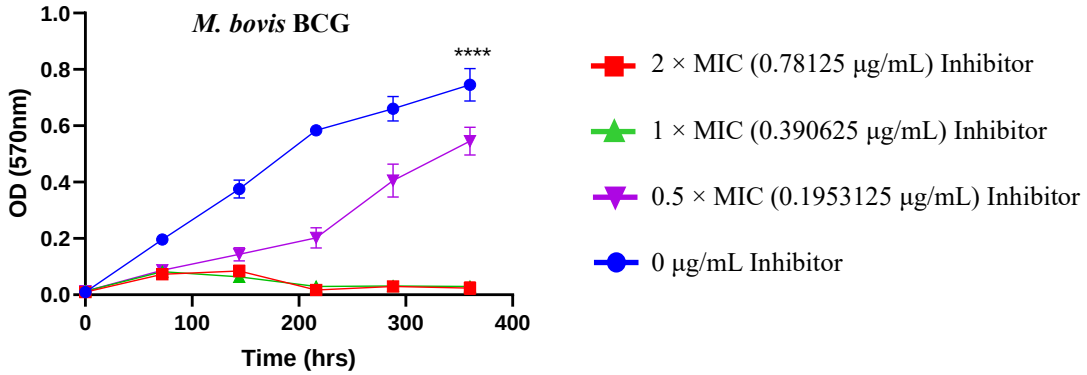

Figure 2.11: Optical density of *M. bovis* BCG incubated with antibiotic **193**.

Monfluoro-cyclopropane β-lactam **193** was re-assayed in unison with trifluoro-cyclopropane β-lactams **144** and **181** as an antibiotic against multiple variants of *M. abscessus* and *M. bovis BCG Pasteur 1173P2*. The MIC and MBC values which were calculated from these assays are illustrated in Table 2.2

Table 2.2: MIC and MBC of selected β-lactams against *M. abscessus* variants and *M. bovis*.

Bacteria	Variant	Compound					
		193		**144**		**181**	
		MIC (µg/mL)	MBC (µg/mL)	MIC (µg/mL)	MBC (µg/mL)	MIC (µg/mL)	MBC (µg/mL)
M. abscessus	***Subsp. abscessus***	50	50	>200	>200	>200	>200
	Subsp. bolletii	100	100	>200	>200	>200	>200
	Subsp. massiliense	100	>200	>200	>200	>200	>200
	NCTC 13031 smooth	100	>200	>200	>200	>200	>200
	NCTC 13031 rough	100	100	>200	>200	>200	>200
M. bovis	***BCG Pasteur 1173P2***	0.39	0. 39	100	100	>200	>200

When compared to trifluoro-cyclopropanes **144** and **181** the MIC of monfluoro-cyclopropane **193** is significantly lower against all screened bacteria. This is most clearly observed with *M. bovis*, as the MIC of β-lactam **193** (0.39 µg/mL) is over 100-fold lower than that of β-lactam **144** (100 µg/mL) and **181** (>200 µg/mL). The MBC values for β-lactam **193** against almost all of the screened bacteria are lower than β-lactams **144** and **181**, with the exception of *Subsp. massiliense* and *NCTC 13031* smooth. For these bacteria, all three tested compounds have an MBC of >200 µg/mL, indicating that none of the tested β-lactams are able to kill these bacteria. In all, Table 2.2 indicates that monofluoro-cyclopropane **193** shows relatively high antibacterial activity against *M. bovis BCG Pasteur 1173P2* and certain variants of *M. abscessus* compared to trifluoro-cyclopropanes **144** and **181**.

2.2.5 – Monofluoro-cyclopropane ring opening experiments

Given that this monofluorinated cyclopropane had higher activity than the trifluoro-cyclopropane, the monofluorinated lactam **193** may also be inherently more reactive. Therefore, the chemical hydrolysis of **193** was explored in a similar manner to that previously described for the earlier series of β-lactams. Drawing from previous experiments, hydrolysis of lactam **193** was attempted using methoxide as a nucleophile. In an initial experiment, 1 mg of β-lactam **193** was dissolved in deuterated methanol and then sodium methoxide (1 M, 1.5 equiv.) was added. ^{1}H and $\{^{1}H\}^{19}F$ NMR experiments were run at multiple time intervals over a 48 h time period to monitor the reaction progression (for further detail see Chapter 7.4). Figure 2.12 shows stacked $\{^{1}H\}^{19}F$ NMR spectra taken from time intervals throughout the experiment.

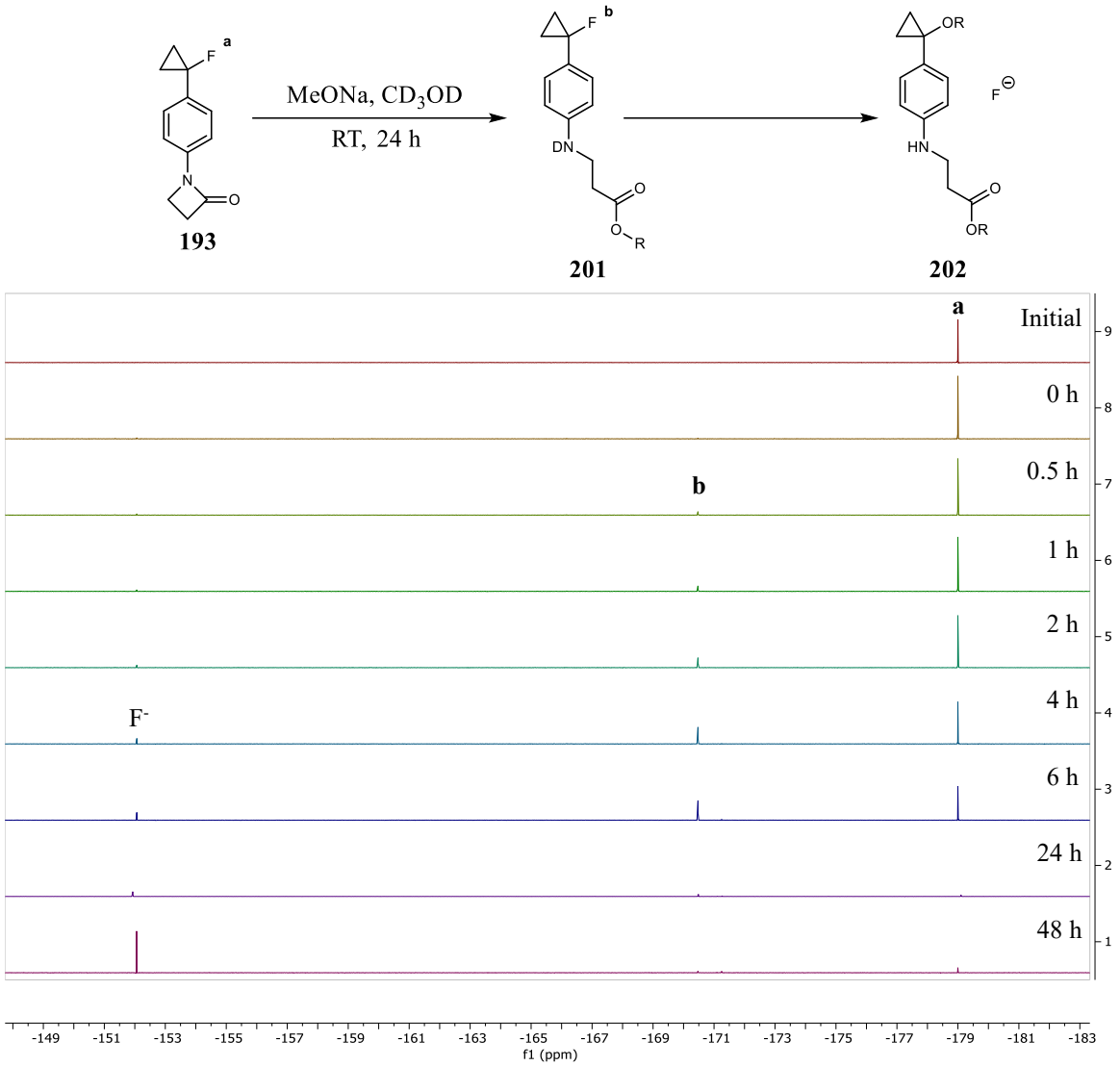

Figure 2.12: Stacked $\{^{1}H\}^{19}F$ NMR spectra taken at time intervals from a treatment of β-lactam **193** with sodium methoxide.

The data in Figure 2.12 indicated that lactam **193** is converted to a new compound over several hours, presumably as the β-lactam ring is hydrolysed, however, unlike the previous ring opening experiments with trifluoro-cyclopropanes, fluoride elimination is now observed (after 4 hours).

The stacked $\{^1H\}^{19}F$ NMR spectra show the gradual decrease in intensity of the starting signal corresponding to fluorine **a** of **193** and an increased intensity of a new signal at -171 ppm. This is an aliphatic fluorine and is consistent with a shift (Δ 8 ppm) in the cyclopropane fluorine environment. This change in peak intensity is consistent with methoxide hydrolysis of the β-lactam **193** to aniline **201**. This intermediate peak (**b**) then decreases in intensity and a new signal appears at -152 ppm, which is consistent with the presence of fluoride ions. To support the identity of the fluoride ion, an ^{19}F NMR experiment without proton decoupling was performed, which showed that there was no proton-fluorine coupling to the signal at -152 ppm. Finally, the reaction was treated with hydrochloric acid (1 M) to neutralize the pH. This resulted in a significant shift in ppm from -152 to -182 (Figure 2.13), typical of a free hydrogen fluoride in solution.[64]

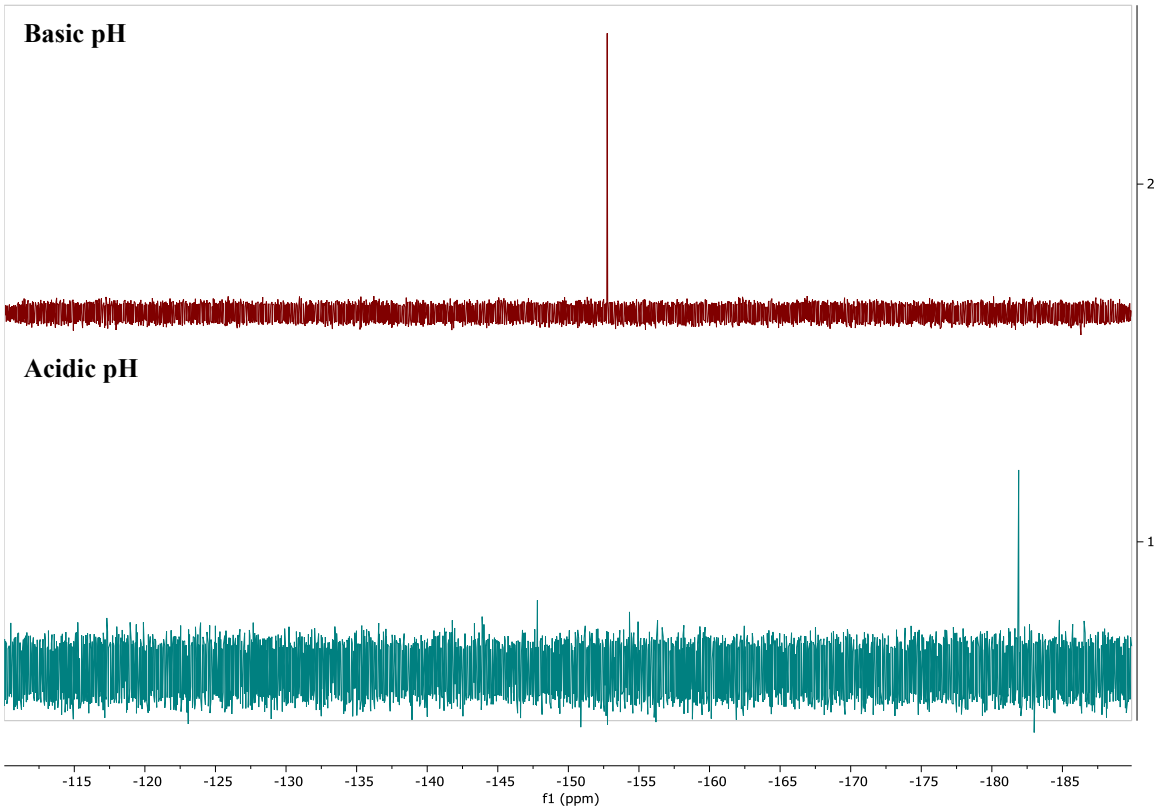

Figure 2.13: ^{19}F NMR spectra after sodium methoxide treatment of cyclopropane **193** in (a) basic and (b) acid conditions, indicating the presence of fluoride ion.

The ^1H NMR time course also supports the release of a fluoride ion from the cyclopropane in **193**. Figure 2.14 shows the stacked ^1H NMR spectra taken from the ring opening experiment over the course of 48 h.

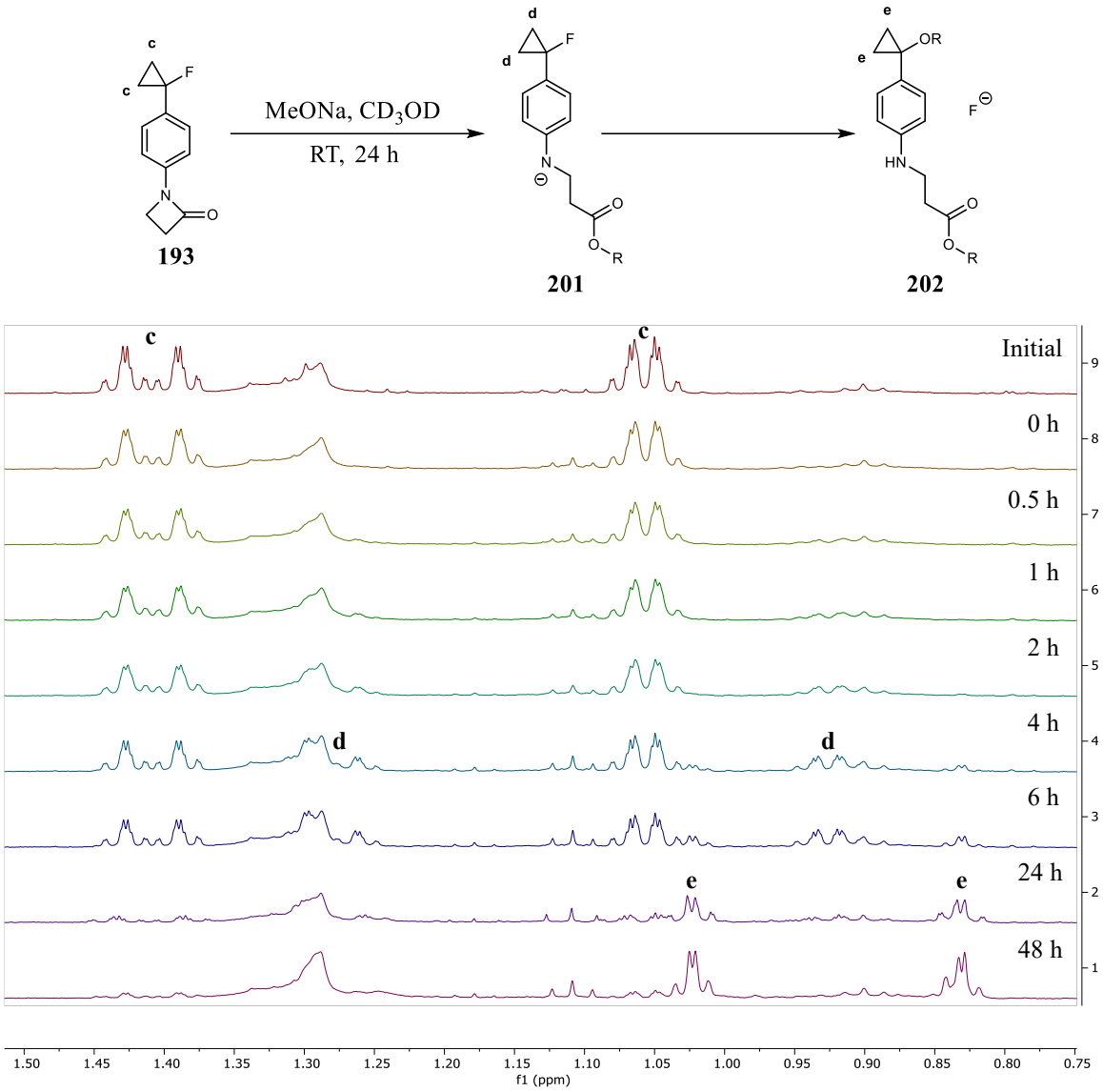

Figure 2.14: Stacked ^{1}H NMR spectra taken at specified time points over 48 h from a ring opening experiment with β-lactam **193** with sodium methoxide.

Three different pairs of signals are observed increasing and decreasing in intensity over the 48 h time period. Importantly, the signals corresponding to the cyclopropane environment from putative aniline **201** (1.29 and 0.92 ppm (**d**)) have an identical coupling pattern to the cyclopropane of lactam **193** (1.41 and 1.06 ppm (**c**)). This indicates a coupling between the cyclopropane protons and indicates the presence of a fluorine. However, after 4 h a set of signals corresponding to the cyclopropane protons without fluorine appear (1.02 and 0.83 ppm (**e**)). The coupling pattern has changed from a doublet of doublet of doublets (ddd) to a doublet of doublets (dd), indicating the removal of the spin active fluorine, and supporting fluoride ion elimination.

As there is no formation of any defluorinated cyclopropane **202** before an apparent ring opening, it is assumed that the ring opened aniline **201** is an intermediate, and that fluoride ejection occurred after ring opening.

Although fluoride ejection was observed, the resulting organic product could not be isolated. The methoxide nucleophile was also difficult to distinguish from the methanol solvent by the ^{1}H NMR spectrum and any possible methyl ether or methyl ester products proved difficult to identify and isolate. Therefore, the experiment was repeated with a more ^{1}H NMR distinct nucleophile; sodium benzyl alkoxide, as this was anticipated to give a more readily isolatable product, and easier detection by ^{1}H NMR spectroscopy (Scheme 2.18).

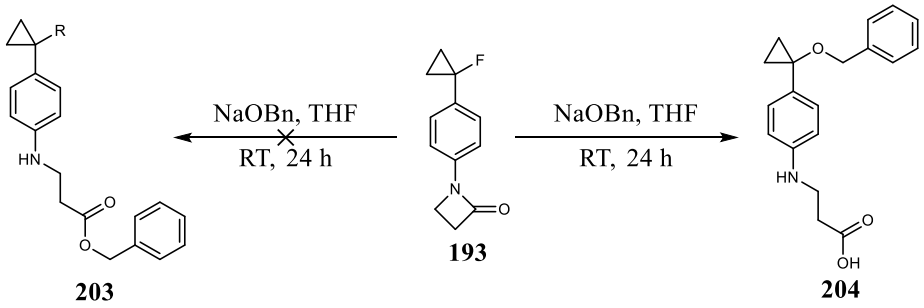

203 **193** **204**

Scheme 2.18: Ring opening and subsequent fluoride ion elimination of monofluoro-cyclopropane **193** with sodium benzyl alkoxide.

When the reaction was repeated with sodium benzyl alkoxide the major product that was isolated was carboxylic acid **204**, which contained a benzyl ether moiety attached to the cyclopropane. Conversely, there was no evidence for the formation of a benzyl ester **203**, despite the reaction being carried out under apparent anhydrous conditions. This was concluded from the ^{1}H NMR of lactam **193** after treatment with sodium benzyl alkoxide. The outcome was also supported by the ^{1}H-^{13}C 2D NMR spectrum and High-Resolution Mass Spectrometry (HRMS) of the isolated product, shown in Figure 2.15.

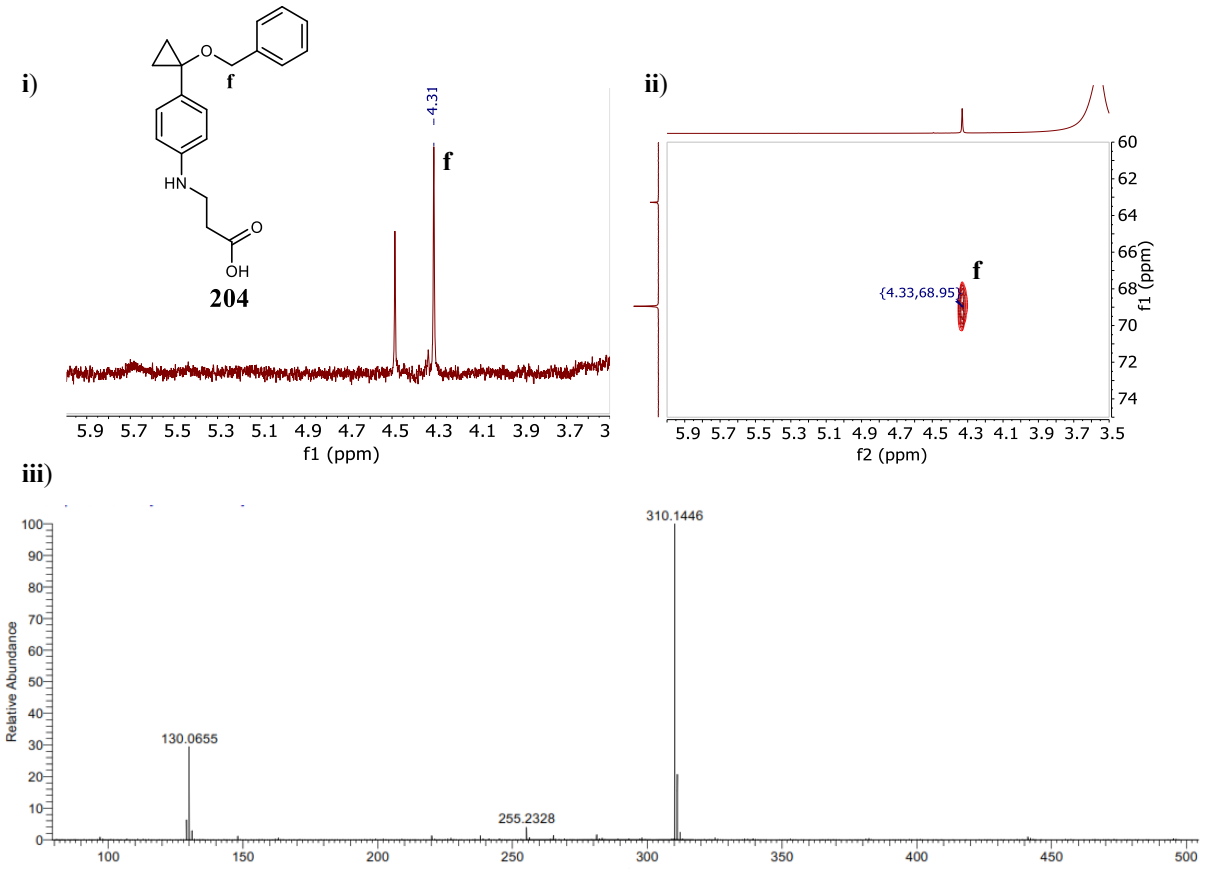

Figure 2.15: i) ^{1}H NMR spectra taken of lactam **193** treated with sodium benzyl alkoxide after 48 h. **ii)** ^{1}H-^{13}C 2D NMR of the isolated product. **iii)** HRMS of isolated product.

The ^{1}H NMR of carboxylic acid **204** taken after 48 h (**i**) shows two singlets, one at 4.5 ppm correlating to unreacted benzyl alcohol and another at 4.3 ppm, correlating to a different benzylic environment. The corresponding carbon associated with this benzylic proton environment, which can be assigned from the ^{1}H-^{13}C 2D NMR of the isolated product (**ii**), is at 68.1 ppm. Both the ^{1}H and ^{13}C NMR shifts correspond to a benzyl ether,[65] as opposed to a benzyl ester **203**, which would be anticipated to have an ^{1}H NMR shift of ~5.1 ppm, and a ^{13}C NMR shift of ~66 ppm,[66] neither of which are detectable in the ring opening experiment.

The outcome clearly confirmed that there is an elimination of a fluoride ion when the β-lactam **193** is treated with an alkoxide nucleophile, however, the presence of the carboxylic acid **204** and not the benzyl ester **203** was unexpected.

The formation of the carboxylic acid could clearly arise from adventitious water hydrolysing the β-lactam ring, despite best efforts in keeping the reaction anhydrous. To validate the role of water as a nucleophile, a sodium benzyloxide ring opening experiment was performed, however, this time it was spiked with one equivalent of $H_2{}^{18}O$ [^{18}O-97 atom %] as an additive (Scheme 2.19).

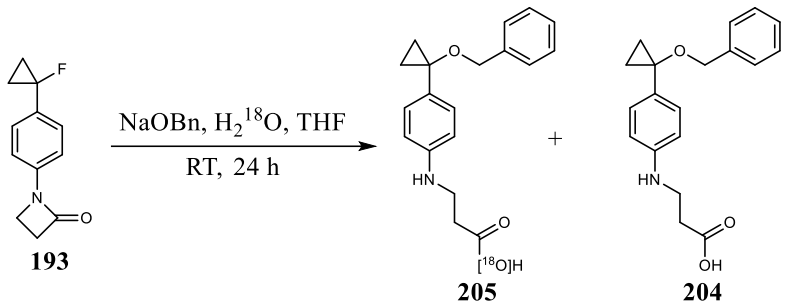

Scheme 2.19: Reaction of monofluoro-cyclopropane **193** with sodium hydroxide spiked with $H_2{}^{18}O$ [^{18}O-97 atom %] additive.

In order to observe the incorporation of oxygen-18 from $H_2{}^{18}O$ [^{18}O-97 atom %] into the carboxylic acid, HRMS was used, and the outcome is illustrated in Figure 2.16.

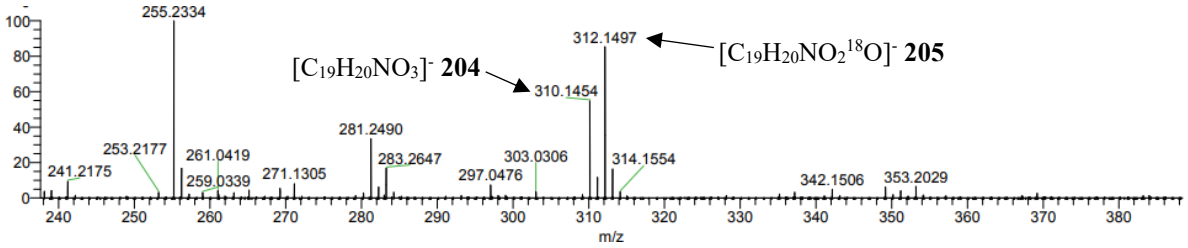

Figure 2.16: HRMS spectra of ring opening products **204** and **205** showing isotope enrichment.

Two peaks were observed corresponding to natural abundance oxygen-16 carboxylic acid **204** (310.1454 = $[M-H]^-$) and also the enriched oxygen-18 carboxylic acid **205** (312.1497 = $[M-H]^-$), differing by a molecular weight of 2.0043. From the relative intensities of these ions, it can be concluded that there was approximately a 60% incorporation of oxygen-18 into the product. Given that the oxygen-18 water was 97% enriched, this indicates a substantial incorporation, but also the presence of some oxygen-16 water too. There was no evidence of a dibenzyl product observed by HRMS.

Perhaps the monofluoro-cyclopropane **193** is formed as a hydrate complex, and the residual water from this complex becomes deprotonated by sodium benzylate. This then acts as the nucleophile for the hydrolysis of the β-lactam ring. This finalised hypothesised mechanism is illustrated in Scheme 2.20.

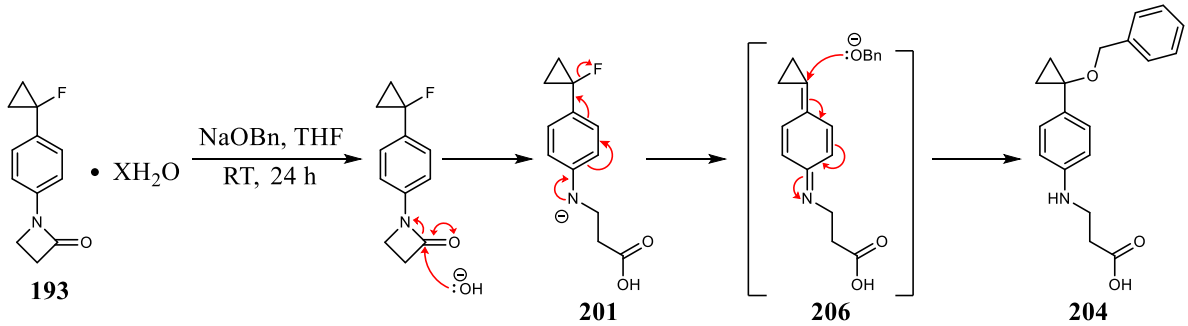

Scheme 2.20: Putative mechanism for nucleophilic attack of β-lactam **193** to give benzyl ether **204**.

2.2.6 – Log *P* of β-lactams

Log *P* values (see Chapter 1.2.1) are used in medicinal chemistry as a metric to determine how lipophilic a compound is. This value is a significant pharmacokinetic parameter in medicinal chemistry. To this end, measuring the log *P* of the synthesised β-lactams provides additional data, useful for determining their use as potential antibiotics or β-lactamase inhibitors. It is also of interest to explore the effects of fluorine substitution on polarity.

The log *P*'s of the synthesised β-lactams were measured using reverse phase HPLC.[67] In brief, the capacity factor (*k*) of the β-lactams were calculated from their retention time (R_t) on a C_{18} reverse phase column using Equation 2.1, where T_0 is the column "dead time" (time taken for an unretained compound to pass through a column).

$$k = \frac{R_t - T_0}{T_0} \qquad 2.1$$

The log *P* values of the lactams were then calculated from a straight-line graph constructed from reference compounds with known log *P* values (for further details, see Chapter 7.5). The average retention times (R_t), capacity factor (*k*) and log *P* of selected lactams are shown in Table 2.3. Each is an average of three measurements.

Table 2.3: Average retention time (R_t), capacity factor (*k*) and log *P* of β-lactams.

B-Lactam	Average R_t min^{-1}	Capacity Factor (*k*)	Calc. Log P
144	8.59	0.970	2.74 ± 0.01
181	8.91	1.044	2.89 ± 0.01
182	8.79	1.015	2.83 ± 0.01
183	9.08	1.083	2.96 ± 0.01
190	8.33	0.911	2.61 ± 0.01
193	8.68	0.991	2.78 ± 0.01

Figure 2.17 illustrates these β-lactams on a scale of increasing log *P.* β-lactam **183** has the highest log *P* of 2.96, which is consistent with the hydrophobic aryl CF_3 group, on the other hand, β-lactam **190** has the lowest log *P* of 2.61, which, although not so obvious, may result from an increased dipole moment across the molecule caused by the aryl difluoro motif. The β-lactams as a series have values which lie narrowly between 2.6 and 3.0, a log *P* range which falls under Lipinski's value of 5 for an ideal drug candidate.[68]

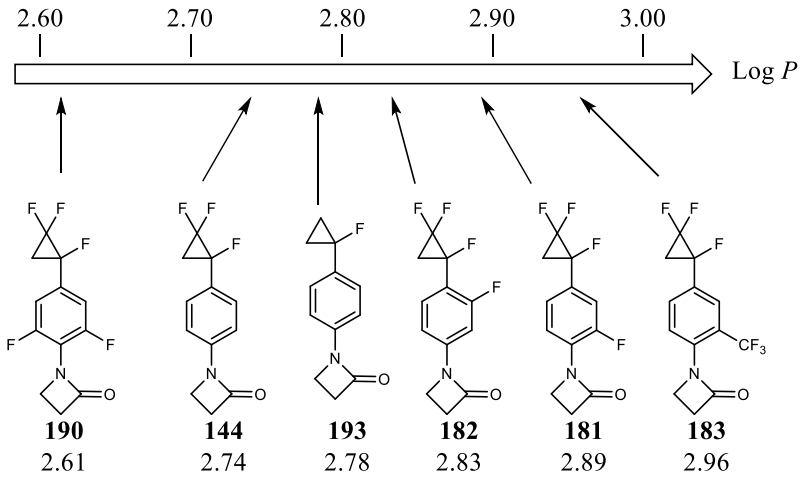

Figure 2.17: Novel β-lactams and their comparative log *P* value.

2.2.7 – Drug metabolism and pharmacokinetics of β-Lactams

In order to gain a better understanding of how these β-lactams may perform *in vivo*, a selection (**144**, **181 – 183**, and **193**) was sent to the Drug Discovery Unit at the University of Dundee to be screened for human and mouse toxicology and metabolic clearance assays. The β-lactams were screened for intrinsic clearance (the ability of the liver to metabolise the drug) in both mouse and human microsomal liver proteins (g/min/mg) and their toxicity against HepG2, a human liver cancer cell line commonly used for drug metabolism studies.[69] The results from theses screens are summarised in Table 2.4.

Table 2.4: Mouse and human intrinsic clearance and HepG2 toxicity assay results for **144**, **181 – 183**, and **193**. *Based on scaling factor of 48 mg of microsomal protein per g liver. **Based on scaling factor of 39.7mg of microsomal protein per g liver. † $\mathbf{pXC_{50} = 6 - \log(XC_{50})}$.

Compound	Mouse Intrinsic Clearance		Human Intrinsic Clearance		HepG2 Toxicity	
	Microsomal Protein (mL/min/mg)	Liver* (mL/min/g)	Microsomal Protein (mL/min/mg)	Liver** (mL/min/g)	XC_{50} (μM)	pXC_{50}†
144	>1	>48	Chemically unstable		>100	<4
181	>1	>48	Chemically unstable		>100	<4
182	Chemically unstable		Chemically unstable		56	4.3
183	>1	>48	Chemically unstable		>100	<4
193	>1	>48	>1	>40	1.2	5.9

Clearance relates to how quickly a compound is cleared from the body *in vivo*, and compounds can be categorised as having high, medium, or low clearance. Highly cleared compounds are typically poor drug candidates as they are likely to be rapidly cleared resulting in a short duration of action. For intrinsic clearance of microsomal liver proteins, the upper limit for low

clearance classification is 0.02 mL/min/mg and the lower limit for high clearance classification is 0.1 mL/min/mg.[70]

All of the screened β-lactams except **193** were metabolically unstable when incubated with human microsomal proteins, and β-lactam **182** was similarly unstable in a mouse microsomal protein assay. This indicates that the β-lactams were rapidly metabolised, and they could not be detected in the assay, most likely resulting from an immediate hydrolysis of the β-lactam ring. For every other entry, the intrinsic clearance for mice and human microsomal proteins is recorded as above 1 mL/min/mg, a value substantially above the lower limit for high clearance classification. This means that the screened β-lactam drugs will be cleared rapidly *in vivo*, resulting in an extremely short duration of action.

HepG2 is a human hepatic cell line and is often used as a model of healthy liver cells to test the cytotoxicity of substances on the liver.[71] β-Lactams **144**, **181**, and **183** all show an XC_{50} (half-maximal inhibitory/effective concentration, in this instance the concentration needed to kill half the HepG2 cell line) of above 100 μM and were essentially nontoxic. **182** however was toxic, with an XC_{50} of 56 μM. However, the lack of significant activity against *M. abscessus* at high concentrations (see Chapter 2.2.2) indicates that even if the compound were administrated at low dosages, it would not have any effect on *M. abscessus* growth. Finally, the most active β-lactam of the series, **193**, appears to be toxic at low concentrations (XC_{50} = 1.2 μM), over 50-fold lower than any of the other β-lactams. This result suggests that β-lactam **193**'s good activity against bacteria is due to the compound acting as a general cytotoxin in cells. This toxicity limited the progression of these compounds as pharmaceuticals and drugs.

2.3 – Conclusions

This chapter has described the design and synthesis of seven novel fluoro-cyclopropane β-lactams as candidate mechanism based β-lactamase inhibitors. Their efficacy as antibiotic enhancers were explored, with almost all of the novel compounds showing a good degree of inhibition against *M. abscessus* when paired with amoxicillin. Monofluoro-cyclopropane **193** in particular was shown to display good activity as an antibiotic against several antibiotic resistance bacteria, and with greatest activity against *M. bovis*.

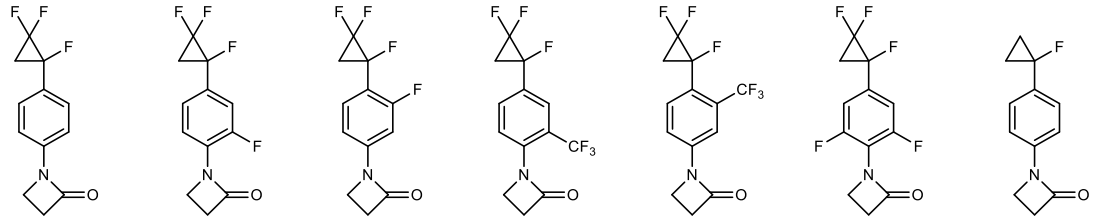

144 **181** **182** **183** **184** **190** **193**

Figure 2.18: β-Lactams explored in this chapter.

Hydrolysis of these compounds was explored under nucleophilic β-lactam ring opening experiments. All of the β-lactams are hydrolysed rapidly under basic conditions, and monofluoro-cyclopropane **193** shows fluoride elimination over the course of 24 hours, after addition of a base (sodium methoxide or sodium benzyloxide). The resulting ring-opened defluorinated product was isolated and characterised.

The log *P* of β-lactams **144**, **181** – **183**, **190**, and **193** was measured by reverse phase HPLC, with the values lying in an acceptable range between log *P* = 2.61 and 2.96. β-Lactams **144**, **181 – 183**, and **193** were screened for intrinsic clearance and toxicology, in assays conducted at the Dundee Drug Discovery Unit. It was found that the β-lactams were either chemically unstable or had high clearance rates. β-Lactam **193**, the most active antibiotic, was found to be toxic against the human hepatic cell line HepG2, halting the progression of this compound as a pharmaceutical drug.

2.4 – References

1 M. Moore and J. B. Frerichs, *J. Invest. Dermatol.*, 1953, **20**, 133–169.

2 F. Ripoll, S. Pasek, C. Schenowitz, C. Dossat, V. Barbe, M. Rottman, E. Macheras, B. Heym, J.-L. Herrmann, M. Daffé, R. Brosch, J.-L. Risler and J.-L. Gaillard, *PLOS ONE*, 2009, **4**, e5660.

3 R. Nessar, E. Cambau, J. M. Reyrat, A. Murray and B. Gicquel, *J. Antimicrob. Chemother.*, 2012, **67**, 810–818.

4 K. Ryan and T. F. Byrd, *Front. Microbiol.*, 2018, **9**, 2642.

5 M.-R. Lee, W.-H. Sheng, C.-C. Hung, C.-J. Yu, L.-N. Lee and P.-R. Hsueh, *Emerg. Infect. Dis.*, 2015, **21**, 1638–1646.

6 M. D. Johansen, J.-L. Herrmann and L. Kremer, *Nat. Rev. Microbiol.*, 2020, **18**, 392–407.

7 E. A. Misch, C. Saddler and J. M. Davis, *Curr. Infect. Dis. Rep.*, 2018, **20**, 6.

8 C. R. Esther, D. A. Esserman, P. Gilligan, A. Kerr and P. G. Noone, *J. Cyst. Fibros.*, 2010, **9**, 117–123.

9 D. E. Griffith, W. M. Girard and R. J. Wallace, *Am. Rev. Respir. Dis.*, 1993, **147**, 1271–1278.

10 I. Sermet-Gaudelus, M. Le Bourgeois, C. Pierre-Audigier, C. Offredo, D. Guillemot, S. Halley, C. Akoua-Koffi, V. Vincent, V. Sivadon-Tardy, A. Ferroni, P. Berche, P. Scheinmann, G. Lenoir and J.-L. Gaillard, *Emerg. Infect. Dis.*, 2003, **9**, 1587–1591.

11 D. K. Radhakrishnan, Y. Yau, M. Corey, S. Richardson, P. Chedore, F. Jamieson and S. D. Dell, *Pediatr. Pulmonol.*, 2009, **44**, 1100–1106.

12 I. K. Park and K. N. Olivier, *Semin. Respir. Crit. Care Med.*, 2015, **36**, 217–224.

13 E. Abraham, *Am. J. Respir. Crit. Care Med.*, 2007, **175**, 744b–7745.

14 S. M. Chernenko, A. Humar, M. Hutcheon, C.-W. Chow, C. Chaparro, S. Keshavjee and L. G. Singer, *J. Heart Lung Transplant.*, 2006, **25**, 1447–1455.

15 C. *Via*na-Niero, K. V. B. Lima, M. L. Lopes, M. C. da S. Rabello, L. R. Marsola, V. C. R. Brilhante, A. M. Durham and S. C. Leão, *J. Clin. Microbiol.*, 2008, **46**, 850–855.

16 S.-J. Koh, T. Song, Y. A. Kang, J. W. Choi, K. J. Chang, C. S. Chu, J. G. Jeong, J.-Y. Lee, M.-K. Song, H.-Y. Sung, Y. H. Kang and J.-J. Yim, *Clin. Microbiol. Infect.*, 2010, **16**, 895–901.

17 S. C. Leao, E. Tortoli, C. *Via*na-Niero, S. Y. M. Ueki, K. V. B. Lima, M. L. Lopes, J. Yubero, M. C. Menendez and M. J. Garcia, *J. Clin. Microbiol.*, 2009, **47**, 2691–2698.

18 R. R. Falsey, M. H. Kinzer, S. Hurst, A. Kalus, P. S. Pottinger, J. S. Duchin, J. Zhang, J. Noble-Wang and M. M. Shinohara, *Clin. Infect. Dis.*, 2013, **57**, e143–e147.

19 A.-L. Roux, E. Catherinot, F. Ripoll, N. Soismier, E. Macheras, S. Ravilly, G. Bellis, M.-A. Vibet, E. L. Roux, L. Lemonnier, C. Gutierrez, V. Vincent, B. Fauroux, M. Rottman, D. Guillemot, J.-L. Gaillard and J.-L. H. for the O. Group, *J. Clin. Microbiol.*, 2009, **47**, 4124–4128.

20 E. Tortoli, T. A. Kohl, B. A. Brown-Elliott, A. Trovato, S. C. Leão, M. J. Garcia, S. Vasireddy, C. Y. Turenne, D. E. Griffith, J. V. Philley, R. Baldan, S. Campana, L. Cariani, C. Colombo, G. Taccetti, A. Teri, S. Niemann, R. J. Wallace Jr. and D. M. Cirillo, *Int. J. Syst. Evol. Microbiol.*, 2016, **66**, 4471–4479.

21 T. Adékambi, P. Berger, D. Raoult and M. Drancourt, *Int. J. Syst. Evol. Microbiol.*, 2006, **56**, 133–143.

22 E. Macheras, A.-L. Roux, F. Ripoll, V. Sivadon-Tardy, C. Gutierrez, J.-L. Gaillard and B. Heym, *J. Clin. Microbiol.*, 2009, **47**, 2596–2600.

23 H.-Y. Kim, B. J. Kim, Y. Kook, Y.-J. Yun, J. H. Shin, B.-J. Kim and Y.-H. Kook, *Microbiol. Immunol.*, 2010, **54**, 347–353.

24 N. Kwak, M. P. Dalcolmo, C. L. Daley, G. Eather, R. Gayoso, N. Hasegawa, B. W. Jhun, W.-J. Koh, H. Namkoong, J. Park, R. Thomson, J. van Ingen, S. M. H. Zweijpfenning and J.-J. Yim, *Eur. Respir. J.*

25 R. C. Lopeman, J. Harrison, M. Desai and J. A. G. Cox, *Microorg.*, 2019, **7**, 90.

26 M. Sanguinetti, F. Ardito, E. Fiscarelli, M. L. Sorda, P. D'Argenio, G. Ricciotti and G. Fadda, *J. Clin. Microbiol.*, 2001, **39**, 816–819.

27 J. Trias, V. Jarlier and R. Benz, *Science*, 1992, **258**, 1479–1481.

28 G. E. Louw, R. M. Warren, G. van Pittius, C. R. E. McEvoy, P. D. V. Helden and T. C. Victor, *Antimicrob. Agents. Chemother.*, 2009, **53**, 3181–3189.

29 E. D. Rossi, J. A. Aínsa and G. Riccardi, *FEMS Microbiol. Rev.*, 2006, **30**, 36–52.

30 I. Guillemin, V. Jarlier and E. Cambau, *Antimicrob. Agents. Chemother.*, 1998, **42**, 2084–2088.

31 S. Luthra, A. Rominski and P. Sander, *Front. Microbiol.*, 2018, **9**, DOI:10.3389/fmicb.2018.02179.

32 D. Soroka, V. Dubée, O. Soulier-Escrihuela, G. Cuinet, J.-E. Hugonnet, L. Gutmann, J.-L. Mainardi and M. Arthur, *J. Antimicrob. Chemother.*, 2014, **69**, 691–696.

33 R. Fernandes, P. Amador and C. Prudêncio, *Rev. Res. Med. Microbiol.*, 2013, **24**, 7.

34 A. Ramírez, M. Ruggiero, C. Aranaga, A. Cataldi, G. Gutkind, J. H. de Waard, M. Araque and P. Power, *Microb. Drug Resist.*, 2017, **23**, 294–300.

35 M. Lavollay, V. Dubée, B. Heym, J.-L. Herrmann, J.-L. Gaillard, L. Gutmann, M. Arthur and J.-L. Mainardi, *Clin. Microbiol. Infect.*, 2014, **20**, O297–O300.

36 A.-L. Lefebvre, V. Dubée, M. Cortes, D. Dorchêne, M. Arthur and J.-L. Mainardi, *J. Antimicrob. Chemother.*, 2016, **71**, 1556–1563.

37 A. Rominski, P. Selchow, K. Becker, J. K. Brülle, M. Dal Molin and P. Sander, *J. Antimicrob. Chemother.*, 2017, **72**, 2191–2200.

38 M.-L. Wu, D. B. Aziz, V. Dartois and T. Dick, *Drug Discov. Today*, 2018, **23**, 1502–1519.

39 V. Dubée, A. Bernut, M. Cortes, T. Lesne, D. Dorchene, A.-L. Lefebvre, J.-E. Hugonnet, L. Gutmann, J.-L. Mainardi, J.-L. Herrmann, J.-L. Gaillard, L. Kremer and M. Arthur, *J. Antimicrob. Chemother.*, 2015, **70**, 1051–1058.

40 D. Y. Wang, M. I. Abboud, M. S. Markoulides, J. Brem and C. J. Schofield, *Future Med. Chem.*, 2016, **8**, 1063–1084.

41 N. P. Krishnan, N. Q. Nguyen, K. M. Papp-Wallace, R. A. Bonomo and F. van den Akker, *PLOS ONE*, 2015, **10**, e0136813.

42 D. E. Ehmann, H. Jahić, P. L. Ross, R.-F. Gu, J. Hu, G. Kern, G. K. Walkup and S. L. Fisher, *Proc. Natl. Acad. Sci.*, 2012, **109**, 11663–11668.

43 T. Stachyra, M.-C. Péchereau, J.-M. Bruneau, M. Claudon, J.-M. Frère, C. Miossec, K. Coleman and M. T. Black, *Antimicrob. Agents. Chemother.*, 2010, **54**, 5132–5138.

44 M. S. Hanes, K. M. Jude, J. M. Berger, R. A. Bonomo and T. M. Handel, *Biochem.*, 2009, **48**, 9185–9193.

45 T. A. Blizzard, H. Chen, S. Kim, J. Wu, R. Bodner, C. Gude, J. Imbriglio, K. Young, Y.-W. Park, A. Ogawa, S. Raghoobar, N. Hairston, R. E. Painter, D. Wisniewski, G. Scapin, P. Fitzgerald, N. Sharma, J. Lu, S. Ha, J. Hermes and M. L. Hammond, *Bioorg. Med. Chem. Lett.*, 2014, **24**, 780–785.

46 E. Le Run, H. Atze, M. Arthur and J.-L. Mainardi, *J. Antimicrob. Chemother.*, 2020, **75**, 379–383.

47 A. Kaushik, N. C. Ammerman, J. Lee, O. Martins, B. N. Kreiswirth, G. Lamichhane, N. M. Parrish and E. L. Nuermberger, *Antimicrob. Agents. Chemother.*, 2019, **63**, DOI:10.1128/AAC.02623-18.

48 B. A. Brown-Elliott, J. Killingley, S. Vasireddy, L. Bridge and R. J. Wallace, *J. Clin. Microbiol.*, 2016, **54**, 1586–1592.

49 R. C. Lopeman, J. Harrison, D. L. Rathbone, M. Desai, P. A. Lambert and J. A. G. Cox, *Sci. Rep.*, 2020, **10**, 928.

50 O. of the Commissioner, FDA approves new treatment for complicated urinary tract and complicated intra-abdominal infections, https://www.fda.gov/news-events/press-announcements/fda-approves-new-treatment-complicated-urinary-tract-and-complicated-intra-abdominal-infections, (accessed 23 September 2020).

51 A. Bricheux, L. Lenggenhager, S. Hughes, A. Karmime, P. Lescuyer and A. Huttner, *Clin. Microbiol. Infect.*, 2019, **25**, 383.e1-383.e4.

52 S. E. Schliamser, K.-A. Broholm, A.-L. Liljedahl and S. R. Norrby, *J. Antimicrob. Chemother.*, 1988, **22**, 687–695.

53 R. Pandey, L. Chen, C. Manca, S. Jenkins, L. Glaser, C. Vinnard, G. Stone, J. Lee, B. Mathema, E. L. Nuermberger, R. A. Bonomo and B. N. Kreiswirth, *mBio*, 2019, **10**, DOI:10.1128/mBio.02895-18.

54 C. J. Thomson, Q. Zhang, N. Al-Maharik, M. Bühl, D. B. Cordes, A. M. Z. Slawin and D. O'Hagan, *Chem. Commun.*, 2018, **54**, 8415–8418.

55 S. J. Harris, A. M. Kinahan, M. J. Meegan and R. C. Prendergast, *J. Chem. Res., Miniprint*, 1994, **9**, 1832–1845.

56 K.-C. Lin, *J. Chem. Educ.*, 1988, **65**, 857.

57 D. R. McKean, G. Parrinello, A. F. Renaldo and J. K. Stille, *J. Org. Chem.*, 1987, **52**, 422–424.

58 S. Hruschka, T. C. Rosen, S. Yoshida, K. L. Kirk, R. Fröhlich, B. Wibbeling and G. Haufe, *Bioorg. Med. Chem. Lett.*, 2008, **16**, 7148–7166.

59 G. K. S. Prakash, R. Krishnamurti and G. A. Olah, *J. Am. Chem. Soc.*, 1989, **111**, 393–395.

60 T. Hanamoto and T. Kobayashi, *J. Org. Chem.*, 2003, **68**, 6354–6359.

61 H. E. Simmons and R. D. Smith, *J. Am. Chem. Soc.*, 1958, **80**, 5323-5324

62 L.G.Menchikov, E.V.Shulishov and Yu.V.Tomilov *Russ. Chem. Rev.*, 2021, **90** 199-230

63 G. Kingsley-Moore, Masters Thesis, University of St. Andrews, 2023.

64 M. Gerken, J. A. Boatz, A. Kornath, R. Haiges, S. Schneider, T. Schroer and K. O. Christe, *J. Fluoro. Chem.*, 2002, **116**, 49–58.

65 W. Chen, X. Xie, J. Zhang, J. Qu, C. Luo, Y. Lai, F. Jiang, H. Yu and Y. Wei, *Green Chem.*, 2021, **23**, 9140–9146.

66 Y. Sun, J. A. Kaplan, A. Shieh, H.-L. Sun, C. M. Croce, M. W. Grinstaff and J. R. Parquette, *Chem. Commun.*, 2016, **52**, 5254–5257.

67 A. De Kock and D. A. Lord, *Chemosphere*, 1987, **16**, 133–142.

68 C. A. Lipinski, *Drug Discov. Today Technol.*, 2004, **1**, 337–341.

69 M. T. Donato, L. Tolosa and M. J. Gómez-Lechón, *Methods Mol. Biol.*, 2015, **1250**, 77–93.

70 J. Brian Houston, *Biochem. Pharm.*, 1994, **47**, 1469–1479.

71 V. A. Arzumanian, O. I. Kiseleva and E. V. Poverennaya, *Int. J. Mol. Sci.*, 2021, **22**, 13135.

Chapter 3

Interaction of Janus cyclohexanes with DNA

3.1 – Introduction

3.1.1 – Förster Resonance Energy Transfer (FRET)

Förster resonance energy transfer (FRET) is a phenomenon in which an excited state donor fluorophore transfers energy to an acceptor molecule *via* dipole-dipole coupling, in turn exciting the acceptor molecule.[1] This leads to an enhanced acceptor emission whilst simultaneously decreasing, or quenching, the donor fluorescence. This quenching can only occur when the donor and acceptor are in close proximity, and if the emission region of the donor overlaps with the absorption region of the acceptor. The distance required for FRET to occur is related to Equation 3.1.[1]

$$E_{FRET} = \frac{1}{1 + (r/R_0)^6} \qquad 3.1$$

E_{FRET} is the FRET efficiency (the proficiency of FRET quenching), and is defined as the proportion of the donor molecules that have transferred excitation state energy to the acceptor molecules.[2] r is the distance between the donor and acceptor and R_0 is the Förster distance, at which 50% of the donor energy has been transferred to the acceptor. R_0 is dependent on the pair of fluorophores used and the distance range to be measured, but is generally between 10 and 70 Å; a suitable distance for most structural and molecular interactions. Figure 3.1 illustrates an example E_{FRET} versus fluorophore distance curve as defined by Equation 3.1.[3]

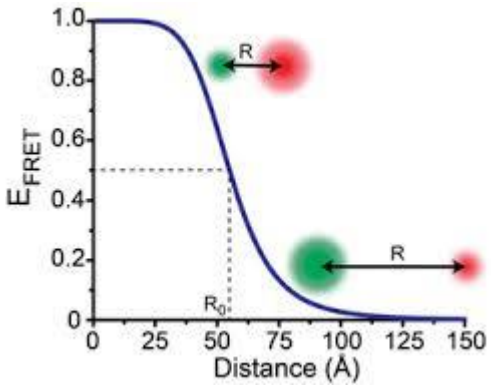

Figure 3.1: Example of a E_{FRET} versus distance (r) graph, where the green and red dots represent the donor and accepter fluorophores. Reprinted with permission from Springer Nature.[3] *Copyright © 2008, Springer Nature America, Inc.*

In a typical donor quenching experiment by FRET the donor fluorophore is excited by light at the absorption band, and both donor and acceptor emission are observed. When there is a reduction in the donor emission and a simultaneous increase in acceptor emission then FRET

from the donor to the acceptor has taken place, and it can be concluded that the donor and acceptor have come into close proximity. In an ideal FRET experiment, there will be little to no overlap between the wavelength used to excite the donor and the excitation wavelength of the acceptor, as this overlap will lead to direct excitation of the acceptor. Figure 3.2 shows the excitation (λ_{exc}) and emission (λ_{emm}) wavelengths for a cyanine 3 dye (Cy3, donor) and a cyanine 5 dye (Cy5, acceptor), the overlap integral (the spectral overlap between absorption of the donor and emission of the acceptor), and a decrease in donor and the concomitant increase in acceptor as a result of energy transfer.[4]

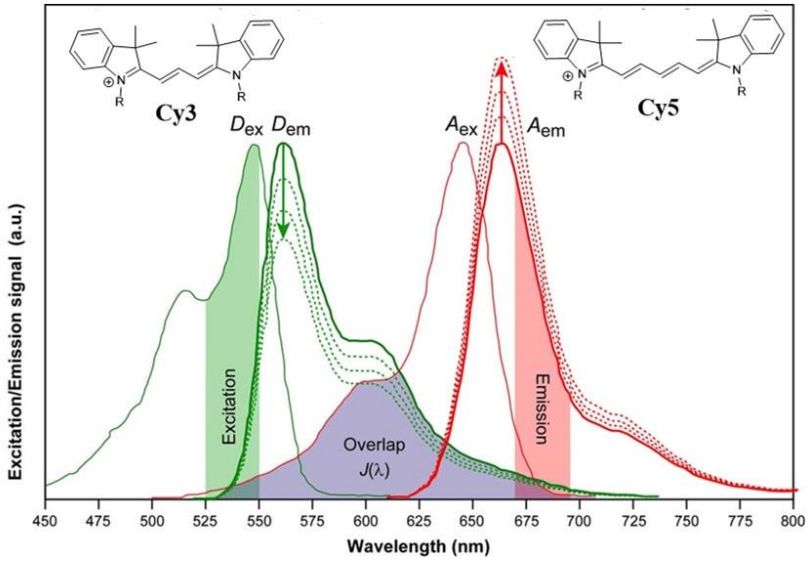

Figure 3.2: UV-Vis spectra of the excitation and emission ranges of both Cy3 (donor) and Cy5 (acceptor). Reprinted with permission from MDPI (Basel, Switzerland).[4] *Copyright © 2012 by the authors.*

E_{FRET} is a value used to measure the degree of energy transfer from donor to acceptor in an experiment. An approximation for this value is represented in Equation 3.2.[5]

$$E_{FRET} = 1 - \frac{I_D A}{I_D} \qquad 3.2$$

Where I_DA is the intensity of the donor in the presence of an acceptor and I_D is the intensity of a donor without an acceptor. If no FRET occurs then $I_DA = I_D$ and $E_{FRET} = 0$, whereas if the donor transfers its energy completely to the acceptor, then $I_DA = 0$ and $E_{FRET} = 1$. This approximation, however, assumes the difference between $I_DA = I_D$ is solely caused by FRET and does not consider variation in the expression level of the donor, self-quenching, or photobleaching.

FRET can be used to determine affinity between biomolecules in solution. As an illustrative example, Murade *et. al*.[6] demonstrated the use of FRET for studying electrostatic interactions between DNA and positively charged ligands (Figure 3.3).

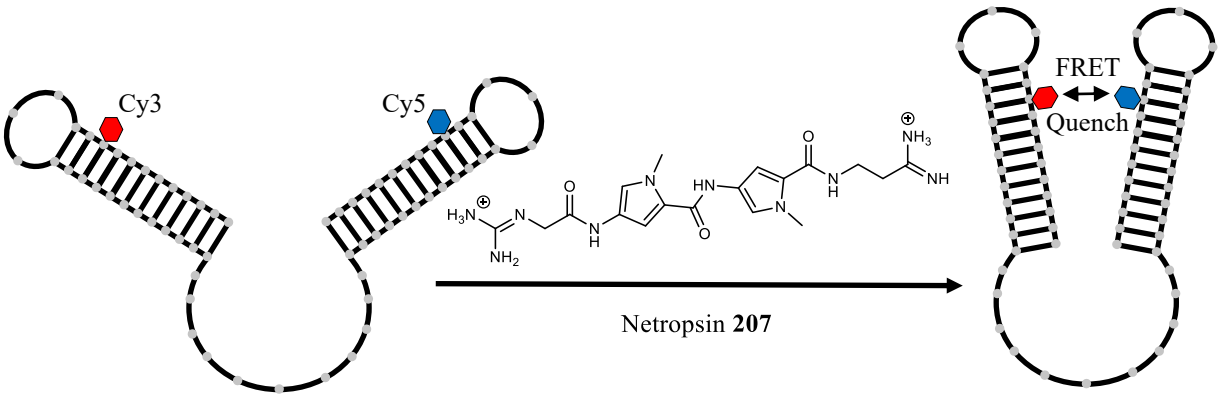

Figure 3.3: Introduction of the intercalating antibiotic netropsin **207** causes arms of hybridized nucleotide to come together (due to neutralisation of negatively charged phosphate backbone) allowing FRET quenching between Cy3 and Cy5 probes.[6]

A single DNA oligonucleotide strand which folds into a "tong" shape with two rigid double stranded arms (12 base-pairs) was equipped with a Cy3 probe on one arm, and a Cy5 on the other. When in buffer the single-strand connector results in the two arms being removed from one another, due to the repulsion created by the negatively charged phosphate backbone (see Chapter 1.5 for DNA-ligand binding). When the intercalating antibiotic netropsin **207** is introduced to the solution, the drug binds to the DNA arms and partially neutralizes this negative charge. This decreases the effective repulsion between the arms and allows the fluorophores to come closer, allowing for donor quenching by FRET to happen. The extent of FRET taking place is therefore proportional to the amount of the netropsin **207** bound to the DNA.

3.1.2 – Isothermal Titration Calorimetry (ITC)

Isothermal titration calorimetry (ITC) is a biophysical technique used to measure the thermodynamics of the formation and dissociation of molecular complexes.[7] This is achieved through the measurement of temperature changes created by binding events, allowing for the determination of the corresponding Gibbs energy, enthalpy, entropy, and heat capacity changes.[8] These values can in turn determine not only if a binding event has occurred, but also the strength of binding, and can help determine the method of binding between a ligand and a macromolecule. Fundamentally, an ITC instrument is a heat-flux calorimeter that measures the amount of energy required to maintain a constant temperature difference between a sample cell (a complexation between a ligand and macromolecule) and a reference cell (containing only the medium of a sample cell).[8] A schematic illustrating the ICT instrument is shown in Figure 3.4**.**

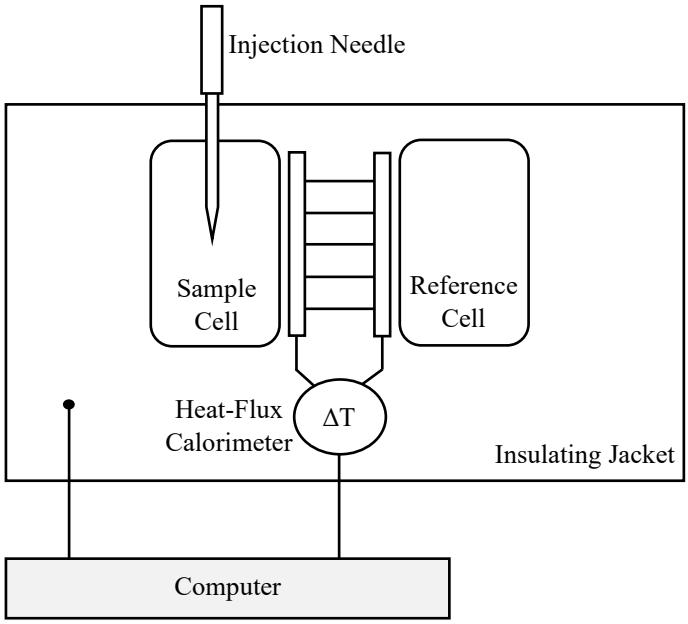

Figure 3.4: Schematic of an ITC machine.[8]

A baseline level is first established by applying continuous power to the sample cell. The ligand solution is then injected into the sample cell (already containing a macromolecule in solution) which causes complexation. This in turn releases or absorbs heat (depending on if complexation is exothermic or endothermic) and causes a temperature change between the sample and the reference cell. The feedback system then compensates for the imbalance by raising or lowering the temperature to reach baseline equilibrium. This process is repeated multiple times. Each injection produces a recorded signal in the form of a peak, which when the area under the peak is integrated, reveals the total heat change associated with the injection. With each injection, the change in heat diminishes due to ligand saturation of the macromolecule, in turn producing a titration curve from which thermodynamic parameters of the complexation can be deduced (binding affinity, binding enthalpy, and ligand-macromolecule stoichiometry).[8]

3.1.3 – Single-Molecule FRET (smFRET)

Single-molecule FRET (smFRET) is a microscopy method used to study the conformational dynamics and interactions of individual biomolecules. smFRET is an application of FRET where the energy transfer mechanism is observed and measured on a single molecule basis.[9] The technique is sensitive enough to detect the change in distance of biomolecules probed with fluorophores (a 1 – 10 nm range). This sensitivity allows smFRET to be used as a "spectroscopic ruler", where the distance between fluorophore probed biomolecules can be calculated based on FRET efficiency (see Equation 3.2).[10] smFRET has shown utility in the investigation of protein interactions with DNA.[11–13] A study carried out by Coats *et. al.* demonstrated how smFRET can be used to observe the binding and dissociation of the yeast protein yNhp6A to 18 base-pair DNA (Figure 3.5).[14]

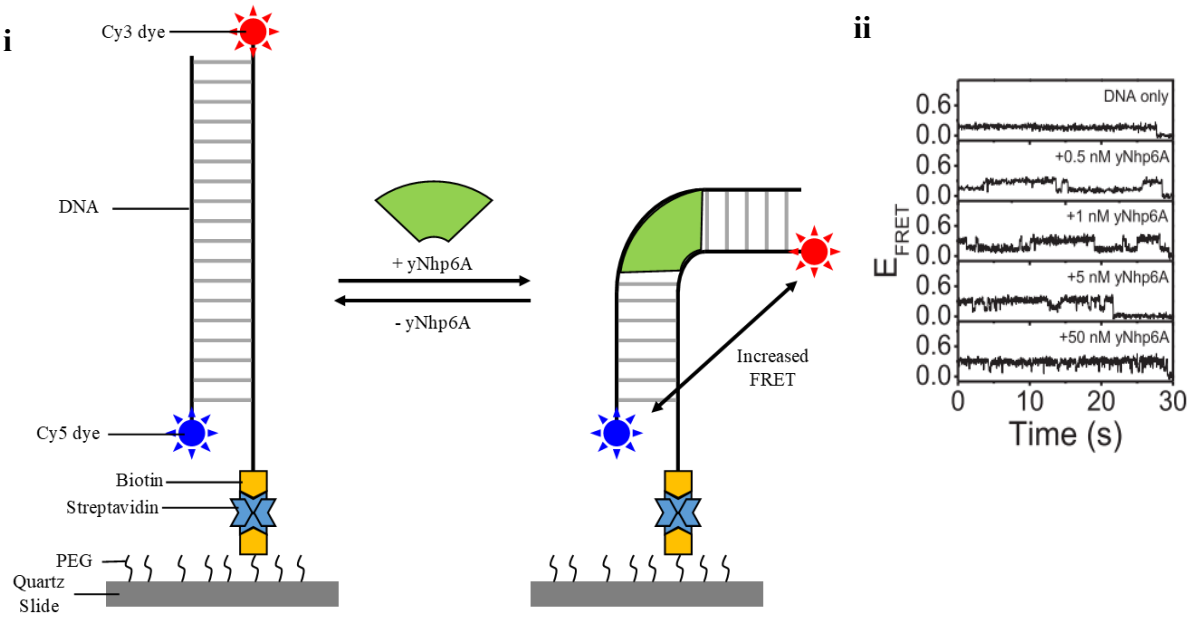

Figure 3.5: i) Schematic design of smFRET experiment **ii)** Corresponding FRET efficiency time traces showing ranging from DNA only to +50 mM yNhp6A. Reprinted with permission from Oxford University Press.[14] *Copyright © 2012, © The Author(s) 2012. Published by Oxford University Press.*

Figure 3.5.i illustrates the addition of protein yNhp6A to the dsDNA, which causes a kink to form in the DNA, in turn bringing the Cy5 and Cy3 dyes closer. This results in an increased FRET interaction between the fluorophore pair, which is shown in the corresponding FRET efficiency time traces (Figure 3.5.i). The time traces show FRET efficiency over the course of 30 seconds, which show the transition between the low ($E_{FRET} = 0.17$) and high ($E_{FRET} = 0.30$) FRET states in the presence of yNhp6A. As the concentration of yNhp6A increases, so does the duration of the high FRET state, suggesting that at higher concentrations of yNhp6A the DNA takes on a kinked form for a longer duration.

Figure 3.6 gives a generalised schematic of a prism-type total internal reflection fluorescence microscope set-up used for smFRET.[15]

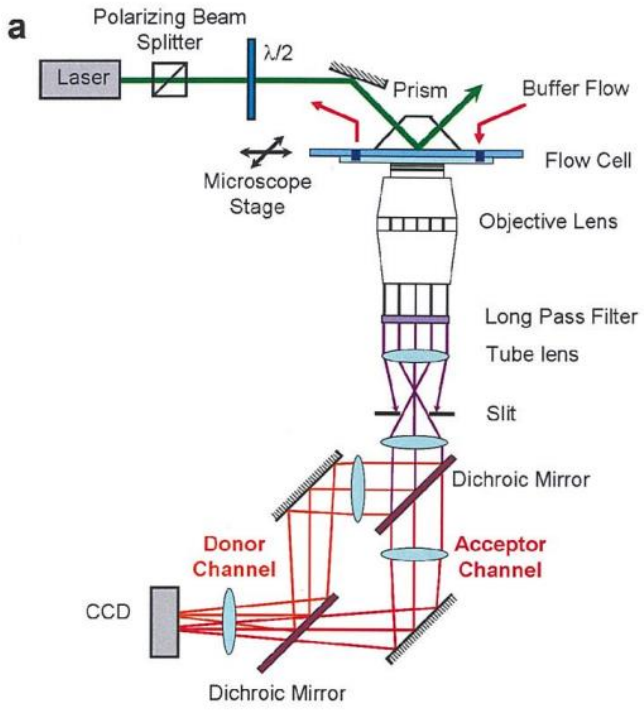

Figure 3.6: Schematic of a prism-type total internal reflection fluorescence microscope set-up. Reprinted with permission from the University of St Andrews Library.[15] *Copyright © 2014, © University of St Andrews Library.*

The outline of the home-built microscope used to collect FRET information at the level of single molecules is shown in Figure 3.6. In brief, the 532 nm laser beam is modulated by a polarizing beam splitter to decrease or increase its intensity to values sufficient to visualize the molecules, but not so intense that molecules immediately photobleach. The beam travels through the prism, index-matching oil, and the quartz slides before reaching the upper interface between the quartz slide and the sample (aqueous solution). The beam is made incident to a prism at an angle of ~65°. At this angle the beam mostly gets reflected, however, a small proportion of the laser beam penetrates the sample (~100 nm into the aqueous solution). This small layer of light excites the molecules that are attached to the quartz slide without illuminating the rest of the solution. This enables a high signal-to-noise ratio that is required to detect individual molecules. The fluorescence light emitted by the excited fluorophores is collected by a high numerical aperture (the range of angles over which the microscope can absorb light) objective (1.45 NA) and directed towards an electron-multiplying charge coupled device (CCD) detector with high sensitivity to collect low levels of light. Along the path between the objective and detector a series of dichroic mirrors allow separation of the light above (Cy5 acceptor) and below (Cy3 emission) 645 nm. Each of these Cy3 and Cy5 beams is directed towards the left (Cy3) and right halves of the CCD imaging area. This allows detection of the intensities arising from Cy3 and Cy5 in the same molecule simultaneously. The images are then processed using home-made scripts written in MATLAB.[16]

3.1.4 – Aims and objectives

As described (Chapter 1.4), the Janus face cyclohexane is a highly polarised organic motif, with a "sticky" quality. Non-covalent interactions play a critical part in biochemical processes, from hydrogen bonds of protein-substrate complexes to the hydrophilic/hydrophobic interactions of cell membranes.[17] A polar motif such as the Janus face cyclohexane may be expected to form electrostatic interactions with these biomolecules. This would allow the Janus face motif to be incorporated into biomolecular probes, facilitating transport of the probe to specific biomolecules.

This chapter will detail attempts to use the methods described above to study the degree to which the Janus face motif selectively binds to a series of chosen biomolecules, most prominently, DNA. The mode of DNA binding is explored, and the differential affinity between the Janus face motif and both single strand and double strand DNA (ssDNA and dsDNA respectively) is also described. The synthesis of the various Janus face probes used in these experiments is also presented.

3.2 – Results and discussion

3.2.1 – Development of a FRET-based assay to explore Janus cyclohexane-DNA interactions in solution

An initial experiment explored if the Janus face cyclohexane motif will form non-covalent interactions with DNA. It was hypothesised that the electropositive hydrogen face of the Janus cyclohexane may form electrostatic interactions with the negatively charged phosphate backbone of DNA.

To this end, an inter-molecular FRET assay was developed to investigate the potential interaction between a Janus face acceptor-probe molecule and a DNA duplex, labelled with the Cy3 FRET donor attached to the DNA. It was assumed that if a relatively short DNA duplex (15-18 nucleotides, an end-to-end length of 5.2-6.3 nm) was used, binding of the Janus face-Cy5 molecule to the DNA-Cy3 molecule should be within distance range for efficient energy transfer, considering that the R_o for the Cy3-Cy5 pair is 5.6 nm (see Figure 3.1).[3] With DNA tagged with a terminal Cy3 dye and the Janus face coupled to a Cy5 dye, quenching of the donor due to FRET would be observed if the Janus cyclohexane was localised on the DNA. This would give an initial insight into any interaction between the Janus cyclohexane and DNA. A schematic of the proposed experiment is illustrated in Figure 3.7.

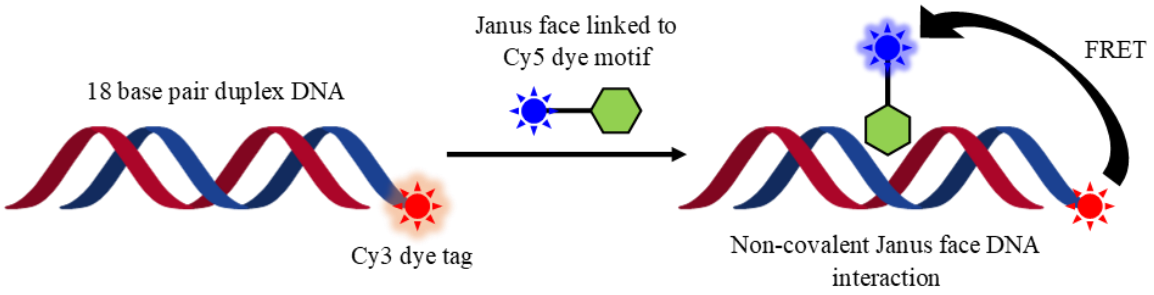

Figure 3.7: Schematic illustrating proposed solution-based FRET quenching experiment to investigate interactions between the Janus face motif and DNA.

With this initial experiment in mind, a synthetic route towards Janus-Cy5 **208** was explored. A retrosynthetic analysis of Janus-Cy5 **208** is illustrated in Scheme 3.1.

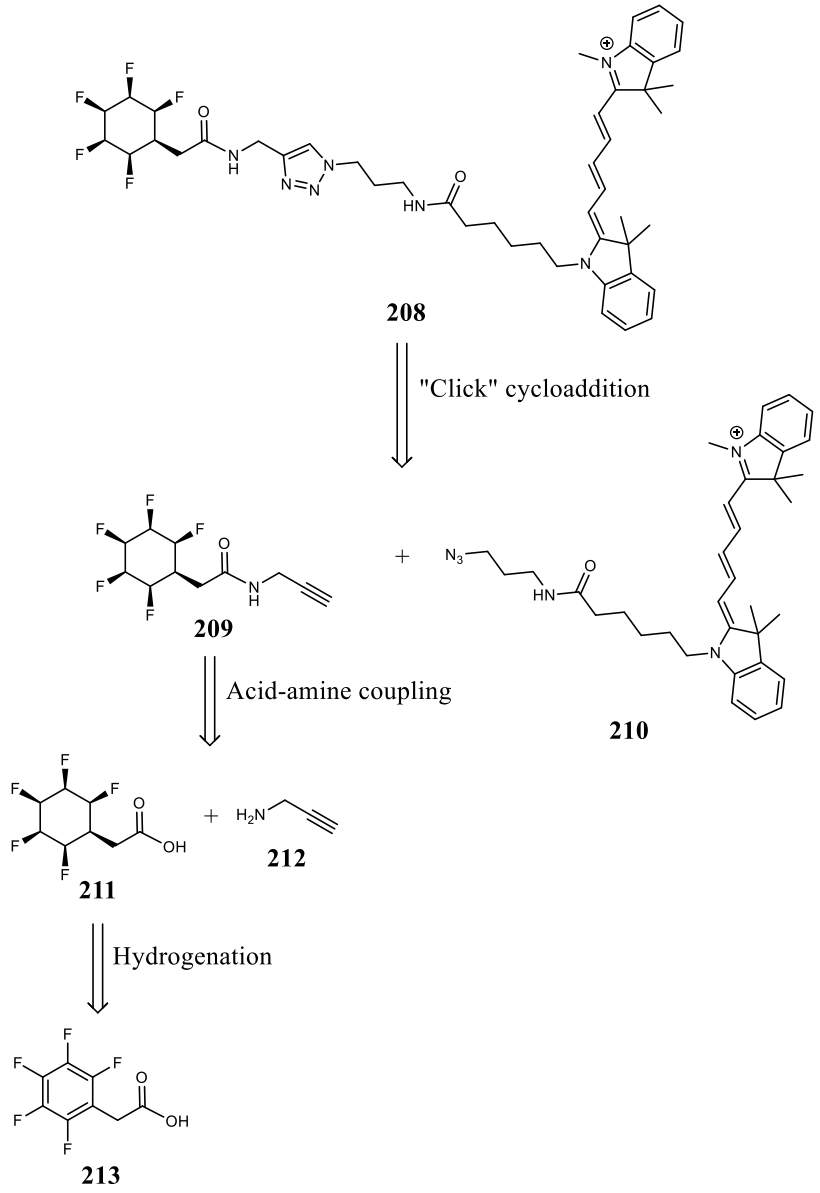

Scheme 3.1: Retrosynthetic analysis of Janus-Cy5 **208**.

Janus-Cy5 **208** could be synthesised from a click CuAAC coupling between Cy3-azide **210** and Janus face alkyne **209**. The latter would be synthesised from the coupling of propargylamine

212 to carboxylic acid **211**. Using a synthetic route previously described in the St Andrews group,[18] work began towards the synthesis of an alkyne **209** as a unit to couple to a Cy5 azide dye (Scheme 3.2).

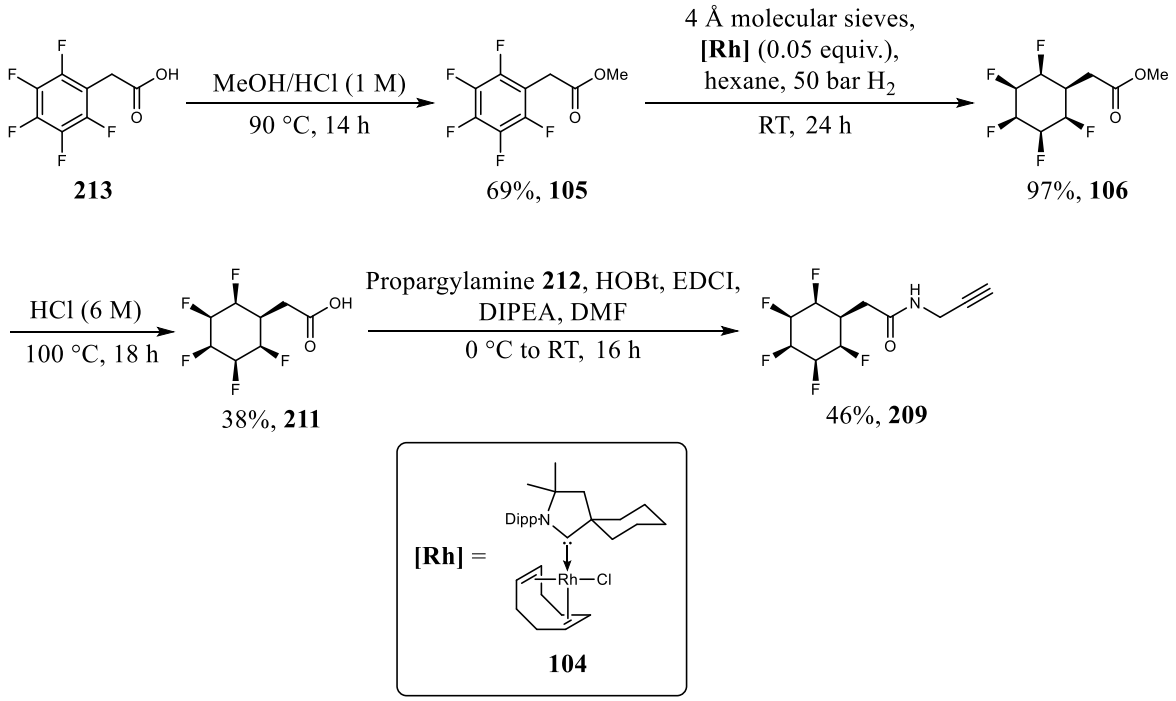

Scheme 3.2: Synthesis of Janus alkyne **209** over four steps.[18]

Commercially available perfluorinated aryl carboxylic acid **213** was esterified with acidic methanol to give perfluorinated aryl ester **105**. This was subjected to an aryl hydrogenation (50 bar H_2) using the Zeng catalyst **104** to give the all *syn* cyclohexane ester **106**. Finally, hydrolysis of ester **106** was achieved under forcing acidic conditions with 6 M hydrochloric acid to yield carboxylic acid **211**. Base hydrolysis was not used for this step to avoid any dehydrofluorination. With carboxylic acid **211** in hand, a strategy towards attaching a terminal acetylene was explored. Amide formation with propargylamine using classical coupling reagents gave Janus face alkyne **209**. Finally, the Cy5 motif, with an azide attached, underwent a successful click CuAAC reaction to generate the desired adduct (Scheme 3.3).

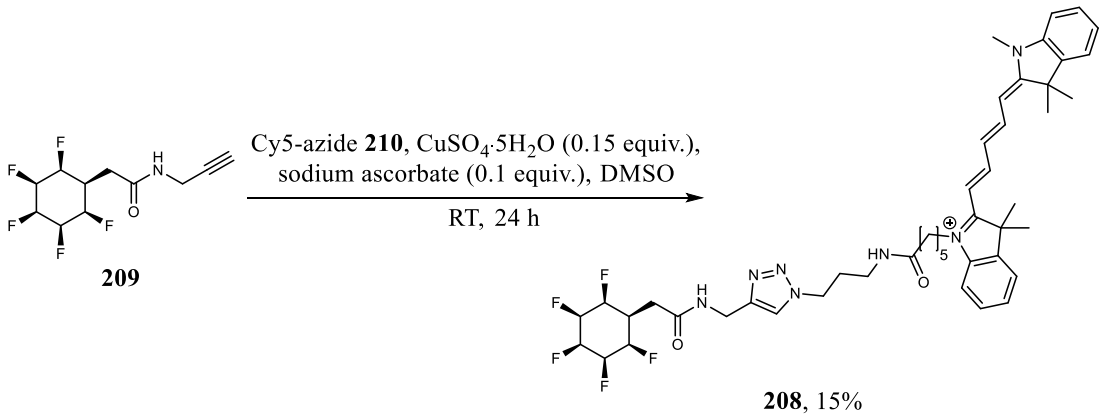

Scheme 3.3: Synthesis of Janus-Cy5 **208** *via* click cycloaddition of Cy5 azide **210** with **209**.

The required Janus-Cy5 **208** was prepared on a nanomolar scale, amounts which did not allow for characterization by NMR spectroscopy. However, the compound was securely identified by HRMS and showed a single peak by HPLC, indicating that a homogeneous product with the correct mass had been isolated. This is illustrated in Figure 3.8.

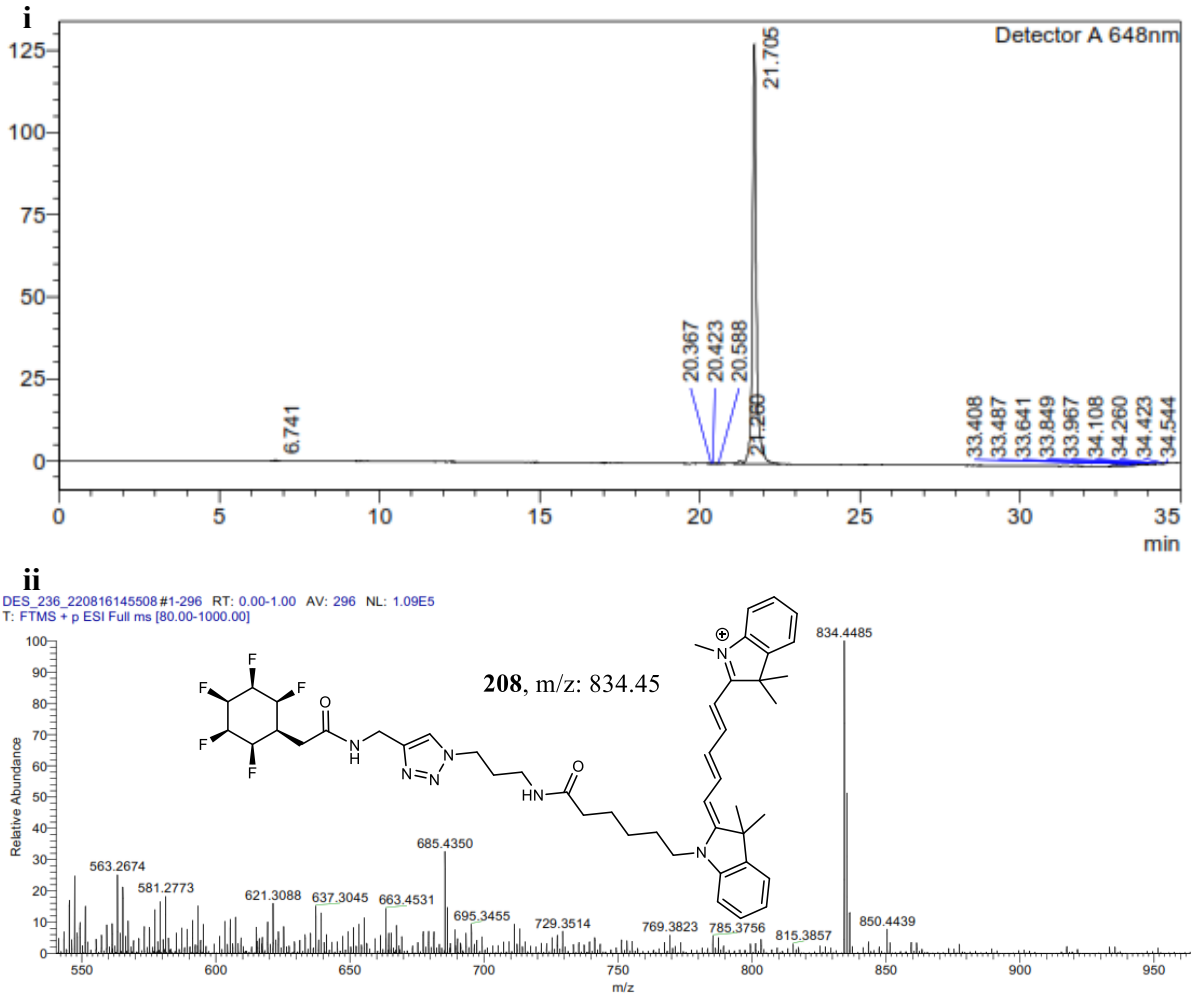

Figure 3.8: HPLC trace **(i)** and HRMS spectrum **(ii)** of Janus face-Cy5 **208**.

A control compound was also synthesized, in order to validate any interactions observed between the Janus cyclohexane probe and DNA. It was judged that a terminal acetamide-Cy5 molecule **215** would offer a suitable control, as it possessed all other functional groups except the Janus cyclohexane itself. The synthesis of the control **215** is shown in Scheme 3.4.

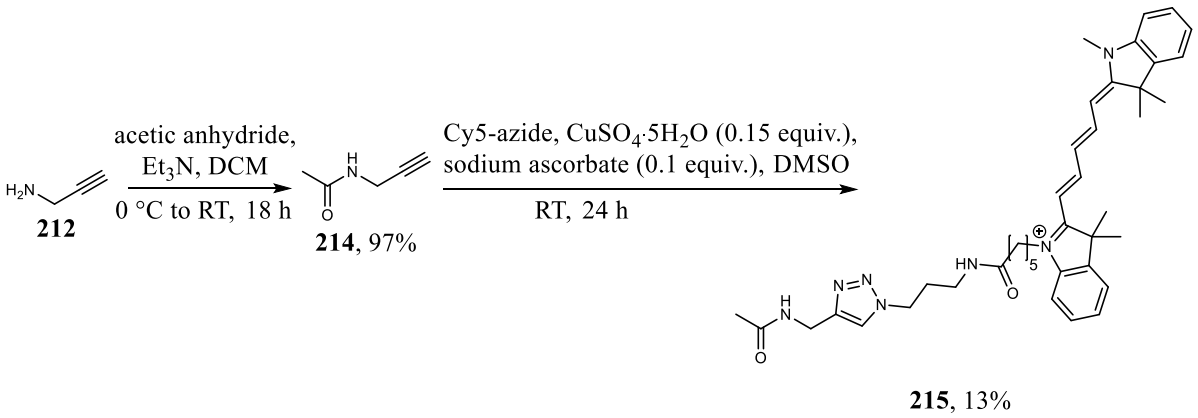

Scheme 3.4: Synthesis of acetamide-Cy5 **215** *via* click CuAAC.

The Cy3-DNA sequence was purchased from Integrated DNA Technologies (see Chapter 7.6.1) with the Cy3 dye already incorporated at one end of the duplex. With both the Janus cyclohexane-Cy5 **208**, acetamide-Cy5 control **215**, and DNA at hand, interactions between DNA and the Janus face motif were now explored by fluorescence spectroscopy.

In brief, a cuvette was filled with a 50 nM solution of 18 base pair duplex DNA carrying a terminal Cy3 motif. Using a fluorimeter (an instrument which simultaneously excites and observes fluorophores) the Cy3 motif was excited at a wavelength of 545 nm, which corresponds to the absorption maximum of the Cy3 fluorophore (λ_{Exc}^{D}). The emitted fluorescence was measured from 555 nm to 750 nm. The cuvette was then titrated with a solution containing the Cy5-Janus cyclohexane probe **208**, and the sample was excited at the same 545 nm wavelength. This process was repeated with increasing concentrations of Cy5-Janus face **208** (for a more detailed method, see Chapter 7.6). Figure 3.9 shows the fluorescence spectra for the titration experiments with both Cy5-Janus cyclohexane **208** and the control Cy5-acetamide **215**.

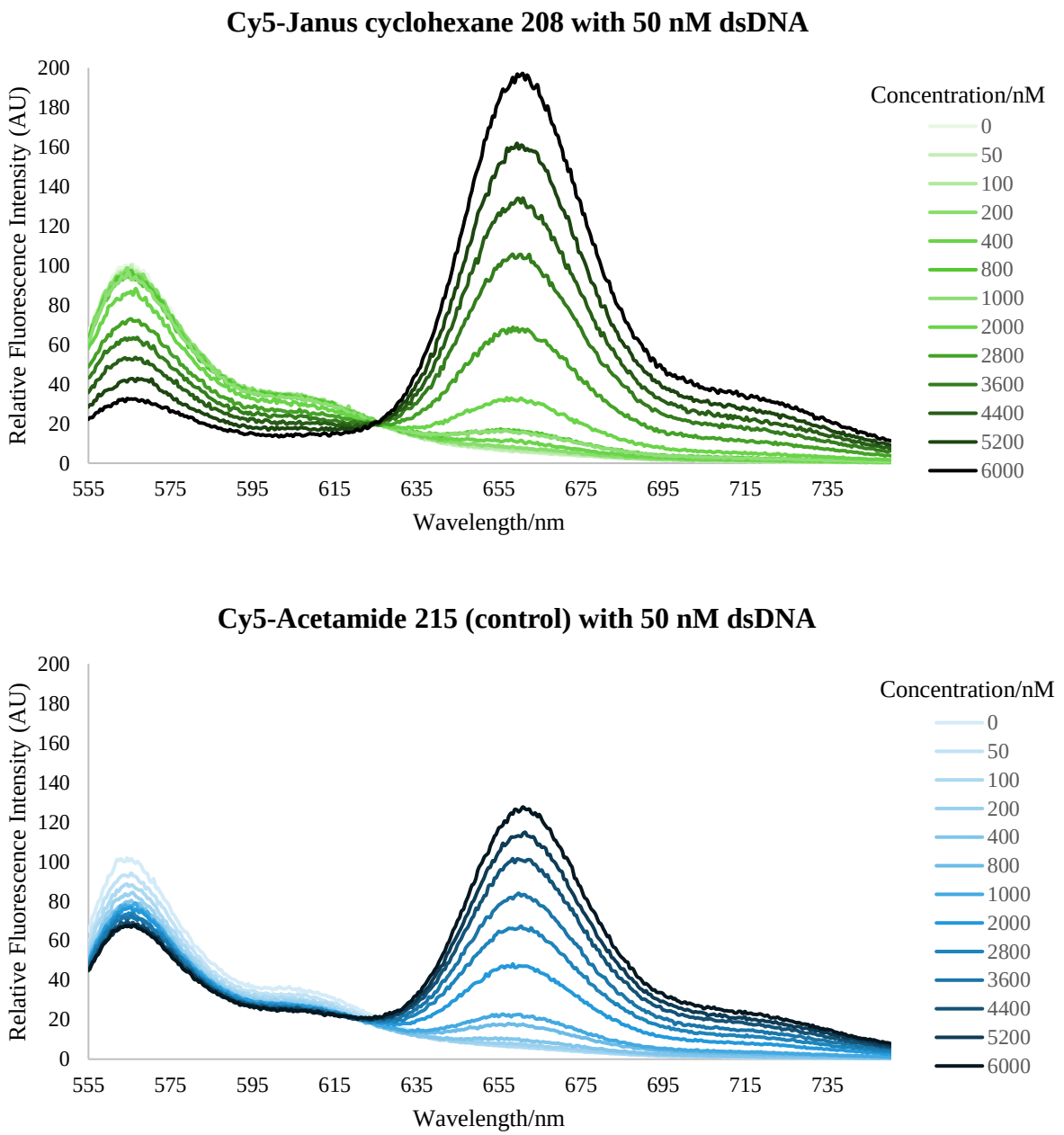

Figure 3.9: Fluorescence emission spectra recorded for the titration of an 18 bp dsDNA-Cy3 with increasing concentrations of Cy5-Janus ligand **208** (top) and Cy5-acetamide ligand **215** (bottom). Excitation wavelength 545 nm, [DNA-Cy3] = 50 nM.

The stacked fluorescence spectra of the titration with Cy5-Janus **208** with dsDNA shows a decrease in relative fluorescence intensity around 565 nm (λ_{Emm}^{D}) and an increase in relative fluorescence intensity around 665 nm (λ_{Emm}^{A}) as the concentration of **208** increases. The observed decrease in the Cy3 emission intensity is caused by donor quenching of the Cy3 tag attached to the dsDNA by the Cy5 motif of **208**. This indicates an interaction between the dsDNA and the Janus face cyclohexane. The observed increase of Cy5 acceptor intensity at 665 nm (λ_{Emm}^{A}) arises from two effects: i) potential FRET transfer from the donor Cy3 fluorophore and/or ii) direct excitation due to the absorption of Cy5 being non-zero at 545 nm. Because of both effects, only the quenching of the Cy3 donor, after correction for dilution, is used to

quantify the FRET efficiency using Equation 3.2. For the Cy5-acetamide **215** titration experiment, the decrease in fluorescence intensity around 565 nm is less, indicating a weaker capacity for FRET.

Figure 3.10 shows the concentration of Cy5-acetamide **215** and Cy5-Janus face **208** against the maximum fluorescence intensity at 564 nm (λ^{D}_{Emm}) for dsDNA (left), and the approximate E_{FRET} against ligand concentration (right).

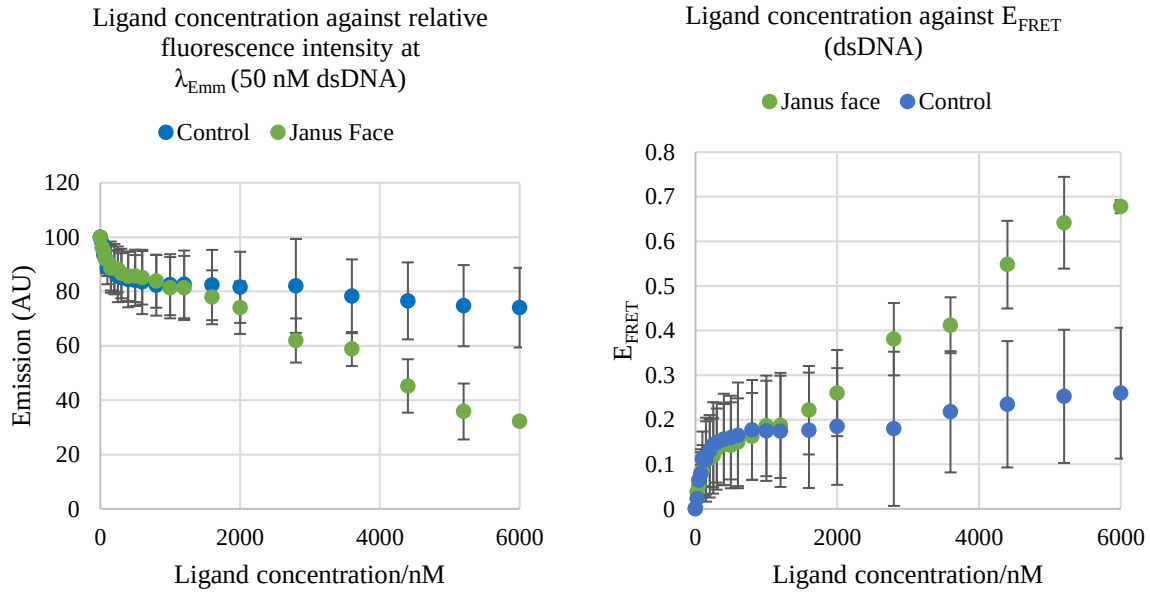

Figure 3.10: Left: Ligand concentration (Janus face **208** green, control **215** blue) against the relative fluorescence intensity at 564 nm for dsDNA. Right: Ligand concentration (Janus face **208** green, control **215** blue) against E_{FRET} for dsDNA.

Both the drop in relative fluorescence intensity with Cy5-Janus cyclohexane **208** and the approximate E_{FRET} value is greater than that of the control **215** at higher concentrations. The relative fluorescence intensity of the control titration experiment plateaus after 1000 nM, indicating a saturation of the dsDNA molecules by the Cy5-acetamide **215** ligand, whilst the fluorescence intensity from the Cy5-Janus cyclohexane **208** titration continues to decrease at higher concentrations. This is also true for approximate E_{FRET}, and only at concentrations above 2000 nM do the two experiments appear to diverge, with the Janus cyclohexane possessing a larger E_{FRET}. The relative fluorescence and E_{FRET} data suggest that Janus probe **208** has a greater affinity for dsDNA compared to control **215** at high concentrations. However, the large error range for the control indicates a degree of uncertainty in these solution-based experiments.

The same titration experiments were conducted again with single strand DNA in place of double strand DNA. Figure 3.11 shows the fluorescence spectra with the titration experiments carried out with both Cy5-Janus probe **208** and Cy5-acetamide **215** with single strand DNA.

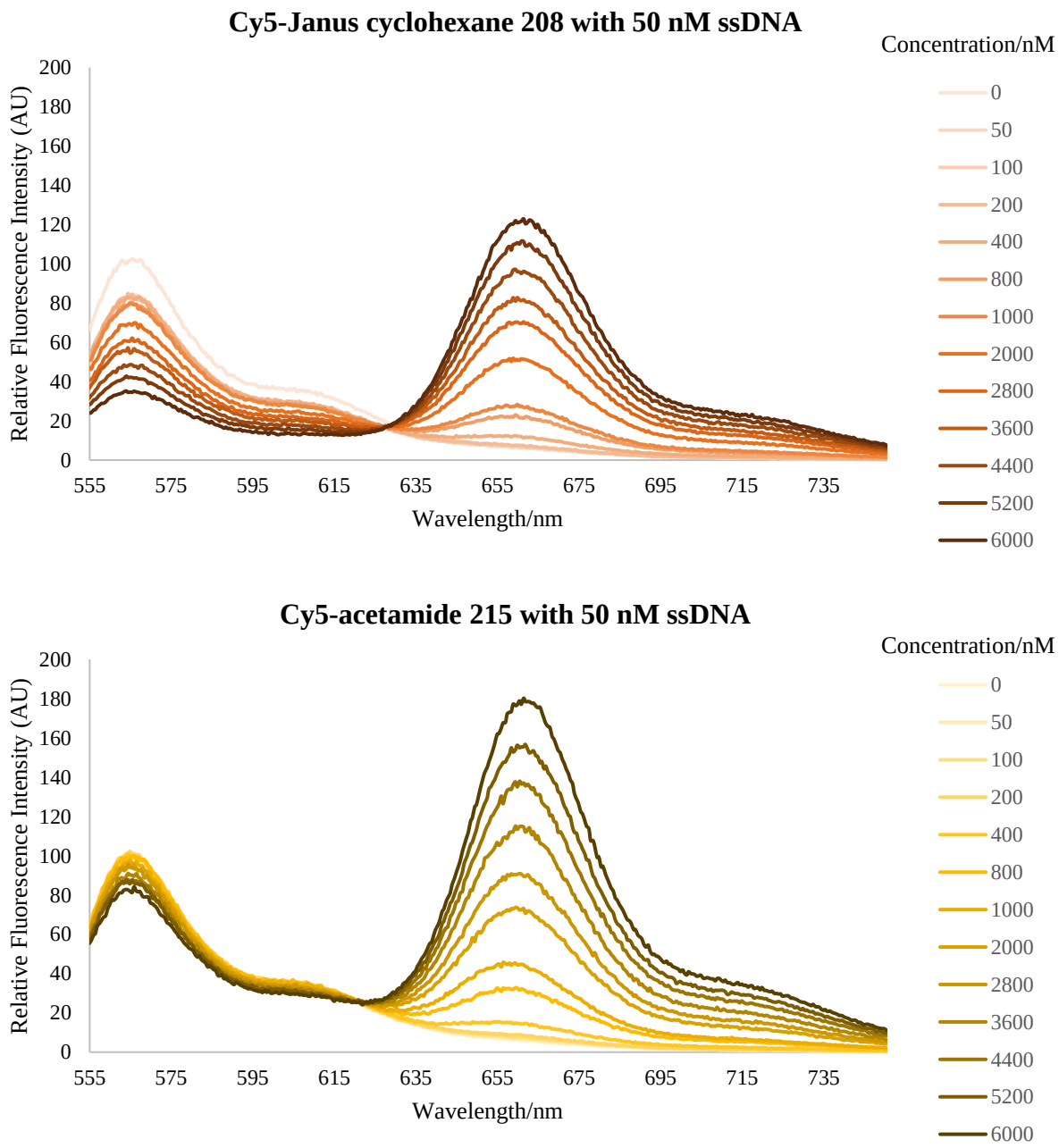

Figure 3.11: Fluorescence emission spectra recorded for the titration of an 18 bp ssDNA-Cy3 with increasing concentrations of Cy5-Janus face ligand **208** (top) and Cy5-acetamide ligand **215** (bottom). Excitation wavelength 545 nm, [DNA-Cy3] = 50 nM.

As with the titration experiment with dsDNA, the above stacked fluorescence spectra of Cy5-Janus cyclohexane **208** with ssDNA shows a decrease in relative fluorescence intensity around 565 nm (λ^{D}_{Emm}) with increased concentration of **208**. This again shows a FRET interaction between the Cy3 of the ssDNA and Cy5 of the Janus cyclohexane **215**, which indicates that the Janus motif is more localised to the ssDNA. Again, the Cy5-acetamide **215** titration with ssDNA does not show the same degree of FRET quenching, with the relative intensity around 565 nm (λ^{D}_{Emm}) staying somewhat constant. However, the relative intensity at 665 nm (λ^{A}_{Emm}) increases clearly and consistently with concentration. This is due to direct excitation of the Cy5 acceptor

by 545 nm light, due to the overlap between the Cy3 and Cy5 excitation wavelengths (see Figure 3.2).

Figure 3.12 shows the concentration of Cy5-acetamide **215** and Cy5-Janus cyclohexane **208** against the maximum fluorescence intensity at 564 nm (λ_{Emm}) and E_{FRET} for ssDNA.

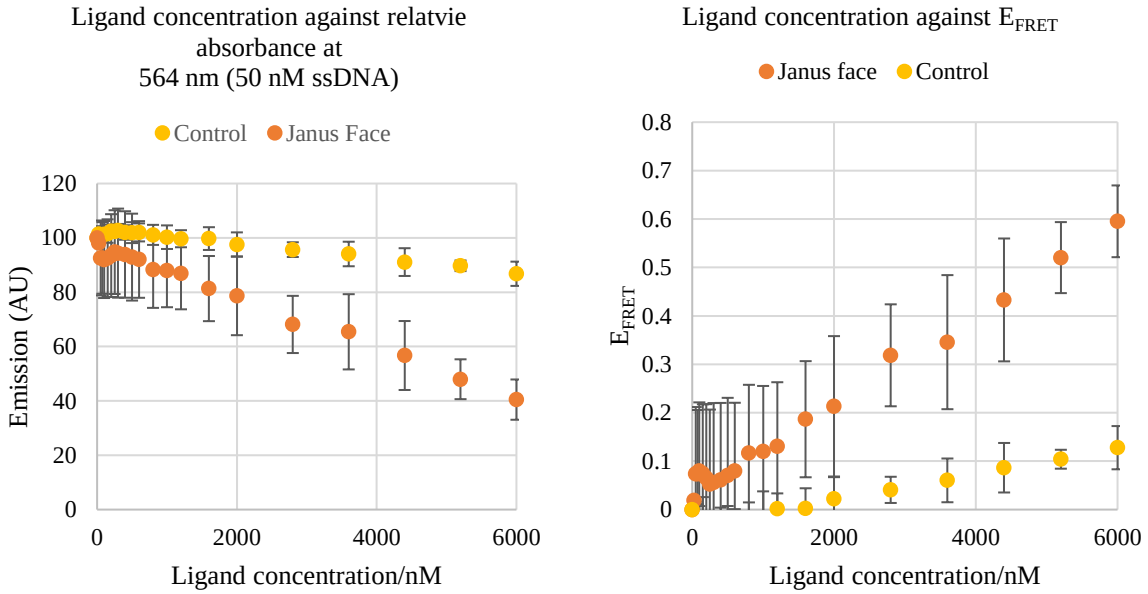

Figure 3.12: Left: Ligand concentration (Janus face **208** orange, control **215** yellow) against the relative fluorescence intensity at 564 nm for ssDNA. Right: Ligand concentration (Janus face **208** orange, control **215** yellow) against E_{FRET} for ssDNA.

Again, the decrease in relative intensity at 565 nm (λ^{D}_{Emm}) through donor quenching is greater for the Janus ligand **208** compared to the acetamide ligand. The E_{FRET} appears to be greater for the Janus ligand **208** over the control **215**, and at ligand concentrations above 2000 nM the two ligands diverge, with the Janus cyclohexane showing a much higher E_{FRET} and in turn a greater degree of donor quenching. This shows that at higher concentrations the Janus motif interacts with ssDNA to a greater extent than the control **215**.

These experiments suggest that the Janus cyclohexane **208** forms non-covalent interactions with both single strand and double strand DNA at relatively high concentrations. There is also a larger E_{FRET} between the Janus motif and double strand DNA compared to single strand DNA (E_{FRET} = 0.7 vs 0.6 respectively at 6000 nm). This indicates a small bias in binding with dsDNA over ssDNA in solution.

3.2.2 – Single Molecule FRET (smFRET) to explore Janus cyclohexane-DNA interactions

The FRET-based inter-molecular assays developed in the previous section showed a specific interaction of the Janus face-Cy5 molecule **208** to nucleic acid sequences when compared to a

control **215**, and a preference for dsDNA over ssDNA. However, these methods do not provide dynamic information regarding the lifetime of the interaction and potential differences between ssDNA and dsDNA. Therefore, FRET measurements were performed at the single molecule level using the same inter-molecular FRET concept but on surface-immobilized DNA substrates. For these experiments, the 18 nucleotide DNA substrate was identical to that used in the solution-based FRET experiments, but with biotin attached at the other end of the DNA structure. Biotin was used for surface-immobilization to a streptavidin-coated quartz slide. The interaction between biotin and streptavidin is one of the strongest in nature with an affinity constant in the femtomolar range,[19] thus providing a robust and stable anchoring point to immobilize biomolecules. Moreover, to avoid non-specific interactions between the Janus cyclohexane probes and the quartz surface, the slides were passivated by incorporating PEG chains of which 1% contains a biotin molecule to immobilized streptavidin. In these experiments, the concentration of immobilized DNA is between 10-50 pM and the concentration of Janus face-Cy5 **208** is 50 nM (see Chapter 7.8 for further details).

The first experiment constituted affixing dsDNA, tagged with Cy3 dye, to a slide and exciting the sample with 545 nm (λ_{Exc}^{D}) light. The Cy5-Janus cyclohexane **208** is passed over the surface in solution. If there is a non-covalent interaction between the Janus face and dsDNA then the Cy5 dye attached to the ligand will be localised next to the Cy3 dye, allowing for FRET to occur. This will be observed by smFRET as points of fluorescence intensity on the right-hand side of the Electron Multiplying Charge-Coupled Device (EMCCD) camera which detects Cy5 emission. Figure 3.13 illustrates the proposed experiment (for more details, see Chapter 7.8).

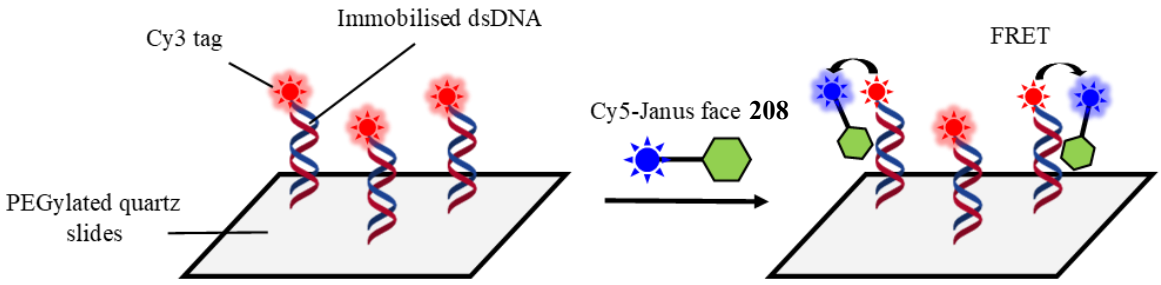

Figure 3.13: Schematic of proposed smFRET experiment to observe FRET between immobilised dsDNA and a Janus face ligand **208**.

The ligands were prepared, and the experiment was carried out by Prof. Carlos Penedo from the School of Physics and Astronomy (University of St. Andrews). Selected results are illustrated in Figure 3.14**.**

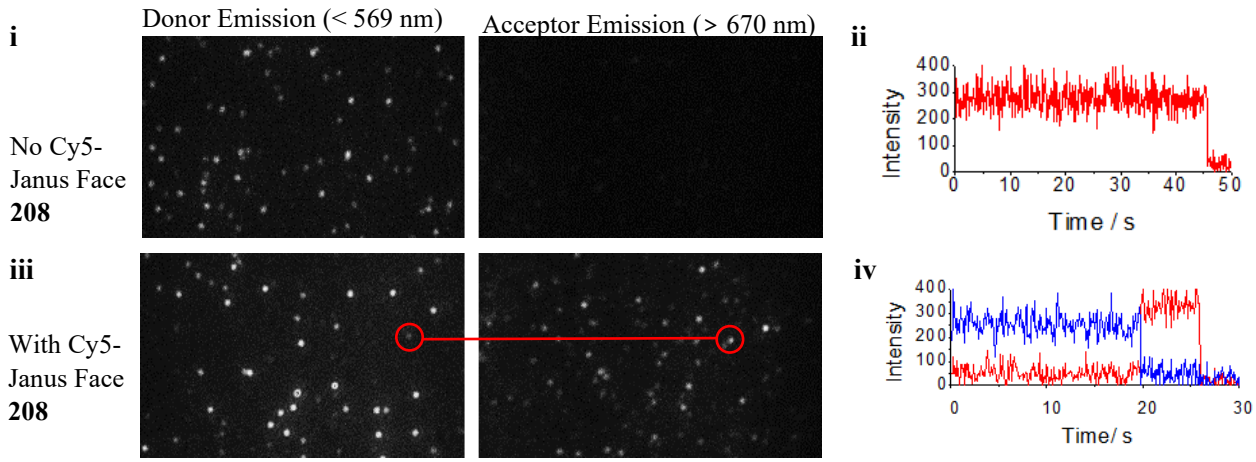

Figure 3.14: smFRET observed quenching between Cy3 tagged dsDNA immobilised on a surface and Cy5-Janus **208**. **i)** Control, no Cy5-Janus ligand **208** added. **ii)** Light intensity of a specific pixel over the course of a given time period for the control. **iii)** Cy5-Janus **208** present. **iv)** Light intensity of a specific pixel over the course of a given time period for the Janus cyclohexane. Red indicates < 569 nm light (donor) and blue indicates > 670 nm light (acceptor).

Spots emitting in the Cy3 camera channel (Figure 3.14.i, < 569 nm) corresponding to Biotin-dsDNA-Cy3 immobilized constructs were observed in the absence of Janus-Cy5 **208**. No signal was observed in the Cy5 camera channel (Figure 3.14.i, > 670 nm). The intensity profile over time for each spot shows stable emission until Cy3 photobleaching occurred. For instance, the red trace shown in Figure 3.14.ii displays a photobleaching step at ~47 seconds where the intensity of the Cy3 fluorophores decreases to background as a result of light induced Cy3 degradation. However, emission spots on the Cy5 channel (> 670 nm) could be observed for the Janus face experiment (Figure 3.14.iii). This is indicative of binding of Janus **208** to the immobilized dsDNA-Cy3. Excitation of the Cy3 and the close proximity of the Janus face-Cy5 on the dsDNA results in efficient energy transfer. The single molecule intensity trajectories confirm the presence of FRET from Cy3 and Cy5 and the specificity of the interaction as shown in the smFRET trace are shown in Figure 3.14.iv. The trace shows a high intensity of Cy5 (blue) and low intensity of the Cy3 donor (red) due to energy transfer. At approximately 20 seconds, the Cy5 is photobleached. As there is no possibility of FRET from Cy3 to Cy5 anymore, the Cy3 emission is not quenched and its intensity recovers (red) until the Cy3 motif is photobleached, at approximately 27 seconds. This anti-correlated behaviour of the Cy3 and Cy5 is indicative of the Janus **208** ligand bound to the Cy3 labelled dsDNA in turn placing both dyes in close proximity for efficient FRET. This is consistent with a stable interaction of the Janus cyclohexane with dsDNA.

A second assay was designed to investigate the interaction between Janus face motifs and labelled dsDNA. In this case, the Janus molecule was secured on the surface with dsDNA as

the solute. The Janus cyclohexane was functionalised with a biotin group using a PEG chain as the linker between both motifs. The biotin motif will attach to the PEGylated quartz slide surface through a biotin-streptavidin interaction. A schematic for this experiment is illustrated in Figure 3.15.

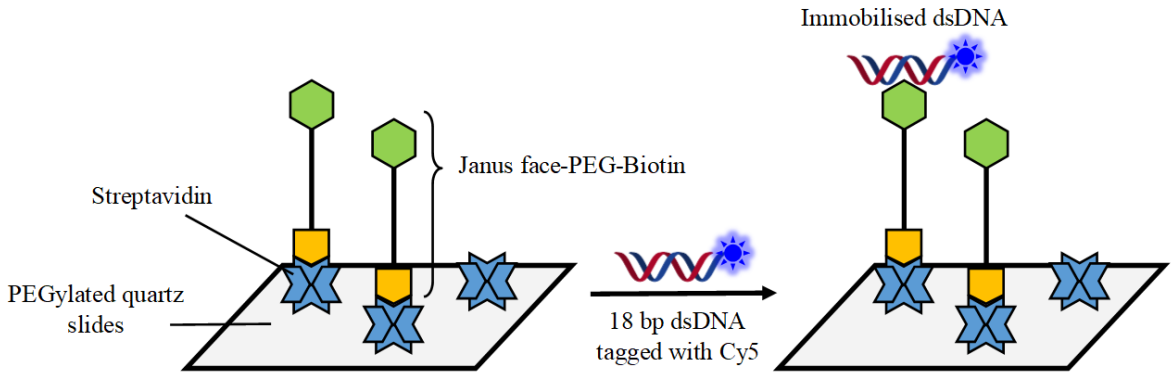

Figure 3.15: Schematic of proposed smFRET experiment to observe immobilised dsDNA through a Janus face-dsDNA non-covalent interaction. Green represents the Janus motif, yellow represents the biotin motif.

Attention therefore turned to the synthesis of Janus face-PEG-biotin molecule **216**. The approach taken involved attaching the Janus cyclohexane to one end of the PEG chain *via* an azide-acetylene click reaction, with the biotin motif attached to the other terminus *via* an amide. The target and retrosynthetic strategy is shown in Scheme 3.5.

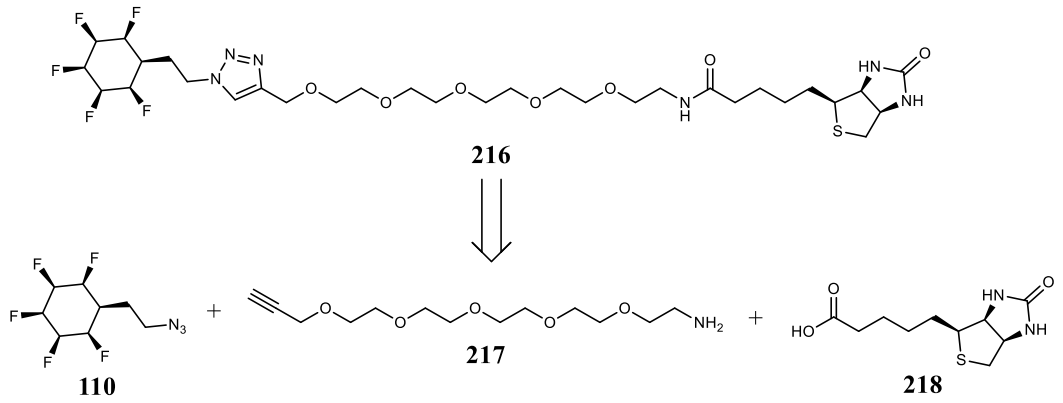

Scheme 3.5: Target and retrosynthetic strategy for the synthesis of Janus face-PEG-Biotin **216.**

This required preparation of Janus azide **110**. The route started from methyl ester **106** (see Scheme 3.2) and involved a series of functional group interconversions to generate the azide **110** (Scheme 3.6).

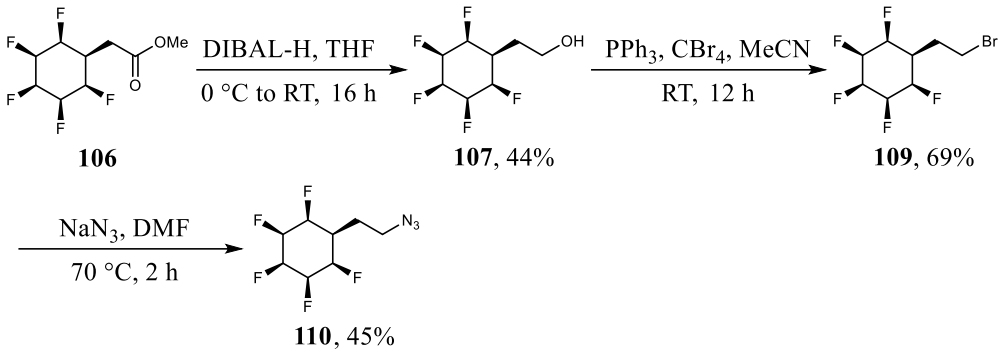

106 **107**, 44% **109**, 69% **110**, 45%

Scheme 3.6: Synthesis of azide **110** from ester **106** over three steps.[18]

Using protocols previously developed in St Andrews,[18] the methyl ester **106** was reduced with diisobutylaluminium hydride (DIBAL-H) to give alcohol **107**. The alcohol **107** was then subject to an Appel halogenation to generate alkyl bromide **109**, which was then treated with sodium azide to generate azide **110**. This sequence was conducted in an overall yield of 14% over the three steps. The PEG chain required to attach azide **110** was prepared as outlined in Scheme 3.7.[20–22]

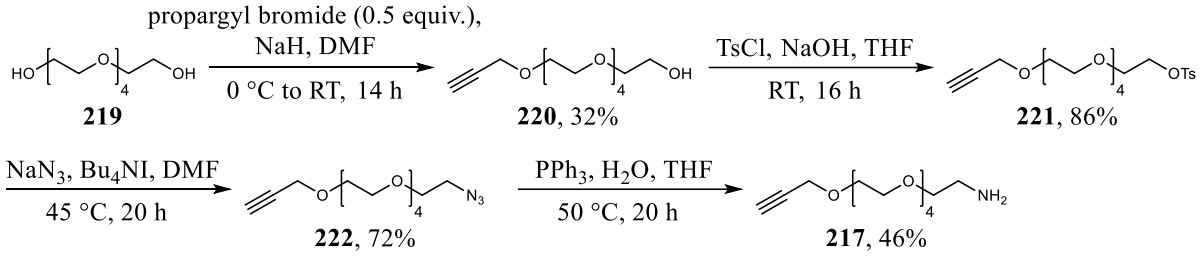

219 **220**, 32% **221**, 86% **222**, 72% **217**, 46%

Scheme 3.7: Four step synthesis of acetylene amine PEG **217** from glycol **219**.[20–22]

Alkylation of glycol **219** with propargyl bromide gave mono acetylene PEG **220**. This product was treated with tosyl chloride to generate PEG tosyl **221**. Treatment then with sodium azide generated PEG azide **222** which was finally reduced *via* a Staudinger reaction,[23] to yield acetylene-PEG-amine **217**. The synthesis sequence was achieved in an overall yield of 10% over the four steps. The biotin and the Janus motifs were then subsequently attached to either side of the PEG chain (Scheme 3.8). The biotin **218** motif was attached to **217** *via* a peptide coupling reaction to give PEG-biotin **223**. The terminal acetylene was then reacted with azide **110** in a click CuAAC to give the required Janus face-PEG-biotin **216**.

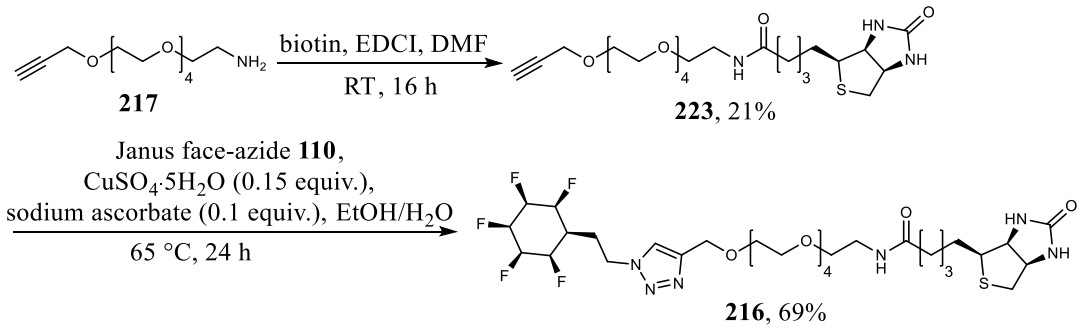

Scheme 3.8: Synthesis of Janus face-PEG-biotin **216**.

With target probe **216** in hand, the previously described smFRET experiment between **216** and Cy3 tagged DNA (Figure 3.15) was performed, again by Prof. Carlos Penedo. The results are shown in Figure 3.16.

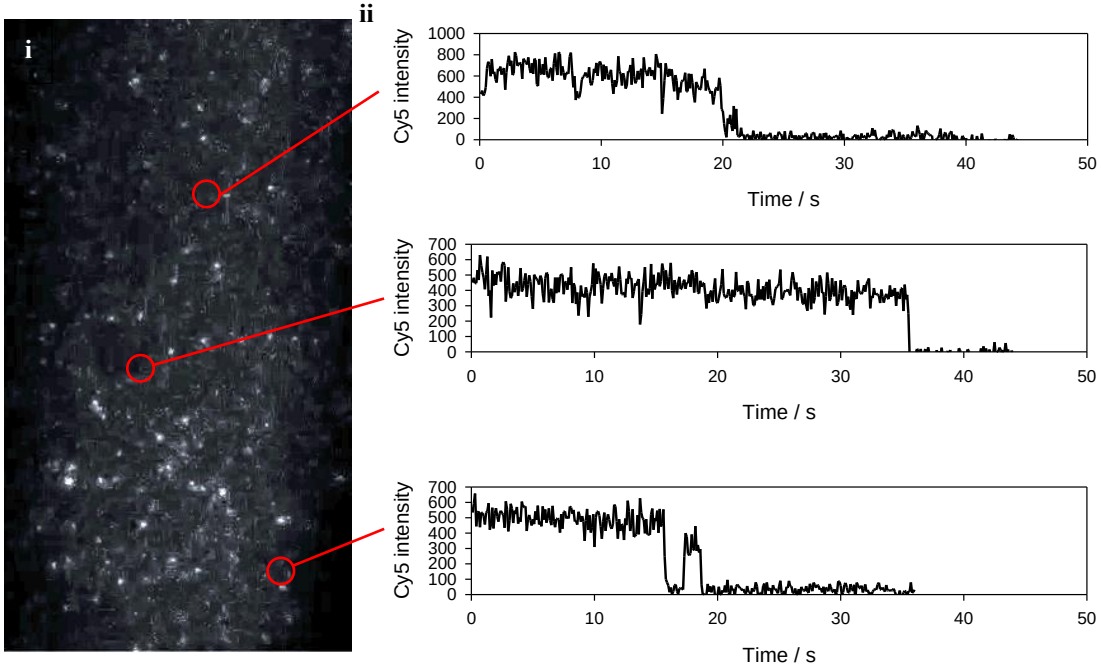

Figure 3.16: Light intensity at 670 nm from smFRET experiment between immobilised Janus face and dsDNA tagged with Cy5. **i)** Direct image from the slide. **ii)** Time course of Cy5 intensity of a given pixel.

Discrete fluorescence spots (i) and representative intensity trajectories (ii) for three of these spots are shown on the right-hand side in a time course in Figure 3.16. The graphs shown in Figure 3.16.ii show two states; "on" (where Cy5 intensity is >100), which indicates the immobilisation of the Cy5 tagged dsDNA, and "off" (Cy5 intensity <100), which indicates a lack of dsDNA. The presence of two discrete states suggests that the dsDNA and Janus probe **216** form a 1:1 complex, as opposed to a multi-ligand complex which would show more than two discrete states. Additionally, the on state is long lasting, with a lifetime ranging from 14 to 35 seconds, indicating that the interaction between the Janus probe **216** and dsDNA is stable and long-lasting, as was also observed in the reciprocal reaction. It is clear from the smFRET

results that the immobilized Janus motif **216** acts as an anchor and binds to dsDNA. The experiment was repeated using ssDNA tagged with Cy5. The results are shown in Figure 3.17.

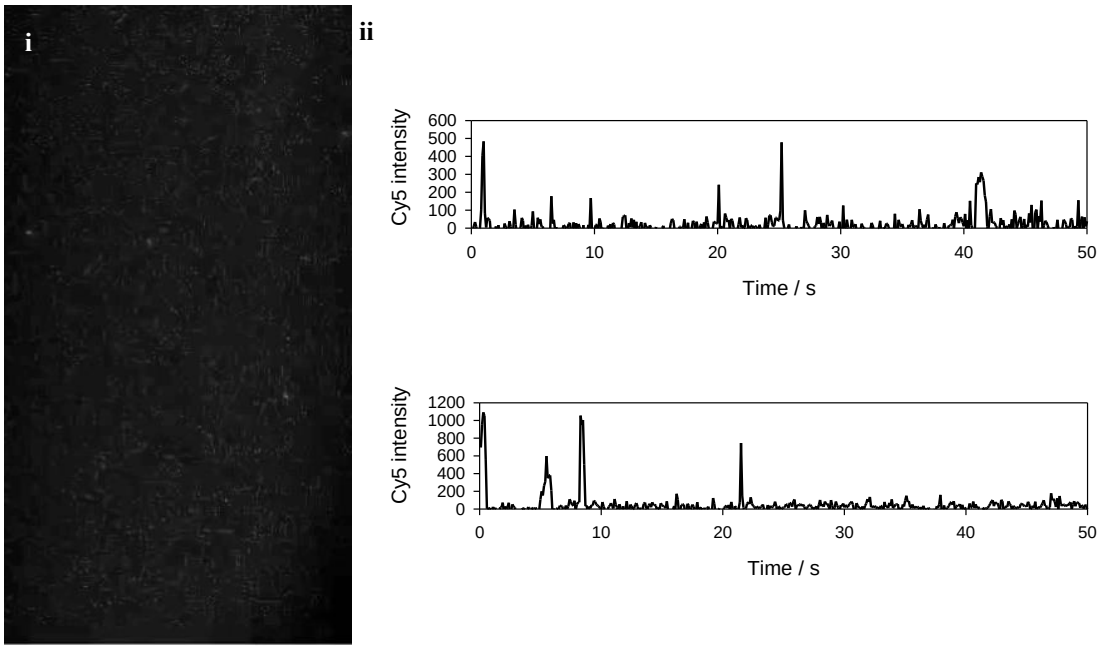

Figure 3.17: Light intensity at 670 nm from smFRET experiment between immobilised Janus face and ssDNA tagged with Cy5.i) Direct image from the slide. ii) Time course of Cy5 intensity of a given pixel.

By contrast, there is no observed stationary fluorescence from the Cy5 tag. Any observed fluorescence is brief, and lasts for milliseconds, as shown by the light intensity time courses (Figure 3.17.ii). This suggests that the Janus face probe **216** does not form stable, long lasting, non-covalent interactions with ssDNA. This represents a significant difference compared to the previous smFRET experiment with dsDNA (Figure 3.16) where there is a clear association with dsDNA.

It has been shown using smFRET techniques that the Janus motif forms stable, long-lasting interactions (up to 35 seconds) with dsDNA on a picomolar scale. smFRET also showcases that the Janus face motif forms a 1:1 complex with the 18 bp oligomer, which indicates that the dsDNA is saturated after binding to only one Janus motif. However, using the same smFRET experiments, there is a distinct lack of evidence for interactions between ssDNA and the Janus face motif. Although the previous solution-based FRET experiments (see Figure 3.12) indicate an interaction between ssDNA and the Janus face at high concentrations, the single molecule scale of smFRET (picomolar vs micromolar) highlights a clear preference for Janus face-dsDNA binding over Janus face-ssDNA binding at very low concentrations.

3.2.3 – Isothermal Titration Calorimetry (ITC) to explore Janus cyclohexane-DNA interactions

In an effort to further explore Janus cyclohexane-DNA interactions through a physical method, attention turned towards ITC. Three different Janus face ligands were selected to explore how both solubility and functionalisation of the Janus motif might impact any degree of interaction. The selected ligands, and their respective solubilities in water at room temperature, are shown in Figure 3.18.

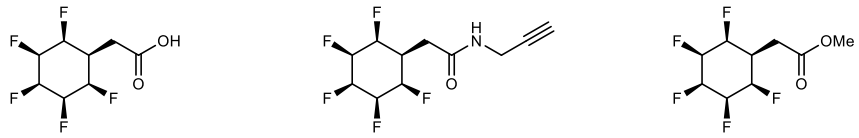

211, 2.55 g/L **209**, 0.90 g/L **106**, 0.44 g/L

Figure 3.18: Janus cyclohexane used as ligands for ITC and their associated solubilities in water at room temperature.

Solubilities were calculated by saturating a volume of deionised water (5 mL) with a chosen ligand before heating the mixture to 100 °C. The mixture was then cooled to room temperature before all of the remaining precipitate was allowed to settle. An aliquot (1 mL) of a clear solution was extracted and lyophilised to give the mass of the solute in 1 mL and in turn the compound's solubility. As expected, the carboxylic acid **211** had the highest solubility in water, followed by amide **209**, and finally ester **106**, which has no obvious oxygen to hydrogen bonding capability.

As a positive control for ITC experiments, a known dsDNA intercalator, proflavine **224**, was used with an 18 base pair DNA sequence (Figure 3.19).

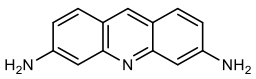

Proflavine, **224**

5' – GCG AGA TGG CGA GTC ACG – 3'
3' – CGC TCT ACC GCT CAG CGT – 5'

Figure 3.19: dsDNA intercalator proflavine **244** and the sequence of DNA used.

In brief, the ITC sample cell was filled with 20 mM of the dsDNA in a solution of tris buffer at pH 8. Proflavine **224** (500 μM) dissolved in the same buffer was loaded into the syringe (for full details, see Chapter 7.7). The results of the ITC experiment are shown in Figure 3.20.

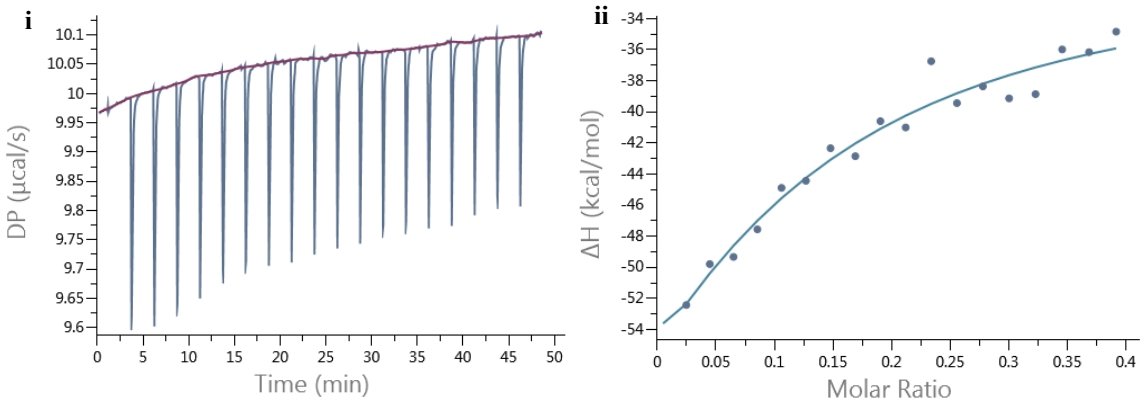

Figure 3.20: Thermograms from proflavine **224** dsDNA binding experiment; **i)** Heat of binding over time with each spike representing an injection and **ii)** Titration curve.

The thermogram (Figure 3.20.i**)** depicts the differential power (DP) (energy required to maintain similar temperature between reference and sample cell) over time. Each spike represents an injection of proflavine **224** to the dsDNA solution (adjusted for enthalpy of dilution), with an adjustment to the DP requiring a significant change in energy. As the dsDNA becomes more saturated, the DP diminishes with each sequential injection, representing a smaller change in enthalpy due to less ligands binding. This change in enthalpy can be plotted against the molar ratio of ligand **224** to dsDNA, generating a titration curve.

With this positive control data, attention turned to ITC experiments between the Janus face molecules and dsDNA. In a manner similar to the proflavine **224** ITC experiment, the sample cell was filled with dsDNA (20 µM) in tris buffer, and the syringe was loaded with ligand **106** (500 µM) dissolved in the same buffer. Figure 3.21 shows the resulting thermograms.

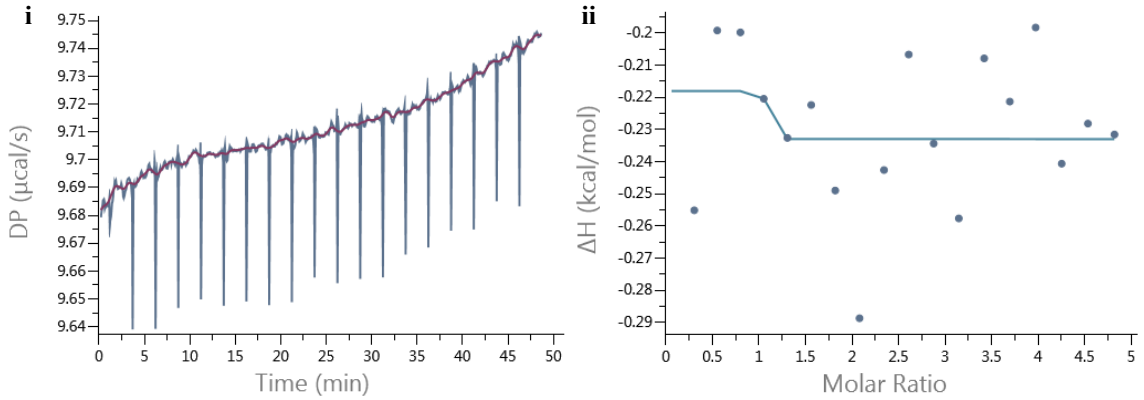

Figure 3.21: Thermograms from Janus face ester **106** dsDNA binding experiment; **i)** Heat of binding over time and **ii)** Titration curve.

The thermograms indicate that there is no obvious correlation between molar ratio and the change in enthalpy, indicating that there is no observable enthalpy change when Janus face ester **106** is added to dsDNA. The experiment was repeated with the Janus face amide **209** and

carboxylic acid **211**. The resulting thermograms can be seen in Figure 3.22 and Figure 3.23 respectively.

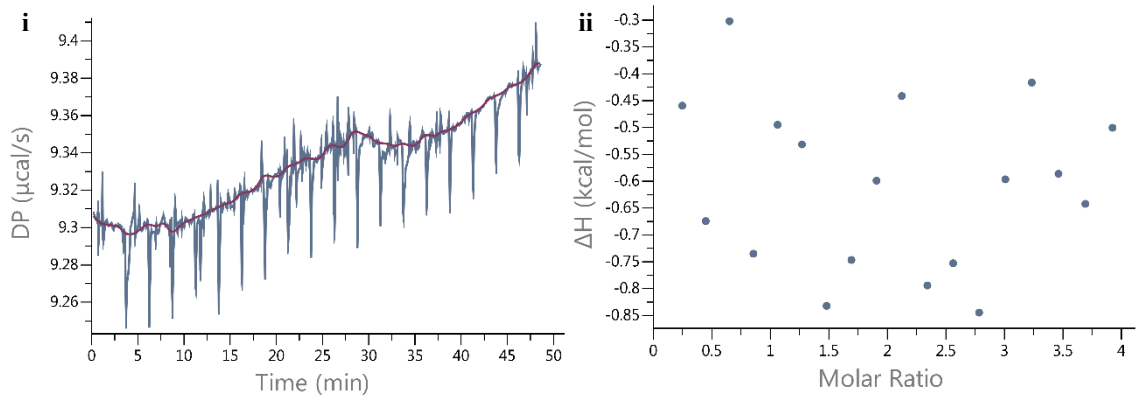

Figure 3.22: Thermograms from Janus face amide **209** dsDNA binding experiment; **i)** Heat of binding over time and **ii)** Titration curve.

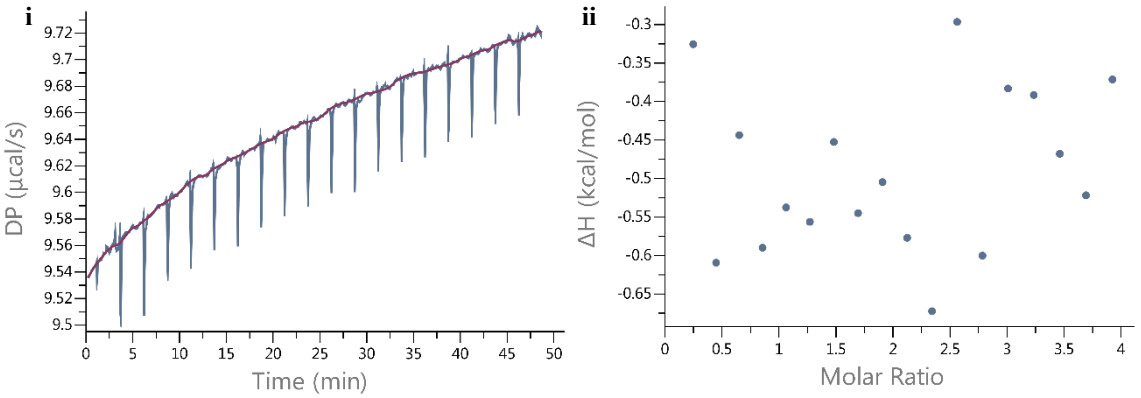

Figure 3.23: Thermograms from Janus face acid **211** dsDNA binding experiment; **i)** Heat of binding over time and **ii)** Titration curve.

Both the ITC experiments which titrate the amide **209** and carboxylic acid **211** with dsDNA gave similar negative results to the previously described Janus ester **106**. This indicates that even with a change in functional group that there is no observed enthalpy change when the Janus probes interact with dsDNA.

The concentration of sodium chloride in the buffer could clearly inhibit electrostatic interactions between the ligands and DNA, therefore this was explored further. Experiments were repeated with tris buffers which differed in concentrations of sodium chloride (10 mM, 50 mM, and 100 mM). However, there was an insignificant change in DP with no obvious correlation between the molar ratio and the change in enthalpy. This correlates to a lack of binding between the Janus face motif and dsDNA, even at different salt concentrations.

Although a binding enthalpy between dsDNA and the Janus probes were not obvious in bulk solution (observed by ITC), interactions observed in smFRET experiments with dsDNA were clear. At this stage it is not clear why there is a difference between the bulk solvent and single

molecule surface experiments. Perhaps the polarity of the solvent is screening interactions between the probes and DNA.

3.3 – Conclusions

This chapter has explored the interaction of the Janus face motif and DNA. A series of experiments have been designed and carried out, with solution-based FRET and smFRET showing that the Janus face motif forms long lasting non-covalent one-to-one interactions with dsDNA. These experiments also show that the Janus face motif preferentially binds to dsDNA over ssDNA at a single molecule level. This provides an exciting avenue for the Janus face motif to be explored as a tool to transport drugs, proteins, and analytical compounds to DNA.

The lack of an enthalpy change in ITC suggests that there is a lack of substantial water molecule displacement by the Janus face motif during a Janus face-DNA binding event. The enthalpy change caused by DNA-Janus face binding may be smaller than that detectable by ITC techniques.

This chapter also describes the synthesis of molecular probes which possess a Janus face motif, demonstrating the ability to incorporate the Janus cyclohexane into a range of larger, complex molecules for analysis of biological systems.

3.4 – References

1 B. Fang, Y. Shen, B. Peng, H. Bai, L. Wang, J. Zhang, W. Hu, L. Fu, W. Zhang, L. Li and W. Huang, *Angew. Chem., Int. Ed.*, 2022, **61**, e202207188.

2 H. Chen, H. L. Puhl, S. V. Koushik, S. S. Vogel and S. R. Ikeda, *Biophysical J.,* 2006, **91**, L39–L41.

3 R. Roy, S. Hohng and T. Ha, *Nat. Methods*, 2008, **5**, 507–516.

4 H. Ishikawa-Ankerhold, R. Ankerhold and G. Drummen, *Molecules*, 2012, **17**, 4047–132.

5 Á. Szabó, J. Szöllősi and P. Nagy, *Curr. Protoc.*, 2022, **2**, e625.

6 C. U. Murade and G. T. Shubeita, *Biomed. Opt. Express*, 2022, **13**, 159–167.

7 R. Ghai, R. J. Falconer and B. M. Collins, *J. Mol. Recognit.*, 2012, **25**, 32–52.

8 A. Velázquez-Campoy, H. Ohtaka, A. Nezami, S. Muzammil and E. Freire, *Curr. Protoc. Cell Bio.*, 2004, **23**, 17.8.1-17.8.24.

9 D. K. Sasmal, L. E. Pulido, S. Kasal and J. Huang, *Nanoscale*, 2016, **8**, 19928–19944.

10 H. P. Lu, *Acc. Chem. Res.*, 2005, **38**, 557–565.

11 Š. Ivanovaitė, J. Paksaitė, A. Kopūstas, G. Karzaitė, D. Rutkauskas, A. Silanskas, G. Sasnauskas, M. Zaremba, S. K. Jr. Jones and M. Tutkus, *J. Phys. Chem. B*, 2023, **127**, 6470–6478.

12 C. Phelps, B. Israels, D. Jose, M. C. Marsh, P. H. von Hippel and A. H. Marcus, *Proc. Natl. Acad. Sci. U.S.A.*, 2017, **114**, E3612–E3621.

13 L. Schärfen and M. Schlierf, *Methods*, 2019, **169**, 11–20.

14 J. E. Coats, Y. Lin, E. Rueter, L. J. Maher and I. Rasnik, *Nucleic Acids Res.*, 2013, **41**, 1372–1381.

15 S. D. Quinn, PhD Thesis, University of St Andrews, 2013.

16 C. Penedo, MATLAB (version version: 9.13.0 (R2022b)) The MathWorks Inc., Natick, Massachusetts, United States 2023.

17 K. E. Riley and P. Hobza, *Wiley Interdiscip. Rev. Comput. Mol. Sci.*, 2011, **1**, 3–17.

18 J. L. Clark, R. M. Neyyappadath, C. Yu, A. M. Z. Slawin, D. B. Cordes and D. O'Hagan, *Chem. Eur. J.*, 2021, **27**, 16000–16005.

19 N. Green, *Biochem. J.*, 1963, **89**, 585–591.

20 J. Diot, M. I. García-Moreno, S. G. Gouin, C. O. Mellet, K. Haupt and J. Kovensky, *Org. Biomol. Chem.*, 2008, **7**, 357–363.

21 R. Zamboni, R. Henning, A. Ji, T. Smith, B. Heller, T. J. Reddy, S. Rocheleau, M. A. Beaulieu, US Pat. 15 965 506, 2018.

22 F. Tran, A. V. Odell, G. E. Ward and N. J. Westwood, *Molecules*, 2013, **18**, 11639–11657.

23 H. Staudinger, J. Meyer, *Helv. Chim. Acta.,* 1919, 2, 635-646.

Chapter 4

^{18}F-Radiolabelling of a Janus cyclohexane probe

4.1 – Introduction and aims

4.1.1 – Positron Emission Tomography (PET)

Positron emission tomography (PET) is an imaging technique which monitors and visualises physiological activities in three-dimensions, in turn allowing for the diagnoses and monitoring of tumours and cancers, as well as brain diseases such as Alzheimer's and epilepsy.[1,2] This is conducted through the use of radiotracers; molecules that possess a positron-emitting isotope bound to an organic ligand which interacts with relevant biomolecules. The radioactive isotope, most commonly ^{11}C or ^{18}F, undergoes positive beta decay involving the transformations of a proton to a neutron, in turn releasing a positron (an electron antiparticle) and a neutrino (a chargeless and near massless particle). The collision between an electron and a positron emits two photons (or γ-rays) which travel in equal and opposite directions. When these photons are detected by opposed γ-ray detectors a coincidence event is recorded and the annihilation is assumed to have occurred along the line of response (LOR), allowing for the pinpointing of the annihilation event and in turn the location of the radiotracer in the body (Figure 4.1).[2]

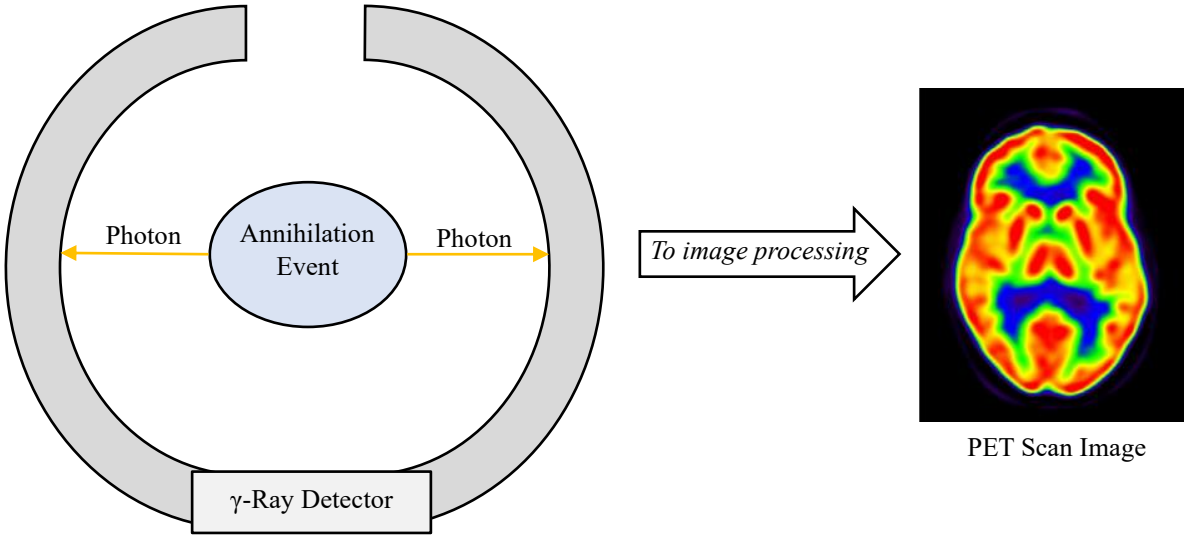

Figure 4.1: Basic overview of the PET scanning process. The collision of an electron and neutron emits two photons which when detected allow for the pinpointing of the annihilation event and in turn the production of a PET scan image.[2]

An advantage of using PET as a diagnostic method is that only a trace level of radiotracer is required to develop a quality image. For example the most common radiotracer, [^{18}F]-2-fluoro-2-deoxyglucose ([^{18}F]FDG),[3] is used on a nanogram scale emitting 8 mSv, an amount of radiation exposure a patient would receive from everyday background radiation sources.[4] This

nanogram scale used is also beneficial for radiotracer production, as sources of radioactive isotopes such as ^{18}F, which are used in radiotracer synthesis, are expensive.

The most common radiotracer isotope used in the clinical setting is fluorine-18 (^{18}F).[5] This is a consequence of several factors, including; a relatively long half-life ($t_{1/2}$ = 109.8 min) allowing for more complex radiosynthesis, fluorine's bioisostere properties (Chapter 1.2.4), and a low positron energy (0.64 Mev), resulting in the generation of high-resolution images.[5] Table 4.1 lists a series of commonly used radionuclides in PET imaging.

Table 4.1: Common radionuclides used in PET.[5]

Radionuclide	Half-Life/min	Max. Positron Energy/MeV
^{11}C	20.3	0.97
^{13}N	10.0	1.20
^{15}O	2.00	1.74
^{18}F	**109.8**	**0.64**
^{64}Cu	762	0.66
^{68}Ga	68.1	1.90
^{79}Br	972	4.00
^{124}I	60,192	2.14

4.1.2 – Brief overview of ^{18}F-radiolabelling

Fluorine-18 is not a naturally occurring isotope. The primary source of ^{18}F as [^{18}F]fluoride, is generated in a cyclotron from an accelerated proton beam irradiation of commercially available ^{18}O in a heavy water [$H_2{}^{18}O$] target.[6] Both electrophilic and nucleophilic sources of ^{18}F can be produced *via* this method. In the first instance the process generates an aqueous solution of [^{18}F]-fluoride (nucleophile). Alternatively when $^{18}O_2$ gas is used as the target, this generates [^{18}F]F_2 gas (electrophile).[7,8] The synthesis of ^{18}F compounds for PET applications has been extensively reviewed.[7,9–11] This work will briefly outline two of the most common radiosynthetic methods.

The most frequently used radiotracer for PET is [^{18}F]2-deoxy-2-fluoro-D-glucose, or [^{18}F]FDG **227a** (Scheme 4.1). [^{18}F]FDG **227a** can be synthesized both through nucleophilic or electrophilic fluorination, as detailed in Scheme 4.1.[12]

Electrophilic Fluorination

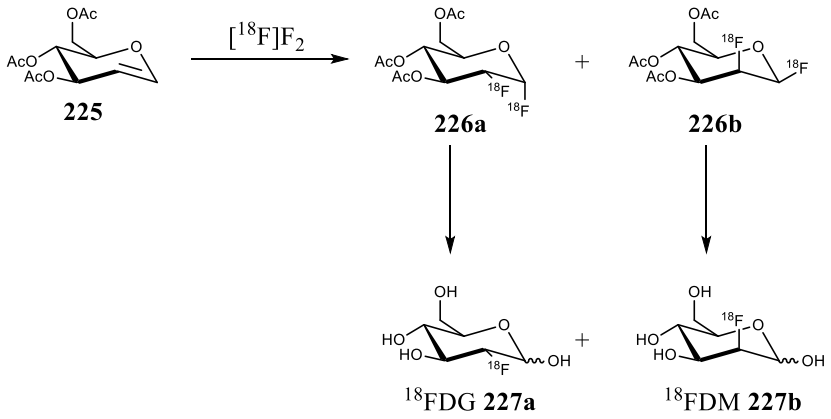

Nucleophilic Substitution

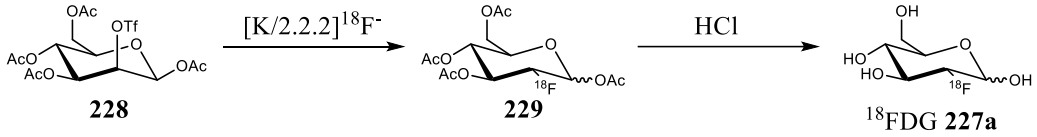

Scheme 4.1: Synthesis of ^{18}FDG (**227a**) *via* electrophilic and nucleophilic substitution protocols.[12]

The original synthesis of [^{18}F]FDG **227a** in 1977 was accomplished using gaseous [^{18}F]F_2 *via* electrophilic fluorination (Scheme 4.1).[13] Electrophilic attack across the alkene of glycal **225** gives a 3:1 mixture of [^{18}F]FDG **227a**:[^{18}F]FDM **227b**, with [^{18}F]FDM **227b** being the mannose with an axial ^{18}F. [^{18}F]FDM **227b** appears to have a 20% reduction in apparent cerebral metabolic rates for glucose when compared to [^{18}F]FDG **227a**.[14] This in turn leads to an underestimation of the metabolic rate of the radiotracer when a mixture of [^{18}F]FDG **227a** and [^{18}F]FDM **227b** is used, producing inaccurate PET data.[14]

The synthesis of [^{18}F]FDG **227a** *via* nucleophilic substitution uses mannopyranose **228** as a substrate in a reaction with ^{18}F-fluoride (derived from the dehydration of $H_2{}^{18}O/{}^{18}F^-$) and then subsequent deprotection with hydrochloric acid. Kryptofix [2.2.2] is used to complex the potassium counterion and in turn increase the reactivity of ^{18}F-fluoride.[15]

4.1.3 – Fluorinase and late-stage enzymatic fluorination of adenosine

The synthetic routes available for the preparation of radiotracers are numerous, however, the use of elemental [^{18}F]F_2 and $^{18}F^-$-fluoride present challenges with functional group tolerance in late-stage fluorination. Work done by the O'Hagan group has presented an alternative approach to radiolabelling which utilizes a fluorination enzyme. The enzyme works in an aqueous medium at neutral pH and under ambient conditions.[16]

The fluorinase enzyme was isolated in 2002 and it catalyses the reaction between S-adenosyl-L-methionine (AdoMe) and fluoride ion to give 5'fluoro-5'-deoxyadenosine (FDA) and L-

methionine (L-Met).[17] This enzymatic transformation can be utilised for the formation of C-^{18}F bonds to synthesise radiotracers for PET with L-Met substituted for the more reactive additive L-selenomethionine (L-SeMet), as shown in Scheme 4.2.[16]

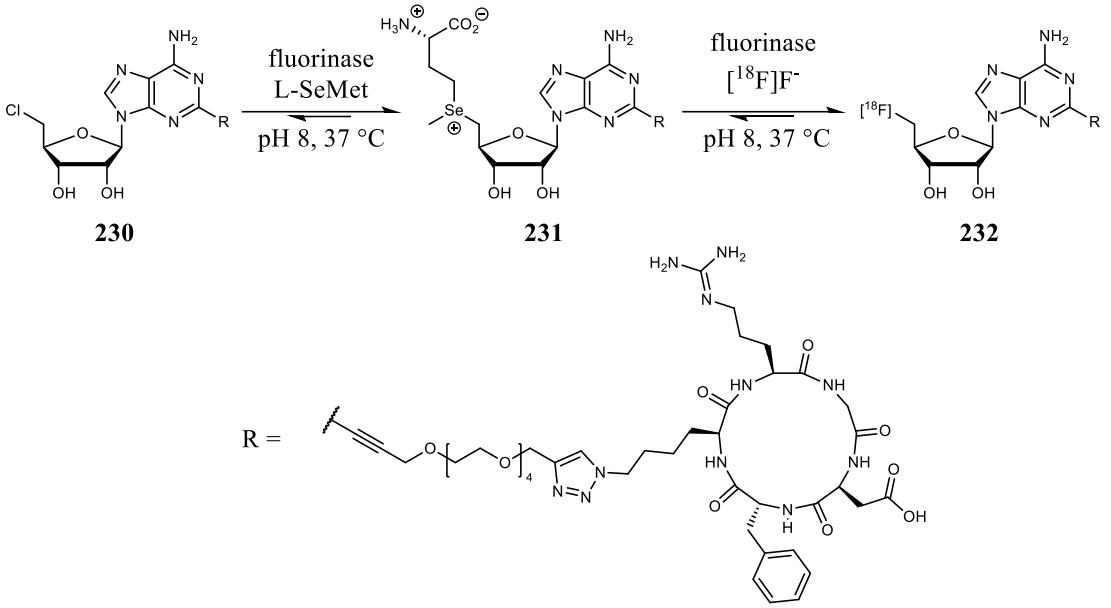

Scheme 4.2: Fluorinase catalysed transformation of 5'-chloro-'5-deoxy-2-ethynyladenosine motif (ClDEA, **230**) to 5'-[^{18}F]-fluorodeoxy-2-ethynyladenosine ([^{18}F]FDEA, **232**).[16]

Scheme 4.2 shows the transformation of ClDEA-PEG-RGD **230** (ClDEA = 5'-chlorodeoxy-2-ethynyladenosine) to AdoSeMet **231** through substitution of the 5'-chlorine by ^{18}F-fluoride to give the radioactive product [^{18}F]FDEA-PEG-RGD **232** (FDEA = 5'-fluorodeoxy-2-ethynyladenosine). Radiolabelling is carried out under aqueous conditions, using a $H_2{}^{18}O/{}^{18}F^-$ solution, at ambient temperature. The site-specific enzymatic reaction has high functional group tolerance and allows for the radiolabelling of complex molecules when compared to traditional ^{18}F radiolabelling methods. However, the fluorinase enzyme is highly specific to the adenosine motif, and all atoms are required for the reaction to proceed.

4.1.4 – RGD peptide drug delivery systems

Arginine-glycine-aspartic acid (RGD) containing peptides have high affinity to the transmembrane $\alpha_v\beta_3$ receptor, protein epitopes that are over-expressed in tumour-associated cells.[18] Because of this, RGD peptides have been used as tumour targeting ligands, facilitating the selective delivery of anti-tumour drugs to cancer cells.[19] This is achieved through non-covalent linking of the anti-tumour drug to the RGD peptide, localising the drug to targeted areas, increasing the drugs potency and reducing harmful side effects.[20,21] An example of this was conducted by Lin *et. al*., who incorporated doxorubicin (DOX, **234**) into a RGD-conjugated polypeptide zwitterion **233** through ionic bonding, increasing the accumulation of the drug in the tumour and decreasing systemic toxicity when compared to the free drug (Figure 4.2).[21]

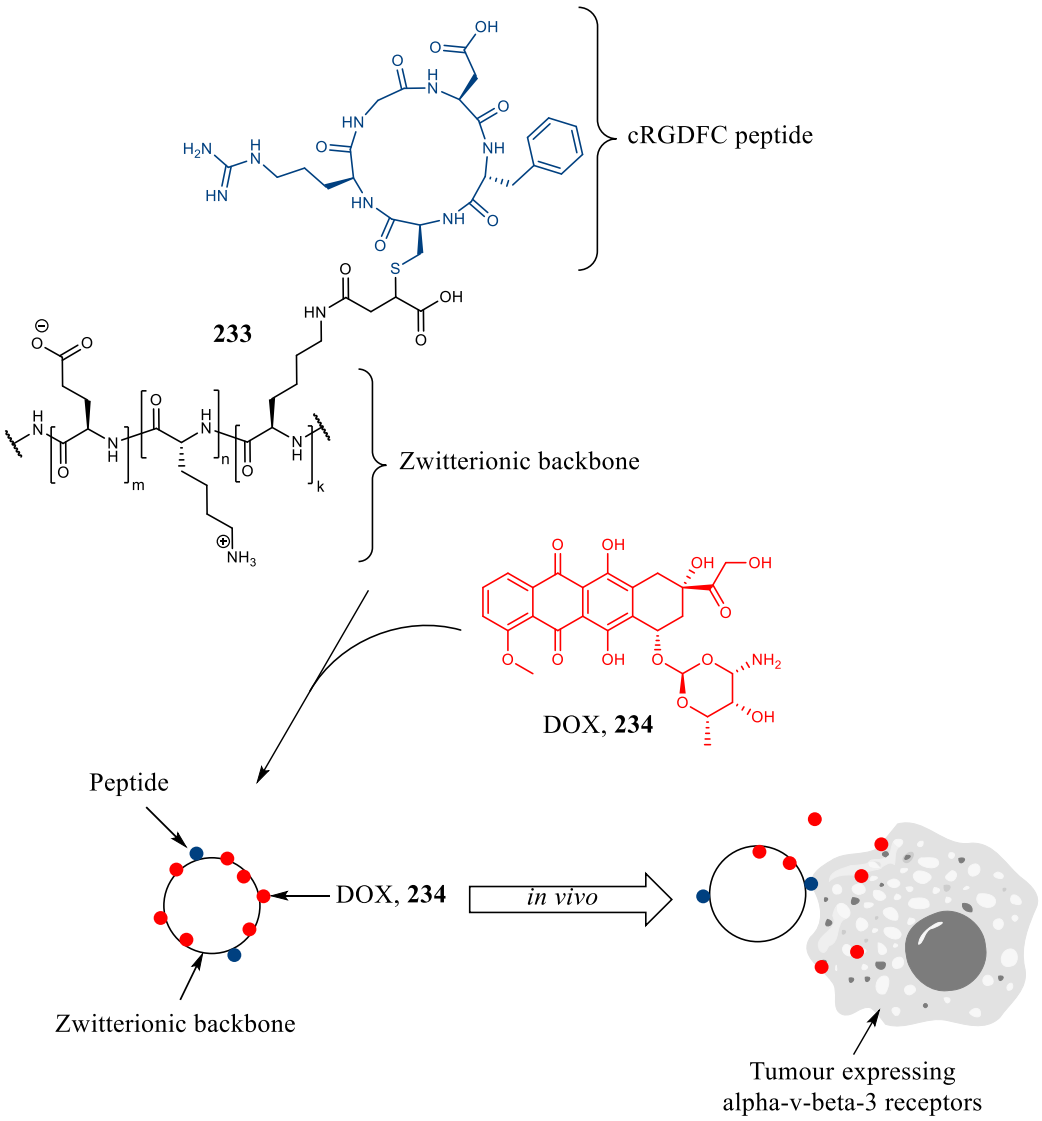

Figure 4.2: Schematic detailing a drug-delivery system using RGDs. The antitumour drug DOX **234** is embedded in the zwitterionic backbone containing RGD peptide units (**233**) which binds to the $\alpha_v\beta_3$ receptor expressing tumour cells, localising DOX **234** to the target area.[21]

4.1.5 – Aims and objectives

This project aims to radiolabel a molecule containing a Janus motif, to explore how robust the fluorocyclohexane is under radiolabelling conditions. Success would open up prospects for the further study of the Janus motif in biological systems using PET, perhaps for the design of co-localising and/or aggregation agents. For example, functionalised Janus motifs should have a tendency to complex to each other, and this offers a new strategy for the delivery of a drug or probe to particular cell types *via* Janus-Janus interactions of differently functionalised probes. As a first step, the following protocol aimed to explore the possibility of localising Janus rings on the surface of cancer cells through the $\alpha_v\beta_3$ integrin by linking a Janus cyclohexane to a c(RGDfK) ring. Success here would then allow investigation of co-locating a ^{18}F-fluoride labelled Janus probe on the surface of the cancer cells, and to explore a novel strategy for contrast imaging (Figure 4.3).

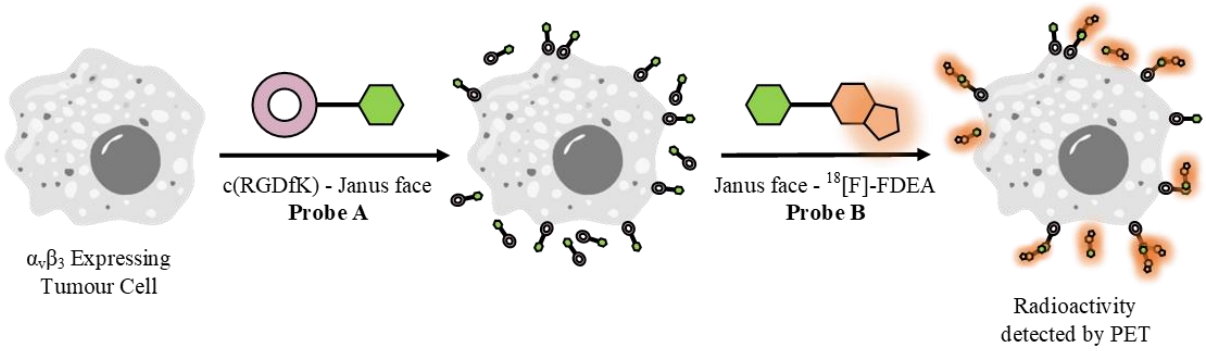

Figure 4.3: Schematic illustrating a strategy for ^{18}F-contrast imaging of cancer cells through Janus– Janus complexation.

First, a tumour cell expressing $\alpha_v\beta_3$ receptors would be saturated with a probe containing a c(RGDfK) peptide at one end and a free Janus motif on the other (probe A). The c(RGDfK) peptide should bind to the $\alpha_v\beta_3$ receptors potentially leaving the Janus motif exposed on the surface of the tumour cell. Next, an ^{18}[F]FDEA-Janus probe (probe B) would be introduced, and the Janus motif of probe A should bind to the Janus cyclohexane of probe B within the cell. This would localise the radioactive ^{18}[F]FDEA motif at the $\alpha_v\beta_3$ receptor expressing cell, which would then be detected by γ-ray detector in PET scans.

In this chapter a synthetic route towards a ClDEA-Janus molecule is detailed, and the method for its subsequent transformation to a FDEA control analogue is presented. Radiolabelling of the ClDEA-Janus molecule using the fluorinase enzyme and $^{18}F^-/H_2{}^{18}O$ is also detailed. Synthesis of a cyclic Arg-Gly-Asp-D-Phe-Lys protein (c(RGDfK)) linked to a Janus cyclohexane is described as an integral probe for this protocol.

4.2 – Results and discussion

4.2.1 – Synthesis of Janus radiotracer precursor

The original route envisioned the synthesis of a molecule that possesses a ClDEA motif tethered to a Janus ring through a PEG (polyethylene glycol) chain **235**. The PEG chain would provide separation between the ClDEA fluorinase substrate motif and the Janus ring, preventing any interference with the enzyme reaction. The synthesis combines three parts; preparation of the ClDEA unit, assembly of the PEG linker, and synthesis of the Janus unit (Scheme 4.3).

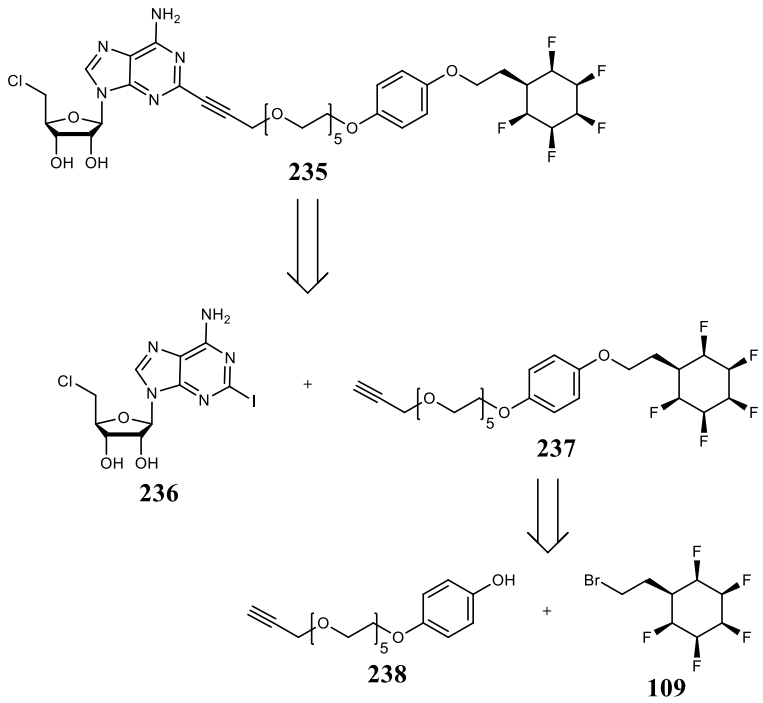

Scheme 4.3: Retrosynthetic analysis of ClDEA-PEG-Janus molecule **235**.

The coupling of the Janus ring and the PEG chain would be achieved through substitution of alkyl bromide **109** by phenol **238**. The coupling of the PEG chain to ClDEA would then be carried out *via* a Sonogashira cross coupling reaction of intermediate product **237** with 5'chloro-iodoadenosine **236**. The resulting ethynyl adenosine unit should be relatively well tolerated by the active site of the fluorinase enzyme as the chain attached to the acetylene group projects from the enzyme active site.[16]

Alkyl bromide **109** was required and its synthesis followed the reported route which was previously used in Chapter 3 and illustrated again in Scheme 4.4.[22]

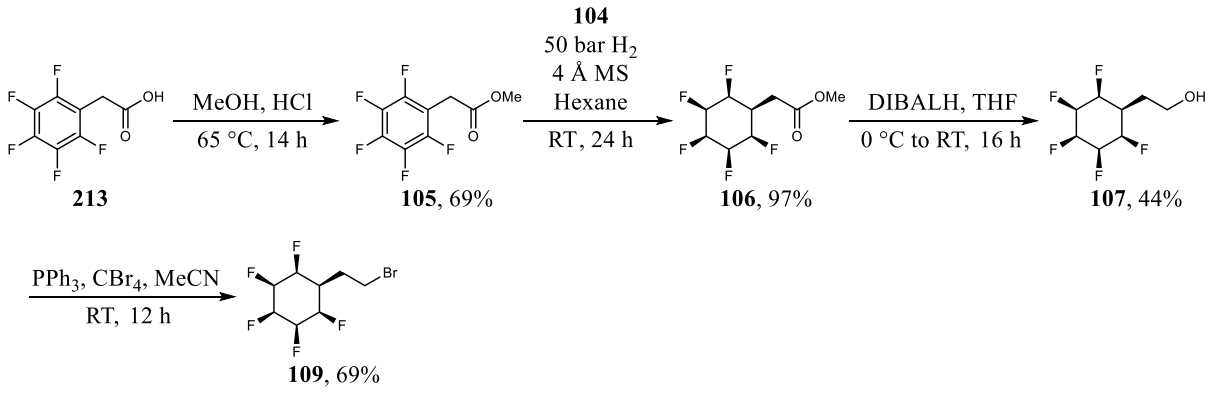

Scheme 4.4: Synthesis route to Janus face alkylbromide **109**.[22]

Synthesis of PEG-phenol **238** (Scheme 4.5) was carried out in a similar manner to that described in Scheme 3.7 (Chapter 3.2.2).[23,24]

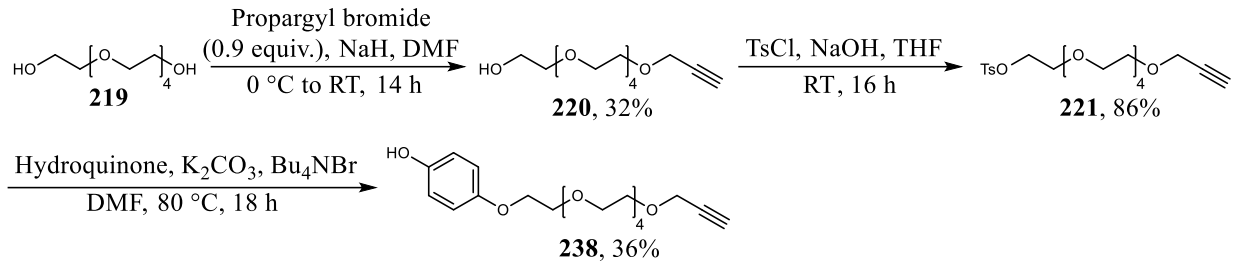

Scheme 4.5: Synthesis route to PEG linker **238**.[23,24]

Mono-alkylation of glycol **219** gave propargyl ether **220**. The terminal alcohol was activated by tosylation to give **221,** and then a substitution reaction with hydroquinone gave the PEG substituted free phenol **238**. Finally, 5'chloro-iodoadenosine **236** was required to be prepared (illustrated in Scheme 4.6). The route was previously established in St Andrews and was followed without any significant modifications.[16,25]

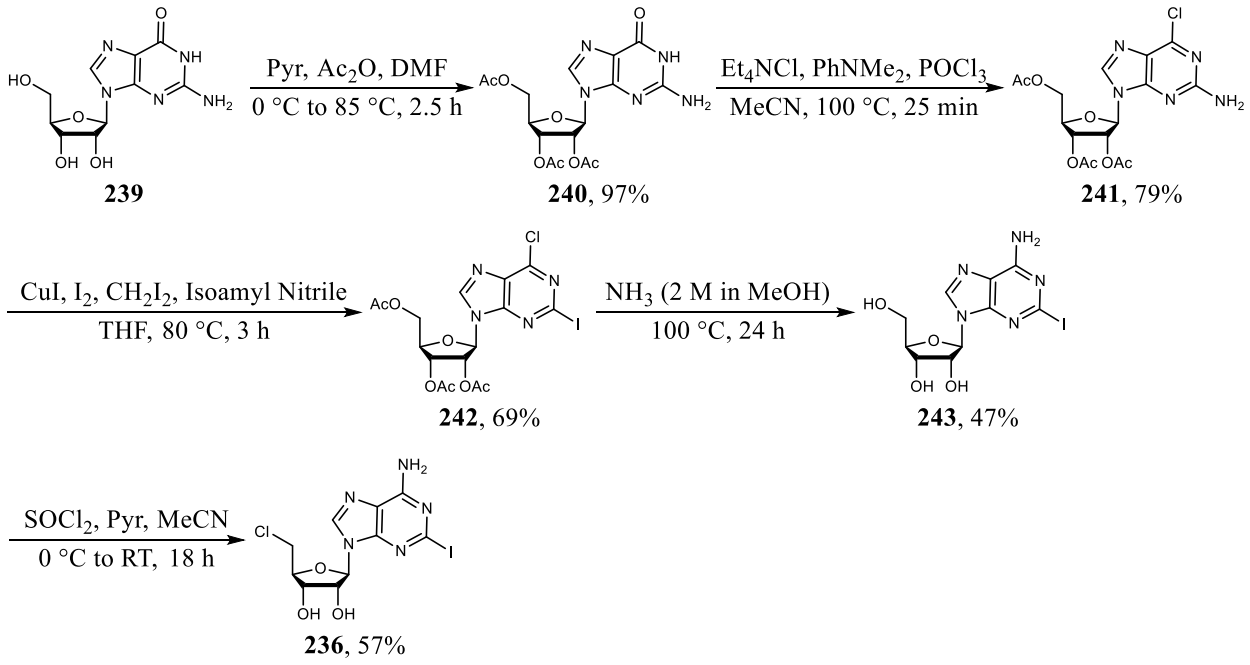

Scheme 4.6: Synthesis route to 5'chloro-iodoadenosine **236**.[16,25]

Guanosine **239** was first acylated, using acetic anhydride, to give guanine **240**, in order to protect the free hydroxyl groups from interfering with the following steps. The carbonyl of the purine was then chlorinated to generate **241**. The free amine of the purine was then converted to the corresponding iodide using a protocol described by Nair and Richardson *via* free radical iodination.[26] This generated purine **242**. Nucleophilic aromatic substitution with ammonia at C6 was accompanied by a simultaneous deprotection of the acetyl groups, to give iodoadenosine **243**. Finally, thionyl chloride was used to convert the primary alcohol of iodoadenosine **243** to a chloromethyl group generating 5'-chloro-iodoadenosine **236**.

With the three desired building blocks in hand, work commenced towards linking them together. First, a substitution reaction between alkylbromide **109** and PEG phenol **238** was conducted as illustrated in Scheme 4.7.

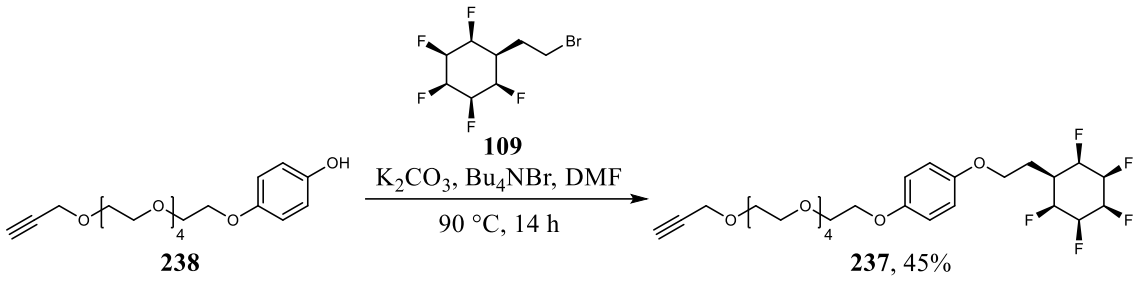

Scheme 4.7: Combination of phenol **238** and alkylbromide **109** to generate PEG-Janus **237**.

The synthesis of PEG-Janus **237** was achieved in a similar manner. The potassium hydrogen carbonate base did not cause any defluorination of the Janus cyclohexane, however, the modest yield suggests that the phenol was not an ideal nucleophile for this substitution reaction. Finally, a Sonogashira cross coupling reaction between PEG-Janus **237** and ClDEA **236** was explored as illustrated in Scheme 4.8 following the conditions reported for related reactions.[16,25]

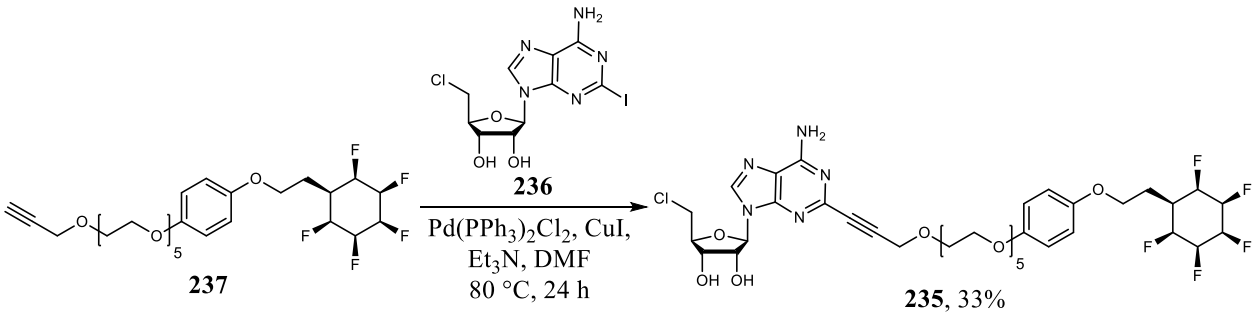

Scheme 4.8: Synthesis of ClDEA-PEG-Janus **235** from PEG-Janus **237** *via* Sonogashira cross coupling.[25]

Purification of the product ClDEA-PEG-Janus **235** proved challenging, and the product could not be recovered after flash column chromatography. In an attempt to resolve this issue, purification was explored by semi-prep HPLC. This required reverse phase chromatography, however, the product was poorly soluble in acetonitrile/water. This also suggested that this compound would be a challenging substrate for fluorinase enzyme reactions if its aqueous solubility was poor.

Accordingly, a revision was made in order to design a more aqueous soluble ClDEA-PEG-Janus substrate but retaining a biorthogonal PEG linker. It appeared that the phenol residue, whilst offering a good linker strategy, was conferring lipophilicity on **235**. Thus, a new ClDEA-PEG-Janus target **244** was designed which utilized a triazole group in place of the phenol in an effort to increase water solubility (Scheme 4.9).

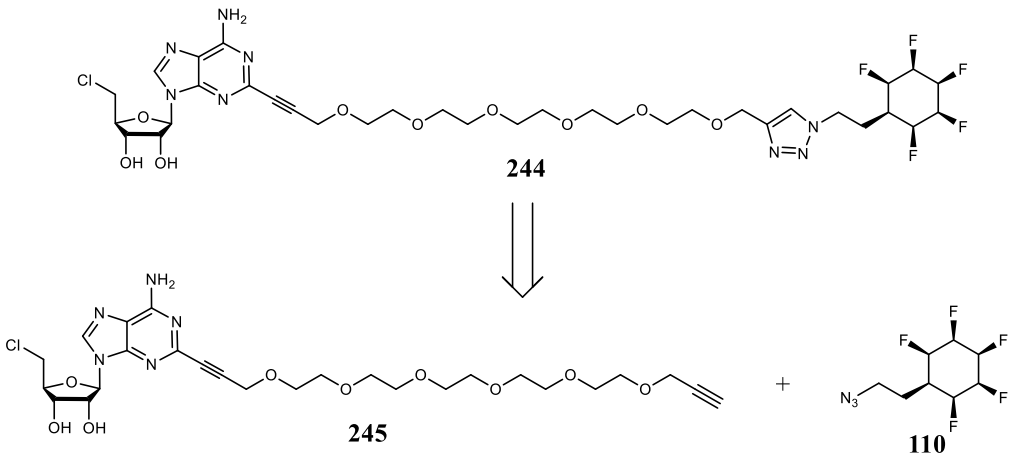

Scheme 4.9: Reterosynthetic analysis of second generation ClDEA-PEG-Janus **244**.

It was envisaged that the new target **244** could be synthesised by linking together a terminal acetylene of a ClDEA-PEG chain **245** with a Janus ring containing azide **110**, utilizing CuAAC click chemistry to combine them. The synthesis of ClDEA-PEG-Janus **244** would require only a minor modification to the original synthesis route (see Scheme 4.3) and would also use previously prepared building blocks.

The synthesis commenced with the assembly of the ClDEA-PEG unit **245** and again used Sonogashira chemistry, however, to avoid addition of ClDA **236** to both terminal acetylenes, one end of the chain required protection. The approach taken to the desired PEG unit **247** is illustrated in Scheme 4.10.[27]

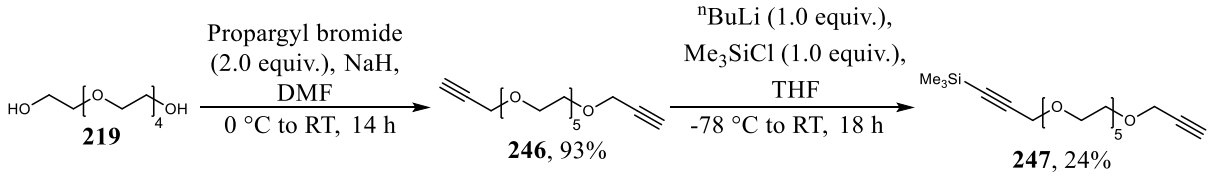

Scheme 4.10: Monoprotection to generate PEG **247**.[27]

Using previously described reaction conditions (see Scheme 4.5), glycol **219** underwent a dialkylation to generate diacetylene **246**. Limiting conditions were selected to try to only achieve a single alkylation, however the product mixture also contained starting material and some di-silylated product. Purification by chromatography of this mixture proved challenging, as the difference in polarity between the mono- and di-silylated products was low, however after repeated chromatography the mono-protected PEG **247** was isolated, but in a modest 24% yield.

Sonogashira coupling of ClDA unit **236** and the mono-protected PEG chain **245** was carried as previously reported and as illustrated in Scheme 4.11.[25]

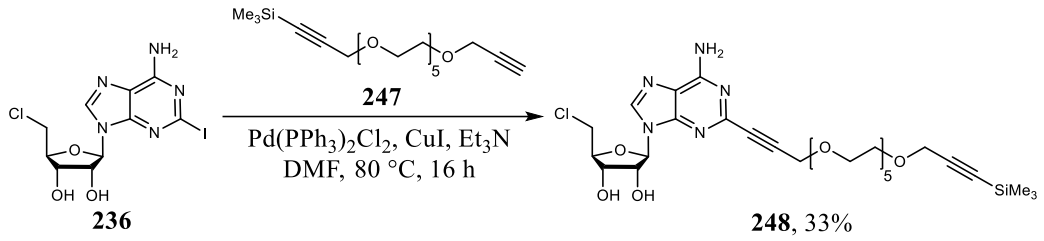

Scheme 4.11: Synthesis of ClDEA-PEG **248**.[25]

The reaction proceeded without evidence of any bis-acetylene coupling and the product was successfully purified by chromatography. With the ClDEA-PEG unit **248** at hand, attention turned to preparation of the Janus azide coupling partner **110**. This involved treating alkyl bromide **109** with sodium azide as illustrated in Scheme 4.12.[28]

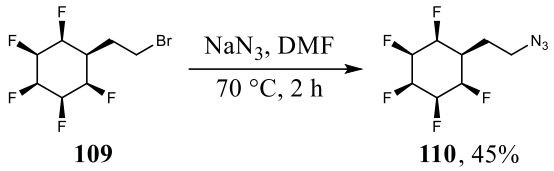

Scheme 4.12: Synthesis of Janus azide **110**.[28]

Finally, a click' reaction between azide **110** and ClDEA-PEG **248** was required to complete synthesis of target **244**. The approach involved deprotection and then a direct CuAAC without purification, to minimise any loss of product **248** during purification. The telescoped reaction is illustrated in Scheme 4.13.

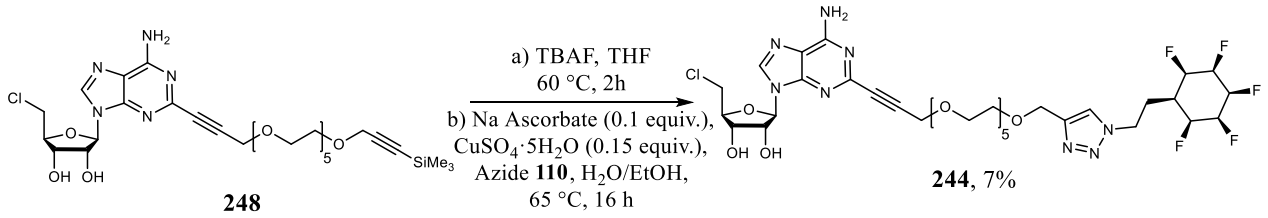

Scheme 4.13: Synthesis of ClDEA-PEG-Janus **244**.

The silyl deprotection used tetra-*n*-butylammonium fluoride (TBAF) as a source of a fluoride ion. After TBAF treatment the reaction was concentrated *in vacuo* and was then taken directly to the click reaction, with Janus azide **110**. The reaction was monitored by TLC, and upon completion, was purified by HPLC. Five milligrams of the final product **244** was isolated by HPLC elution, giving an indication that this product was at least partially soluble in water.

With the synthesis of a water-soluble Janus fluorinase substrate **244** in hand, attention turned to the preparation of FDEA **253**. This was required as a reference compound to confirm the identity of the product of enzymatic fluorination. The synthesis of FDEA **253**, is illustrated in Scheme 4.14.[16]

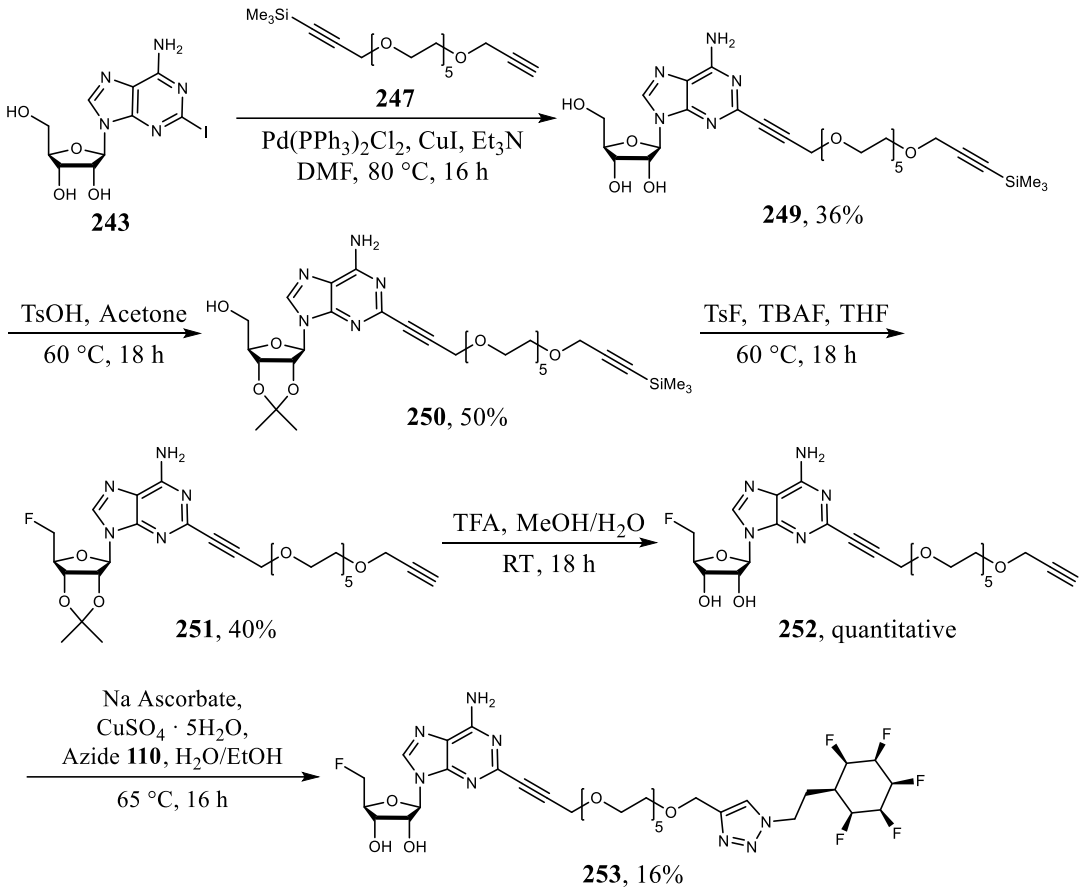

Scheme 4.14: Synthesis of FDEA **253**.[16]

Although FDEA **253** only differs from ClDEA **244** in terms of the halogen, the route is significantly longer. This compound had been prepared before in the research group from iodoadenosine **243** in five steps.[16] An initial Sonogashira cross coupling of iodoadenosine **243** with mono-silylated PEG chain **247** gave PEGylated adenosine **249**. In order to ensure only the primary alcohol is fluorinated, the adjacent secondary alcohols were protected in the form of acetal **250**. Activation of the alcohol with tosyl fluoride and treatment with TBAF then generated 5'-fluoroadenosine-PEG **251**. Acetal deprotection used acidic methanol/water, to give FDEA-PEG **252**, and this product was coupled with Janus azide **110** to generate the desired product **253**.

4.2.2 – "Cold" enzymatic fluorination

With both the fluorinase substrate ClDEA-PEG-Janus **244** and the accompanying reference product **253** in hand, attention turned to the enzymatic fluorination reaction. To test the fluorinase enzyme's tolerance to the Janus motif, ClDEA-PEG-Janus **244** was first explored in a "cold" enzymatic fluorination, with fluoride-19. A successful transformation here is required before enzymatic experiments with "hot" radioactive ^{18}F-fluoride could take place. The reaction conditions for the cold enzymatic fluorination reaction are detailed below (Table 4.2).

Table 4.2: Reaction conditions for cold enzymatic fluorination of ClDEA-PEG-Janus **244**.

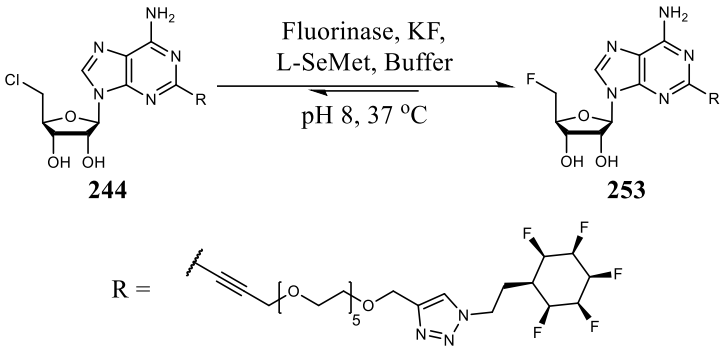

	Experiment		Control	
	Vol (µL)	**Conc (mM)**	**Vol (µL)**	**Conc (mM)**
Substrate 244 (1 mM)	30	0.2	0	-
5'-ClDEA (4 mM)	0	-	30	0.2
Fluorinase (370 µM)	80	0.05	80	0.05
Potassium Fluoride (0.5 M)	96	80	96	80
L-SeMet (2 mM)	30	0.1	30	0.1
Tris Phosphate Buffer (50 mM)	464	50	464	50
Total Vol	700	-	700	-

The cold fluorinase reaction was monitored by HPLC. Figure 4.4 shows the stacked HPLC traces taken from the reaction at time points between 0 h and 24 h.

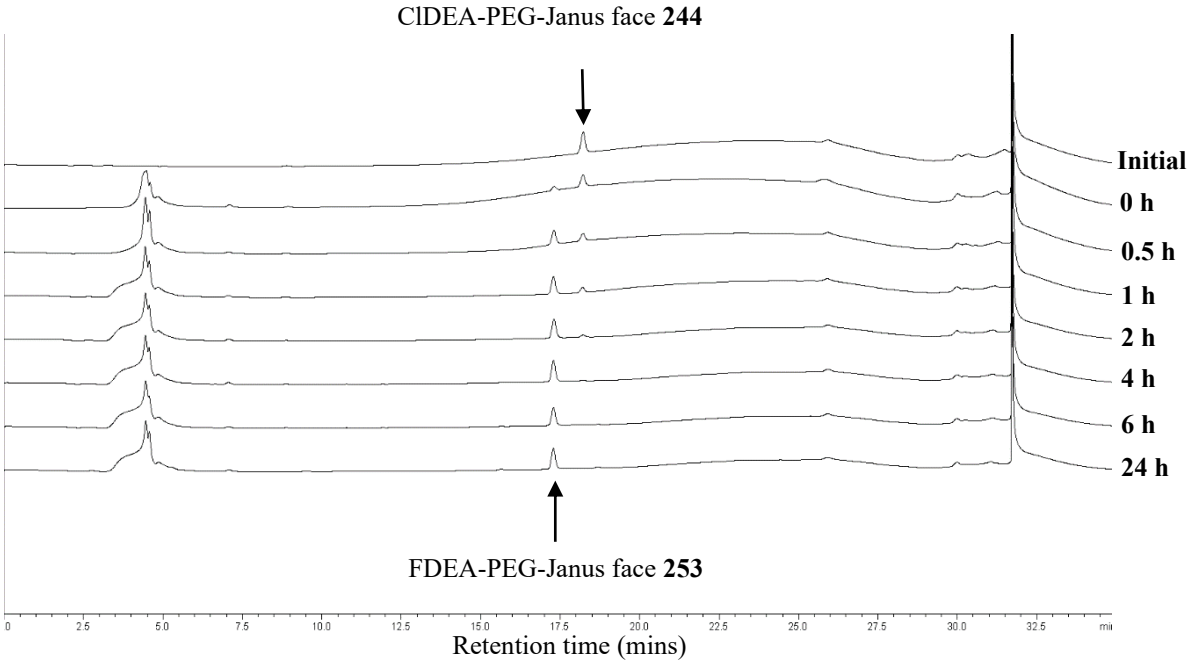

Figure 4.4: Time course showing stacked HPLC traces for enzymatic fluorination of ClDEA-PEG-Janus **244** over 24 h.

Figure 4.4 indicates a complete conversion of ClDEA-PEG-Janus **244** to FDEA-PEG-Janus **253** after 6 h under these conditions. The first HPLC trace (initial) was taken before the addition

of fluorinase to the reaction and did not show the presence of any FDEA-PEG-Janus **244**, however, the second HPLC trace (0 h) taken moments after fluorinase addition indicates the immediate presence of FDEA-PEG-Janus **253**. After 0.5 h, over half of the ClDEA-PEG-Janus substrate **244** had been converted, and at 6 h it appears that there is no substrate **244** left. The HPLC trace taken at 24 h coincided with the HPLC trace of the synthesised reference **253** (data not shown), which in conjunction with HRMS, validated the new peak as FDEA-PEG-Janus **253**. This experiment demonstrates that fluorinase tolerates the ClDEA-PEG-Janus **244** as a substrate.

4.2.3 –^{18}F Fluorination of the Janus probe

Having established that **244** is a suitable substrate, attention was now directed towards a hot enzymatic fluorination of ClDEA-PEG-Janus **244**. In collaboration with Dr Sergio Dall'Angelo, radiolabelling work was conducted at the John Mallard PET Centre in Aberdeen based at the Royal Infirmary and associated with the University of Aberdeen. Table 4.3 details the reaction conditions used for the ^{18}F enzymatic fluorination of ClDEA-PEG-Janus **244**.

Table 4.3: Reaction conditions for hot enzymatic radiolabelling of ClDEA-PEG-Janus **244**.

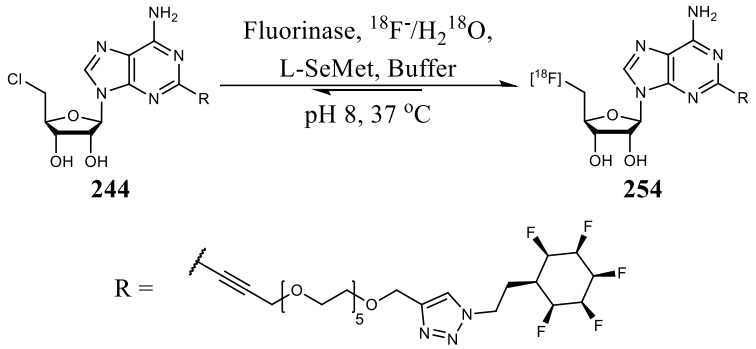

	Volume/µL	Assay Concentration
Substrate 244	50	9.6 mM
Fluorinase	-	5 mg
$^{18}F^-/H_2{}^{18}O$	50	205 mBq
L-SeMet	40	2 mM
Tris Phosphate Buffer	60	50 mM
Total Volume	200	-

The amount of substrate **244** used for the hot radiolabelling experiment is nearly 20-fold of that used in the radiolabelling experiment. This, paired with the excess of fluorinase over ^{18}F fluoride ions, will allow for maximum uptake of the available ^{18}F-fluoride, and should improve the conversion rate. Once the reaction was conducted, an HPLC radio-trace was taken after 30

minutes. Figure 4.5 shows the HPLC radio-trace from the hot fluorination and the HPLC trace of the FDEA-PEG-Janus reference **253**.

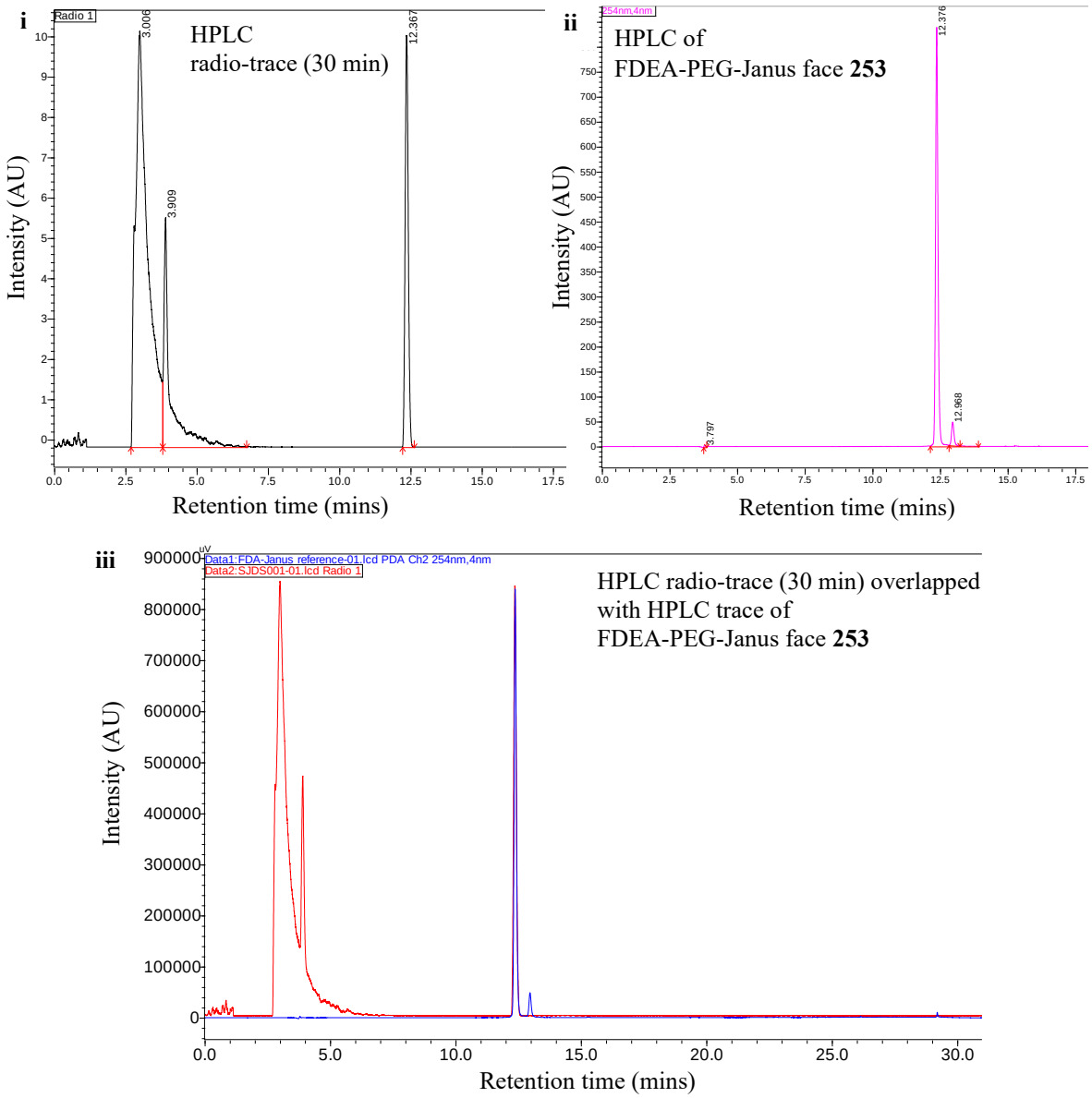

Figure 4.5: i) HPLC radio-trace take from hot fluorinase reaction after 30 min. **ii)** HPLC trace of FDEA-PEG-Janus **253**. **iii)** Overlap of both HPLC traces.

The HPLC radio-trace taken from the hot fluorination after 30 mins coincided with the HPLC retention time for the FDEA-PEG-Janus reference **253** and is consistent with [^{18}F]FDEA-PEG-Janus **254** being generated as a product of the fluorinase reaction.

A HPLC radio-trace was recorded from the hot fluorination reaction again after 60 min. The intensity of the peak corresponding to [^{18}F]FDEA-PEG-Janus **254** had dropped significantly, due to the decay of ^{18}F ($t_{1/2}$ = 110 min). The reaction was stopped at this point, and the conversion was calculated from the radio-trace taken at 30 min. By measuring the area under the peak of interest, the conversion was calculated to 17% (uncorrected). In order to correct for radioactive decay, Equation 4.1 was used.[29]

$$A_t = A_0\, e^{-\lambda t} \qquad 4.1$$

Where A_0 is the original activity at time 0, A_t is the activity after the elapsed time; t (30 min for this experiment), and λ is the decay constant, calculated by Equation 4.2.

$$\lambda = \frac{\ln (2)}{t_{1/2}} \qquad 4.2$$

Where $t_{1/2}$ is the half-life of the isotope used, in this case 109.8 mins. When substituting the known values (A_t = 0.17, t = 30 min, λ = 6.35 × 10^{-3} min^{-1}), the original activity at time 0 is calculated to be 0.21, giving a decay corrected conversion of 21%.

4.2.4 – Synthesis of c(RGDfK)-Janus probe

With [^{18}F]FDEA-PEG-Janus **254** in hand, work began on the synthesis of the counterpart probe A (see Figure 4.3). The retrosynthetic analysis used for the assembly of the first c(RGDfK)-Janus probe **255** is illustrated in Scheme 4.15.

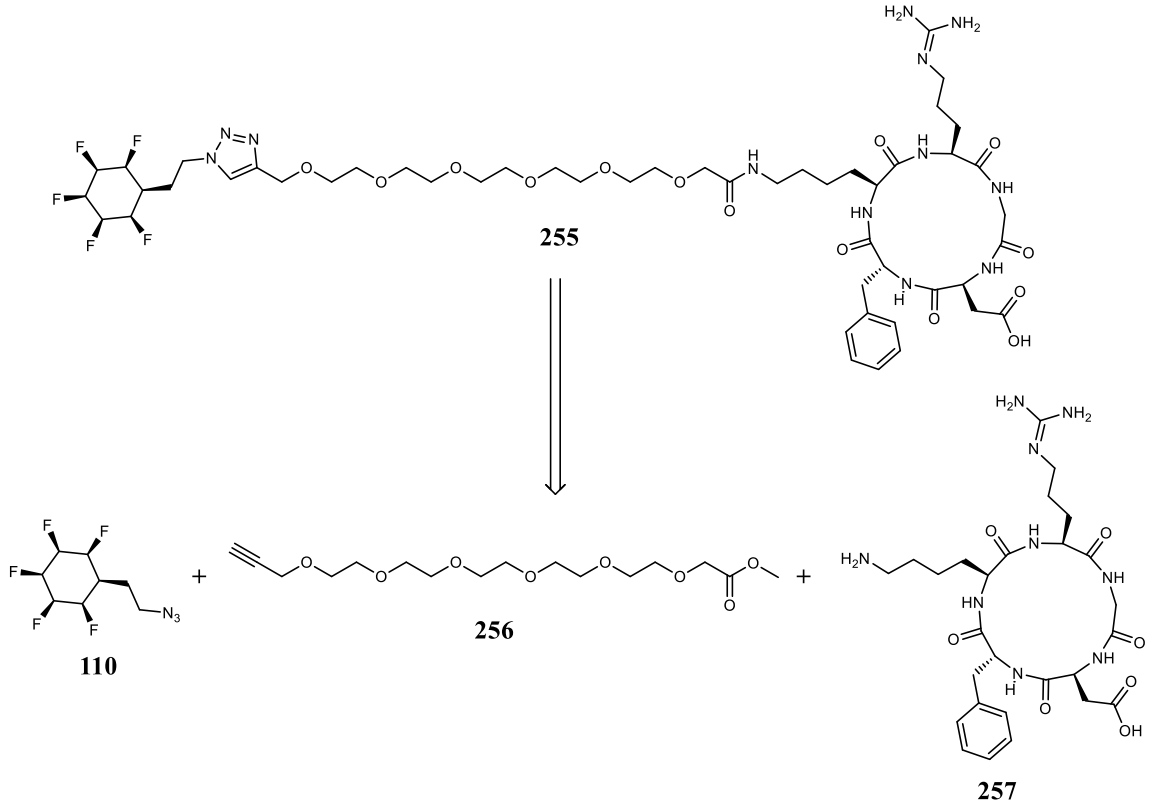

Scheme 4.15: Retrosynthetic analysis for the assembly of c(RGDfK)-Janus probe **255**.

It was envisaged that the probe could be synthesised from three building blocks. These were the Janus azide **110**, the PEG ester **256**, and commercially available c(RGDfK) peptide **257**. The synthesis of PEG **256** is detailed in Scheme 4.16.

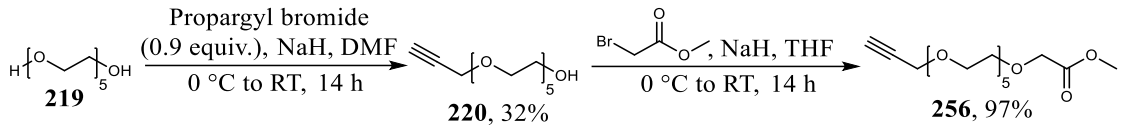

Scheme 4.16: Synthesis of PEG methyl ester **256**.

Accordingly, glycol **219** was mono-alkylated with propargyl bromide to give alkyne **220**. The alkyne was then alkylated with methyl bromoacetate through the residual alcohol moiety to generate the extended methyl ester **256**. The linking of the three building blocks is illustrated in Scheme 4.17 (for synthesis of azide **110**, see Scheme 4.12).

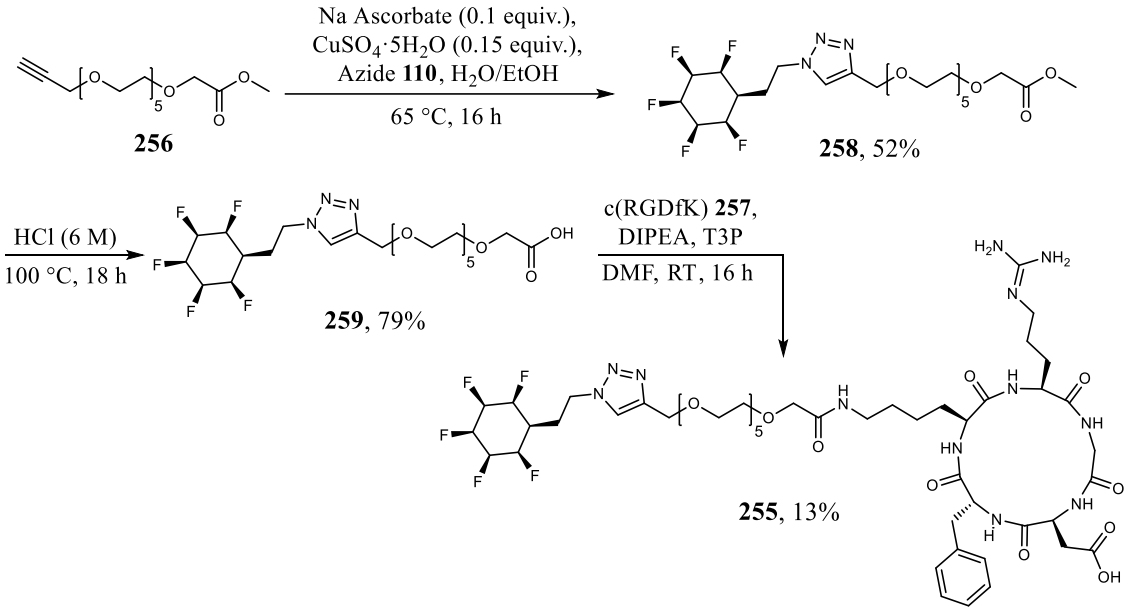

Scheme 4.17: Synthesis of Janus-c(RGDfK) **255**.

A click CuAAC reaction between azide **110** and alkyne **256** gave Janus-PEG **258**. This product was then hydrolysed using forcing acidic conditions to generate carboxylic acid **259**. Finally, the c(RGDfK) peptide **257** was coupled through its free amine, to carboxylic acid **259**, to generate the target probe **255**. Finally, the product was purified by HPLC to give **255** in a 13% isolated yield.

A control molecule which possessed an aliphatic cyclohexane ring in place of the Janus cyclohexane **264** was also synthesised. The route is outlined in Scheme 4.18.

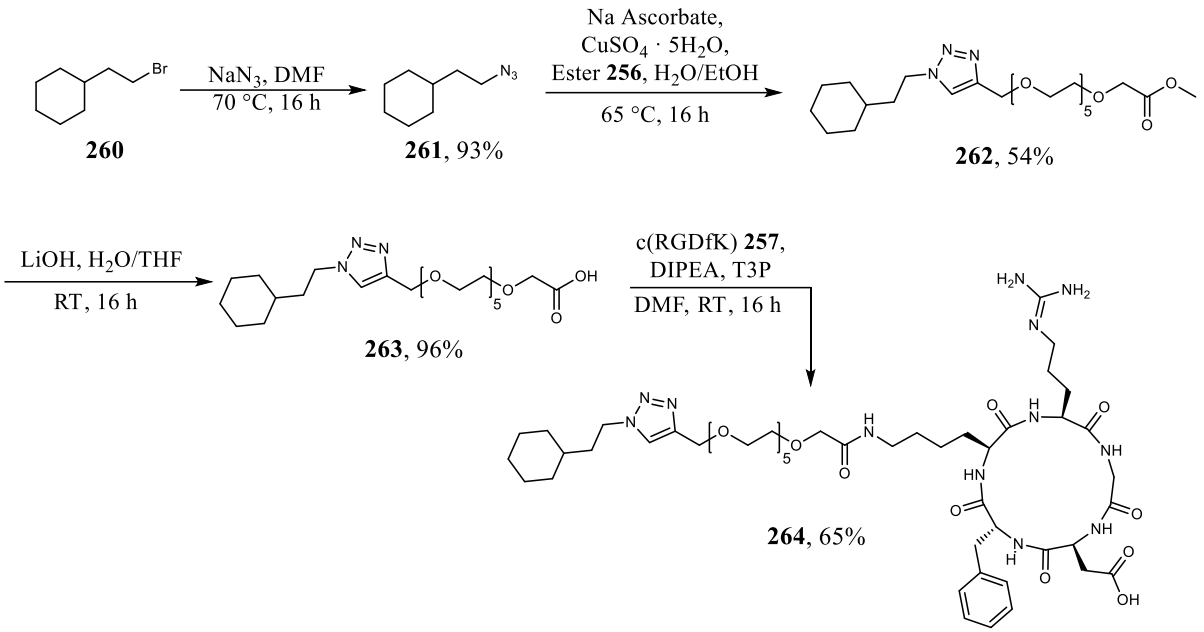

Scheme 4.18: Synthesis of control probe **264**.

This synthesis was accomplished in a similar manner to that of **255**. Thus, bromo-cyclohexane **260** was converted to azide **261**, and this product was then clicked with alkyne **256** to generate ester **262**. Hydrolysis of the methyl ester with lithium hydroxide gave carboxylic acid **263**, which was again coupled to the c(RGDfK) peptide **257** through the amine moiety, to give the desired product **264**.

Janus-PEG-c(RGDfK) probe **255** was synthesized over 10-steps, and a saturated cyclohexane control **264** over 6-steps. These two probes can now be used in experiments with $\alpha v\beta_3$ receptor expressing cells, such as the experiment detailed in Figure 4.3. This constitutes an ongoing collaboration between St Andrews and the University of Aberdeen.

4.3 – Conclusions

In this chapter, a 13-step synthesis campaign was undertaken to prepare the ClDEA-PEG-Janus fluorinase substrate **244**. A 15-step synthesis was required to prepare the FDEA-PEG-Janus reference **253**. The ClDEA-PEG-Janus precursor **244** emerged as a successful substrate for the fluorinase enzyme, demonstrating that the enzyme will accept this rather unusual substrate. This opens up the prospects of radiolabelling Janus ring probes for future chemical biology studies. A radiolabelling experiment was demonstrated using $^{18}F^-/H_2{}^{18}O$ and the product was generated in 21% (decay corrected) conversion.

4.4 – References

1 D. K. Leung and R. L. Van Heertum, *Semin. Nucl. Med.*, 2009, **39**, 195–203.

2 K. Lameka, M. D. Farwell and M. Ichise, *Handbook of Clinical Neurology*, ed. J. C. Masdeu and R. G. González, Elsevier, Amsterdam, 1st edn, 2016, vol. 135, ch. 11, pp. 209–227.

3 S. Purser, P. R. Moore, S. Swallow and V. Gouverneur, *Chem. Soc. Rev.*, 2008, **37**, 320–330.

4 M. Kapoor and A. Kasi, *StatPearls*, StatPearls Publishing, Treasure Island, FL, 2023.

5 S. L. Pimlott and A. Sutherland, *Chem. Soc. Rev.*, 2011, **40**, 149–162.

6 A. J. Palmer, J. C. Clark and R. W. Goulding, *Int. J. Appl. Radiat. Isot.*, 1977, **28**, 53–65.

7 O. Jacobson, D. O. Kiesewetter and X. Chen, *Bioconjugate Chem.*, 2015, **26**, 1–18.

8 C. Vito, T. Ido, A. P. Wolf, J. S. Fowler, R. R. MacGregor and T. J. Ruth, *J. Nucl. Med.*, 1980, **21**, 750–757.

9 E. L. Cole, M. N. Stewart, R. Littich, R. Hoareau and P. J. H. Scott, *Curr. Top. Med. Chem.*, 2014, **14**, 875–900.

10 F. Sobrio, *J. Label. Compd. Radiopharm.*, 2013, **56**, 180–186.

11 J. Ajenjo, G. Destro, B. Cornelissen and V. Gouverneur, *EJNMMI Radiopharm. Chem.*, 2021, **6**, 33.

12 J. S. Fowler and T. Ido, *Semin. Nucl. Med.*, 2002, **32**, 6–12.

13 B. M. Gallagher, A. Ansari, H. Atkins, V. Casella, D. R. Christman, J. S. Fowler, T. Ido, R. R. MacGregor, P. Som, C. N. Wan, A. P. Wolf, D. E. Kuhl and M. Reivich, *J. Nucl. Med.*, 1977, **18**, 990–996.

14 A. R. Braun, R. E. Carson, H. R. Adams, R. D. Finn, B. E. Francis and P. Herscovitch, *Nucl. Med. Biol.*, 1994, **21**, 857–863.

15 K. Hamacher, H. H. Coenen and G. Stöcklin, *J. Nucl. Med.*, 1986, **27**, 235–238.

16 S. Thompson, Q. Zhang, M. Onega, S. McMahon, I. Fleming, S. Ashworth, J. H. Naismith, J. Passchier and D. O'Hagan, *Angew. Chem., Int. Ed.*, 2014, **53**, 8913–8918.

17 D. O'Hagan, C. Schaffrath, S. L. Cobb, J. T. G. Hamilton and C. D. Murphy, *Nature*, 2002, **416**, 279–279.

18 L. Yin, X. Li, R. Wang, Y. Zeng, Z. Zeng and T. Xie, *Int. J. Pept. Res. Ther.*, 2023, **29**, 53.

19 B. M. Dicheva, T. L. M. ten Hagen, A. L. B. Seynhaeve, M. Amin, A. M. M. Eggermont and G. A. Koning, *Pharm. Res.*, 2015, **32**, 3862–3876.

20 X. Li, N. Yu, J. Li, J. Bai, D. Ding, Q. Tang and H. Xu, *ACS Appl. Mater. Interfaces*, 2020, **12**, 10096–10106.

21 W. Lin, G. Ma, Z. Yuan, H. Qian, L. Xu, E. Sidransky and S. Chen, *Langmuir*, 2019, **35**, 1273–1283.

22 J. L. Clark, A. Taylor, A. Geddis, R. M. Neyyappadath, B. A. Piscelli, C. Yu, D. B. Cordes, A. M. Z. Slawin, R. A. Cormanich, S. Guldin and D. O'Hagan, *Chem. Sci.*, 2021, **12**, 9712–9719.

23 J. Diot, M. I. García-Moreno, S. G. Gouin, C. O. Mellet, K. Haupt and J. Kovensky, *Org. Biomol. Chem.*, 2008, **7**, 357–363.

24 R. Zamboni, R. Henning, A. Ji, T. Smith, B. Heller, T. J. Reddy, S. Rocheleau, M. A. Beaulieu, US Pat. 15 965 506, 2018.

25 S. Thompson, I. N. Fleming and D. O'Hagan, *Org. Biomol. Chem.*, 2016, **14**, 3120–3129.

26 V. Nair and S. G. Richardson, *J. Org. Chem.*, 1980, **45**, 3969–3974.

27 Z. Li, Y. Li, Y. Zhao, H. Wang, Y. Zhang, B. Song, X. Li, S. Lu, X.-Q. Hao, S.-W. Hla, Y. Tu and X. Li, *J. Am. Chem. Soc.*, 2020, **142**, 6196–6205.

28 J. L. Clark, R. M. Neyyappadath, C. Yu, A. M. Z. Slawin, D. B. Cordes and D. O'Hagan, *Chem. Eur. J.*, 2021, **27**, 16000–16005.

29 M. Dawood, X. Jiang and K. Schäfers, *Correction Techniques in Emission Tomography*, CRC Press, Boca Raton Fl, 2012.

Chapter 5

Novel A_{2A} receptor agonists

5.1 – Introduction

5.1.1 – Adenosine A_{2A} receptor

The adenosine A_{2A} receptor is a member of the G-protein-coupled receptor (GPCR) family,[1] the largest group of membrane proteins which are responsible for vision, olfaction, and taste.[2] GPCRs are characterised by seven membrane spanning α-helical segments separated by alternating intracellular and extracellular loop regions.[2] GPCRs are usually divided into five families based on their structural similarities; rhodopsin (family A) which is by far the largest family and the family to which the A_{2A} receptor belongs to, secretin (family B), glutamate (family C), adhesion, and Frizzled/Taste2.[3]

A_{2A} receptors are expressed in a multitude of important regions in the mammalian body, including but not limited to; leukocytes, blood pallets, spleen, lungs, brain, and heart.[4] The function of the A_{2A} receptor is complicated by the fact that the receptor physically associates to other unrelated G-protein-coupled receptors to form heterodimers and heterotrimers.[5] This in turn makes isolating the function of the A_{2A} receptor as a monomer, challenging. However, it is known that the A_{2A} receptor plays a role in vasodilation, blood vessel synthesis, indirect pathway of the basal ganglia (responsible for motor control), and inflammatory damage.[5] The structure of an A_{2A} receptor is shown in Figure 5.1, with the dotted lines representing the extent of the cell membrane.[6]

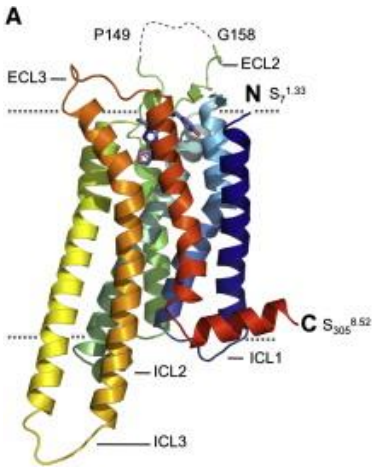

Figure 5.1: Structure of A_{2A} receptor coordinating to ZM-241,385, a high affinity agonist ligand of the A_{2A} receptor. Reprinted with permission from Elsevier.[6]

5.1.2 – A_{2A} Receptor agonists

Over the past decade A_{2A} receptors have been the focus of increasing interest due to their association with pathogenic, myocardial, and neurological diseases. Because of this, the receptor has become a therapeutic target for the treatment of numerous disorders, including insomnia, depression, CNS disorders, and Parkinson's disease.[7–9]

Structural activity relationships (SAR) of adenosine-based ligands have established a pharmacophore which is required for an A_{2A} receptor agonist to show activity.[10–12] Although modifications to the substituents of the adenosine core have resulted in ligands with increased affinity and selectivity, a core structural motif remains relatively constant. Figure 5.2 shows this pharmacophore and a selection of developed A_{2A} receptor agonists.[13]

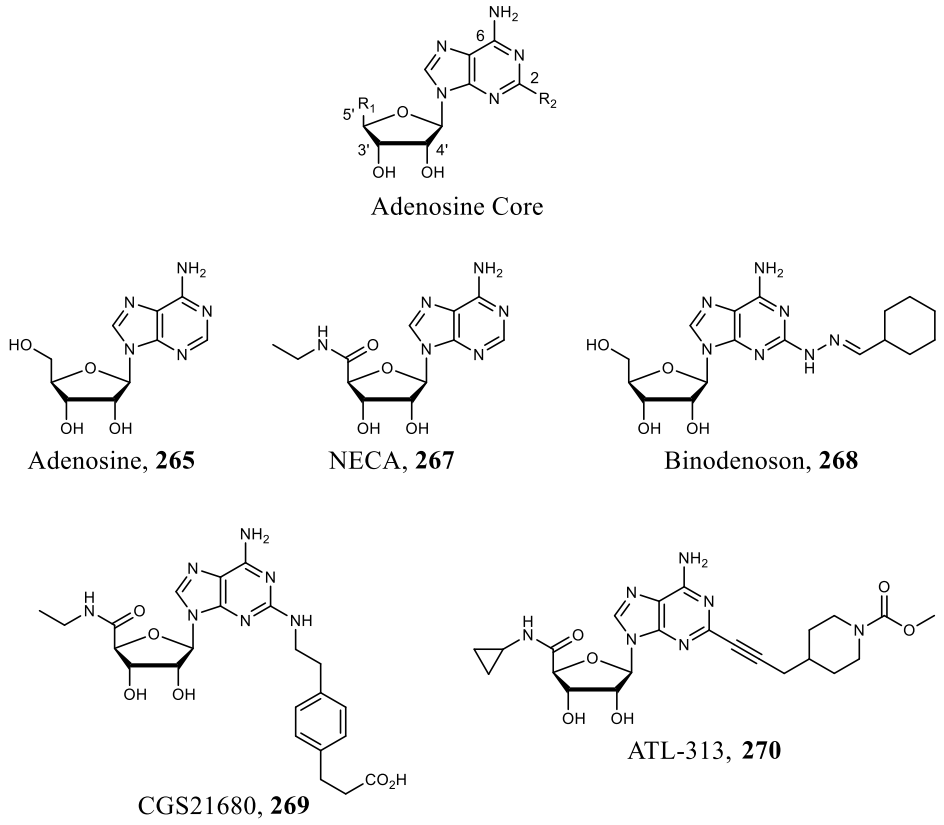

Figure 5.2: Examples of A_{2A} adenosine agonist ligands.[5,13]

The substituents which are most often modified are the 5' secondary alcohol (R_1) of the ribose and at C2 of the adenine ring (R_2). Retention of the 2',3'-diol from the ribose core is important in retaining agonist activity, whilst nitrogen substitution (C6) decreases A_{2A} receptor potency.[13]

5.2 – Aims and objectives

5.2.1 – Previous work in St Andrews

Previously in St Andrews a new class of fluorinated A_{2A} adenosine receptor agonists were developed; FDA-PP1 **271** and FDA-PP2 **272**.[13] They were designed around the previously

reported agonist ATL-313 **270** however there was a significant difference in that a 5'-fluoromethyl motif replaced the cyclopropane amide motif of ATL-313 **270**. This was not an obvious SAR change, but instead was driven by the desire to generate an agonist, or class of agonists, that had the potential to be radiolabelled directly with the fluorinase enzyme (see Chapter 4.2.2 for a similar protocol). Therefore a 5'chloromethyl-adenosine precursor was also required in the event the A_{2A} receptor affinity of 5'fluoromethyl-adenosine **271** or **272** was high. As a positive control, CGS26180 **269**, a clinically used agonist developed by GSK, was used, as illustrated in Figure 5.3.

The most active new agonist **271** could therefore be prepared directly from its chloromethyl analogue in a last step ^{18}F fluorination using the fluorinase enzyme. This opened up the prospect of accessing a novel agonist as a PET imaging agent, which could be conveniently prepared from ^{18}F-fluoride ions, as a product of a fluorinase reaction.[13]

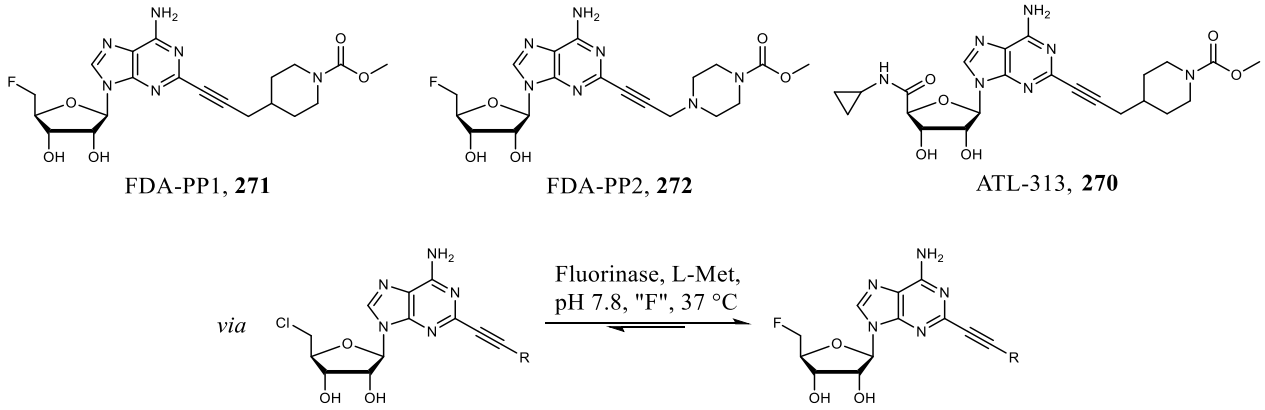

Scheme 5.1: Preparation of A_{2A} receptor agonists FDA-PP1 **271** and FDA-PP2 **272** *via* late stage enzymatic fluorination.[13]

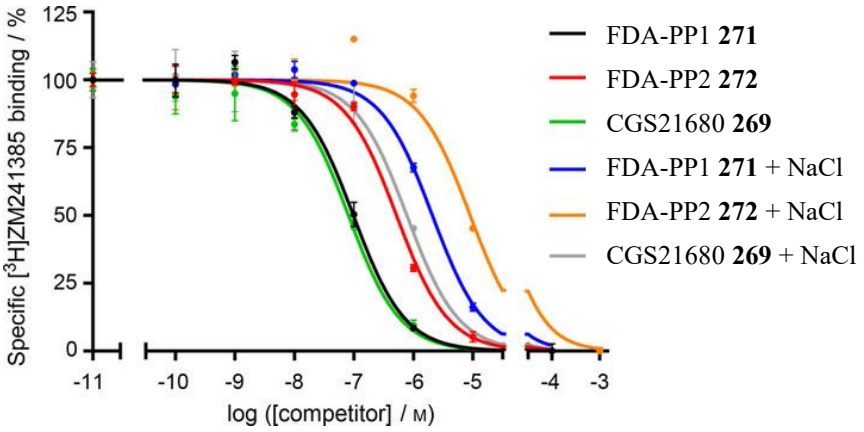

Ligand	pK_i ± SEM (without NaCl)	pK_i ± SEM (with NaCl)
FDA-PP1 **271**	7.42 ± 0.07	6.19 ± 0.02
FDA-PP2 **272**	6.76 ± 0.01	5.52 ± 0.06
CGS21680 **269**	7.43 ± 0.09	6.56 ± 0.07

Figure 5.3: Concentration-response curves for the action of FDA-PP1 **271** and FDA-PP2 **272** on HEK293 cell membranes expressing the A_{2A} receptor. Reprinted with permission from John Wiley and Sons.[13] *Copyright © 2017 Wiley-VCH Verlag GmbH & Co. KGaA, Weinheim.*

5.2.2 – Project Aims

The aim of this project was to design and prepare a potential A_{2A} receptor agonist which carried a Janus face motif. Pharmacokinetics indicate that the Janus cyclohexane lowers Log *P* relative to aliphatic motifs and thus such derivatives fulfil some basic lipophilicity criteria regarding drug design.[14] Additionally, no Janus cyclohexane containing compounds have been prepared and assessed as a bioactive; this would be the first investigation of the tolerance of a receptor-protein to this large polar motif.

5.3 – Results and discussion

5.3.1 – Synthesis of Janus face adenosines

Three initial Janus face A_{2A} receptor agonist candidates were envisioned as targets, as shown in Figure 5.4.

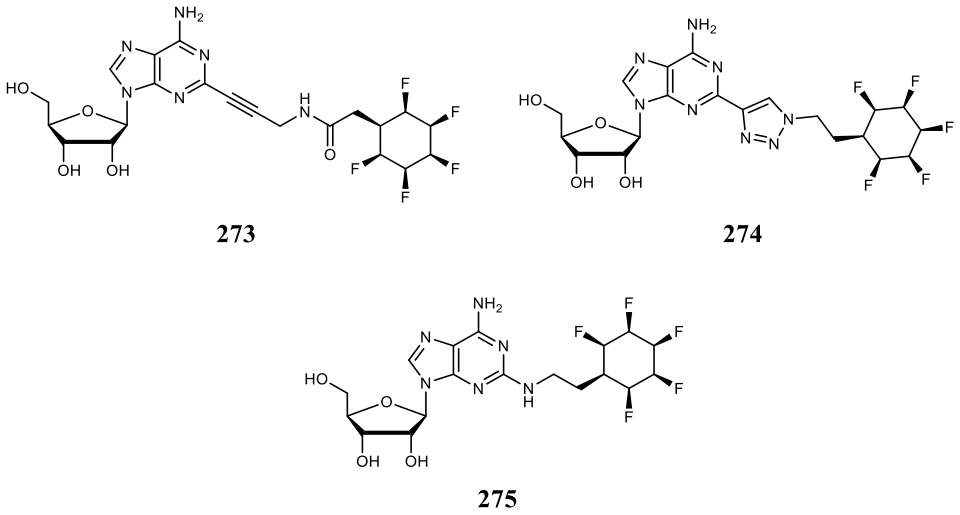

Figure 5.4: Candidate Janus face A_{2A} receptor agonists.

All three candidates possess the same active adenosine pharmacophore with a Janus cyclohexane attached to the core *via* different methods. These comprised of a Sonogashira coupling (to **273**), a [3+2] click cycloaddition reaction (to **274**), and a S_NAr reaction protocol (to **275**). It is anticipated that trialling agonist candidates with different linkers, to the adenosine core would allow exploration of what functional groups (with an adjacent Janus face motif) are tolerated by active site of the A_{2A} receptor, if any at all.

The first synthesis involved a Sonogashira cross coupling between alkyne **209** and iodoadenosine **243**. Accordingly, iodoadenosine was re-synthesised using the route described in Scheme 4.6.

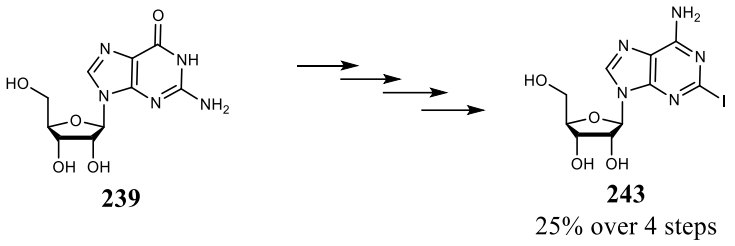

Scheme 5.2: Iodoadenosine **243** can be prepared in four steps from **239**.[13]

The Sonogashira cross-coupling between iodoadenosine **243** and alkyne **209** was accomplished in a 33% yield (Scheme 5.3).

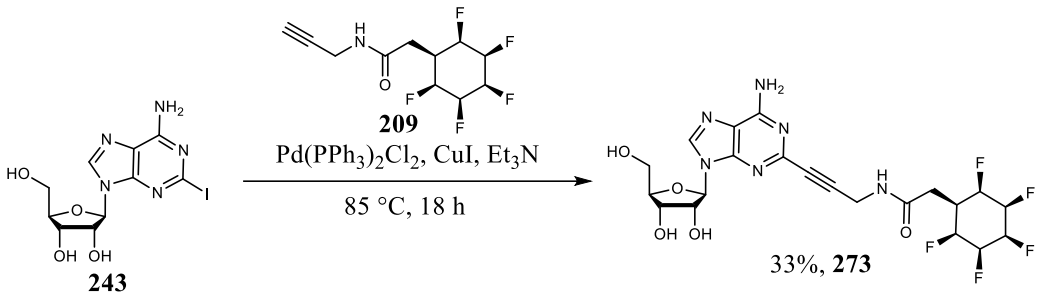

Scheme 5.3: Synthesis of A_{2A} receptor agonist candidate **273** *via* Sonogashira coupling.

Attention was then turned to synthesis of the triazole A_{2A} receptor agonist candidate **274**. A first approach to acetylene **273**, required as the click coupling partner, is illustrated in Scheme 5.4.

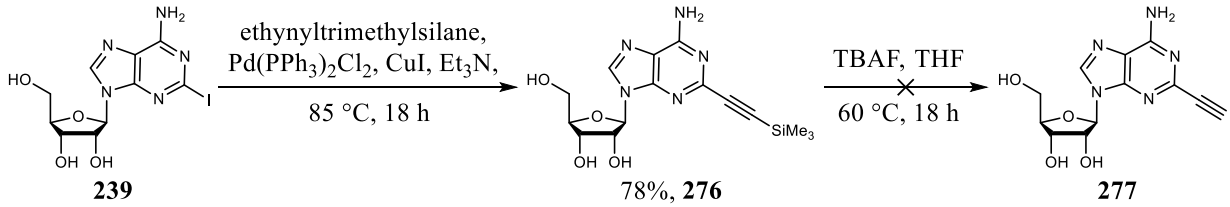

Scheme 5.4: Attempted synthesis of acetylene **277** from iodoadenosine **239**.

The silyl protected alkyl-adenosine **276** was prepared by a straightforward Sonogashira cross-coupling reaction with ethynyltrimethylsilane, however, attempts to remove the trimethylsilyl group using TBAF (60 °C) proved to be too harsh. Although silane hydrolysis was achieved, the anomeric C-N bond between the ribose and the adenine ring was also cleaved, leading to degradation of the product. Alternatively, treatment with ammonia successfully removed the trimethylsilyl protecting group, generating terminal alkyne **277** in nearly quantitative yield. With **277** in hand, the click reaction could be explored (Scheme 5.5).

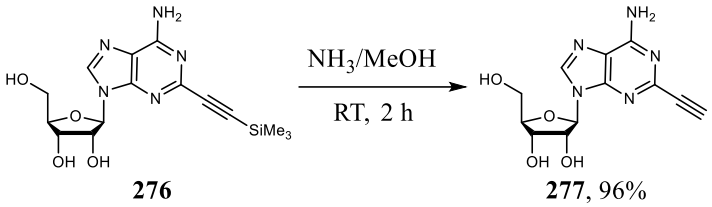

276 **277**, 96%

Scheme 5.5: Synthesis of alkyne **277**.

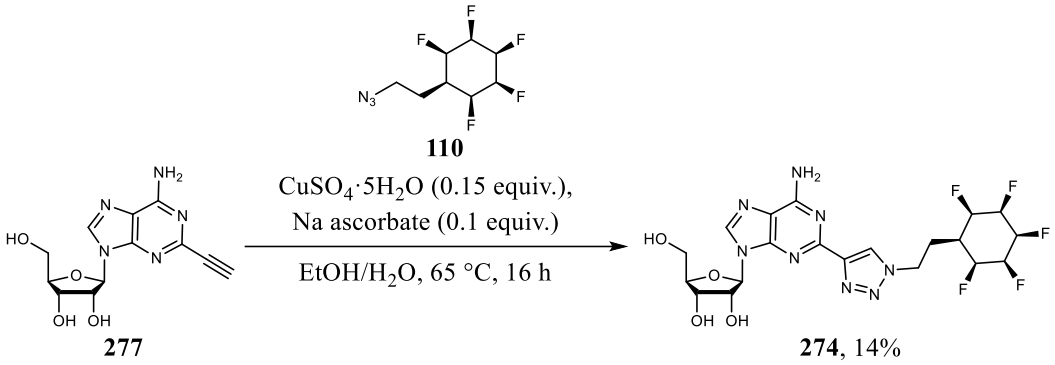

277 **274**, 14%

Scheme 5.6: Synthesis of A_{2A} receptor agonist candidate **274**.

A CuAAC reaction between the previously prepared Janus face azide **110** (see Scheme 3.6) and alkyne **277** gave the desired product **274** in a 14% yield.

Attention turned then to the synthesis of the last of the three targets **275**. First, a suitable Janus cyclohexane functionalised amine was prepared as the nucleophile for an S_NAr reaction with iodoadenosine **239**.

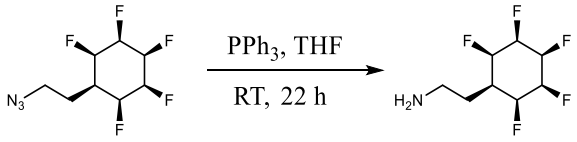

110 **111**, 66%

Scheme 5.7: Synthesis of amine **111**.

Azide **110** was reduced using triphenylphosphine to give amine **111** using a Staudinger protocol. This was accomplished in 66% yield as illustrated in Scheme 5.7. With amine **111** in hand, an initial S_NAr reaction with iodoadenosine **239** was explored (Scheme 5.8).

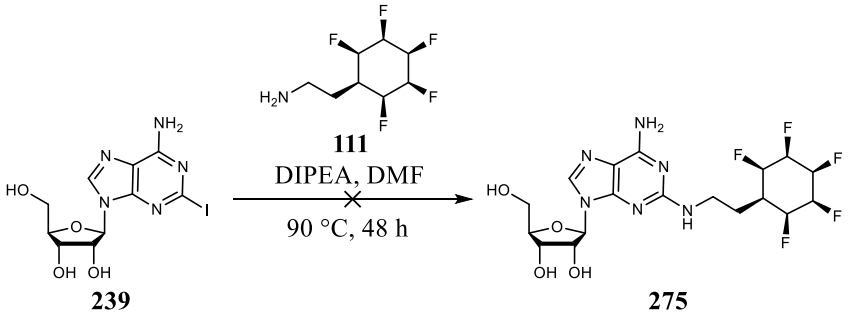

239 **275**

Scheme 5.8: Attempted synthesis of A_{2A} receptor agonist **275** from iodoadenosine **239**.

This S_NAr reaction used DIPEA as the base and DMF as the solvent, however, there was no evidence of product (by ^1H NMR spectroscopy), even when left for 48 h. There was no indication of any conversion of starting materials, suggesting that iodoadenosine **239** was not electrophilic enough to undergo the S_NAr reaction with amine **111**. Although iodine is considered to be a good leaving group in S_N2 reactions, this does not follow through to S_NAr reactions where the trend is often reversed (F > Cl > I). The reactions are promoted when the carbon is most electropositive because nucleophilic attack is rate limiting (for more information see Chapter 1.1.3).[15] With this in mind, chloroadenosine **278** was then explored as a substrate, and the reaction was carried out under similar conditions (Scheme 5.9).

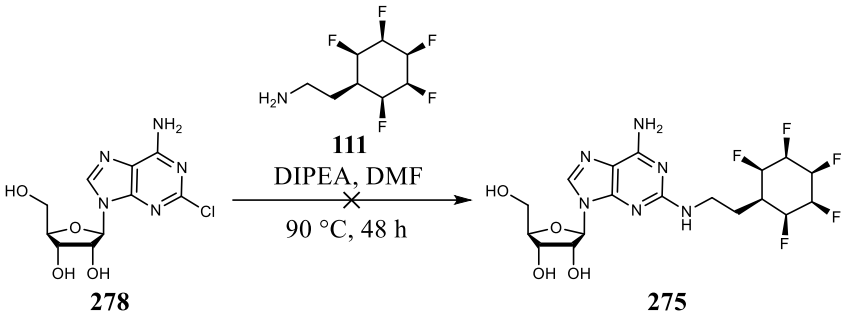

Scheme 5.9: Attempted synthesis of A_{2A} receptor agonist candidate **275** from chloroadenosine **278**.

Again, there was no apparent formation of product **275** and again no conversion of chloroadenosine **278**. In an attempt to force the reaction, other conditions were explored with higher temperatures and different solvents which have previously been described for the S_NAr of chloroadenosine **278** with a primary amine (summarised in Table 5.1).[16–18] However, these conditions proved unsuccessful too.

Table 5.1: Reaction conditions for the synthesis of A_{2A} receptor agonist candidate **275**. * Reaction was performed in a thick walled screw-cap sealed round bottom flasks.[16–18]

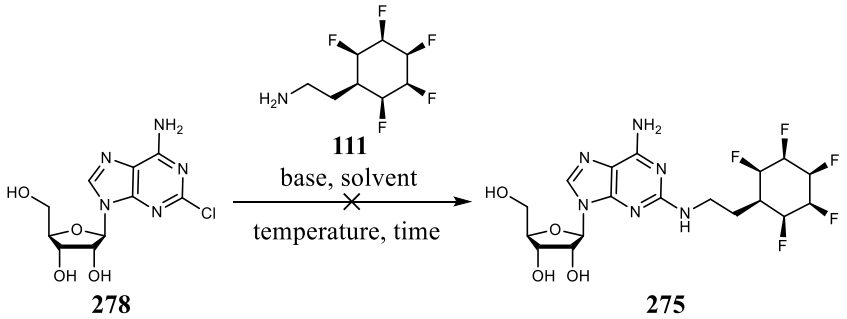

Entry	Base	Solvent	Time/h	Temperature	Yield
1	DIPEA	DMF	48	90 °C	0%
2	TEA	3-methylbutan-1-ol	48	150 °C	0%
3	DIPEA	Ethanol	48	120 °C*	0%

As the synthesis of A_{2A} receptor agonist candidate **275** proved unsuccessful, it was decided to move forward toward the assay with the two agonist candidates **273** and **274**.

5.3.2 – A_{2A} Receptor radioligand-displacement assay

The relative affinities of **273** and **274** for the A_{2A} receptor were evaluated using radioligand-displacement assays. The assays were conducted in a manner similar to the A_{2A} receptor agonists previously tested for ligands FDA-PP1 **271** and FDA-PP2 **272**. These assays were performed by the Heitman group at the University of Lieden in the Netherlands. In brief, human A_{2A} receptors were saturated with [^{3}H]ZM241385 **279**, a radiolabelled high affinity A_{2A} receptor antagonist ligand. The new A_{2A} receptor agonist candidates **273** and **274** were then introduced over a range of concentrations.

The assays were conducted both with and without sodium chloride, as the binding of a sodium ion to the allosteric site of the A_{2A} receptor stabilises the inactive conformation, reducing the binding of the agonists to the active site.[19] A reduction in the ligand affinity with high sodium chloride concentrations indicates that an agonist is binding to the active site and not an allosteric site.

As a positive control, the known agonist with high A_{2A} receptor affinity, CGS21680 **269**, was included in the assays (for more detail, see Chapter 7.11). Figure 5.5 shows the resulting titration curve from the preformed radioligand-displacement assays.

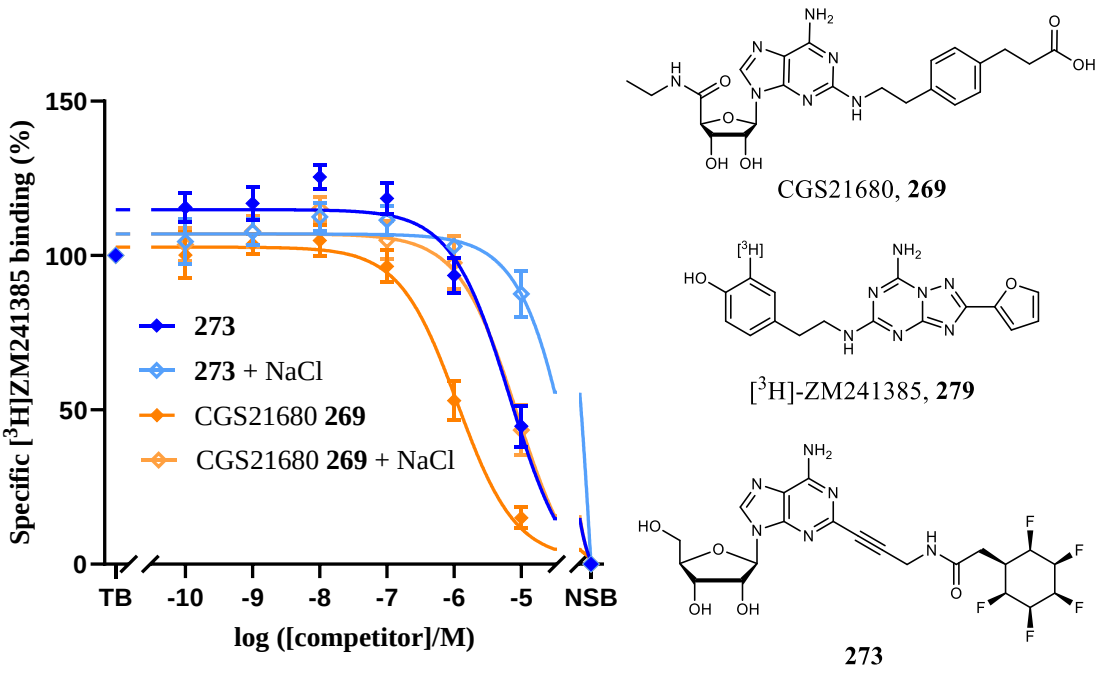

Figure 5.5: Resulting titration curve from radioligand-displacement assays of human A_{2A} receptors saturated with [^{3}H]ZM241385 against A_{2A} receptor agonist candidate **273**.

The resulting titration curve from Figure 5.5 illustrates that **273** displaces [^{3}H]ZM241385 from A_{2A} receptors at -7 log M ([**273**]), and then shows clear displacements with successive concentration increases. This indicates that **273** with a Janus cyclohexane, has a comparable affinity to agonist CGS21680 **269** for the human A_{2A} receptor. Also, the presence of 1 M NaCl decreased the affinity of **273** to above micromolar values, which is consistent with **273** acting as an active site binding agonists on the receptor.

Table 5.2: Comparison of A_{2A} receptor affinities between **273** and control agonist CGS21680 **269**.

Ligand	pK_i ± SEM (without NaCl)	pK_i ± SEM (with NaCl)
273	5.67 ± 0.12	3.79 ± 0.91
CGS21680 **269**	6.44 ± 0.08	5.57 ± 0.12

On the other hand, agonist candidate **274** did not show any displacement, suggesting very poor affinity for the A_{2A} receptor. Table 5.2 shows the respective binding affinities (pK_i) of Janus cyclohexane agonist **273** against the control CGS21680 **269**.

The Janus cyclohexane containing ligand **273** appears to possess only 10% less affinity when compared to the control CGS21680 **269** (without NaCl). However, when in the presence of NaCl, the affinity drops roughly by two orders of magnitude. These experiments showcase the first instance of a Janus face motif being incorporated into a drug like molecule, which show good levels of affinity for the target protein when compared to a control drug.

5.4 – Conclusions

Synthesis of two novel A_{2A} receptor agonist candidates containing a Janus cyclohexane motif, **273** and **274**, were synthesized *via* multistep synthesis pathways. The agonist candidate **273** was found to possess a good level of affinity for the A_{2A} receptor when compared to a known agonist with high affinity. This was determined using A_{2A} receptor radioligand-displacement assays. This study helps validate the potential for using the Janus face cyclohexyl motif in medicinal chemistry programmes for the discovery of new bioactives.

5.5 – References

1 F. Libert, M. Parmentier, A. Lefort, C. Dinsart, J. Van Sande, C. Maenhaut, M.-J. Simons, J. E. Dumont and G. Vassart, *Science*, 1989, **244**, 569–572.

2 D. M. Rosenbaum, S. G. F. Rasmussen and B. K. Kobilka, *Nature*, 2009, **459**, 356–363.

3 R. Fredriksson, M. C. Lagerström, L.-G. Lundin and H. B. Schiöth, *Mol. Pharmacol.*, 2003, **63**, 1256–1272.

4 B. Fredholm, A. Ijzerman, K. Jacobson, K.-N. Klotz and J. Linden, *Pharmacol. Rev.*, 2001, **53**, 527–552.

5 M. de Lera Ruiz, Y.-H. Lim and J. Zheng, *J. Med. Chem.*, 2014, **57**, 3623–3650.

6 A. S. Doré, N. Robertson, J. C. Errey, I. Ng, K. Hollenstein, B. Tehan, E. Hurrell, K. Bennett, M. Congreve, F. Magnani, C. G. Tate, M. Weir and F. H. Marshall, *Structure*, 2011, **19**, 1283–1293.

7 K. A. Jacobson and Z.-G. Gao, *Nat. Rev. Drug Discov.*, 2006, **5**, 247–264.

8 G. Haskó, J. Linden, B. Cronstein and P. Pacher, *Nat. Rev. Drug Discov.*, 2008, **7**, 759–770.

9 M. T. Armentero, A. Pinna, S. Ferré, J. L. Lanciego, C. E. Müller and R. Franco, *Pharmacol. Therap.*, 2011, **132**, 280–299.

10 S. Basu, D. A. Barawkar, S. Thorat, Y. D. Shejul, M. Patel, M. Naykodi, V. Jain, Y. Salve, V. Prasad, S. Chaudhary, I. Ghosh, G. Bhat, A. Quraishi, H. Patil, S. Ansari, S. Menon, V. Unadkat, R. Thakare, M. S. Seervi, A. V. Meru, S. De, R. K. Bhamidipati, S. R. Rouduri, V. P. Palle, A. Chug and K. A. Mookhtiar, *J. Med. Chem.*, 2017, **60**, 681–694.

11 J. M. Rieger, M. L. Brown, G. W. Sullivan, J. Linden and T. L. Macdonald, *J. Med. Chem.*, 2001, **44**, 531–539.

12 O. Saku, M. Saki, M. Kurokawa, K. Ikeda, S. Uchida, T. Takizawa and N. Uesaka, *Bioorg. Med. Chem. Lett.*, 2010, **20**, 3768–3771.

13 P. T. Lowe, S. Dall'Angelo, T. Mulder-Krieger, A. P. IJzerman, M. Zanda and D. O'Hagan, *ChemBioChem*, 2017, **18**, 2156–2164.

14 A. Rodil, S. Bosisio, M. Salah Ayoup, L. Quinn, D. B. Cordes, A. M. Z. Slawin, C. D. Murphy, J. Michel and D. O'Hagan, *Chem. Sci.*, 2018, **9**, 3023–3028.

15 J. F. Bunnett, E. W. Jr. Garbisch and K. M. Pruitt, *J. Am. Chem. Soc.*, 1957, **79**, 385–391.

16 J. E. Francis, R. L. Webb, G. R. Ghai, A. J. Hutchison, M. A. Moskal, R. DeJesus, R. Yokoyama, S. L. Rovinski and N. Contardo, *J. Med. Chem.*, 1991, **34**, 2570–2579.

17 K. Tatani, M. Hiratochi, Y. Nonaka, M. Isaji and S. Shuto, *ACS Med. Chem. Lett.*, 2015, **6**, 244–248.

18 D. Baranowski, G. Framski, E. Wyszko and T. Ostrowski, *J. Mol. Struct.*, 2019, **1195**, 110–118.

19 Z.-G. Gao and A. P. Ijzerman, *Biochem. Pharmacol.*, 2000, **60**, 669–676.

Chapter 6

Conclusions and future work

6.1 – Conclusions

This thesis describes the synthesis of a library of selectively fluorinated compounds, with a focus on incorporating the Janus cyclohexyl motif, as bioactive drug-like molecules and biomolecular probes. Chapter 2 describes the synthesis of novel fluorocyclopropane β-lactam molecules and details their utility as β-lactamase inhibitors and antibiotics. The synthesis of a library of Janus face biomolecular probes and their ability to bind to double stranded and single stranded DNA was explored in Chapter 3. This was built upon in Chapter 4 with the ^{18}F radiolabelling of a Janus face molecule *via* enzymatic fluorination and synthesis of c(RGDfK) probes **255** and **264** for use in $\alpha_v\beta_3$ receptor experiments. Finally, Chapter 5 details the synthesis and receptor affinity of novel Janus face A_{2A} receptor agonists.

6.2 – Future work

6.2.1 – β-Lactam antibiotics and β-lactamase inhibitors

In an effort to develop a less toxic β-lactam antibiotic, the structural activity relationship of β-lactam **193** could be explored further. By modifying the structure of the β-lactam, aryl, or cyclopropane, the toxicity and intrinsic clearance rate of the compound may be lowered whilst still maintaining antibacterial activity. This is required to be done in a way which maintains the core mechanism for triggered β-lactam ring opening and subsequent fluoride elimination from the cyclopropane ring. γ-Lactam **280** may provide lower intrinsic clearance, as the 5-membered lactam ring would undergo a hydrolysis slower. In an effort to reduce toxicity, a difluoro-cyclopropane ring could be installed (**281**) which may provide a compromise between the less active and toxic trifluoro-cyclopropane **144** and more active and toxic monofluoro-cyclopropane ring **193**. In this case relative and absolute stereochemistry would require to be attended to, and that presents a synthesis challenge.

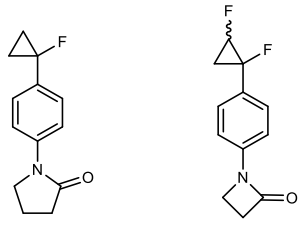

280 **281**

Figure 6.1: Candidate lactam-based antibiotics.

6.2.2 – Janus face DNA interactions

In order to determine the nature of the Janus face-DNA interaction, it would be beneficial to investigate with co-crystallisation studies. This would potentially allow for structural data which would reveal the mode of binding and key interactions between DNA and the Janus cyclohexane ring.

A clear progression of the current work would be to carry out FRET experiments using a negatively charged sulfo-Cy5 dye, tagged to a Janus cyclohexane probe eg **282**, as opposed to the positively charged probe **208** used in this work. This would eliminate the possibility of interactions between the negatively charged phosphate backbone of the DNA and the positively charged amine of the Cy5 motif, which would further validate any interaction between DNA and the probe involves a Janus cyclohexyl-DNA interaction. It should be noted however that interactions between positively charged Cy5 dyes and DNA and not generally considered to be significant in FRET studies with DNA over many years.

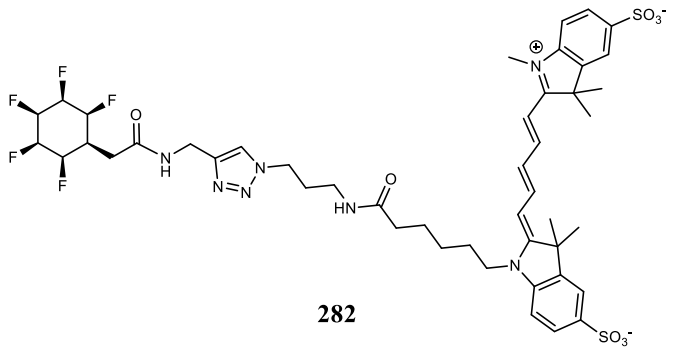

282

Figure 6.2: Candidate Cy5-Janus face bio-probe.

6.2.3 – Radiolabelled Janus face probe experiments

Chapter 4.1.5 described an experiment utilising Janus cyclohexyl-PEG-^{18}[F]FDEA **254** and c(RDGfK) probes **255** and **264** (Figure 6.3). Moving forward, a tumour cell expressing $\alpha_v\beta_3$ receptors could be saturated with probe **255** which would bind to the $\alpha_v\beta_3$ receptors leaving the Janus cyclohexyl motifs exposed on the surface of the tumour cell. Next, a radiolabelled probe such as [^{18}F]FDEA **254** could be introduced, to explore if **254** also co-locates on the cell surface due to associations between the Janus cyclohexane rings. Localisation of the radioactive [^{18}F]FDEA motif around $\alpha_v\beta_3$ epitopes on the cancer cells would offer a new imaging modality.

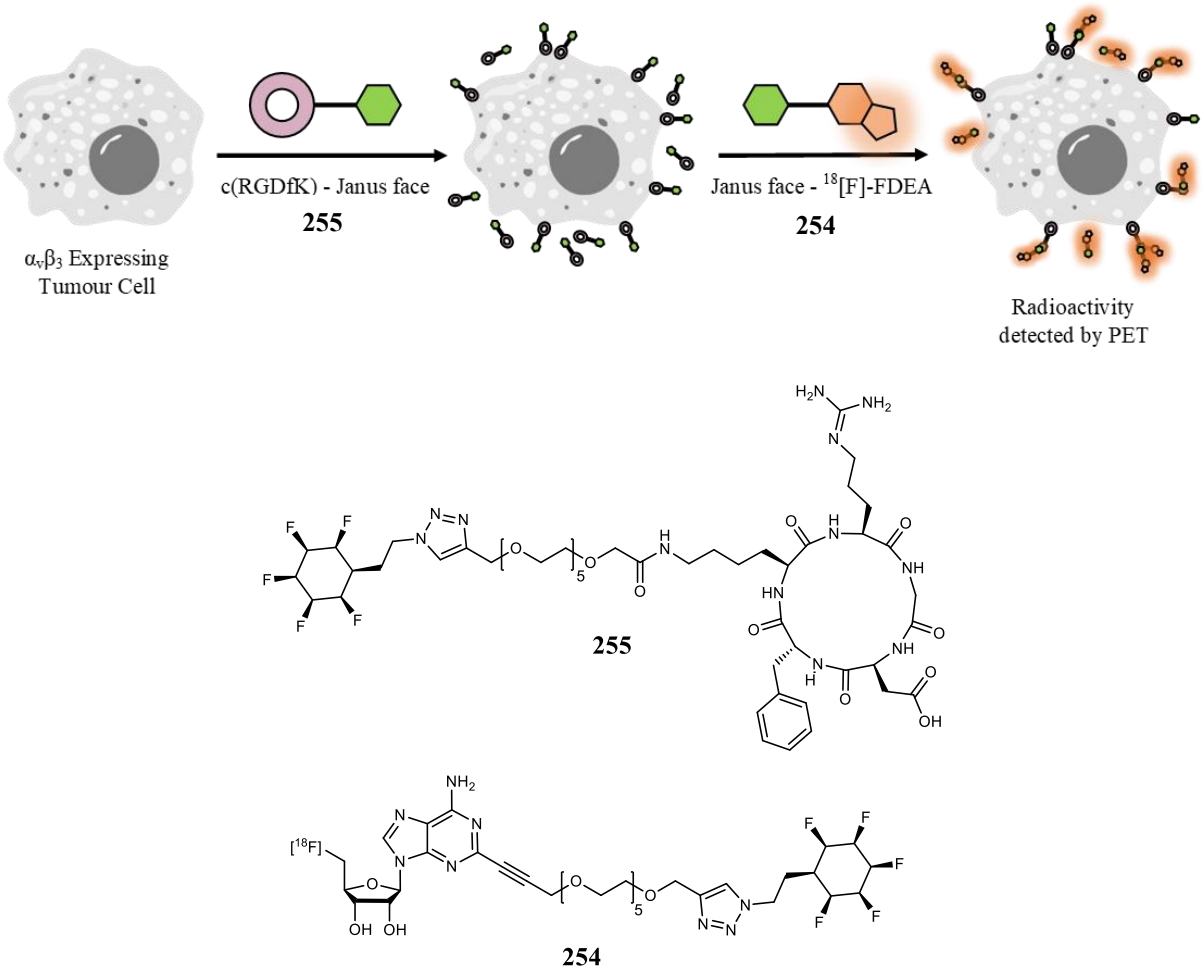

Figure 6.3: Schematic illustrating a proposed probe co-location experiment utilizing a Janus face – Janus face complexation of probes **255** and **254** on the surface of a (cancer) cell.

Chapter 7
Experimental

7.1 – General experimental

All reactions involving air- or moisture-sensitive reagents or intermediates were carried out in oven-dried glassware or a PTFE flask under an atmosphere of nitrogen or argon. Room temperature (RT) is between 18 °C and 22 °C. Flash column chromatography was performed using silica gel 60 (250-400 mesh, Merck Geduran) under a positive pressure of compressed air (5 – 10 bar) eluting with the appropriate solvent. All chemicals which have not been reported for synthesis are commercial reagents, supplied by: Acros Organics, Alfa Aesar, Apollo Scientific, Fisher Scientific, Fluorochem, Lumiprobe, Merck, Manchester Organics, Sigma-Aldrich, TCI Chemicals, or Thermo Scientific. Anhydrous solvents (THF, DCM, hexane, diethyl ether, and toluene) were dispensed from an MBraun SPS-800 solvent system. Anhydrous methanol, DMF, and acetonitrile were purchased from Sigma-Aldrich and 1,4-Dioxane was distilled before use.

^{1}H NMR, ^{13}C NMR and ^{19}F NMR spectra were recorded on a Bruker AV 300, Bruker AV 400, Bruker AVII 400, Bruker AVIII-HD 500, Bruker AVIII 500 or Bruker AV III-HD 700 instrument. For ^{1}H and ^{13}C NMR the chosen deuterated solvent ($CDCl_3$, CD_3OD, CD_3CN, $OS(CD_3)_2$, $OC(CD_3)_2$ or D_2O) was used for an internal deuterium lock and chemical shifts were referenced to the residual protic solvent. ^{1}H NMR were recorded at 400, 500 or 700 MHz and chemical shifts are reported to two decimal places. ^{13}C NMR were recorded at 100, 126 or 176 MHz and chemical shifts are reported to one decimal place. ^{19}F NMR were recorded at 376, 470, 471, or 659 MHz and chemical shifts are reported to one decimal place. Chemical shifts (δ) are reported in parts per million (ppm) relative to an external standard, which is tetramethylsilane (TMS, 0.00 ppm) for ^{1}H and ^{13}C, and trichlorofluoromethane (0.00 ppm) for ^{19}F NMR. Coupling constants (J) are reported in Hz to one decimal place. Data processing was done using MestReNova 12.0.3. Signal multiplicities are abbreviated as such: s singlet, d doublet, dd, doublet of doublets, ddd doublet of doublet of doublets, dt, doublet of triplets, dq doublet of quartets, t triplet, q quartet, m multiplet, br broad. Two-dimensional experiments (HSQC, COSY) were used where applicable.

Retention factor (R_f) was obtained by running thin layer chromatography (TLC) on aluminium backed TLC silica gel 60 F_{254} (Sigma-Aldrich). Melting points were determined using a Griffin MPA350 melting point apparatus. Mass spectra was obtained by electrospray (ESI) and electron impact (EI) ionisation modes. These spectra were obtained by Caroline Horsburgh (University

of St Andrews) and Alan Taylor (University of Edinburgh). Electrospray ionisation was achieved using a Micromass LCT spectrometer. Electron impact ionisation was achieved using a Micromass GCT spectrometer, a Finnigan MAT 95 XP and a ThermoElectron MAT 900. Reported m/z values have units of Daltons. Infrared spectra were acquired on a Shimadzu IRAffinity-1S spectrometer with a diamond ATR attachment. Appropriate signals are reported in units of wavenumbers (cm^{-1}).

7.2 – Experimental procedures and characterisation

7.2.1–General procedures for preparations of phenyl amides (A)

A flame-dried round-bottomed flask equipped with a magnetic stir bar was sealed, evacuated, and backfilled with nitrogen before anhydrous THF and 3-bromopropanoyl chloride (1.2 equiv.) were added sequentially *via* syringe before being stirred and cooled to 0 °C. A separate flame-dried round-bottomed flask was charged with 4-dimethylaminopyridine (0.5 equiv.) and the appropriate iodoaniline (1.0 equiv.). The reaction vessel was sealed, evacuated, and backfilled with nitrogen thrice before anhydrous THF was added *via* syringe. The iodoaniline solution was added dropwise to the stirring 3-bromopropanoyl chloride solution under nitrogen at 0 °C. The solution was left to stir at 0 °C until no starting material was observed *via* TLC. After completion, the reaction was worked-up with deionised water (10 mL), the aqueous layer was separated and extracted with ethyl acetate (3 × 10 mL) and the combined organic layers were sequentially washed with sat. brine solution (10 mL) followed by drying over anhydrous magnesium sulphate. After filtration, the solvent was removed *in vacuo*. Purification by flash column chromatography afforded the appropriate phenyl amide.

7.2.2–General procedures for preparations of iodophenyl lactams (B)

A suspension of the appropriate phenyl amide (1.0 equiv.) in dichloromethane:acetonitrile (19:1) was added dropwise to a stirring solution of pulv. potassium hydroxide (2.0 equiv.) and TBAB (0.4 equiv.) in DCM:acetonitrile (19:1) *via* dropping funnel over the course of 6 h at RT. After addition the solution was left to stir for 30 min at RT. After completion the reaction was worked-up with deionised water (50mL). The aqueous layer was separated and extracted with ethyl acetate (3 × 30 mL) and the combined organic layers were sequentially washed with sat. brine solution (50 mL) followed by drying with anhydrous magnesium sulphate. After filtration the solvent was removed *in vacuo*. Purification by flash column chromatography afforded the appropriate phenyl amide.

7.2.3–General procedures for preparations of vinylphenyls (C)

A flame-dried round-bottomed flask equipped with a magnetic stirrer bar was charged with the appropriate iodophenyl lactam (1.0 equiv.), butylated hydroxytoluene (10 mol%), and tetrakis(triphenylphosphine)palladium (0) (5 mol%). The reaction vessel was sealed, evacuated, and backfilled with nitrogen thrice before degassed anhydrous toluene was added *via* syringe. Tributyl(vinyl)stannane (1.2 equiv.) was added to the stirring solution *via* syringe before being heated to 100 °C under nitrogen and stirred until no starting material was observed by TLC. After completion, the reaction was worked-up with deionised water (10 mL). The aqueous layer was separated and extracted with ethyl acetate (3 × 10 mL) and the combined organic layers were sequentially washed with sat. brine solution (10 mL) followed by drying over anhydrous magnesium sulphate. After filtration the solvent was removed *in vacuo*. Purification by flash column chromatography afforded the appropriate phenyl amide.

7.2.4–General procedures for preparations of bromofluorides (D)

A PTFE round-bottomed flask equipped with a magnetic stirrer bar was charged with the appropriate vinylphenyl (1.0 equiv.). The reaction vessel was sealed, evacuated, and backfilled with nitrogen before anhydrous DCM was added *via* syringe and cooled to 0 °C. Triethylamine trihydrofluoride (1.1 equiv.) was added dropwise to the stirring solution before N-bromosuccinimide (1.1 equiv.) was carefully added portion-wise to the stirring solution at 0 °C. The reaction was brought to room temperature and left to stir under nitrogen until no starting material was observed by TLC. After completion, the reaction was quenched by adding sat. sodium carbonate dropwise, until no further carbonation was observed. The aqueous layer was separated and extracted with ethyl acetate (3 × 10 mL) and the combined organic layers were sequentially washed with sat. brine solution (10 mL) followed by drying of anhydrous magnesium sulphate. After filtration the solvent was removed *in vacuo*. Purification by flash column chromatography afforded the appropriate bromofluoride.

7.2.5–General procedures for preparations of fluorovinyls (E)

A flame-dried round-bottomed flask equipped with a magnetic stirrer bar was charged with the appropriate bromofluoride (1.0 equiv.). The reaction vessel was sealed, evacuated, and backfilled with nitrogen before anhydrous THF was added *via* syringe and cooled to 0 °C. Potassium *tert*-butoxide (1.05 equiv.) was then carefully added portion-wise to the stirring solution at 0 °C. The reaction was left to stir under nitrogen until no starting material was observed by TLC. After completion, the reaction was worked-up with water (10 mL). The aqueous layer was separated and extracted with ethyl acetate (3 × 10 mL) and the combined organic layers were sequentially washed with sat. brine solution (10 mL) followed by drying of

anhydrous magnesium sulphate. After filtration the solvent was removed *in vacuo*. Purification by flash column chromatography afforded the appropriate fluorovinyl.

7.2.6–General procedures for preparations of trifluorocyclopropanes (F)

A flame-dried round-bottomed flask equipped with a magnetic stirrer bar was charged with the appropriate fluorovinyl (1.0 equiv.) and sodium iodide (2.5 equiv.). The reaction vessel was sealed, evacuated, and backfilled with nitrogen thrice before anhydrous THF was added *via* syringe. Trifluoromethyltrimethylsilane (2.5 equiv.) was added to the stirring solution and then heated to reflux. The reaction was left to stir under nitrogen at reflux until no starting material was observed by TLC (18 h). After completion, the reaction was worked-up with water (10 mL). The aqueous layer was separated and extracted with ethyl acetate (3 × 10 mL) and the combined organic layers were sequentially washed with sat. brine solution (10 mL) followed by drying of anhydrous magnesium sulphate. After filtration the solvent was removed *in vacuo*. Purification by flash column chromatography followed by recrystallization from pentane/ethyl acetate afforded the appropriate trifluorocyclopropane.

7.2.7 –Compound synthesis and characterisation

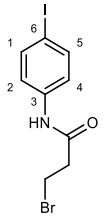

150

3-Bromo-N-(4-iodophenyl)propenamide (150) was prepared by following general procedure A, using 4-iodoaniline **148** (3.00 g, 13.7 mmol, 1.0 equiv), 3-bromopropionyl chloride **149** (1.66 mL, 16.4 mmol, 1.2 equiv.) and 4-dimethylaminopyridine (873 mg, 6.85 mmol, 0.5 equiv.) in THF (2 × 5 mL), and left to stir for 90 min. The product was obtained by flash column chromatography (silica gel, DCM) as a white solid (3.69 g, 73%); R_f 0.26 (DCM); ^{1}H NMR (500 MHz, $CDCl_3$) δ: 7.63 (2H, d, *J* = 8.7 Hz, C[1]H and C[2]H), 7.31 (2H, d, *J* = 8.7 Hz, C[2]H and C[4]H), 7.72 (1H, br s, NH), 3.70 (2H, t, *J* = 6.5 Hz, CH_2Br), 2.93 (2H, t, *J* = 6.5 Hz, $COCH_2$);^{13}C NMR (126 MHz, $CDCl_3$) δ_C 168.1 (CO), 138.2 (C[1]H and C[5]H), 137.3 (C[3]), 122.0 (C[2]H and C[4]H), 88.1 (C[6]), 40.8 ($COCH_2$), 27.0 (CH_2Br); HRMS (ESI): calcd. For $C_9H_9{}^{79}BrINONa$, 375.8804. Found: $[MNa]^+$, 375.8800 (-1.17 ppm error). Spectroscopic data matched that reported in the literature.[2]

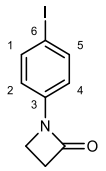

151

1-(4-Iodophenyl)azetidin-2-one (151) was prepared by following general procedure B, using 3-bromo-N-(4-iodophenyl)propenamide **150** (3.69 g, 10.5 mmol, 1.0 equiv), pulv. KOH (1.17 g, 20.9 mmol, 2.0 equiv.) and TBAB (1.35 g, 4.18 mmol, 0.4 equiv.) in DCM:acetonitrile (19:1) (2 × 50 mL). The product was obtained by flash column chromatography (silica gel, DCM) as a white solid (1.72 g, 60%); ^{1}H NMR (500 MHz, $CDCl_3$) δ_H 7.63 – 7.60 (2H, m, C[1]H and C[5]H), 7.13 – 7.10 (2H, m, C[2]H and C[4]H), 3.60 (2H, t, *J* = 4.5 Hz, NCH_2), 3.13 (2H, t, *J* = 4.5 Hz, $OCCH_2$). ^{13}C NMR (126 MHz, $CDCl_3$) δ_C 164.6 (CO), 138.2 (C[3]), 138.1 (C[1]H and C[5]H), 118.1 (C[2]H and C[4]H), 86.9 (C[6]), 38.2 (NCH_2), 36.5 ($COCH_2$); HRMS (ESI): calcd. For C_9H_8INONa, 295.9548. Found: $[MNa]^+$, 295.9538 (-1.70 ppm error). Spectroscopic data matched that reported in the literature.[2]

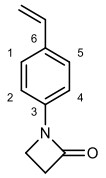

152

1-(4-Vinylphenyl)azetidin-2-one (152) was prepared following general procedure C, using 1-(4-iodophenyl)azetidin-2-one **151** (1.00 g, 3.66 mmol, 1.0 equiv.), butylated hydroxytoluene (81 mg, 0.37 mmol, 10 mol%), tetrakis(triphenylphosphine)palladium (0) (208 mg, 0.18 mmol, 5 mol%), and tributyl(vinyl)stannane (1.29 mL, 4.40 mmol, 1.2 equiv.) in toluene (18 mL). The reaction was refluxed for 1 h. The product was obtained by flash column chromatography (silica gel, DCM) as a white solid (633mg, >99%); Mp. 96–98 ºC; R_f 0.18 (DCM); ν_{max}/cm^{-1} (neat) 2965 (C-H alkene stretch), 1734 (C=O stretch), 1609 (C=C alkene stretch), 1514 (C-C aromatic stretch); ^{1}H NMR (500 MHz, $CDCl_3$) δ_H δ 7.40 (2H, d, *J* = 8.6 Hz, C[2]H and C[4]H), 7.33 (2H, d, *J* = 8.6 Hz, C[1]H and C[5]H), 6.66 (1H, dd, *J* = 17.6, 10.9 Hz, HC=CH'H"), 5.67 (1H, dd, *J* = 17.6, 0.9 Hz, HC=CH'H"), 5.19 (1H, dd, *J* = 10.9, 0.9 Hz, HC=CH'H"), 3.61 (2H, t, *J* = 4.5 Hz, NCH_2), 3.10 (2H, t, *J* = 4.5 Hz, $OCCH_2$); ^{13}C NMR (126 MHz, $CDCl_3$) δ_C 164.3 (CO), 138.0 (C[3]), 136.0 (HC=CH'H"), 133.2 (C[6]), 126.9 (C[2]H and C[4]H), 116.1 (C[1]H and C[5]H), 112.9 (HC=CH'H"), 38.0 (NCH_2), 36.1 ($OCCH_2$); HRMS (ESI): calcd. For $C_{11}H_{11}NONa$, 196.0738. Found: $[MNa]^+$, 196.0731 (-0.96 ppm error).

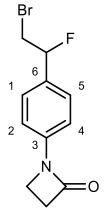

153

1-(4-(2-Bromo-1-fluoroethyl)phenyl)azetidin-2-one (153) was prepared following general procedure D, using 1-(4-vinylphenyl)azetidin-2-one **152** (230 mg, 1.33 mmol, 1.0 equiv.), triethylamine trihydrofluoride (238 µL, 1.46 mmol, 1.1 equiv.), and N-bromosuccinimide (260 mg, 1.46 mmol, 1.1 equiv.) in (5 mL). The reaction was stirred for 5 h. The product was obtained by flash column chromatography (silica gel, DCM) as a colourless oil (227 mg, 63%); R_f 0.18 (DCM); ν_{max}/cm^{-1} (neat) 1730 (C=O stretch), 1512 (C-C aromatic stretch); ^1H NMR (500 MHz, $CDCl_3$) δ_H 7.28 (2H, d, *J* = 8.4 Hz, C[2]H and C[4]H), 7.22 (2H, d, *J* = 8.4 Hz, C[1]H and C[5]H), 5.48 (1H, ddd, *J* = 46.6, 7.7, 4.2 Hz, FCHCH$_2$Br), 3.61 – 3.45 (4H, m, FCHCH$_2$Br and NCH$_2$), 3.01 (2H, t, *J* = 4.5 Hz, OCCH$_2$); ^{13}C NMR (126 MHz, $CDCl_3$) δ_C 164.6 (CO), 139.2 (C[3]), 132.1 (d, *J* = 20.7 Hz, C[6]), 126.8 (d, *J* = 6.3 Hz, C[1]H and C[5]H), 116.2 (C[2]H and C[4]H), 92.3 (d, *J* = 177.4 Hz, CF), 38.1 (NCH$_2$), 36.2 (OCCH$_2$), 34.2 (d, *J* = 29.1 Hz, CH$_2$Br); $^{19}F\{^1H\}$ NMR (470 MHz, $CDCl_3$) δ_F -171.6 (CF); HRMS (ESI): calcd. For $C_{11}H_{11}{}^{79}BrFNONa$, 293.9906. Found: $[MNa]^+$, 293.9911 (1.70 ppm error).

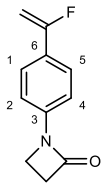

154

1-(4-(1-Fluorovinyl)phenyl)azetidin-2-one (154) was prepared following general procedure E, using 1-(4-(2-bromo-1-fluoroethyl)phenyl)azetidin-2-one **153** (50 mg, 0.18 mmol, 1.0 equiv.) and potassium *tert*-butoxide (27 mg, 0.19 mmol, 1.05 equiv.) in DMF (2 mL). The product was obtained by flash column chromatography (silica gel, DCM) as a colourless oil (21 mg, 61%); R_f 0.29 (DCM); ν_{max}/cm^{-1} (neat) 3131 (C-H alkene stretch), 1728 (C=O stretch), 1607 (C=C alkene stretch), 1516 (C-C aromatic stretch); ^1H NMR (500 MHz, $CDCl_3$) δ_H 7.52 (2H, d, *J* = 8.7 Hz, C[1]H and C[5]H), 7.36 (2H, d, *J* = 8.7 Hz, C[2]H and C[4]H), 4.96 (1H, dd, *J* = 49.9, 3.5 Hz, FC=CH'H"), 4.80 (1H, dd, *J* = 18.0, 3.5 Hz, FC=CH'H"), 3.66 (2H, t, *J* = 4.6 Hz, NCH$_2$), 3.15 (2H, t, *J* = 4.6 Hz, OCCH$_2$); ^{13}C NMR (126 MHz, $CDCl_3$) δ_C 164.7 (CO), 162.6 (d, *J* = 249.3 Hz, H$_2$C=CF), 139.3 (C[3]), 127.6 (d, *J* = 29.8 Hz, C[6]), 125.7 (d, *J* = 7.2 Hz, C[1]H and C[5]H), 116.2 (d, *J* = 1.7 Hz, C[2]H and C[4]H), 88.9 (d, *J* = 22.7 Hz, H$_2$C=CF),

38.3 (N<u>C</u>H$_2$), 36.5 (OC<u>C</u>H$_2$); ^{19}F NMR (470 MHz, CDCl$_3$) δ_F -107.9 (dd, *J* = 49.8, 17.9 Hz, H$_2$C=C<u>F</u>); HRMS (ESI): calcd. For $C_{11}H_{11}FNO$, 192.0825 Found: $[MH]^+$, 192.0818 (-3.64 ppm error).

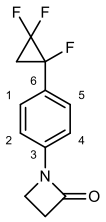

154

1-(4-(1,2,2-Trifluorocyclopropyl)phenyl)azetidin-2-one (**154**) was prepared by following general procedure F, using 1-(4-(1-fluorovinyl)phenyl)azetidin-2-one **153** (100 mg, 0.52 mmol, 1.0 equiv.), sodium iodide (194 mg, 1.31 mmol, 2.5 equiv.), and trifluoromethyltrimethylsilane (192 µL, 1.31 mmol, 2.5 equiv.) in THF (5 mL). The product was obtained by flash column chromatography (silica gel, 20% ethyl acetate in hexane) as a white solid (73 mg, 58%); Mp. 81–83 °C; R_f 0.56 (DCM); ν_{max}/cm^{-1} (neat) 1732 (C=O stretch), 1523 (C-C aromatic stretch); ^{1}H NMR (500 MHz, CDCl$_3$) δ_H 7.41 (4H, s, 4 × ArC<u>H</u>), 3.66 (2H, t, *J* = 4.5 Hz, NC<u>H$_2$</u>), 3.15 (2H, t, *J* = 4.5 Hz, OCC<u>H$_2$</u>), 2.17 – 1.98 (2H, m, F$_2$CC<u>H$_2$</u>CF); ^{13}C NMR (126 MHz, CDCl$_3$) δ_C 164.8 (<u>C</u>O), 139.6 (d, *J* = 1.9 Hz, <u>C[3]</u>), 128.6 (d, *J* = 4.5 Hz, <u>C[1]</u>H and <u>C[5]</u>H), 126.2 (d, *J* = 19.6 Hz, <u>C[6]</u>), 116.4 (<u>C[2]</u>H and <u>C[4]</u>H), 109.4 (ddd, *J* = 296.8, 293.9, 11.9 Hz, <u>C</u>F$_2$), 78.6 (ddd, *J* = 233.3, 12.7, 10.6 Hz, <u>C</u>F), 38.3 (N<u>C</u>H$_2$), 36.5 (OC<u>C</u>H$_2$), 22.3 (dt, *J* = 13.8, 10.3 Hz, F$_2$C<u>C</u>H$_2$CF); ^{19}F{^{1}H} NMR (470 MHz, CDCl$_3$) δ_F -136.2 (dd, *J* = 166.7, 8.9 Hz, CFC<u>F</u>'F"), -142.2 (dd, *J* = 166.7, 4.5 Hz, CFCF'<u>F</u>"), -178.3 (dd, *J* = 8.9, 4.5 Hz, C<u>F</u>CF'F"); HRMS (ESI): calcd. For $C_{12}H_{11}F_3NO$, 242.0793. Found $[MH]^+$, 242.0785 (-0.79 ppm error).

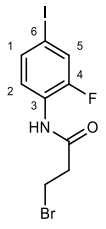

142

3-Bromo-N-(2-fluoro-4-iodophenyl)propanamide (161) was prepared by following general procedure A, using 2-fluoro-4-iodoaniline **157** (2.00 g, 8.44 mmol, 1.0 equiv), 3-bromopropionyl chloride (1.02 mL, 10.1 mmol, 1.2 equiv.) and 4-dimethylaminopyridine (515 mg, 4.22 mmol, 0.5 equiv.) in THF (2 × 6 mL), stirring for 1 h. The product was obtained by flash column chromatography (silica gel, DCM) as a white solid (2.61 g, 82%); Mp. 136–138 ºC; R_f 0.51 (DCM); ν_{max}/cm^{-1} (neat) 3298 (N-H stretch), 3260 (C-H aromatic stretch), 1678

(C=O stretch), 1651 (N-H bend), 1520 (C-C aromatic stretch); ^{1}H NMR (500 MHz, $CDCl_3$) δ_H 8.11 (1H, t, *J* = 8.5 Hz, C[1]H), 7.47 – 7.43 (2H, m, C[5]H and C[2]H), 7.41 (1H, br s, NH), 3.70 (2H, t, *J* = 6.5 Hz, BrCH_2), 2.99 (2H, t, *J* = 6.5 Hz, NCH_2); ^{13}C NMR (126 MHz, $CDCl_3$) δ_C 168.0 (CO), 151.9 (d, *J* = 249 Hz, C[4]F), 134.0 (d, *J* = 3.6 Hz, C[2]H), 126.1 (d, *J* = 10.0 Hz, C[3]), 124.1 (d, *J* = 21.6 Hz, C[5]H), 123.2 (C[1]H), 86.1 (d, *J* = 8.0 Hz, C[6]I), 40.8 (NC(O)CH_2), 26.6 (CH_2Br); ^{19}F{^{1}H} NMR (470 MHz, $CDCl_3$) δ_F -128.6 (C[4]F); HRMS (ESI): calcd. For $C_9H_8{}^{79}BrFINONa$, 393.8710. Found: $[MNa]^+$, 393.8705 (-1.32 ppm error).

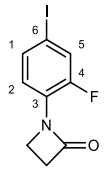

165

1-(2-Fluoro-4-iodophenyl)azetidin-2-one (165) was prepared by following general procedure B, using 3-bromo-N-(2-fluoro-4-iodophenyl)propenamide **161** (600 mg, 1.62 mmol, 1.0 equiv), pulv. potassium hydroxide (182 mg, 3.24 mmol, 2.0 equiv.) and TBAB (210 mg, 0.65 mmol, 0.4 equiv.) in DCM:acetonitrile (19:1) (2 × 32 mL). The product was obtained by flash column chromatography (silica gel, DCM) as a white solid (434 mg, 92%); Mp. 122–124 °C; R_f 0.24 (DCM); ν_{max}/cm^{-1} (neat) 2974 (C-H alkane stretch), 1730 (C=O stretch); ^{1}H NMR (400 MHz, $CDCl_3$) δ_H 7.80 (1H, apparent t, *J* = 8.5 Hz, C[1]H), 7.47 – 7.34 (2H, m, C[2]H and C[5]H), 3.90 (2H, apparent q, *J* = 4.5 Hz, NCH_2), 3.17 (2H, t, *J* = 4.5 Hz, C(O)CH_2); ^{13}C NMR (126 MHz, $CDCl_3$) δ_C 165.6 (CO), 151.5 (d, *J* = 250.2 Hz, C[4]F), 133.8 (d, *J* = 3.4 Hz, C[2]H), 126.5 (d, *J* = 10.3 Hz, C[3]), 125.4 (d, *J* = 21.9 Hz, C[5]H), 122.5 (d, *J* = 2.4 Hz, C[1]H), 85.5 (d, *J* = 7.4 Hz, C[6]I), 42.3 (d, *J* = 6.6 Hz, NCH_2), 38.6 (d, *J* = 2.1 Hz, C(O)CH_2); ^{19}F NMR (471 MHz, $CDCl_3$) δ_F -128.2 (m, C[4]F); HRMS (ESI): calcd. For $C_9H_7FINONa$, 313.9449. Found: $[MNa]^+$, 313.9439 (-3.05 ppm error).

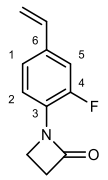

169

1-(2-Fluoro-4-vinylphenyl)azetidin-2-one (169) was prepared by following general procedure C, using 1-(2-fluoro-4-iodophenyl)azetidin-2-one **165** (102 mg, 0.35 mmol, 1.0 equiv.), butylated hydroxytoluene (9 mg, 0.04 mmol, 10 mol%), tetrakis(triphenylphosphine)palladium (0) (23 mg, 0.02 mmol, 5 mol%), and tributyl(vinyl)stannane (123 µL, 0.42 mmol, 1.2 equiv.) in toluene (2 mL) and refluxing for 1 h. The product was obtained by flash column

chromatography (silica gel, DCM) as a white solid (48 mg, 72%); Mp. 71–73 ºC; R_f 0.28 (DCM); ν_{max}/cm^{-1} (neat) 1732 (C=O stretch), 1514 (C-C aromatic stretch); ^1H NMR (500 MHz, $CDCl_3$) δ_H 7.99 (1H, apparent t, *J* = 8.2 Hz, C[1]H), 7.24 – 7.04 (2H, m, C[2]H and C[5]H), 6.63 (1H, dd, *J* = 17.5, 10.8 Hz, HC=H'H"), 5.70 (1H, apparent d, *J* = 17.5 Hz, HC=H'H"), 5.27 (1H, apparent d, *J* = 10.8, HC=H'H"), 3.93 (2H, apparent q, *J* = 4.5 Hz, NCH_2), 3.19 (2H, t, *J* = 4.5 Hz, $OCCH_2$); ^{13}C NMR (126 MHz, $CDCl_3$) δ_C 165.5 (CO), 152.1 (d, *J* = 244.6 Hz, C[4]F), 135.2 (d, *J* = 1.8 Hz, $HC=CH_2$), 134.5 (d, *J* = 6.9 Hz, C[6]), 125.8 (d, *J* = 10.9 Hz, C[3]), 122.7 (d, *J* = 2.7 Hz, C[2]H), 121.1 (d, *J* = 2.8 Hz, C[1]H), 114.4 ($HC=CH_2$), 113.4 (d, *J* = 20.0 Hz, C[5]H), 42.1 (d, *J* = 6.6 Hz, NCH_2), 38.3 (d, *J* = 1.6 Hz ,$OCCH_2$); ^{19}F NMR (471 MHz, $CDCl_3$) δ_F -130.7 (td, *J* = 8.6, 4.0 Hz, C[4]F); HRMS (ESI): calcd. For $C_{11}H_{10}FNONa$, 214.0639. Found: $[MNa]^+$, 214.0631 (-3.57 ppm error).

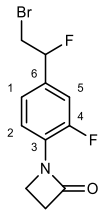

173

1-(4-(2-Bromo-1-fluoroethyl)-2-fluorophenyl)azetidin-2-one (173) was prepared by following general procedure D, using 1-(2-fluoro-4-vinylphenyl)azetidin-2-one **169** (206 mg, 1.08 mmol, 1.0 equiv.), triethylamine trihydrofluoride (194 µL, 1.19 mmol, 1.1 equiv.), and N-bromosuccinimide (212 mg, 1.19 mmol, 1.1 equiv.) in DCM (5 mL) stirring for 5 h. The product was obtained by flash column chromatography (silica gel, DCM) as a white solid (136 mg, 44%); Mp. 80–82 °C; R_f 0.42 (DCM); ν_{max}/cm^{-1} 1732 (C=O stretch), 1516 (C-C aromatic stretch); ^1H NMR (500 MHz, $CDCl_3$) δ_H 8.09 (1H, td, *J* = 8.0, 1.2 Hz C[1]H), 7.14 (1H, dd, *J* = 12.0, 1.2 Hz, C[5]H) 7.10 (1H, d, *J* = 8.0 Hz, C[2]H), 5.56 (1H, ddd, *J* = 46.3, 7.3, 4.5 Hz, $FCHCH_2Br$), 3.94 (2H, td, *J* = 4.5, 3.4 Hz, NCH_2), 3.78 – 3.36 (2H, m, CH_2Br), 3.19 (2H, t, *J* = 4.5 Hz, $OCCH_2$); ^{13}C NMR (126 MHz, $CDCl_3$) δ_C 165.7 (CO), 151.7 (d, *J* = 246.3 Hz, C[4]F), 133.5 (dd, *J* = 21.1, 6.6 Hz, C[6]), 127.2 (dd, *J* = 10.6, 1.7 Hz, C[3]), 122.2 (dd, *J* = 6.5, 3.3 Hz, C[2]H), 121.4 (d, *J* = 3.0 Hz, C[1]H), 113.9 (dd, *J* = 21.2, 7.3 Hz, C[5]H), 91.6 (dd, *J* = 179.0, 1.5 Hz, $FCCH_2Br$), 42.2 (d, *J* = 6.8 Hz, NCH_2), 38.5 (d, *J* = 2.1 Hz, $OCCH_2$), 33.7 (d, *J* = 28.9 Hz, CH_2Br); ^{19}F NMR (470 MHz, $CDCl_3$) δ_F -129.4 (ddt, *J* = 12.0, 8.0, 3.4 Hz, C[4]F), -172.9 (ddd, *J* = 46.3, 23.4, 15.7 Hz, HCF); HRMS (ESI): calcd. For $C_{11}H_{10}{}^{79}BrF_2NONa$, 331.9806. Found: $[MNa]^+$, 331.9796 (-3.22 ppm error).

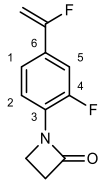

177

1-(2-Fluoro-4-(1-fluorovinyl)phenyl)azetidin-2-one (177) was prepared by following general procedure E, using 1-(4-(2-bromo-1-fluoroethyl)-2-fluorophenyl)azetidin-2-one **173** (200 mg, 0.69 mmol, 1.0 equiv.) and potassium *tert*-butoxide (82 mg, 0.73 mmol, 1.05 equiv.) in THF (5 mL) and stirring for 15 min. The product was obtained by flash column chromatography (silica gel, 15% ethyl acetate in petroleum ether) as a white solid (91 mg, 63%); Mp. 82–84 °C; R_f 0.69 (DCM); ν_{max}/cm^{-1} (neat) 1734 (C=O stretch), 1647 (C=C stretch), 1518 (C-C aromatic stretch); ^1H NMR (500 MHz, $CDCl_3$) δ_H 8.05 (1H, dt, J = 8.5, 1.5 Hz, C[1]H), 7.28 (1H, dd, J = 8.5, 2.0 Hz, C[2]H), 7.24 (1H, dd, J = 12.3, 1.5 Hz, C[5]H), 4.98 (1H, dd, J = 49.4, 3.7 Hz, FC=CH'H"), 4.85 (1H, dd, J = 17.7, 3.7 Hz, FC=CH'H"), 3.94 (2H, q, J = 4.2 Hz, NCH_2), 3.19 (2H, t, J = 4.6 Hz, $OCCH_2$); ^{13}C NMR (126 MHz, $CDCl_3$) δ_C 165.8 (CO), 161.4 (dd, J = 249.6, 2.6 Hz, $FC=CH_2$), 151.7 (dd, J = 249.5, 2.6 Hz, C[4]F), 128.5 (dd, J = 30.7, 7.4 Hz, C[6]), 127.3 (d, J = 10.6 Hz, C[3]), 121.1 – 121.0 (m, C[1]H and C[2]H), 112.7 (dd, J = 22.0, 7.6 Hz, C[5]H), 90.1 (d, J = 22.3 Hz, $FC=CH_2$), 42.3 (d, J = 6.7 Hz, NCH_2), 38.6 (d, J = 1.4 Hz, $OCCH_2$); ^{19}F NMR (659 MHz, $CDCl_3$) δ_F -108.1 (apparent ddd, J = 49.4, 17.7, 3.5 Hz, $FC=CH_2$), -130.4 (apparent ddt, J = 12.3, 7.7, 4.2 Hz, C[4]F); HRMS (ESI): calcd. For $C_{11}H_9F_2NONa$, 232.0544. Found: $[MNa]^+$, 232.0536 (-3.63 ppm error).

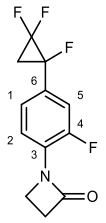

181

1-(2-Fluoro-4-(1,2,2-trifluorocyclopropyl)phenyl)azetidin-2-one (181) was prepared by following general procedure F, using 1-(2-fluoro-4-(1-fluorovinyl)phenyl)azetidin-2-one **177** (60 mg, 0.29 mmol, 1.0 equiv.), sodium iodide (113 mg, 0.73 mmol, 2.5 equiv.), and trifluoromethyltrimethylsilane (107 µL, 0.73 mmol, 2.5 equiv.) in THF (2 mL). The product was obtained by flash column chromatography (silica gel, DCM) as a white solid (45 mg, 60%); Mp. 66–68 °C; R_f 0.35 (DCM); ν_{max}/cm^{-1} 1746 (C=O stretch), 1524 (C-C aromatic stretch); ^1H NMR (500 MHz, $CDCl_3$) δ_H 8.11 (1H, ddd, J = 8.2, 1.0, 1.0 Hz, C[1]H), 7.17 (1H, apparent d, J = 12.2 Hz, C[5]H), 7.13 (1H, apparent d, J = 8.2 Hz, C[2]H), 3.95 (2H, apparent q, J = 4.3 Hz, NCH_2), 3.20 (2H, t, J = 4.3 Hz, $OCCH_2$), 2.14 (1H, dddd, J = 25.0, 16.8, 10.6, 5.8 Hz,

FCC<u>H</u>'H"CF_2), 2.02 (1H, dddd, *J* = 14.6, 12.6, 10.6, 6.7 Hz, FCCH'<u>H</u>"CF_2); ^{13}C NMR (126 MHz, $CDCl_3$) δ_C 165.9 (<u>C</u>O), 151.7 (d, *J* = 246.1 Hz, <u>C[4]</u>F), 127.5 (dd, *J* = 10.1, 0.8 Hz, <u>C[6]</u>), 127.4 (d, *J* = 8.8 Hz, <u>C[3]</u>), 123.3 (<u>C[2]</u>H), 121.4 (d, *J* = 3.0 Hz, <u>C[1]</u>H), 115.3 (dd, *J* = 21.6, 5.3 Hz, <u>C[5]</u>H), 110.2 (ddd, *J* = 297.9, 294.3, 11.6 Hz, <u>C</u>F_2), 42.3 (d, *J* = 6.8 Hz, N<u>C</u>H_2), 38.6 (d, *J* = 2.0 Hz, OC<u>C</u>H_2), 22.6 (ddd, *J* = 13.5, 10.7, 9.5 Hz, F_2C<u>C</u>H_2)*; ^{19}F NMR (659 MHz, $CDCl_3$) δ_F -129.7 (apparent ddt, *J* = 12.2, 8.2, 4.3 Hz, C[4]<u>F</u>), -136.8 (dddd, *J* = 167.3, 14.6, 8.6, 5.8 Hz, C<u>F</u>'F"), -141.8 (dddd, *J* = 167.3, 16.8, 6.7, 4.2 Hz, CF'<u>F</u>"), -181.2 (dddd, *J* = 25.0, 12.6, 8.6, 4.2 Hz, <u>F</u>CCF_2); HRMS (ESI): calcd. For $C_{12}H_9F_4NONa$, 282.0518. Found: $[MNa]^+$, 282.0511 (-0.68 ppm error). *CF_2<u>C</u>F peak was hidden by deuterated chloroform peak.

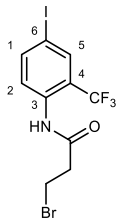

163

3-Bromo-N-(4-iodo-2-(trifluoromethyl)phenyl)propanamide (163) was prepared by following general procedure A, using 4-iodo-2-(trifluoromethyl)aniline **159** (0.50 mL, 3.73 mmol, 1.0 equiv), 3-bromopropionyl chloride (450 µL, 4.48 mmol, 1.2 equiv.) and 4-dimethylaminopyridine (229 mg, 1.87 mmol, 0.5 equiv.) in THF (2 × 3 mL). The reaction mixture was stirred for 1 h. The product was obtained by flash column chromatography (silica gel, DCM) as a white solid (1.29 g, 82%); Mp. 142–144 ºC; R_f 0.65 (DCM); ν_{max}/cm^{-1} (neat) 3242 (N-H stretch), 1659 (C=O stretch), 1531 (C-C aromatic stretch); ^{1}H NMR (500 MHz, $CDCl_3$) 8.02 (1H, d, *J* = 8.8 Hz, C[2]<u>H</u>), 7.94 (1H, d, *J* = 2.0 Hz, C[5]<u>H</u>), 7.89 (1H, dd, *J* = 8.8, 2.0 Hz, C[1]<u>H</u>), 7.44 (1H, br s, N<u>H</u>), 3.72 (2H, t, *J* = 6.5 Hz, BrC<u>H</u>$_2$), 3.01 (2H, t, *J* = 6.5 Hz, COC<u>H</u>$_2$); ^{13}C NMR (101 MHz, $CDCl_3$) δ_C 168.1 (<u>C</u>O), 141.9 (<u>C[1]</u>H), 134.9 (q, *J* = 5.1 Hz, <u>C[5]</u>H), 134.6 (q, *J* = 2.3 Hz, <u>C[3]</u>), 126.4 (<u>C[2]</u>H), 122.9 (apparent d, *J* = 273.7 Hz, <u>C</u>F_3), 121.9 (d, *J* = 30.6 Hz, <u>C[4]</u>), 84.8, (<u>C[6]</u>I), 40.9 (C(O)<u>C</u>H_2), 26.3 (<u>C</u>H_2Br); ^{19}F{^{1}H} NMR (471 MHz, $CDCl_3$) δ_F -60.7 (C<u>F</u>$_3$); HRMS (ESI): calcd. For $C_{10}H_8{}^{79}BrF_3INO$, 445.8658. Found: $[MNa]^+$, 445.8649 (-1.97 ppm error).

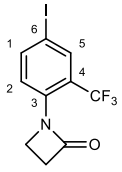

167

1-(4-Iodo-2-(trifluoromethyl)phenyl)azetidin-2-one (167) was prepared by following general procedure B, using 3-bromo-N-(4-iodo-2-(trifluoromethyl)phenyl)propanamide **163**

(1.47 g, 3.48 mmol, 1.0 equiv.), pulv. potassium hydroxide (390 mg, 6.96 mmol, 2.0 equiv.) and TBAB (448 mg, 1.39 mmol, 0.4 equiv.) in DCM:acetonitrile (19:1) (2 × 70 mL). The product was obtained by flash column chromatography (silica gel, 10% ethyl acetate in hexane) as a white solid (1.06 g, 89%); Mp. 50–52 ºC; R_f 0.41 (DCM); ν_{max}/cm^{-1} (neat) 2920 (C-H alkane stretch), 1749 (C=O stretch), 1593 (C-C aromatic stretch); ^1H NMR (500 MHz, $CDCl_3$) δ_H 7.89 (1H, d, J = 2.1 Hz, C[5]H), 7.83 (1H, d, J = 8.7 Hz, C[2]H), 7.75 (1H, dd, J = 8.7, 2.1 Hz, C[1]H), 3.81 (2H, tt, J = 4.8, 1.6 Hz, NCH_2), 3.11 (2H, t, J = 4.8 Hz, $OCCH_2$); ^{13}C NMR (126 MHz, $CDCl_3$) δ_C 166.6 (CO), 141.7 (C[1]H), 135.8 (d, J = 1.8 Hz, C[3]), 135.5 (q, J = 6.2 Hz, C[5]), 126.3 (C[2]), 122.3 (q, J = 272.9 Hz, CF_3), 121.1 (q, J = 31.8 Hz, C[4]), 87.9 (C[6]I), 43.8 (q, J = 4.9 Hz, NCH_2), 37.3 ($OCCH_2$); $^{19}F\{^1H\}$ NMR (470 MHz, $CDCl_3$) δ_F -58.4 (CF_3); HRMS (ESI): calcd. For $C_{10}H_7F_3INONa$, 363.9417. Found: $[MNa]^+$, 363.9405 (-3.19 ppm error).

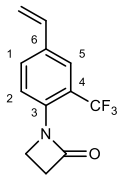

171

1-(2-(Trifluoromethyl)-4-vinylphenyl)azetidin-2-one (171) was prepared by following general procedure C, using 1-(4-iodo-2-(trifluoromethyl)phenyl)azetidin-2-one **167** (144 mg, 0.422 mmol, 1.0 equiv.), butylated hydroxytoluene (10 mg, 0.04 mmol, 10 mol%), tetrakis(triphenylphosphine)palladium (0) (23 mg, 0.02 mmol, 5 mol%), and tributyl(vinyl)stannane (148 µL, 0.506 mmol, 1.2 equiv.) in toluene (3 mL). The reaction was refluxed for 4 h. The product was obtained by flash column chromatography (silica gel, DCM) as a colourless oil (73 mg, 69%); R_f 0.32 (DCM); ν_{max}/cm^{-1} (neat) 2918 (C-H alkene stretch), 1748 (C=O stretch), 1611 (C=C alkene stretch), 1503 (C-C aromatic stretch); ^1H NMR (500 MHz, $CDCl_3$) δ_H 8.00 (1H, d, J = 8.4 Hz, C[2]H), 7.65 (1H, d, J = 2.1 Hz, C[5]H), 7.56 (1H, dd, J = 8.4, 2.1 Hz, C[1]H), 6.68 (1H, dd, J = 17.6, 10.9 Hz, HC=CH'H"), 5.77 (1H, apparent d, J = 17.6 Hz, HC=CH'H"), 5.34 (1H, apparent d, J = 10.9 Hz, HC=CH'H"), 3.86 (2H, td, J = 4.7, 1.3 Hz, NCH_2), 3.16 (2H, t, J = 4.7 Hz, $OCCH_2$); ^{13}C NMR (126 MHz, $CDCl_3$) δ_C 166.9 (CO), 135.2 (d, J = 3.0 Hz, C[3]), 135.0 (HC=CH'H"), 134.9 (C[6]), 130.2 (C[1]H), 125.5 (C[2]H), 124.9 (q, J = 5.8 Hz, C[5]H), 123.6 (q, J = 272.9 Hz, CF_3), 120.7 (apparent d, J = 31.2 Hz, C[4]), 115.7 (HC=CH'H"), 43.9 (q, J = 4.6 Hz, NCH_2), 37.3 ($OCCH_2$); $^{19}F\{^1H\}$ NMR (470 MHz, $CDCl_3$) δ_F -58.7 (CF_3); HRMS (ESI): calcd. For $C_{12}H_{10}F_3NONa$, 264.0607. Found: $[MNa]^+$, 264.0597 (-3.67 ppm error).

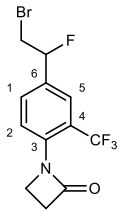

175

1-(4-(2-Bromo-1-fluoroethyl)-2-(trifluoromethyl)phenyl)azetidin-2-one (175) was prepared by following general procedure D, using 1-(2-(trifluoromethyl)-4-vinylphenyl)azetidin-2-one **171** (336 mg, 1.39 mmol, 1.0 equiv.), triethylamine trihydrofluoride (250 µL, 1.53 mmol, 1.1 equiv.), and N-bromosuccinimide (272 mg, 1.53 mmol, 1.1 equiv.) in DCM (3 mL). The reaction was stirred for 24 h. The product was obtained by flash column chromatography (silica gel, dichloromethane) as a white solid (288 mg, 56%); Mp. 68–70 °C; R_f 0.26 (DCM); ν_{max}/cm^{-1} (neat) 1744 (C=O stretch), 1501 (C-C aromatic stretch); ^1H NMR (700 MHz, $CDCl_3$) δ_H 8.18 (1H, d, *J* = 8.5 Hz, C[2]H), 7.65 (1H, d, *J* = 2.0 Hz, C[5]H), 7.52 (1H, dd, *J* = 8.5, 2.0 Hz, C[1]H), 5.64 (1H, ddd, *J* = 46.1, 7.1, 4.7 Hz, FCHCH$_2$Br), 3.90 (2H, td, *J* = 4.7, 1.5 Hz, NCH$_2$), 3.71 – 3.54 (2H, m, FCHCH$_2$Br), 3.18 (2H, t, *J* = 4.7 Hz, OCCH$_2$); ^{13}C NMR (126 MHz, $CDCl_3$) δ_C 166.9 (CO), 136.9 (C[3]), 134.0 (d, *J* = 21.1 Hz, C[6]), 130.3 (d, *J* = 6.2 Hz, C[1]H), 125.3 (C[2]H), 124.7 (qd, *J* = 6.2, 6.2 Hz, C[5]H), 123.3 (q, *J* = 272.8 Hz, CF$_3$), 120.2 (q, *J* = 32.0 Hz, C[4]), 91.6 (d, *J* = 179.4 Hz, BrCH$_2$CFH), 44.0 (q, *J* = 4.8 Hz, NCH$_2$), 37.4 (OCCH$_2$), 33.6 (d, *J* = 28.7 Hz, CH$_2$Br); ^{19}F NMR (659 MHz, $CDCl_3$) δ_F -58.3 (CF$_3$), -173.9 (ddd, *J* = 46.1, 22.4, 16.1 Hz, FCH); HRMS (ESI): calcd. For $C_{12}H_{10}{}^{79}BrF_3NONa$, 361.9774. Found: $[MNa]^+$, 361.9767 (-3.34 ppm error).

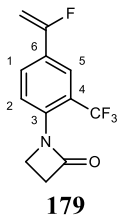

179

1-(4-(1-Fluorovinyl)-2-(trifluoromethyl)phenyl)azetidin-2-one (179) was prepared by following general procedure E, using 1-(4-(2-bromo-1-fluoroethyl)-2-(trifluoromethyl)phenyl)azetidin-2-one **175** (289 mg, 0.85 mmol, 1.0 equiv.) and potassium *tert*-butoxide (105 mg, 1.14 mmol, 1.05 equiv.) in THF (3 mL). The reaction was stirred for 15 min. The product was obtained by flash column chromatography (silica gel, DCM) as a colourless oil (106 mg, 48%). R_f 0.31 (DCM); ν_{max}/cm^{-1} 1755 (C=O stretch), 1505 (C-C aromatic stretch); ^1H NMR (500 MHz, $CDCl_3$) δ_H 8.18 (1H, d, *J* = 8.6 Hz, C[2]H), 7.82 (1H, d, *J* = 2.2 Hz, C[5]H), 7.68 (1H, dd, *J* = 8.6, 2.2 Hz, C[1]H), 5.07 (1H, dd, *J* = 49.2, 3.9 Hz, FC=CH'H"), 4.94 (1H, dd, *J* = 17.7, 3.9 Hz, FC=CH'H"), 3.91 (2H, apparent ddt, *J* = 4.8, 3.2,

1.4 Hz, NC$\underline{H}_2$), 3.15 (2H, t, *J* = 4.8 Hz, OC$\underline{C}H_2$); ^{13}C NMR (126 MHz, $CDCl_3$) δ_C 166.9 ($\underline{C}$O), 161. 2 (d, *J* = 250.1 Hz, H_2C=$\underline{C}$F), 136.9 ($\underline{C}$[3]), 128.9 (d, *J* = 6.5 Hz, $\underline{C}$[1]H), 128.7 (d, *J* = 29.8 Hz, $\underline{C}$[6]), 124.9 (d, *J* = 1.6 Hz, $\underline{C}$[2]H), 123.35 (q, *J* = 272.5 Hz, $\underline{C}F_3$), 123.32 (qd, *J* = 6.2, 6.2 Hz, $\underline{C}$[5]H), 120.0 (q, *J* = 30.2 Hz, $\underline{C}$[4]), 91.0 (d, *J* = 22.1 Hz, FC=$\underline{C}H_2$), 44.0 (q, *J* = 5.0 Hz, N$\underline{C}H_2$), 27.4 (OC$\underline{C}H_2$); ^{19}F NMR (470 MHz, $CDCl_3$) δ_F -58.3 (C$\underline{F}_3$), -108.5 (H_2C=CH$\underline{F}$); HRMS (ESI): calcd. For $C_{12}H_9F_4NONa$, 282.0512. Found: $[MNa]^+$, 282.0502 (-3.72 ppm error).

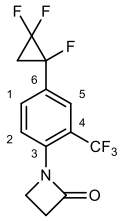

183

1-(4-(1,2,2-Trifluorocyclopropyl)-2-(trifluoromethyl)phenyl)azetidin-2-one (183) was prepared following general procedure F, using 1-(4-(1-fluorovinyl)-2-(trifluoromethyl)phenyl)azetidin-2-one **179** (106 mg, 0.41 mmol, 1.0 equiv.), sodium iodide (151 mg, 1.02 mmol, 2.5 equiv.), and trifluoromethyltrimethylsilane (150 µL, 1.02 mmol, 2.5 equiv.) in THF (5 mL). The product was obtained by flash column chromatography (silica gel, 20% ethyl acetate in hexane) as a colourless oil (90 mg, 71%); R_f 0.38 (DCM); ν_{max}/cm^{-1} 1749 (C=O stretch), 1506 (C-C aromatic stretch); ^{1}H NMR (500 MHz, $CDCl_3$) δ_H 8.24 (1H, d, *J* = 8.6 Hz, C[2]$\underline{H}$), 7.72 (1H, apparent t, *J* = 1.5 Hz, C[5]$\underline{H}$), 7.55 (1H, apparent dt, *J* = 8.6, 1.5 Hz, C[1]$\underline{H}$), 3.92 (2H, apparent ddt, *J* = 4.8, 3.9, 1.4 Hz, N$\underline{C}H_2$), 3.19 (2H, t, *J* = 4.8 Hz, OCC$\underline{H}_2$), 2.37 – 1.88 (2H, m, FCC$\underline{H}_2CF_2$); ^{13}C NMR (126 MHz, $CDCl_3$) δ_C 167.0 ($\underline{C}$O), 137.2 ($\underline{C}$[3]), 131.2 (d, *J* = 3.7 Hz, $\underline{C}$[1]H), 127.9 (d, *J* = 20.4 Hz, $\underline{C}$[6]), 125.8 (q, *J* = 5.5 Hz, $\underline{C}$[5]H), 125.1 ($\underline{C}$[2]H), 123.2 (q, *J* = 272.7 Hz, $\underline{C}F_3$), 119.9 (q, *J* = 31.5 Hz, $\underline{C}$[4]), 108.9 (ddd, *J* = 298.1, 294.0, 11.8 Hz, $F_2\underline{C}$CF), 78.9 – 76.9 (m, $\underline{C}FCF_2$)* 44.0 (q, *J* = 5.1 Hz, N$\underline{C}H_2$), 37.5 (OC$\underline{C}H_2$), 22.7 (dt, *J* = 14.0, 10.3 Hz, $F_2C\underline{C}H_2$CF); ^{19}F{^{1}H} NMR (659 MHz, $CDCl_3$) δ_F -58.2 (C$\underline{F}_3$), -136.7 (dd, *J* = 168.1, 8.8 Hz, C$\underline{F}$'F"), -141.8 (dd, *J* = 168.1, 3.8 Hz, CF'$\underline{F}$"), -182.4 (dd, *J* = 8.8, 3.8 Hz, C$\underline{F}$); HRMS (ESI): calcd. For $C_{13}H_9F_6NONa$, 332.0486. Found: $[MNa]^+$, 332.0477 (-1.05 ppm error).

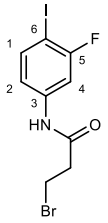

162

3-Bromo-N-(3-fluoro-4-iodophenyl)propanamide (162) was prepared by following general procedure A, using 3-fluoro-4-iodoaniline **158** (1.00 g, 4.22 mmol, 1.0 equiv), 3-bromopropionyl chloride (630 µL, 6.33 mmol, 1.5 equiv.) and 4-dimethylaminopyridine (258 mg, 2.11 mmol, 0.5 equiv.) in THF (2 × 2 mL). The reaction was stirred for 30 min. The product was obtained by flash column chromatography (silica gel, DCM) as a white solid (1.37 g, 88%); Mp. 136–138 ºC; R_f 0.50 (DCM); ν_{max}/cm^{-1} (neat) 3260 (N-H stretch), 1663 (C=O stretch), 1597 (N-H bend); ^{1}H NMR (400 MHz, $CDCl_3$) δ_H 7.65 (1H, dd, *J* = 8.6, 7.0 Hz, C[1]H), 7.56 (1H, dd, *J* = 9.8, 2.4 Hz, C[4]H), 7.33 (1H, br s, NH), 6.98 (1H, dd, *J* = 8.6, 2.4 Hz, C[2]H), 3.70 (2H, t, *J* = 6.5 Hz, BrCH_2), 2.95 (2H, t, *J* = 6.5 Hz, NCH_2); ^{13}C NMR (126 MHz, $CDCl_3$) δ_C 168.1 (CO), 162.0 (d, *J* = 244.5 Hz, C[5]F), 139.3 (d, *J* = 2.8 Hz, C[1]H), 139.2 (C[3]), 116.9 (d, *J* = 2.5 Hz, C[2]H), 107.8 (d, *J* = 30.0 Hz, C[4]H), 74.8 (d, *J* = 26.1, C[6]I), 40.8 (NCH_2), 26.8 (CH_2Br); ^{19}F{^{1}H} NMR (376 MHz, $CDCl_3$) δ_F -91.7 (CF); HRMS (ESI): calcd. For $C_9H_8{}^{79}BrFINO$, 393.8710. Found: $[MNa]^+$, 393.8699 (-2.84 ppm error).

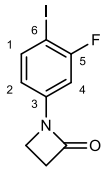

166

1-(3-Fluoro-4-iodophenyl)azetidin-2-one (166) was prepared following general procedure B, using 3-bromo-N-(3-fluoro-4-iodophenyl)propenamide **162** (1.37 g, 3.69 mmol, 1.0 equiv), pulv. potassium hydroxide (415 mg, 7.39 mmol, 2.0 equiv.) and TBAB (477 mg, 1.48 mmol, 0.4 equiv.) in DCM:acetonitrile (19:1) (2 × 74 mL). The product was obtained by flash column chromatography (silica gel, DCM) as a white solid (955 mg, 89%); Mp. 110 -112 ºC; R_f 0.35 (DCM); ν_{max}/cm^{-1} (neat) 1732 (C=O stretch), 1559 (C-C aromatic stretch); ^{1}H NMR (500 MHz, $CDCl_3$) δ_H 7.62 (1H, dd, *J* = 8.5, 6.9 Hz, C[1]H), 7.13 (1H, dd, *J* = 9.2, 2.4 Hz, C[4]H), 6.86 (1H, dd, *J* = 8.5, 2.4 Hz, C[2]H), 3.60 (2H, t, *J* = 4.6 Hz, NCH_2), 3.12 (2H, t, *J* = 4.6 Hz, OCCH_2); ^{13}C NMR (126 MHz, $CDCl_3$) δ_C 164.65 (CO), 161.9 (d, *J* = 245.2 Hz, CF), 140.0 (d, *J* = 9.7 Hz C[3]), 139.5 (d, *J* = 2.7 Hz, C[1]H), 113.5 (d, *J* = 3.1 Hz, C[2]H), 104.2 (d, *J* = 28.4 Hz, C[4]H), 73.6 (d, *J* = 26.0 Hz, C[6]I), 38.5 (NCH_2), 36.6 (COCH_2); ^{19}F{^{1}H} NMR (470

MHz, $CDCl_3$) δ_F -91.8 (C<u>F</u>); HRMS (ESI): calcd. For $C_9H_7FINONa$, 313.9449. Found: $[MNa]^+$, 313.9445 (-1.27 ppm error).

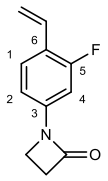

170

1-(3-Fluoro-4-vinylphenyl)azetidin-2-one (170) was prepared by following general procedure C, using 1-(2-fluoro-4-iodophenyl)azetidin-2-one **166** (955 mg, 3.28 mmol, 1.0 equiv.), butylated hydroxytoluene (71 mg, 0.32 mmol, 10 mol%), tetrakis(triphenylphosphine)palladium (0) (185 mg, 0.16 mmol, 5 mol%), and tributyl(vinyl)stannane (1.16 mL, 3.94 mmol, 1.2 equiv.) in toluene (16 mL). The reaction was refluxed for 20 h. The product was obtained by flash column chromatography (silica gel, 30% ethyl acetate in hexane) as a white solid (525 mg, 84%); Mp. 98–100 ºC; R_f 0.36 (30% ethyl acetate in hexane); ν_{max}/cm^{-1} (neat) 1732 (C=O stretch), 1622 (C=C alkene stretch), 1508 (C-C aromatic stretch); ^1H NMR (500 MHz, $CDCl_3$) δ_H 7.44 (1H, apparent t, J = 8.3 Hz, C[1]<u>H</u>), 7.20 – 6.90 (2H, m, C[2]<u>H</u> and C[4]<u>H</u>), 6.80 (1H, dd, J = 17.8, 11.2 Hz, <u>H</u>C=H'H"), 5.75 (1H, dd, J = 17.8, 1.1 Hz, HC=<u>H</u>'H"), 5.31 (1H, dd, J = 11.2, 1.1 Hz, HC=H'<u>H</u>"), 3.63 (2H, t, J = 4.5 Hz, NC<u>H</u>$_2$), 3.14 (2H, t, J = 4.5 Hz, OCC<u>H</u>$_2$); ^{13}C NMR (126 MHz, $CDCl_3$) δ_C 164.6 (<u>C</u>O), 160.6 (d, J = 250.1 Hz, <u>C[5]</u>F), 139.0 (d, J = 11.0 Hz, <u>C[3]</u>), 128.9 (d, J = 3.4 Hz, H<u>C</u>=CH'H"), 127.9 (d, J = 5.1 Hz, <u>C[1]</u>H), 121.1 (d, J = 12.5 Hz, <u>C[6]</u>), 115.5 (d, J = 4.6 Hz, HC=<u>C</u>H'H"), 111.9 (d, J = 3.1 Hz, <u>C[2]</u>H), 104.1 (d, J = 26.9 Hz, <u>C[4]</u>H), 38.5 (N<u>C</u>H$_2$), 36.5 (OC<u>C</u>H$_2$); ^{19}F NMR (471 MHz, $CDCl_3$) δ_F -116.4 (dd, J = 11.5, 8.3 Hz, C<u>F</u>); HRMS (ESI): calcd. For $C_{11}H_{10}FNONa$, 214.0639. Found: $[MNa]^+$, 214.0634 (-2.10 ppm error).

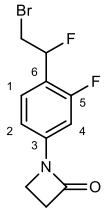

174

1-(4-(2-Bromo-1-fluoroethyl)-3-fluorophenyl)azetidin-2-one (174) was prepared by following general procedure D, using 1-(3-fluoro-4-vinylphenyl)azetidin-2-one **170** (525 mg, 2.75 mmol, 1.0 equiv.), triethylamine trihydrofluoride (492 µL, 3.02 mmol, 1.1 equiv.), and N-bromosuccinimide (538 mg, 3.02 mmol, 1.1 equiv.) in DCM (5 mL). The reaction was stirred for 20 h. The product was obtained by flash column chromatography (silica gel, 30% ethyl acetate in hexane) as a white solid (480 mg, 60%); Mp. 50–52 °C; R_f 0.17 (30% ethyl acetate

in hexane); ν_{max}/cm^{-1} 1738 (C=O stretch), 1512 (C-C aromatic stretch); ^{1}H NMR (700 MHz, $CDCl_3$) δ_H 7.40 (1H, apparent t, *J* = 8.2 Hz, C[1]H), 7.22 (1H, dt, *J* = 11.4, 1.8 Hz, C[4]H), 7.10 (1H, dd, *J* = 8.2, 1.8 Hz, C[2]H), 5.86 (1H, dt, *J* = 45.8, 5.7 Hz, FCHCH'H"Br), 3.70 (1H, d, *J* = 5.7 Hz, FCHCH'H"Br), 3.67 (1H, d, *J* = 5.7 Hz, FCHCH'H"Br), 3.65 (2H, t, *J* = 4.6 Hz, NCH_2), 3.16 (2H, t, *J* = 4.6 Hz, $OCCH_2$); ^{13}C NMR (126 MHz, $CDCl_3$) δ_C 164.8 (CO), 159.9 (dd, *J* = 248.0, 5.6 Hz, C[5]F), 140.5 (d, *J* = 11.1 Hz, C[3]), 128.4 (dd, *J* = 7.5, 5.0 Hz, C[1]H), 119.6 (dd, *J* = 22.2, 13.6 Hz, C[6]), 111.8 (d, *J* = 3.1 Hz, C[2]H), 104.2 (d, *J* = 25.9 Hz, C[4]H), 87.3 (dd, *J* = 177.9, 1.9 Hz, FCHCH'H"Br), 38.6 (NCH_2), 36.6 ($OCCH_2$), 33.2 (d, *J* = 28.2 Hz, FCHCH'H"); ^{19}F NMR (659 MHz, $CDCl_3$) δ_F -116.2 (dd, *J* = 11.4, 8.2 Hz, C[5]F), -179.1 (dt, 45.8, 21.0 Hz, $FCHCH_2Br$); HRMS (ESI): calcd. For $C_{11}H_{11}{}^{81}BrF_2NO$, 291.9966. Found: $[MH]^+$, 291.9957 (-3.13 ppm error).

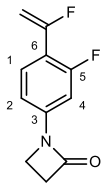

178

1-(3-Fluoro-4-(1-fluorovinyl)phenyl)azetidin-2-one (178) was prepared following general procedure E, using 1-(4-(2-bromo-1-fluoroethyl)-2-fluorophenyl)azetidin-2-one **174** (455 mg, 1.58 mmol, 1.0 equiv.) and potassium *tert*-butoxide (183 mg, 1.63 mmol, 1.05 equiv.) in THF (5 mL). The reaction was stirred for 15 min. The product was obtained by flash column chromatography (silica gel, 30% ethyl acetate in hexane) as a white solid (164 mg, 50%); Mp. 94–96 °C; R_f 0.32 (30% ethyl acetate in hexanes); ν_{max}/cm^{-1} 1734 (C=O stretch), 1622 (C=C alkene stretch), 1514 (C-C aromatic stretch); ^{1}H NMR (500 MHz, $CDCl_3$) δ_H 7.51 (1H, apparent t, *J* = 8.5 Hz, C[1]H), 7.23 (1H, ddd, *J* = 12.6, 2.0, 1.3 Hz, C[4]H), 7.07 (1H, dd, *J* = 8.5, 2.0 Hz, C[2]H), 5.18 (1H, ddd, *J* = 52.6, 3.3, 1.0 Hz, FC=CH'H"), 5.05 (1H, apparent dt, *J* = 20.2, 3.1 Hz, FC=CH'H"), 3.66 (2H, t, *J* = 4.6 Hz, NCH_2), 3.17 (2H, t, *J* = 4.6 Hz, $OCCH_2$); ^{13}C NMR (126 MHz, $CDCl_3$) δ_C 164.8 (CO), 160.3 (dd, *J* = 253.3, 6.3 Hz, C[5]F), 157.1 (dd, *J* = 253.3, 5.0 Hz, $FC=CH_2$), 140.0 (d, *J* = 11.3 Hz, C[3]), 128.0 (dd, *J* = 8.7, 3.5 Hz, C[1]H), 111.4 (dd, *J* = 3.3, 1.4 Hz, C[2]H), 104.7 (dd, *J* = 27.3, 2.8 Hz, C[4]H), 94.8 (dd, *J* = 21.1, 13.1 Hz, $FC=CH_2$), 38.6 (NCH_2), 36.7 ($OCCH_2$);* ^{19}F NMR (659 MHz, $CDCl_3$) δ_F -103.9 (ddd, *J* = 52.6, 20.2, 6.4 Hz, $FC=CH_2$), -109.5 – -109.6 (m, C[5]F); HRMS (ESI): calcd. For $C_{11}H_{10}F_2NO$, 210.0730. Found: $[MH]^+$, 210.0719 (-2.61 ppm error). *C[6] peak was undetectable by ^{13}C NMR.

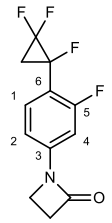

182

1-(3-Fluoro-4-(1,2,2-trifluorocyclopropyl)phenyl)azetidin-2-one (182) was prepared following general procedure F, using 1-(3-fluoro-4-(1-fluorovinyl)phenyl)azetidin-2-one **178** (130 mg, 0.62 mmol, 1.0 equiv.), sodium iodide (230 mg, 1.54 mmol, 2.5 equiv.), and trifluoromethyltrimethylsilane (228 µL, 1.54 mmol, 2.5 equiv.) in THF (5 mL). The product was obtained by flash column chromatography (silica gel, 20% ethyl acetate in hexane) as a white solid (45 mg, 60%); Mp. 110–112 °C; R_f 0.16 (30% ethyl acetate in hexane); ν_{max}/cm^{-1} 1744 (C=O stretch), 1522 (C-C aromatic stretch); ^1H NMR (500 MHz, $CDCl_3$) δ_H 7.44 (1H, td, *J* = 8.2, 1.9 Hz, C[1]H), 7.21 (1H, dd, *J* = 11.1, 2.1 Hz, C[4]H), 7.14 (1H, dd, *J* = 8.2, 2.1 Hz, C[2]H), 3.66 (2H, t, *J* = 4.7 Hz, NCH_2), 3.17 (2H, t, *J* = 4.7 Hz, $OCCH_2$), 2.13 (1H, dddd, *J* = 23.0, 16.0, 10.7, 5.4 Hz, $F_2CCH'H''CF$), 1.99 (1H, dtd, *J* = 14.6, 10.7, 6.5 Hz, $F_2CCH'H''CF$); ^{13}C NMR (126 MHz, $CDCl_3$) δ_C 164.9 (CO), 162.7 (d, *J* = 253.5 Hz, C[5]F), 141.9 (dd, *J* = 10.9, 2.5 Hz, C[3]), 132.4 (d, *J* = 1.3 Hz, C[1]H), 112.9 (dd, *J* = 20.5, 16.3 Hz, C[6]), 111.7 (C[2]H), 108.7 (td, *J* = 293.6, 12.1 Hz, $CFCF_2$), 104.4 (dd, *J* = 25.5, 1.4 Hz, C[4]H), 74.3 (dt, *J* = 235.1, 11.3 Hz, $CFCF_2$), 38.6 (NCH_2), 36.7 ($OCCH_2$), 22.0 (apparent q, *J* = 10.7 Hz, F_2CCH_2CF); $^{19}F\{^1H\}$ NMR (659 MHz, $CDCl_3$) δ_F -111.9 (t, *J* = 2.8 Hz, C[5]F), -134.6 (ddd, *J* = 167.2, 8.0, 4.1 Hz, CF'F"), -144.2 (dd, *J* = 167.2, 3.7 Hz, CF'F"), -173.5 (dt, *J* = 8.0, 3.7 Hz $FCCF_2$); HRMS (ESI): calcd. For $C_{12}H_{10}F_4NO$, 260.0693. Found: $[MH]^+$, 260.0687 (-2.32 ppm error).

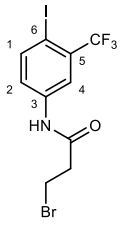

164

3-Bromo-N-(4-iodo-3-(trifluoromethyl)phenyl)propanamide (164) was prepared following general procedure A, using 4-iodo-3-(trifluoromethyl)aniline **160** (526 µL, 3.49 mmol, 1.0 equiv), 3-bromopropionyl chloride (520 µL, 5.24 mmol, 1.5 equiv.) and 4-dimethylaminopyridine (213 mg, 1.75 mmol, 0.5 equiv.) in THF (2 × 2 mL). The reaction was stirred for 30 min. The product was obtained by flash column chromatography (silica gel, DCM) as a white solid (1.24 g, 85%); Mp. 78–80 ºC; R_f 0.49 (DCM); ν_{max}/cm^{-1} (neat) 3265 (N-H

stretch), 1665 (C=O stretch), 1585 (N-H bend); ^{1}H NMR (500 MHz, $CDCl_3$) 7.94 (1H, d, *J* = 8.6 Hz, C[1]H), 7.81 (1H, d, *J* = 2.6 Hz, C[4]H), 7.50 (1H, dd, *J* = 8.6, 2.6 Hz, C[2]H), 7.45 (1H, br s, NH), 3.70 (2H, t, *J* = 6.4 Hz, CH_2Br), 2.97 (2H, t, *J* = 6.4 Hz, $COCH_2$); ^{13}C NMR (126 MHz, $CDCl_3$) δ_C 168.4 (CO), 142.7 (C[1]H), 137.7 (C[3]), 134.3 (q, *J* = 31.7 Hz, C[5]CF_3), 124.1 (C[2]H), 122.5 (q, *J* = 273.9 Hz, CF_3), 119.2 (q, *J* = 5.8 Hz, C[4]H), 84.4 (C[6]I), 40.7 ($COCH_2$), 26.7 (CH_2Br); ^{19}F{^{1}H} NMR (470 MHz, $CDCl_3$) δ_F -63.1 (CF_3); HRMS (ESI): calcd. For $C_{10}H_8{}^{79}BrF_3INO$, 421.8859. Found: $[MH]^+$, 421.8857 (-0.43 ppm error).

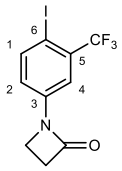

168

1-(4-Iodo-3-(trifluoromethyl)phenyl)azetidin-2-one (168) was prepared following general procedure B, using 3-bromo-N-(4-iodo-3-(trifluoromethyl)phenyl)propenamide **164** (1.17 g, 2.78 mmol, 1.0 equiv.), pulv. potassium hydroxide (312 mg, 5.56 mmol, 2.0 equiv.) and TBAB (358 mg, 1.11 mmol, 0.4 equiv.) in DCM:acetonitrile (19:1) (2 × 56 mL). The product was obtained by flash column chromatography (silica gel, 30% ethyl acetate in hexane) as a white solid (820 mg, 87%); Mp. 86–88 ºC; R_f 0.57 (DCM); ν_{max}/cm^{-1} (neat) 1744 (C=O stretch), 1601 (C-C aromatic stretch); ^{1}H NMR (500 MHz, $CDCl_3$) δ_H 7.94 (1H, d, *J* = 8.5 Hz, C[1]H), 7.54 (1H, d, *J* = 2.6 Hz, C[4]H), 7.31 (1H, dd, *J* = 8.5, 2.6 Hz, C[2]H), 3.67 (2H, t, *J* = 4.6 Hz, NCH_2), 3.18 (2H, t, *J* = 4.6 Hz, $OCCH_2$); ^{13}C NMR (126 MHz, $CDCl_3$) δ_C 164.8 (CO), 142.8 (C[1]H), 138.5 (C[3]), 134.4 (apparent d, *J* = 31.2 Hz, C[5]CF_3), 122.5 (q, *J* = 274.0 Hz, CF_3), 120.6 (C[2]H), 115.2 (q, *J* = 5.8 Hz, C[4]H), 82.9 (q, *J* = 1.6 Hz, C[6]I), 38.3 (NCH_2), 36.7 ($OCCH_2$); ^{19}F{^{1}H} NMR (470 MHz, $CDCl_3$) δ_F -63.1 (CF_3); HRMS (ESI): calcd. For $C_{10}H_8F_3INONa$, 341.957. Found: $[MH]^+$, 341.9589 (-2.39 ppm error).

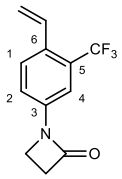

172

1-(3-(Trifluoromethyl)-4-vinylphenyl)azetidin-2-one (172) was prepared following general procedure C, using 1-(4-iodo-2-(trifluoromethyl)phenyl)azetidin-2-one **168** (770 mg, 2.26 mmol, 1.0 equiv.), butylated hydroxytoluene (51 mg, 0.23 mmol, 10 mol%), tetrakis(triphenylphosphine)palladium (0) (127 mg, 0.11 mmol, 5 mol%), and tributyl(vinyl)stannane (795 µL, 2.71 mmol, 1.2 equiv.) in toluene (11 mL). The reaction was

refluxed for 48 h. The product was obtained by flash column chromatography (silica gel, 30% ethyl acetate in hexane) as a white solid (400 mg, 73%); Mp. 82–84 ºC; R_f 0.32 (30% ethyl acetate in hexane); ν_{max}/cm^{-1} (neat) 1753 (C=O stretch), 1611 (C=C alkene stretch), 1501 (C-C aromatic stretch); ^1H NMR (500 MHz, $CDCl_3$) δ_H 7.65 (1H, d, *J* = 8.5 Hz, C[1]H), 7.60 (1H, dd, *J* = 8.5, 2.2 Hz, C[2]H), 7.48 (1H, d, *J* = 2.2 Hz, C[4]H), 7.03 (1H, ddq, *J* = 16.5, 11.0, 2.5 Hz, HC=CH'H"), 5.70 (1H, apparent d, *J* = 16.5 Hz, HC=CH'H"), 5.37 (1H, dd, *J* = 11.0, 1.1 Hz, HC=CH'H"), 3.68 (2H, t, *J* = 4.6 Hz, NCH_2), 3.17 (2H, t, *J* = 4.6 Hz, $OCCH_2$); ^{13}C NMR (126 MHz, $CDCl_3$) δ_C 164.7 (CO), 137.8 (C[3]), 132.4 (apparent d, *J* = 1.5 Hz, HC=CH'H"), 132.0 (C[5]CF_3), 128.3 (C[1]H), 123.2 (q, *J* = 1.3 Hz, C[6]) 124.0 (q, *J* = 274.2 Hz, CF_3), 119.7 (C[2]H), 117.3 (HC=CH'H"), 113.1 (q, *J* = 5.9 Hz, C[4]H), 38.4 (NCH_2), 36.6 ($OCCH_2$); $^{19}F\{^1H\}$ NMR (470 MHz, $CDCl_3$) δ_F -59.7 (CF_3); HRMS (ESI): calcd. For $C_{12}H_{11}F_3NONa$, 242.0787. Found: $[MH]^+$, 242.0779 (-3.41 ppm error).

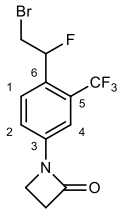

176

1-(4-(2-Bromo-1-fluoroethyl)-3-(trifluoromethyl)phenyl)azetidin-2-one (176) was prepared following general procedure D, using 1-(3-(trifluoromethyl)-4-vinylphenyl)azetidin-2-one **172** (380 mg, 1.58 mmol, 1.0 equiv.), triethylamine trihydrofluoride (282 µL, 1.73 mmol, 1.1 equiv.), and N-bromosuccinimide (308 mg, 1.73 mmol, 1.1 equiv.) in DCM (4 mL). The reaction was stirred for 2 h. The product was obtained by flash column chromatography (silica gel, 30% ethyl acetate in hexane) as a white solid (323 mg, 60%); Mp. 102–104 °C; R_f 0.22 (30% ethyl acetate in hexane); ν_{max}/cm^{-1} (neat) 2965 (C-H alkane stretch), 1744 (C=O stretch), 1512 (C-C aromatic stretch); ^1H NMR (700 MHz, $CDCl_3$) δ_H 7.63 (1H, d, *J* = 8.5 Hz, C[1]H), 7.63 (1H, dd, *J* = 8.5, 2.2 Hz, C[2]H), 7.61 (1H, d, *J* = 2.2 Hz, C[4]H), 5.97 (1H, ddd, *J* = 46.0, 7.9, 1.6 Hz, FCH), 3.70 (1H, t, *J* = 4.6 Hz, NCH_2), 3.66 – 3.56 (2H, m, CH_2Br), 3.20 (2H, t, *J* = 4.6 Hz, $OCCH_2$); ^{13}C NMR (126 MHz, $CDCl_3$) δ_C 164.8 (CO), 139.3 (C[3]), 130.4 (apparent d, *J* = 21.5 Hz, C[5]CF_3), 128.9 (d, *J* = 9.1 Hz, C[1]H), 128.3 (dd, *J* = 35.7, 4.4 Hz, C[6]), 123.6 (q, *J* = 274.3 Hz, CF_3), 119.6 (C[2]H), 113.5 (q, *J* = 5.8 Hz, C[4]H), 90.2 – 85.6 (dd, *J* = 177.6, 2.4 Hz, FCH), 38.4 (NCH_2), 36.7 ($OCCH_2$), 33.9 (d, *J* = 27.7 Hz, CH_2Br); ^{19}F NMR (659 MHz, $CDCl_3$) δ_F -58.6 (CF_3), -175.1 (ddd, *J* = 46.0, 28.5, 17.3 Hz, FCH); HRMS (ESI): calcd. For $C_{12}H_{11}{}^{79}BrF_3NO$, 339.9955. Found: $[MH]^+$, 339.9946 (-2.55 ppm error).

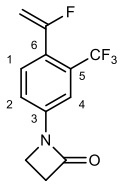

180

1-(4-(1-Fluorovinyl)-3-(trifluoromethyl)phenyl)azetidin-2-one (180) was prepared following general procedure E, using 1-(4-(2-bromo-1-fluoroethyl)-3-(trifluoromethyl)phenyl)azetidin-2-one **176** (282 mg, 0.83 mmol, 1.0 equiv.) and potassium *tert*-butoxide (98 mg, 0.87 mmol, 1.05 equiv.) in THF (3 mL). The product was obtained by flash column chromatography (silica gel, 30% ethyl acetate in hexanes) as a colourless oil (164 mg, 52%); R_f 0.25 (30% ethyl acetate in hexanes); ν_{max}/cm^{-1} (neat) 1748 (C=O stretch), 1616 (C=C alkene stretch), 1506 (C-C aromatic stretch); ^1H NMR (500 MHz, $CDCl_3$) δ_H 7.60 (1H, d, J = 8.5 Hz, C[2]H), 7.56 (1H, d, J = 1.6 Hz, C[4]), 7.50 (1H, d, J = 8.5 Hz, C[1]H), 5.00 (1H, dd, J = 15.4, 3.4 Hz, FC=CH'H"), 4.75 (1H, dd, J = 46.7, 3.4 Hz, FC=CH'H"), 3.70 (2H, t, J = 4.6 Hz, NCH_2), 3.20 (2H, t, J = 4.6 Hz, OCCH_2); ^{13}C NMR (126 MHz, $CDCl_3$) δ_C 164.8 (CO), 161.4 (d, J = 255.5 Hz, H_2C=CF), 139.5 (C[3]), 132.4 (d, J = 3.6 Hz, C[1]H), 129.7 (q, J = 32.1 Hz, C[5]CF_3), 126.3 (d, J = 29.7 Hz, C[6]), 123.3 (q, J = 274.0 Hz, CF_3), 119.4 (C[2]H), 113.9 (q, J = 5.4 Hz, C[4]H), 95.2 (d, J = 22.3 Hz, H_2C=CF), 38.5 (NCH_2), 36.8 (OCCH_2); $^{19}F\{^1H\}$ NMR (470 MHz, $CDCl_3$) δ_F -60.3 (d, J = 14.3 Hz, CF_3), -87.5 (q, J = 14.3 Hz, H_2C=CF); HRMS (ESI): calcd. For $C_{12}H_9F_4NONa$, 282.0518 Found: $[MNa]^+$, 282.0511 (-0.68 ppm error).

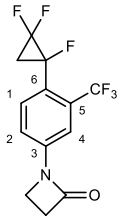

184

1-(4-(1,2,2-Trifluorocyclopropyl)-3-(trifluoromethyl)phenyl)azetidin-2-one (184) was prepared following general procedure F, using 1-(4-(1-fluorovinyl)-3-(trifluoromethyl)phenyl)azetidin-2-one **180** (90 mg, 0.35 mmol, 1.0 equiv.), sodium iodide (130 mg, 0.87 mmol, 2.5 equiv.), and trifluoromethyltrimethylsilane (129 µL, 0.87 mmol, 2.5 equiv.) in THF (3 mL). The product was obtained by flash column chromatography (silica gel, 10% ethyl acetate in petroleum spirits 40-60) as a colourless oil (49 mg, 45%); R_f 0.11 (30% ethyl acetate in hexane); ν_{max}/cm^{-1} 1751 (C=O stretch), 1518 (C-C aromatic stretch); ^1H NMR (500 MHz, $CDCl_3$) δ_H 7.65 – 7.64 (2H, m, C[1]H and C[4]H), 7.57 (1H, dd, J = 9.0, 2.2 Hz, C[2]H), 3.72 (2H, t, J = 4.7 Hz, NCH_2), 3.21 (2H, t, J = 4.7 Hz, OCCH_2), 2.22 – 1.99 (2H, m, F_2CCH_2); ^{13}C NMR (126 MHz, $CDCl_3$) δ_C 164.9 (CO), 140.6 (C[3]), 133.6 (C[2]H), 132.5 (q, J = 32.4

Hz, C[5]CF_3), 123.3 (q, J = 274.0 Hz, CF_3), 122.1 (apparent d, J = 18.3 Hz, C[6]), 119.2 (C[4]H), 115.4 – 114.4 (m, C[1]H), 108.9 (td, J = 292.8, 12.5 Hz, CF_2), 77.6 (dt, J = 235.3, 11.1 Hz, FCCF_2), 38.6 (NCH_2), 36.9 (OCCH_2), 22.12 (apparent q, J = 11.4 Hz, F_2CCH_2); ^{19}F NMR (659 MHz, $CDCl_3$) δ_F -60.5 (dd, J = 9.9, 3.9 Hz, CF_3), -132.2 – -133.0 (m, CF'F"), -143.8 (ddt, J = 168.5, 15.0, 4.5 Hz, CF'F"), -168.2 – -168.4 (m, CF); HRMS (ESI): calcd. For $C_{13}H_9F_6NONa$, 332.0481. Found: $[MNa]^+$, 332.0474 (-1.97 ppm error).

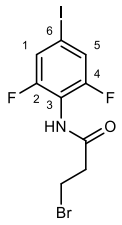

187

3-Bromo-N-(2,6-difluoro-4-iodophenyl)propanamide (187) was prepared by following general procedure A, using 2,6-difluoro-4-iodoaniline **186** (1 g, 3.92 mmol, 1.0 equiv.), 3-bromopropionyl chloride (470 µL, 4.71 mmol, 1.2 equiv.) and 4-dimethylaminopyridine (240mg, 1.96 mmol, 0.5 equiv.) in THF (2 × 5 mL). The reaction was stirred for 2 h. The product was obtained by flash column chromatography (silica gel, DCM) as a white solid (1.27 g, 84%); Mp. 159–161 ºC; R_f 0.51 (DCM); ν_{max}/cm^{-1} (neat) 3165 (N-H stretch), 3005 (C-H aromatic stretch), 1665 (C=O stretch); ^{1}H NMR (500 MHz, $CDCl_3$) δ_H 7.35 (2H, d, J = 6.9 Hz, C[1]H and C[5]H), 6.79 (1H, br s, NH), 3.69 (2H, t, J = 6.7 Hz, $BrCH_2CH_2$), 3.01 (2H, t, J = 6.7 Hz, $HNOCH_2CH_2$); ^{13}C NMR (126 MHz, MeOD) δ_C 171.5 (CO), 159.1 (dd, J = 255.1, 5.3 Hz, C[2]F and C[4]F), 122.6 (dd, J = 21.3, 5.2 Hz, C[5]H and C[1]H), 115.6 (t, J = 16.9 Hz, C[3]) 90.2 (t, J = 9.9 Hz, C[6]I), 39.7 ($COCH_2$), 27.4 (CH_2Br); ^{19}F{^{1}H} NMR (471 MHz, $CDCl_3$) δ_F -116.4 (2 × CF); HRMS (ESI): calcd. For $C_9H_8{}^{79}BrF_2INO$, 389.8797. Found: $[MH]^+$, 389.8795 (-0.39 ppm error)

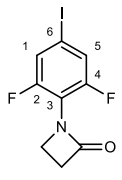

188

1-(2,6-Difluoro-4-iodophenyl)azetidin-2-one (188) was prepared by following general procedure B, using 3-bromo-N-(2,6-difluoro-4-iodophenyl)propanamide **187** (1.27 g, 3.28 mmol, 1.0 equiv.), pulv. potassium hydroxide (368 mg, 6.55 mmol, 2.0 equiv.) and TBAB (53 mg, 0.16 mmol, 0.4 equiv.) in DCM:acetonitrile (19:1) (2 × 66 mL). The product was obtained by flash column chromatography (silica gel, DCM) as a white solid (761 mg, 75%); Mp. 108–

110 ºC; R_f 0.42 (DCM); ν_{max}/cm^{-1} (neat) 1732 (C=O stretch), 1499 (C=C aromatic stretch); ^1H NMR (500 MHz, $CDCl_3$) δ_H 7.33 – 7.30 (2H, m, C[1]H and C[5]H), 3.78 (2H, t, *J* = 4.6 Hz, NCH_2), 3.21 (2H, t, *J* = 4.6 Hz, $COCH_2$); ^{13}C NMR (126 MHz, $CDCl_3$) δ_C 165.0 (CO), 156.8 (dd, *J* = 257.2, 6.3 Hz, C[2]F and C[4]F), 121.8 (dd, *J* = 20.7, 5.1 Hz, C[1]H and C[5]H), 114.6 (t, *J* = 16.0 Hz, C[3]), 88.3 (t, *J* = 9.7 Hz, C[6]I), 41.9 (NCH_2), 38.3 ($COCH_2$); $^{19}F\{^1H\}$ NMR (471 MHz, $CDCl_3$) δ_F -115.9 (d, *J* = 6.3 Hz, CF); HRMS (ESI): calcd. For $C_9H_7F_2INO$, 309.95404. Found: $[MH]^+$, 309.9532 (-0.82 ppm error).

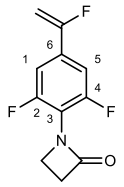

189

1-(2,6-Difluoro-4-(1-fluorovinyl)phenyl)azetidin-2-one (189) was prepared by charging a flame-dried round-bottomed flask equipped with a magnetic stirrer bar with 1-(2,6-difluoro-4-iodophenyl)azetidin-2-one **188** (200 mg, 0.65 mmol, 1.0 equiv.), tetrakis(triphenylphosphine)palladium(0) (37 mg, 32.4 µmol, 5 mol%), copper iodide (6 mg, 32.4 µmol, 5 mol%), and caesium fluoride (198 mg, 1.30 mmol, 2.4 equiv.). The reaction vessel was sealed, evacuated, and backfilled with nitrogen thrice before anhydrous DMF was added *via* syringe. (1-fluorovinyl)(methyl)diphenylsilane **185** (123 µL, 0.54 mmol, 1.5 equiv.) was then added *via* syringe before the stirring solution was heated to 90 °C. The reaction was refluxed under nitrogen until no starting material was observed by TLC (18 h). The reaction was cooled to RT then directly concentrated *in vacuo*. Purification by flash column chromatography (silica gel, DCM) yielded the product as an orange solid (120 mg, 82%); Mp. 77 – 79 ºC; R_f 0. 41 (DCM); ν_{max}/cm^{-1} (neat) 3134 – 2924 (C-H aromatics/alkene stretch), 1744 (C=O stretch), 1651 (C=C alkene stretch), 1514 (C-C aromatic stretch); ^1H NMR (500 MHz, $CDCl_3$) δ_H 7.12 (2H, ddd, *J* = 12.5, 6.1, 2.6 Hz, C[1]H and C[5]H), 5.04 (1H, dd, *J* = 61.0, 4.0 Hz, HH'C=CF), 4.97 (1H, dd, *J* = 29.7, 4.0 Hz, HH'C=CF), 3.81 (2H, t, *J* = 4.6 Hz, NCH_2), 3.22 (1H, t, *J* = 4.6 Hz, $COCH_2$); ^{13}C NMR (126 MHz, $CDCl_3$) δ_C 165.0 (CO), 160.5 (dt, *J* = 250.3, 2.8 Hz, H_2C=CF), 157.0 (ddd, *J* = 251.9, 6.3, 2.3 Hz, C[2]F and C[4]F), 131.5 (dt, *J* = 31.8, 9.5 Hz, C[6]), 115.1 (t, *J* = 17.1 Hz, C[3]), 108.5 (ddd, *J* = 26.3, 12.6, 7.2 Hz, C[1]H and C[5]H), 92.1 (d, *J* = 21.9 Hz, H_2C=CF), 42.1 (NCH_2), 38.3 ($OCCH_2$); $^{19}F\{^1H\}$ NMR (470 MHz, $CDCl_3$) δ_F -108.2 (t, *J* = 4.1 Hz, H_2C=CF), -116.4 (d, *J* = 4.1 Hz, ArF); HRMS (ESI): calcd. For $C_{11}H_9ONF_3$, 228.0636. Found: $[MH]^+$, 228.0629 (-0.60 ppm error).

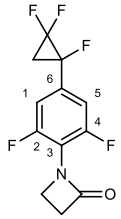

190

1-(2,6-Difluoro-4-(1,2,2-trifluorocyclopropyl)phenyl)azetidin-2-one (190) was prepared following general procedure F, using 1-(2,6-difluoro-4-(1-fluorovinyl)phenyl)azetidin-2-one **189** (120 mg, 0.53 mmol, 1.0 equiv.), sodium iodide (198 mg, 1.32 mmol, 2.5 equiv.), and trifluoromethyltrimethylsilane (195 µL, 1.32 mmol, 2.5 equiv.) in THF (10 mL). The product was obtained by flash column chromatography (silica gel, 1% methanol in DCM) as an amber oil (45 mg, 60%); R_f 0.21 (DCM); ν_{max}/cm^{-1} (neat) 3009-2920 (br, C-H aromatics stretch), 1757 (C=O stretch), 1522 (C-C aromatics stretch); ^{1}H NMR (500 MHz, $CDCl_3$) δ_H 6.99 (2H, d, J = 8.4 Hz, C[1]H and C[5]H), 3.82 (2H, t, J = 4.6 Hz, NCH_2), 3.23 (2H, t, J = 4.6 Hz, $COCH_2$), 2.21 (1H, dddd, J = 25.3, 16.7, 10.8, 6.2 Hz, $F_2CCHH'CF$), 2.04 (1H, dddd, J = 15.0, 12.4, 10.8, 6.7 Hz, $F_2CCHH'CF$); ^{13}C NMR (126 MHz, $CDCl_3$) δ_C 165.0 (CO), 157.1 (dd, J = 253.1, 6.4 Hz, C[2]F and C[4]F), 131.5 (dt, J = 19.3, 8.8 Hz, C[6]), 115.1 (t, J = 17.2 Hz, C[3]), 110.3 (dd, J = 25.9, 6.0 Hz, C[1]H and C[5]H), 108.7 (ddd, J = 298.6, 294.6, 11.3 Hz, CF_2), 78.7 (ddd, J = 235.3, 11.3, 8.9 Hz, $CFCF_2$), 42.0 (NCH_2), 38.4 ($OCCH_2$), 23.2 (dt, J = 12.8, 10.2 Hz, CH_2CF_2); ^{19}F{^{1}H} NMR (470 MHz, $CDCl_3$) δ_F –155.6 (C[2]F and C[4]F), -137.3 (dd, J = 168.2, 9.3 Hz, CFF'CF), -141.1 (dd, J = 168.2, 3.3 Hz, CFF'CF), -185.2 (dd, J = 9.3, 3.3 Hz, CF_2CF); HRMS (ESI): calcd. For $C_{12}H_9F_5NO$, 278.0604. Found: $[MH]^+$, 278.0595 (-1.38 ppm error).

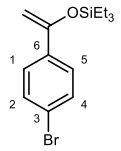

198

((1-(4-Bromophenyl)vinyl)oxy)triethylsilane (198) was prepared by evacuating and backfilling a sealed flame-dried round-bottomed flask equipped with a magnetic stir bar thrice before lithium bis(trimethylsilyl)amide (1 M in THF) (11 mL, 11 mmol, 1.1 equiv.) was added *via* syringe. The vessel was cooled to -78 °C before THF (80 mL) was added *via* syringe. A solution of 4-bromoacetophenone **197** (2 g, 10 mmol, 1.0 equiv.) dissolved in THF (10 mL) was added dropwise to the stirring solution at -78 °C and stirred for 30 min. Chlorotriethylsilane (1.86 mL, 11 mmol, 1.1 equiv.) was then added dropwise to the solution before the reaction was warmed to RT and left to stir for 18 h. The reaction was quenched with a sat. sodium carbonate solution (40 mL) before the aqueous phase was separated then extracted with diethyl ether (3 ×

30 mL). The combined organic layers were washed with sat. brine (5 mL), dried over anhydrous magnesium sulphate, filtered, and concentrated *in vacuo*. Purification by flash column chromatography (silica gel, 5% ethyl acetate in hexane) afforded the product as a yellow oil (2.90 g, 93%); ^{1}H NMR (500 MHz, $CDCl_3$) δ_H 7.49 – 7.43 (4H, C[1]H, C[2]H, C[4]H, and C[5]H), 4.87 (1H, d, J = 1.9 Hz, C=CHH'), 4.44 (1H, d, J = 1.9 Hz, C=CHH'), 1.00 (9H, t, J = 8.0 Hz, $Si(CH_2CH_3)_3$), 0.76 (6H, q, J = 1.9 Hz, $Si(CH_2CH_3)_3$); ^{13}C NMR (126 MHz, D_3COD) δ_C 155.0 (C=CH_2), 136.8 (C[6]), 131.3 (C[2]H and C[4]H), 127.0 (C[1]H and C[5]H), 122.3 (C[3]), 91.0 (C=CH_2), 6.9 ($Si(CH_2CH_3)_3$), 5.0 ($Si(CH_2CH_3)_3$); HRMS (ESI): calcd. For $C_{14}H_{21}{}^{79}BrOSi$, 313.0545. Found: $[MH]^+$, 313.0543 (-0.64 ppm error). Reported data is in accordance with literature.[3]

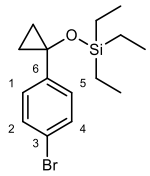

199

(1-(4-Bromophenyl)cyclopropoxy)triethylsilane (199) was prepared by charging a flame-dried round-bottomed flask with (1-(4-bromophenyl)vinyl)oxy)triethylsilane **198** (2.90 g, 9.29 mmol, 1.0 equiv.) and was then equipped with a magnetic stir bar before being sealed, evacuated and backfilled with nitrogen thrice. Anhydrous DCM (20 mL) was added *via* syringe before the solution was cooled to 0 °C. Diiodomethane (1.16 mL, 18.85 mmol, 2.0 equiv.) and diethylzinc (1 M in hexanes) (18.5 mL, 18.58 mmol, 20 equiv.) were added before the solution was warmed to RT and stirred for 16 h. The reaction was quenched *slowly* with a sat. NH_4Cl solution until no gas was evolved. The precipitate was filtered off and the aqueous layer was separated and extracted with DCM (3 × 15 mL). The combined organic layers were washed with sat. brine solution (10 mL), dried over anhydrous $MgSO_4$, filtered, and concentrated *in vacuo*. Purification by flash column chromatography (silica gel, hexane to 1% ethyl acetate in hexane) afforded the product as an amber oil (2.15 g, 71%); R_f 0.66 (1% ethyl acetate in hexane); ν_{max}/cm^{-1} (neat) 2955 (C-H aromatic stretch), 1489 (C-C aromatic stretch); ^{1}H NMR (500 MHz, $CDCl_3$) δ_H 7.41 (2H, d, J = 8.5 Hz, C[2]H and C[4]H), 7.16 (2H, d, J = 8.5 Hz, C[1]H and C[5]H), 1.22 (2H, dt, J = 7.3, 1.7 Hz, CCHH'CHH'C), 0.98 (2H, dt, J = 7.3, 1.7 Hz, CHH'CHH'C), 0.89 (9H, t, J = 8.0 Hz, 3 × $SiCH_2CH_3$), 0.59–0.54 (6H, q, J = 8.0 Hz, 3 × $SiCH_2CH_3$); ^{13}C NMR (126 MHz, $CDCl_3$) δ_C 144.2 (C[6]), 131.1 (C[2]H and C[4]H), 126.3 (C[1]H and C[5]H), 119.9 (C[3]Br), 57.3 ($C(CH_2)_2$), 17.4 ($C(CH_2)_2$), 6.8 (3 × $SiCH_2CH_3$), 5.6 (3 × $SiCH_2CH_3$); HRMS (ESI): calcd. For $C_{16}H_{27}{}^{79}BrO_2SiNa$, 381.0862. Found: $[MMeOHNa]^+$, 381.0857 (-1.31 ppm error).

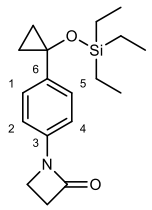

200

1-(4-(1-((Triethylsilyl)oxy)cyclopropyl)phenyl)azetidin-2-one (200) was prepared by charging a flame-dried round-bottomed flask equipped with a magnetic stir bar with (1-(4-bromophenyl)cyclopropoxy)triethylsilane **199** (100 mg, 0.31 mmol, 1.0 equiv.), azetidin-2-one (26 mg, 0.37 mmol, 1.2 equiv.), caesium carbonate (140 mg, 0.43 mmol, 1.4 equiv.), tris(dibenzylideneacetone)dipalladium (0) (1.4 mg, 1.53 μmol, 0.5 mol%), and xantphos (2.7 mg, 4.60 μmol, 1.5 mol%). The vessel was then sealed, evacuated, and backfilled with nitrogen thrice. Degassed anhydrous 1,4-dioxane (1 mL) was added *via* syringe before the solution was heated to reflux and stirred for 16 h. The reaction was diluted with DCM (1 mL) then filtered before concentrating the filtrate *in vacuo*. Purification by flash column chromatography (silica gel, 5% ethyl acetate in hexane to 20% ethyl acetate in hexane) afforded the product as a colourless oil (85 mg, 87%); R_f 0.17 (5% ethyl acetate in hexane); ν_{max}/cm^{-1} (neat) 2955 (C-H alkane stretch), 1738 (C=O stretch); ^{1}H NMR (500 MHz, $CDCl_3$) δ_H 7.28 (4H, d, J = 3.5 Hz, C[1]H, C[2]H, C[4]H, an C[5]H), 3.62 (2H, t, J = 4.5 Hz, NCH_2), 3.10 (2H, t, J = 4.5 Hz, CH_2CO), 1.18 (2H, dd, J = 7.2, 5.3 Hz, CHH'CHH'C), 0.96 (2H, dd, J = 7.2, 5.3 Hz, CHH'CHH'C), 0.88 (9H, t, J = 8.0 Hz, 3 × $SiCH_2CH_3$), 0.54 (6H, q, J = 8.0 Hz, 3 × $SiCH_2CH_3$); ^{13}C NMR (126 MHz, $CDCl_3$) δ_C 164.5 (CO), 140.5 (C[3]), 137.0 (C[6]), 126.1 (C[1]H and C[5]H), 116.0 (C[2]H and C[4]H), 57.7 ($C(CH_2)_2O$), 38.2 (NCH_2), 36.2 (CH_2CO), 17.1 ($C(CH_2)_2O$), 7.0 (3 × $SiCH_2CH_3$), 5.7 (3 × $SiCH_2CH_3$); ^{29}Si NMR (99 MHz, $CDCl_3$) δ_{Si} 20.0 ($OSiEt_3$); HRMS (ESI): calcd. For $C_{18}H_{27}NO_2SiNa$, 340.1703. Found $[MNa]^+$, 340.1693 (-3.02 ppm error).

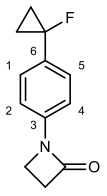

193

1-(4-(1-Fluorocyclopropyl)phenyl)azetidin-2-one (193) was prepared by charging a PTFE round-bottomed flask equipped with a magnetic stir bar with 1-(4-(1-((triethylsilyl)oxy)cyclopropyl)phenyl)azetidin-2-one **200** (180 mg, 0.57 mmol, 1.0 equiv.). The vessel was sealed, evacuated, and backfilled with nitrogen thrice. Anhydrous DCM (3 mL)

was added *via* syringe and the solution was cooled to -78 °C before DAST (150 µL, 1.14 mmol, 2.0 equiv.) was added slowly *via* syringe. After addition the reaction was stirred for 1 h at -78 °C before heating to RT and stirring for an additional hour. The reaction was slowly quenched with sodium hydrogen carbonate until no gas was evolved (5 mL). The aqueous layer was separated and extracted with DCM (3 × 5 mL) and the combined organic layers were washed with sat. brine (5 mL), dried over anhydrous magnesium sulphate, filtered, and concentrated *in vacuo*. The crude mixture was then reconstituted in DCM (5 mL) before ozone gas was bubbled through the solution until the solvent turned pale blue (5 min). The solution was then degassed, reconcentrated *in vacuo* and purified by flash column chromatography (silica gel, 20% ethyl acetate in hexane to 40% ethyl acetate in hexane) to afford the product as a white solid (51 mg, 44%); Mp. 98 – 100 °C; R_f 0.18 (20% ethyl acetate in hexane); ν_{max}/cm^{-1} (neat) 1726 (C=O stretch); ^{1}H NMR (500 MHz, $CDCl_3$) δ_H 7.35 (2H, d, *J* = 8.5 Hz, C[2]H and C[4]H), 7.27 (2H, d, *J* = 8.5 Hz, C[1]H and C[5]H), 3.64 (2H, t, *J* = 4.5 Hz, NCH_2), 3.13 (2H, t, *J* = 4.5 Hz, CH_2CO), 1.49 – 1.42 (2H, m, CHH'CHH'CF'), 1.05 – 1.00 (2H, m, CHH'CHH'CF'); ^{13}C NMR (126 MHz, $CDCl_3$) δ_C 164.6 (CO), 138.0 (C[3]), 135.0 (d, *J* = 21.4 Hz, C[6]), 125.8 (d, *J* = 6.4 Hz, C[1]H and C[5]H), 116.2 (C[2]H and C[4]H), 78.9 (d, *J* = 213.3 Hz, CF), 38.2 (NCH_2), 36.3 (CH_2CO), 14.2 (d, *J* = 12.9 Hz, $(CH_2)_2CF$); ^{19}F NMR (470 MHz, $CDCl_3$) δ_F -176.8 (tt, *J* = 18.5, 8.8 Hz, CF); HRMS (ESI): calcd. For $C_{12}H_{13}NOF$, 206.0981. Found $[MH]^+$, 206.0972 (-1.61 ppm error).

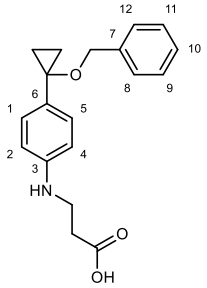

204

3-((4-(1-(Benzyloxy)cyclopropyl)phenyl)amino)propanoic acid (204) was prepared by charging a flame-dried round-bottomed flask equipped with a magnetic stir bar with 1-(4-(1-Fluorocyclopropyl)phenyl)azetidin-2-one **193** (20 mg, 97.5 µmol, 1.0 equiv.) before dry THF (1 mL) was then added and the flask sealed under nitrogen. A solution of benzyl alcohol (22 µL, 214.5 µmol, 2.2 equiv.) and sodium metal (5 mg, 214.5 µmol, 2.2 equiv.) in dry THF (1 mL) was subsequently added *via* syringe and the reaction was stirred at RT for 48 h. The crude mixture was concentrated *in vacuo* before being taken directly to purification by semipreparative HPLC on a Shimadzu Prominence system using a Phenomenex Synergi® Polar-RP 80Å (250 x 10.0 mm, 4µ) and a guard cartridge; Mobile phase: 0.05% TFA in water

(solvent A) and 0.05% TFA in MeCN (solvent B); linear gradient: 20% solvent B to 60% solvent B over 20 min, then hold 60% B over 5 min, then back to 20% B over 5 min, then 20% B for 5 min to re-equilibrate the column. Flow rate: 2.5 mL/min; detection: 254 nm. The relevant fractions were collected (tR = 21.221 min), concentrated and lyophilized affording the product as a white solid (5.6 mg, 18%); ν_{max}/cm^{-1} (neat) 3333 (O-H stretch), 2973 (C-H alkane stretch); ^{1}H NMR (500 MHz, $(CD_3)_2SO$) δ_H 7.32 – 7.24 (5H, m, 5 × BnAr<u>H</u>), 7.71 (2H, d, *J* = 8.2 Hz, C[2]<u>H</u> and C[4]<u>H</u>), 6.67 (2H, d, *J* = 8.2 Hz, C[1]<u>H</u> and C[5]<u>H</u>), 4.32 (2H, s, O<u>C</u>H_2Ph), 3.27 (2H, t, *J* = 6.9 Hz, NH<u>C</u>H_2), 2.50 (2H, t, *J* = 6.9 Hz, <u>C</u>H_2OOH), 1.11 (2H, dd, *J* = 4.7 Hz, CC<u>H</u>H'C<u>H</u>H'), 0.88 (2H, dd, *J* = 4.7 Hz, CCH<u>H'</u>CH<u>H'</u>); ^{13}C NMR (126 MHz, $(CD_3)_2SO$) δ_C 173.1 (<u>C</u>O_2H), 158.1 (<u>C[3]</u>), 146.1 (<u>C[7]</u>), 138.6 (<u>C[6]</u>), 128.2 (<u>C[11]</u>H and <u>C[9]</u>H), 127.8 (<u>C[2]</u>H and <u>C[4]</u>H), 127.5 (<u>C[8]</u>H and <u>C[12]</u>H), 127.3 (<u>C[10]</u>H), 113.5 (<u>C[1]</u>H and <u>C[4]</u>H), 68.6 (O<u>C</u>H_2Ph), 62.9 (CH_2<u>C</u>CH_2), 40.2* (NH<u>C</u>H_2), 33.4 (<u>C</u>H_2OOH), 14.2 (C<u>C</u>H_2<u>C</u>H_2); HRMS (ESI): calcd. For $C_{19}H_{20}NO_3$, 310.1443. Found $[M-H]^-$, 310.1446 (-0.86 ppm error). *Peak detectable by ^{1}H-^{13}C HSQC.

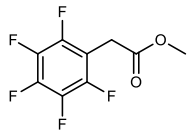

105

Methyl 2-(perfluorophenyl)acetate (105) was prepared by charging a round-bottom flask equipped with a stir bar with 2-(perfluorophenyl)acetic acid **213** (5 g, 22.1 mmol, 1.0 equiv.). The vessel was sealed before methanol (10 mL) and hydrochloric acid (1 M) (0.5 mL) were subsequently added. The reaction was stirred at 70 °C for 16 h. The reaction was directly concentrated *in vacuo* before the crude residue was basified to pH 8 with sat. sodium hydrogen carbonate and the solution extracted with ethyl acetate (3 × 10 mL). The combined organic layers were washed with a sat. brine solution, dried over magnesium sulphate, filtered, and concentrated *in vacuo* to afford the product as a white solid (3.66 g, 69%); ν_{max}/cm^{-1} (neat) 1748 (C=O stretch), 1504 (C-C aromatic stretch); ^{1}H NMR (500 MHz, $CDCl_3$) δ_H 3.75 (3H, s, CO_2C<u>H</u>$_3$), 3.73 (2H, s, <u>C</u>H_2CO_2); ^{13}C NMR (126 MHz, $CDCl_3$) δ_C 168.9 (<u>C</u>O_2), 145.5 (dddt, *J* = 248.1, 11.9, 8.3, 4.2 Hz, 2 × *m*-<u>C</u>F), 140.9 (dd, *J* = 251.1, 13.8 Hz, *p*-<u>C</u>F), 137.7 (dt, *J* = 249.6, 14.6 Hz, 2 × *o*-<u>C</u>F), 108.2 (dd, *J* = 20.7, 3.5 Hz, <u>C</u>CH_2CO_2), 52.9 (CO_2<u>C</u>H_3), 27.7 (<u>C</u>H_2CO_2); $^{19}F\{^{1}H\}$ NMR (470 MHz, $CDCl_3$) δ_F -142.3 (dd, *J* = 21.8, 8.9 Hz, 2 × *o*-C<u>F</u>), -155.2 (t, *J* = 20.8 Hz, *p*-C<u>F</u>), -162.2 – -162.3 (m, 2 × *m*-C<u>F</u>); HRMS (ESI): calcd. For $C_9H_6F_5O_2$, 241.0288. Found: $[MH]^+$, 241.0284 (-1.62 ppm error).

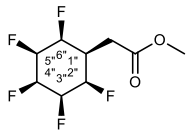

106

Methyl 2-((*1r,2R,3R,4s,5S,6S*)-2,3,4,5,6-pentafluorocyclohexyl)acetate (106) was prepared by charging an oven-dried vial with activated 4 Å molecular sieves (9.5 g), methyl 2-(perfluorophenyl)acetate **105** (950 mg, 3.95 mmol), and chloro[2-(2,6-diisopropylphenyl)-3,3-dimethyl-2-azaspiro[4.5]dec-1-ylidene][1,2,5,6-η-1,5cyclooctadiene]rhodium **104** (23 mg, 0.040 mmol, 1 mol%). The reagents were suspended in hexane (40 mL) and the vial placed inside an autoclave. The autoclave was pressurised with hydrogen to 50 Bar and the reaction mixture stirred at room temperature for 16 h. After depressurising and removing the vial, the suspension was filtered, concentrated *in vacuo* and purified by flash column chromatography (silica gel, 50% ethyl acetate in hexane) to afford the product as a white solid (945 mg, 97%); ^{1}H NMR (500 MHz, $(CD_3)_2CO$) δ_H 5.43 (1H, br dt, J = 52.3, 6.2 Hz, C[4"]H), 5.14 – 4.89 (4H, m, C[2"]H, C[3"]H, C[5"]H, and C[6"]H), 3.70 (3H, s, CO_2CH_3), 2.85 (2H, d, J = 7.2 Hz, CH_2CO_2), 2.55 (1H, br t, J = 33.4 Hz, C[1"]H); ^{13}C NMR (126 MHz, $(CD_3)_2CO$) δ_C 172.3 (CO_2), 89.5 – 88.0 (m, C[2"]H and C[6"]H), 88.3 (dd, J = 214.3, 18.5 Hz, C[4"]H), 88.1 – 86.5 (m, C[3"]H and C[5"]H), 52.2 (CO_2CH_3), 36.1 – 35.7 (m, C[1"]H), 31.0 (CH_2CO_2); ^{19}F{^{1}H} NMR (470 MHz, $(CD_3)_2CO$) δ_F -205.5 (C[3"]F and C[5"]F), -212.5 (d, J = 16.1 Hz, C[2"]F and C[6"]F), -217.6 (C[4"]F); HRMS (ESI): calcd. For $C_9H_{11}F_5O_2Na$, 269.0577. Found: $[MNa]^+$, 269.0570 (-0.71 ppm error). Reported data is in accordance with literature.[4]

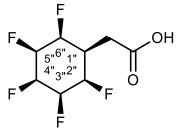

211

2-((*1r,2R,3R,4s,5S,6S*)-2,3,4,5,6-Pentafluorocyclohexyl)acetic acid (211) was prepared by charging a round-bottom flask with methyl 2-((*1r,2R,3R,4s,5S,6S*)-2,3,4,5,6-pentafluorocyclohexyl)acetate **106** (200 mg, 0.81 mmol). The vessel was sealed before hydrochloric acid (6 M) (30 mL, 180 mmol) was added and the solution stirred at 100 °C for 18 h. The reaction was basified to pH 8 with sat. sodium hydrogen carbonate solution and residual starting material was extracted using ethyl acetate (3 x 50 mL). The aqueous phase was re-acidified using hydrochloric acid (1M) and extracted with ethyl acetate (3 x 100 mL). The combined re-acidified organic layers washed with sat. brine solution, dried over magnesium sulphate, filtered, concentrated *in vacuo*, and purified by flash column chromatography (silica gel, 10% methanol in ethyl acetate to 20% methanol in ethyl acetate) to afford the product as a

white solid (71 mg, 38%); Mp. 136 – 138 ºC; R_f 0.06 (10% methanol in DCM); ν_{max}/cm^{-1} (neat) 1678 (C=O stretch); ^1H NMR (500 MHz, $(CD_3)_2SO$) δ_H 12.54 (1H, br s, $CO_2\underline{H}$), 5.39 (1H, br dt, *J* = 54.5, 5.6 Hz, C[4"]H), 5.04 – 5.84 (4H, m, C[2"]H, C[3"]H, C[5"]H, and C[6"]H), 2.68 (2H, d, *J* = 7.2 Hz, $C\underline{H_2}CO_2H$), 2.40 (1H, br t, *J* = 35.2 Hz, C[1"]H); ^{13}C NMR (126 MHz, $(CD_3)_2SO$) δ_C 172.5 (CO), 87.8 (dd, *J* = 190.1, 17.2 Hz, C[2"]H and C[6"]H), 87.3 (dt, *J* = 87.4, 18.1 Hz, C[4"]H), 86.1 (dd, *J* = 185.4, 10.2 Hz, C[3"]H and C[5"]H), 34.3 (t, *J* = 23.8 Hz, C[1"]H), 30.2 (d, *J* = 3.0 Hz, $C\underline{H_2}CO_2H$); $^{19}F\{^1H\}$ NMR (470 MHz, $(CD_3)_2SO$) δ_F -203.9 (FC[3"]H and FC[5"]H), -211.2 (d, *J* = 17.0 Hz, FC[2"]H and FC[6"]H), -216.3(C[4"]F); HRMS (ESI): calcd. For $C_8H_8F_5O_2$, 231.0444. Found: $[M-H]^-$, 231.0449 (-1.99 ppm error).

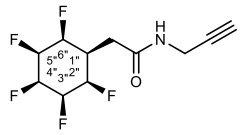

209

2-((*1r,2R,3R,4s,5S,6S*)-2,3,4,5,6-Pentafluorocyclohexyl)-N-(prop-2-yn-1-yl)acetamide (209) was prepared by charging a flame-dried round-bottom flask with 2-((*1r,2R,3R,4s,5S,6S*)-2,3,4,5,6-pentafluorocyclohexyl)acetic acid **211** (70 mg, 0.32 mmol, 1.0 equiv), prop-2-yn-1-amine **212** (22.4 μL, 0.35 mmol, 1.1 equiv.), EDCI (123 mg, 0.64 mmol, 2.0 equiv.) , and HOBt (87 mg, 0.64 mmol, 2.0 equiv.). The vessel was sealed, evacuated, and backfilled with nitrogen thrice before anhydrous DMF (10 mL) was added *via* syringe. The reaction was stirred at RT for 16 h. The reaction was directly concentrated *in vacuo* before reconstituting in ethyl acetate (10 mL) and diluted with deionised water (5 mL). The aqueous layer was separated and extracted with ethyl acetate (3 × 10 mL) before the combined organic layers were washed with sat. brine solution, dried over magnesium sulphate, filtered, concentrated *in vacuo*, and purified by flash column chromatography (silica gel, DCM to 5% methanol in DCM) to afford the product as a white solid (40 mg, 46%); Mp. 236 – 238 ºC; R_f 0.61 (10% methanol in DCM); ν_{max}/cm^{-1} (neat) 3304 (N-H stretch), 2360 (C≡C stretch), 1641 (C=O stretch); ^1H NMR (500 MHz, $(CD_3)_2CO$) δ_H 7.68 (C(O)N\underline{H}), 5.42 (1H, dt, *J* = 53.8, 7.8 Hz, C[4"]H), 5.06 – 4.86 (4H, m, C[2"]H, C[3"]H, C[5"]H, and C[6"]H), 4.03 (2H, dd, *J* = 5.5, 2.5 Hz, CONHC$\underline{H_2}$), 2.73 (2H, d, *J* = 7.2 Hz, C[1"]HC$\underline{H_2}$), 2.64 (1H, t, *J* = 2.5 Hz, C≡C\underline{H}), 2.61 – 2.48 (1H, m, C[1"]H); ^{13}C NMR (126 MHz, $(CD_3)_2CO$) δ_C 170.3 (CO), 89.0 (dd, *J* = 189.0, 17.6 Hz, C[2"]H and C[6"]H), 88.5 (dt, *J* = 193.0, 18.6 Hz, C[4"]H), 88.1 – 86.6 (m, C[3"]H and C[5"]H), 80.3 (C≡CH)*, 72.0 (C≡CH), 36.1 (t, *J* = 18.3 Hz, C[1"]H), 32.5 (C[1"]$\underline{C}H_2CO$), 29.0 ($\underline{C}H_2C\equiv CH$); $^{19}F\{^1H\}$ NMR (470 MHz, $(CD_3)_2CO$) δ_F -205.3 (FC[3"]H and FC[5"]H), -212.0 (d, *J* = 21.5 Hz, FC[2"]H and FC[6"]H), -217.5 (FC[4"]H); HRMS (ESI): calcd. For $C_{11}H_{13}F_5NO$, 270.0917. Found: $[MH]^+$, 270.0911 (-0.12 ppm error). *Peak detected by HSQC.

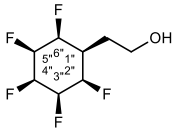

107

2-((*1r,2R,3R,4s,5S,6S*)-2,3,4,5,6-Pentafluorocyclohexyl)ethan-1-ol (107) was prepared by charging a flame-dried round-bottom flask equipped with a magnetic stir bar with methyl 2-((*1r,2R,3R,4s,5S,6S*)-2,3,4,5,6-pentafluorocyclohexyl)acetate **106** (373 mg, 1.52 mmol, 1.0 equiv.). The vessel was sealed, evacuated, and backfilled with nitrogen thrice before anhydrous THF (15 mL) was added *via* syringe and the reaction cooled to 0 °C. DIBAL-H (1 M in THF) (3.35 mL, 3.35 mmol, 2.2 equiv.) was then added dropwise *via* syringe and the reaction was warmed to RT and stirred for 16 h. The reaction was then cooled to 0 °C before being diluted with diethyl ether (50 mL) and subsequently quenched with deionised water (0.2 mL). A solution of sodium hydroxide in water (15% w/w) (0.2 mL) was then added followed by additional deionised water (0.4 mL) before the reaction was stirred at RT for 15 min. Anhydrous magnesium sulphate (500 mg) was then added and the reaction was stirred for an additional 15 min before being filtered and concentrated *in vacuo*. Purification by flash column chromatography (silica gel, DCM to 5% methanol in DCM) afford the product as a white solid (146 mg, 44%); ^{1}H NMR (500 MHz, CD_3OD) δ_H 5.27 (1H, br dt, J = 53.6, 7.2 Hz, C[4"]H), 4.98 – 4.86 (2H, m, C[2"]H and C[6"]H), 4.67 (2H, br dt, J = 34.5, 25.1 Hz, C[3"]H and C[5"]H), 3.74 (2H, t, J = 6.0 Hz, CH_2OH), 2.10 – 1.94 (3H, m, C[1"]H and C[1"]CH_2); ^{13}C NMR (126 MHz, CD_3OD) δ_C 89.3 (dd, J = 190.5, 18.2 Hz, C[2"]H and C[6"]H), 89.1 (d, J = 194.4 Hz, C[4"]H), 87.9 (dd, J = 188.4, 12.8 Hz, C[3"]H and C[5"]H), 59.4 (CH_2OH), 56.3 – 55.9 (m, C[1"]H), 29.8 (C[1"]CH_2); ^{19}F{^{1}H} NMR (470 MHz, CD_3OD) δ_F -205.8 – -205.9 (m, C[3"]F and C[5"]F), -213.2 (dt, J = 25.9, 4.8 Hz, C[2"]F and C[6"]F), -218.2 (tt, J = 24.9, 10.8 Hz, C[4"]F); HRMS (ESI): calcd. For $C_8H_{11}F_5ONa$, 241.0628. Found: $[MNa]^+$, 241.0625 (1.02 ppm error). Reported data is in accordance with literature.[4]

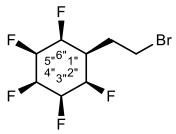

109

(*1r,2R,3R,4s,5S,6S*)-1-(2-Bromoethyl)-2,3,4,5,6-pentafluorocyclohexane (109) was prepared by charging a flame-dried round-bottom flask equipped with a magnetic stir bar with 2-((*1r,2R,3R,4s,5S,6S*)-2,3,4,5,6-pentafluorocyclohexyl)ethan-1-ol **107** (504 mg, 2.31 mmol, 1.0 equiv.), triphenylphosphine (1.27 g, 4.85 mmol, 2.1 equiv.), and carbon tetrabromide (1.60 g, 4.85 mmol, 2.1 equiv.). The vessel was sealed, evacuated, and backfilled with nitrogen thrice

before anhydrous acetonitrile (23 mL) was added *via* syringe. The reaction was stirred at RT for 12 h. The reaction was directly concentrated *in vacuo* before being purified by flash column chromatography (silica gel, 50% DCM in hexane) to afford the product as a white solid (444 mg, 69%); ^{1}H NMR (500 MHz, CD_3OD) δ_H 5.30 (1H, d, J = 53.2 Hz, C[4"]H), 5.08 – 4.59 (4H, m, C[2"]H, C[3"]H, C[5"]H, and C[6"]H), 3.68 (2H, t, J = 6.7 Hz, CH_2Br), 2.36 (2H, apparent q, 6.7 Hz, C[1"]CH_2), 2.24 – 2.09 (1H, m, C[1"]H); ^{13}C NMR (126 MHz, CD_3OD) δ_C 89.8 – 88.6 (m, C[4"]H), 88.7 (dd, J = 193.3, 18.3 Hz, C[2"]H and C[6"]H), 88.6 – 86.8 (m, C[3"]H and C[5"]H), 38.2 – 37.7 (m, C[1"]H), 31.0 (CH_2Br), 30.2 (C[1"]CH_2); ^{19}F{^{1}H} NMR (470 MHz, CD_3OD) δ_F -206.1 (C[3"]F and C[5"]F), -213.0 (d, J = 25.7 Hz, C[2"]F and C[6"]F), -218.3 (tt, J = 25.6, 10.0 Hz, C[4"]F); HRMS (ESI): calcd. For $C_8H_{10}{}^{79}BrF_5Na$, 302.9784. Found: $[MNa]^+$, 302.9778 (-0.18 ppm error). Reported data is in accordance with literature.[4]

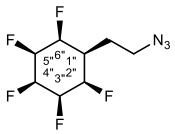

110

(*1r,2R,3R,4s,5S,6S*)-1-(2-Azidoethyl)-2,3,4,5,6-pentafluorocyclohexane (110) was prepared by charging a flame-dried round-bottom flask equipped with a magnetic stir bar with (*1r,2R,3R,4s,5S,6S*)-1-(2-bromoethyl)-2,3,4,5,6-pentafluorocyclohexane **109** (308 mg, 1.1 mmol, 1.0 equiv.) and sodium azide (143 mg, 2.2 mmol, 2.0 equiv.). The vessel was sealed, evacuated, and backfilled thrice with nitrogen before anhydrous DMF (5 mL) was added *via* syringe. The reaction was stirred at 70 °C for 2 h. The reaction was diluted with deionised water (5 mL) and extracted with ethyl acetate (3 × 10 mL). The combined organic layers were washed with a sat. brine solution, dried over magnesium sulphate, filtered, and concentrated *in vacuo*. Purification by flash column chromatography (silica gel, 50% hexane in DCM to DCM) afforded the product as a white solid (121 mg, 45%); ^{1}H NMR (400 MHz, $(CD_3)_2CO$) δ_H 5.42 (1H, dt, J = 53.8, 7.2 Hz, C[4"]H), 5.16 – 5.03 (2H, m, C[2"]H and C[6"]H), 4.94 (2H, dt, J = 39.5, 28.1 Hz, C[3"]H and C[5"]H), 3.64 (2H, t, J = 6.6 Hz, CH_2N_3), 2.08 (2H, apparent q, J = 6.6 Hz, C[1"]CH_2); ^{13}C NMR (126 MHz, $(CD_3)_2CO$) δ_C 88.6 – 86.3 (m, C[3"]H and C[5"]H), 88.5 (dt, J = 194.2, 18.0 Hz, C[4"]H), 88.5 (dd, J = 191.6, 17.5 Hz, C[2"]H and C[6"]H), 49.0 (CH_2N_3), 36.2 (tt, J = 18.1, 4.3 Hz, C[1"]H), 26.1 (C[1"]CH_2); ^{19}F{^{1}H} NMR (470 MHz, $(CD_3)_2CO$) δ_F -205.11 (dd, J = 13.6, 7.6 Hz, C[3"]F and C[5"]F), -212.67 (dt, J = 25.2, 4.9 Hz, C[2"]F and C[6"]F), -217.55 (tt, J = 25.2, 10.7 Hz, C[4"]F); HRMS (ESI): calcd. For $C_8H_{10}N_3F_5Na$, 266.0692. Found: $[MNa]^+$, 266.0681 (-2.40 ppm error). Reported data is in accordance with literature.[4]

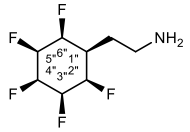

111

2-((*1r,2R,3R,4s,5S,6S*)-2,3,4,5,6-Pentafluorocyclohexyl)ethan-1-amine (111) was prepared by charging a round-bottom flask equipped with a magnetic stir bar with (*1r,2R,3R,4s,5S,6S*)-1-(2-azidoethyl)-2,3,4,5,6-pentafluorocyclohexane **110** (198 mg, 0.85 mmol, 1.0 equiv.) and triphenylphosphine (448 mg, 1.71 mmol, 2.0 equiv.). The vessel was sealed before THF (4 mL) and deionised water (0.5 mL) were subsequently added *via* syringe. The reaction was stirred at 50 °C for 22 h before being directly concentrated *in vacuo*. Purification by flash column chromatography (silica gel, 1% triethylamine in 20% methanol in DCM) afford the product as a white solid (123 mg, 66%); ^{1}H NMR (500 MHz, D_3COD) δ_H 5.28 (1H, dt, J = 54.5, 7.1 Hz, C[4"]H), 4.96 – 4.56 (4H, m, C[2"]H, C[3"]H, C[5"]H, and C[6"]H), 2.88 (2H, t, J = 7.2 Hz, CH_2NH_2), 2.00 – 1.87 (3H, m, C[1"]H and C[1"]CH_2); ^{13}C NMR (126 MHz, D_3COD) δ_C 89.9 – 88.2 (m, C[4"]H), 89.1 (dd, J = 191.8, 17.9 Hz, C[2"]H and C[6"]H), 88.7 – 87.0 (m, C[3"]H and C[5"]H), 39.0 (CH_2NH_2), 36.9 – 36.5 (m, C[1"]H), 29.0 (C[1"]CH_2); ^{19}F{^{1}H} NMR (470 MHz, $(CD_3)_2CO$) δ_F -205.9 (C[3"]F and C[5"]F), -213.4 (d, J = 25.5 Hz, C[2"]F and C[6"]F), -218.3 (tt, J = 25.5, 11.0 Hz, C[4"]F); HRMS (ESI): calcd. For $C_8H_{10}F_5N_3Na$, 266.0692. Found: $[MNa]^+$, 266.0681 (-2.40 ppm error). Reported data is in accordance with literature.[4]

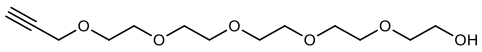

220

3,6,9,12,15-Pentaoxaoctadec-17-yn-1-ol (220) was prepared by charging a flame-dried round-bottom flask equipped with a magnetic stir bar with 3,6,9,12-tetraoxatetradecane-1,14-diol **219** (1.8 mL, 8.51 mmol, 1.0 equiv.) before adding anhydrous DMF (160 mL). The solution was cooled to 0 °C before sodium hydride (60% w/w dispersion in mineral oil) (375 mg, 9.36 mmol, 1.1 equiv.) was added portion-wise. The vessel was sealed and the reaction was stirred at 0 °C for 30 min before propargyl bromide (0.71 mL, 9.36 mmol, 1.1 equiv.) was added dropwise *via* syringe. The reaction was stirred at RT for 14 h. The reaction was diluted with methanol (20 mL) before being stirred for an additional 20 min. The reaction was concentrated *in vacuo* before being reconstituted in ethyl acetate (80 mL) and washed with a sat, ammonium chloride solution (50 mL). The aqueous layer was separated and extracted with ethyl acetate (3 × 40 mL) before the combined organic layers were dried over magnesium sulphate, filtered, concentrated *in vacuo*, and purified by flash column chromatography (silica gel, ethyl acetate to 5% methanol

in ethyl acetate) to afford the product as an amber oil (750 mg, 32%); ^{1}H NMR (400 MHz, $CDCl_3$) δ_H 4.19 (2H, d, J = 2.4 Hz, HC≡CC$\underline{H}_2$), 3.72 – 3.63 (18H, m, 9 × OC$\underline{H}_2$CH_2O), 3.61 – 3.59 (2H, m, OCH_2C$\underline{H}_2$O), 2.66 (1H, br s, O$\underline{H}$), 2.42 (1H, t, J = 2.4 Hz, $\underline{H}$C≡C); ^{13}C NMR (126 MHz, $CDCl_3$) δ_C 79.7 (HC≡$\underline{C}$), 74.5 (H$\underline{C}$≡C), 72.5 (O$\underline{C}H_2CH_2O$), 70.6 (m, 5 × O$\underline{C}H_2CH_2O$), 70.4 (O$\underline{C}H_2CH_2O$), 70.4 (O$\underline{C}H_2CH_2O$), 69.1 (O$\underline{C}H_2CH_2O$), 61.8 ($\underline{C}H_2$OH), 58.4 (C≡C$\underline{C}H_2$); HRMS (ESI): calcd. For $C_{13}H_{24}O_6Na$, 299.1471. Found: $[MNa]^+$, 299.1464 (-0.37 ppm error). Reported data is in accordance with literature.[5]

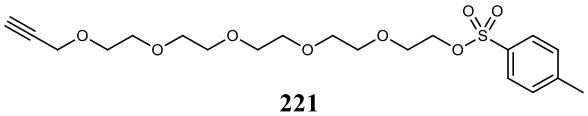

221

3,6,9,12,15-Pentaoxaoctadec-17-yn-1-yl 4-methylbenzenesulfonate (221) was prepared by charging a round-bottom flask equipped with a magnetic stir bar with 3,6,9,12,15-pentaoxaoctadec-17-yn-1-ol **220** (200 mg, 0.73 mmol, 1.0 equiv.) before subsequently adding THF (5 mL) and a sodium hydroxide solution (5 mL/g) (0.5 mL, 2.54 mmol, 3.5 equiv.). 4-toluenesulfonyl chloride (165 mg, 0.87 mmol, 1.2 equiv.) was added portion-wise before the vessel was sealed and the reaction stirred at RT for 16 h. The reaction was quenched with sat. ammonium chloride (5 mL) before the aqueous layer was separated and extracted with DCM (3 × 5 mL). The combined organic layers were dried over anhydrous magnesium sulphate, filtered, and concentrated *in vacuo* to afford the product as a colourless oil (267 mg, 86%); ^{1}H NMR (500 MHz, $CDCl_3$) δ_H 7.79 (2H, d, J = 8.3 Hz, *m*-ArC$\underline{H}$), 7.33 (2H, d, J = 8.3 Hz, *o*-ArC$\underline{H}$), 4.19 (2H, d, J = 2.4 Hz, C≡CC$\underline{H}_2$), 4.16 – 4.14 (2H, m, C$\underline{H}_2$OSO_2), 3.70 – 3.57 (18H, m, 9 × OC$\underline{H}_2$CH_2O), 2.44 (3H, s, *p*-ArCC$\underline{H}_3$), 2.42 (1H, t, J = 2.4 Hz, $\underline{H}$C≡C); ^{13}C NMR (126 MHz, $CDCl_3$) δ_C 144.9 ($SO_2\underline{C}$), 133.1 (*p*-Ar$\underline{C}CH_3$), 129.9 (*m*-Ar$\underline{C}$H), 128.1 (*o*-Ar$\underline{C}$H), 79.8 (HC≡$\underline{C}$), 74.7 (H$\underline{C}$≡C), 70.9 (O$\underline{C}H_2CH_2O$), 70.7 – 70.6 (m, 5 × O$\underline{C}H_2CH_2O$), 70.5 (O$\underline{C}H_2CH_2O$), 69.4 (O$\underline{C}H_2CH_2O$), 69.2 (O$\underline{C}H_2CH_2O$), 68.8 (O$\underline{C}H_2CH_2O$), 58.5 (C≡C$\underline{C}H_2$), 21.8 (*p*-ArC$\underline{C}H_3$); HRMS (ESI): calcd. For $C_{20}H_{31}O_8S$, 431.1734. Found: $[MH]^+$, 431.1735 (0.20 ppm error). Reported data is in accordance with literature.[6]

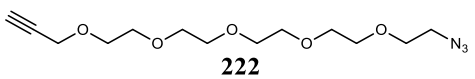

222

1-Azido-3,6,9,12,15-pentaoxaoctadec-17-yne (222) was prepared by charging a flame-dried round-bottom flask equipped with a magnetic stir bar with 3,6,9,12,15-pentaoxaoctadec-17-yn-1-yl 4-methylbenzenesulfonate **221** (250 mg, 0.58 mmol, 1.0 equiv.), sodium azide (42 mg, 0.64 mmol, 1.1 equiv.), and TBAI (21 mg, 58 μmol, 10 mol%). The vessel was sealed, evacuated, and backfilled with nitrogen thrice before anhydrous DMF (5 mL) was added *via*

syringe. The reaction was stirred at 45 °C for 20 h before being directly concentrated *in vacuo*. The crude reaction mixture was triturated with diethyl ether and subsequently filtered. The filtrate was concentrated *in vacuo* before being reconstituted in toluene and concentrated *in vacuo* once more to afford the product as a colourless oil (126 mg, 72%); ^{1}H NMR (500 MHz, $CDCl_3$) δ_H 4.19 (2H, d, J = 2.1 Hz, C≡CC$\underline{H_2}$), 3.68 – 3.65 (18H, m, 9 × OC$\underline{H_2}$CH_2O), 3.38 (2H, t, J = 4.9 Hz, C$\underline{H_2}$N$_3$), 2.42 (1H, t, J = 2.1 Hz, C≡CC$\underline{H_2}$); ^{13}C NMR (126 MHz, $CDCl_3$) δ_C 79.8 (HC≡$\underline{C}$), 74.6 (H$\underline{C}$≡C), 70.8 – 70.7 (7 × O$\underline{C}$H$_2$CH$_2$O), 70.5 (O$\underline{C}$H$_2$CH$_2$O), 70.1 (O$\underline{C}$H$_2$CH$_2$O), 69.2 (O$\underline{C}$H$_2$CH$_2$O), 58.5 (C≡$\underline{C}$CH$_2$), 50.8 ($\underline{C}$H$_2$N$_3$); HRMS (ESI): calcd. For $C_{13}H_{23}O_5N_3Na$, 324.1530. Found: $[MNa]^+$, 324.1523 (-2.13 ppm error). Reported data is in accordance with literature.[7]

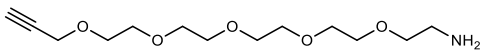

217

3,6,9,12,15-Pentaoxaoctadec-17-yn-1-amine (217) was prepared by charging a round-bottom flask equipped with a magnetic stir bar with 1-azido-3,6,9,12,15-pentaoxaoctadec-17-yne **222** (617 mg, 2.05 mmol, 1.0 equiv.) and triphenylphosphine (645 mg, 2.46 mmol, 1.2 equiv.). The vessel was sealed before THF (10 mL) and deionised water (1.5 mL) were subsequently added *via* syringe. The reaction was stirred at 50 °C for 20 h before being directly concentrated *in vacuo*. Purification by flash column chromatography (silica gel, 1% triethylamine in 20% methanol in DCM) afford the product as a white solid (265 mg, 46%); ^{1}H NMR (400 MHz, $CDCl_3$) δ_H 4.20 (2H, d, J = 2.4 Hz, HC≡CC$\underline{H_2}$), 3.71 – 3.61 (16H, m, 8 × OC$\underline{H_2}$CH_2O), 3.52 (2H, t, J = 5.2 Hz, OC$\underline{H_2}$CH_2NH$_2$), 3.47 – 3.46 (2H, m, N$\underline{H_2}$), 2.87 (2H, t, J = 5.2 Hz, C$\underline{H_2}$NH$_2$), 2.43 (1H, t, J = 2.4 Hz, $\underline{H}$C≡C); ^{13}C NMR (126 MHz, $CDCl_3$) δ_C 79.8 (HC≡$\underline{C}$), 74.7 (H$\underline{C}$≡C), 72.8 (O$\underline{C}$H$_2$CH$_2$O), 70.7 – 70.4 (m, 8 × O$\underline{C}$H$_2$CH$_2$O), 69.2 (O$\underline{C}$H$_2$CH$_2$O), 58.5 (C≡$\underline{C}$CH$_2$), 41.7 ($\underline{C}$H$_2$NH$_2$); HRMS (ESI): calcd. For $C_{13}H_{26}O_5N$, 276.1811. Found: $[MH]^+$, 276.1812 (2.29 ppm error). Reported data is in accordance with literature.[7]

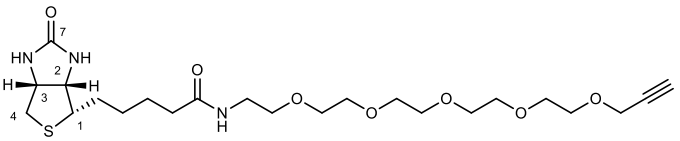

223

N-(3,6,9,12,15-Pentaoxaoctadec-17-yn-1-yl)-5-((*4S*)-2-oxohexahydro-1H-thieno[3,4-d]imidazol-4-yl)pentanamide (223) was prepared by charging a flame-dried round-bottom flask equipped with a magnetic stir bar with 3,6,9,12,15-pentaoxaoctadec-17-yn-1-amine **217** (238 mg, 0.87 mmol, 1.0 equiv.), biotin **218** (254 mg, 1.04 mmol, 1.2 equiv.), and EDCI (200 mg, 1.04 mmol, 1.2 equiv.). The vessel was sealed, evacuated, and backfilled with nitrogen

thrice. Anhydrous DMF (5 mL) was added *via* syringe before the reaction was stirred at RT for 16 h. The reaction was worked up with a sat. sodium hydrogen carbonate solution (5 mL) and the aqueous layer was extracted with ethyl acetate (3 × 5 mL). The combined organic layers were washed with sat. brine (5 mL), dried over anhydrous magnesium sulphate, filtered, and concentrated *in vacuo*. Purification by flash column chromatography (silica gel, 10% methanol in ethyl) afforded the product as a colourless oil (51 mg, 21%); R_f 0.12 (10% methanol in ethyl acetate); ν_{max}/cm^{-1} (neat) 3246 (N-H amide stretch/C-H alkyne stretch), 3868 (C-H alkane stretch), 1703 (C=O stretch); ^{1}H NMR (500 MHz, CD_3OD) δ_H 4.50 (1H, ddd, *J* = 8.0, 5.0, 0.8 Hz, C[3]H), 4.31 (1H, dd, *J* = 8.0, 4.5 Hz, C[2]H), 4.19 (2H, d, *J* = 2.4 Hz, $H_2CC{\equiv}CH$), 3.69 – 3.61 (16H, m, 8 × OCH_2), 3.55 (2H, t, *J* = 5.5 Hz, OCH_2CH_2NH), 3.36 (2H, t, *J* = 5.5 Hz, OCH_2CH_2NH), 3.21 (1H, dt, *J* = 10.1, 5.6 Hz, C[1]H), 2.93 (dd, *J* = 12.7, 5.0 Hz, C[4]HH'), 2.86 (1H, t, *J* = 2.4 Hz, C≡CH), 2.71 (1H, apparent d, *J* = 12.7, C[4]HH'), 2.23 (2H, t, *J* = 2.4 Hz, $CH_2CH_2C(O)NH$), 1.78 – 1.57 (4H, m, C[1]HCH_2CH_2 and $CH_2CH_2C(O)NH$), 1.48 – 1.42 (2H, apparent p, *J* = 7.9, 7.7 Hz, SCH$CH_2CH_2CH_2$); ^{13}C NMR (126 MHz, CD_3OD) δ_C 176.1 (CH_2CONH), 166.1 (C[7]O), 80.6 (HC≡C), 76.0 (HC≡C), 71.5 (5 × OCH_2), 71.5 (OCH_2), 71.3 (OCH_2), 70.6 (OCH_2), 70.1 (OCH_2), 63.4 (C[2]H), 61.6 (C[3]H), 59.0 ($OCH_2C{\equiv}CH$), 57.0 (C[1]H), 41.1 (C[4]H_2), 40.4 (C(O)NHCH_2), 36.7 ($CH_2C(O)NH$), 29.8 (C[1]H$CH_2CH_2CH_2$), 29.5 (C[1]HCH_2), 26.9 ($CH_2CH_2CH_2$); HRMS (ESI): calcd. For $C_{23}H_{40}N_3O_7S$, 502.2587. Found: $[MH]^+$, 502.2573 (-1.6571 ppm error).

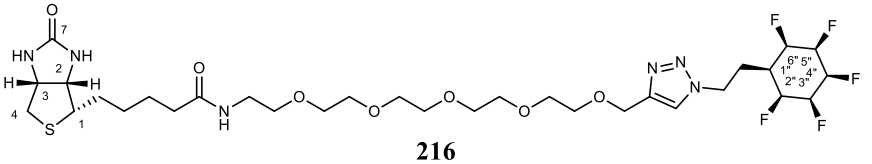

216

2-(2-Oxohexahydro-1H-thieno[3,4-d]imidazol-4-yl)-N-(1-(1-(2-((*2R,3R,4s,5S,6S*)-2,3,4,5,6-pentafluorocyclohexyl)ethyl)-1H-1,2,3-triazol-4-yl)-2,5,8,11,14-pentaoxahexadecan-16-yl)acetamide (216) was prepared by charging a round-bottomed flask equipped with a magnetic stir bar with N-(3,6,9,12,15-pentaoxaoctadec-17-yn-1-yl)-2-(2-oxohexahydro-1H-thieno[3,4-d]imidazol-4-yl)acetamide **223** (51 mg, 0.10 mmol, 1.0 equiv.), (*1r,2R,3R,4s,5S,6S*)-1-(2-azidoethyl)-2,3,4,5,6-pentafluorocyclohexane **110** (28 mg, 0.11 mmol, 1.1 equiv.), sodium ascorbate (3 mg, 15 μmol, 15 mol%), and copper (II) sulfate pentahydrate (0.8 mg, 3.1 μmol, 3 mol%). Ethanol (1 mL) and deionised water (1 mL) were subsequently added *via* syringe before heating to 65 °C for 24 h. Purification by flash column chromatography (silica gel, 50% methanol in ethyl acetate) afforded the product as a colourless oil (52 mg, 69%); R_f 0.23 (50% methanol in ethyl acetate); ν_{max}/cm^{-1} (neat) 2992 (C-H alkene), 2855 (C-H alkane), 1697 (C=O amide), 1647 (C=C alkene); ^{1}H NMR (700 MHz, CD_3OD) δ_H

8.07 (1H, s, HC=C), 5.32–5.23 (1H, m, FC[4"]H), 5.04–4.95 (2H, m, FC[2"]H and FC[6"]H), 4.70 – 4.55 (6H, m, NNNCH_2CH_2, OCH_2CNNN, C[3"]H, and C[5"]H), 4.49 (1H, dd, *J* = 7.9, 5.0 Hz, C[3]H), 4.30 (1H, dd, *J* = 7.9, 4.5 Hz, C[2]H), 3.68 – 3.60 (16H, m, 8 × OCH_2), 3.53 (2H, t, *J* = 5.5 Hz, C(O)NHCH_2CH_2O), 3.35 (2H, t, *J* = 5.5 Hz, C(O)NHCH_2CH_2O), 3.20 (1H, ddd, *J* = 9.0, 5.8, 4.5 Hz, C[1]H), 2.92 (1H, dd, *J* = 12.8, 5.0 Hz, C[4]HH'), 2.70 (1H, d, *J* = 12.8 Hz, C[4]HH'), 2.41 (2H, q, *J* = 7.1 Hz, CH_2C[1"]H), 2.22 (2H, td, *J* = 7.4, 1.8 Hz, CH_2CH_2C(O)NH), 1.88 – 1.79 (1H, m, C[1"]H), 1.74 (1H, ddt, *J* = 13.2, 9.3, 6.2 Hz, C[1]HCHH'), 1.70 – 1.57 (3H, m, C[1]HCHH' and CH_2CH_2C(O)NH), 1.44 (2H, apparent p, *J* = 8.8, 8.3 Hz, CH_2CH_2CH_2C(O)NH);^{13}C NMR (176 MHz, CD_3OD) δ_C 176.2 (CH_2C(O)NH), 166.1 (C[7]O), 146.3 (CH_2C=CH), 125.3 (CH_2C=CH), 88.88 (dd, *J* = 193.4, 18.1 Hz, FC[2"]H and FC[6"]H), 88.8 (d, *J* = 187.8 Hz, C[4"]H)*, 86.8 – 85.8 (m, C[3"]H and C[5"]H)*, 71.6 – 71.5 (m, 6 × OCH_2), 71.2 (OCH_2), 70.9 (OCH_2), 70.6 (OCH_2), 65.0 (OCH_2C=C), 63.4 (C[2]H), 61.6 (C[3]H), 57.0 (C[1]H), 48.3 (NNNCH_2CH_2), 41.1 (C[4]H_2), 40.4 (C(O)NHCH_2), 36.8 (m, C[1"]H), 36.7 (CH_2C(O)NH), 29.8 (CH_2CH_2CH_2C(O)NH), 29.5 (C[1]HCH_2), 28.0 (CH_2C[1"]H), 26.8 (CH_2CH_2C(O)NH);^{19}F{^{1}H} NMR (470 MHz, CD_3OD) δ_F -206.0 (C[3"]F and C[5"]F), -213.2 (d, *J* = 20.6 Hz, C[2"]F and C[6"]F), -218.2 – -218.3 (m, C[4"]F); HRMS (ESI): calcd. For $C_{31}H_{49}F_5N_6O_7SNa$, 767.3196. Found: $[MNa]^+$, 767.3186 (-1.28 ppm error). *Peaks detected by HSQC.

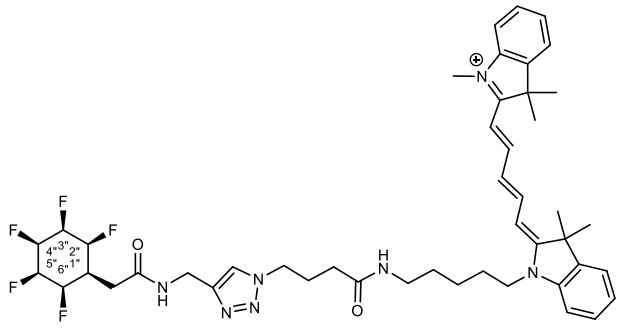

208

2-((1E,3E)-5-((E)-3,3-Dimethyl-1-(5-(4-(4-((2-((*1r,2R,3R,4s,5S,6S*)-2,3,4,5,6-pentafluorocyclohexyl)acetamido)methyl)-1H-1,2,3-triazol-1-yl)butanamido)pentyl)indolin-2-ylidene)penta-1,3-dien-1-yl)-1,3,3-trimethyl-3H-indol-1-ium (208) was prepared by flame-drying a microwave vial equipped with a magnetic stir bar before sealing, evacuating, and backfilling with nitrogen thrice. DMSO (1 mL), cyanine5 azide **210** (1 mg/mL in DMSO) (0.17 mL, 0.30 μmol, 1.0 equiv.), 2-((*1r,2R,3R,4s,5S,6S*)-2,3,4,5,6-pentafluorocyclohexyl)-N-(prop-2-yn-1-yl)acetamide **209** (1 mg/mL in DMSO) (0.16 mL, 0.60 μmol, 2.0 equiv.), copper(I) sulphate pentahydrate (1 M in water) (0.9 μL, 0.9 μmol, 3.0 equiv.), and sodium ascorbate (1 M in water) (1.8 μL, 1.8 μmol, 6.0 equiv.) were subsequently added to the vial *via* syringe before nitrogen was bubbled through the solution for 10 min. The reaction

was stirred at RT for 24 h in the absence of light. The reaction was taken directly to purification by semipreparative HPLC on a Shimadzu Prominence system using a Phenomenex Synergi® Polar-RP 80Å (250 x 10.0 mm, 4µ) and a guard cartridge; Mobile phase: 0.05% TFA in water (solvent A) and 0.05% TFA in MeCN (solvent B); linear gradient: 20% solvent B to 80% solvent B over 20 min, then to 95% B over 5 min, then back to 20% B over 5 min, then 20% B for 5 min to re-equilibrate the column. Flow rate: 2.5 mL/min; detection: 648 nm. The relevant fractions were collected (tR = 21.71 min), concentrated and lyophilized affording the product (38 µg*, 15%) as a blue solid; HRMS (ESI): calcd. For $C_{46}H_{57}F_5N_7O_2^+$, 834.4494. Found: $[M]^+$, 834.4485 (-1.08 ppm error). *Mass was calculated from measured absorbance (648 nm).

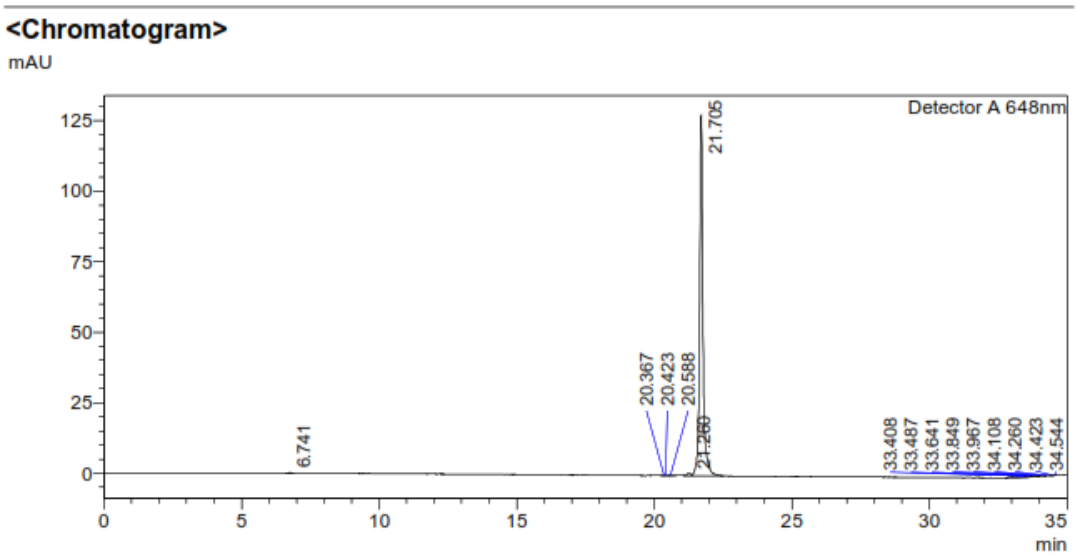

<Peak Table>

Detector A 648nm

Peak#	Ret. Time	Area	Height	Conc.	Unit	Mark	Name
6	21.705	1089545	127573	0.000	mg/L	V	RT:21.705
Total		1089545	127573				

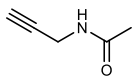

214

N-(Prop-2-yn-1-yl)acetamide (214) was prepared by cooling a solution of prop-2-yn-1-amine **212** (200 mg, 3.63 mmol, 1.0 equiv.) in DCM (15 mL) to 0 °C in a sealed flame-dried round-bottom flask equipped with a magnetic stir bar. Triethylamine (556 mg, 5.45 mmol, 1.5 equiv.) and acetic anhydride (1.11g, 11.0 mmol, 3.0 equiv.) were subsequently added *via* syringe before the reaction was stirred at 0 °C for 1 h. The reaction was then warmed to RT and stirred for a further 10 h before being quenched with deionised water (10 mL). The organic layer was separated, dried over magnesium sulphate, filtered, and concentrated *in vacuo* to afford the product as an orange solid (343 mg, 97%); ^{1}H NMR (500 MHz, $CDCl_3$) δ_H 6.10 (1H, br s, NH),

4.02 (2H, dd, J = 5.3, 2.6 Hz, C≡CC<u>H</u>$_2$), 2.21 (1H, t, J = 2.6 Hz, <u>H</u>C≡C), 2.00 (3H, s, COC<u>H</u>$_3$); ^{13}C NMR (126 MHz, $CDCl_3$) δ_C 170.0 (<u>C</u>O), 79.7 (HC≡<u>C</u>), 71.6 (H<u>C</u>≡C), 29.3 (C≡C<u>C</u>H$_2$), 23.1 (CO<u>C</u>H$_3$); HRMS (ESI): calcd. For C_5H_7ON, 97.0522. Found: $[M]^+$, 97.0524 (1.77 ppm error). Reported data is in accordance with literature.[9]

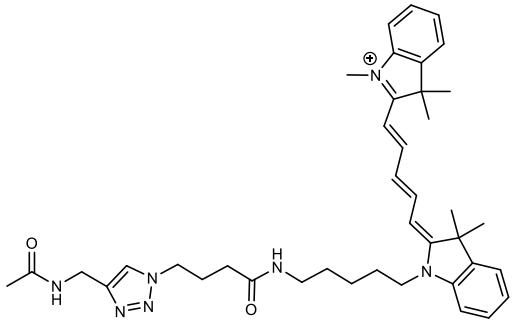

215

2-((1E,3E)-5-((E)-1-(5-(4-(4-(Acetamidomethyl)-1H-1,2,3-triazol-1-yl)butanamido)pentyl)-3,3-dimethylindolin-2-ylidene)penta-1,3-dien-1-yl)-1,3,3-trimethyl-3H-indol-1-ium (215) was prepared by flame-drying a microwave vial equipped with a magnetic stir bar before sealing, evacuating, and backfilling with nitrogen thrice. DMSO (0.5 mL), deionised water (0.5 mL), cyanine5 azide **210** (5 mg/mL in DMSO) (34 µL, 0.30 µmol, 1.0 equiv.), N-(prop-2-yn-1-yl)acetamide **214** (1 mg/mL in DMSO) (58 µL, 0.60 µmol, 2.0 equiv.), copper(I) sulphate pentahydrate (1 M in water) (0.9 µL, 0.9 µmol, 3.0 equiv.), and sodium ascorbate (1 M in water) (1.8 µL, 1.8 µmol, 6.0 equiv.) were subsequently added to the vial *via* syringe before nitrogen was bubbled through the solution for 10 min. The reaction was stirred at 70 °C for 24 h in the absence of light. The reaction was taken directly to purification by semipreparative HPLC on a Shimadzu Prominence system using a Phenomenex Synergi® Polar-RP 80Å (250 x 10.0 mm, 4µ) and a guard cartridge; Mobile phase: 0.05% TFA in water (solvent A) and 0.05% TFA in MeCN (solvent B); linear gradient: 20% solvent B to 80% solvent B over 20 min, then to 95% B over 5 min, then back to 20% B over 5 min, then 20% B for 5 min to re-equilibrate the column. Flow rate: 2.5 mL/min; detection: 648 nm. The relevant fractions were collected (tR = 21.170 min), concentrated and lyophilized affording the product (26 µg*, 13%) as a blue solid; HRMS (ESI): calcd. For $C_{40}H_{52}N_7O_2^+$, 662.4177. Found: $[M]^+$, 662.4173 (-0.60 ppm error). *Mass was calculated from measured absorbance (648 nm).

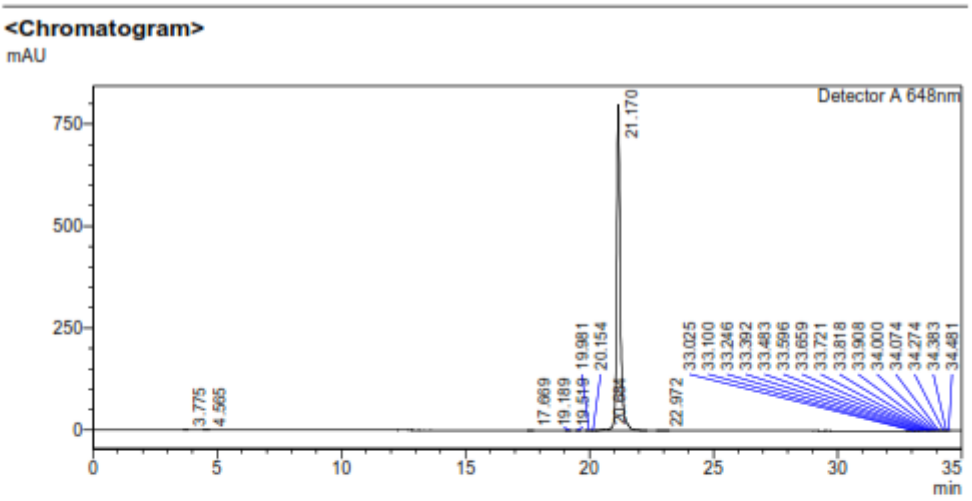

<Peak Table>

Detector A 648nm

Peak#	Ret. Time	Area	Height	Conc.	Unit	Mark	Name
1	3.775	1021	123	0.000		V	
2	4.565	1425	136	0.000		V	
3	17.669	1561	190	0.000		V	
4	19.189	1732	180	0.000		V	
5	19.519	1025	128	0.000		V	
6	19.981	2901	298	0.000		V	
7	20.154	1418	179	0.000		V	
8	20.684	50449	3588	0.000		V	
9	21.170	8106604	798868	0.000	mg/L	SV	RT:21.170
10	22.972	4924	486	0.000			
11	33.025	7068	568	0.000			
12	33.100	1936	572	0.000		V	
13	33.246	5738	581	0.000		V	
14	33.392	4595	527	0.000		V	
15	33.483	2904	503	0.000		V	
16	33.596	2169	503	0.000		V	
17	33.659	1345	455	0.000		V	
18	33.721	2554	456	0.000		V	
19	33.818	1713	406	0.000		V	
20	33.908	1859	388	0.000		V	
21	34.000	2120	363	0.000		V	
22	34.074	3196	358	0.000		V	

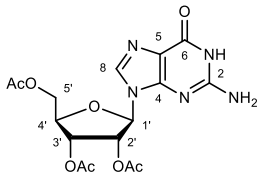

240

(*2R,3S,4S,5R*)-2-(Acetoxymethyl)-5-(2-amino-6-oxo-1,6-dihydro-9H-purin-9-yl)tetrahydrofuran-3,4-diyl diacetate (240) was prepared by charging a flame-dried round-bottom flask equipped with a magnetic stir bar with guanosine **239** (3.00 g, 10.6 mmol, 1.0 equiv.). DMF (40 mL) was added *via* syringe and the solution cooled to 0 °C before pyridine (4.70 mL, 58.3 mmol, 5.5 equiv.) and acetic anhydride (7.01 mL, 74.1 mmol, 7.0 equiv.) were subsequently added. The reaction was stirred at 85 °C for 2.5 h before being cooled to RT and concentrated *in vacuo* to give a crude resin. The resin was suspended in isopropanol (70 mL) and heated under reflux for 1 h. After cooling, the reaction mixture was filtered and the precipitate was washed with diethyl ether (20 mL), collected, and dried under vacuum to afford

the product as a white powder (4.20 g, 97%); ^{1}H NMR (500 MHz, $(CD_3)_2SO$) δ_H 10.8 (1H, br s, NH), 7.94 (1H, s, C[8]H), 6.57 (2H, br s, NH_2), 5.99 (1H, d, J = 6.1 Hz, C[1']H), 5.79 (1H, apparent t, J = 6.0 Hz, C[2']H), 5.50 (1H, apparent t, J = 5.1 Hz, C[3']H), 4.39 – 4.24 (3H, m, C[4']H and C[5']H_2), 2.10 (3H, s, CO_2CH_3), 2.04 (3H, s, CO_2CH_3), 2.03 (3H, s, CH_3CO_2); ^{13}C NMR (126 MHz, $(CD_3)_2SO$) δ_C 170.2 (CH_3CO_2), 169.6 (CH_3CO_2), 169.4 (CH_3CO_2), 156.8 (C[6]), 154.0 (C[2]), 151.2 (C[4]), 135.8 (C[8]H), 116.9 (C[5]), 84.5 (C[1']H), 79.6 (C[4']H), 72.1 (C[2']H), 70.4 (C[3']H), 63.2 (C[5']H_2), 20.6 (CH_3CO_2), 20.5 (CH_3CO_2), 20.3 (CH_3CO_2); HRMS (ESI): calcd. For $C_{16}H_{19}O_8N_5Na$, 432.1132. Found: $[MNa]^+$, 432.1122 (-0.78 ppm error). Reported data is in accordance with literature.[10]

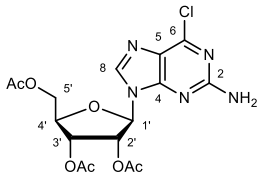

241

(*2R,3R,4R,5R*)-2-(Acetoxymethyl)-5-(2-amino-6-chloro-9H-purin-9-yl)tetrahydrofuran-3,4-diyl diacetate (241) was prepared by charging a flame-dried round bottom flask equipped with a magnetic stir bar (*2R,3S,4S,5R*)-2-(acetoxymethyl)-5-(2-amino-6-oxo-1,6-dihydro-9H-purin-9-yl)tetrahydrofuran-3,4-diyl diacetate **240** (4.44 g, 10.9 mmol. 1.0 equiv.) and tetraethylammonium chloride (3.61 g, 21.8 mmol, 2.0 equiv.). The vessel was sealed, evacuated, and backfilled with nitrogen thrice before anhydrous acetonitrile (120 mL) and N,N-dimethylaniline (1.38 mL, 10.9 mmol, 1.0 equiv.) were subsequently added *via* syringe. Phosphoryl chloride (6.12 mL, 65.4 mmol, 6.0 equiv.) was then added **dropwise** before the reaction was stirred at 100 °C for 25 min. The reaction was concentrated *in vacuo* before being reconstituted in a chloroform (120 mL) and ice water (120 mL) mixture. The solution was stirred for 30 min before the aqueous layer was separated and extracted with ethyl acetate (3 × 50 mL). The combined organic layers were washed with a sat. sodium hydrogen carbonate (50 mL), dried over magnesium sulphate, filtered, concentrated *in vacuo*, and purified by flash column chromatography (silica gel, DCM to 5% methanol in DCM) to afford the product as an off white solid (3.66 g, 79%);^{1}H NMR (500 MHz, $CDCl_3$) δ_H 7.86 (1H, s, C[8]H), 5.98 (1H, d, J = 4.9 Hz, C[1']H), 5.90 (1H, apparent t, J = 5.1 Hz, C[2']H), 5.69 (1H, apparent t, J = 5.0 Hz, C[3']H), 5.53 (2H, br s, NH_2), 4.41 – 4.38 (2H, m, C[4']H and C[5']HH'), 4.31 (1H, dd, J = 13.1, 5.9 Hz, C[5']HH'), 2.09 (3H, s, CH_3CO_2), 2.05 (3H, s, CH_3CO_2), 2.03 (3H, s, CH_3CO_2); ^{13}C NMR (126 MHz, $CDCl_3$) δ_C 170.5 (CO_2), 169.6 (CO_2), 169.4 (CO_2), 159.3 (C[2]), 153.1 (C[6]), 151.7 (C[4]), 140.7 (C[8]H), 125.6 (C[5]), 86.5 (C[1']H), 80.0 (C[4']H), 72.7 (C[2']H), 70.5 (C[3']H), 62.9 (C[5']H_2), 20.7 (CH_3CO_2), 20.6 (CH_3CO_2), 20.4 (CH_3CO_2); HRMS (ESI):

calcd. For $C_{16}H_{18}O_7N_5ClNa$, 450.0787. Found: $[MNa]^+$, 450.0772 (-3.33 ppm error). Reported data is in accordance with literature.[10]

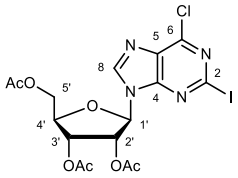

242

(*2R,3R,4R,5R*)-2-(Acetoxymethyl)-5-(6-chloro-2-iodo-9H-purin-9-yl)tetrahydrofuran-3,4-diyl diacetate (242) was prepared charging a flame-dried round-bottom flask equipped with a magnetic stir bar with (*2R,3R,4R,5R*)-2-(acetoxymethyl)-5-(2-amino-6-chloro-9H-purin-9-yl)tetrahydrofuran-3,4-diyl diacetate **241** (3.25 g, 7.61 mmol, 1.0 equiv.), copper(I) iodide (2.90 g, 15.2 mmol, 2.0 equiv.), and iodine (1.93 g, 7.61 mmol, 1.0 equiv.). The vessel was sealed, evacuated, and backfilled with nitrogen thrice before anhydrous degassed THF (80 mL) was added *via* syringe. Diiodomethane (6.13 mL, 76.1 mmol, 10.0 equiv.) and isoamyl nitrite (3.1 mL, 22.8 mmol. 3.0 equiv.) were subsequently added dropwise before the reaction was stirred at 80 °C for 3 h. The reaction was then cooled to RT before being filtered through celite, concentrated *in vacuo*, and purified by flash column chromatography (silica gel, DCM to 2% methanol in DCM) to afford the product as a yellow solid (2.81 g, 69%); ^{1}H NMR (400 MHz, $CDCl_3$) δ_H 8.20 (1H, s, C[8]H), 6.20 (1H, d, J = 5.4 Hz, C[1']H), 5.78 (1H, apparent t, J = 5.5 Hz, C[2']H), 5.59 (1H, dd, J = 5.5, 4.4 Hz, C[3']H), 4.48 (1H, td, J = 4.3, 3.2 Hz, C[4']H), 4.45 – 4.37 (2H, m, C[5']H_2), 2.18 (CH_3CO_2), 2.14 (CH_3CO_2), 2.10 (CH_3CO_2); ^{13}C NMR (126 MHz, $CDCl_3$) δ_C 170.3 (CH_3CO_2), 169.7 (CH_3CO_2), 169.5 (CH_3CO_2), 152.1 (C[6]), 151.2 (C[4]), 143.2 (C[8]H), 132.4 (C[2]), 117.2 (C[5]), 86.8 (C[1']H), 81.0 (C[4']H), 73.5 (C[2']H), 70.7 (C[3']H), 63.1 (C[5']H_2), 21.0 (CH_3CO_2), 20.7 (CH_3CO_2), 20.6 (CH_3CO_2); HRMS (ESI): calcd. For $C_{16}H_{17}O_7N_4ClI$, 538.9825. Found: $[MH]^+$, 538.9836 (2.05 ppm error). Reported data is in accordance with literature.[10]

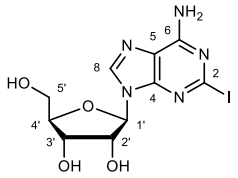

243

2-Iodoadenosine (243) was prepared by charging a flame-dried thick-walled round-bottom pressure flask equipped with a magnetic stir bar with (*2R,3R,4R,5R*)-2-(acetoxymethyl)-5-(6-chloro-2-iodo-9H-purin-9-yl)tetrahydrofuran-3,4-diyl diacetate **242** (2.20 g, 4.09 mmol, 1.0 equiv.) before adding ammonia (2 M in methanol) (50 mL). The vessel was sealed with a screw

cap before being stirred at 100 °C for 48 h. The vessel was first cooled to RT before being opened and degassed with nitrogen for 10 min. The solution was concentrated *in vacuo* before being recrystalised from ethanol and dried under vacuum to afford the product as a white solid (748 mg, 47%); ^{1}H NMR (500 MHz, $(CD_3)_2SO$) δ_H 8.29 (1H, s, C[8]H), 7.72 (2H, s, NH_2), 5.80 (1H, d, *J* = 6.2 Hz, C[1']H), 5.47 (1H, d, *J* = 6.1 Hz, C[2']OH), 5.21 (1H, d, *J* = 4.7 Hz, C[3']OH), 5.05 (1H, t, *J* = 5.7 Hz, C[5']OH), 4.52 (1H, apparent q, 5.5 Hz, C[2']H), 4.11 (1H, dt, *J* = 6.4, 3.0 Hz, C[3']H), 3.93 (1H, apparent q, *J* = 3.0 Hz, C[4']H), 3.64 (1H, dd, *J* = 12.3, 3.5 Hz, C[5']HH'), 3.56 – 3.53 (1H, m, C[5']HH'); ^{13}C NMR (126 MHz, $(CD_3)_2SO$) δ_C 156.0 (C[6]), 149.8 (C[2]), 139.5 (C[8]H), 120.9 (C[4]), 119.1 (C[5]), 87.2 (C[1']H), 85.9 (C[4']H), 73.6 (C[2']H), 70.6 (C[3']H), 61.5 (C[5']H_2); HRMS (ESI): calcd. For $C_{10}H_{13}O_4N_5I$, 394.0012. Found: $[MH]^+$, 394.0004 (-0.81 ppm error). Reported data is in accordance with literature.[10]

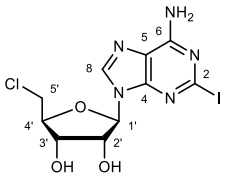

236

5'-Chloro-2-iodoadenosine (236) was prepared by charging a flame-dried round-bottom flask equipped with a magnetic stir bar with 2-iodoadenosine **243** (534 mg, 1.34 mmol, 1.0 equiv.). The vessel was sealed, evacuated, and backfilled with nitrogen thrice before anhydrous acetonitrile (20 mL) was added *via* syringe and the solution cooled to 0 °C. Pyridine (222 µL, 2.68 mmol, 2.0 equiv.) and thionyl chloride (300 µL, 4.01 mmol, 3.0 equiv.) were subsequently added before the reaction was stirred at 0 °C for 4 h. The reaction was then warmed to RT before being stirred for an additional 16 h. The reaction was concentrated *in vacuo* before the crude mixture was suspended in a methanol/water/aqueous ammonia solution (35% v/v) (10:2:1, 20 mL) and the solution stirred for 2 h. The solution was once more concentrated *in vacuo* before being purified by flash column chromatography (silica gel, 5% methanol in DCM) to afford the product as a white foam (318 mg, 57%); ^{1}H NMR (500 MHz, D_3COD) δ_H 8.15 (1H, s, C[8]H), 5.95 (1H, d, *J* = 5.1 Hz, C[1']H), 4.77 (1H, apparent t, *J* = 5.1 Hz, C[2']H), 4.40 (1H, dd, *J* = 5.1, 4.2 Hz, C[3']H), 4.26 (!H, apparent q, *J* = 5.1 Hz, C[4']H), 3.95 (1H, dd, *J* = 11.9, 5.1 Hz, C[5']HH'), 3.85 (1H, dd, *J* = 11.9, 5.2 Hz, C[5']HH'); ^{13}C NMR (126 MHz, D_3COD) δ_C 157.1 (C[6]), 150.9 (C[4]), 141.1 (C[8]H), 120.7 (C[5]), 120.5 (C[2]), 90.5 (C[1']H), 85.5 (C[4']H), 74.8 (C[2']H), 72.7 (C[3']H), 45.0 (C[5']H_2); HRMS (ESI): calcd. For $C_{10}H_{12}O_3N_5ICl$, 411.9668. Found: $[MH]^+$, 411.9675 (1.73 ppm error). Reported data is in accordance with literature.[11]

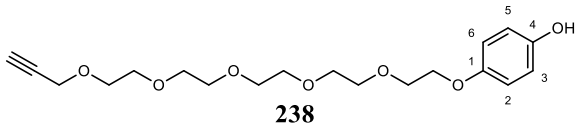

238

4-((3,6,9,12,15-Pentaoxaoctadec-17-yn-1-yl)oxy)phenol (238) was prepared by charging a flame-dried round-bottom flask equipped with a stir bar with potassium carbonate (353 mg, 2.56 mmol, 1.1 equiv.), hydroquinone (512 mg, 4.65 mmol, 2.0 equiv.), and TBAB (75 mg, 0.23 mmol, 0.1 equiv.). Anhydrous DMF (4 mL) was added *via* syringe and the solution was stirred under nitrogen for 10 min. A solution of 3,6,9,12,15-pentaoxaoctadec-17-yn-1-yl 4-methylbenzenesulfonate **221** (1.0 g, 2.33 mmol, 1.0 equiv.) dissolved in anhydrous DMF (12 mL) was added to the reaction mixture before being stirred at 80 °C for 16 h. The reaction was directly concentrated *in vacuo* before being reconstituted in ethyl acetate (10 mL) and subsequently diluted with hydrochloric acid (1 M) (5 mL). The organic layer was separated, washed with hydrochloric acid (1 M) (2 × 5 mL), washed again with a sat. brine solution (2 × 5 mL), dried over magnesium sulphate, filtered, concentrated *in vacuo*, and purified by flash column chromatography (silica gel, 50 % ethyl acetate in hexane) to afford the product as a brown oil (307 mg, 36%); R_f 0.59 (ethyl acetate); ν_{max}/cm^{-1} (neat) 3206 (C-H alkyne stretch), 2938 (C-H alkane stretch), 1647 (C≡C stretch); ^1H NMR (500 MHz, $CDCl_3$) δ_H 6.79 – 6.74 (4H, m, C[2]H, C[3]H, C[5]H, and C[6]H), 4.19 (2H, d, J = 2.4 Hz, C≡CCH_2), 4.04 (2H, dd, J = 5.4, 4.3 Hz, OCH_2CH_2OC[1]), 3.81 (2H, dd, J = 5.4, 4.3 Hz, OCH_2CH_2OC[1]), 3.72 – 3.64 (16H, m, 8 × OCH_2CH_2O), 2.42 (1H, t, J = 2.4 Hz, HC≡C); ^{13}C NMR (126 MHz, $CDCl_3$) δ_C 152.9 (C[1]), 150.1 (C[4]), 116.2 (C[5]H and C[3]H), 116.0 (C[2]H and C[6]H), 79.7 (HC≡C), 74.7 (HC≡C), 70.9 (OCH_2CH_2O), 70.8 (OCH_2CH_2O), 70.8 (OCH_2CH_2O), 70.7 (3 × OCH_2CH_2O), 70.7 (OCH_2CH_2O), 70.5 (OCH_2CH_2O), 70.1 (OCH_2CH_2OC[1]), 69.3 (OCH_2CH_2O), 68.3 (OCH_2CH_2OC[1]), 58.6 (C≡CCH_2); HRMS (ESI): calcd. For $C_{19}H_{28}O_7Na$, 391.1727. Found: $[MNa]^+$, 391.1712 (-3.90 ppm error).

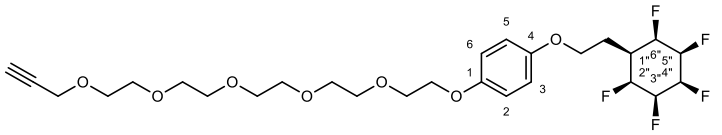

237

1-(4-(2-((*1r,2R,3R,4s,5S,6S*)-2,3,4,5,6-Pentafluorocyclohexyl)ethoxy)phenoxy)-3,6,9,12,15-pentaoxaoctadec-17-yne (237) was prepared by charging a flame-dried round-bottom flask equipped with a stir bar with potassium carbonate (122 mg, 0.88 mmol, 1.05 equiv.), 4-((3,6,9,12,15-Pentaoxaoctadec-17-yn-1-yl)oxy)phenol **238** (512 mg, 0.83 mmol, 1.0 equiv.), and TBAB (26 mg, 0.08 mmol, 0.1 equiv.). Anhydrous DMF (4 mL) was added *via* syringe and the solution was stirred under nitrogen for 10 min. A solution of

(*1r,2R,3R,4s,5S,6S*)-1-(2-bromoethyl)-2,3,4,5,6-pentafluorocyclohexane **109** (235 mg, 0.83 mmol, 1.0 equiv.) dissolved in anhydrous DMF (10 mL) was added to the reaction mixture before being stirred at 80 °C for 16 h. The reaction was directly concentrated *in vacuo* before being reconstituted in ethyl acetate (10 mL) and subsequently diluted with hydrochloric acid (1 M) (5 mL). The organic layer was separated, washed with hydrochloric acid (1 M) (2 × 5 mL), washed again with a sat. brine solution (2 × 5 mL), dried over magnesium sulphate, filtered, concentrated *in vacuo*, and purified by flash column chromatography (silica gel, 80 % ethyl acetate in hexane) to afford the product as a white solid (215 mg, 45%); Mp. 48–50 ºC; R_f 0.22 (1% methanol in DCM); ν_{max}/cm^{-1} (neat) 3239 (C-H alkyne stretch), 2897 (C-H alkane stretch), 2868 (C-H alkane stretch), 1508 (C-C aromatic stretch); ^{1}H NMR (500 MHz, $CDCl_3$) δ_H 6.87 – 6.78 (4H, m, C[2]H, C[3]H, C[5]H, and C[6]H), 5.34 (1H, br dt, *J* = 52.9, 6.7 Hz, C[4"]H), 4.99 (2H, br d, *J* = 48.6 Hz, C[2"]H and C[6"]H), 4.48 (2H, br dt, *J* = 41.1, 27.0 Hz, C[3"]H and C[5"]H), 4.19 (2H, d, *J* = 2.3 Hz, HC≡CCH_2), 4.11 – 4.06 (4H, m, OCH_2CH_2OC[1] and C[4]OCH_2), 3.83 (2H, dd, *J* = 5.4, 4.3 Hz, OCH_2CH_2OC[1]), 3.72 – 3.65 (16H, m, 8 × OCH_2CH_2O), 2.42 (1H, t, *J* = 2.3 Hz, HC≡C), 2.31 (2H, apparent q, *J* = 6.0 Hz, CH_2C[1"]), 2.09 (1H, br tt, *J* = 33.9, 6.0 Hz, C[1"]H); ^{13}C NMR (126 MHz, $CDCl_3$) δ_C 153.5 (C[1] **or** C[4])*, 152.7 (C[1] **or** C[4])*, 115.9 (C[6]H and C[2]H **or** C[3]H and C[5]H)*, 115.3 (C[6]H and C[2]H **or** C[3]H and C[5]H)*, 87.3 (dt, *J* = 197.5, 19.2 Hz, C[4"]H), 87. 3 (dd, *J* = 195.2, 17.7 Hz, C[2"]H and C[6"]H), 87.3 – 85.4 (m, C[3"]H and C[5"]H), 79.8 (HC≡C), 74.7 (HC≡C), 70.9 (OCH_2CH_2O), 70.8 – 70.7 (m, 5 × OCH_2CH_2O), 70.5 (OCH_2CH_2O), 70.0 (OCH_2CH_2OC[1]), 69.3 (OCH_2CH_2O), 68.3 (OCH$_2$CH_2OC[1]), 64.3 (C[4]OCH_2), 58.5 (C≡CCH_2), 35.0 (tt, *J* = 20.2, 5.5 Hz, C[1"]H), 26.0 (CH_2C[1"]); ^{19}F{^{1}H} NMR (470 MHz, $CDCl_3$) δ_F -203.4 (m, C[3"]F and C[5"]F), -211.7 (m, C[2"]F and C[6"]F), -216.7 (tt, *J* = 26.5, 11.1 Hz, C[4"]F); HRMS (ESI): calcd. For $C_{27}H_{37}O_7F_5Na$, 591.2352. Found: $[MNa]^+$, 591.2332 (-3.32 ppm error). *Unable to fully assign peaks due to indistinguishable environments.

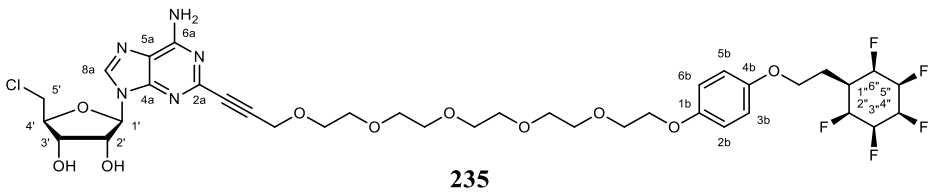

235

(*2R,3R,4S,5S*)-2-(6-Amino-2-(1-(4-(2-((*1r,2R,3R,4s,5S,6S*)-2,3,4,5,6-pentafluorocyclohexyl)ethoxy)phenoxy)-3,6,9,12,15-pentaoxaoctadec-17-yn-18-yl)-9H-purin-9-yl)-5-(chloromethyl)tetrahydrofuran-3,4-diol (235) was prepared by charging a flame-dried round-bottom flask equipped with a stir bar with 1-(4-(2-((*1r,2R,3R,4s,5S,6S*)-2,3,4,5,6-pentafluorocyclohexyl)ethoxy)phenoxy)-3,6,9,12,15-pentaoxaoctadec-17-yne **237**

(100 mg, 0.18 mmol, 1.0 equiv.), 5'-chloro-2-iodoadenosine **236** (80 mg, 0.19 mmol, 1.1 equiv.), bis(triphenylphosphine)palladium(II) dichloride (12 mg, 17.6 μmol, 10 mol%), and copper(I) iodide (3 mg, 17.6 μmol, 10 mol%). The vessel was sealed, evacuated, and backfilled with nitrogen thrice before degassed DMF (10 mL) and triethylamine (74 μL, 0.53 mmol, 3.0 equiv.) were added sequentially *via* syringe. The reaction was heated to 85 °C and stirred under nitrogen at for 24 h. The reaction was directly concentrated *in vacuo* before the crude solid was diluted in ethyl acetate (10 mL) and washed with EDTA solution (0.5 M) (2 × 5 mL). The organic layer was separated, dried over magnesium sulphate, filtered, concentrated *in vacuo*, and purified by flash column chromatography (silica gel, 50 % DCM in acetone) to afford the product as an amber oil (50 mg, 33%); ^{1}H NMR (700 MHz, $(CD_3)_2CO$) δ_H 8.25 (1H, s, C[8a]H), 6.87 (4H, s, C[2b]H, C[3b]H, C[5b]H, and C[6b]H), 6.69 (1H, br s, NH$_2$), 6.04 (1H, d, *J* = 4.0 Hz, C[1']H), 5.42 (1H, br dt, *J* = 54.5, 7.4 Hz, C[4"]H), 5.13 (2H, br d, *J* = 49.1 Hz, C[2"]H and C[6"]H), 5.02 – 4.89 (4H, m, C[2']H, C[3']OH, C[3"]H and C[5"]H), 4.60 (2H, d, *J* = 5.1 Hz, C[3']OH), 4.50 (1H, apparent q, *J* = 4.4 Hz, C[3']H), 4.42 (2H, s, C≡CCH$_2$), 4.27 (1H, apparent q, *J* = 5.0 Hz, C[4']H), 4.15 (2H, t, *J* = 6.0 Hz, C[4b]OCH$_2$), 4.07 – 4.06 (2H, m, CH$_2$OC[1b]), 3.99 (1H, dd, *J* = 11.7, 5.1 Hz, C[5']HH'), 3.90 (1H, dd, *J* = 11.7, 5.5 Hz, C[5']HH'), 3.79 – 3.78 (2H, m, CH$_2$CH$_2$OC[1b]), 3.74 (2H, dd, *J* = 5.6, 3.6 Hz, C≡CCH$_2$OCH$_2$), 3.67 – 3.59 (14H, m, 7 × OCH$_2$CH$_2$O), 2.36 (1H, br t, *J* = 35.3 Hz, C[1"]H), 2.25 (2H, apparent q, *J* = 5.5 Hz, CH$_2$C[1"]); ^{13}C NMR (176 MHz, $(CD_3)_2CO$) δ_C 156.9 (C[6a]), 154.1 (C[1b] **or** C[4b])*, 154.0 (C[1b] **or** C[4b])*, 150.7 (C[4a]), 146.7 (C[2a]), 141.4 (C[8a]), 120.3 (C[5a]), 116.4 (m, C[2b]H, C[3b]H, C[5b]H, and C[6b]H), 89.5 (C[1']H), 89.2 – 88.0 (m, C[4"]H), 88.8 (dd, *J* = 189.6, 16.3 Hz, C[2"]H and C[6"]H), 88.1 – 87.0 (m, C[3"]H and C[5"]H), 87.1 (C[2a]C≡CCH$_2$), 85.0 (C[4']H), 81.0 (C[2a]C≡CCH$_2$), 74.6 (C[2']H), 72.6 (C[3']H), 71.2 (OCH$_2$CH$_2$O), 71.0 – 70.9 (m, 5 × OCH$_2$CH$_2$O), 70.9 (OCH$_2$CH$_2$O), 70.4 (CH$_2$CH$_2$OC[1b]), 69.9 (C≡CCH$_2$OCH$_2$), 68.9 (CH$_2$OC[1b]), 66.1 (C[4b]OCH$_2$), 59.1 (C≡CCH$_2$), 45.4 (C[5']H$_2$), 36.1 (t, *J* = 20.9 Hz, C[1"]H), 26.8 (CH$_2$C[1"]H); ^{19}F{^{1}H} NMR (470 MHz, $CDCl_3$) δ_F -205.0 (C[3"]F and C[5"]F), -212.5 (d, *J* = 25.5 Hz, C[2"]F and C[6"]F), -217.4 (tt, *J* = 24.9, 10.5 Hz, C[4"]F); HRMS (ESI): calcd. For $C_{37}H_{48}O_{10}F_5Cl$, 852.3004. Found: $[MH]^+$, 852.2991 (-1.57 ppm error). *Unable to fully assign peaks due to indistinguishable environments.

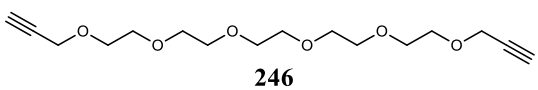

246

4,7,10,13,16,19-Hexaoxadocosa-1,21-diyne (246) was prepared by charging a flame-dried round-bottom flask equipped with a magnetic stir bar with 3,6,9,12-tetraoxatetradecane-1,14-

diol **219** (1.78 mL, 8.40 mmol, 1.0 equiv.) before adding anhydrous THF (42 mL). The solution was cooled to 0 °C before sodium hydride (60% w/w dispersion in mineral oil) (740 mg, 18.5 mmol, 2.2 equiv.) was added portion-wise. The vessel was sealed, and the reaction was stirred at 0 °C for 30 min before propargyl bromide (1.4 mL, 18.5 mmol, 2.2 equiv.) was added dropwise *via* syringe. The reaction was stirred at RT for 14 h. The reaction was diluted with methanol (10 mL) before being stirred for an additional 20 min. The reaction was concentrated *in vacuo* before being reconstituted in ethyl acetate (80 mL) and washed with a sat, ammonium chloride solution (50 mL). The aqueous layer was separated and extracted with ethyl acetate (3 × 40 mL) before the combined organic layers were dried over magnesium sulphate, filtered, concentrated *in vacuo*, and purified by flash column chromatography (silica gel, ethyl acetate) to afford the product as an amber oil (2.45 g, 93%); ^{1}H NMR (500 MHz, $CDCl_3$) δ_H 4.19 (4H, d, J = 2.4 Hz, 2 × C≡CC$\underline{H}_2$), 3.70 – 3.64 (20H, m, 5 × OC$\underline{H}_2$C$\underline{H}_2$O), 2.42 (2H, t, J = 2.4 Hz, 2 × $\underline{H}$C≡C); ^{13}C NMR (126 MHz, $CDCl_3$) δ_C 79.8 (2 × HC≡$\underline{C}$), 74.6 (2 × H$\underline{C}$≡C), 70.7 – 70.5 (8 × O$\underline{C}$H$_2$$\underline{C}H_2$O), 69.2 (2 × O$\underline{C}H_2CH_2$O), 58.5 (2 × C≡C$\underline{C}H_2$); HRMS (ESI): calcd. For $C_{16}H_{26}O_6Na$, 337.1611. Found: $[MNa]^+$, 337.1627 (-3.14 ppm error). Reported data is in accordance with literature.[12]

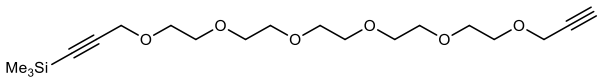

247

2,2-Dimethyl-6,9,12,15,18,21-hexaoxa-2-silatetracosa-3,23-diyne (247) was prepared by charging a flame-dried round bottom flask equipped with a magnetic stir bar with 4,7,10,13,16,19-hexaoxadocosa-1,21-diyne **246** (2.72 g, 8.66 mmol, 1.0 equiv). The vessel was then sealed, evacuated, and backfilled with nitrogen thrice before anhydrous THF (25 mL) was added *via* syringe. The solution was cooled to -78 °C before n-butyllithium (2.5 M in hexanes) (3.81 mL, 9.52 mmol, 1.1 equiv.) was added dropwise *via* syringe. After stirring at -78 °C for 1 h under nitrogen trimethylsilyl chloride (1.2 mL, 9.52 mmol, 1.1 equiv.) was added dropwise. After stirring at -78 °C for an additional hour the reaction was warmed to RT and stirred for 16 h. After completion the reaction was slowly exposed to air before being directly concentrated *in vacuo*. Purification by flash column chromatography (silica gel, hexane to 50% ethyl acetate in hexane) afforded to product as a brown oil (813 mg, 24%); R_f 0.51 (ethyl acetate); ν_{max}/cm^{-1} (neat) 2868 (C-H alkane stretch); ^{1}H NMR (500 MHz, $CDCl_3$) δ_H 4.21 – 4.18 (4H, m, 2 × $\underline{H}_2$CC≡C), 3.73 – 3.64 (20H, m, 10 × OC$\underline{H}_2$), 2.42 (1H, t, J = 2.4 Hz, $\underline{H}$C≡C), 0.17 (9H, s, SiC$\underline{H}_3$); ^{13}C NMR (126 MHz, $CDCl_3$) δ_C 101.6 ($\underline{C}$≡CSi), 91.5 (C≡$\underline{C}$Si), 79.8 ($\underline{C}$≡CH), 74.6 (C≡$\underline{C}$H), 70.8 – 70.7 (m, O$\underline{C}$H$_2$CH$_2$O), 70.6 (O$\underline{C}$H$_2$CH$_2$O), 69.3 (O$\underline{C}$H$_2$CH$_2$O). 69.2

(O<u>C</u>H$_2$CH$_2$O), 59.3 (<u>C</u>H$_2$C≡CH), 58.5 (<u>C</u>H$_2$C≡CSi), 0.03 (Si<u>C</u>H$_3$); HRMS (ESI): calcd. For $C_{19}H_{34}O_6SiNa$, 409.2007. Found: $[MNa]^+$, 409.2017 (-2.41 ppm error).

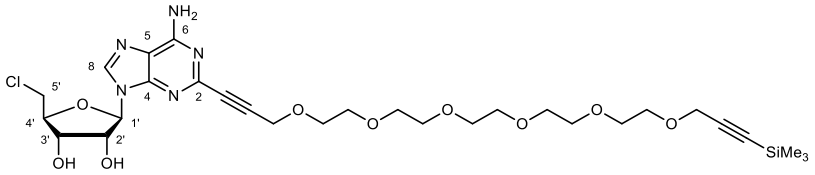

248

(*2R,3R,4S,5S*)-2-(6-Amino-2-(2,2-dimethyl-6,9,12,15,18,21-hexaoxa-2-silatetracosa-3,23-diyn-24-yl)-9H-purin-9-yl)-5-(chloromethyl)tetrahydrofuran-3,4-diol (248) was prepared by charging a flame-dried round-bottom flask equipped with a magnetic stir bar with 5'-chloro-2-iodoadenosine **236** (230 mg, 0.56 mmol, 1.0 equiv.), 2,2-dimethyl-6,9,12,15,18,21-hexaoxa-2-silatetracosa-3,23-diyne **247** (432 mg, 1.12 mmol, 2.0 equiv), copper(I) iodide (11 mg, 56 μmol, 10 mol%), and bis(triphenylphosphine)palladium(II) dichloride (37 mg, 56 μmol, 10 mol%). The vessel was sealed, evacuated, and backfilled with nitrogen thrice before degassed DMF (9 mL) and triethylamine (117 μL, 0.84 mmol, 1.5 equiv.) were added sequentially *via* syringe. The reaction was heated to 85 °C and stirred under nitrogen for 16 h. The reaction was directly concentrated *in vacuo* before the crude solid was triturated in ethyl acetate (10 mL) and washed with EDTA solution (0.5 M) (2 × 5 mL). The organic layer was separated, dried over magnesium sulphate, filtered, concentrated *in vacuo*, and purified by flash column chromatography (silica gel, DCM to 10% methanol in DCM) to afford the product as an amber oil (125 mg, 33%); R_f 0.55 (10% methanol in DCM); ν_{max}/cm^{-1} (neat) 2874 (C-H alkane stretch), 1099 (C-O stretch); ^{1}H NMR (400 MHz, $CDCl_3$) δ_H 8.18 (1H, s, C[8]<u>H</u>); 6.76 (2H, br s, N<u>H</u>$_2$), 6.14 (1H, d, *J* = 5.0 Hz, C[1']<u>H</u>), 5.28 – 5.27 (2H, m, C[3']O<u>H</u> and C[2']O<u>H</u>), 4.83 (1H, apparent t, *J* = 5.0 Hz, C[2']<u>H</u>), 4.51 (1H, apparent t, *J* = 4.0 Hz, C[3']<u>H</u>), 4.43 (1H, q, *J* = 4.0 Hz, C[4']<u>H</u>), 4.37 (2H, d, *J* = 3.2 Hz, C<u>H</u>$_2$C≡CC), 4.18 (2H, s, C<u>H</u>$_2$C≡CSi), 3.92 (1H, dd, *J* = 12.0, 4.0 Hz, C[5']<u>H</u>H'), 3.85 (1H, dd, *J* = 12.0, 4.0 Hz, C[5']H<u>H'</u>), 3.76 – 3.48 (20H, m, 10 × OC<u>H</u>$_2$CH$_2$), 0.15 (9H, s, Si(C<u>H</u>$_3$)$_3$); ^{13}C NMR (126 MHz, $CDCl_3$) δ_C 155.5 (<u>C[6]</u>), 148.9 (<u>C[4]</u>), 145.1 (<u>C[2]</u>), 140.1 (<u>C[8]</u>H), 119.0 (<u>C[5]</u>), 101.5 (<u>C</u>≡CSi), 91.6 (C≡<u>C</u>Si), 89.0 (<u>C[1']</u>H), 84.9 (CC≡<u>C</u>CH$_2$), 84.0 (<u>C[4']</u>H), 82.0 (C<u>C</u>≡CCH$_2$), 75.2 (<u>C[2']</u>H), 71.9 (<u>C[3']</u>H), 70.7 – 70.5 (m, 8 × OC<u>H</u>$_2$CH$_2$O), 69.7 (OC<u>H</u>$_2$CH$_2$O), 69.1 (OC<u>H</u>$_2$CH$_2$O), 59.3 (<u>C</u>H$_2$C≡CSi), 58.9 (<u>C</u>H$_2$C≡CC), 44.8 (<u>C[5']</u>H$_2$),–0.06 (Si<u>C</u>H$_3$); HRMS (ESI): calcd. For $C_{29}H_{45}ClN_5O_9Si$, 670.2660. Found: $[MH]^+$, 670.2670 (-1.43 ppm error).

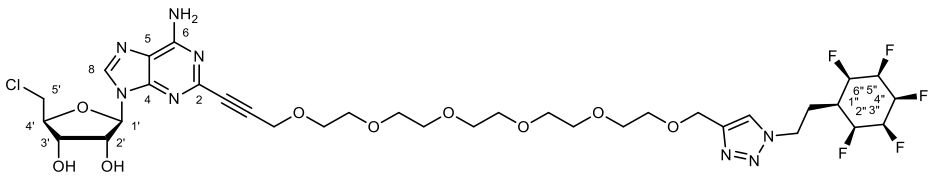

244

(*2R,3R,4S,5S*)-2-(6-Amino-2-(1-(1-(2-((*1r,2R,3R,4s,5S,6S*)-2,3,4,5,6-pentafluorocyclohexyl)ethyl)-1H-1,2,3-triazol-4-yl)-2,5,8,11,14,17-hexaoxaicos-19-yn-20-yl)-9H-purin-9-yl)-5-(chloromethyl)tetrahydrofuran-3,4-diol (244) was prepared by charging a PTFE round-bottom flask equipped with a magnetic stir bar with (*2R,3R,4S,5S*)-2-(6-amino-2-(2,2-dimethyl-6,9,12,15,18,21-hexaoxa-2-silatetracosa-3,23-diyn-24-yl)-9H-purin-9-yl)-5-(chloromethyl)tetrahydrofuran-3,4-diol **248** (100 mg, 0.15 mmol, 1.0 equiv.). The vessel was sealed, evacuated, and backfilled with nitrogen thrice before anhydrous THF (10 mL) was added *via* syringe and cooled to 0 °C. TBAF (165 µL, 0.16 mmol, 1.1 equiv.) was added dropwise to the stirring solution *via* syringe and the reaction was stirred at 0 °C for 1 h. The reaction was brought to RT before being quenched with deionised water (5 mL) and the aqueous layer separated and extracted with ethyl acetate (3 × 5 mL). The organic layer was separated, dried over magnesium sulphate, filtered, and concentrated *in vacuo*. The crude mixture was transferred to a round-bottom flask which was subsequently charged with (*1r,2R,3R,4s,5S,6S*)-1-(2-azidoethyl)-2,3,4,5,6-pentafluorocyclohexane **110** (22 mg, 92.1 µmol). The vessel was sealed before ethanol (2 mL), deionised water (2 mL), copper(II) sulphate pentahydrate (1 M in water) (2.5 µL, 2.5 µmol), and sodium ascorbate (1 M in water) (12.6 µL, 12.6 µmol) were added *via* syringe. The reaction was heated to 65 °C and stirred for 16 h. The crude reaction mixture was purified by semipreparative HPLC on a Shimadzu Prominence system using a Phenomenex Synergi® Polar-RP 80Å (250 x 10.0 mm, 4µ) and a guard cartridge; Mobile phase: 0.05% TFA in water (solvent A) and 0.05% TFA in acetonitrile (solvent B); linear gradient: 20% solvent B to 65% solvent B over 20 min, then to 95% B over 2 min, then 95% B over 3 min, back to 20% B over 2 min, then 20% B for 8 min to re-equilibrate the column. Flow rate: 2.5 mL/min; detection: 254 nm. The relevant fractions were collected (tR = 11.53 min), concentrated and lyophilized affording the product as a white solid (5 mg, 7%); R_f 0.23 (5% methanol in DCM); ^{1}H NMR (700 MHz, CD_3OD) δ_H 8.31 (1H, s, C[8]H), 8.06 (1H, s, NNHC=C), 6.01 (1H, d, *J* = 5.0 Hz, C[1']H), 5.32 – 5.20 (1H, m, F[C4"]H), 5.04 − 4.93 (2H, m, FC[2"]H and FC[6"]H), 4.76 (1H, apparent t, *J* = 5.0 Hz, C[2']H), 4.68 – 4.56 (6H, m, FC[3"]H, FC[5"]H, NNNCH_2, and C≡CCH_2O), 4.44 (2H, s, OCH_2C=CH), 4.39 (1H, apparent t, *J* = 5.0 Hz, C[3']H), 4.28 (1H, apparent q, *J* = 5.0 Hz, C[4']H), 3.97 (1H, dd, *J* = 11.9, 5.0 Hz, C[5']HH'), 3.86 (1H, dd, *J* = 11.9, 5.0 Hz, C[5']HH') 3.78 – 3.77 (2H, m,

OC$\underline{H_2}$CH$_2$O), 3.70 – 3.69 (2H, m, OC$\underline{H_2}$CH$_2$O), 3.66 – 3.60 (16H, m, 8 × OC$\underline{H_2}$CH$_2$O), 2.59 – 2.54 (1H, m, C[1"]$\underline{H}$), 2.40 (2H, apparent q, J = 7.0 Hz, C$\underline{H_2}$C[1"]H); ^{13}C NMR (176 MHz, CD$_3$OD) δ_C 157.2 (C[6]), 150.7 (C[2]), 147.1 (C[4]), 146.3 (H$_2$C$\underline{C}$=CHN), 142.0 (C[8]H), 125.3 (C=CHNNN), 120.16 (C[5]), 90.3 (C[1']H), 88.8 (dd, J = 191.5, 19.9 Hz, C[2"]F and C[6"]F), 88.6 (d, J = 177.8 Hz, C[4"]F)*, 88.1 – 87.0 (m, C[3"]F and C[5"]F)*, 86.3 (C≡CCH$_2$), 85.3 (C[4']H), 82.5 (C≡CCH$_2$), 75.0 (C[2']H), 72.6 (C[3']H), 71.5 – 71.4 (8 × OCH$_2$CH$_2$O), 70.8 (OCH$_2$CH$_2$O), 70.5 (OCH$_2$CH$_2$O), 65.0 (CH$_2$C=CH), 59.4 (C≡CCH$_2$), 48.3 (NNNCH$_2$CH$_2$), 45.2 (C[5']H$_2$), 36.7 (C[1"]H), 27.9 (CH$_2$C[1"]H); ^{19}F{^{1}H} NMR (659 MHz, CD$_3$OD) δ_{F-}206.1 (FC[3"]H and FC[5"]H),–213.3 (FC[2"]H and FC[6"]H),–218.3 (FC[4"]H); HRMS (ESI): calcd. For $C_{34}H_{46}ClF_5N_8O_9Na$, 863.2882. Found: $[MNa]^+$, 863.2889 (-0.77 ppm error). *Peaks detected by HSQC.

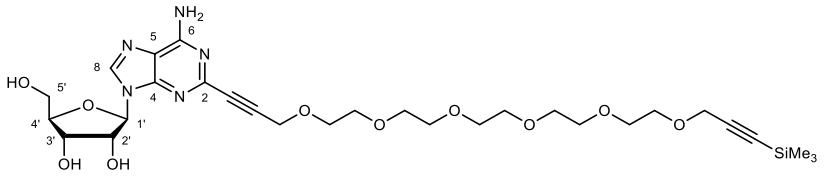

249

(*2R,3R,4S,5R*)-2-(6-Amino-2-(2,2-dimethyl-6,9,12,15,18,21-hexaoxa-2-silatetracosa-3,23-diyn-24-yl)-9H-purin-9-yl)-5-(hydroxymethyl)tetrahydrofuran-3,4-diol (249) was prepared by charging a flame-dried round-bottom flask equipped with a magnetic stir bar with 4-iodoadenosine **243** (176 mg, 0.45 mmol, 1.0 equiv.), 2,2-dimethyl-6,9,12,15,18,21-hexaoxa-2-silatetracosa-3,23-diyne **247** (346 mg, 0.90 mmol, 2.0 equiv), copper(I) iodide (9 mg, 45 μmol, 10 mol%), and bis(triphenylphosphine)palladium(II) dichloride (32 mg, 45 μmol, 10 mol%). The vessel was sealed, evacuated, and backfilled with nitrogen thrice before degassed DMF (2 mL) and triethylamine (94 μL, 0.67 mmol, 1.5 equiv.) were added sequentially *via* syringe. The reaction was heated to 85 °C and stirred under nitrogen at for 90 min. The reaction was directly concentrated *in vacuo* before the crude solid was diluted in ethyl acetate (5 mL) and washed with EDTA solution (0.5 M) (2 × 5 mL). The organic layer was dried over magnesium sulphate, filtered, concentrated *in vacuo*, and purified by flash column chromatography (silica gel, DCM to 10% methanol in DCM) to afford the product as an amber oil (104 mg, 36%); R_f 0.05 (10% methanol in DCM); ν_{max}/cm^{-1} (neat) 2874 (C-H alkane stretch), 1099 (C-O stretch); ^{1}H NMR (500 MHz, (CD$_3$)$_2$CO) δ_H 8.29 (1H, s, C[8]$\underline{H}$), 6.95 (2H, s, N$\underline{H_2}$), 5.96 (1H, d, J = 6.0 Hz, C[1']$\underline{H}$), 5.38 (1H, dd, J = 9.0, 2.2 Hz, C[5']O$\underline{H}$), 4.88 – 4.86 (2H, m, C[2']O$\underline{H}$ and C[2']$\underline{H}$), 4.48 – 4.41 (4H, m, C[3']O$\underline{H}$, C[3']$\underline{H}$, and C$\underline{H_2}$C≡CC), 4.19 – 4.17 (3H, m, C$\underline{H_2}$C≡CSi and C[4']$\underline{H}$), 3.85 (1H, apparent dt, J = 12.1, 1.8 Hz, C[5']$\underline{H}$H'), 3.78 (2H, dd, J = 5.8, 3.8 Hz, OC$\underline{H_2}$CH$_2$), 3.71 (1H, apparent dt, J = 9.6, 1.8 Hz, C[5']H$\underline{H}$'), 3.69

(2H, dd, *J* = 5.8, 3.8 Hz, OC$\underline{H}_2$CH$_2$), 3.65 – 3.59 (16H, m, 8 × OC$\underline{H}_2$CH$_2$), 0.15 (9H, s, Si(C$\underline{H}_3$)$_3$); ^{13}C NMR (126 MHz, (CD$_3$)$_2$CO) δ_C 157.2 (C[6]), 149.9 (C[4]), 146.3 (C[2]), 142.4 (C[8]H), 120.9 (C[5]), 103.3 (C≡CSi), 91.1 (C≡CSi), 90.9 (C[1']H), 88.0 (C[4']H), 86.3 (CC≡CCH$_2$), 82.1 (CC≡CCH$_2$), 75.0 (C[2']H), 72.6 (C[3']H), 71.2 – 70.9 (m, 8 × OCH$_2$CH$_2$O), 70.0 (OCH$_2$CH$_2$O), 69.7 (OCH$_2$CH$_2$O), 63.3 (C[5']H$_2$), 59.4 (CH$_2$C≡CSi), 59.0 (CH$_2$C≡CC), -0.1 (Si(CH$_3$)$_3$); HRMS (ESI): calcd. For $C_{29}H_{46}N_5O_{10}Si$, 652.3015. Found: $[MH]^+$, 652.3007 (-1.15 ppm error).

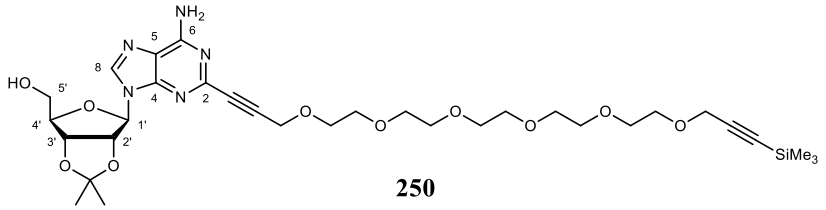

250

((*3aR,4R,6R,6aR*)-6-(6-Amino-2-(2,2-dimethyl-6,9,12,15,18,21-hexaoxa-2-silatetracosa-3,23-diyn-24-yl)-9H-purin-9-yl)-2,2-dimethyltetrahydrofuro[3,4-d][1,3]dioxol-4-yl)methanol (250) was prepared by was prepared by charging a flame-dried round-bottom flask equipped with a magnetic stir bar with (*2R,3R,4S,5R*)-2-(6-amino-2-(2,2-dimethyl-6,9,12,15,18,21-hexaoxa-2-silatetracosa-3,23-diyn-24-yl)-9H-purin-9-yl)-5-(hydroxymethyl)tetrahydrofuran-3,4-diol **249** (100 mg, 0.15 mmol, 1.0 equiv.) and *p*-toluenesulfonic acid (293 mg, 1.54 mmol, 10.0 equiv.). The vessel was sealed, evacuated, and backfilled with nitrogen thrice before anhydrous acetone (50 mL) was added *via* syringe. The reaction was heated to 60 °C and stirred under nitrogen for 16 h. Upon completion the reaction was cooled to 0 °C and a sat. sodium hydrogen carbonate solution (25 mL) was added dropwise until no further effervescence was observed. The aqueous layer was separated and extracted with DCM (3 × 20 mL) before the combined organic layers were separated, dried over magnesium sulphate, filtered, concentrated *in vacuo*, and purified by flash column chromatography (silica gel, 5% methanol in DCM) to afford the product as a colourless oil (53 mg, 50%); R_f 0.37 (10% methanol in DCM); ν_{max}/cm^{-1} (neat) 3325 (O-H stretch), 2880 (C-H alkane stretch); ^{1}H NMR (500 MHz, CDCl$_3$) δ_H 7.84 (1H, s, C[8]H), 6.38 (2H, s, N$\underline{H}_2$), 5.85 (1H, s, C[5']O$\underline{H}$), 5.82 (1H, d, *J* = 5.0 Hz, C[1']H), 5.18 (1H, apparent t, *J* = 5.0 Hz, C[2']H), 5.09 (1H, dd, *J* = 5.0, 1.4 Hz, C[3']H), 4.48 (1H, apparent s, C[4']H), 4.43 (2H, s, CC≡CC$\underline{H}_2$), 4.18 (2H, s, C$\underline{H}_2$C≡CSi), 3.94 (1H, apparent d, *J* = 11.9 Hz, C[5']HH'), 3.81 – 3.79 (2H, m, OC$\underline{H}_2$CH$_2$O), 3.76 (1H, apparent d, *J* = 9.3 Hz, C[5']HH'), 3.71 (2H, dd, *J* = 5.5, 3.8 Hz, OC$\underline{H}_2$CH$_2$O), 3.68 – 3.62 (16H, m, 8 × OC$\underline{H}_2$CH$_2$O), 1.61 (3H, s, OCC$\underline{H}_3$), 1.35 (3H, s, OCC$\underline{H}_3$), 0.15 (9H, s, Si(C$\underline{H}_3$)$_3$); ^{13}C NMR (126 MHz, CDCl$_3$) δ_C 156.0 (C[6]), 148.6 (C[4]), 145.7 (C[2]), 141.0 (C[8]H), 120.6 (C[5]), 114.1 (C(CH$_3$)$_2$), 101.6 (C≡CSi), 94.1 (C[1']H), 91.5

(C≡CSi), 86.3 (C[4']H), 84.9 (CC≡CCH$_2$), 83.1 (C[2']H), 82.8 (CC≡CCH$_2$), 81.8 (C[3']H), 70.7 – 70.5 (m, 8 × OCH$_2$CH$_2$O), 69.5 (OCH$_2$CH$_2$O), 69.2 (OCH$_2$CH$_2$O), 63.4 (C[5']H$_2$), 59.3 (CH$_2$C≡CSi), 58.9 (CC≡CCH$_2$), 27.7 (OCCH$_3$), 25.4 (OCCH$_3$), -0.1 (Si(CH$_3$)$_3$); HRMS (ESI): calcd. For $C_{32}H_{50}N_5O_{10}Si$, 692.3328. Found: $[MH]^+$, 692.3314 (-1.14 ppm error).

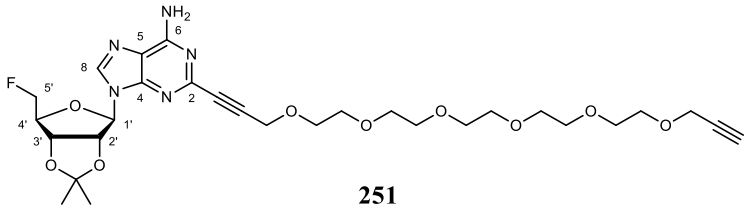

251

2-(4,7,10,13,16,19-Hexaoxadocosa-1,21-diyn-1-yl)-9-((*3aR,4R,6S,6aS*)-6-(fluoromethyl)-2,2-dimethyltetrahydrofuro[3,4-d][1,3]dioxol-4-yl)-9H-purin-6-amine (251) was prepared by charging a flame-dried round-bottom flask equipped with a magnetic stir bar with ((*3aR,4R,6R,6aR*)-6-(6-amino-2-(2,2-dimethyl-6,9,12,15,18,21-hexaoxa-2-silatetracosa-3,23-diyn-24-yl)-9H-purin-9-yl)-2,2-dimethyltetrahydrofuro[3,4-d][1,3]dioxol-4-yl)methanol **250** (50 mg, 72.3 μmol, 1.0 equiv.) and *p*-toluenesulfonyl fluoride (38 mg, 0.22 mmol, 3.0 equiv.). The vessel was sealed, evacuated, and backfilled with nitrogen thrice before anhydrous THF (5 mL) and TBAF (1 M in THF) (723 μL, 0.72 mmol, 10.0 equiv.) were subsequently added *via* syringe. The reaction was heated to 60 °C and stirred under nitrogen for 16 h. The reaction was cooled to RT and directly concentrated *in vacuo* before being purified by flash column chromatography (silica gel, ethyl acetate to 20% methanol in ethyl acetate) to afford the product as an amber oil (18 mg, 40%); R_f 0.42 (10% methanol in ethyl acetate); ^{1}H NMR (500 MHz, $CDCl_3$) δ_H 7.95 (1H, s, C[8]H), 6.20 (1H, d, J = 1.8 Hz, C[1']H), 5.95 (2H, s, NH$_2$), 5.72 (1H, dd, J = 6.1, 1.8 Hz, C[2']H), 5.09 (1H, dd, J = 6.1, 3.3 Hz, C[3']H), 4.68 (1H, ddd, J = 33.1, 10.3, 4.2 Hz, C[5']HH'), 4.59 (1H, ddd, J = 32.6, 10.3, 4.2 Hz, C[5']HH'), 4.51 – 4.44 (1H, m, C[4']H), 4.45 (2H, s, CC≡CCH$_2$), 4.19 – 4.17 (3H, m, CH$_2$C≡CH and C[4']H), 3.79 (2H, dd, J = 5.7, 3.6 Hz, OCH$_2$CH$_2$O), 3.72 – 3.64 (18H, m, 9 × OCH$_2$CH$_2$O), 2.42 (1H, t, J = 2.2 Hz, C≡CH), 1.62 (3H, s, C(CH$_3$)), 1.39 (3H, s, C(CH$_3$)); ^{13}C NMR (126 MHz, $CDCl_3$) δ_C 155.5 (C[6]), 149.6 (C[4]), 146.1 (C[2]), 140.2 (d, J = 3.6 Hz, C[8]H), 119.7 (C[5]), 114.8 (C(CH$_3$)$_2$), 90.5 (C[1']H), 85.7 (d, J = 19.4 Hz, C[4']H), 85.7 (CC≡CCH$_2$), 84.7 (C[2']H), 83.0 (d, J = 171.7 Hz, C[5']H$_2$), 81.7 (CC≡CCH$_2$ and CH$_2$C≡CH), 80.9 (d, J = 6.9 Hz, C[3']H), 74.6 (C≡CH), 72.7 (OCH$_2$CH$_2$O), 70.8 – 70.5 (7 × OCH$_2$CH$_2$O), 69.6 (OCH$_2$CH$_2$O), 69.3 (OCH$_2$CH$_2$O), 59.0 (CC≡CCH$_2$), 58.5 (CH$_2$C≡CH), 27.3 (C(CH$_3$)), 25.6 (C(CH$_3$)); ^{19}F{^{1}H} NMR (470 MHz, $CDCl_3$) δ_F -228.7 (FC[5']H$_2$); HRMS (ESI): calcd. For $C_{29}H_{41}N_5O_9F$, 622.2888. Found: $[MH]^+$, 622.2869 (-2.29 ppm error).

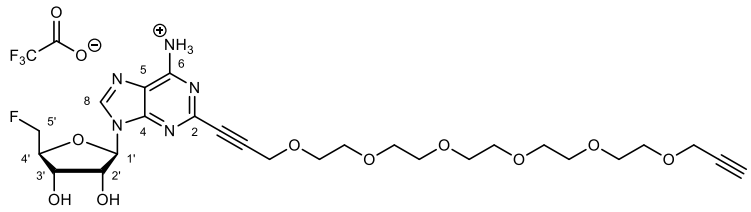

252

(*2R,3R,4S,5S*)-2-(6-Amino-2-(4,7,10,13,16,19-hexaoxadocosa-1,21-diyn-1-yl)-9H-purin-9-yl)-5-(fluoromethyl)tetrahydrofuran-3,4-diol (252) was prepared by charging a round-bottom flask equipped with a magnetic stir bar with 2-(4,7,10,13,16,19-hexaoxadocosa-1,21-diyn-1-yl)-9-((*3aR,4R,6S,6aS*)-6-(fluoromethyl)-2,2-dimethyltetrahydrofuro[3,4-d][1,3]dioxol-4-yl)-9H-purin-6-amine **251** (18 mg, 29.0 μmol, 1.0 equiv.). The vessel was sealed, evacuated, and backfilled with nitrogen thrice before methanol (2 mL), deionised water (2 mL), and TFA (0.2 mL) were subsequently added *via* syringe. The reaction was stirred at RT for 18 h before being directly concentrated *in vacuo*. Purification by flash column chromatography (silica gel, 10% methanol in ethyl acetate) afforded the product as a white solid (17 mg, > 99%), Mp. 264 – 266 ºC (decomp.); R_f 0.25 (10% methanol in ethyl acetate); ν_{max}/cm^{-1} (neat) 2359 (C≡C stretch); ^{1}H NMR (400 MHz, $OC(CD_3)_2$) δ_H 8.21 (1H, s, C[8]H), 6.78 (3H, br s, NH_3^+), 6.08 (1H, dd, *J* = 4.3 Hz, C[1']H), 5.40 (1H, br s, C[3']OH), 5.08 (1H, br s, C[2']H), 4.79 (1H, apparent t, *J* = 3.3 Hz, C[5']HH'), 4.71 (1H, apparent t, *J* = 4.4 Hz, C[2']H), 4.67 (1H, apparent t, *J* = 3.3 Hz, C[5']HH'), 4.50 (1H, apparent t, *J* = 5.2 Hz, C[3']H), 4.45 (2H, s, CC≡CCH_2), 4.31 – 4.21 (1H, m, C[4']H), 4.21 (2H, d, *J* = 2.3 Hz, CH_2C≡CH), 3.77 (2H, dd, *J* = 5.9, 3.2 Hz, OCH_2CH_2O), 3.71 – 3.59 (18H, m, 9 × OCH_2CH_2O), 2.97 – 2.95 (1H, m, C≡CH); ^{13}C NMR (126 MHz, $OC(CD_3)_2$) δ_C 156.9 (C[6]), 150.7 (C[4]), 146.7 (C[2]), 140.9 (d, *J* = 2.3 Hz, C[8]H), 120.1 (C[5]), 89.5 (C[1']H), 87.0 (C[2]C≡C), 83.9 (d, *J* = 18.5 Hz, C[4']H), 83.7 (d, *J* = 169.8 Hz, C[5']H_2), 81.0 (C≡CH), 76.0 (C[2]C≡C), 76.0 (C≡CH), 75.2 (C[2']H), 72.9 (OCH_2CH_2O), 71.0 – 70.5 (m, 8 × OCH_2CH_2O and C[3']H), 70.0 (OCH_2CH_2O), 69.6 (OCH_2CH_2O), 59.1 (CC≡CCH_2), 58.6 (CH_2C≡CH); ^{19}F{^{1}H} NMR (376 MHz, $CDCl_3$) δ_F -230.2 (FC[5']H_2); HRMS (ESI): calcd. For $C_{26}H_{36}N_5O_9FNa$, 604.2395. Found: $[MNa]^+$, 604.2389 (-0.03 ppm error).

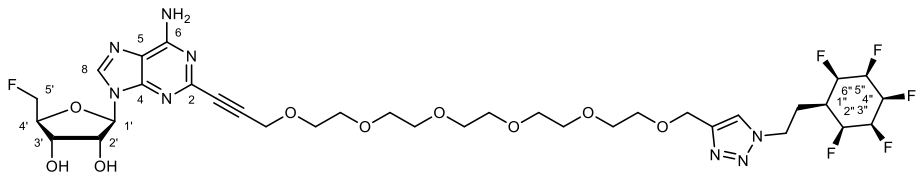

253

(*2R,3R,4S,5S*)-2-(6-Amino-2-(1-(1-(2-((*1r,2R,3R,4s,5S,6S*)-2,3,4,5,6-pentafluorocyclohexyl)ethyl)-1H-1,2,3-triazol-4-yl)-2,5,8,11,14,17-hexaoxaicos-19-yn-20-yl)-9H-purin-9-yl)-5-(fluoromethyl)tetrahydrofuran-3,4-diol (253) was prepared by charging a round-bottom flask equipped with a magnetic stir bar with 2-(4,7,10,13,16,19-hexaoxadocosa-1,21-diyn-1-yl)-9-((*2R,3R,4S,5S*)-5-(fluoromethyl)-3,4-dihydroxytetrahydrofuran-2-yl)-9H-purin-6-aminium **252** (26 mg, 44.7 μmol, 1.0 equiv.), (*1r,2R,3R,4s,5S,6S*)-1-(2-azidoethyl)-2,3,4,5,6-pentafluorocyclohexane **110** (12 mg, 49.2 μmol, 1.1 equiv.), sodium ascorbate (1 mg, 5 μmol), and copper(II) sulfate pentahydrate (1 mg, 6 μmol). The vessel was sealed before ethanol (1 mL) and deionised water (1 mL) were added *via* syringe. The reaction was stirred at 65 °C for 18 h before being directly concentrated *in vacuo*. The crude reaction mixture was purified by semipreparative HPLC on a Shimadzu Prominence system using a Phenomenex Synergi® Polar-RP 80Å (250 x 10.0 mm, 4μ) and a guard cartridge; Mobile phase: 0.05% TFA in water (solvent A) and 0.05% TFA in acetonitrile (solvent B); linear gradient: 20% solvent B to 65% solvent B over 20 min, then to 95% B over 2 min, then 95% B over 3 min, back to 20% B over 2 min, then 20% B for 8 min to re-equilibrate the column. Flow rate: 2.5 mL/min; detection: 254 nm. The relevant fractions were collected (tR = 17.37 min), concentrated and lyophilized affording the product as a white solid (6 mg, 16%); R_f 0.06 (5% methanol in DCM); ν_{max}/cm^{-1} (neat) 2920 (C-H alkane stretch); ^{1}H NMR (500 MHz, CD_3OD) δ_H 8.24 (1H, s, C[8]H), 8.06 (NC=CH), 6.04 (1H, d, *J* = 4.1 Hz, C[1']H), 5.32 – 5.21 (1H, m, C[4"]H), 5.04 – 4.94 (2H, m, C[3"]H and C[5"]H), 4.77 (1H, ddd, *J* = 37.1, 10.6, 2.8 Hz, FC[5']HH'), 4.67 (1H, ddd, *J* = 32.9, 14.8, 2.8 Hz, FC[5']HH'), 4.74 – 4.62 (6H, m, C[2"]H, C[6"]H and CH_2CNNN, CH_2CH_2C[1']H), 4.56 (1H, apparent t, *J* = 4.5 Hz, C[2']H), 4.44 (2H, s, C[2]C≡CCH_2), 4.39 (1H, apparent t, *J* = 5.3 Hz, C[3']H), 4.24 (1H, ddt, *J* = 28.1, 6.0, 3.1 Hz, C[4']H), 3.77 (2H, dd, *J* = 5.7, 3.5 Hz, OCH_2CH_2O), 3.69 (2H, dd, *J* = 5.7, 3.5 Hz, OCH_2CH_2O), 3.66 – 3.60 (16H, m, 8 × OCH_2CH_2O), 2.40 (2H, q, *J* = 7.0 Hz, CH_2C[1"]H), 1.88 – 1.75 (1H, m, C[1"]H); ^{13}C NMR (126 MHz, CD_3OD) δ_C 157.1 (C[6]), 150.6 (C[4]), 147.2 (C[2]), 146.3 (NC=CHN), 141.3 (C[8]H), 125.3 (NC=CHN), 120.0 (C[5]), 90.2 (C[1']H), 88.8 (dd, *J* = 193.0, 17.1 Hz, FC[2"]H and FC[6"]H), 88.6 – 86.9 (m, FC[3"]H and FC[5"]H), 88.2 – 86.5 (m, FC[4"]H)*, 86.3 (C[2]C≡C), 84.5 (d, *J* = 18.5 Hz, C[4']H), 83.6 (d, *J* = 170.5 Hz, C[5']H_2), 82.6 (C[2]C≡C), 75.8 (C[2']H), 71.5 – 71.5 (m, 8 × OCH_2CH_2), 70.9 (C[3']H), 70.8 (OCH_2CH_2), 70.5 (OCH_2CH_2), 65.0 (CH_2CNNN), 59.4 (C[2]C≡CCH_2), 48.0

(CH$_2$CH$_2$C[1']H)*, 37.0 – 36.6 (m, C[1"]H), 27.9 (CH$_2$C[1"]H); ^{19}F{^{1}H} NMR (376 MHz, CD$_3$OD) δ_F –206.1 (FC[3"]H and FC[5"]H), –213.3 (d, J = 24.6 Hz, FC[2"]H and FC[6"]H), -218.2 – -218.4 (m, FC[4"]H), -232.5 (FC[5']H$_2$); HRMS (ESI): calcd. For $C_{34}H_{46}N_8O_9F_6Na$, 847.3184. Found: [MNa]$^+$, 847.3171 (-1.55 ppm error). *Peaks detected by HSQC.

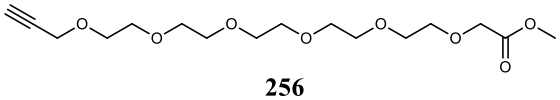

256

Methyl 3,6,9,12,15,18-hexaoxahenicos-20-ynoate (256) was prepared by charging a flame-dried round-bottom flask equipped with a magnetic stir bar with 3,6,9,12,15-pentaoxaoctadec-17-yn-1-ol **220** (750 mg, 2.15 mmol, 1.0 equiv.) before adding anhydrous THF (30 mL). The solution was cooled to 0 °C before sodium hydride (60% w/w dispersion in mineral oil) (120 mg, 3.016 mmol, 1.4 equiv.) was added portion-wise. The vessel was sealed and the reaction was stirred at 0 °C for 30 min before methyl 3-bromopropanoate (285 μL, 3.01 mmol, 1.4 equiv.) was added dropwise *via* syringe. The reaction was stirred at RT for 14 h. The reaction was diluted with methanol (10 mL) before being stirred for an additional 20 min. The reaction was concentrated *in vacuo* before being reconstituted in ethyl acetate (20 mL) and washed with a sat. ammonium chloride solution (10 mL). The aqueous layer was separated and extracted with ethyl acetate (3 × 10 mL) before the combined organic layers were dried over magnesium sulphate, filtered, concentrated *in vacuo*, and purified by flash column chromatography (silica gel, 70% ethyl acetate in hexane) to afford the product as a colourless oil (725 mg, 97%); ^{1}H NMR (400 MHz, CDCl$_3$) δ_H 4.20 (2H, d, J = 2.4 Hz, C≡CCH$_2$), 4.16 (2H, s, CH$_2$CO$_2$), 3.74 (3H, s, CO$_2$CH$_3$), 3.74 – 3.64 (20H, m, 5 × OCH$_2$CH$_2$O), 2.43 (1H, t, J = 2.4 Hz, HC≡C); ^{13}C NMR (101 MHz, CDCl$_3$) δ_C 171.0 (CO$_2$), 77.4 (HC≡C), 74.7 (HC≡C), 71.0 (OCH$_2$CH$_2$O), 70.8 – 70.7 (m, 7 × OCH$_2$CH$_2$O), 70.5 (OCH$_2$CH$_2$O), 69.2 (OCH$_2$CH$_2$O), 68.8 (CH$_2$CO$_2$), 58.5 (C≡CCH$_2$), 51.9 (CO$_2$CH$_3$); HRMS (ESI): calcd. For $C_{16}H_{28}O_8Na$, 371.1676. Found: [MNa]$^+$, 371.1672 (-1.18 ppm error).

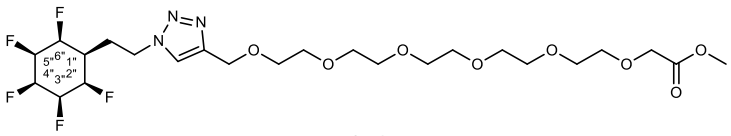

258

Methyl 1-(1-(2-((*1r,2R,3R,4s,5S,6S*)-2,3,4,5,6-pentafluorocyclohexyl)ethyl)-1H-1,2,3-triazol-4-yl)-2,5,8,11,14,17-hexaoxanonadecan-19-oate (258) was prepared by charging a round-bottom flask with (*1r,2R,3R,4s,5S,6S*)-1-(2-azidoethyl)-2,3,4,5,6-pentafluorocyclohexane **110** (37 mg, 0.15 mmol, 1.0 equiv.), methyl 3,6,9,12,15,18-hexaoxahenicos-20-ynoate **256** (58 mg, 0.17 mmol, 1.1 equiv.), sodium ascorbate (5 mg, 22.8

μmol, 15 mol%), and copper sulphate pentahydrate (1 mg, 4.5 μmol, 3 mol%). The vessel was sealed before ethanol (2 mL) and deionised water (2 mL) were added *via* syringe. The reaction was stirred at 65 °C for 16 h. The reaction was diluted with deionised water (5 mL) before being extracted with ethyl acetate (3 × 5 mL). The combined organic layers were washed with sat. brine solution, dried over magnesium sulphate, filtered, concentrated *in vacuo*, and purified by flash column chromatography (silica gel, ethyl acetate to 20% methanol in ethyl acetate) to afford the product as an amber oil (46 mg, 52%); R_f 0.14 (10% methanol in ethyl acetate); ν_{max}/cm^{-1} (neat) 2947 (C-H alkane stretch), 1749 (C=O stretch); ^1H NMR (500 MHz, $CDCl_3$) δ_H 7.73 (HC=C), 5.27 (1H, br d, J = 52.5 Hz, C[4"]H), 4.97 (2H, br d, J = 49.4 Hz, C[2"]H and C[6"]H), 4.70 – 4.51 (2H, m, C[3"]H and C[5"]H), 4.62 (2H, s, $CH_2CO_2CH_3$), 4.55 (2H, t, J = 6.5 Hz, CH_2CH_2NNN), 4.12 (2H, s, $HC{\equiv}CCH_2$), 3.71 (3H, s, CO_2CH_3), 3.68 – 3.59 (20H, m, 10 × OCH_2CH_2O), 2.39 (2H, apparent q, J = 6.5 Hz, C[1"]CH_2), 1.84 (1H, br t, J = 34.1 Hz, C[1"]H); ^{13}C NMR (126 MHz, $CDCl_3$) δ_C 171.1 (CO), 145.4 (HC=CNNN), 123.3 (HC=CNNN), 88.2 – 86.6 (m, C[4"]H), 87.4 (dd, J = 192.6, 17.9 Hz, C[2"]H and C[6"]H), 86.1 (dd, J = 193.7, 12.6 Hz, C[3"]H and C[5"]H), 70.9 (OCH_2CH_2O), 70.44 (8 × OCH_2CH_2O), 69.8 (OCH_2CH_2O), 68.5 (HC=CCH_2), 64.6 ($CH_2CO_2CH_3$), 51.9 (CO_2CH_3), 46.8 (CH_2NNN), 35.1 (t, J = 18.3 Hz, C[1"]H), 26.8 (C[1"]CH_2), $^{19}F\{^1H\}$ NMR (470 MHz, $CDCl_3$) δ_F -204.3 (FC[3"]H and FC[5"]H), -212.0 (d, J = 24.0 Hz, FC[2"]H and FC[6"]H), -216.7 – -216.8 (m, FC[4"]H); HRMS (ESI): calcd. For $C_{24}H_{38}F_5N_3O_8Na$, 614.2471. Found: $[MNa]^+$, 614.2449 (-3.63 ppm error).

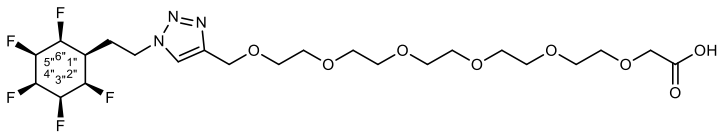

259

1-(1-(2-((*1r,2R,3R,4s,5S,6S*)-2,3,4,5,6-Pentafluorocyclohexyl)ethyl)-1H-1,2,3-triazol-4-yl)-2,5,8,11,14,17-hexaoxanonadecan-19-oic acid (259) was prepared by charging a round-bottom flask with methyl 1-(1-(2-((*1r,2R,3R,4s,5S,6S*)-2,3,4,5,6-pentafluorocyclohexyl)ethyl)-1H-1,2,3-triazol-4-yl)-2,5,8,11,14,17-hexaoxanonadecan-19-oate **258** (40 mg, 67.65 μmol) before adding hydrochloric acid (6 M) (8 mL). The vessel was sealed and the reaction stirred at 100 °C for 18 h. The reaction was basified to pH 8 with sat. sodium hydrogen carbonate solution and residual starting material was extracted using ethyl acetate (3 x 5 mL). The aqueous phase was separated and re-acidified using hydrochloric acid (1M) before being extracted with ethyl acetate (3 x 10 mL). The combined re-acidified organic layers washed with sat. brine solution, dried over magnesium sulphate, filtered, and concentrated *in vacuo* to afford the product as a colourless oil (31 mg, 79%); R_f 0.23 (20% methanol in DCM); ν_{max}/cm^{-1} (neat) 2926 (O-H

stretch), 1600 (C=O stretch); ^{1}H NMR (500 MHz, CD_3OD) δ_H 8.07 (1H, s, HC=CNNN), 5.27 (1H, br d, J = 53.5 Hz, C[4"]H), 4.99 (2H, br d, J = 50.0 Hz, C[2"]H and C[6"]H), 4.74 – 4.64 (2H, m, C[3"]H and C[5"]H), 4.65 (2H, s, CH_2CO_2H), 4.63 (2H, t, J = 7.1 Hz, CH_2NNN), 3.87 (2H, s, C≡CCH_2), 3.68 – 3.64 (20H, m, 10 × OCH_2CH_2O), 2.41 (2H, apparent q, J = 7.1 Hz, C[1"]CH_2), 1.95 – 1.82 (1H, m, C[1"]H); ^{13}C NMR (126 MHz, CD_3OD) δ_C 177.5 (CO_2H), 146.2 (HC=CNNN), 125.2 (HC=CNNN), 89.45 – 87.8 (m, C[4"]H)*, 88.9 (dd, J = 192.6, 17.5 Hz, C[2"]H and C[6"]H), 87.7 (dd, J = 189.2, 6.3 Hz, C[3"]H and C[5"]H), 71.6 (CH_2CO_2H), 71.0 (OCH_2CH_2O), 70.9 (OCH_2CH_2O), 70.8 (OCH_2CH_2O), 70.7 (2 × OCH_2CH_2O), 70.6 (OCH_2CH_2O), 70.5 (OCH_2CH_2O), 70.5 (OCH_2CH_2O), 70.5 (OCH_2CH_2O), 70.4 (OCH_2CH_2O), 64.9 (HC=CCH_2), 48.4 (CH_2NNN), 36.9 (m, C[1"]H), 28.0 (C[1"]CH_2); ^{19}F{^{1}H} NMR (470 MHz, CD_3OD) δ_F -206.1 (FC[3"]H and FC[5"]H), -213.2 (d, J = 22.7 Hz, FC[2"]H and FC[6"]H), -218.2 (FC[4"]H); HRMS (ESI): calcd. For $C_{23}H_{36}F_5N_3O_8Na$, 600.2315. Found: $[MNa]^+$, 600.2317 (0.37 ppm error).*Peak detected by HSQC

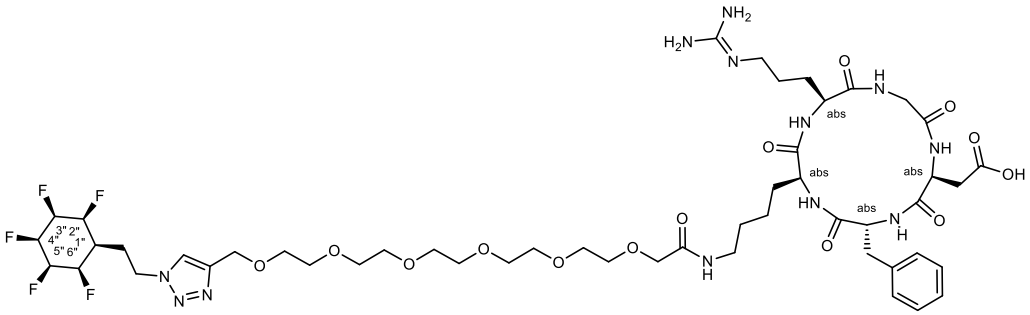

255

2-((*2S,5R,8S,11S*)-5-Benzyl-11-(3-((diaminomethylene)amino)propyl)-3,6,9,12,15-pentaoxo-8-(19-oxo-1-(1-(2-((*1r,2R,3R,4s,5S,6S*)-2,3,4,5,6-pentafluorocyclohexyl)ethyl)-1H-1,2,3-triazol-4-yl)-2,5,8,11,14,17-hexaoxa-20-azatetracosan-24-yl)-1,4,7,10,13-pentaazacyclopentadecan-2-yl)acetic acid (255) was prepared by charging a flame-dried round-bottom flask equipped with a magnetic stir bar with 1-(1-(2-((*1r,2R,3R,4s,5S,6S*)-2,3,4,5,6-Pentafluorocyclohexyl)ethyl)-1H-1,2,3-triazol-4-yl)-2,5,8,11,14,17-hexaoxanonadecan-19-oic acid **259** (6 mg, 9.93 μmol, 1.2 equiv.) and cylco(-RGDfK) **257** (5 mg, 8.28 μmol, 1.0 equiv.). The vessel was sealed, evacuated, and backfilled with nitrogen thrice before anhydrous DMF (2 mL), DIPEA (4 μL, 24.8 μmol, 3.0 equiv.), and T3P (10 μL, 16.6 μmol, 2.0 equiv.) were subsequently added. The reaction was stirred at RT for 16 h. The reaction was diluted with deionised water (2 mL) before being extracted with ethyl acetate (3 × 5 mL). The combined organic layers were dried over magnesium sulphate, filtered, and concentrated *in vacuo*. The crude reaction mixture was purified by semipreparative HPLC on a Shimadzu Prominence system using a Phenomenex Synergi® Polar-RP 80Å (250 x 10.0 mm, 4μ) and a guard cartridge; Mobile phase: 0.05% TFA in water (solvent A) and 0.05% TFA in

MeCN (solvent B); linear gradient: 10% solvent B to 55% solvent B over 25 min, then to 95% B over 0.1 min, then held at 95% solvent B over 5 mins, back to 10% B over 0.1 min, then 10% B for 5 min to re-equilibrate the column. Flow rate: 2.5 mL/min; detection: 220 nm. The relevant fractions were collected (tR = 23.40 min), concentrated and lyophilized affording the product (1.2 mg, 13%) as a white powder; ^{1}H NMR (700 MHz, D_2O) δ_H 8.11 (1H, s, HC=CNNN), 7.37 (2H, apparent t, *J* = 7.2 Hz, Phe *m*-ArCH), 7.31 (1H, t, *J* = 7.3 Hz, Phe *p*-ArCH), 7.25 (2H, d, *J* = 7.6 Hz, Phe *o*-ArCH), 5.52 (1H, br dt, *J* = 54.5, 6.8 Hz, C[4"]H), 5.13 (2H, br d, *J* = 50.0 Hz, C[6"]H and C[2"]H), 4.91 – 4.84 (2H, m, C[5"]H and C[3"]H), 4.75 (Asp α-CH)*, 4.69 (2H, s, CH_2CONH), 4.67 (2H, t, *J* = 7.1 Hz, CH_2NNN), 4.64 (1H, dd, *J* = 9.1, 6.4 Hz, Phe α-CH), 4.36 (1H, dd, *J* = 8.7, 5.7 Hz, Arg α-CH), 4.22 (1H, d, *J* = 15.0 Hz, Gly CH^aH^b), 4.08 (2H, s, C≡CCH_2), 3.88 (1H, ddd, *J* = 10.3, 4.6, 1.5 Hz, Lys α-CH), 3.74 – 3.68 (20H, m, 5 × OCH_2CH_2O), 3.51 (1H, d, *J* = 15.0 Hz, Gly CH^aH^b), 3.24 – 3.13 (4H, m, Lys ε-CH_2, Arg δ-CH_2), 3.07 (1H, dd, *J* = 13.4, 6.2 Hz, Phe β-CH^aH^b), 2.97 (1H, dd, *J* = 13.4, 9.9 Hz, Phe β-CH^aH^b), 2.91 (1H, dd, *J* = 16.6, 7.9 Hz, Asp β-CH^aH^b), 2.74 – 2.71 (1H, m, Asp β-CH^aH^b), 2.44 (2H, q, *J* = 7.1 Hz, C[1"]CH_2), 1.99 (1H, br t, *J* = 35.3 Hz, C[1"]H), 1.87 (1H, dq, *J* = 12.9, 5.8 Hz, Arg β-CH^aH^b), 1.69 – 1.63 (2H, m, Lys δ-CH^aH^b and Arg β-CH^aH^b), 1.56 – 1.48 (3H, m, Lys β-CH^aH^b, Arg γ-CH_2), 1.42 – 1.38 (2H, m, Lys δ-CH_2), 0.97 (2H, dq, *J* = 15.4, 7.7 Hz, Lys γ-CH_2); ^{19}F NMR (659 MHz, D_2O) δ_F -204.6 – -204.7 (m, C[3"]F and C[5"]F), -211.5 – -211.6 (m, C[2"]F and C[6"]F), -216.6 – -216.8 (m, C[4"]F); HRMS (ESI): calcd. For $C_{50}H_{76}F_5N_{12}O_{14}$, 1163.5525. Found: $[MNa]^+$, 1163.5517 (-0.14 ppm error). *Obscured by H_2O signal, detected by COSY NMR.

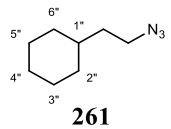

261

(2-Azidoethyl)cyclohexane (261) was prepared by charging a flame-dried round-bottom flask equipped with a magnetic stir bar with (2-bromoethyl)cyclohexane **260** (409 µL, 2.63 mmol, 1.0 equiv.) and sodium azide (365 mg, 5.26 mmol, 2.0 equiv.). The vessel was sealed, evacuated, and backfilled thrice with nitrogen before anhydrous DMF (20 mL) was added *via* syringe. The reaction was stirred at 70 °C for 16 h. The reaction was diluted with deionised water (15 mL) and extracted with diethyl ether (3 × 10 mL). The combined organic layers were washed with a sat. brine solution, dried over magnesium sulphate, filtered, and concentrated *in vacuo* to afford the product as a colourless oil (375 mg, 93%); ^{1}H NMR (500 MHz, $CDCl_3$) δ_H 3.29 (2H, t, *J* = 7.2 Hz, CH_2N_3), 1.72 – 1.64 (5H, m, C[4"]HH', C[6"]HH', C[5"]HH', C[3"]HH', and C[2"]HH'), 1.50 (2H, apparent q, *J* = 7.1 Hz, C[1"]HCH_2), 1.41 – 1.32 (1H, m, C[1"]H), 1.28

– 1.11 (3H, m, C[5"]HH', C[4"]HH', and C[3"]HH'), 0.96 – 0.88 (2H, m, C[6"]HH' and C[2"]HH'); ^{13}C NMR (126 MHz, $CDCl_3$) δ_C 49.4 ($\underline{C}H_2N_3$), 36.1 (C[1"]H$\underline{C}H_2$), 35.2 ($\underline{C[1"]}$H), 33.2 ($\underline{C[6"]}H_2$ and $\underline{C[2"]}H_2$), 26.6 ($\underline{C[4"]}$H), 26.3 ($\underline{C[5"]}H_2$ and $\underline{C[3"]}H_2$). Reported data is in accordance with literature.[8]

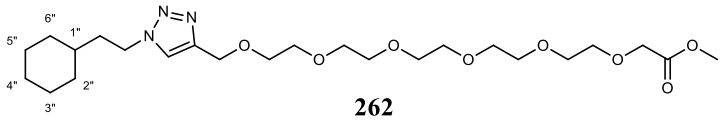

262

Methyl 1-(1-(2-cyclohexylethyl)-1H-1,2,3-triazol-4-yl)-2,5,8,11,14,17-hexaoxanonadecan-19-oate (262) was prepared by charging a round-bottom flask with (2-azidoethyl)cyclohexane **261** (100 mg, 0.65 mmol, 1.0 equiv.), methyl 3,6,9,12,15,18-hexaoxahenicos-20-ynoate **256** (250 mg, 0.728 mmol, 1.1 equiv.), sodium ascorbate (19 mg, 97.9 μmol, 15 mol%), and copper sulphate pentahydrate (5 mg, 19.6 μmol, 3 mol%). The vessel was sealed before *tert*-butyl alcohol (2 mL) and deionised water (2 mL) were added *via* syringe. The reaction was stirred at 70 °C for 16 h. The reaction was diluted with deionised water (5 mL) before being extracted with diethyl ether (3 × 10 mL). The combined organic layers were washed with sat. brine solution, dried over magnesium sulphate, filtered, concentrated *in vacuo*, and purified by flash column chromatography (silica gel, ethyl acetate to 10% methanol in ethyl acetate) to afford the product as a colourless oil (177 mg, 54%); R_f 0.21 (10% methanol in ethyl acetate); ν_{max}/cm^{-1} (neat) 2920 (O-H stretch), 2856 (C-H alkane stretch), 1751 (C=O stretch); ^{1}H NMR (500 MHz, $CDCl_3$) δ_H 7.55 (1H, s, $\underline{H}$C=CNNN), 4.68 (2H, s, $C\underline{H_2}CO_2CH_3$), 4.36 (2H, t, J = 7.6 Hz, $C\underline{H_2}$NNN), 4.16 (2H, s, C=C$C\underline{H_2}$), 3.74 (3H, s, $CO_2C\underline{H_3}$), 3.72 – 3.64 (20H, m, 10 × $OC\underline{H_2}CH_2O$), 1.78 (2H, apparent q, J = 7.6 Hz, $C\underline{H_2}CH_2NNN$), 1.77 – 1.64 (5H, m, C[4"]$\underline{H}$H', C[6"]$\underline{H}$H', C[5"]$\underline{H}$H', C[3"]$\underline{H}$H', and C[2"]$\underline{H}$H'), 1.32 – 1.10 (4H, m, C[5"]H$\underline{H}$', C[4"]H$\underline{H}$', C[3"]H$\underline{H}$', C[1"]$\underline{H}$), 0.99 – 0.92 (2H, m, C[6"]H$\underline{H}$' and C[2"]H$\underline{H}$'); ^{13}C NMR (126 MHz, $CDCl_3$) δ_C 171.0 ($\underline{C}O_2$), 145.3 (HC=$\underline{C}$NNN), 122.4 (H$\underline{C}$=CNNN), 71.1 (O$\underline{C}H_2CH_2O$), 70.8 (O$\underline{C}H_2CH_2O$), 70.7 (6 × O$\underline{C}H_2CH_2O$), 70.6 (O$\underline{C}H_2CH_2O$), 69.8 (O$\underline{C}H_2CH_2O$), 68.8 (C=$C\underline{C}H_2$), 64.9 ($\underline{C}H_2CO_2CH_3$), 51.9 ($CO_2\underline{C}H_3$), 48.4 ($\underline{C}H_2$NNN), 37.8 ($\underline{C}H_2CH_2$NNN), 35.0 ($\underline{C[1"]}$H), 33.01 ($\underline{C[6"]}H_2$ and $\underline{C[2"]}H_2$), 26.5 ($\underline{C[4"]}H_2$), 26.1 ($\underline{C[5"]}H_2$ and $\underline{C[3"]}H_2$); HRMS (ESI): calcd. For $C_{24}H_{44}N_3O_8$, 502.3129. Found: $[MH]^+$, 502.3123 (-0.08 ppm error).

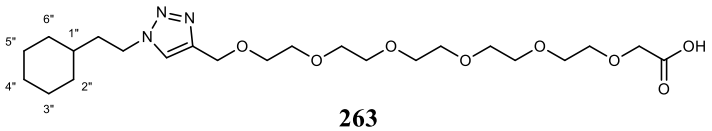

263

1-(1-(2-Cyclohexylethyl)-1H-1,2,3-triazol-4-yl)-2,5,8,11,14,17-hexaoxanonadecan-19-oic acid (263) was prepared by charging a round-bottom flask with methyl 1-(1-(2-cyclohexylethyl)-1H-1,2,3-triazol-4-yl)-2,5,8,11,14,17-hexaoxanonadecan-19-oate **262** (150 mg, 0.30 mmol, 1.0 equiv.). The vessel was sealed before THF (3 mL) and a lithium hydroxide solution (0.5 M in water) (3 mL, 1.50 mmol, 5.0 equiv.) were subsequently added before the reaction was stirred at RT for 16 h. The reaction was acidified to pH 3 with hydrochloric acid (1 M) before the solution was extracted with ethyl acetate (3 × 5 mL). The combined organic layers were washed with sat. brine solution, dried over magnesium sulphate, filtered, and concentrated *in vacuo* to afford the product as a colourless oil (140 mg, 96%); R_f 0.34 (20% methanol in ethyl acetate); R_f 0.21 (10% methanol in ethyl acetate); ν_{max}/cm^{-1} (neat) 3397 (O-H stretch), 2922 (C-H alkane stretch), 1719 (C=O stretch), 1647 (C=C stretch); ^{1}H NMR (500 MHz, CD_3OD) δ_H 7.99 (1H, s, HC=CNNN), 4.63 (2H, s, CH_2CO_2H), 4.44 (2H, t, J = 7.4 Hz, CH_2NNN), 4.11 (2H, d, J = 1.8 Hz, HC=CCH_2), 3.70 – 3.63 (20H, m, 10 × OCH_2CH_2O), 1.80 (2H, apparent q, J = 7.0 Hz, CH_2CH_2NNN), 1.79 – 1.65 (5H, m, C[4”]HH’, C[6”]HH’, C[5”]HH’, C[3”]HH’, and C[2”]HH’), 1.34 – 1.18 (4H, m, C[5”]HH’, C[4”]HH’, C[3”]HH’, C[1”]H), 0.99 (2H, qd, J = 12.1, 11.3, 2.7 Hz, C[6”]HH’ and C[2”]HH’); ^{13}C NMR (126 MHz, CD_3OD) δ_C 174.4 (CO_2H), 146.0 (HC=CNNN), 125.0 (HC=CNNN), 71.6 – 71.5 (m, 9 × OCH_2CH_2O), 70.7 (OCH_2CH_2O), 69.3 (HC=CCH_2), 65.0 (CH_2CO_2H), 49.2 (CH_2NNN), 38.8 (CH_2CH_2NNN), 36.1 (C[1”]H_2), 34.0 (C[6”]H_2 and C[2”]H_2), 27.5 (C[4”]H_2), 27.1 (C[5”]H_2 and C[3”]H_2); HRMS (ESI): calcd. For $C_{23}H_{41}N_3O_8Na$, 510.2786. Found: $[MNa]^+$, 510.2777 (-1.74 ppm error).

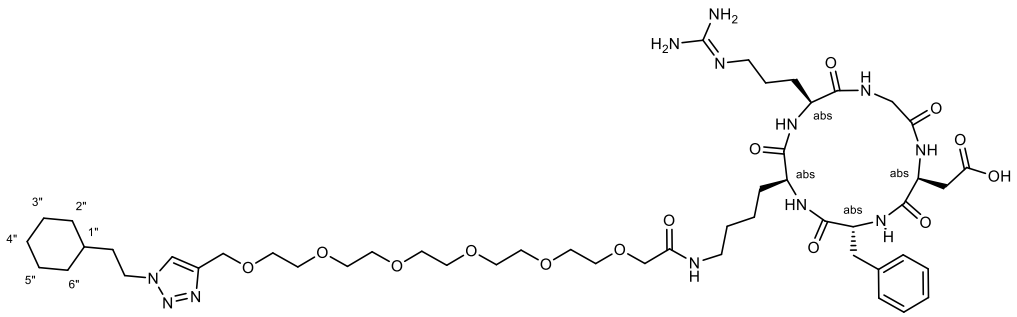

264

2-((*2S,5R,8S,11S*)-5-Benzyl-8-(1-(1-(2-cyclohexylethyl)-1H-1,2,3-triazol-4-yl)-19-oxo-2,5,8,11,14,17-hexaoxa-20-azatetracosan-24-yl)-11-(3-((diaminomethylene)amino)propyl)-3,6,9,12,15-pentaoxo-1,4,7,10,13-pentaazacyclopentadecan-2-yl)acetic acid (264) was prepared by charging a flame-dried round-bottom flask equipped with a magnetic stir bar with 1-(1-(2-cyclohexylethyl)-1H-1,2,3-triazol-4-yl)-2,5,8,11,14,17-hexaoxanonadecan-19-oic acid **263** (3 mg, 3.98 μmol, 1.2 equiv.) and cylco(-RGDfK) **257** (2 mg, 3.31 μmol, 1.0 equiv.). The vessel was sealed, evacuated, and backfilled with nitrogen thrice before anhydrous DMF (1 mL), DIPEA (2 μL, 12.4 μmol, 3.0 equiv.), and T3P (5 μL, 8.3 μmol, 2.0 equiv.) were subsequently added. The reaction was stirred at RT for 16 h. The reaction was diluted with deionised water (2 mL) before being extracted with ethyl acetate (3 × 5 mL). The combined organic layers were dried over magnesium sulphate, filtered, and concentrated *in vacuo*. The crude reaction mixture was purified by semipreparative HPLC on a Shimadzu Prominence system using a Phenomenex Synergi® Polar-RP 80Å (250 x 10.0 mm, 4μ) and a guard cartridge; Mobile phase: 0.05% TFA in water (solvent A) and 0.05% TFA in MeCN (solvent B); linear gradient: 10% solvent B to 55% solvent B over 25 min, then to 95% B over 0.1 min, then held at 95% solvent B over 5 mins, back to 10% B over 0.1 min, then 10% B for 5 min to re-equilibrate the column. Flow rate: 2.5 mL/min; detection: 220 nm. The relevant fractions were collected (tR = 26.72 min), concentrated and lyophilized affording the product (2.3 mg, 65%) as a white powder; ^{1}H NMR (700 MHz, D_2O) δ_H 8.00 (1H, s, HC=CNNN), 7.33 (2H, apparent t, J = 7.2 Hz, Phe *m*-ArH), 7.37 (1H, t, J = 7.3 Hz, Phe *p*-ArH), 7.21 (2H, d, J = 7.6 Hz, Phe *o*-ArH), 4.74 (1H, dd, J = 8.0, 6.6 Hz, Asp α-CH), 4.64 (2H, s, CH_2CONH), 4.61 (1H, dd, J = 9.8, 6.2 Hz, Phe α-CH), 4.42 (2H, t, J = 7.1 Hz, CH_2NNN), 4.32 (1H, dd, J = 9.2, 5.6 Hz, Arg α-CH), 4.18 (1H, d, J = 15.1 Hz, Gly CH^{a}H^b), 4.04 (2H, s, C≡CCH_2), 3.84 (1H, dd, J = 10.3, 4.6 Hz, Lys α-H), 3.71 – 3.62 (20H, m, 5 × OCH_2CH_2O), 3.47 (1H, d, J = 15.1 Hz, Gly CH^{a}H^b), 3.21 – 3.10 (4H, m, Lys ε-CH_2, Arg δ-CH_2), 3.03 (1H, dd, J = 13.2, 6.2 Hz, Phe β-CH^{a}H^b), 2.95 – 2.87 (2H, m, Phe β-CH^{a}H^b and Asp β-CH^{a}H^b), 2.71 (1H, dd, J = 16.8, 6.4 Hz, Asp β-CH^{a}H^b), 1.87 – 1.80 (1H, m, Arg β-CH^{a}H^b), 1.75 (2H, q, J = 7.0 Hz, C[1"]CH_2), 1.66 – 1.54 (7H, m, Arg β-CH^{a}H^b, Lys β-CH^{a}H^b, 5 ×

cyclohexane C<u>H</u>), 1.54 – 1.46 (3H, m, Lys β-CH^{a}<u>H</u>^{b}, Arg γ-C<u>H$_2$</u>), 1.37 – 1.33 (2H, m, Lys δ-C<u>H$_2$</u>), 1.16 – 1.05 (4H, m, 4 × cyclohexane C<u>H</u>), 0.97 – 0.87 (4H, m, Lys γ-C<u>H$_2$</u> and 2 × cyclohexane C<u>H</u>); HRMS (ESI): calcd. For $C_{50}H_{76}F_5N_{12}O_{14}$, 1163.5525. Found: $[MNa]^+$, 1163.5517 (-0.14 ppm error).

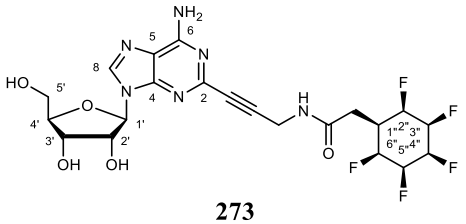

273

N-(3-(6-Amino-9-((*2R,3R,4S,5R*)-3,4-dihydroxy-5-(hydroxymethyl)tetrahydrofuran-2-yl)-9H-purin-2-yl)prop-2-yn-1-yl)-2-((*1r,2R,3R,4S,5S,6S*)-2,3,4,5,6-pentafluorocyclohexyl)acetamide (273) was prepared by charging a flame-dried round-bottom flask equipped with a magnetic stir bar with 2-iodoadenosine **243** (100 mg, 0.26 mmol, 1.0 equiv.), 2-((*1r,2R,3R,4s,5S,6S*)-2,3,4,5,6-pentafluorocyclohexyl)-N-(prop-2-yn-1-yl)acetamide **209** (69 mg, 0.26 mmol, 1.0 equiv.), copper(I) iodide (5 mg, 25.5 μmol, 10 mol%), and bis(triphenylphosphine)palladium(II) dichloride (18 mg, 25.5 μmol, 10 mol%). The reaction vessel was sealed, evacuated, and backfilled with nitrogen thrice before degassed anhydrous DMF (5 mL) and triethylamine (53 μL, 0.38 mmol, 1.5 equiv.) were subsequently added *via* syringe. The reaction was stirred at 85 °C for 18 h before being concentrated *in vacuo*. The crude material was reconstituted in ethyl acetate (10 mL) before being washed with an EDTA solution (0.5 M) (15 mL). The organic layer was separated, washed with sat. brine solution, dried over magnesium sulphate, filtered, and concentrated *in vacuo*. The crude reaction mixture was purified by semipreparative HPLC on a Shimadzu Prominence system using a Phenomenex Synergi® Polar-RP 80Å (250 x 10.0 mm, 4μ) and a guard cartridge; Mobile phase: 0.05% TFA in water (solvent A) and 0.05% TFA in acetonitrile (solvent B); linear gradient: 20% solvent B to 40% solvent B over 20 min, then to 95% B over 5 min, back to 20% B over 5 min, then 20% B for 5 min to re-equilibrate the column. Flow rate: 2.5 mL/min; detection: 260 nm. The relevant fractions were collected (tR = 13.43 min), concentrated and lyophilized affording the product as a white solid (45 mg, 33%); Mp. 200 – 202 ºC (dec.); R_f 0.47 (20% methanol in DCM); ν_{max}/cm^{-1} (neat) 3283 (O-H stretch), 3206 (N-H stretch), 2945 (C-H alkane stretch), 1713 (C=O stretch), 1638 (N-H bend), 1545 (C-C aromatic stretch); ^{1}H NMR (700 MHz, $(CD_3)_2SO$) δ_H 8.73 (1H, t, *J* = 5.5 Hz, N<u>H</u>CO), 8.43 (1H, s, C[8]<u>H</u>), 7.49 (2H, br s, N<u>H$_2$</u>), 5.85 (1H, d, *J* = 5.6 Hz, C[1']<u>H</u>), 5.43–5.35 (1H, m, C[4"]<u>H</u>), 5.01–4.88 (4H, m, C[2"]<u>H</u>, C[3"]<u>H</u>, C[5"]<u>H</u>, and C[6"]<u>H</u>), 4.50 (1H, dd, *J* = 5.6, 4.6 Hz, C[2']<u>H</u>), 4.16 (2H, d, *J* = 5.5 Hz, C≡CC<u>H$_2$</u>NH), 4.12 (1H, dd, *J* = 4.6, 3.5 Hz, C[3']<u>H</u>), 3.94 (1H, td, *J* = 3.7, 3.5 Hz, C[4']<u>H</u>),

3.66 (1H, dd, *J* = 12.1, 3.7 Hz, C[5']HH'), 3.55 (1H, dd, *J* = 12.1, 3.7 Hz, C[5']HH'), 2.63 (2H, d, *J* = 7.3 Hz, COCH_2CH), 2.02–1.99 (1H, m, C[1"]H); ^{13}C NMR (176 MHz, $(CD_3)_2SO$) δ_C 169.5 (CO), 155.8 (C[6]), 149.3 (C[2]), 145.1 (C[4]), 140.4 (C[8]H), 118.7 (C[5]), 88.1 (dd, *J* = 189.5, 17.4 Hz, C[2"]F and C[6"]F), 88.1–86.6 (m, C[4"]F), 86.7–85.7 (m, C[3"]F and C[5"]F), 87.3 (C[1']H), 85.6 (C[4']H), 81.8 (C≡CCH$_2$NH), 81.5 (C≡CCH$_2$NH), 73.8 (C[2']H), 70.3 (C[3']H), 61.4 (C[5']H$_2$), 34.4 (C[1"]H), 34.4 (C[1"]F), 31.2 (COCH$_2$CH), 28.3 (C≡CCH$_2$NH); ^{19}F{^{1}H} NMR (470 MHz, $(D_3C)_2SO$) δ_F -203.8 (t, *J* = 12.6 Hz, C[3"]F and C[5"]F), -210.5 (d, *J* = 23.0 Hz, C[2"]F and C[6"]F), -216.2 (dt, *J* = 23.0, 12.6 Hz, C[4"]F); HRMS (ESI): calcd. For $C_{21}H_{23}F_5N_6O_5Na$, 557.1542. Found: $[MNa]^+$, 557.1544 (-0.31 ppm error).

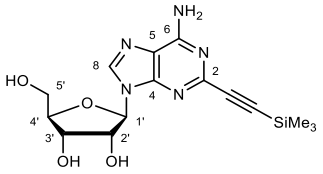

276

(*2R,3S,4R,5R*)-2-(6-Amino-2-((trimethylsilyl)ethynyl)-9H-purin-9-yl)-5-(hydroxymethyl)tetrahydrofuran-3,4-diol (276) was prepared by charging a flame-dried round-bottom flask equipped with a magnetic stir bar with iodoadenosine **243** (200 mg, 0.51 mmol, 1.0 equiv.), ethynyltrimethylsilane (145 μL, 1.02 mmol, 2.0 equiv), copper(I) iodide (10 mg, 51 μmol, 10 mol%), and bis(triphenylphosphine)palladium(II) dichloride (36 mg, 51 μmol, 10 mol%). The vessel was sealed, evacuated, and backfilled with nitrogen thrice before degassed DMF (5 mL) and triethylamine (106 μL, 0.76 mmol, 1.5 equiv.) were added sequentially *via* syringe. The reaction was heated to 85 °C and stirred under nitrogen at for 16 h. The reaction was directly concentrated *in vacuo* before the crude solid was diluted in ethyl acetate (10 mL) and washed with EDTA solution (0.5 M) (2 × 5 mL). The organic layer was separated, dried over magnesium sulphate, filtered, concentrated *in vacuo*, and purified by flash column chromatography (silica gel, 2% methanol in DCM to 5% methanol in DCM) to afford the product as an off white solid (151 mg, 78%); ^{1}H NMR (500 MHz, $(CD_3)_2SO$) δ_H 8.45 (1H, s, C[8]H), 7.53 (2H, s, NH$_2$), 5.87 (1H, d, *J* = 6.0 Hz, C[1']H), 5.48 (1H, br s, C[2']OH), 5.20 (1H, br s, C[3']OH), 5.14 (1H, br s, C[5']OH), 4.48 (1H, apparent t, *J* = 5.5 Hz, C[2']H), 4.11 (1H, dd, *J* = 4.9, 3.4 Hz, C[3']H), 3.94 (1H, apparent q, *J* = 3.7 Hz, C[4']H), 3.66 (1H, dd, *J* = 12.1, 3.9 Hz, C[5']HH'), 3.56 (1H, dd, *J* = 12.1, 3.7 Hz, C[5']HH'), 0.24 (9H, s, Si(CH$_3$)$_3$); ^{13}C NMR (126 MHz, $(CD_3)_2SO$) δ_C 155.9 (C[6]), 149.3 (C[4]), 144.8 (C[2]), 140.3 (C[8]H), 118.8 (C[5]), 104.5 (C≡CSi), 88.7 (C≡CSi), 87.0 (C[1']H), 85.6 (C[4']H), 73.9 (C[2']H), 70.4

(C[3']H), 61.4 (C[5']H_2), -0.36 (Si(CH_3)$_3$); HRMS (ESI): calcd. For $C_{15}H_{22}O_4N_5Si$, 364.1436. Found: $[MH]^+$, 364.1428 (-2.08 ppm error). Reported data is in accordance with literature.[10]

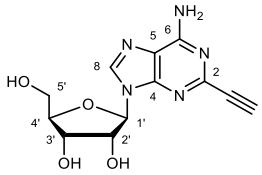

277

(*2R,3R,4S,5R*)-2-(6-Amino-2-ethynyl-9H-purin-9-yl)-5-(hydroxymethyl)tetrahydrofuran-3,4-diol (277) was prepared by charging a flame-dried round-bottom flask equipped with a magnetic stir bar with (*2R,3S,4R,5R*)-2-(6-amino-2-((trimethylsilyl)ethynyl)-9H-purin-9-yl)-5-(hydroxymethyl)tetrahydrofuran-3,4-diol **276** (75 mg, 0.21 mmol, 1.0 equiv.). The vessel was sealed, evacuated, and backfilled with nitrogen thrice before ammonia (2 M in methanol) (5 mL) was added *via* syringe and the reaction stirred at RT for 2 h. The reaction was directly concentrated *in vacuo* and the crude solid recrystalised from ethanol to afford the product as an off white solid (59 mg, 96%); ^{1}H NMR (500 MHz, $(CD_3)_2SO$) δ_H 8.43 (1H, s, C[8]H), 7.54 (2H, s, NH_2), 5.85 (1H, d, J = 6.1 Hz, C[1']H), 5.48 (1H, br s, C[2']OH), 5.21 (1H, br s, C[3']OH), 5.19 (1H, br s, C[5']OH), 4.55 (1H, apparent q, J = 5.3 Hz, C[2']H), 4.13 (1H, apparent q, J = 3.5 Hz, C[3']H), 4.03 (1H, s, C≡CH), 3.95 (1H, apparent q, J = 3.7 Hz, C[4']H), 3.66 (1H, dt, J = 12.2, 4.4 Hz, C[5']HH'), 3.57 – 3.52 (1H, m, C[5']HH'); ^{13}C NMR (126 MHz, $(CD_3)_2SO$) δ_C 155.9 (C[6]), 149.1 (C[4]), 144.7 (C[2]), 140.7 (C[8]H), 119.1 (C[5]), 87.5 (C[1']H), 85.8 (C[4']H), 83.2 (C≡CH), 75.1 (C≡CH), 73.6 (C[2']H), 70.5 (C[3']H), 61.5 (C[5']H_2); HRMS (ESI): calcd. For $C_{12}H_{13}O_4N_5Na$, 314.0860. Found: $[MNa]^+$, 314.0856 (-1.19 ppm error).

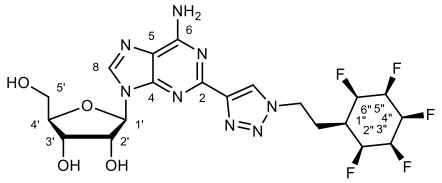

274

(*2R,3R,4S,5R*)-2-(6-Amino-2-(1-(2-((*1r,2R,3R,4S,5S,6S*)-2,3,4,5,6-pentafluorocyclohexyl)ethyl)-1H-1,2,3-triazol-4-yl)-9H-purin-9-yl)-5-(hydroxymethyl)tetrahydrofuran-3,4-diol (274) was prepared by charging a round-bottom flask equipped with a magnetic stir bar with (*2R,3R,4S,5R*)-2-(6-amino-2-ethynyl-9H-purin-9-yl)-5-(hydroxymethyl)tetrahydrofuran-3,4-diol **277** (20 mg, 68 μmol, 1.0 equiv.), (*1r,2R,3R,4s,5S,6S*)-1-(2-azidoethyl)-2,3,4,5,6-pentafluorocyclohexane **110** (18 mg, 76 μmol, 1.1 equiv.), sodium ascorbate (2.0 mg, 10 μmol, 15 mol%), and copper(I) sulphate pentahydrate

(0.5 mg, 2.1 μmol, 3 mol%). The vessel was sealed before ethanol (1 mL) and deionised water (1 mL) were added. The reaction was stirred at 65 °C for 16 h. The reaction was directly concentrated *in vacuo* and was directly purified by semipreparative HPLC on a Shimadzu Prominence system using a Phenomenex Synergi® Polar-RP 80Å (250 x 10.0 mm, 4μ) and a guard cartridge; Mobile phase: 0.05% TFA in water (solvent A) and 0.05% TFA in acetonitrile (solvent B); linear gradient: 20% solvent B to 40% solvent B over 20 min, then to 95% B over 5 min, back to 20% B over 5 min, then 20% B for 5 min to re-equilibrate the column. Flow rate: 2.5 mL/min; detection: 260 nm. The relevant fractions were collected (tR = 12.23 min), concentrated and lyophilized affording the product as a white solid (5 mg, 14%); Mp. 188 – 190 ºC (dec.); R_f 0. 27 (20% methanol in DCM); ν_{max}/cm^{-1} (neat) 3206 (O-H stretch), 2938 (C-H alkane stretch), 1674 (C=C alkene stretch); ^{1}H NMR (400 MHz, $(CD_3)_2SO$) δ_H 8.70 (1H, s, C=C<u>H</u>N), 8.45 (1H, s, C[8]<u>H</u>), 7.70 (2H, br s, N<u>H$_2$</u>), 5.96 (1H, d, *J* = 6.3 Hz, C[1']<u>H</u>), 5.43–5.29 (1H, m, C[4"]<u>H</u>), 5.16–5.03 (2H, m, C[6"]<u>H</u> and C[2"]<u>H</u>), 4.99–4.75 (2H, m, C[3"]<u>H</u> and C[5"]<u>H</u>), 4.67–4.62 (3H, m, NC<u>H$_2$</u>CH$_2$ and C[2']<u>H</u>), 4.18 (1H, dd, *J* = 5.0, 3.2 Hz, C[3']<u>H</u>), 3.96 (1H, td, *J* = 3.9, 3.2 Hz, C[4']<u>H</u>), 3.68 (1H, dd, *J* = 12.0, 3.9 Hz, C[5']<u>H</u>H'), 3.57 (1H, dd, *J* = 12.0, 3.9 Hz, C[5']H<u>H</u>'), 2.31 (2H, q, *J* = 7.1 Hz, NCH$_2$C<u>H$_2$</u>), 1.99–1.98 (1H, m, C[1"]<u>H</u>); ^{13}C NMR (101 MHz, $(CD_3)_2SO$) δ_C 155.3 (<u>C[6]</u>), 150.2 (<u>C[2]</u>), 146.0 (<u>C[4]</u>), 140.7 (<u>C[8]</u>H), 126.3 (C=<u>C</u>HN), 118.4 (<u>C[5]</u>), 117.4 (<u>C</u>=CHN), 88.2 – 86.2 (m, <u>C[4"]</u>H)*, 87.5 (dd, *J* = 189.0, 17.9 Hz, <u>C[2"]</u>H and <u>C[6"]</u>H), 86.8 – 85.2 (m, <u>C[3"]</u>H and <u>C[5"]</u>H), 87.1 (<u>C[1']</u>H), 85.9 (<u>C[4']</u>H), 73.7 (<u>C[2']</u>H), 70.7 (<u>C[3']</u>), 61.6 (<u>C[5']</u>H$_2$), 46.6 (N<u>C</u>H$_2$CH$_2$CH), 34.7 (<u>C[1"]</u>H), 26.4 (NCH$_2$<u>C</u>H$_2$C); ^{19}F{^{1}H} NMR (376 MHz, $(CD_3)_2SO$) δ_F -203.6 (t, *J* = 12.6 Hz, C[3"]<u>F</u> and C[5"]<u>F</u>), -211.6 (d, *J* = 23.0 Hz, C[2"]<u>F</u> and C[6"]<u>F</u>), -216.3 (dt, *J* = 23.0, 12.6 Hz, C[4"]<u>F</u>); HRMS (ESI): calcd. For $C_{20}H_{24}F_5N_8O_4$, 535.1841. Found: $[MH]^+$, 535.1833 (-1.50 ppm error). *Peak detected by HSQC.

7.3 – β-Lactam assays

7.3.1 – Growth of bacteria cultures

The following bacterial cultures; *M. abscessus* subsp. *abscessus*; a clinical isolate of *M. abscessus* subsp. *bolettii;* a clinical isolate of *M. abscessus* subsp. *massiliense; M. abscessus* NCTC 13031 (smooth morphotype), M. abscessus NCTC 13031 (rough morphotype), *Escherichia coli* ATCC 25922, J53 2138E, J53 2140E, 1496 ESBL, *Pseudomonas aeruginosa* ATCC, *M. bovis BCG* Pasteur 1173P2, and *Salmonella sp*. were grown at 37 °C for 72 h from 40% glycol stocks, shaking at 180 rpm. The media used was Middlebrook 7H9 + 10% albumin-dextrose-catalase + 0.05% Tween-80 (Sigma-Aldrich).

7.3.2 – Inhibition assays without accompanying amoxicillin

In a 96-well microtitre plate a stock solution of a chosen β-lactam (**144**, **181**, and **193**) (10 mg/mL in DMSO) was serially diluted two-fold in DMSO to concentrations ranging from 10 mg/mL to 0.076 mg/mL (18 dilutions total). This was done across two rows of the plate, filling nine wells per row with the tenth filled with DMSO. From each well 2 μL was transferred to a separate 96-well plate at n=4. Three of the concentrations were combined with 98 μL of bacterial culture adjusted to OD (600 nm) 0.1. This resulted in final compound concentrations ranging from 200 μg/mL to 0.001525878906 μg/mL with additional 0 μg/mL which contained only DMSO. The remaining repeat of each concentration was combined with media only to provide a media control that would be used to normalise each OD and media colour. The final two columns were inoculated with 100 μL of bacteria and 100 μL of media respectively as positive and negative controls. Each plate was incubated aerobically at 37 °C for 96 h, and optical density was observed at given time points using an absorbance spectrophotometric plate reader at 570 nm (BioTek EL808) to establish growth curves. At endpoint, each well was stamped onto 7H11 agar plates and incubated at 37 °C for 72 hours, in order to ascertain MBC. 30 μL (0.1%) resazurin solution (filter sterile) was then added to each well of the 96 well plate, and incubated at 37 °C for 24 hours. The next day, plates were observed for a purple colour to determine MIC. This entire process was done three times per species to allow three biological replicates. Three technical replicates are included per plate corresponding to a final n number = 9. All assays were performed by Emily Baker from the Cox group at Aston University.

7.3.3 – Inhibition assays with accompanying amoxicillin

In a 96-well microtitre plate a stock solution of a chosen β-lactam (**144**, **181 – 184**, and **190**) (10 mg/mL in DMSO) was serially diluted two-fold in DMSO to concentrations ranging from 5 mg/mL to 0.038 mg/mL (18 dilutions total). This was done across two rows of the plate, filling nine wells per row with the tenth filled with DMSO. From each well 2 μL was transferred to a

separate 96-well plate at n=4. Three of the concentrations were combined with 2 μL of Amoxicillin (5 mg/mL) and 96 μL of bacterial culture adjusted to OD (600 nm) 0.1. This resulted in final compound concentrations ranging from 100 μg/mL to 0.001525878906 μg/mL with additional 0 μg/mL which contained only DMSO. The remaining repeat of each concentration was combined with media only to provide a media control that would be used to normalise each OD and media colour. The final two columns were inoculated with 100 μL of bacteria and 100 μL of media respectively as positive and negative controls. Each plate was incubated aerobically at 37 °C for 96 h, and optical density was observed at given time points using an absorbance spectrophotometric plate reader at 570 nm (BioTek EL808) to establish growth curves. This entire process was done three times per species to allow three biological replicates. Three technical replicates are included per plate corresponding to a final n number = 9. All assays were performed by Dr. James Harrison from the Cox group at Aston University.

7.4 – Ring opening experiments

7.4.1 – Materials and methods

To a flame dried NMR tube was added the appropriate β-lactam (**144**, **181 – 184**, **190** and **193**) (2 mg, 1.0 equiv.) dissolved in deuterated methanol (0.5 mL). A ^{1}H and $\{^{1}H\}^{19}F$ NMR experiment was taken as an initial reference. A premade solution of either sodium methoxide in methanol (1 M, 1.5 equiv.) or hydrochloric acid in water (1 M, 1.5 equiv.) was then added to the NMR tube before being shaken and a ^{1}H and $\{^{1}H\}^{19}F$ NMR experiment was immediately taken (0 hours). The reaction was left in the tube at RT and further ^{1}H and $\{^{1}H\}^{19}F$ NMR experiments were taken at 30 min, 1 h, 2 h, 5 h, and/or 24 h. After 24 h, a further 10 equiv. of either sodium methoxide or hydrochloric acid was added to selected NMR tubes before the solution was left for an additional 24 h and a final ^{1}H and $\{^{1}H\}^{19}F$ NMR experiment was taken.

7.4.2 – Resulting ^{1}H and $\{^{1}H\}^{19}F$ NMR spectra

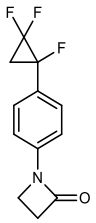

144

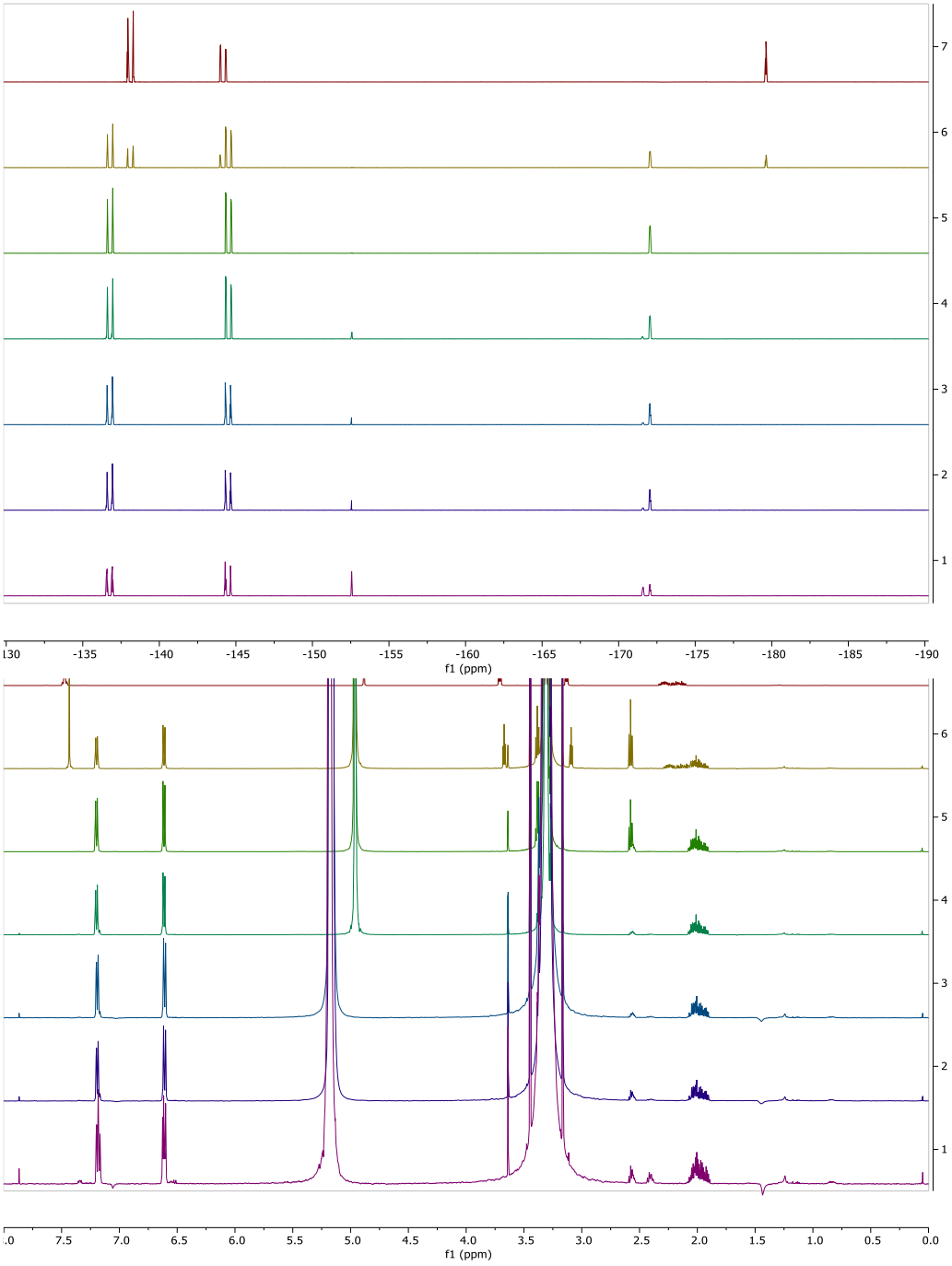

Figure 7.1: Stacked $\{^{1}H\}^{19}F$ NMR (top) and ^{1}H NMR (bottom) spectra of sodium methoxide ring hydrolysis of β-lactam **144**. From top to bottom: Initial, 0 h, 30 min, 1 h, 2 h, 5 h, 24 h.

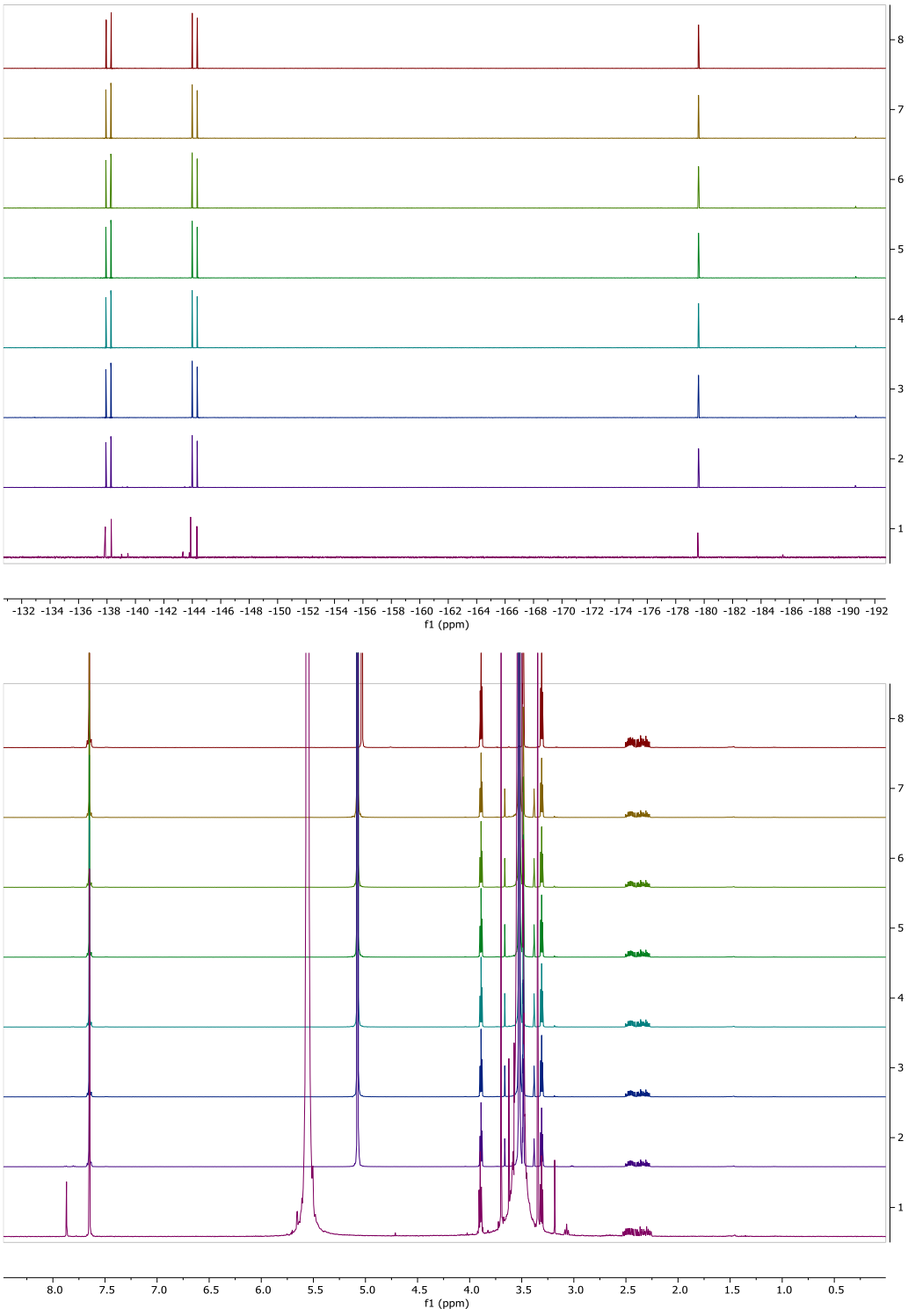

Figure 7.2: Stacked $\{^{1}H\}^{19}F$ NMR (top) and ^{1}H NMR (bottom) spectra of hydrochloric acid ring hydrolysis of β-lactam **144**. From top to bottom: Initial, 0 h, 30 min, 1 h, 2 h, 5 h, 24 h, 48 h (+ 10 equiv.).

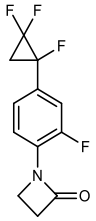

181

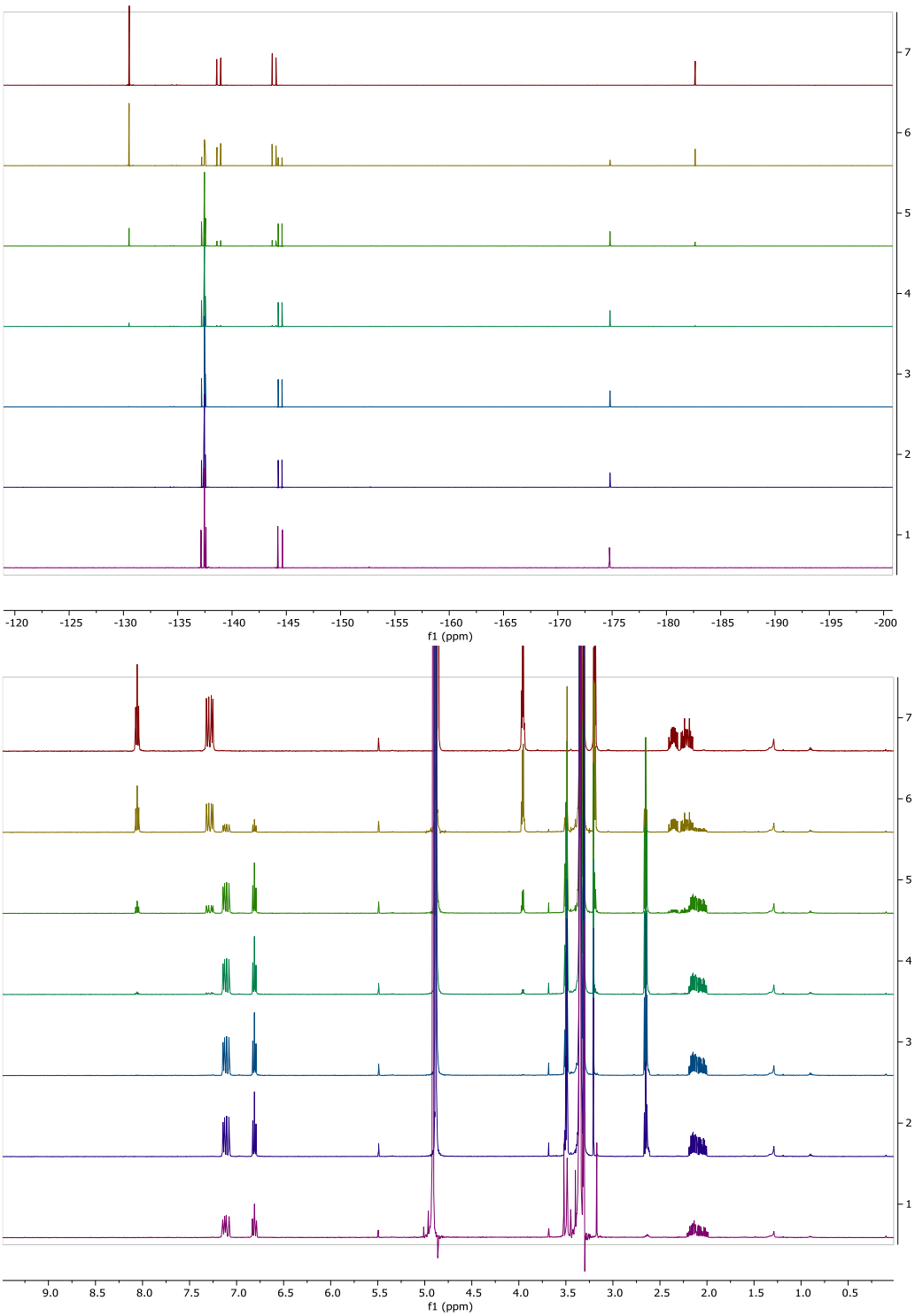

Figure 7.3: Stacked {^{1}H}^{19}F NMR (top) and ^{1}H NMR (bottom) spectra of sodium methoxide ring hydrolysis of β-lactam **181**. From top to bottom: Initial, 0 h, 30 min, 1 h, 2 h, 5 h, 24 h.

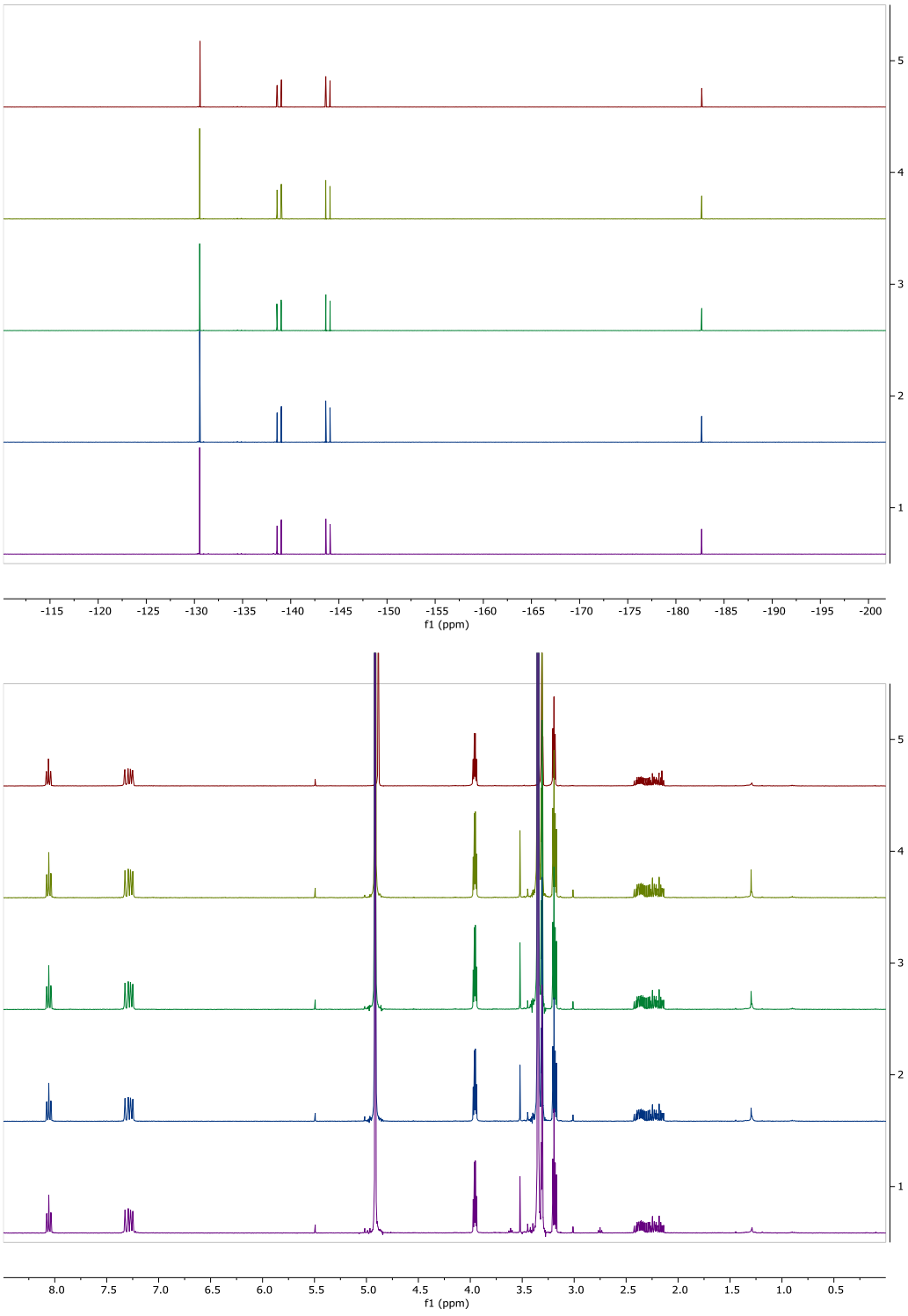

Figure 7.4: Stacked {^{1}H}^{19}F NMR (top) and ^{1}H NMR (bottom) spectra of hydrochloric acid ring hydrolysis of β-lactam **181**. From top to bottom: Initial, 0 h, 30 min, 1 h, 24 h.

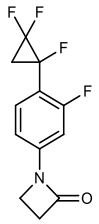

182

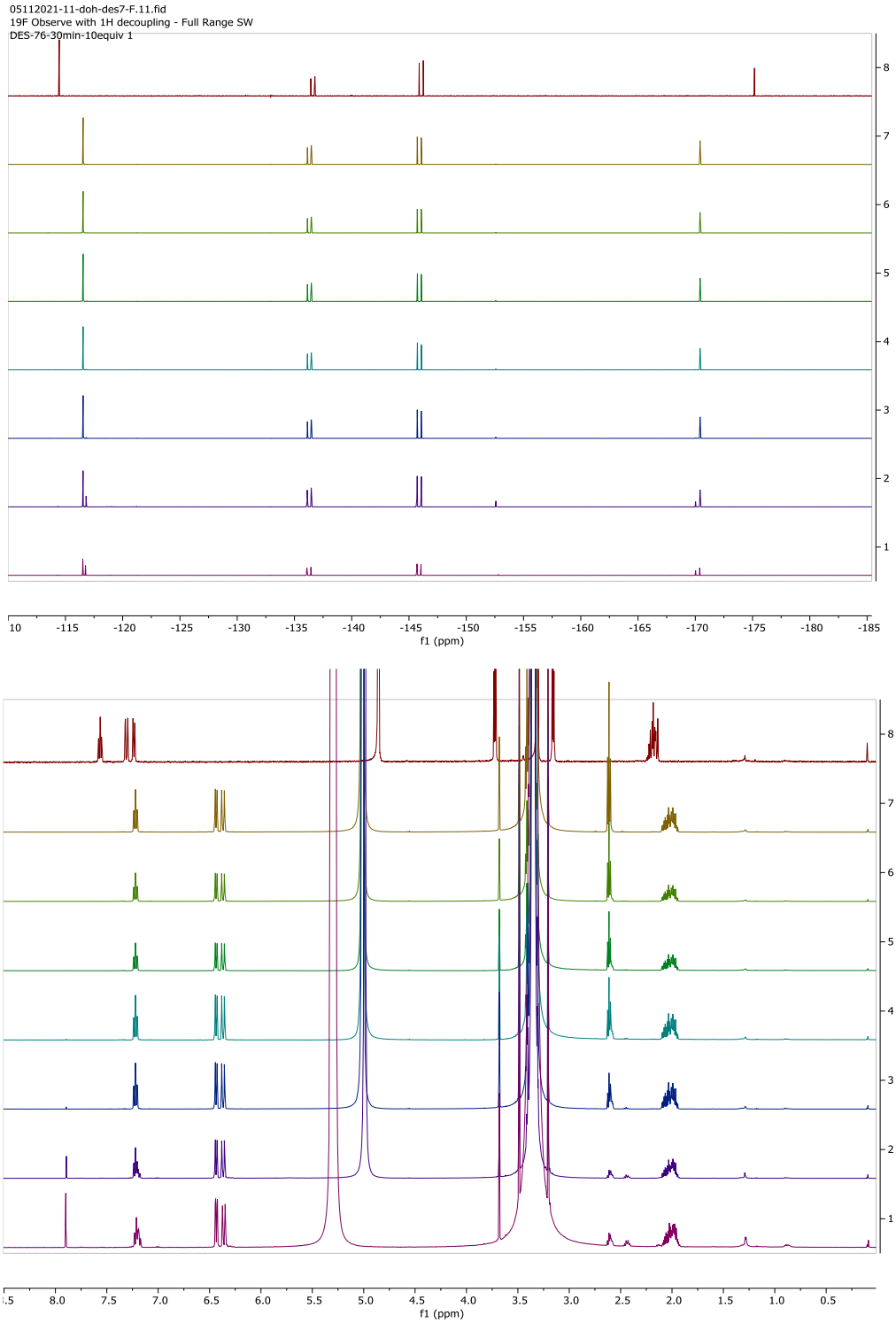

Figure 7.5: Stacked $\{^{1}H\}^{19}F$ NMR (top) and ^{1}H NMR (bottom) spectra of sodium methoxide ring hydrolysis of β-lactam **182**. From top to bottom: Initial, 0 h, 30 min, 1 h, 2 h, 5 h, 24 h, 48 h (+ 10 equiv.).

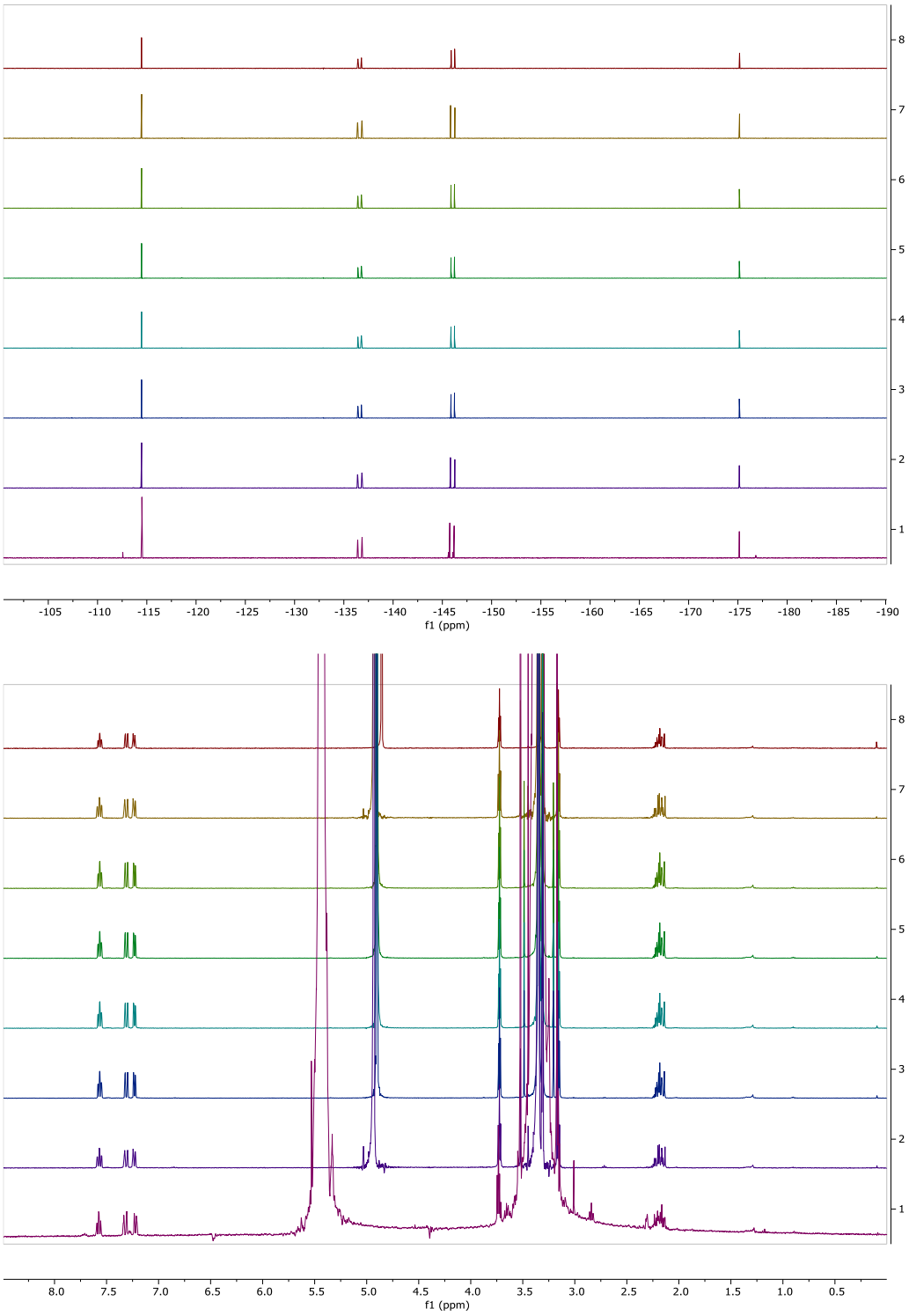

Figure 7.6: Stacked {^{1}H}^{19}F NMR (top) and ^{1}H NMR (bottom) spectra of hydrochloric acid ring hydrolysis of β-lactam **182**. From top to bottom: Initial, 0 h, 30 min, 1 h, 2 h, 5 h, 24 h, 48 h (+ 10 equiv.).

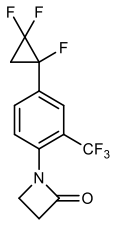

183

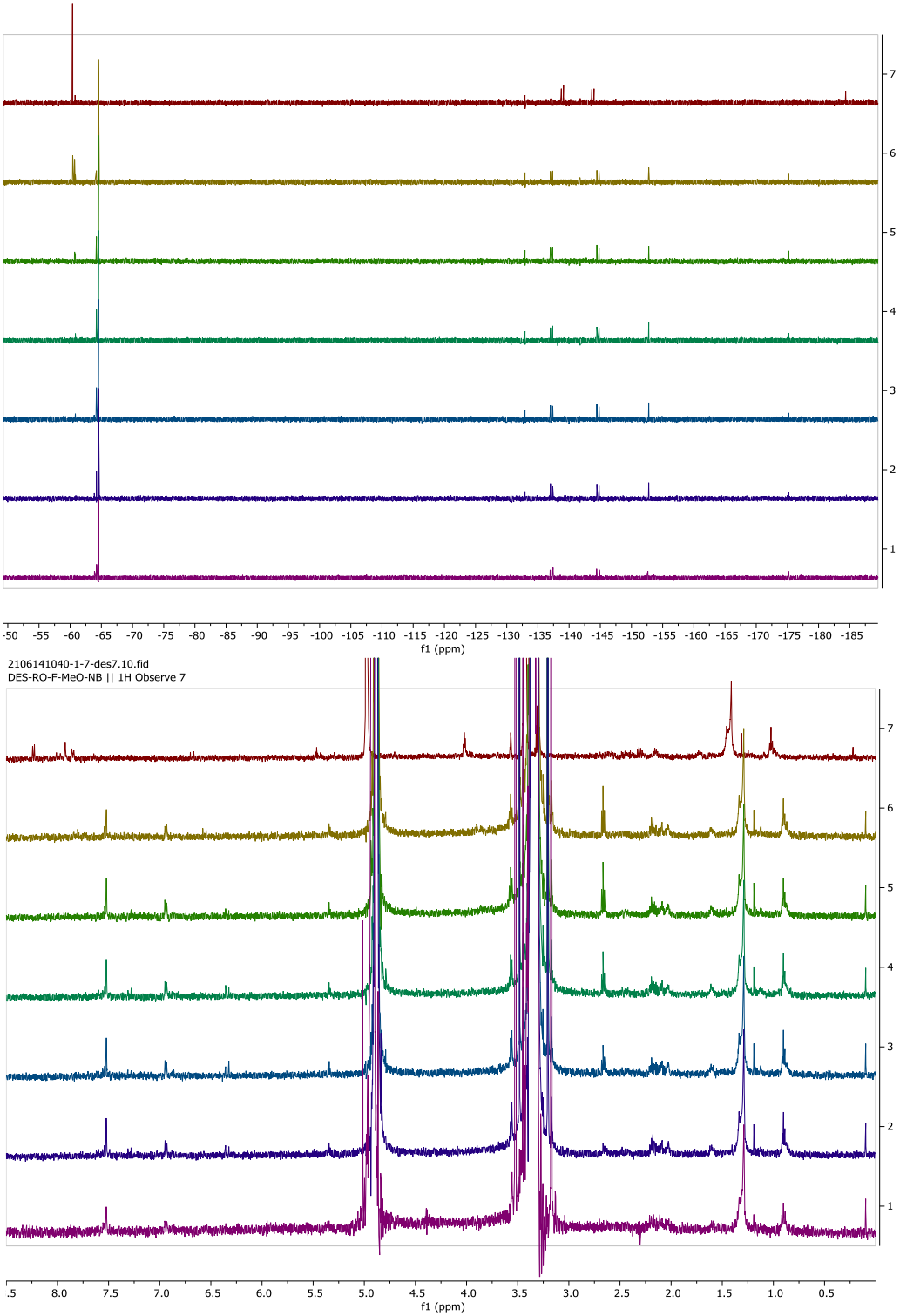

Figure 7.7: Stacked $\{^{1}H\}^{19}F$ NMR (top) and ^{1}H NMR (bottom) spectra of sodium methoxide ring hydrolysis of β-lactam **183**. From top to bottom: Initial, 0 h, 30 min, 1 h, 2 h, 5 h, 24 h.

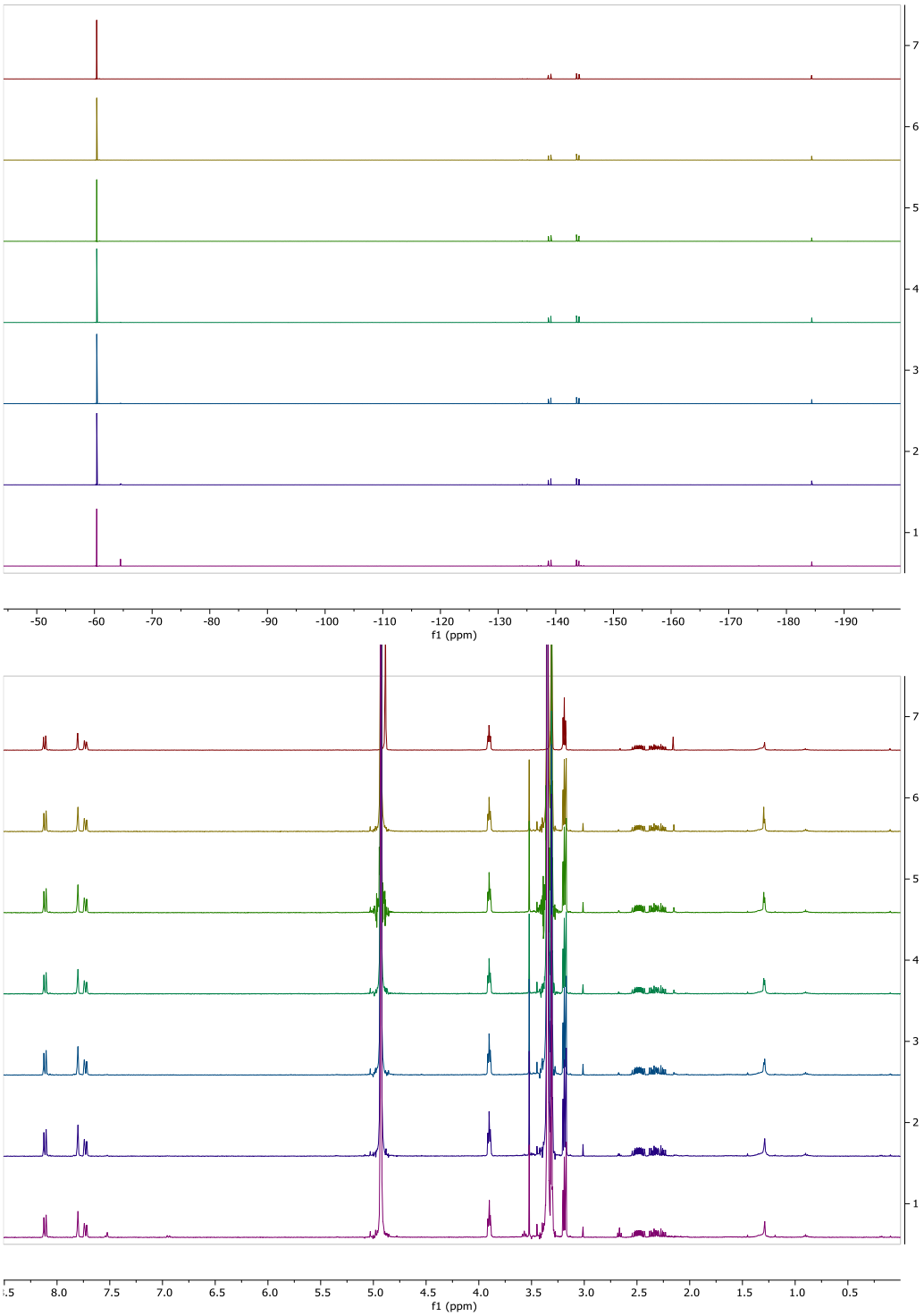

Figure 7.8: Stacked $\{^{1}H\}^{19}F$ NMR (top) and ^{1}H NMR (bottom) spectra of hydrochloric acid ring hydrolysis of β-lactam **183**. From top to bottom: Initial, 0 h, 30 min, 1 h, 2 h, 5 h, 24 h.

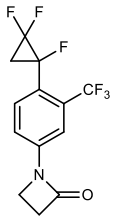

184

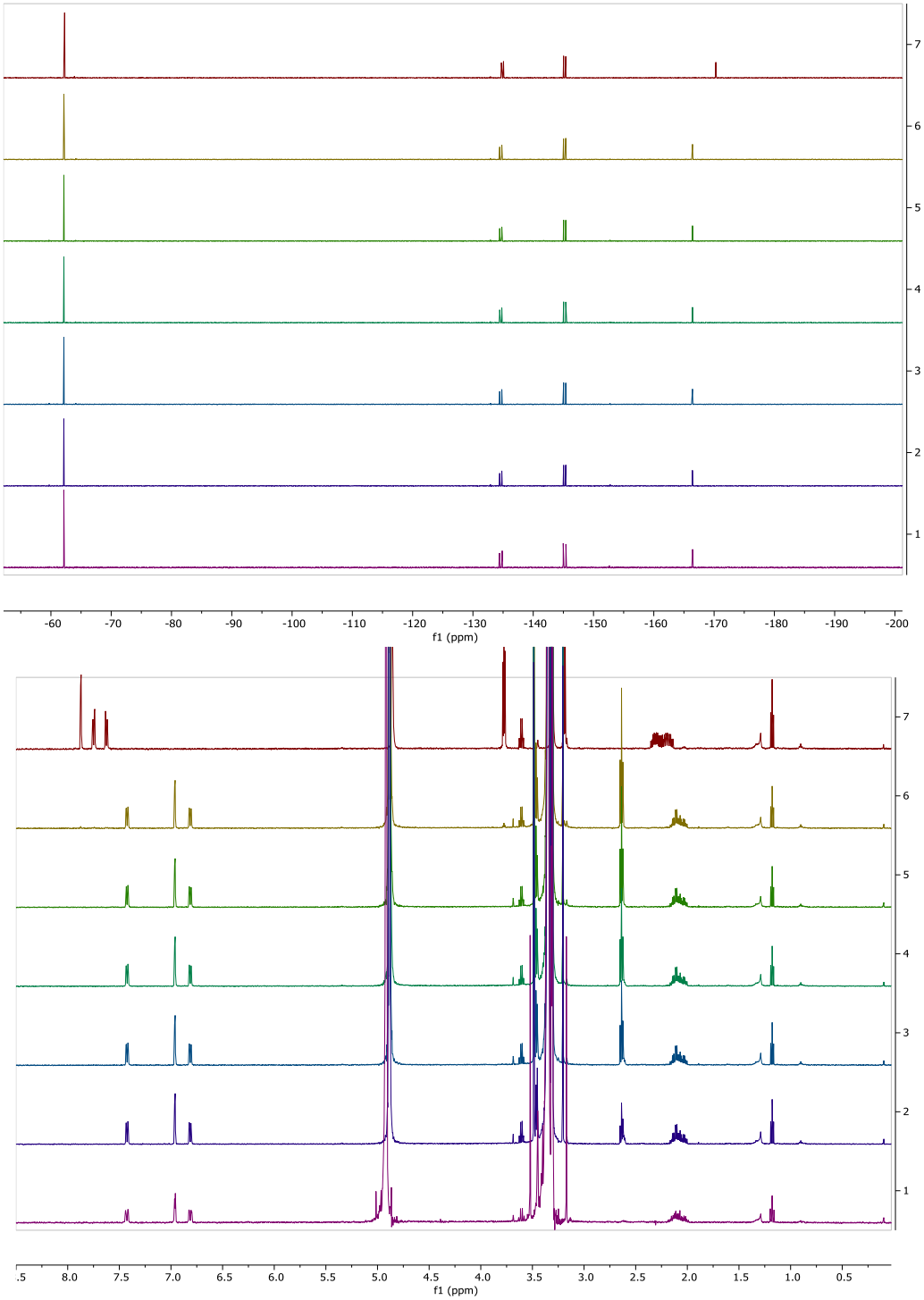

Figure 7.9: Stacked $\{^{1}H\}^{19}F$ NMR (top) and ^{1}H NMR (bottom) spectra of sodium methoxide ring hydrolysis of β-lactam **184**. From top to bottom: Initial, 0 h, 30 min, 1 h, 2 h, 5 h, 24 h.

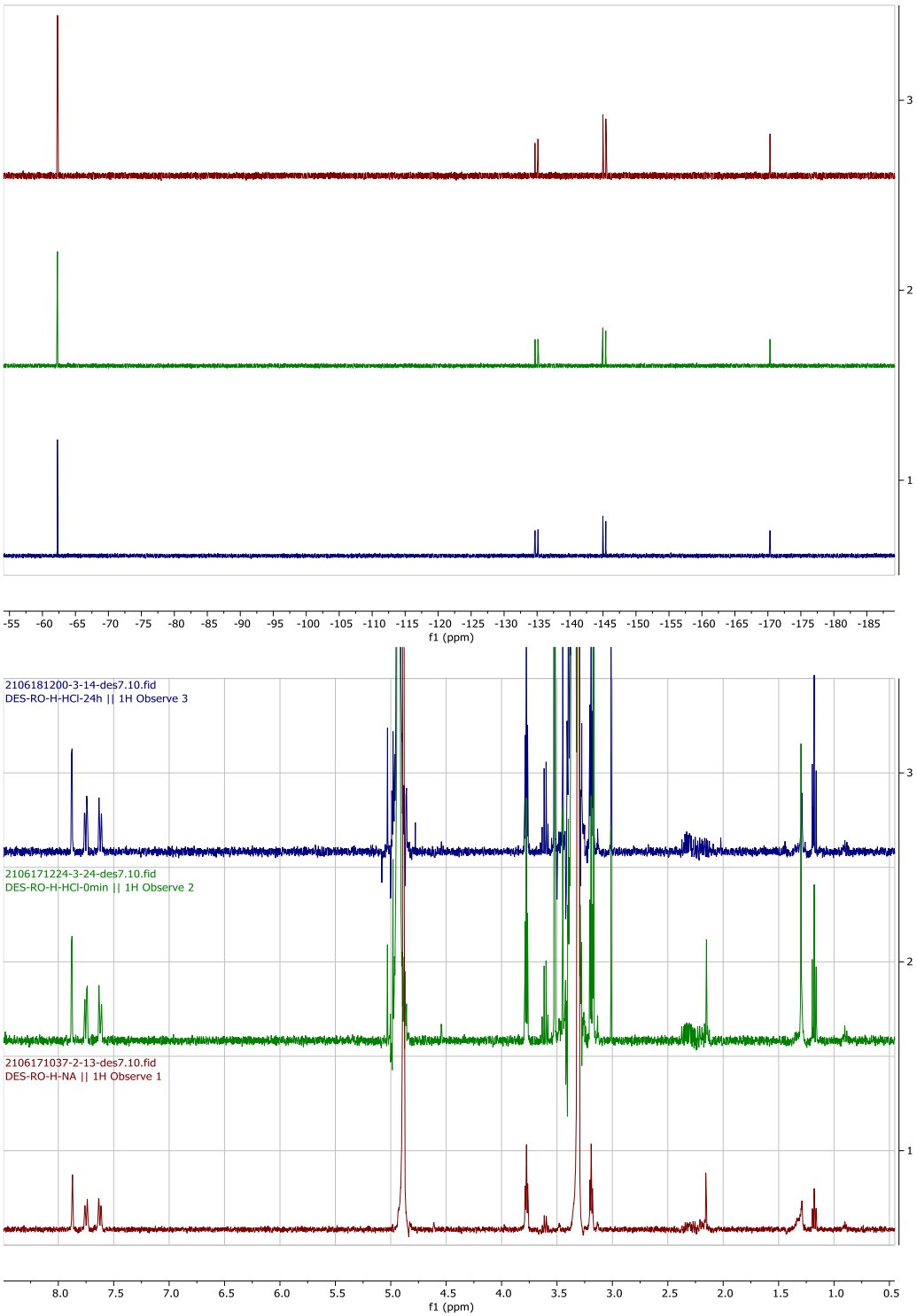

Figure 7.10: Stacked $\{^{1}H\}^{19}F$ NMR (top) and ^{1}H NMR (bottom) spectra of hydrochloric acid ring hydrolysis of β-lactam **184**. From top to bottom: Initial, 0 h, 24 h.

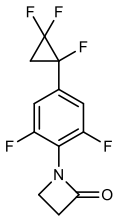

190

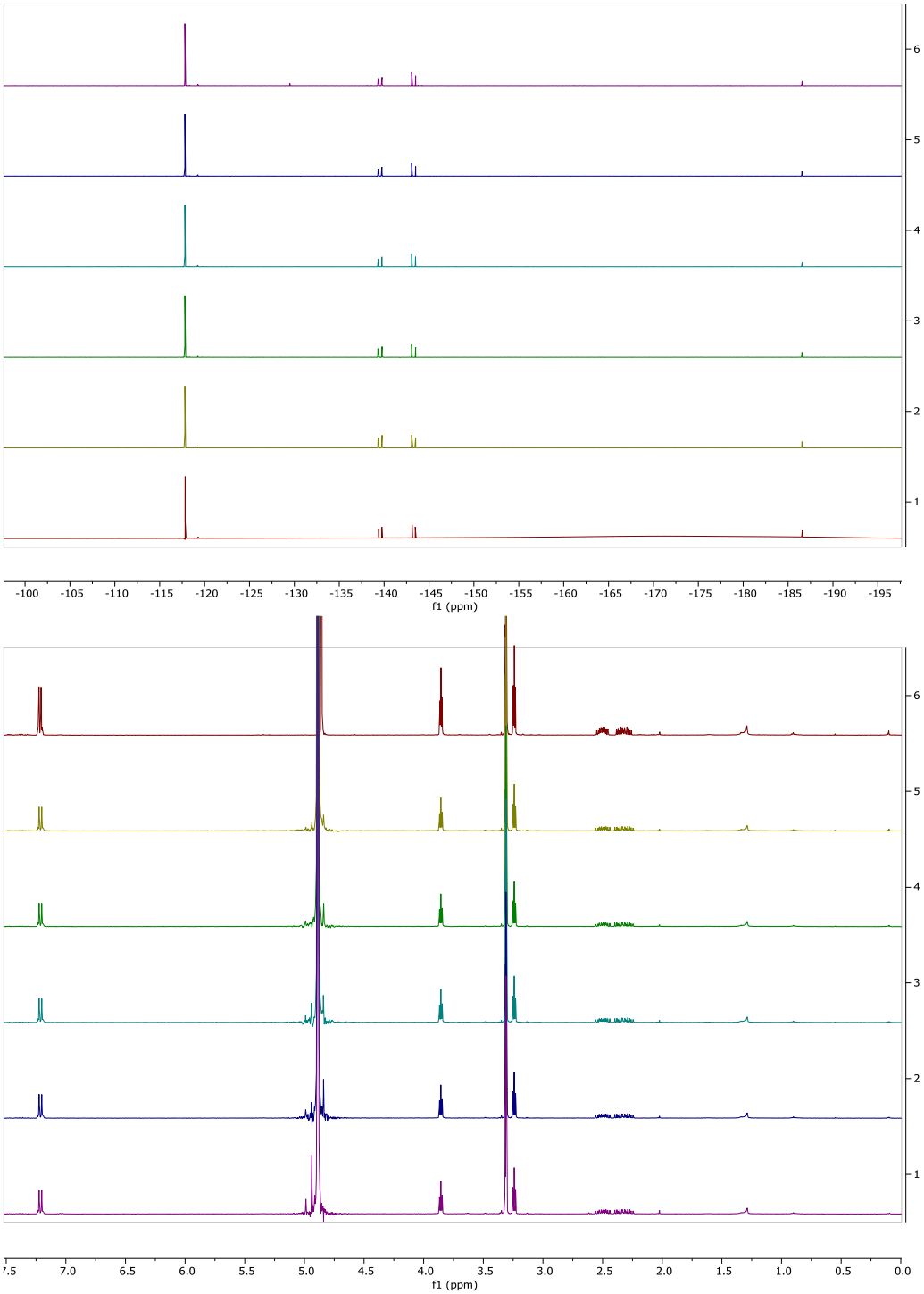

Figure 7.11: Stacked $\{^{1}H\}^{19}F$ NMR (top) and ^{1}H NMR (bottom) spectra of hydrochloric acid ring hydrolysis of β-lactam **190**. From top to bottom: Initial, 0 h, 30 min, 1 h, 2 h, and 24 h.

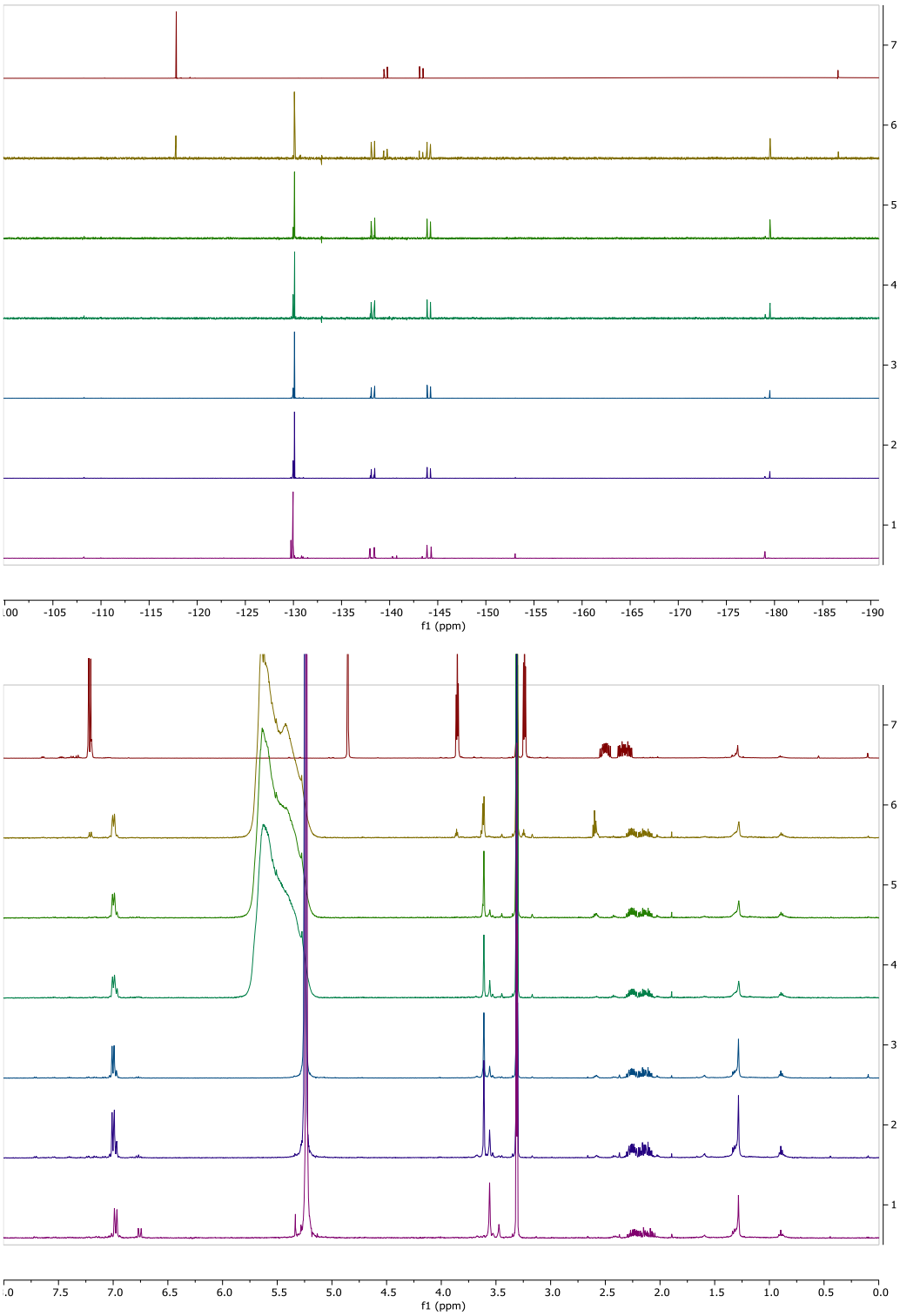

Figure 7.12: Stacked $\{^{1}H\}^{19}F$ NMR (top) and ^{1}H NMR (bottom) spectra of sodium methoxide ring hydrolysis of β-lactam **190**. From top to bottom: Initial, 0 h, 30 min, 1 h, 2 h, 5 h, 24 h.

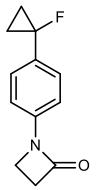

193

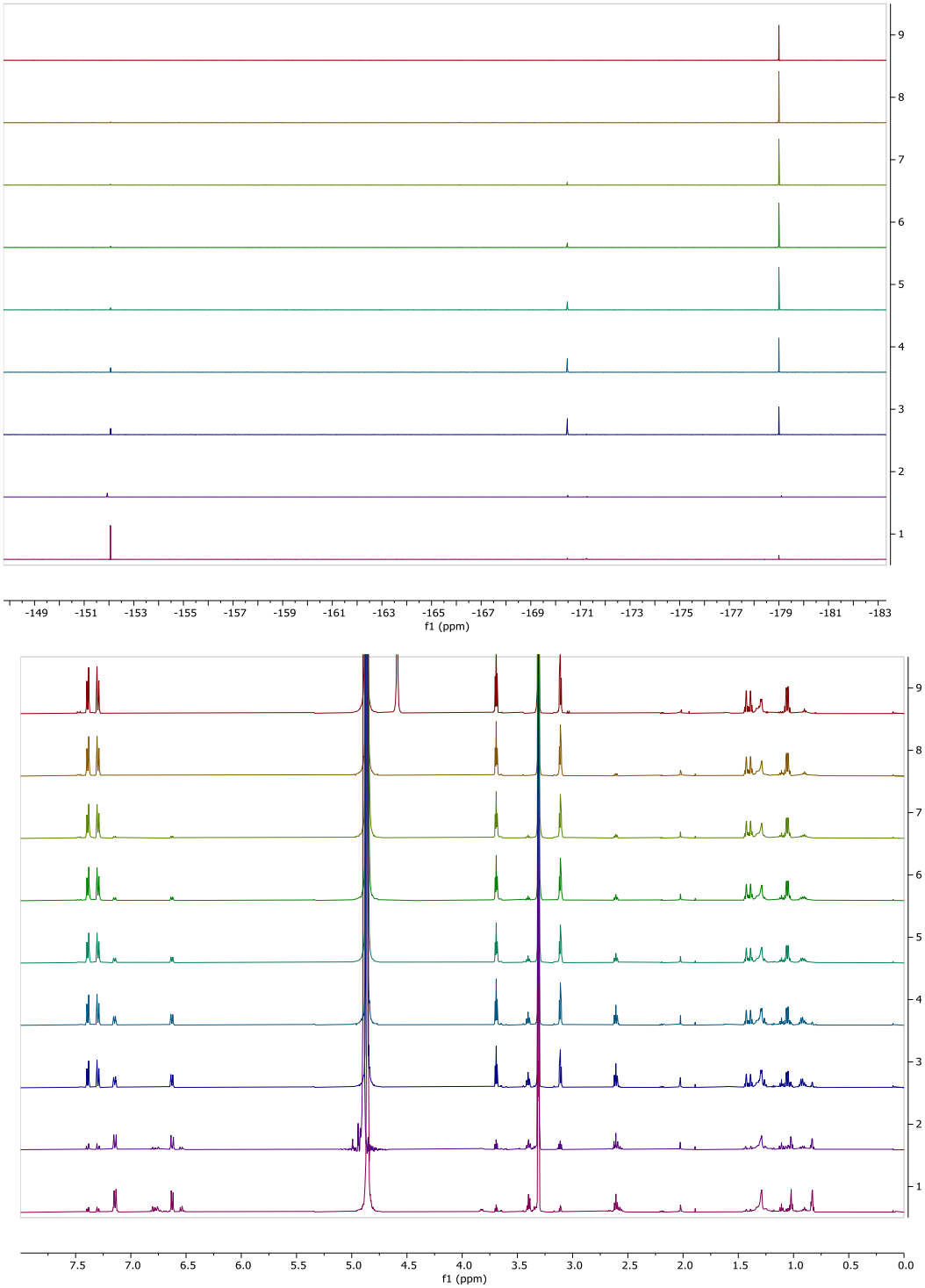

Figure 7.13: Stacked $\{^{1}H\}^{19}F$ NMR (top) and ^{1}H NMR (bottom) spectra of sodium methoxide ring hydrolysis of β-lactam **193**. From top to bottom: Initial, 0 h, 30 min, 1 h, 2 h, 4 h, 6 h, 24 h, 48 h.

7.5 – Estimation of log *P* values

Estimation of lipophilicity values were conducted using a Shimadzu Prominence system using a Phenomenex Synergi® Polar-RP 80Å (250 x 10.0 mm, 4μ) and a guard cartridge; Mobile phase: 0.05% TFA in water (solvent A) and 0.05% TFA in MeCN (solvent B); isocratic: 60% solvent B for 20 min. Flow rate: 2.5 mL/min; detection: 254 nm. A series of reference compounds with known Log *P* values were injected (10 μL, 1 mg/mL in acetonitrile) and their retention time (R_t) plotted against Log *P* to obtain a straight-line equation which was used to obtain Log *P* values for lactams (**144**, **181 – 183**, **190**, and **193**). The literature Log *P* values for the reference compounds were obtained from A. Rodil Garcia.[1]

The R_t of each reference compound was used to calculate their respective capacity factor (*K*) using Equation 7.1.

$$k = \frac{R_t - T_0}{T_0} \qquad 7.1$$

Where T_0 is column dead time (the time taken for an unretained compound to pass through the column), which for the used HPLC setup is 4.36 mins. Table 7.1 shows the measured retention time (R_t) (measured in triplicate), capacity factor (k) (calculated from average R_t), Log k, and the literature Log *P* of the standards used.[1]

Table 7.1: Measured retention time (R_t), capacity factor (k) and Log k of reference compounds against their literature Log *P*.[1]

Standards							
Reference Compound	R_t min^{-1}			Average R_t min^{-1}	Capacity Factor (k)	Log k	Lit. Log *P*
	Triplicate 1	Triplicate 2	Triplicate 3				
Phenol	6.53	6.54	6.54	6.54	0.499235474	-0.30169	1.50
Toluene	9.14	9.13	9.13	9.13	1.094801223	0.039335	2.73
Cumene	10.70	10.70	10.70	10.70	1.45412844	0.162603	3.66
Pyrene	16.24	16.22	16.23	16.23	2.722477064	0.434964	4.88

The Log k was plotted against the respective literature Log *P* for each reference compound to construct a reference line graph and obtain the corresponding straight-line equation (Figure 7.14).

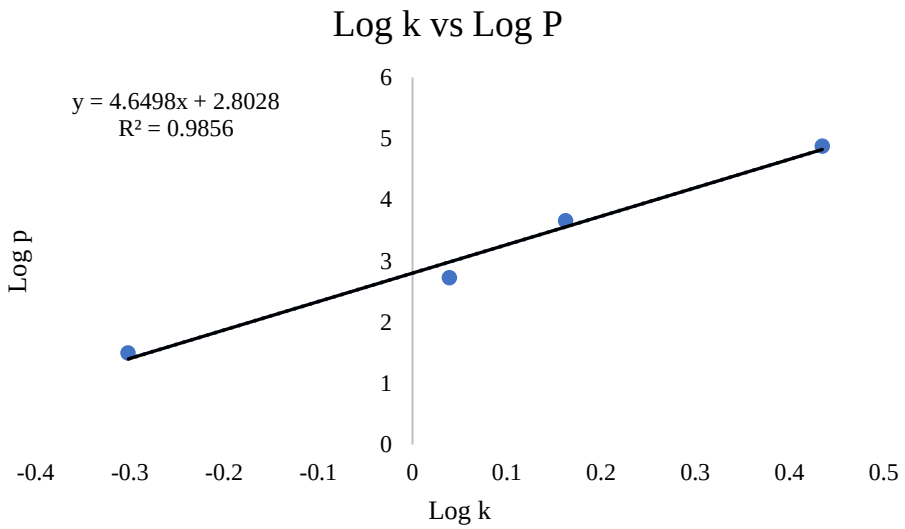

Figure 7.14: Log *P* vs Log k of compound standards with straight-line equation.

Using the straight-line equation produced by the line of best fit, the approximate Log *P* of the β-lactams were calculated from their retention time and in turn Log k value (Table 7.2).

Table 7.2: Measured retention time (R_t), capacity factor (k) and Log k of β-lactams and their calculated Log *P*.

β-Lactams							
Compound	R_t min^{-1}			Average R_t min^{-1}	Capacity Factor (k)	Log k	**Calc. Log P**
	Triplicate 1	Triplicate 2	Triplicate 3				
144	8.59	8.59	8.59	8.59	0.970183486	-0.01315	**2.74**
181	8.91	8.91	8.92	8.91	1.044342508	0.018843	**2.89**
182	8.79	8.79	8.78	8.79	1.01529052	0.00659	**2.83**
183	9.08	9.08	9.08	9.08	1.082568807	0.034456	**2.96**
190	8.33	8.33	8.33	8.33	0.910550459	-0.0407	**2.61**
193	8.68	8.68	8.68	8.68	0.990825688	-0.004	**2.78**

7.6 – Solution FRET

7.6.1 – Materials and methods

Two complementary ssDNA oligonucleotides were purchased (Integrated DNA Technologies) for use in the solution FRET quenching experiments (Table 7.3).

Table 7.3: Purchased ssDNA oligonucleotides.

Name	**Sequence**	**Molecular Weight/ g mol^{-1}**
Oligo 1	5'- GCG AGA TGG CGA GTC ACG -3'	5,589.7
Oligo 2	5'- CGT GAC TCG CCA TCT CGC – **Cyanine 3**	6,042.3
Oligo 3	**Biotin**–GCG AGA TGG CGA GTC ACG -3'	5,816.01

dsDNA was made by making stock solutions of Oligo 1 to 127 μM and Oligo 2 to 61 μM in buffer (50 mM Tris, 50 mM NaCl, pH 8). 0.315 μL of Oligo 1 solution and 0.656 μL of Oligo 2 solution were combined with 19 μL of buffer (50 mM Tris, 50 mM NaCl, pH 8) in an Eppendorf to make 20 μL of a 2 μM solution of dsDNA. The Eppendorf was sealed, and the solution mixed on a vortex before being heated to 95 °C for three minutes *via* heating block. The Eppendorf was then removed and allowed to cool to RT overnight to give annealed dsDNA. Integrity of the dsDNA was compared against Oligo 1 using SDS-PAGE. For ssDNA experiments, a stock solution of Oligo 2 was used.

Solution-based fluorescence emission spectra were collected using a Varian Eclipse fluorescence spectrophotometer. A Xenon flash lamp was used as an excitation source and all fluorescence emission spectra were corrected for fluctuations in excitation intensity. All solution-based samples were done in a quartz cuvette (path length = 1 cm) and all measurements were collected at a 90 ° angle relative to the incident light. A long pass filter was used to avoid excitation light entering the photomultiplier tube. Spectra were recorded using excitation wavelengths (λ_{exc}) of 545 nm and the recorded range was 550 nm to 750 nm and fluorescence intensity was measured every 0.5 nm.

Solution-based FRET experiments were performed as follows: a 50 nM solution (150 μL) of either dsDNA (3.75 μL) or ssDNA (0.122 μL) in buffer (50 mM Tris, 50 mM NaCl, pH 8) was made up in a cuvette before an initial measurement was recorded. A specific concentration of either the Janus face **208** or control **215** molecule in buffer (50 mM Tris, 50 mM NaCl, pH 8) was pipetted directly into the cuvette before an additional measurement was recorded (for specific volumes and concentrations, see Table 7.4 – Table 7.7). This process was repeated until the ligand (**208** or **215**) concentration in the cuvette reached 6000 nM. Each experiment was repeated thrice. Relative intensities at 545 nm and E_{FRET} values were calculated from an average of the triplicates. Control against ssDNA repeat 3 was not included in these averages due to a ten-fold discrepancy, likely caused by degradation of the ligand.

Table 7.4: Volumes and concentrations of titrated ligand Janus face **208** against dsDNA.

Janus Face 208 to dsDNA			
Ligand Vol. Added / µL	**Total Vol. In Cuvette / µL**	**Stock Ligand Conc. / µM**	**Ligand Conc. In Cuvette / nM**
0	150	-	0
0.274	150.274	13.7	25
0.274	150.548	13.7	50
0.274	150.822	13.7	75
0.274	151.096	13.7	100
0.547	151.643	13.7	150
0.547	152.190	13.7	200
0.547	152.737	13.7	250
0.547	153.284	13.7	300
1.094	154.378	13.7	400
1.094	155.472	13.7	500
1.094	156.566	13.7	600
2.189	158.755	13.7	800
2.189	160.944	13.7	1000
2.189	163.133	13.7	1200
0.438	163.571	137	1600
0.438	164.009	137	2000
0.876	164.885	137	2800
0.876	165.761	137	3600
0.876	166.637	137	4400
0.876	167.513	137	5200
0.876	168.389	137	6000

Table 7.5: Volumes and concentrations of titrated ligand Janus face **208** against ssDNA.

Janus Face 208 to ssDNA			
Ligand Vol. Added / µL	**Total Vol. In Cuvette / µL**	**Stock Ligand Conc. / µM**	**Ligand Conc. In Cuvette / nM**
0	150	-	0
0.680	150.680	5.5	25
0.680	151.360	5.5	50
0.680	152.040	5.5	75
0.680	152.720	5.5	100
1.360	154.080	5.5	150
1.360	155.440	5.5	200
1.360	156.800	5.5	250
1.360	158.160	5.5	300
0.273	158.433	55	400
0.273	158.706	55	500
0.273	158.979	55	600
0.546	159.525	55	800
0.546	160.071	55	1000
0.546	160.617	55	1200
1.091	161.708	55	1600
1.091	162.799	55	2000
2.182	164.981	55	2800
2.182	167.163	55	3600
2.182	169.345	55	4400
2.182	171.527	55	5200
2.182	173.709	55	6000

Table 7.6: Volumes and concentrations of titrated ligand control **215** against dsDNA.

Control 215 to dsDNA			
Ligand Vol. Added / µL	**Total Vol. In Cuvette / µL**	**Stock Ligand Conc. / µM**	**Ligand Conc. In Cuvette / nM**
0	150	-	0
0.276	150.276	13.6	25
0.276	150.552	13.6	50
0.276	150.828	13.6	75
0.276	151.104	13.6	100
0.552	151.656	13.6	150
0.552	152.208	13.6	200
0.552	152.760	13.6	250
0.552	153.312	13.6	300
1.102	154.414	13.6	400
1.102	155.516	13.6	500
1.102	156.618	13.6	600
0.220	156.838	136	800
0.220	157.058	136	1000
0.220	157.278	136	1200
0.440	157.718	136	1600
0.440	158.158	136	2000
0.880	159.038	136	2800
0.880	159.918	136	3600
0.880	160.798	136	4400
0.880	161.678	136	5200
0.880	162.558	136	6000

Table 7.7: Volumes and concentrations of titrated ligand Janus face **215** against ssDNA.

Control 215 to ssDNA			
Ligand Vol. Added / µL	**Total Vol. In Cuvette / µL**	**Stock Ligand Conc. / µM**	**Ligand Conc. In Cuvette / nM**
0	150	-	0
0.286	150.286	13.1	25
0.286	150.572	13.1	50
0.286	150.858	13.1	75
0.286	151.144	13.1	100
0.572	151.716	13.1	150
0.572	152.288	13.1	200
0.572	152.86	13.1	250
0.572	153.432	13.1	300
0.114	153.546	131	400
0.114	153.66	131	500
0.114	153.774	131	600
0.230	154.004	131	800
0.230	154.234	131	1000
0.230	154.464	131	1200
0.458	154.922	131	1600
0.458	155.38	131	2000
0.916	156.296	131	2800
0.916	157.212	131	3600
0.916	158.128	131	4400
0.916	159.044	131	5200
0.916	159.96	131	6000

The resulting spectra from the solution-based FRET quench experiments are shown below (n = 3).

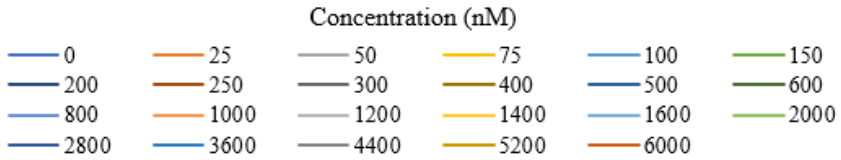

Figure 7.15: Ligand concentration legend for collected fluorescence spectra.

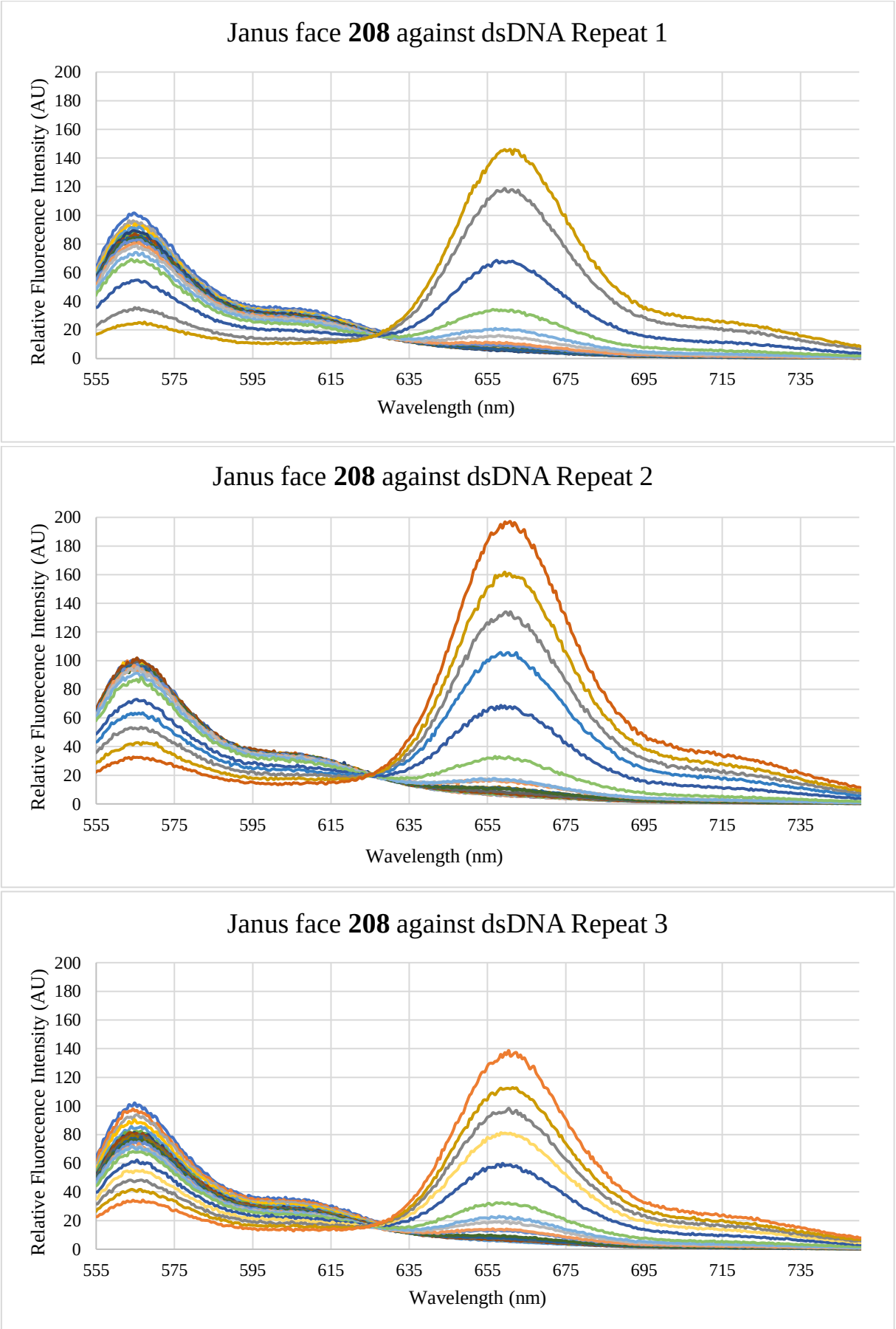

Figure 7.16: Triplicated fluorescence spectra from Janus face **208** against dsDNA.

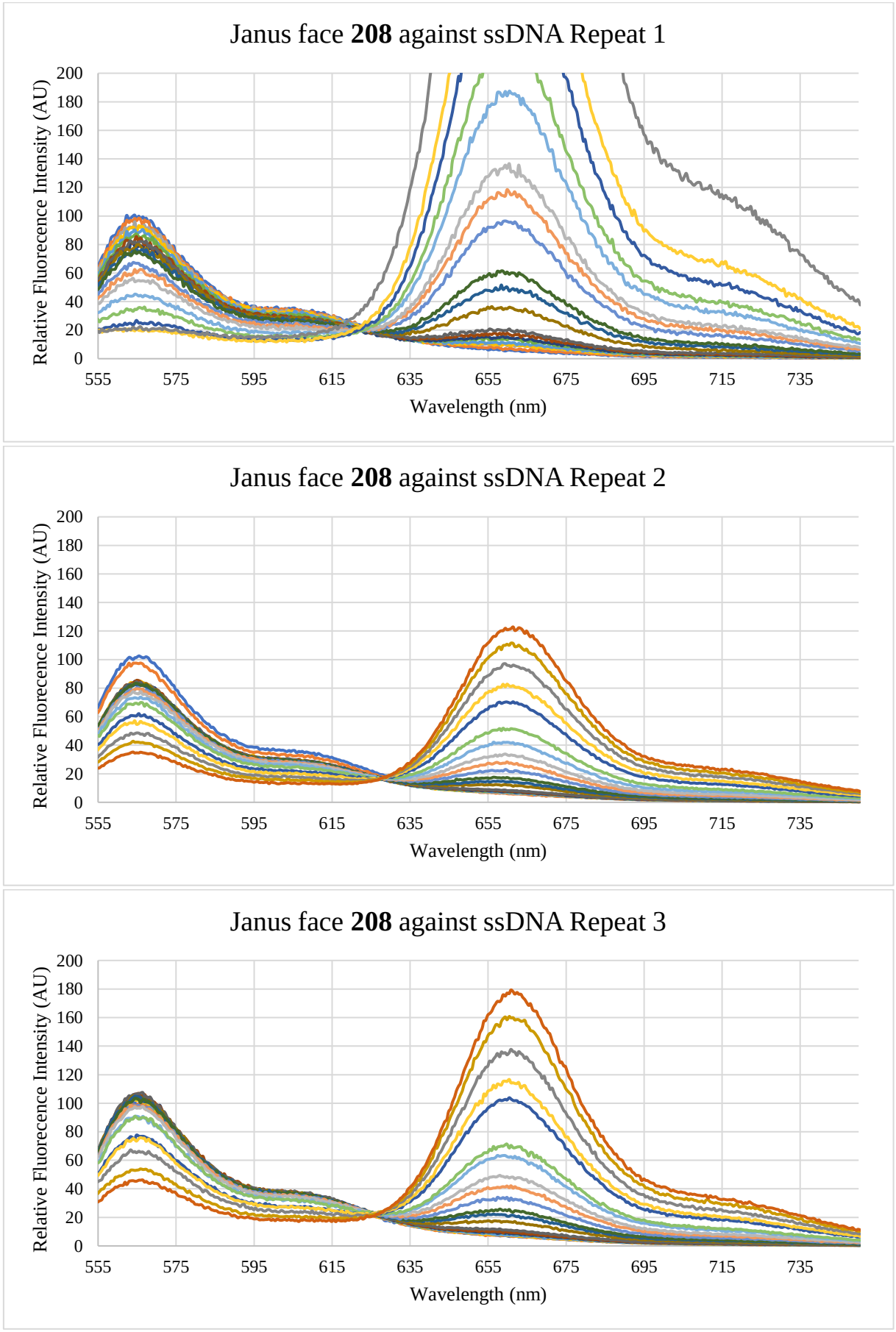

Figure 7.17: Triplicated fluorescence spectra from Janus face **208** against ssDNA.

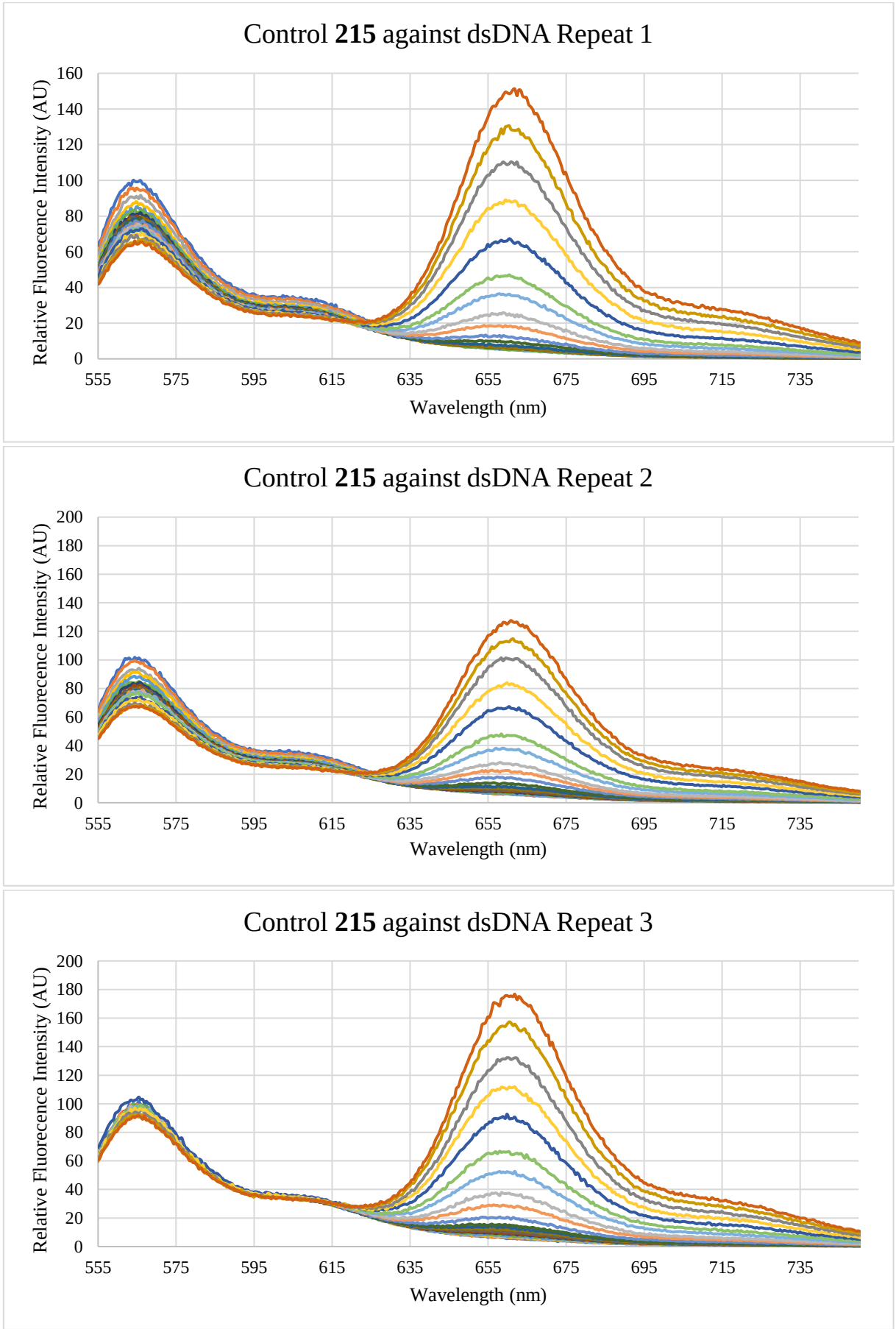

Figure 7.18: Triplicated fluorescence spectra from control **215** against dsDNA.

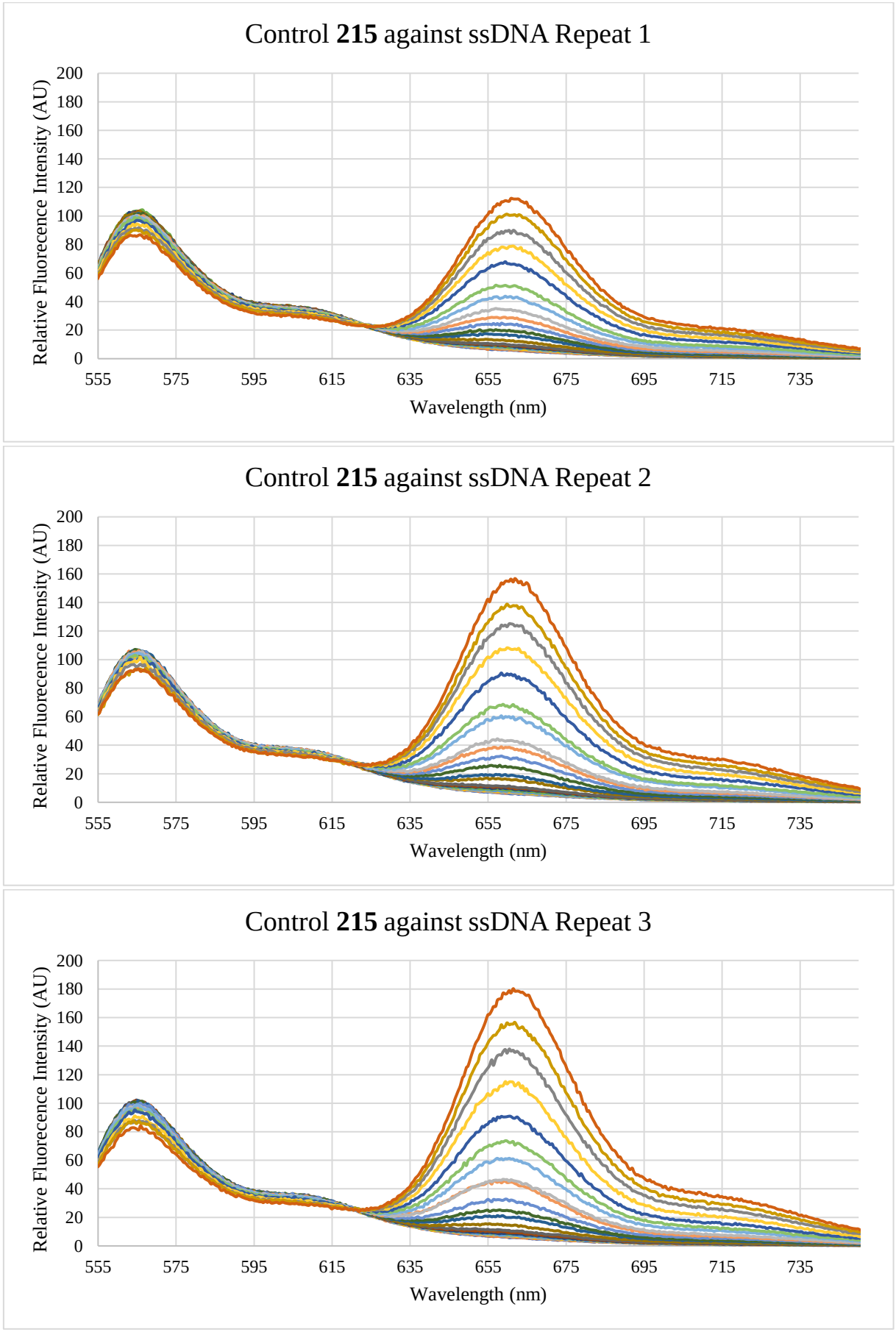

Figure 7.19: Triplicated fluorescence spectra from control **215** against ssDNA.

7.6.2 – Data processing

To compensate for increased dilution of the DNA solution (and in turn reduction of Cy3 emissions) during titration, all recorded fluorescence intensity points on the spectra were adjusted for dilution using Equation 7.2.

$$Int_{dillution} = Int\left(\frac{Vol_{total}}{Vol_{initial}}\right) \quad 7.2$$

Where Vol_{total} is the current volume in the cuvette and $Vol_{initial}$ is the starting volume in the cuvette (150 µL). To calibrate fluorescence intensity points across different spectra, a relative intensity ($Int_{relative}$) was then obtained for each spectrum using Equation 7.3.

$$Int_{relative} = Int_{dillution}\left(\frac{100}{Int_{Initial}^{564\,nm}}\right) \quad 7.3$$

Where $Int_{Initial}^{564\,nm}$ is the fluorescence intensity value of initial run (with no ligand) at 564 nm. This gives a fluorescence intensity value relative to the initial highest fluorescence intensity, which is set to 100 AU, allowing for easier comparison between spectra.

7.7 – ITC materials and methods

Two complementary ssDNA oligonucleotides were purchased (Integrated DNA Technologies) for use in the ITC experiments (Table 7.8).

Table 7.8: Purchased ssDNA oligonucleotides.

Name	Sequence	Molecular Weight/ g mol^{-1}
Oligo 1	5'- GCG AGA TGG CGA GTC ACG -3'	5,589.7
Oligo 4	5'- CGT GAC TCG CCA TCT CGC -3'	5,411.5

dsDNA was made by making stock solutions of Oligo 1 to 1 mM and Oligo 4 to 1 mM in buffer (50 mM Tris, 50 mM NaCl, pH 8). 0.6 mL of Oligo 1 solution and 0.6 mL of Oligo 4 solution were combined with 18.8 mL of buffer (50 mM Tris, 50 mM NaCl, pH 8) in a Falcon tube to make 20 mL of a 500 µM solution of dsDNA. The Falcon tube was sealed, and the solution mixed on a vortex before being heated to 95 °C for three minutes *via* heating block. The Falcon tube was then removed and allowed to cool to RT overnight to give annealed dsDNA. Integrity of the dsDNA was compared against Oligo 1 using SDS-PAGE (120 v, 50 min).

ITC measurements were performed at 20 °C in a MicroCal PEAQ-ITC calorimeter (Malvern Instruments). Janus face (**106**, **209**, and **211**) or proflavine **224** ligands were made up to 2.5 mM in buffer (50 mM Tris, 50 mM NaCl, pH 8). An initial injection of 0.4 μL was performed, followed by 18 successive injections of 2 μl of the chosen ligand into 400 μL of 20 μM dsDNA with 150 s interval between successive injections and a reference power of 10 μcal s^{-1}. The heat of dilution for each experiment was measured by titrating the chosen ligand into 400 μL of buffer and subtracted from the corresponding binding curve. Binding curves were fitted to a multi-site binding model as implemented in the PEAQ-ITC analysis software (Malvern Instruments).

7.8 – smFRET materials and methods

The dsDNA and ssDNA used for smFRET experiments were the same as that used for solution-based FRET quenching, with Cy3 replaced with Cy5 where appropriate (Chapter 7.6.1).

All single molecule imaging experiments were performed by Prof. Carlos Penedo. Quartz slides were passivated with a 30:1 mixture of PEG and biotinylated PEG (Molecular weight = 5,000) followed by a second passivation step with a short MS(PEG)4. Either Cy3 tagged dsDNA-biotin or Janus face-PEG-biotin **216** were added to the slide in a concentration of ~ 250 pM to which they are tethered *via* a biotin-streptavidin interaction. The imaging was carried out in 5 mM transcription buffer (50 mM Tris buffer, 50 mM NaCl) to which were added 5 mM protocatechuic acid (PCA), 100 nM protocatechuate 3,4-dioxygenase (PCD), and 2 mM 6-hydroxy-2,5,7,8-tetramethylchroman-2-carboxylic acid (TROLOX). Experiments were conducted at RT on a home-built prism-type total internal reflection (TIR) microscope (Olympus IX71) equipped with a 50 mW continuous wave laser operating at 532 nm. Donor and acceptor fluorescence emissions were separated using longpass dichroic mirrors (645 DCRLP, Chroma Technology) and simultaneously imaged onto the left and right half-chip of a back-illuminated Ixon EMCCD camera. Experimental movies were collected with an integration of 50 ms.

The mapping and processing of raw movies are performed by using custom-built routines in IDL 6.0 (Exelis, Boulder, USA). Calibration is done using carboxylated fluorescent polystyrene beads (Crimson Fluorescent Fluospheres, 0.2 μm) that are non-specifically bound to the surface of the slide. The representation of single-molecule trajectories is done using laboratory written routines in Matlab (Mathworks, Natick, USA).

7.9 – Fluorination materials and methods

In a total reaction volume of 800 μL, recombinant fluorinase (5 mg/mL) in phosphate buffer (pH 7.8) was incubated with phosphate buffer (50 mM), Janus face-PEG-ClDEA **244** (0.2 mM) or ClDA for the control (0.2 mM), L-SeMet (0.1 mM), and potassium fluoride (80 mM) at 37 °C. Samples (100 μL) were periodically removed, denatured by heating at 95 °C for 3 min, before being clarified by centrifugation (13 000 rpm, 10 min). Samples of the supernatant (60 μL) were removed for analysis by HPLC. HPLC analysis was performed on a Varian Prostar system equipped with a Varian 400 autosampler, Varian Prostar 230 solvent delivery system, Varian Prostar 235 UV-Vis detector using a Kinetix 5 μm XB-C18 100A (150 mm × 4.6 mm) column and a guard cartridge. Mobile phase: 0.05% TFA in water (solvent A) and 0.05% TFA in acetonitrile (solvent B); Linear gradient: 5% solvent B for 2 min, then from 5% to 25% of solvent B in 10 min, from 25% to 50% of solvent B in 3 min and finally 95% solvent B to flush the column; Flow rate: 1 mL/min; Detection: 260 nm; Injection volume: 20 μL.

7.10 – Radiolabelling materials and methods

^{18}F Fluoride was produced using a Siemens RDS-111 Eclipse cyclotron equipped with a fluoride target loaded with oxygen-18 enriched water by means of the ^{18}O(p,n)^{18}F reaction. The ^{18}F fluoride solution in oxygen-18 enriched water was transferred with a sweep of argon gas from the cyclotron target to the hot cell containing the reaction equipment. Radioactivity was measured using an ion chamber (ISOMED 2000 Dose Calibrator).

50 μL of ^{18}F fluoride solution in [^{18}O]water (205 MBq) was added to an Eppendorf containing Janus face-PEG-ClDEA **244** (9.6 mM), L-SeMet (2 mM) and freeze dried fluorinase/phosphate buffer (5 mg protein, 0.59 mM). The contents were well mixed and incubated at 37 °C for 30 min. After this time, the reaction mixture was heated at 95 °C for 5 min and the denatured protein was removed by centrifugation (13,000 rpm, 5 min). An aliquot (20 μL) of the supernatant was analysed by HPLC on a 1100 series Agilent equipped with a binary pump, a degasser, a flow cell detector and a diode array detector using a Phenomenex Luna 5 μm, C-18 100A (250 × 4.6 mm) column and a guard cartridge; Mobile phase: 0.05% TFA in water (solvent A) and 0.05% TFA in acetonitrile (solvent B); Linear gradient: 25-51% B in 15 min, 95% B in 20 min and then return to initial condition (25% B); Flow rate: 1 mL.min-1 . The supernatant was also analysed against a synthetic standard of Janus face-PEG-FDEA **253**, confirming the production of Janus face-PEG-[^{18}F]FDEA **254**. Conversion was calculated by area under curve of the HPLC trace.

7.11 – A_{2A} Receptor assay materials and methods

7.11.1 Cell culture and membrane preparation

$HEK_{293}hA_{2A}R$ cells were grown in culture medium consisting of Dulbecco's Modified Eagles Medium (DMEM) supplemented with 10% newborn calf serum, 50 µg/mL streptomycin, 50 IU/mL penicillin, and 500 µg/mL G418 at 37 ºC and 7% CO_2. Cells were subcultured twice a week at a ratio of 1:7 on 10 cm Ø plates or 1:6 on 15 cm Ø plates. $HEK_{293}hA_{2A}$ cells were grown to 80-90% confluency and detached from plates by scraping them into 5 mL phosphate-buffered saline (PBS). Detached cells were collected and centrifuged at 0.2 × g for 5 min. Pellets derived from 100 15 cm Ø plates were pooled and resuspended in 70 mL of Ice-cold 50 mM Tris-HCl buffer, pH 7.4. A Heidolph Diax 900 homogenizer was used to homogenize the cell suspension. Membranes and the cytosolic fraction were separated by centrifugation at 100,000x g in a Beckman Optima LE-80 K ultracentrifuge (Beckman Coulter, Fullerton, CA) at 4 ˚C for 20 min. The pellet was resuspended in 35 mL of the Tris-HCl buffer, and the homogenization and centrifugation step was repeated. Tris-HCl buffer (25 mL) was used to resuspend the pellet, and ADA was added (0.8 U/mL) to break down endogenous adenosine. Membranes were stored in 250 µL and 500 µL aliquots at -80 ˚C. Concentrations of the membrane protein were measured using the bicinchoninic acid method.

7.11.2 Radioligand displacement assay

Radioligand displacement experiments were performed using 6 concentrations of competing ligand in the presence of 1.7 nM [^{3}H]-ZM241385 **279**. At this concentration total radioligand binding did not exceed 10% of that added to prevent ligand depletion. The incubations are performed under standard conditions and in the presence of 1M NaCl to test the effect of NaCl on agonist affinity. Nonspecific binding was determined in the presence of 100 µM NECA (5′-(NEthylcarboxamido)adenosine) **269**. Membrane aliquots containing 25 µg of protein were incubated in a total volume of 100 µL of assay buffer (25 mM Tris-HCl, pH 7.4) at 25 ºC for 2 h to ensure the equilibrium was reached. Incubations were terminated by rapid vacuum filtration to separate the bound and free radioligand through prewetted 96-well GF/C filter plates using a PerkinElmer Filtermate-harvester (Perkin Elmer, Groningen, the Netherlands) after the indicated incubation time. Filters were subsequently washed 12 times with ice-cold wash buffer (25 mM Tris-HCl, pH 7.4). The plates were dried at 55 ºC and Microscint^{TM} -20 cocktail (Perkin Elmer, Groningen, The Netherlands). After 3 h the filter-bound radioactivity was determined by scintillation spectrometry using a 2450 MicroBeta Microplate Counter (Perkin Elmer, Groningen, The Netherlands).

7.11.3 Data analysis

All experimental data was analysed using GraphPad Prism 9.0 (GraphPad, Software, Inc., San Diego, CA). All values obtained are means of three independent experiments performed in duplicate. The K_D value of [^{3}H]ZM241385 **279** at the hA_{2A} membranes was obtained by computational analysis of saturation curves. IC_{50} values obtained from competition displacement binding data were converted into K_i values using the Cheng-Prusoff equation.

7.12 – References

1 A. Rodil Garcia, PhD Thesis, University of St Andrews, 2019.

2 M. S. Manhas and S. J. Jeng, *J. Org. Chem.*, 1967, **32**, 1246–1248.

3 B. Hurlocker, M. R. Miner and K. A. Woerpel, *Org. Lett.*, 2014, **16**, 4280–4283.

4 J. L. Clark, R. M. Neyyappadath, C. Yu, A. M. Z. Slawin, D. B. Cordes and D. O'Hagan, *Chem. Eur. J.*, 2021, **27**, 16000–16005.

5 J. Diot, M. I. García-Moreno, S. G. Gouin, C. O. Mellet, K. Haupt and J. Kovensky, *Org. Biomol. Chem.*, 2008, **7**, 357–363.

6 R. Zamboni, R. Henning, A. Ji, T. Smith, B. Heller, T. J. Reddy, S. Rocheleau, M. A. Beaulieu, US Pat. 15 965 506, 2018.

7 F. Tran, A. V. Odell, G. E. Ward and N. J. Westwood, *Molecules*, 2013, **18**, 11639–11657.

8 T. Suzuki, Y. Ota, M. Ri, M. Bando, A. Gotoh, Y. Itoh, H. Tsumoto, P. R. Tatum, T. Mizukami, H. Nakagawa, S. Iida, R. Ueda, K. Shirahige and N. Miyata, *J. Med. Chem.*, 2012, **55**, 9562–9575.

9 S.-C. Lu, F.-Q. Wen and X.-D. Guan, *Green Chem.*, 2021, **23**, 8964–8968.

10 S. Thompson, Q. Zhang, M. Onega, S. McMahon, I. Fleming, S. Ashworth, J. H. Naismith, J. Passchier and D. O'Hagan, *Angewandte Chemie Int. Ed.*, 2014, **53**, 8913–8918.

11 S. Thompson, I. N. Fleming and D. O'Hagan, *Org. Biomol. Chem.*, 2016, **14**, 3120–3129.

12 Z. Li, Y. Li, Y. Zhao, H. Wang, Y. Zhang, B. Song, X. Li, S. Lu, X.-Q. Hao, S.-W. Hla, Y. Tu and X. Li, *J. Am. Chem. Soc.*, 2020, **142**, 6196–6205.